frontiers | Research Topics

Molecular mechanisms of substance abuse and its neurotoxicity

Edited by
Jie Yan, Jianfeng Liu, Qian Ren and Qi Wang

Published in
Frontiers in Molecular Neuroscience

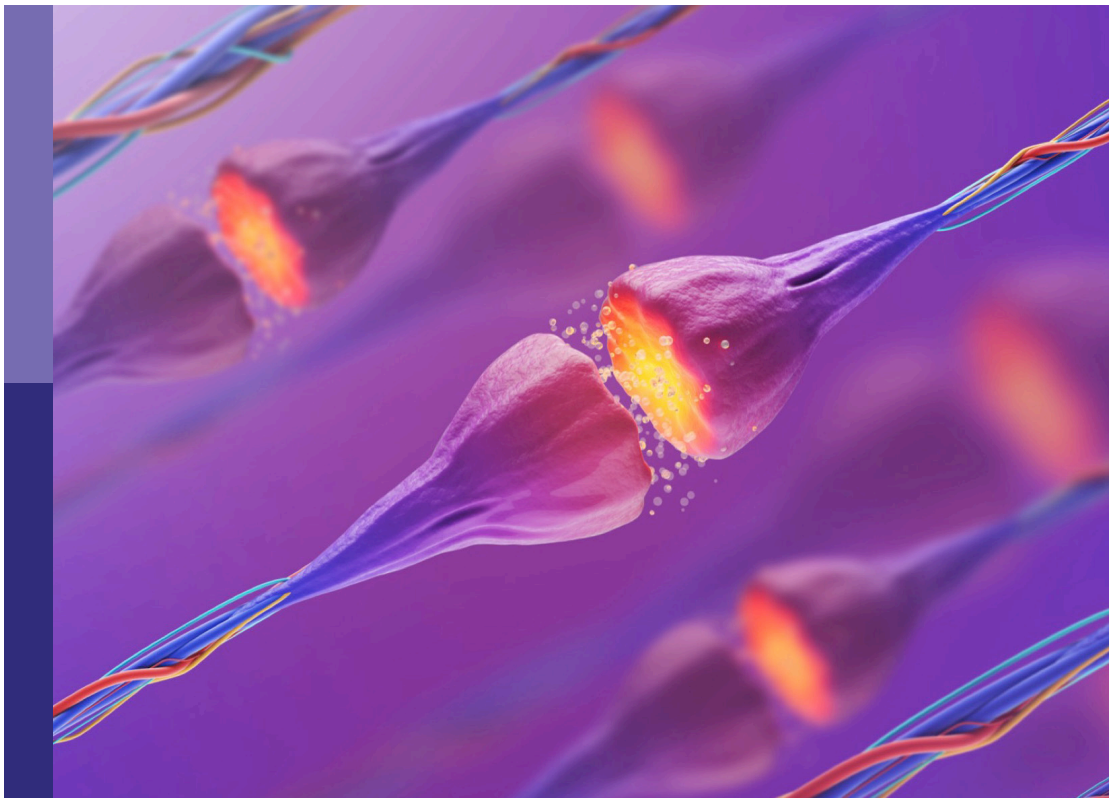

ISSN 1664-8714
ISBN 978-2-83251-141-1
DOI 10.3389/978-2-83251-141-1

About Frontiers

Frontiers is more than just an open access publisher of scholarly articles: it is a pioneering approach to the world of academia, radically improving the way scholarly research is managed. The grand vision of Frontiers is a world where all people have an equal opportunity to seek, share and generate knowledge. Frontiers provides immediate and permanent online open access to all its publications, but this alone is not enough to realize our grand goals.

Frontiers journal series

The Frontiers journal series is a multi-tier and interdisciplinary set of open-access, online journals, promising a paradigm shift from the current review, selection and dissemination processes in academic publishing. All Frontiers journals are driven by researchers for researchers; therefore, they constitute a service to the scholarly community. At the same time, the *Frontiers journal series* operates on a revolutionary invention, the tiered publishing system, initially addressing specific communities of scholars, and gradually climbing up to broader public understanding, thus serving the interests of the lay society, too.

Dedication to quality

Each Frontiers article is a landmark of the highest quality, thanks to genuinely collaborative interactions between authors and review editors, who include some of the world's best academicians. Research must be certified by peers before entering a stream of knowledge that may eventually reach the public - and shape society; therefore, Frontiers only applies the most rigorous and unbiased reviews. Frontiers revolutionizes research publishing by freely delivering the most outstanding research, evaluated with no bias from both the academic and social point of view. By applying the most advanced information technologies, Frontiers is catapulting scholarly publishing into a new generation.

What are Frontiers Research Topics?

Frontiers Research Topics are very popular trademarks of the *Frontiers journals series*: they are collections of at least ten articles, all centered on a particular subject. With their unique mix of varied contributions from Original Research to Review Articles, Frontiers Research Topics unify the most influential researchers, the latest key findings and historical advances in a hot research area.

Find out more on how to host your own Frontiers Research Topic or contribute to one as an author by contacting the Frontiers editorial office: frontiersin.org/about/contact

Molecular mechanisms of substance abuse and its neurotoxicity

Topic editors

Jie Yan — Central South University China

Jianfeng Liu — Wuhan University of Science and Technology, China

Qian Ren — Hebei Medical University, China

Qi Wang — Southern Medical University, China

Citation

Yan, J., Liu, J., Ren, Q., Wang, Q., eds. (2023). *Molecular mechanisms of substance abuse and its neurotoxicity*. Lausanne: Frontiers Media SA.

doi: 10.3389/978-2-83251-141-1

Table of contents

frontiers in Molecular Neuroscience

ORIGINAL RESEARCH
published: 04 January 2022
doi: 10.3389/fnmol.2021.808807

The Role of Hyperthermia in Methamphetamine-Induced Depression-Like Behaviors: Protective Effects of Coral Calcium Hydride

Xintao Wang[1,2,3†], Bonan Tong[1,2,3†], Rongji Hui[1,2,3], Congcong Hou[1,2,3], Zilu Zhang[4], Ludi Zhang[1,2,3], Bing Xie[1,2,3], Zhiyu Ni[5], Bin Cong[1,2,3], Chunling Ma[1,2,3] and Di Wen[1,2,3]**

[1] College of Forensic Medicine, Hebei Medical University, Shijiazhuang, China, [2] Hebei Key Laboratory of Forensic Medicine, Collaborative Innovation Center of Forensic Medical Molecular Identification, Shijiazhuang, China, [3] Research Unit of Digestive Tract Microecosystem Pharmacology and Toxicology, Chinese Academy of Medical Sciences, Shijiazhuang, China, [4] The First Clinical Medical College of Peking University Health Science Center, Peking University, Beijing, China, [5] School of Basic Medical Sciences, Hebei University, Baoding, China

OPEN ACCESS

Edited by:
Jie Yan,
Central South University, China

Reviewed by:
Kun Xiong,
Independent Researcher, Changsha, China
Xisheng Yan,
Wuhan Third Hospital, China

***Correspondence:**
Chunling Ma
chunlingma@126.com
Di Wen
wendi01125@126.com

[†]These authors have contributed equally to this work

Specialty section:
This article was submitted to Molecular Signalling and Pathways, a section of the journal Frontiers in Molecular Neuroscience

Received: 04 November 2021
Accepted: 06 December 2021
Published: 04 January 2022

Citation:
Wang X, Tong B, Hui R, Hou C, Zhang Z, Zhang L, Xie B, Ni Z, Cong B, Ma C and Wen D (2022) The Role of Hyperthermia in Methamphetamine-Induced Depression-Like Behaviors: Protective Effects of Coral Calcium Hydride. Front. Mol. Neurosci. 14:808807. doi: 10.3389/fnmol.2021.808807

Methamphetamine (METH) abuse causes irreversible damage to the central nervous system and leads to psychiatric symptoms including depression. Notably, METH-induced hyperthermia is a crucial factor in the development of these symptoms, as it aggravates METH-induced neurotoxicity. However, the role of hyperthermia in METH-induced depression-like behaviors needs to be clarified. In the present study, we treated mice with different doses of METH under normal (NAT) or high ambient temperatures (HAT). We found that HAT promoted hyperthermia after METH treatment and played a key role in METH-induced depression-like behaviors in mice. Intriguingly, chronic METH exposure (10 mg/kg, 7 or 14 days) or administration of an escalating-dose (2 ∼ 15 mg/kg, 3 days) of METH under NAT failed to induce depression-like behaviors. However, HAT aggravated METH-induced damage of hippocampal synaptic plasticity, reaction to oxidative stress, and neuroinflammation. Molecular hydrogen acts as an antioxidant and anti-inflammatory agent and has been shown to have preventive and therapeutic applicability in a wide range of diseases. Coral calcium hydride (CCH) is a newly identified hydrogen-rich powder which produces hydrogen gas gradually when exposed to water. Herein, we found that CCH pretreatment significantly attenuated METH-induced hyperthermia, and administration of CCH after METH exposure also inhibited METH-induced depression-like behaviors and reduced the hippocampal synaptic plasticity damage. Moreover, CCH effectively reduced the activity of lactate dehydrogenase and decreased malondialdehyde, TNF-α and IL-6 generation in hippocampus. These results suggest that CCH is an efficient hydrogen-rich agent, which has a potential therapeutic applicability in the treatment of METH abusers.

Keywords: methamphetamine, hyperthermia, depression, coral calcium hydride, oxidative stress, neuroinflammation

HIGHLIGHTS

- Hyperthermia plays a key role in METH-induced depression-like behaviors.
- High ambient temperature aggravates METH-induced depressive behaviors.
- CCH pretreatment inhibits METH-induced depression-like behaviors.
- CCH reduces METH-induced hippocampal synaptic plasticity damage.
- CCH has a potential therapeutic applicability in the treatment of METH abusers.

INTRODUCTION

Methamphetamine (METH) is a widely abused psychoactive substance all over the world (De-Carolis et al., 2015). Long-term or large dose use of METH leads to serious abnormalities in the cardiovascular, digestive, and immune system, and especially causes irreversible damage to the central nervous system (CNS) (Papageorgiou et al., 2019). As such, METH abusers are susceptible to neurodegenerative diseases, such as Parkinson's (Arab et al., 2019), Alzheimer's (Panmak et al., 2021), and Huntington's disease (Johnson et al., 2006), and generally present with a variety of psychiatric symptoms, such as depression and schizophrenia (Pogorelov et al., 2012).

Studies have shown that dopamine oxidative stress, excitotoxicity, and neuroinflammation are the most important mechanisms in METH-induced neurotoxicity (Halpin et al., 2014; Shaerzadeh et al., 2018; Pan et al., 2020). Additionally, hyperthermia is also a critical factor, and METH caused hyperthermia occurs in a dose- and ambient temperature-dependent manner (Molkov et al., 2014). A single medium or high dose of METH can cause a rapid rise of core body temperature, which is maintained for several hours, and this persistent hyperthermia aggravates METH-induced oxidative stress, excitotoxicity and neuroinflammation (Matsumoto et al., 2014; Liao et al., 2021). Immunohistochemistry index of tyrosine hydroxylase (Hotchkiss and Gibb, 1980; Kaewsuk et al., 2009), dopamine transporter (Sambo et al., 2018), glial fibrillary acidic protein (Castelli et al., 2014), and c-Fos in mice brain samples taken 6 days after METH administration confirmed that exposure to hot ambient temperature increases the neurotoxicity of METH (Cornish et al., 2012). However, whether hyperthermia plays a role in METH-induced psychiatric symptoms remains elusive.

Increasing evidence has indicated that treatment with antioxidant and anti-inflammatory agents is an effective intervention strategy that can effectively reduce the incidence of METH-induced neurotoxic complications (Murakami et al., 2018; Xie et al., 2018). Molecular hydrogen, as a novel healthcare product for a wide range of diseases, has recently become increasingly popular because of its unique anti-oxidative capability of selectively scavenging highly cytotoxic oxygen radicals and its anti-inflammatory properties (Qi et al., 2021). Our previous studies have revealed that molecular hydrogen delivered by *ad libitum* hydrogen-rich water (HRW) consumption significantly inhibited METH-induced spatial memory impairment in the Barnes and Morris water maze tests (Wen et al., 2019). In addition, hydrogen-rich saline (HRS) injections attenuated symptoms of low dose METH-induced behavioral sensitization (Wen et al., 2020). Up to now, drinking or bathing with HRW and inhalation of hydrogen gas (HG) have been used as the routes for administering hydrogen to humans (Zhu et al., 2018; Mikami et al., 2019). However, these methods hardly lead to the long-term effective accumulation of hydrogen owing to its low solubility in water. Coral calcium hydride (CCH), a porous powder made of coral calcium reacting with hydrogen at high temperature, generates HG gradually, when exposed to water (Ueda et al., 2010). Previous studies have reported that the maximum concentration of HG generated reached nearly 600 ppb in 5 $\sim$ 10 g CCH/L suspension. Moreover, this hydrogen could be steadily released for at least 24-h before its generation gradually declined (Hou et al., 2016). Herein, we hypothesized that the administration of CCH used to produce pure hydrogen may alleviate hyperthermia and prevent depression-like behaviors caused by high dose of METH exposure.

In this study, animals were treated with METH in different ambient temperatures to investigate the role of hyperthermia in METH-induced depression-like behaviors *via* tail suspension test (TST), forced swimming test (FST), and locomotion test (LMT). In addition, the effect of CCH on METH-induced hyperthermia and depression-like behaviors was also explored. As the damage of hippocampal neurons plays a key role in plasticity regulation of synapses and a critical role in the mechanism of depression, Golgi staining in hippocampus was conducted, and the index of oxidative stress and neuroinflammation were also measured by the detection of lactate dehydrogenase (LDH), malondialdehyde (MDA), IL-6 and TNF-α levels.

MATERIALS AND METHODS

Animals

Three hundred and ninety C57BL/6 mice, initially weighing 20–22 g (8 weeks old) were ordered from Beijing Vital River Laboratory Animal Technology Co., Ltd., China. All the mice were provided with food and water *ad libitum* and were kept in a climate controlled environment, at a consistent temperature ($22 \pm 1°C$), humidity (approximately 60%), and a 12-h light/dark cycle (lights off at 7:00 a.m.). All experimental procedures were approved by the Local Animal Use Committee of Hebei Medical University and performed in accordance with the National Institutes of Health Guide for the Care and Use of Laboratory Animals.

Drugs

DL-METH was provided by Beijing Municipal Public Security Bureau, China. CCH was provided by Shanghai Quanren Biological Technology Co., Ltd. (Shanghai, China). The stock solution of METH (1 g/mL) was dissolved in 0.9% sterile saline, and CCH was suspended in pure water

before use. The concentration of METH was adjusted to an appropriate injection volume of 10 mL/kg of body weight in each experiment.

Behavioral Testing

Tail Suspension Test

The procedure of behavioral testing was consistent with previous studies (Hao et al., 2019; Zhao et al., 2019; Luo et al., 2021). Four brightly lit 20 cm × 20 cm × 35 cm white, plexiglass arenas were used for the TST. The tail of each mouse was attached to a hook placed 3 cm from the top of each box using adhesive tape placed 1 cm away from the tip of the tail for a duration of 6 min. Immobility was defined as the absence of movement of limb or body when hung passively, and the immobility time during the last 5 min were measured. The behavioral tests were videotaped and analyzed using Noldus Video Tracking Software (Wageningen, Netherlands). Animals were separated from each other to prevent visual and acoustic interplay. The arena was cleaned with 75% alcohol between each test.

Forced Swim Test

Four transparent resin cylinders with a diameter of 10 cm and a height of 23 cm were filled with 15 cm of 23–25°C warm water for performing the FST. Each mouse was placed in a cylinder and videotaped for 6 min to record the immobility time. The immobility in the last 5 min was measured and analyzed using Noldus Video Tracking Software. Immobility was defined as the absence of limb or body movements, except for what is necessary to keep the body from sinking. During the test, mice were separated from each other to prevent visual and acoustic interplay. The used water was replaced with fresh water after each test.

Locomotion Test

The mice were placed in a brightly lit 40 cm × 40 cm white plexiglass arenas. The movement and location of the mice were recorded. The total distance traveled within the arena was recorded for a single 5 min session, which was used to measure the motor ability of the mice. The arena was cleaned with 75% alcohol between each test.

Experimental Design

Effect of Ambient Temperature on Methamphetamine-Induced Hyperthermia and Depression-Like Behaviors

The drug exposure regimen and dose described in previous studies were used in the present study. As shown in **Figure 1A**, two batches of mice kept at normal ambient temperature (NAT) of 22°C and high ambient temperature (HAT) of 28°C, respectively, were treated with four doses of 10 mg/kg METH *via* intraperitoneal (i.p.) injections with a 2-h interval in between each injection for 1 or 3 days. Two hours after the last METH injection, animals were placed back to their home cages at normal ambient temperature (22°C). The core body temperature of each mouse was recorded at 1-h after the first and second METH injection. Also, the core body temperature and body weight were measured at 24-h after the first METH injection. The depression-like behaviors were tested 7 and 14 days after METH exposure. All mice were tested in the following order: LMT, TST, and FST.

Effect of Drug Exposure Regimen and Dose on Methamphetamine-Induced Depression-Like Behaviors

Subsequently, the effect of different drug exposure regimens and doses on METH-induced depression-like behaviors was investigated (**Figure 2A**). Two batches of mice were administered 14 and 28 doses of 10 mg/kg METH injections (twice per day with 2-h interval) over 7 and 14 days, respectively. One batch was given four 15 mg/kg METH injections with 2-h interval for 3 days and one batch was given gradually increasing doses (2, 2, 5, 5, 5, 5, 10, 10, 10, 10, 15, and 15 mg/kg) of METH in 3 days (Martins et al., 2011; Ding et al., 2020; Chen et al., 2021). These experiments were all performed under NAT of 22°C. The depression-like behaviors were tested 7 and 14 days after METH exposure.

Effect of Molecular Hydrogen Generated by Coral Calcium Hydride on Methamphetamine-Induced Hyperthermia and Depression-Like Behaviors

Mice were pre-treated with CCH (100 and 200 mg/kg, intragastric route [i.g.]) resuspended in 0.2 mL pure water 1-h before METH exposure (10 mg/kg, once) at 28°C ambient temperature. The core body temperature was determined every 20 min for 2-h. To explore the effect of CCH on METH-induced depression-like behaviors, mice were treated with METH (10 mg/kg × 4) for 3 days and then administered with pure water (0.2 mL, i.g.) or CCH (100 and 200 mg/kg, i.g.) twice per day. The depression-like behaviors were tested 7 and 14 days after METH exposure by TST, FST, and LMT.

Effect of Methamphetamine Exposure and Coral Calcium Hydride Administration on the Hippocampal Synaptic Plasticity and Levels of Oxidative Stress Products and Inflammatory Cytokines

Mice were treated with METH (10 mg/kg × 4) for 3 days and then administered with pure water (0.2 mL, i.g.) or CCH (100 and 200 mg/kg, i.g.) twice per day. Golgi staining was performed to examine the effect of METH exposure and CCH administration on the hippocampal synaptic plasticity. Hippocampal tissues were dissected to detect the level of oxidative stress products (MDA and LDH) and inflammatory cytokines (TNF-α and IL-6) by commercial assay kits.

Golgi Staining

Golgi staining was used to detect the changes of dendritic spines in hippocampal neurons. The commercial Golgi staining kit made by Genmed Medicine Technology Co., Ltd. (Shanghai, China) was used. The mice were anesthetized with isoflurane and perfused with 1 × PBS solution and 4% paraformaldehyde. The brains of these mice were harvested and washed with pure water, then placed in a soak solution for 2 weeks in the dark and subsequently transferred to 30% sucrose solution for 48-h. Sagittal sections (80 ∼ 100 μm thick) were stained

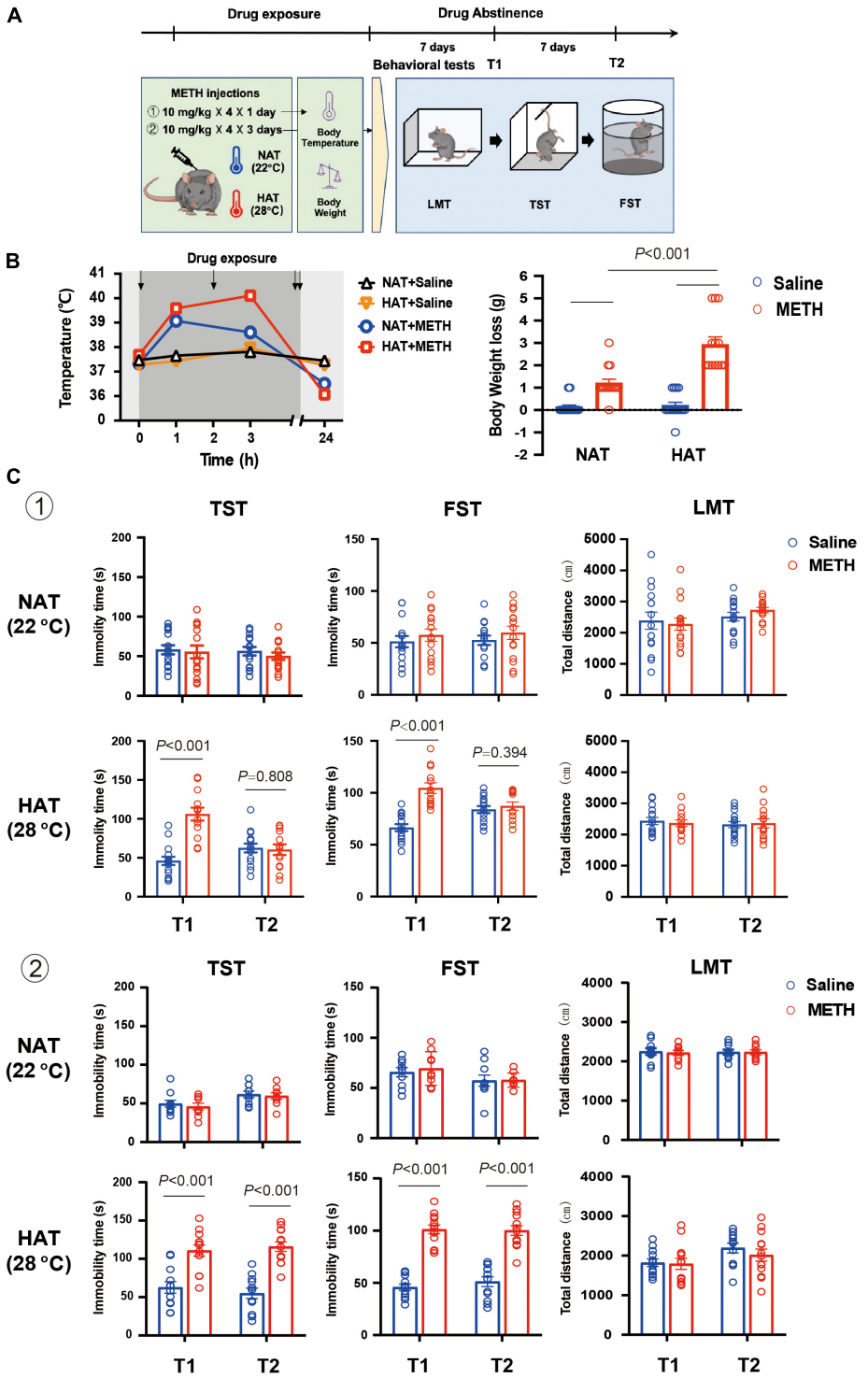

FIGURE 1 | Methamphetamine (METH) exposure induced hyperthermia and depression-like behaviors in an ambient temperature and dose-dependent manner. **(A)** Timeline of drug treatment and behavioral tests. **(B)** High ambient temperature aggravated METH-induced hyperthermia (left) and body weight loss (right). Four doses of METH (10 mg/kg i.p.) treatments were given to mice each within 2-h interval. The arrows represented drug exposure. Body temperature was determined at 0-, 1-, 3-, and 24-h after the first METH treatment, and body weight loss was calculated at 24-h after drug treatment. (n = 15, 15, 15, and 13) **(C)** METH exposure (a: 10 mg/kg × 4 injections × 1 day; b: 10 mg/kg × 4 injections × 3 days) under high ambient temperature (28°C) induced depression-like behaviors in mice. The behavioral tests including locomotion test (LMT), tail suspension test (TST), and forced swimming test (FST) were performed 7 (T1) and 14 (T2) days after METH treatments (**a:** n = 15 and 15 for NAT, n = 15 and 13 for HAT; **b:** n = 10 and 9 for NAT, n = 12 and 13 for HAT). Data are expressed as the mean ± SEM.

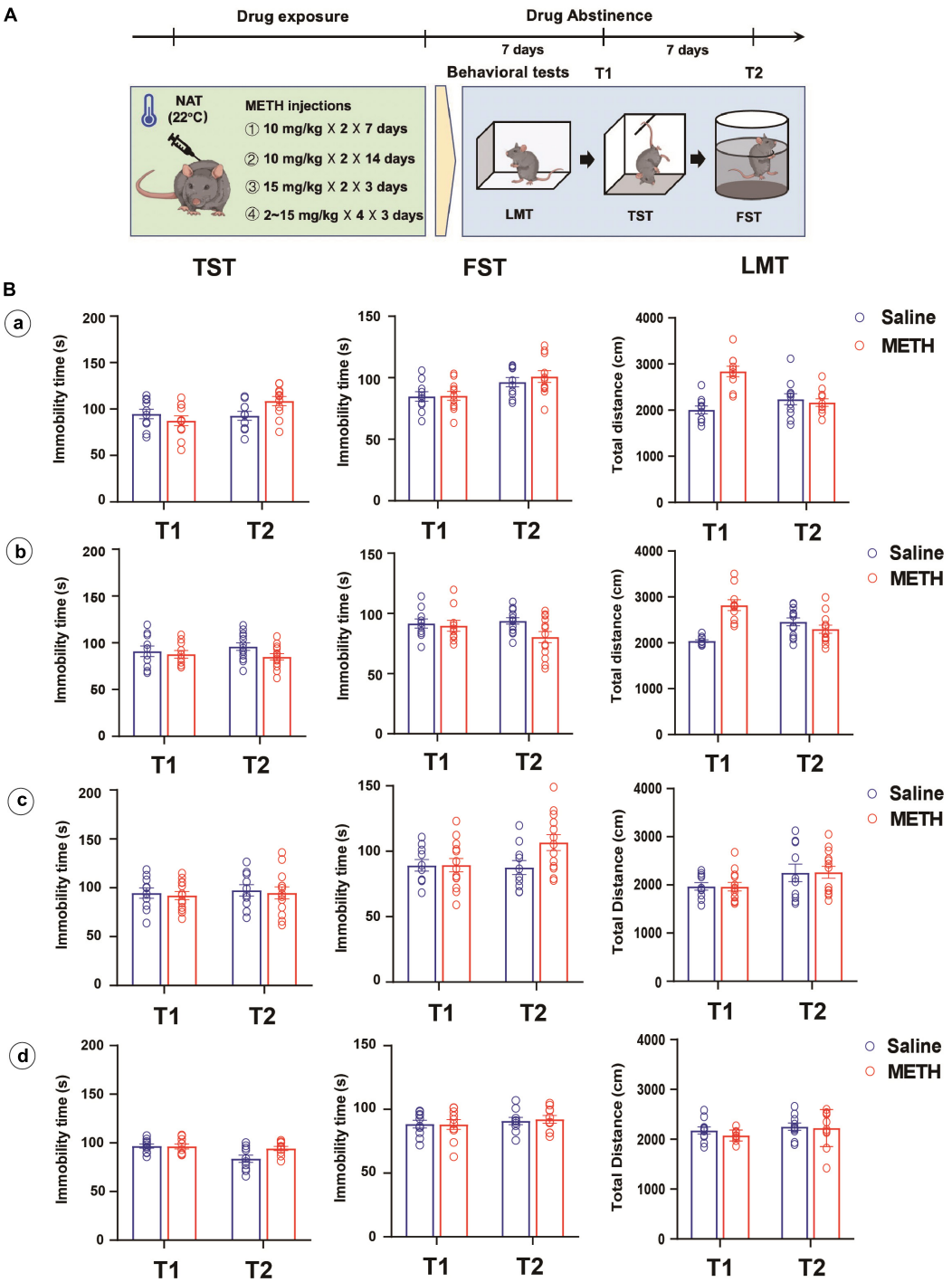

FIGURE 2 | Longer-term (10 mg/kg × 2, 7 and 14 days), higher dose (15 mg/kg × 4, 3 days) or escalating-dose (2–15 mg/kg, 3 days) regimen of METH treatments under normal ambient temperature (22°C) failed to induce depression-like behaviors in mice. **(A)** Timeline of drug treatment and behavioral tests. **(B)** Different METH treatment procedures (**a:** 10 mg/kg × 2, 7 days; **b:** 10 mg/kg × 2, 14 days; **c:** 15 mg/kg × 4, 3 days; **d:** 2, 2, 5, 5, 5, 5, 10, 10, 10, 10, 15, and 15 mg/kg in 3 days) were performed in mice, and the depression-like behaviors and locomotion were tested at 7 (T1) and 14 (T2) days after METH exposure (**a:** n = 10 and 11; **b:** n = 10 and 12; **c:** n = 10 and 13; **d:** n = 10 and 10). Data are expressed as the mean ± SEM.

using the oscillating sectioning technique. One out of every five sections were selected, and a total of three sections were selected from each mouse. After Golgi staining, the changes of dendritic spines were observed under a microscope, and the number of dendritic spines was calculated by two independent observers.

Measurement of TNF-α, IL-6, Malondialdehyde, and Lactate Dehydrogenase Levels

The levels of TNF-α and IL-6 in hippocampal tissues were detected by enzyme-linked immunosorbent assay (ELISA). The experiment was conducted according to the product instruction (ABclonal Technology Co., Ltd., Wuhan, China). The levels of MDA and LDH, which are the markers of lipid peroxidation, were determined using a thiobarbituric acid (TBA) assay kit and 2,4-dinitrophenylhydrazine colorimetric assay kit (Beyotime Technology, Shanghai, China) in accordance with the manufacturer's protocol. After completing the drug treatments, hippocampal tissues of six mice in each group were collected and stored at −80°C until analysis. When performing the experiments, the tissues were homogenized in PBS buffer and centrifuged to collect the supernatant. The total protein content was tested using a Bicinchoninic Acid (BCA) protein assay kit (Solarbio, Beijing, China). The levels of TNF-α, IL-6, MDA and LDH was measured in nanomole per microgram (nmol/mg) of protein.

Data Analysis

Data are presented as means ± standard error of mean (SEM). Analysis of variance (ANOVA) including one-way, two-way, and three-way ANOVA and mixed ANOVA (repeated-measures design) were used for the statistical analyses. Bonferroni's *post hoc* test was performed to assess the differences between groups. Unpaired two-tailed Student's *t*-test was used to compare two independent groups. The threshold for statistical significance was set at $P < 0.05$ (GraphPad, v.8.0, CA, United States).

RESULTS

Animal Exclusion

A total of 390 C57BL/6 mice were initially purchased. With regard to accidental death after METH treatment, especially under HAT, the number of mice in each group was inconsistent in experimental design. In total, 24 mice died during METH treatments, 6 mice died because the failure of intragastric injection, and 5 mice were excluded due to poor general state and low activity in locomotion test. Thus, a total of 355 experimental animals were included in the data analysis.

High Ambient Temperature Aggravated Methamphetamine-Induced Hyperthermia and Body Weight Loss

Mice were treated with four doses of 10 mg/kg METH with 2-h interval in between doses at normal (22°C) and high (28°C) ambient temperatures (Baladi et al., 2014), and the control mice received four saline (10 mg/kg) injections (Zhu et al., 2006; García-Cabrerizo et al., 2018). As shown in **Figure 1B**, METH exposure under HAT led to severe hyperthermia (left) and greater body weight loss (right). The mixed ANOVA (repeated measure) revealed significant effects on body temperature of METH treatment ($F_{1,54} = 57.29$, $P < 0.001$) and ambient temperature ($F_{1,54} = 15.06$, $P < 0.001$), and significant interaction of METH treatment with ambient temperature ($F_{1,54} = 5.68$, $P = 0.021$). In addition, the two-way ANOVA revealed significant main effects on body weight loss for METH treatment ($F_{1,54} = 89.03$, $P < 0.001$), ambient temperature ($F_{1,54} = 19.86$, $P < 0.001$), and interaction of METH treatment and ambient temperature ($F_{1,54} = 17.01$, $P < 0.001$). *Post hoc* comparisons indicated that the body weight loss was much more serious when METH was given under HAT ($P < 0.001$), compared to NAT.

Methamphetamine Exposure Induced Depression-Like Behaviors in an Ambient Temperature and Dose-Dependent Manner

To investigate the potential effects of hyperthermia on depression-like behaviors, mice were treated with METH (10 mg/kg × 4 injections) at NAT (22°C) and HAT (28°C), and the behavioral tests including LMT, TST, and FST were performed 7 (T1) and 14 (T2) days later. As shown in **Figure 1C**, METH treatment under the NAT did not induce any depression-like behaviors in TST (T1: $P = 0.782$; T2: $P = 0.390$) and FST (T1: $P = 0.442$; T2: $P = 0.365$). However, METH treatment given with HAT induced depression-like behaviors both in TST ($P < 0.001$) and FST ($P < 0.001$) at 7 days after METH exposure (T1) but recovered in T2 tests (TST: $P = 0.808$; FST: $P = 0.394$). All the LMT results showed no significant differences between groups in T1 and T2 tests (NAT: $P = 0.753$ and $P = 0.209$; HAT: $P = 0.456$ and $P = 0.853$).

Next, we increased the doses of METH treatments to 10 mg/kg × 12 injections (in 3 days). The results of behavioral tests also showed no difference between groups in T1 (TST: $P = 0.568$; FST: $P = 0.611$) and T2 (TST: $P = 0.707$; FST: $P = 0.938$) tests when METH treatment was performed under NAT. However, METH treatment given with HAT induced long-lasting depression-like behaviors at least for 14 days. The results of FST and TST test revealed significant differences between saline and METH group in T1 (TST: $P < 0.001$; FST: $P < 0.001$) and T2 (TST: $P < 0.001$; FST: $P < 0.001$) tests. Moreover, METH treatments under NAT and HAT did not affect the locomotion of animals in T1 and T2 procedures (NAT: $P = 0.749$ and $P = 0.979$; HAT: $P = 0.797$ and $P = 0.460$).

Interestingly, we involved different METH exposure regimens and doses under NAT with the aim to induce depression-like behaviors. As shown in **Figure 2B**, long-term (a and b), higher dose (c), or escalating-dose (d) regimen of METH exposure failed to induce depression-like behaviors and locomotion deficit in mice, only except for the total distance traveled by mice in LMT, which increased after 7 or 14 days of METH treatments and 7 days of drug abstinence when compared to that of control mice ($P < 0.001$).

Inhibition of Methamphetamine-Induced Hyperthermia and Depression-Like Behaviors Using Coral Calcium Hydride Generated Molecular Hydrogen

Since CCH interaction with water under acidic conditions leads to gradual HG production, mice were administrated with

CCH intragastrically before and after METH treatments to investigate the preventative and therapeutic effect of molecular hydrogen on METH-induced hyperthermia and depression-like behaviors, respectively. Mice were pretreated with CCH (100 and 200 mg/kg, i.g.), and received METH injection (10 mg/kg, i.p.) 1-h later under HAT (28°C) (**Figure 3A**). The core body temperature was determined every 20 min for next 2-h. As shown in **Figure 3B**, CCH pretreatment significantly attenuated METH-induced hyperthermia. The two-way ANOVA indicated significant main effects on body temperature for drug treatment ($F_{3,35} = 4.007$, $P = 0.015$) and time ($F_{3.256,114} = 35.58$, $P < 0.001$), and interaction of drug treatment and time ($F_{18,210} = 4.90$, $P < 0.001$). Moreover, the one-way ANOVA revealed significant difference in body temperature at 60 min after METH treatment between groups ($F_{3,35} = 14.06$, $P < 0.001$). *Post hoc* comparisons indicated a rise in body temperature in METH-treated mice ($P < 0.001$), and an inhibitory effect of CCH pretreatment at doses of 200 mg/kg ($P = 0.002$), but not 100 mg/kg ($P = 0.801$) on METH-induced increase of body temperature (**Figure 3C**).

To examine the therapeutic effect of CCH on METH-induced depression, CCH (100 and 200 mg/kg, i.g.) treatments were given to mice for 7 days (once per day) after METH injections (10 mg/kg × 4 × 3 days, i.p.) (**Figure 3D**). As shown in **Figure 3E**, the results of one-way ANOVA revealed significant differences between groups in the immobility time in TST ($F_{3,28} = 18.74$, $P < 0.001$) and FST ($F_{3,28} = 39.34$, $P < 0.001$). *Post hoc* comparisons indicated significant therapeutic effect of 100 mg/kg (TST: $P = 0.002$; FST: $P < 0.001$) and 200 mg/kg (TST: $P < 0.001$; FST: $P < 0.001$) CCH on METH-induced depression-like behaviors. Furthermore, there were no differences noted on the total distance in LMT between groups ($F_{3,28} = 1.473$, $P = 0.2432$).

Coral Calcium Hydride Induced Reversal of Methamphetamine-Induced Hippocampal Synaptic Plasticity Damage and Attenuation of Degree of Oxidative Stress and Neuroinflammation

Golgi staining showed that METH elicited hippocampal synaptic plasticity damage in mice, and this change was more severe when METH was given under HAT ($P = 0.027$, **Figure 4A**). The two-way ANOVA indicated significant main effects on spine number for METH treatment ($F_{1,8} = 176.20$, $P < 0.001$) and ambient temperature ($F_{1,8} = 13.52$, $P = 0.006$), but no interaction of METH treatment and ambient temperature ($F_{1,8} = 3.353$, $P = 0.104$). Furthermore, METH induced oxidative stress and neuroinflammation in a time-dependent manner. The one-way

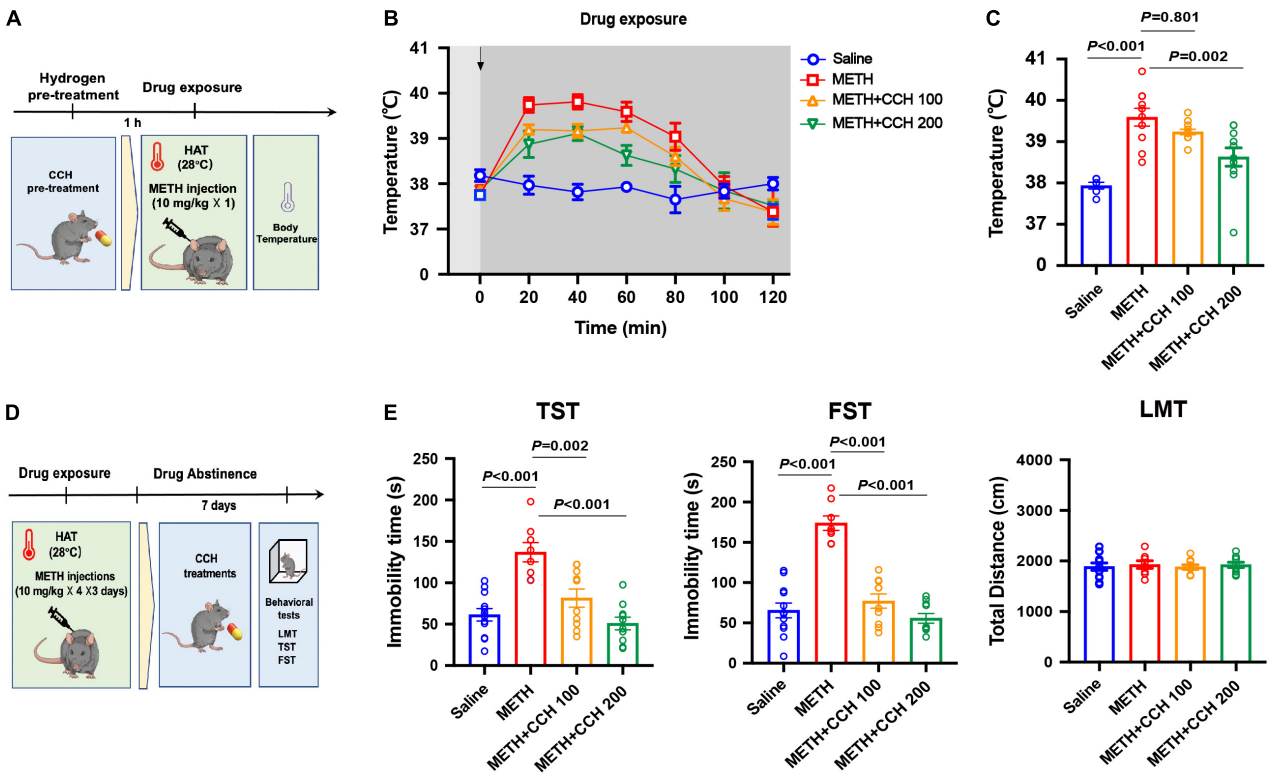

FIGURE 3 | Coral calcium hydride (CCH) administration inhibited METH-induced hyperthermia and depression-like behaviors. **(A)** Timeline of CCH pre-treatment, METH exposure and core body temperature determination. **(B)** The core body temperature was determined every 20 min after METH (10 mg/kg, i.p.) injection for 2-h (n = 6, 10, 12, and 11). The arrows represent drug treatment. **(C)** The body temperature at 60 min after METH treatment was analyzed. **(D)** Timeline of METH exposure, therapeutic CCH treatment and behavioral tests. **(E)** Effect of CCH administration on METH-induced depression-like behaviors (n = 8 per group). Data are expressed as the mean ± SEM.

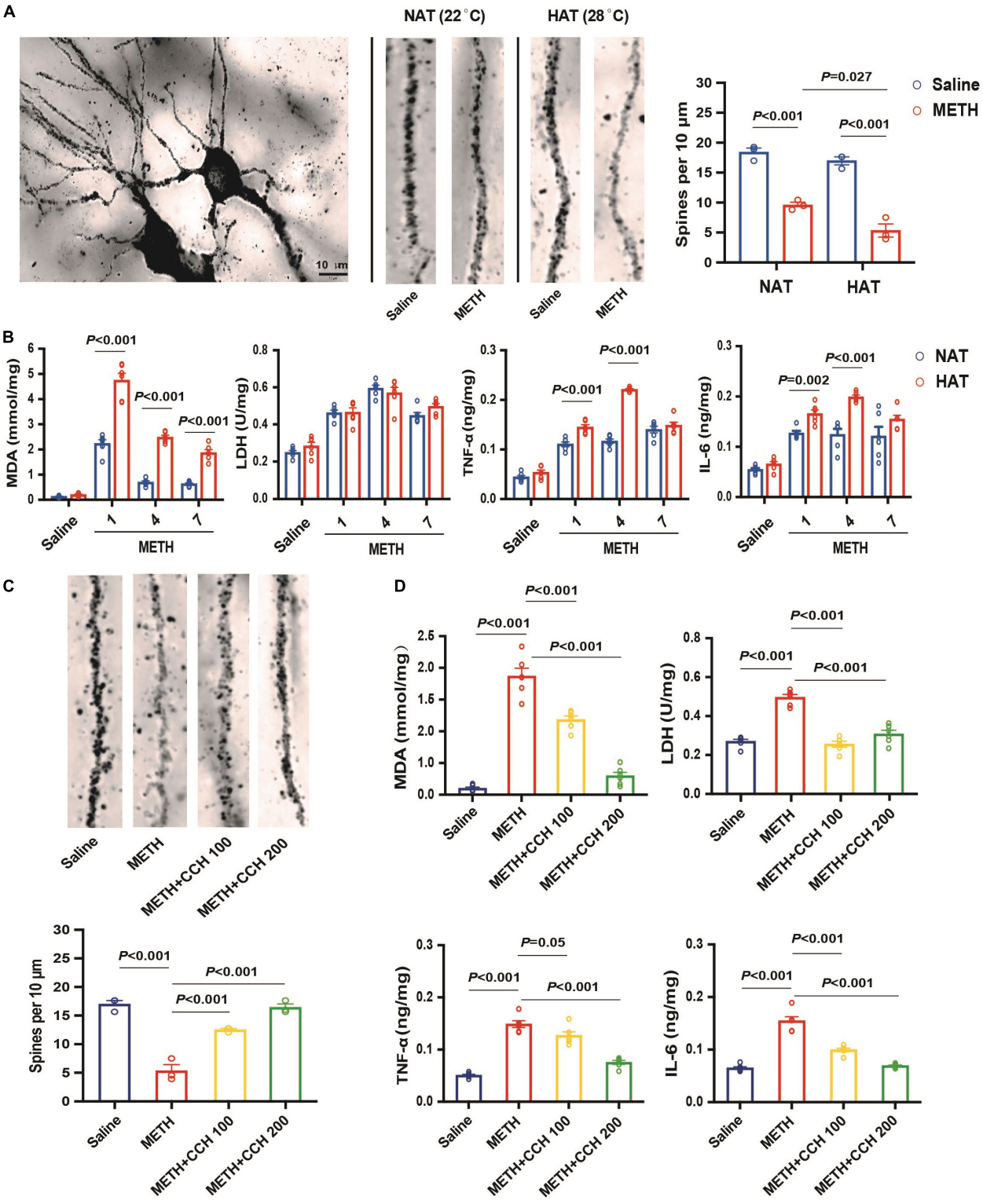

FIGURE 4 | Coral calcium hydride administration inhibited METH-induced hippocampal synaptic plasticity damage, oxidative stress, and neuroinflammation. **(A)** HAT aggravated METH-induced hippocampal synaptic plasticity damage. The number of spines in hippocampal neuron was significantly decreased after METH treatment, especially when it given under HAT. Bar = 10 μm. **(B)** METH elicited time-dependent oxidative stress and neuroinflammation in hippocampus. HAT compounded METH-induced increase of MDA, TNF-α, and IL-6 levels, but did not change the activity of LDH. **(C)** CCH administration attenuated METH-induced hippocampal synaptic plasticity damage. **(D)** CCH administration inhibited METH-induced secretion of oxidative stress products and inflammatory cytokines in hippocampus. Data are expressed as the mean ± SEM (n = 3 per group in Golgi staining; n = 6 per group in measurement of MDA, LDH, TNF-α, and IL-6 levels).

ANOVA indicated significant main effects on MDA levels (NAT: $F_{3,20} = 271.0$, $P < 0.001$; HAT: $F_{3,20} = 137.8$, $P < 0.001$), LDH (NAT: $F_{3,20} = 90.15$, $P < 0.001$; HAT: $F_{3,20} = 26.56$, $P < 0.001$), TNF-α (NAT: $F_{3,20} = 69.17$, $P < 0.001$; HAT: $F_{3,20} = 196.2$, $P < 0.001$), and IL-6 (NAT: $F_{3,20} = 9{,}96$, $P < 0.001$; HAT: $F_{3,20} = 78.03$, $P < 0.001$) for METH treatment. HAT aggravated METH-induced abnormal changes in MDA, TNF-α and IL-6 level (statistical data presented in **Figure 4B**). Interestingly, there was no difference between NAT and HAT group for the activity of LDH at each time point after METH treatments (**Figure 4B**). As shown in **Figure 4C**, the results of one-way ANOVA revealed significant differences between groups on the spine number ($F_{3,28} = 18.74$, $P < 0.001$). *Post hoc* comparisons indicated that CCH administration effectively reversed METH-induced hippocampal synaptic plasticity damage (CCH100: $P < 0.001$, CCH200: $P < 0.001$ compared to METH group). Similar results were revealed in MDA ($F_{3,20} = 115.50$, $P < 0.001$), LDH ($F_{3,20} = 50.66$, $P < 0.001$), TNF-α ($F_{3,20} = 73.14$, $P < 0.001$), and IL-6 ($F_{3,20} = 81.24$, $P < 0.001$) content measurement (**Figure 4D**). *Post hoc* comparisons also indicated an inhibitory effect of CCH administration on METH-induced increase of MDA (CCH100: $P < 0.001$, CCH200: $P < 0.001$), LDH (CCH100: $P < 0.001$, CCH200: $P < 0.001$), TNF-α (CCH100: $P = 0.05$, CCH200: $P < 0.001$), and IL-6 (CCH100: $P < 0.001$, CCH200: $P < 0.001$). Therefore, it can be stated conclusively that CCH administration significantly reversed hippocampal synaptic plasticity damage and alleviated oxidative stress and neuroinflammation induced by METH exposure.

DISCUSSION

Herein, we firstly demonstrated the role of hyperthermia in METH-induced depression-like behaviors in mice. The results of present study revealed that HAT (28°C) aggravates METH-induced hyperthermia and plays a key role in METH-induced depression-like behaviors. Secondly, we further clarified the effect of CCH, on METH-induced hyperthermia and behavioral abnormality. Treatment with CCH significantly inhibited METH-induced hippocampal synaptic plasticity damage and attenuated the rise in oxidative stress products and inflammatory cytokines in the hippocampus. Therefore, our study suggested that CCH used as an efficient hydrogen-rich agent is a novel and effective treatment of METH-induced psychiatric disorders.

It is known that frequent use of psychostimulants causes elevated behavioral and cognitive activity, and can also lead to severe psychiatric symptoms (King et al., 2010). The symptoms, such as psychosis, depression, and anxiety, are predictive of drug relapse, and significantly increase the risk of suicidal behavior and mortality (Archer et al., 2018). Previous studies have revealed that withdrawal of amphetamine-type psychostimulants and major depressive disorder share remarkable behavioral similarities in humans (Durdle et al., 2008; Härtel-Petri et al., 2017). Also, withdrawal from chronic or sub-chronic METH exposure induces anxiety and depression-like behaviors in several animal models (McCoy et al., 2011; North et al., 2013). The dose and duration of chronic METH usage range from 2 to 10 mg/kg and 7 days to 8 weeks, respectively (Ding et al., 2020). In addition, a binge dose (5–10 mg/kg × 4 at 2 h intervals) and the acute bolus drug administration (20–40 mg/kg) of METH have been employed frequently to study its neurotoxicity (Zhu et al., 2006; Melega et al., 2007). Fonseca et al. (2017) reported that a single neurotoxic dose of METH (30 mg/kg) induced a long-lasting depressive behavior in mice. However, the present study found that multiple repeated 10 mg/kg METH-injections paradigm induced depression-like behaviors in an ambient temperature and dose-dependent manner. We also considered that METH-induced hyperthermia is an important factor for the occurrence of depression-like behaviors. In a previous study, the author defined "neutral" as 24–27°C and "warm" as 28–37°C (Sabol et al., 2013). Indeed, 28°C cannot be considered as a high ambient temperature, but we found that most animals died after METH exposure when the ambient temperature was higher than 28°C. Therefore, we defined 28°C as the high ambient temperature in the present study, and the results revealed that HAT (28°C) aggravated METH-induced hyperthermia and lead to depression-like behaviors. No significant alteration in total distance in open field test indicates that METH induced depression-like behaviors do not affect the locomotor activity. Interestingly, the same METH-injections paradigm under NAT (22°C) and chronic METH treatments (10 mg/kg, 7 or 14 days) or escalating-dose (2 ∼ 15 mg/kg, 3 days) of METH exposure failed to induce depression-like behaviors. However, the difference in timescale of behavior tests after METH withdrawal also was a key factor related to the contradictory behavioral results. Indeed, a major pitfall of the present study is that it did not observe the earlier depression-like behaviors (less than 7 days) in these METH-treated mice.

Molecular hydrogen, as a selective antioxidant, was first reported by Ohsawa et al. (2007). Up to now, it has been shown to exhibit distinct potential as a novel therapeutic agent for a wide range of diseases, especially oxidative stress-mediated diseases. We previously found that molecular hydrogen significantly attenuated anxiety-like behaviors in morphine-withdrawn mice, and it was able to inhibit the acquisition and transfer of low dose METH-induced behavioral sensitization to a certain extent (Wen et al., 2020). Drinking or bathing with hydrogen-rich water and inhalation of HG were popular methods used to administer hydrogen to humans, while hydrogen-rich saline injection, *ad libitum* hydrogen-rich water consumption, and inhalation of HG were common methods to deliver molecular hydrogen to animals in experimental research. However, due to the low solubility of hydrogen in water, it is not easy to realize high concentration and long-term accumulation by hydrogen-rich water consumption or hydrogen-rich saline injection to animal model in a particular point of time. Therefore, we only evaluated the inhibitory effect of hydrogen on low dose METH-induced behavioral abnormality and neurotoxicity. Recent studies demonstrated that the hydrogen level released by CCH administration was more reliable and robust than hydrogen-rich water *in vitro* and *in vivo*. Moreover, Ueda et al. (2011) reported that CCH exerted antioxidant activity by enhancing the basal endogenous antioxidant ability in the hippocampus of rats. Consistent with above results, we found that

CCH administration significantly attenuated large dose repeated METH treatment-induced severe hyperthermia and inhibited depression-like behaviors in FST and TST without altering the locomotion in mice. There has a previous study reported that molecular hydrogen potentiates hypothermia and prevents hypotension and fever in LPS-induced systemic inflammation. They found that molecular hydrogen caused a reduction in surges of TNF-α, IL-1β, and prostaglandin E2 (PGE2) in plasma and exerted anti-inflammatory effects strong enough to prevent fever by altering hypothalamic PGE2 production (Saramago et al., 2019). As already known, depressed mood and anhedonia are core symptoms of major depressive disorder (Rizvi et al., 2016). FST and TST are common tests used for assessing despair-like behaviors in laboratory animals (Zhao et al., 2019). In addition to above results, we investigated the effect of METH exposure and CCH treatment on anhedonia-like behavior, and consistent results were revealed in sucrose preference test (see **Supplementary Figure 1**). It is worthy to note that most studies in the past used oral intake of CCH or CCH-rich diet feeding for CCH administration. However, due to the restriction of time for drug treatment and body temperature determination, intragastric CCH treatment was involved in the present study. Meanwhile, we considered that long-term administration of intragastric injection might be a stress to the animals and would create influence on behavioral test, so intragastric CCH treatment was only given for 7 days and then the behavioral tests were subsequently performed. We also determined the effects of CCH treatment on locomotion and depression-like behaviors, as well as the index of oxidative stress and inflammation in hippocampus of naïve mice (see **Supplementary Figure 2**). Furthermore, coral calcium (CC) was used as a controlled treatment to exclude the therapeutic effects of other ingredients (see **Supplementary Figure 3**), and the result showed that administration of CC did not affect METH-induced depression-like behaviors. The previous data also revealed that there were no changes in the serum total Ca^{2+} levels after CCH treatment (Hou et al., 2016). Therefore, we considered that the protective effect of CCH was dependent on molecular hydrogen derived from CCH instead of other ingredients.

Although depressive symptoms and METH withdrawal have common neurobiological symptoms, our search for possible mechanisms of METH-induced depression-like behavior was focused on the METH-induced neurotoxicity and the involvement of hippocampal synaptic plasticity damage (Ren et al., 2017; Papageorgiou et al., 2019; Golsorkhdan et al., 2020). Recent studies have found that hippocampal volume and neuron loss are prominent characters of depression (Barch et al., 2019; Sheline et al., 2019). Accumulating evidence also supports the existence of alteration of hippocampal synaptic plasticity in depressive symptoms (Lu et al., 2014; Liu et al., 2018). Therefore, it has been proposed that increase in METH-induced oxidative stress products and inflammatory factors, results in decreased synaptic proteins synthesis and structural damage, ultimately leading to depressive symptoms (Huang et al., 2013). Likewise, HAT aggravated hyperthermia, and it also induced remarkable increase of MDA, LDH, IL-6, and TNF-α in hippocampus of METH-treated mice. Golgi staining showed corresponding severe damage in hippocampal synaptic plasticity when METH was given under HAT. In addition, CCH administration significantly reduced the damage of METH-induced hippocampal synaptic plasticity and reduced the levels of MDA, LDH, IL-6, and TNF-α in hippocampus of mice.

However, there have two limitations of the present study. Firstly, although the present data revealed the inhibitory effect of CCH on METH-induced severe hyperthermia, whether it affect the hypothalamus or generate peripheral effect thereby causing temperature change in METH-treated mice should be explored. Moreover, since the evidence of CCH toxicity in humans is limited, the possible toxicity should be carefully investigated in future studies.

CONCLUSION

In the present study, we revealed that hyperthermia plays a key role in METH-induced depression-like behaviors. In addition, it was also proved that molecular hydrogen released by CCH effectively ameliorated METH-induced hyperthermia and depression-like behaviors, and this function was possibly elaborated *via* the regulation of hippocampal synaptic plasticity damage mediated by oxidative stress and neuroinflammation. In summary, based on our present study, it can be concluded that CCH acts as a protective antioxidant treatment and may have potential application in reducing the risk of psychiatric symptoms in METH abusers.

DATA AVAILABILITY STATEMENT

The original contributions presented in the study are included in the article/**Supplementary Material**, further inquiries can be directed to the corresponding authors.

ETHICS STATEMENT

The animal study was reviewed and approved by Hebei Medical University.

AUTHOR CONTRIBUTIONS

DW and CM designed the experimental plans. XW, BT, and RH performed the behavioral part of the study. CH and ZZ did the molecular biological experiment in text. LZ and BX analyzed data. ZN and BC wrote and revised the manuscript. All authors contributed to the article and approved the submitted version.

FUNDING

This work was supported by the National Natural Science Foundation of China (grant numbers: 82030057 and 81772019) and the Science and Technology Research Projects for University in Hebei Province (grant numbers: ZD2020307 and BJ2017015).

ACKNOWLEDGMENTS

We thank Shanghai Quanren Biotechnology Co., Ltd. for providing the CCH. We thank Zhimin Kang of Shanghai Huikang Hydrogen Medical Research Center, for her assistance in study design.

SUPPLEMENTARY MATERIAL

The Supplementary Material for this article can be found online at: https://www.frontiersin.org/articles/10.3389/fnmol.2021.808807/full#supplementary-material

Supplementary Figure 1 | Administration of coral calcium hydride (CCH) inhibited methamphetamine (METH)-induced depression-like behavior in sucrose preference test. METH treatment and CCH administration were the same as the procedure presented in **Figure 3D**. After 7 days of CCH administration, sucrose preference test was conducted to assess the anhedonia of mice. Two bottles of 1% (w/v) sucrose solution were provided in each cage to conduct 48 h habituation. Then, mice were deprived of water for 24 h and individually housed before being exposed to sucrose bottle and water bottle for 24 h, and sucrose and water intake were measured. Sucrose preference was calculated as the percentage of sucrose consumption in total liquid consumption. METH exposure under HAT induced the decrease of sucrose intake, and CCH administration significantly inhibited the effect of METH (n = 8 per group). Data are expressed as the mean ± SEM.

Supplementary Figure 2 | Administration of CCH without METH treatment did not induce the depression-like behavior and the activation of oxidative stress and neuroinflammation in hippocampus. **(A)** Timeline of CCH treatment, behavioral test and tissue collection. **(B)** Administration of CCH without METH did not induce the depression-like behavior (n = 8 per group). **(C)** Administration of CCH without METH treatment has no effect on the activity of LDH and the content of MDA, TNF-α, and IL-6 in hippocampus (n = 6 per group). Data are expressed as the mean ± SEM.

Supplementary Figure 3 | Administration of coral calcium (CC) did not affect METH-induced depression-like behaviors. **(A)** Timeline of CC/CCH treatment and behavioral tests. **(B)** Administration of CC after METH treatment did not alter the depression-like behavior. Mice were administered with CC or CCH (200 mg/kg, intragastric route [i.g.]) resuspended in 0.2 mL pure water twice per day after METH exposure (n = 6, 6, 8, and 6). Data are expressed as the mean ± SEM.

REFERENCES

Arab, A., Ruda-kucerova, J., Minsterova, A., Drazanova, E., Szabó, N., Starcuk, Z. Jr., et al. (2019). Diffusion kurtosis imaging detects microstructural changes in a methamphetamine-induced mouse model of parkinson's disease. *Neurotox. Res.* 36, 724–735. doi: 10.1007/s12640-019-00068-0

Archer, G., Kuh, D., Hotopf, M., Stafford, M., and Richards, M. (2018). Adolescent affective symptoms and mortality. *Br. J. Psychiatry* 213, 419–424. doi: 10.1192/bjp.2018.90

Baladi, M. G., Newman, A. H., Nielsen, S. M., Hanson, G. R., and Fleckenstein, A. E. (2014). Dopamine d(3) receptors contribute to methamphetamine-induced alterations in dopaminergic neuronal function: role of hyperthermia. *Eur. J. Pharmacol.* 732, 105–110. doi: 10.1016/j.ejphar.2014.03.023

Barch, D. M., Tillman, R., Kelly, D., Whalen, D., Gilbert, K., and Luby, J. L. (2019). Hippocampal volume and depression among young children. *Psychiatry Res. Neuroimaging* 288, 21–28. doi: 10.1016/j.pscychresns.2019.04.012

Castelli, M. P., Madeddu, C., Casti, A., Casu, A., Casti, P., Scherma, M., et al. (2014). Δ9-Tetrahydrocannabinol prevents methamphetamine-induced neurotoxicity. *PLoS One* 9:e98079. doi: 10.1371/journal.pone.0098079

Chen, L. J., Zhi, X., Zhang, K. K., Wang, L. B., Li, J. H., Liu, J. L., et al. (2021). Escalating dose-multiple binge methamphetamine treatment elicits neurotoxicity, altering gut microbiota and fecal metabolites in mice. *Food Chem. Toxicol.* 148:111946. doi: 10.1016/j.fct.2020.111946

Cornish, J. L., Hunt, G. E., Robins, L., and Mcgregor, I. S. (2012). Regional C-Fos And Fosb/Δfosb expression associated with chronic methamphetamine self-administration and methamphetamine-seeking behavior in rats. *Neuroscience* 206, 100–114. doi: 10.1016/j.neuroscience.2012.01.004

De-Carolis, C., Boyd, G. A., Mancinelli, L., Pagano, S., and Eramo, S. (2015). Methamphetamine abuse and "Meth Mouth" in europe. *Med. Oral Patol. Oral Cir. Bucal.* 20, E205–E210. doi: 10.4317/medoral.20204

Ding, J., Hu, S., Meng, Y., Li, C., Huang, J., He, Y., et al. (2020). Alpha-synuclein deficiency ameliorates chronic methamphetamine induced neurodegeneration in mice. *Toxicology* 438:152461. doi: 10.1016/j.tox.2020.152461

Durdle, H., Lundahl, L. H., Johanson, C. E., and Tancer, M. (2008). Major depression: the relative contribution of gender, mdma, and cannabis use. *Depress Anxiety* 25, 241–247. doi: 10.1002/da.20297

Fonseca, R., Carvalho, R. A., Lemos, C., Sequeira, A. C., Pita, I. R., Carvalho, F., et al. (2017). methamphetamine induces anhedonic-like behavior and impairs frontal cortical energetics in mice. *CNS Neurosci. Ther.* 23, 119–126. doi: 10.1111/cns.12649

García-Cabrerizo, R., Bis-Humbert, C., and García-Fuster, M. J. (2018). Methamphetamine binge administration during late adolescence induced enduring hippocampal cell damage following prolonged withdrawal in rats. *Neurotoxicology* 66, 1–9. doi: 10.1016/j.neuro.2018.02.016

Golsorkhdan, S. A., Boroujeni, M. E., Aliaghaei, A., Abdollahifar, M. A., Ramezanpour, A., Nejatbakhsh, R., et al. (2020). Methamphetamine administration impairs behavior, memory and underlying signaling pathways in the hippocampus. *Behav. Brain Res.* 379:112300. doi: 10.1016/j.bbr.2019.112300

Halpin, L. E., Northrop, N. A., and Yamamoto, B. K. (2014). Ammonia mediates methamphetamine-induced increases in glutamate and excitotoxicity. *Neuropsychopharmacology* 39, 1031–1038. doi: 10.1038/npp.2013.306

Hao, Y., Ge, H., Sun, M., and Gao, Y. (2019). Selecting an appropriate animal model of depression. *Int. J. Mol. Sci.* 20:4827. doi: 10.3390/ijms20194827

Härtel-Petri, R., Krampe-Scheidler, A., Braunwarth, W. D., Havemann-Reinecke, U., Jeschke, P., Looser, W., et al. (2017). Evidence-based guidelines for the pharmacologic management of methamphetamine dependence, relapse prevention, chronic methamphetamine-related, and comorbid psychiatric disorders in post-acute settings. *Pharmacopsychiatry* 50, 96–104. doi: 10.1055/s-0043-105500

Hotchkiss, A. J., and Gibb, J. W. (1980). Long-term effects of multiple doses of methamphetamine on tryptophan hydroxylase and tyrosine hydroxylase activity in rat brain. *J. Pharmacol. Exp. Ther.* 214, 257–262.

Hou, C., Wang, Y., Zhu, E., Yan, C., Zhao, L., Wang, X., et al. (2016). Coral calcium hydride prevents hepatic steatosis in high fat diet-induced obese rats: a potent mitochondrial nutrient and phase ii enzyme inducer. *Biochem. Pharmacol.* 103, 85–97. doi: 10.1016/j.bcp.2015.12.020

Huang, M. C., Lin, S. K., Chen, C. H., Pan, C. H., Lee, C. H., and Liu, H. C. (2013). Oxidative stress status in recently abstinent methamphetamine abusers. *Psychiatry Clin. Neurosci.* 67, 92–100. doi: 10.1111/pcn.12025

Johnson, M. A., Rajan, V., Miller, C. E., and Wightman, R. M. (2006). Dopamine release is severely compromised in the R6/2 mouse model of huntington's disease. *J. Neurochem.* 97, 737–746. doi: 10.1111/j.1471-4159.2006.03762.x

Kaewsuk, S., Sae-Ung, K., Phansuwan-Pujito, P., and Govitrapong, P. (2009). Melatonin attenuates methamphetamine-induced reduction of tyrosine hydroxylase, synaptophysin and growth-associated protein-43 levels in the neonatal rat brain. *Neurochem. Int.* 55, 397–405. doi: 10.1016/j.neuint.2009.04.010

King, G., Alicata, D., Cloak, C., and Chang, L. (2010). Psychiatric symptoms and hpa axis function in adolescent methamphetamine users. *J. Neuroimmune Pharmacol.* 5, 582–591. doi: 10.1007/s11481-010-9206-y

Liao, L. S., Lu, S., Yan, W. T., Wang, S. C., Guo, L. M., Yang, Y. D., et al. (2021). The role Of Hsp90α In methamphetamine/hyperthermia-induced necroptosis in rat striatal neurons. *Front. Pharmacol.* 12:716394. doi: 10.3389/fphar.2021.716394

Liu, W., Xue, X., Xia, J., Liu, J., and Qi, Z. (2018). Swimming exercise reverses cums-induced changes in depression-like behaviors and hippocampal plasticity-related proteins. *J. Affect. Disord.* 227, 126–135. doi: 10.1016/j.jad.2017.10.019

Lu, B., Nagappan, G., and Lu, Y. (2014). Bdnf and synaptic plasticity, cognitive function, and dysfunction. *Handb. Exp. Pharmacol.* 220, 223–250. doi: 10.1007/978-3-642-45106-5_9

Luo, Y., Zhao, P., Dou, M., Mao, J., Zhang, G., Su, Y., et al. (2021). Exogenous microbiota-derived metabolite trimethylamine N-Oxide treatment alters social behaviors: involvement of hippocampal metabolic adaptation. *Neuropharmacology* 191:108563. doi: 10.1016/j.neuropharm.2021.108563

Martins, T., Baptista, S., Gonçalves, J., Leal, E., Milhazes, N., Borges, F., et al. (2011). Methamphetamine transiently increases the blood-brain barrier permeability in the hippocampus: role of tight junction proteins and matrix metalloproteinase-9. *Brain Res.* 1411, 28–40. doi: 10.1016/j.brainres.2011.07.013

Matsumoto, R. R., Seminerio, M. J., Turner, R. C., Robson, M. J., Nguyen, L., Miller, D. B., et al. (2014). Methamphetamine-induced toxicity: an updated review on issues related to hyperthermia. *Pharmacol. Ther.* 144, 28–40. doi: 10.1016/j.pharmthera.2014.05.001

McCoy, M. T., Jayanthi, S., Wulu, J. A., Beauvais, G., Ladenheim, B., Martin, T. A., et al. (2011). Chronic methamphetamine exposure suppresses the striatal expression of members of multiple families of immediate early genes (iegs) in the rat: normalization by an acute methamphetamine injection. *Psychopharmacology (BERL)* 215, 353–365. doi: 10.1007/s00213-010-2146-7

Melega, W. P., Cho, A. K., Harvey, D., and Laæan, G. (2007). Methamphetamine blood concentrations in human abusers: application to pharmacokinetic modeling. *Synapse* 61, 216–220. doi: 10.1002/syn.20365

Mikami, T., Tano, K., Lee, H., Lee, H., Park, J., Ohta, F., et al. (2019). Drinking hydrogen water enhances endurance and relieves psychometric fatigue: a randomized, double-blind, placebo-controlled study (1). *Can. J. Physiol. Pharmacol.* 97, 857–862. doi: 10.1139/cjpp-2019-0059

Molkov, Y. I., Zaretskaia, M. V., and Zaretsky, D. V. (2014). Meth math: modeling temperature responses to methamphetamine. *Am. J. Physiol. Regul. Integr. Comp. Physiol.* 306, R552–R566. doi: 10.1152/ajpregu.00365.2013

Murakami, Y., Kawata, A., Suzuki, S., and Fujisawa, S. (2018). cytotoxicity and pro-/anti-inflammatory properties of cinnamates, acrylates and methacrylates against raw264.7 cells. *In Vivo* 32, 1309–1322. doi: 10.21873/invivo.11381

North, A., Swant, J., Salvatore, M. F., Gamble-George, J., Prins, P., Butler, B., et al. (2013). Chronic methamphetamine exposure produces a delayed, long-lasting memory deficit. *Synapse* 67, 245–257. doi: 10.1002/syn.21635

Ohsawa, I., Ishikawa, M., Takahashi, K., Watanabe, M., Nishimaki, K., Yamagata, K., et al. (2007). Hydrogen acts as a therapeutic antioxidant by selectively reducing cytotoxic oxygen radicals. *Nat. Med.* 13, 688–694. doi: 10.1038/nm1577

Pan, A. L., Hasalliu, E., Hasalliu, M., and Angulo, J. A. (2020). Epigallocatechin gallate mitigates the methamphetamine-induced striatal dopamine terminal toxicity by preventing oxidative stress in the mouse brain. *Neurotox. Res.* 37, 883–892. doi: 10.1007/s12640-020-00177-1

Panmak, P., Nopparat, C., Permpoonpattana, K., Namyen, J., and Govitrapong, P. (2021). Melatonin protects against methamphetamine-induced alzheimer's disease-like pathological changes in rat hippocampus. *Neurochem. Int.* 148:105121. doi: 10.1016/j.neuint.2021.105121

Papageorgiou, M., Raza, A., Fraser, S., Nurgali, K., and Apostolopoulos, V. (2019). Methamphetamine and its immune-modulating effects. *Maturitas* 121, 13–21. doi: 10.1016/j.maturitas.2018.12.003

Pogorelov, V. M., Nomura, J., Kim, J., Kannan, G., Ayhan, Y., Yang, C., et al. (2012). Mutant disc1 affects methamphetamine-induced sensitization and conditioned place preference: a comorbidity model. *Neuropharmacology* 62, 1242–1251. doi: 10.1016/j.neuropharm.2011.02.003

Qi, B., Yu, Y., Wang, Y., Wang, Y., Yu, Y., and Xie, K. (2021). Perspective of molecular hydrogen in the treatment of sepsis. *Curr. Pharm. Des.* 27, 667–678. doi: 10.2174/1381612826666200909124936

Ren, W., Luan, X., Zhang, J., Gutteea, P., Cai, Y., Zhao, J., et al. (2017). Brain-derived neurotrophic factor levels and depression during methamphetamine withdrawal. *J. Affect. Disord.* 221, 165–171. doi: 10.1016/j.jad.2017.06.017

Rizvi, S. J., Pizzagalli, D. A., Sproule, B. A., and Kennedy, S. H. (2016). Assessing anhedonia in depression: potentials and pitfalls. *Neurosci. Biobehav. Rev.* 65, 21–35. doi: 10.1016/j.neubiorev.2016.03.004

Sabol, K. E., Yancey, D. M., Speaker, H. A., and Mitchell, S. L. (2013). Methamphetamine and core temperature in the rat: ambient temperature, dose, and the effect Of A D2 receptor blocker. *Psychopharmacology (BERL)* 228, 551–561. doi: 10.1007/s00213-013-3059-z

Sambo, D. O., Lebowitz, J. J., and Khoshbouei, H. (2018). The sigma-1 receptor as a regulator of dopamine neurotransmission: a potential therapeutic target for methamphetamine addiction. *Pharmacol. Ther.* 186, 152–167. doi: 10.1016/j.pharmthera.2018.01.009

Saramago, E. A., Borges, G. S., Singolani, C. G. Jr., Nogueira, J. E., Soriano, R. N., Cárnio, E. C., et al. (2019). Molecular hydrogen potentiates hypothermia and prevents hypotension and fever in LPS-induced systemic inflammation. *Brain Behav. Immun.* 75, 119–128. doi: 10.1016/j.bbi.2018.09.027

Shaerzadeh, F., Streit, W. J., Heysieattalab, S., and Khoshbouei, H. (2018). Methamphetamine neurotoxicity, microglia, and neuroinflammation. *J. Neuroinflammation* 15:341. doi: 10.1186/s12974-018-1385-0

Sheline, Y. I., Liston, C., and Mcewen, B. S. (2019). Parsing the hippocampus in depression: chronic stress, hippocampal volume, and major depressive disorder. *Biol. Psychiatry* 85, 436–438. doi: 10.1016/j.biopsych.2019.01.011

Ueda, Y., Kojima, T., and Oikawa, T. (2011). Hippocampal gene network analysis suggests that coral calcium hydride may reduce accelerated senescence in mice. *Nutr. Res.* 31, 863–872. doi: 10.1016/j.nutres.2011.09.011

Ueda, Y., Nakajima, A., and Oikawa, T. (2010). Hydrogen-related enhancement of *in vivo* antioxidant ability in the brain of rats fed coral calcium hydride. *Neurochem. Res.* 35, 1510–1515. doi: 10.1007/s11064-010-0204-5

Wen, D., Hui, R., Liu, Y., Luo, Y., Wang, J., Shen, X., et al. (2020). Molecular hydrogen attenuates methamphetamine-induced behavioral sensitization and activation of ERK-ΔFOSB signaling in the mouse nucleus accumbens. *Prog. Neuropsychopharmacol. Biol. Psychiatry* 97:109781. doi: 10.1016/j.pnpbp.2019.109781

Wen, D., Hui, R., Wang, J., Shen, X., Xie, B., Gong, M., et al. (2019). Effects of molecular hydrogen on methamphetamine-induced neurotoxicity and spatial memory impairment. *Front. Pharmacol.* 10:823. doi: 10.3389/fphar.2019.00823

Xie, X. L., He, J. T., Wang, Z. T., Xiao, H. Q., Zhou, W. T., Du, S. H., et al. (2018). Lactulose attenuates meth-induced neurotoxicity by alleviating the impaired autophagy, stabilizing the perturbed antioxidant system and suppressing apoptosis in rat striatum. *Toxicol. Lett.* 289, 107–113. doi: 10.1016/j.toxlet.2018.03.015

Zhao, X., Cao, F., Liu, Q., Li, X., Xu, G., Liu, G., et al. (2019). Behavioral, inflammatory and neurochemical disturbances in Lps And Ucms-induced mouse models of depression. *Behav. Brain Res.* 364, 494–502. doi: 10.1016/j.bbr.2017.05.064

Zhu, J. P., Xu, W., Angulo, N., and Angulo, J. A. (2006). Methamphetamine-induced striatal apoptosis in the mouse brain: comparison of a binge to an acute bolus drug administration. *Neurotoxicology* 27, 131–136. doi: 10.1016/j.neuro.2005.05.014

Zhu, Q., Wu, Y., Li, Y., Chen, Z., Wang, L., Xiong, H., et al. (2018). Positive effects of hydrogen-water bathing in patients of psoriasis and parapsoriasis En plaques. *Sci. Rep.* 8:8051. doi: 10.1038/s41598-018-26388-3

Conflict of Interest: The authors declare that the research was conducted in the absence of any commercial or financial relationships that could be construed as a potential conflict of interest.

Publisher's Note: All claims expressed in this article are solely those of the authors and do not necessarily represent those of their affiliated organizations, or those of the publisher, the editors and the reviewers. Any product that may be evaluated in this article, or claim that may be made by its manufacturer, is not guaranteed or endorsed by the publisher.

frontiers in Molecular Neuroscience

ORIGINAL RESEARCH
published: 20 January 2022
doi: 10.3389/fnmol.2021.810726

Regional Homogeneity Abnormalities and Its Correlation With Impulsivity in Male Abstinent Methamphetamine Dependent Individuals

Yanan Zhou[1,2,3†], Qianjin Wang[1,2†], Honghong Ren[1,2], Xuyi Wang[1,2], Yanhui Liao[4], Zhi Yang[5], Yuzhu Hao[1,2], Yunfei Wang[1,2], Manyun Li[1,2], Yuejiao Ma[1,2], Qiuxia Wu[1,2], Yingying Wang[1,2], Dong Yang[3], Jiang Xin[6], Winson Fu Zun Yang[7], Long Wang[8]* and Tieqiao Liu[1,2]**

[1] National Clinical Research Center for Mental Disorders, and Department of Psychiatry, The Second Xiangya Hospital of Central South University, Changsha, China, [2] Hunan Key Laboratory of Psychiatry and Mental Health, Changsha, China, [3] Department of Psychiatry, Hunan Brain Hospital (Hunan Second People's Hospital), Changsha, China, [4] Department of Psychiatry, Sir Run Run Shaw Hospital, School of Medicine, Zhejiang University, Hangzhou, China, [5] Laboratory of Psychological Heath and Imaging, Shanghai Mental Health Center, Shanghai Jiao Tong University School of Medicine, Institute of Psychological and Behavioral Science, Shanghai Jiao Tong University, Shanghai, China, [6] School of Computer Science and Engineering, Central South University, Changsha, China, [7] Department of Psychological Sciences, College of Arts & Sciences, Texas Tech University, Lubbock, TX, United States, [8] Department of Psychiatry, Sanming City Taijiang Hospital, Sanming, China

Methamphetamine (MA) use affects the brain structure and function. However, no studies have investigated the relationship between changes in regional homogeneity (ReHo) and impulsivity in MA dependent individuals (MADs). The aim of this study was to investigate the changes of brain activity under resting state in MADs and their relationship to impulsivity using ReHo method. Functional magnetic resonance imaging (fMRI) was performed to collect data from 46 MADs and 44 healthy controls (HCs) under resting state. ReHo method was used to investigate the differences in average ReHo values between the two groups. The ReHo values abnormalities of the brain regions found in inter-group comparisons were extracted and correlated with impulsivity. Compared to the HCs, MADs showed significant increased ReHo values in the bilateral striatum, while the ReHo values of the bilateral precentral gyrus and the bilateral postcentral gyrus decreased significantly. The ReHo values of the left precentral gyrus were negatively correlated with the BIS-attention, BIS-motor, and BIS-nonplanning subscale scores, while the ReHo values of the postcentral gyrus were only negatively correlated with the BIS-motor subscale scores in MADs. The abnormal spontaneous brain activity in the resting state of MADs revealed in this study may further improve our understanding of the neuro-matrix of MADs impulse control dysfunction and may help us to explore the neuropathological mechanism of MADs related dysfunction and rehabilitation.

Keywords: methamphetamine, impulsivity, regional homogeneity, resting state, functional magnetic resonance image

OPEN ACCESS

Edited by:
Jianfeng Liu,
Texas A&M University, United States

Reviewed by:
Yixiao Luo,
Hunan Normal University, China
Jiajia Zhu,
First Affiliated Hospital of Anhui Medical University, China
Xiang Yang Zhang,
Institute of Psychology, Chinese Academy of Sciences (CAS), China

***Correspondence:**
Winson Fu Zun Yang
winson.yang@ttu.edu
Long Wang
742978062@qq.com
Tieqiao Liu
liutieqiao123@csu.edu.cn

† These authors have contributed equally to this work

Specialty section:
This article was submitted to Molecular Signaling and Pathways, a section of the journal Frontiers in Molecular Neuroscience

Received: *07 November 2021*
Accepted: *27 December 2021*
Published: *20 January 2022*

Citation:
Zhou Y, Wang Q, Ren H, Wang X, Liao Y, Yang Z, Hao Y, Wang Y, Li M, Ma Y, Wu Q, Wang Y, Yang D, Xin J, Yang WFZ, Wang L and Liu T (2022) Regional Homogeneity Abnormalities and Its Correlation With Impulsivity in Male Abstinent Methamphetamine Dependent Individuals. Front. Mol. Neurosci. 14:810726. doi: 10.3389/fnmol.2021.810726

INTRODUCTION

Methamphetamine (MA), commonly known as "ice," is an amphetamine-type stimulant (ATS) that is one of the most abused new drugs in the world (Shadloo et al., 2017). According to the 2019 China Drug Situation Report released in 2020, MA users in China accounted for 55.2 percent of its 2.148 million registered drug users, making it the largest drug user in the country by far, (China National Narcotic Control Commission, 2020). In addition to the high prevalence of MA use, the high recurrence rates of MA dependent individuals (MADs) exacerbate the problem, creating a huge public health burden worldwide (Jiang et al., 2021). Chronic use of MA has been associated with a variety of physical and mental health problems (e.g., cardiovascular disease, depression) (Schwarzbach et al., 2020; Jiang et al., 2021), daily dysfunction (e.g., impulsivity) (Moallem et al., 2018; Wang et al., 2020) and neurocognitive dysfunction (Basterfield et al., 2019; Mizoguchi and Yamada, 2019), contributing to a considerable global disease burden. Although increasing studies have been conducted on the treating MA use disorders, such as pharmacotherapy (Chan et al., 2019), psychotherapy (Harada et al., 2018), and repetitive transcranial magnetic stimulation (rTMS) (AshaRani et al., 2020), the effectiveness in reducing MA recurrence remains unsatisfactory.

A challenge for treating MA abuse is recurrence during abstinence (Li X. et al., 2019). Although many factors contribute to recurrence of MADs, a possible key predictor is impulsivity (Ahn et al., 2016; Vassileva and Conrod, 2019). Impulsivity is defined as a predisposition toward rapid, unplanned reactions to internal or external stimuli with diminished regard to their negative consequences to themselves or others (Ahn et al., 2016; Psederska et al., 2021). It is considered a key etiological factor in current conceptualizations of substance use disorder (SUD). Moreover, self-reported impulsivity is a strong predictor of poor treatment response (Fernie et al., 2010; Winhusen et al., 2013). Although MA dependence is associated with many neuropsychiatric and behavioral problems, impulsivity has been studied extensively because of its purported importance in initiation and escalation of drug use and the probability of recurrence (Schwartz et al., 2010).

One of the popular methods of investigating impulsivity in MA patients is through resting-state functional magnetic resonance imaging (rs-fMRI). Rs-fMRI is a powerful tool that measures brain activities by detecting changes in blood-oxygen-level-dependent (BOLD) signals in the resting brain (Park et al., 2019). It has been widely used recently because it does not require the involvement of any specific task in the scanner and could reveal the neural substrates of task-independent processes in diseases (Xie et al., 2021). A specific methodology in rs-fMRI is regional homogeneity (ReHo). ReHo evaluates signal synchronization by calculating the consistency of temporal variations of BOLD signals within local brain regions (Liu et al., 2019c), and has been used in many neuropsychiatric disorders (Li H. et al., 2019; Ma et al., 2019), but rarely in addiction (Liao et al., 2012; Qiu et al., 2013). Over the past few decades, several neuroimaging studies have assessed the relationship between abnormal brain function and abnormal behaviors (such as impulsivity) in MADs, but the results have been inconsistent. For instance, abstinent MADs showed less frontal activation during cognitive control compared to healthy controls (HCs) (Salo et al., 2013; Weafer et al., 2020), and showed less delay discounting activation than HCs in the bilateral precuneus, right caudate, anterior cingulate cortex (ACC), and dorsolateral prefrontal cortex (DLPFC) (Hoffman et al., 2008). In contrast, abstinence MADs have greater activation of MA-related cues in the ventral striatum and medial frontal cortex (Malcolm et al., 2016). Moreover, few functional magnetic resonance imaging (fMRI) studies have focused on the relationship between impulsivity and brain dysfunction.

In this study, we used the ReHo method to study the difference in spontaneous brain activity between MADs and HCs in the resting state. Based on our previous studies (Xie et al., 2021), we hypothesized that ReHo values in the resting state would differ in the relevant brain regions between MADs and HCs. We also hypothesized that differences in ReHo values might be related to impulsivity.

MATERIALS AND METHODS

Participants

One hundred Han male participants (50 MADs and 50 HCs, aged 18 – 45, completion of at least 6 years of formal education; fluency in Chinese; right-handed) were enrolled in this study. Data for 3 MADs (2 had contraindications to MRI and 1 had abnormal scan) and 6 HCs (3 were lost to follow-up, 1 had contraindication to MRI, and 2 had abnormal scans) were excluded. Meanwhile, one MADs with maximal head motion exceeding 2 mm or rotations over 2° was excluded from further analysis. A total of 46 MADs and 44 HCs were included in the final analysis. MADs were recruited from the Kangda Voluntary Drug Rehabilitation Centers in Changsha, Hunan Province, while drug-free HCs were recruited *via* local community advertisements. All the MADs were diagnosed with MA use disorders per DSM-5 by two trained senior psychiatrists using the Structured Clinical Interview (SCID) (First et al., 2002). All the MADs were required not to use any psychoactive substances other than tobacco, including alcohol, at least 48 h before the MRI scan. In order to reduce the effects of different stages of abstinence on brain cognition, MADs were assessed 3 months after abstinence, during which time MADs used drugs. Participants were excluded if they met any of following criteria: (1) had any general medical condition or neurological disorders that could confound brain function; (2) had a history of severe head injury with skull fracture or loss of consciousness of more than 10 min; (3) had any current or previous psychiatric disorder or family history of psychiatric disorder; and (4) had contraindications for MRI (including implanted metallic devices or ferromagnetic material or claustrophobia).

Clinical Assessment

All the participants completed the following self-report scales; all the instruments have good reliability and validity.

General Information

Basic demographic information included age, height, weight, education, marital status, employment, and income. We also reported the drinking, smoking, and betel use status in the two groups.

Impulsivity

The level of impulsivity was measured using the Barratt Impulsivity Scale 11 Edition (BIS-11), which is the most extensive self-report scale for this purpose (Subramanian et al., 2020). The Chinese version of BIS-11 was used to measure the cognitive impulsiveness, motor impulsiveness and non-planning impulsiveness of MADs. Items 4, 5, 13, 14, 15, 16, 17, 19, 20, 21, and 26 were reverse scored (Yao et al., 2007). The whole scale consists of 30 items, using a 5-point Likert scale for each item with a higher total score indicating stronger impulsivity (Patton et al., 1995).

Magnetic Resonance Imaging Data Acquisition

Magnetic resonance imaging data of all participants were acquired in the resting condition using a 3.0T MRI scanner (Siemens Skyra, Munich) equipped with a 16-channel head coil at the Magnetic Resonance Imaging Center of Hunan Children's Hospital, Changsha, China. None of the participants were taking any medications on the day of the MRI scan. Participants were instructed to remain awake and still in supine position with eyes closed. During the scanning, foam pads and earplugs were used to restrain head motion and to attenuate noise. Anatomical T1-weighted MRI data were acquired using a 3D magnetization preparing rapid acquisition gradient echo sequence with the following parameters: repetition time (TR) = 2,530 ms, echo time (TE) = 2.98 ms, flip angle = 7°, field of view = 256 × 256 mm, slice thickness = 1 mm, slice gap = 0 mm, voxel size = 1 × 1 × 1 mm^3, number of slices = 176, and scanning time = 363 s. Functional images were obtained using a gradient echo-planar imaging (EPI) sequence with the following parameters: TR = 2,000 ms, TE = 30 ms, flip angle = 78°, field of view = 224 × 224 mm, slice thickness = 3.5 mm, slice gap = 0.7 mm, voxel size = 3.5 × 3.5 × 3.5 mm^3, number of slice = 33, and scanning time = 488 s.

Data Preprocessing

Functional MRI data were preprocessed according to standard procedures with the Data Processing Assistant for Resting-State fMRI (DPARSF, version 4.1) (Chao-Gan and Yu-Feng, 2010),[1] running in MATLAB (version R2013b, The MathWorks, Inc., Natick, MA, United States) (Yan et al., 2016). Functional MRI data preprocessing consisted of the following steps: (1) remove the first 10 time points in case of unstable signal quality, (2) perform slice-timing adjustment, (3) perform realignment, excluding subjects with maximal head motion exceeding 2 mm or rotations over 2°, (4) remove the mean framewise displacement (FD) > 0.2 mm, (5) conduct spatial normalization to the EPI template of Montreal Neurological Institute (MNI) space by resampling to 3 mm × 3 mm × 3 mm, (6) remove linear detrending, (7) temporal band-pass filtering (0.01 – 0.1 Hz), (8) smooth at 8 mm full width at half maximum (FWHM), and (9) nuisance signals were regressed out, including Friston 24 head motion parameters, global signal, white matter signal, and cerebrospinal fluid signal.

Regional Homogeneity Calculation

ReHo calculation was performed with the REST[2] software. In short, this was achieved by calculating Kendall's coefficient of concordance (KCC) of time series of a given voxel with those of its nearest 26 neighbors on a voxel-by-voxel basis (Zang et al., 2004). The KCC value was calculated to this voxel, and a separate KCC map was obtained for each participant. For standardization purpose, the individual ReHo maps were divided by their own global mean KCC within the whole-brain mask. The individual ReHo maps were then spatially smoothed with an 8 mm FWHM Gaussian kernel to reduce noise and residual differences in gyral anatomy.

Statistical Analysis

All statistical analyses were performed using R version 3.5.3. Before statistical analysis, normality, and variance homogeneity were tested. Demographic and clinical data are compared between groups using the Chi-square test, Mann–Whitney U test, or Student's *t*-test, When appropriate. Several one-way analyses of covariances (ANCOVAs) were used to analyze group differences in ReHo values among the pre-defined regions of interest (ROIs). Covariances used were smoking, drinking, and betel use. Bonferroni-correction was used at this stage to reduce the number of type-I errors. ANOVAs were also used to analyze group differences in impulsivity. Significant ReHo results were subsequently used as individual predictors in linear regression for impulsivity. Scores were mean centered before running linear regressions as interaction terms needed to be computed.

RESULTS

Demographics and Clinical Characteristics

MADs were significantly older than HCs with lower weight and higher education levels (**Table 1**). More importantly, MADs smoked more (95.70%) than HCs (45.50%, $p < 0.001$), and had longer smoking duration (12.80 ± 4.85 years) than HCs (7.42 ± 6.73, $p = 0.001$). Although there were no significant differences in drinking ($p = 0.052$), MADs drank for a longer time (3.89 ± 5.44 years) compared to HCs (1.27 ± 3.01, $p = 0.006$). Finally, MADs also use more betel (67.40%) compared to HCs (40.90%, $p = 0.021$) and used betel for a longer duration (9.02 ± 5.17 years) as compared to HCs (3.78 ± 2.16, $p < 0.001$).

[1] http://www.restfmri.net

[2] http://www.resting-fmri.sourceforge.net

Behavioral Results

There were no significant differences between MADs and HCs on BIS-attention at $F_{(1,85)} = 0.11$, $p = 0.74$, BIS-nonplanning at $F_{(1,85)} = 0.29$, $p = 0.59$, or BIS-motor at $F_{(1,85)} = 1.58$, $p = 0.21$.

Neuroimaging Results

Regional Homogeneity

There were significant differences between MADs and HCs on ReHo values of the left caudate at $F_{(1,85)} = 14.79$, $p = 0.017$, right caudate at $F_{(1,85)} = 30.00$, $p < 0.001$, left postcentral gyrus at $F_{(1,85)} = 31.96$, $p < 0.001$, left precentral gyrus at $F_{(1,85)} = 39.21$, $p = 0.0087$, right postcentral gyrus at $F_{(1,85)} = 16.73$, $p < 0.001$, and right precentral gyrus at $F_{(1,85)} = 17.06$, $p = 0.0089$ after Bonferroni correction. See **Figure 1** for more details.

Regression Analysis

Regression analysis of predicting BIS from ReHo values revealed a significant model for left postcentral gyrus for predicting BIS-motor at $F_{(3,86)} = 4.72$, $p = 0.0043$. Although there was a Group × ReHo interaction where higher left postcentral gyrus ReHo values in the MAD group was associated with lower BIS-motor scores, it only approached significance ($B = -3.74$, $p = 0.074$). There was also a significant model for ReHo values of the left precentral gyrus at $F_{(3,86)} = 4.32$, $p = 0.0069$. Although there was a Group × ReHo interaction where higher left precentral gyrus ReHo values in the MAD group was associated with lower BIS-nonplanning scores, it only approached significance ($B = -5.35$, $p = 0.061$). ReHo values of the left precentral gyrus predicted BIS-motor scores at $F_{(3,86)} = 4.32$, $p = 0.001$. There was a Group × ReHo interaction where higher left precentral gyrus ReHo values in the MAD group was associated with lower BIS-motor scores ($B = -6.75$, $p = 0.034$). ReHo values of the left precentral gyrus also predicted BIS-attention scores at $F_{(3,86)} = 3.03$, $p = 0.033$. There was a Group × ReHo interaction where higher left precentral gyrus ReHo values in the MAD group was associated with lower BIS-attention scores ($B = -8.29$, $p = 0.017$). There were no other significant models of ReHo values predicting BIS scores. See **Figure 2** for more details.

TABLE 1 | Demographics and clinical characteristics of participants.

Variables *M* (SD) or *n* (%)		HC (*n* = 44)	MAD (*n* = 46)	*p*-value
Age		26.05 (6.81)	31.37 (5.51)	<0.001
Height		171.66 (5.41)	170.76 (6.65)	0.485
Weight		68.48 (9.40)	73.52 (11.74)	0.027
Education years		14.00 (3.20)	11.46 (3.15)	<0.001
Marital status (%)	Divorced	0 (0.00)	6 (13.00)	<0.001
	Married	10 (22.70)	27 (58.70)	
	Single	34 (77.30)	13 (28.30)	
Employment (%)	Employed	19 (43.20)	25 (54.30)	<0.001
	Freelance	4 (9.10)	12 (26.10)	
	student	21 (47.70)	0 (0.00)	
	Unemployed	0 (0.00)	9 (19.60)	
Income in Yuan (%)	<2,000	18 (40.90)	2 (4.30)	<0.001
	>10,000	2 (4.50)	8 (17.40)	
	2,000–5,000	10 (22.70)	18 (39.10)	
	5,000–10,000	14 (31.80)	18 (39.10)	
Smoking (%)	No	24 (54.50)	2 (4.30)	<0.001
	Yes	20 (45.50)	44 (95.70)	
Smoke years		7.42 (6.73)	12.80 (4.85)	0.001
Drinking (%)	No	30 (68.20)	21 (45.70)	0.052
	Yes	14 (31.80)	25 (54.30)	
Drink years		1.27 (3.01)	3.89 (5.44)	0.006
Betel use (%)	No	26 (59.10)	15 (32.60)	0.021
	Yes	18 (40.90)	31 (67.40)	
Betel years		3.78 (2.16)	9.02 (5.17)	<0.001

M, mean; SD, standard deviation; n, number; %, percentage; MAD, methamphetamine dependent individual; and HC, health control.

DISCUSSION

To our knowledge, this is the first study to explore the relationship between ReHo values of local spontaneous brain activity and impulsivity in MADs. Compared with HCs, MADs showed significantly increased ReHo values in bilateral caudate, and decreased ReHo values in the bilateral postcentral gyrus, and the bilateral precentral gyrus. We further found that the ReHo values of the left precentral gyrus were negatively correlated with the BIS-attention, BIS-motor, and BIS-nonplanning subscale scores, while the ReHo values of the left postcentral gyrus were only negatively correlated with the BIS-motor subscale scores in MADs.

Compared to one of our previous studies, this study focused on the relationship between the abnormal ReHo values of the brain ROIs in MADs and the impulsivity of MADs (Xie et al., 2021). Moreover, most previous studies have focused on exploring the relationship between low-frequency fluctuation (ALFF) (Wang et al., 2013; Liu Y. et al., 2020), fractional amplitude of low frequency fluctuation (fALFF) (Chu et al., 2014; Wang et al., 2017) or structural MRI (Huang et al., 2020; Meade et al., 2020) and clinical variables, rather than ReHo. Furthermore, some studies on ReHo have focused on other addicts (Huang et al., 2020; Meade et al., 2020) and psychiatric patients (Liu P. et al., 2020; Shan et al., 2021), but not on MADs.

The striatum is a continuous mass structure composed of the caudate and putamen (Lerner et al., 2012), which can directly participate in rewards, movement control, regulation, and decision-making, especially action selection and initiation (de la Fuente-Fernández et al., 2002; Liu et al., 2019a). In this study, the increase in the bilateral striatum ReHo of MADs indicates the importance of their spontaneous neural activity in resting brain of MADs. This is consistent with our previous findings that ReHo was increased in the bilateral striatum of MADs compared to HCs (Xie et al., 2021; Yang et al., 2021). To date, only a few rs-fMRI studies have used ReHo to explore spontaneous brain activity changes and synchronization in individuals with SUD. A comparative study in recurring heroin addicts found that ReHo in the right caudate of recurred heroin addicts increased (Chang et al., 2016). It should be noted that compared with HCs, the ReHo of the left dorsal striatum was

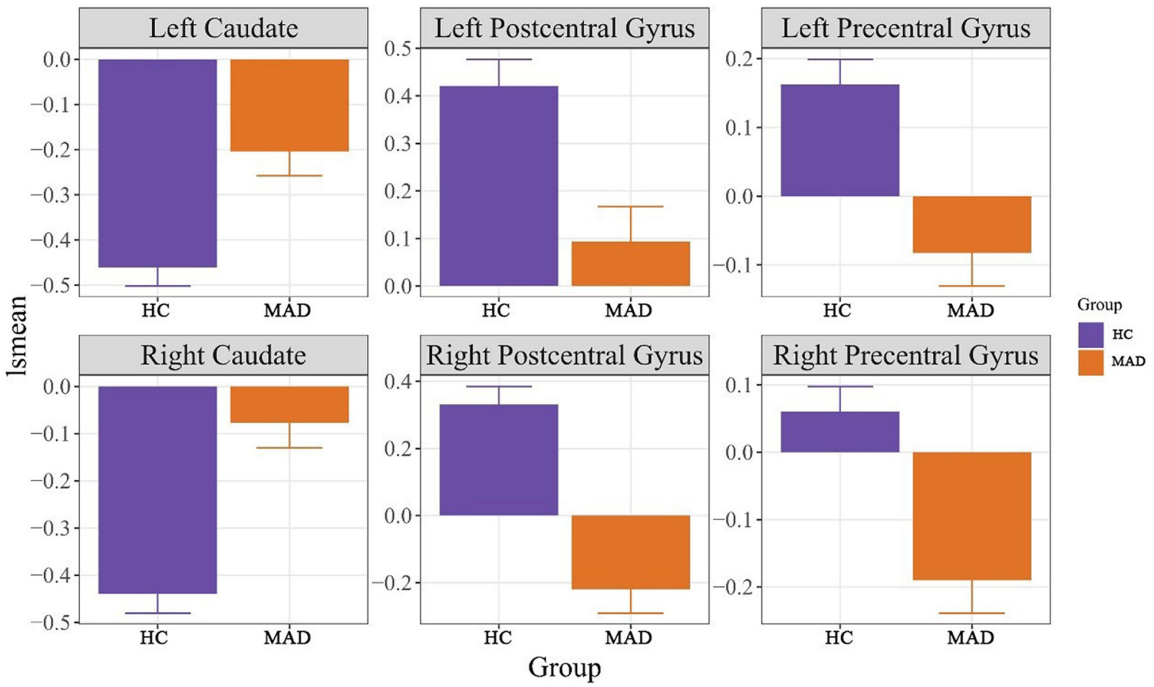

FIGURE 1 | It displays the least square means (lsmeans) among HC and MAD for the significant regions of interest. HC, healthy control, MAD, methamphetamine dependent individual.

reduced in codeine-containing cough syrups (CCS) dependent individuals, and was negatively correlated with the BIS-11 total scores and attentional impulsivity score (Qiu et al., 2013). The reason why our results were inconsistent with this study may be mainly due to the heterogeneity of clinical samples (i.e., different addictive substances, different data collection status, and different sample sizes). Thus, the different mechanisms underlying MA and codeine use may result in representation in the brain. In addition, the ReHo values may change during withdrawal. Using fALFF, it was found that the activity of spontaneous neurons in the caudate of smokers was enhanced (Feng et al., 2016). Meanwhile, structural MRI studies showed a significant increase in gray matter volume in the putamen and caudate nuclei of cocaine users compared to HCs (Ersche et al., 2011). Although the methodologies were different, these findings provide strong support for the theory that the bilateral striatum is a key region in addiction disorders, and our findings support this view.

It is worth noting that the ReHo values of the bilateral postcentral gyrus and the bilateral precentral gyrus were decreased in MADs. It is well known that precentral gyrus, as the primary motor cortex, is involved in somatosensory activity, while postcentral gyrus, as the primary sensory cortex, is involved in the initiation and regulation of spontaneous movement (Javed et al., 2021). However, their relevance to addiction should not be underestimated. Studies have shown that the sensory and motor cortex is involved in various stages of drug addiction (Yalachkov et al., 2010). Meanwhile, the activation of sensory and motor cortex induced by drug-related cues can predict relapse (Kosten et al., 2006). Previous studies have also shown that the ReHo values of MA-associated psychosis (MAP) decreases in the left postcentral gyrus (Yang et al., 2021). Moreover, studies of nicotine addicts have shown a significant increase in the ReHo values of paracentral lobule after 2 weeks of abstinence (Mo et al., 2018). More interestingly, the study further found that the ReHo values of the left precentral gyrus were negatively correlated with the BIS-attention, BIS-motor, and BIS-nonplanning subscales scores, while the ReHo values of the left postcentral gyrus were only negatively correlated with the BIS-motor subscale scores in MADs. It is not difficult to know from the results that the negative correlation with impulsivity is mainly concentrated in the left precentral gyrus, rather than the left postcentral gyrus, which is consistent with the previous research results. For example, a meta-analysis of cue-reactivity in behavioral addictions found increased neural activation in the precentral gyrus (Starcke et al., 2018). Similar results also exist in individual with SUD (such as cannabis, alcohol) (Cheng et al., 2014; Fede et al., 2020). The precentral gyrus is one of the four most important gyrus in the prefrontal cortex. The prefrontal cortex is known to be the higher-order association center of the brain as it is responsible for decision making, regulating impulsivity-related disorders such as drug addiction, reasoning, personality expression, maintaining social appropriateness, and other complex cognitive behaviors (Liu et al., 2019b; El-Baba and Schury, 2021). This may be one of the reasons why the precentral gyrus is more associated with impulsivity than the postcentral gyrus.

We observed that the ReHo values of the left precentral gyrus were negatively correlated with BIS-attention, BIS-motor, and BIS-nonplanning subscales scores in MADs. This may

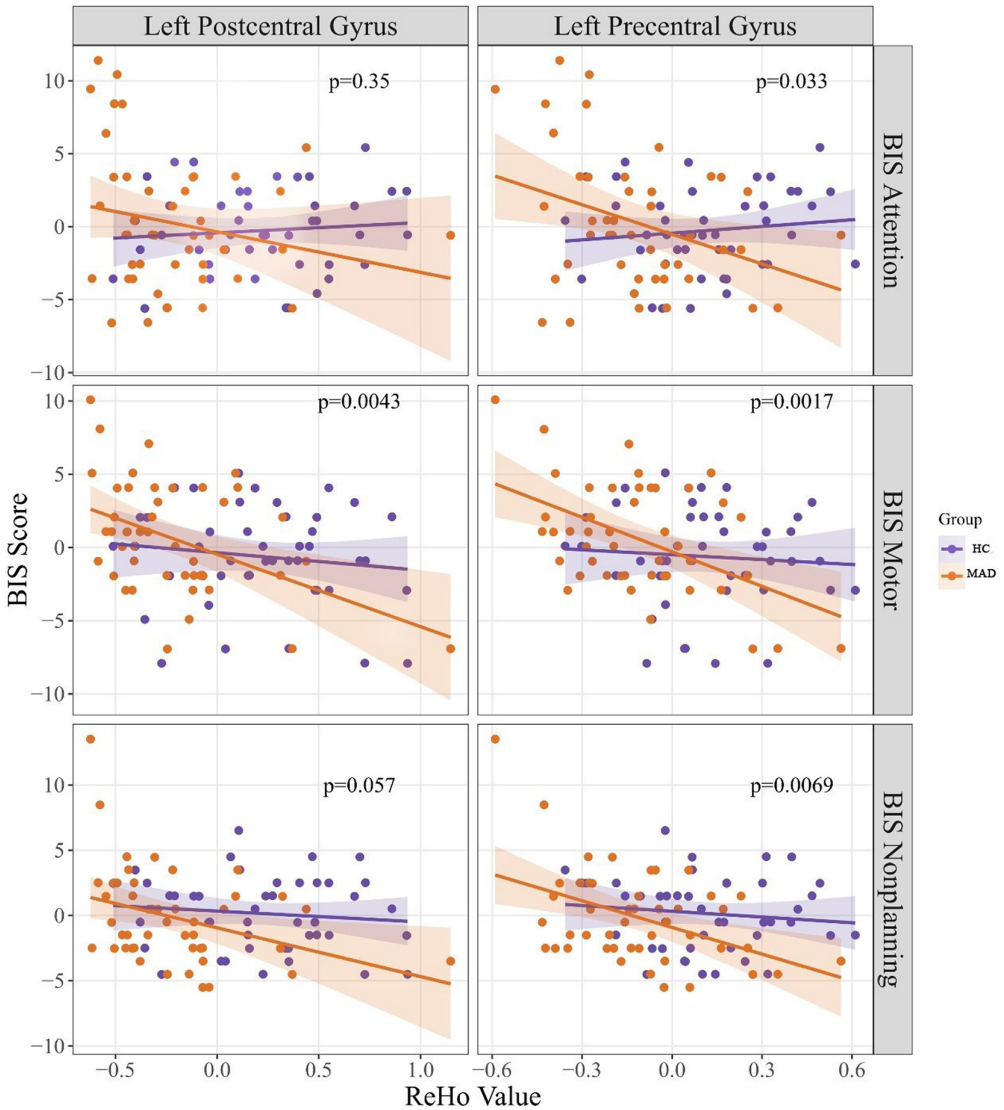

FIGURE 2 | It presents the correlation between BIS scores and ReHo values. The *p*-values presented in this figure were *p*-values of the regression model. BIS, Barratt Impulsivity Scale, ReHo, regional homogeneity, HC, healthy control, and MAD, methamphetamine dependent individual.

indicate that reduced ReHo values in the left precentral gyrus are more closely associated with impulsivity in MADs than in HCs. Also, as presented in this study, ReHo values of the left postcentral gyrus only negatively correlated with BIS-motor subscale scores in MADs. Different brain regions are thought to be preferentially involved in complementary aspects of cognitive control to produce appropriate behavior (Crunelle et al., 2014). The left precentral gyrus may be particularly involved in cognitive control of MAD behavior, behavioral aspect of impulsivity, and temporal impulsivity, while the left postcentral gyrus may only be particularly involved in the behavioral aspect of impulsivity. In addition, no correlation was observed between left precentral gyrus of HCs and BIS subscales scores in the current study. This may indicate that changes in the ReHo values of the left precentral gyrus cannot be a predictor of impulsivity in HCs. Therefore, the reduced ReHo values in the left precentral gyrus might indicate dysfunction in this region in MADs.

While our study provided new insights on the role of ReHo in the left precentral gyrus on impulsive behaviors, some limitations of our study need to be addressed. Firstly, the study was cross-sectional, and causal relationships between variables could not be rigorously evaluated. Therefore, longitudinal studies are needed to help address these issues in the future. Secondly, the study recruited only male MADs, and the results are not representative of brain changes in women. As previous studies have shown that gender is an influential factor of brain dysfunction in MADs, further study on female MADs is needed. Finally, as with all ReHo analyses, it is still debated what higher or lower ReHo represents in terms of biologic functions, or their interpretability toward behavioral change. As ReHo only measures local connectivity,

and the brain consists of connected networks, other analyses are needed to supplement ReHo results. Furthermore, this study did not evaluate other factors related to the ReHo of MADs, such as chronic stress.

CONCLUSION

In conclusion, this study found abnormal ReHo values of MADs in the bilateral striatum, the bilateral precentral gyrus, and the bilateral postcentral gyrus. These brain changes might have to do with self-control and external perception. We also observed that decreased ReHo values in the left precentral gyrus and the left postcentral gyrus were associated with impulsivity. These findings may help to illustrate the pathophysiological mechanism of MADs, particularly in impulsivity, and provide a basis for the urgent formulation of good clinical treatment and prevention strategies to prevent recurrence.

DATA AVAILABILITY STATEMENT

The data analyzed in this study is subject to the following licenses/restrictions: All data in the current study was stored in the PI's affiliation, and is available from the corresponding authors on reasonable request and with completion of data user agreement. Requests to access these datasets should be directed to TL, liutieqiao123@csu.edu.cn.

ETHICS STATEMENT

The studies involving human participants were reviewed and approved by the Ethics Committee of the Second Xiangya Hospital, Central South University (No. S095, 2013). The patients/participants provided their written informed consent to participate in this study.

AUTHOR CONTRIBUTIONS

TL and YL designed and supervised the study. YZ, YH, ML, YfW, and YyW collected the data. YZ, WY, QjW, and JX analyzed and interpreted the data. YZ and QjW drafted the manuscript. HR, XW, WY, YM, QxW, DY, LW, and TL revised the manuscript. All co-authors revised and approved the final version to be published.

FUNDING

This study was supported by the National Key R&D Program of China (2017YFC1310400 to TL), the provincial Natural Science Foundation of Hunan (2020JJ4795 to TL and 2018JJ2221 to DY), the Health and Family Planning Commission of Hunan Province Project (B20180484 to YZ and B20180123 to DY), and the Science and Technology Bureau, Changsha Project (kq2004106 to YZ).

ACKNOWLEDGMENTS

We acknowledged all the staff at Kangda Voluntary Drug Rehabilitation Center for their assistance in data collection, and we would like to express our sincere thanks to all the participants in this work.

REFERENCES

Ahn, W. Y., Ramesh, D., Moeller, F. G., and Vassileva, J. (2016). Utility of machine-learning approaches to identify behavioral markers for substance use disorders: impulsivity dimensions as predictors of current cocaine dependence. *Front. Psychiatry* 7:34. doi: 10.3389/fpsyt.2016.00034

AshaRani, P. V., Hombali, A., Seow, E., Ong, W. J., Tan, J. H., and Subramaniam, M. (2020). Non-pharmacological interventions for methamphetamine use disorder: a systematic review. *Drug Alcohol Depend.* 212:108060. doi: 10.1016/j.drugalcdep.2020.108060

Basterfield, C., Hester, R., and Bowden, S. C. (2019). A meta-analysis of the relationship between abstinence and neuropsychological functioning in methamphetamine use disorder. *Neuropsychology* 33, 739–753. doi: 10.1037/neu0000552

Chan, B., Freeman, M., Kondo, K., Ayers, C., Montgomery, J., Paynter, R., et al. (2019). Pharmacotherapy for methamphetamine/amphetamine use disorder-a systematic review and meta-analysis. *Addiction* 114, 2122–2136. doi: 10.1111/add.14755

Chang, H., Li, W., Li, Q., Chen, J., Zhu, J., Ye, J., et al. (2016). Regional homogeneity changes between heroin relapse and non-relapse patients under methadone maintenance treatment: a resting-state fMRI study. *BMC Neurol.* 16:145. doi: 10.1186/s12883-016-0659-3

Chao-Gan, Y., and Yu-Feng, Z. (2010). DPARSF: a MATLAB toolbox for "pipeline" data analysis of resting-state fMRI. *Front. Syst. Neurosci.* 4:13. doi: 10.3389/fnsys.2010.00013

Cheng, H., Skosnik, P. D., Pruce, B. J., Brumbaugh, M. S., Vollmer, J. M., Fridberg, D. J., et al. (2014). Resting state functional magnetic resonance imaging reveals distinct brain activity in heavy cannabis users - a multi-voxel pattern analysis. *J. Psychopharmacol.* 28, 1030–1040. doi: 10.1177/0269881114550354

China National Narcotic Control Commission (2020). *Drug Situation in China (2019)*. Available online at: http://www.nncc626.com/2020-06/25/c_1210675877.htm (accessed on 25 June 2020).

Chu, S., Xiao, D., Wang, S., Peng, P., Xie, T., He, Y., et al. (2014). Spontaneous brain activity in chronic smokers revealed by fractional amplitude of low frequency fluctuation analysis: a resting state functional magnetic resonance imaging study. *Chin. Med. J. (Engl)* 127, 1504–1509.

Crunelle, C. L., Kaag, A. M., van Wingen, G., van den Munkhof, H. E., Homberg, J. R., Reneman, L., et al. (2014). Reduced frontal brain volume in non-treatment-seeking cocaine-dependent individuals: exploring the role of impulsivity, depression, and smoking. *Front. Hum. Neurosci.* 8:7. doi: 10.3389/fnhum.2014.00007

de la Fuente-Fernández, R., Phillips, A. G., Zamburlini, M., Sossi, V., Calne, D. B., Ruth, T. J., et al. (2002). Dopamine release in human ventral striatum and expectation of reward. *Behav. Brain Res.* 136, 359–363. doi: 10.1016/s0166-4328(02)00130-4

El-Baba, R. M., and Schury, M. P. (2021). *Neuroanatomy, Frontal Cortex [Online]*. Treasure Island, FL: StatPearls Publishing.

Ersche, K. D., Barnes, A., Jones, P. S., Morein-Zamir, S., Robbins, T. W., and Bullmore, E. T. (2011). Abnormal structure of frontostriatal brain systems is associated with aspects of impulsivity and compulsivity in cocaine dependence. *Brain* 134(Pt 7), 2013–2024. doi: 10.1093/brain/awr138

Fede, S. J., Abrahao, K. P., Cortes, C. R., Grodin, E. N., Schwandt, M. L., George, D. T., et al. (2020). Alcohol effects on globus pallidus connectivity: role of

impulsivity and binge drinking. *PLoS One* 15:e0224906. doi: 10.1371/journal.pone.0224906

Feng, D., Yuan, K., Li, Y., Cai, C., Yin, J., Bi, Y., et al. (2016). Intra-regional and inter-regional abnormalities and cognitive control deficits in young adult smokers. *Brain Imaging Behav.* 10, 506–516. doi: 10.1007/s11682-015-9427-z

Fernie, G., Cole, J. C., Goudie, A. J., and Field, M. (2010). Risk-taking but not response inhibition or delay discounting predict alcohol consumption in social drinkers. *Drug Alcohol Depend.* 112, 54–61. doi: 10.1016/j.drugalcdep.2010.05.011

First, M. B., Spitzer, R. L., Gibbon, M., and Williams, J. (2002). *Structured Clinical Interview for DSM-IV-TR Axis I Disorders, Research Version, Patient Edition With Psychotic Screen (SCID-I/P W/ PSY SCREEN)*. New York, NY: New York State Psychiatric Institute.

Harada, T., Tsutomi, H., Mori, R., and Wilson, D. B. (2018). Cognitive-behavioural treatment for amphetamine-type stimulants (ATS)-use disorders. *Cochrane Database Syst. Rev.* 12:Cd011315. doi: 10.1002/14651858.CD011315.pub2

Hoffman, W. F., Schwartz, D. L., Huckans, M. S., McFarland, B. H., Meiri, G., Stevens, A. A., et al. (2008). Cortical activation during delay discounting in abstinent methamphetamine dependent individuals. *Psychopharmacology (Berl)* 201, 183–193. doi: 10.1007/s00213-008-1261-1

Huang, S., Dai, Y., Zhang, C., Yang, C., Huang, Q., Hao, W., et al. (2020). Higher impulsivity and lower grey matter volume in the bilateral prefrontal cortex in long-term abstinent individuals with severe methamphetamine use disorder. *Drug Alcohol Depend.* 212, 108040. doi: 10.1016/j.drugalcdep.2020.108040

Javed, K., Reddy, V., and Lui, F. (2021). *Neuroanatomy, Cerebral Cortex [Online]*. Treasure Island, FL: StatPearls Publishing.

Jiang, P., Sun, J., Zhou, X., Lu, L., Li, L., Huang, X., et al. (2021). Functional connectivity abnormalities underlying mood disturbances in male abstinent methamphetamine abusers. *Hum. Brain Mapp.* 42, 3366–3378. doi: 10.1002/hbm.25439

Kosten, T. R., Scanley, B. E., Tucker, K. A., Oliveto, A., Prince, C., Sinha, R., et al. (2006). Cue-induced brain activity changes and relapse in cocaine-dependent patients. *Neuropsychopharmacology* 31, 644–650. doi: 10.1038/sj.npp.1300851

Lerner, A., Bagic, A., Simmons, J. M., Mari, Z., Bonne, O., Xu, B., et al. (2012). Widespread abnormality of the γ-aminobutyric acid-ergic system in Tourette syndrome. *Brain* 135(Pt 6), 1926–1936. doi: 10.1093/brain/aws104

Li, H., Guo, W., Liu, F., Chen, J., Su, Q., Zhang, Z., et al. (2019). Enhanced baseline activity in the left ventromedial putamen predicts individual treatment response in drug-naive, first-episode schizophrenia: results from two independent study samples. *EBioMedicine* 46, 248–255. doi: 10.1016/j.ebiom.2019.07.022

Li, X., Davis, I. R., Lofaro, O. M., Zhang, J., Cimbro, R., and Rubio, F. J. (2019). Distinct gene alterations between Fos-expressing striatal and thalamic neurons after withdrawal from methamphetamine self-administration. *Brain Behav.* 9:e01378. doi: 10.1002/brb3.1378

Liao, Y., Tang, J., Fornito, A., Liu, T., Chen, X., Chen, H., et al. (2012). Alterations in regional homogeneity of resting-state brain activity in ketamine addicts. *Neurosci. Lett.* 522, 36–40. doi: 10.1016/j.neulet.2012.06.009

Liu, J., Tao, J., Liu, W., Huang, J., Xue, X., Li, M., et al. (2019a). Different modulation effects of Tai Chi Chuan and Baduanjin on resting-state functional connectivity of the default mode network in older adults. *Soc. Cogn. Affect. Neurosci.* 14, 217–224. doi: 10.1093/scan/nsz001

Liu, J., Wu, R., Johnson, B., Vu, J., Bass, C., and Li, J. X. (2019b). The claustrum-prefrontal cortex pathway regulates impulsive-like behavior. *J. Neurosci.* 39, 10071–10080. doi: 10.1523/jneurosci.1005-19.2019

Liu, P., Li, Q., Zhang, A., Liu, Z., Sun, N., Yang, C., et al. (2020). Similar and different regional homogeneity changes between bipolar disorder and unipolar depression: a resting-state fMRI study. *Neuropsychiatr. Dis. Treat.* 16, 1087–1093. doi: 10.2147/ndt.S249489

Liu, Y., Li, M., Chen, H., Wei, X., Hu, G., Yu, S., et al. (2019c). Alterations of regional homogeneity in Parkinson's disease patients with freezing of gait: a resting-state fMRI study. *Front. Aging Neurosci.* 11:276. doi: 10.3389/fnagi.2019.00276

Liu, Y., Zhu, J., Li, Q., Wang, Y., Li, Y., Chen, J., et al. (2020). Differences in the amplitude of low-frequency fluctuation between methamphetamine and heroin use disorder individuals: a resting-state fMRI study. *Brain Behav.* 10:e01703. doi: 10.1002/brb3.1703

Ma, X., Zheng, W., Li, C., Li, Z., Tang, J., Yuan, L., et al. (2019). Decreased regional homogeneity and increased functional connectivity of default network correlated with neurocognitive deficits in subjects with genetic high-risk for schizophrenia: a resting-state fMRI study. *Psychiatry Res.* 281:112603. doi: 10.1016/j.psychres.2019.112603

Malcolm, R., Myrick, H., Li, X., Henderson, S., Brady, K. T., George, M. S., et al. (2016). Regional brain activity in abstinent methamphetamine dependent males following cue exposure. *J. Drug Abuse* 2:16. doi: 10.21767/2471-853x.100016

Meade, C. S., Bell, R. P., Towe, S. L., and Hall, S. A. (2020). Cocaine-related alterations in fronto-parietal gray matter volume correlate with trait and behavioral impulsivity. *Drug Alcohol Depend.* 206:107757. doi: 10.1016/j.drugalcdep.2019.107757

Mizoguchi, H., and Yamada, K. (2019). Methamphetamine use causes cognitive impairment and altered decision-making. *Neurochem. Int.* 124, 106–113. doi: 10.1016/j.neuint.2018.12.019

Mo, S., Feng, S., and Chen, H. (2018). [Research on the rest functional magnetic resonance imaging before and after smoking cessation]. *Sheng Wu Yi Xue Gong Cheng Xue Za Zhi* 35, 87–91. doi: 10.7507/1001-5515.201609026

Moallem, N. R., Courtney, K. E., and Ray, L. A. (2018). The relationship between impulsivity and methamphetamine use severity in a community sample. *Drug Alcohol Depend.* 187, 1–7. doi: 10.1016/j.drugalcdep.2018.01.034

Park, B. Y., Shim, W. M., James, O., and Park, H. (2019). Possible links between the lag structure in visual cortex and visual streams using fMRI. *Sci. Rep.* 9:4283. doi: 10.1038/s41598-019-40728-x

Patton, J. H., Stanford, M. S., and Barratt, E. S. (1995). Factor structure of the Barratt impulsiveness scale. *J. Clin. Psychol.* 51, 768–774. doi: 10.1002/1097-4679(199511)51:6<768::aid-jclp2270510607<3.0.co;2-1

Psederska, E., Thomson, N. D., Bozgunov, K., Nedelchev, D., Vasilev, G., and Vassileva, J. (2021). Effects of psychopathy on neurocognitive domains of impulsivity in abstinent opiate and stimulant users. *Front. Psychiatry* 12:660810. doi: 10.3389/fpsyt.2021.660810

Qiu, Y., Lv, X., Su, H., Jiang, G., Tian, J., Zhuo, F., et al. (2013). Reduced regional homogeneity in bilateral frontostriatal system relates to higher impulsivity behavior in codeine-containing cough syrups dependent individuals. *PLoS One* 8:e78738. doi: 10.1371/journal.pone.0078738

Salo, R., Fassbender, C., Buonocore, M. H., and Ursu, S. (2013). Behavioral regulation in methamphetamine abusers: an fMRI study. *Psychiatry Res.* 211, 234–238. doi: 10.1016/j.pscychresns.2012.10.003

Schwartz, D. L., Mitchell, A. D., Lahna, D. L., Luber, H. S., Huckans, M. S., Mitchell, S. H., et al. (2010). Global and local morphometric differences in recently abstinent methamphetamine-dependent individuals. *Neuroimage* 50, 1392–1401. doi: 10.1016/j.neuroimage.2010.01.056

Schwarzbach, V., Lenk, K., and Laufs, U. (2020). Methamphetamine-related cardiovascular diseases. *ESC Heart Fail.* 7, 407–414. doi: 10.1002/ehf2.12572

Shadloo, B., Amin-Esmaeili, M., Haft-Baradaran, M., Noroozi, A., Ghorban-Jahromi, R., and Rahimi-Movaghar, A. (2017). Use of amphetamine-type stimulants in the Islamic Republic of Iran, 2004-2015: a review. *East Mediterr. Health J.* 23, 245–256. doi: 10.26719/2017.23.3.245

Shan, X., Liao, R., Ou, Y., Pan, P., Ding, Y., Liu, F., et al. (2021). Increased regional homogeneity modulated by metacognitive training predicts therapeutic efficacy in patients with schizophrenia. *Eur. Arch. Psychiatry Clin. Neurosci.* 271, 783–798. doi: 10.1007/s00406-020-01119-w

Starcke, K., Antons, S., Trotzke, P., and Brand, M. (2018). Cue-reactivity in behavioral addictions: a meta-analysis and methodological considerations. *J. Behav. Addict.* 7, 227–238. doi: 10.1556/2006.7.2018.39

Subramanian, K., Menon, V., Sarkar, S., Chandrasekaran, V., and Selvakumar, N. (2020). Study of risk factors associated with suicide attempt in patients with bipolar disorder type I. *J. Neurosci. Rural Pract.* 11:291.

Vassileva, J., and Conrod, P. J. (2019). Impulsivities and addictions: a multidimensional integrative framework informing assessment and interventions for substance use disorders. *Philos. Trans. R. Soc. Lond. B Biol. Sci.* 374:20180137. doi: 10.1098/rstb.2018.0137

Wang, C., Shen, Z., Huang, P., Yu, H., Qian, W., Guan, X., et al. (2017). Altered spontaneous brain activity in chronic smokers revealed by fractional ramplitude of low-frequency fluctuation analysis: a preliminary study. *Sci. Rep.* 7:328. doi: 10.1038/s41598-017-00463-7

Wang, Y., Zhu, J., Li, Q., Li, W., Wu, N., Zheng, Y., et al. (2013). Altered fronto-striatal and fronto-cerebellar circuits in heroin-dependent individuals:

a resting-state FMRI study. *PLoS One* 8:e58098. doi: 10.1371/journal.pone.0058098

Wang, Y., Zuo, J., Hao, W., Shen, H., Zhang, X., Deng, Q., et al. (2020). Quality of life in patients with methamphetamine use disorder: relationship to impulsivity and drug use characteristics. *Front. Psychiatry* 11:579302. doi: 10.3389/fpsyt.2020.579302

Weafer, J., Van Hedger, K., Keedy, S. K., Nwaokolo, N., and de Wit, H. (2020). Methamphetamine acutely alters frontostriatal resting state functional connectivity in healthy young adults. *Addict. Biol.* 25:e12775. doi: 10.1111/adb.12775

Winhusen, T., Lewis, D., Adinoff, B., Brigham, G., Kropp, F., Donovan, D. M., et al. (2013). Impulsivity is associated with treatment non-completion in cocaine- and methamphetamine-dependent patients but differs in nature as a function of stimulant-dependence diagnosis. *J. Subst. Abuse Treat.* 44, 541–547. doi: 10.1016/j.jsat.2012.12.005

Xie, A., Wu, Q., Yang, W. F. Z., Qi, C., Liao, Y., Wang, X., et al. (2021). Altered patterns of fractional amplitude of low-frequency fluctuation and regional homogeneity in abstinent methamphetamine-dependent users. *Sci. Rep.* 11:7705. doi: 10.1038/s41598-021-87185-z

Yalachkov, Y., Kaiser, J., and Naumer, M. J. (2010). Sensory and motor aspects of addiction. *Behav. Brain Res.* 207, 215–222. doi: 10.1016/j.bbr.2009.09.015

Yan, C. G., Wang, X. D., Zuo, X. N., and Zang, Y. F. (2016). DPABI: data processing & analysis for (resting-state) brain imaging. *Neuroinformatics* 14, 339–351. doi: 10.1007/s12021-016-9299-4

Yang, M., Jia, X., Zhou, H., Ren, P., Deng, H., Kong, Z., et al. (2021). Brain dysfunction of methamphetamine-associated psychosis in resting state: approaching schizophrenia and critical role of right superior temporal deficit. *Addict. Biol.* 26:e13044. doi: 10.1111/adb.13044

Yao, S., Yang, H., Zhu, X., Auerbach, R. P., Abela, J. R., Pulleyblank, R. W., et al. (2007). An examination of the psychometric properties of the Chinese version of the Barratt Impulsiveness Scale, 11th version in a sample of Chinese adolescents. *Percept. Mot. Skills* 104(3 Pt 2), 1169–1182. doi: 10.2466/pms.104.4.1169-1182

Zang, Y., Jiang, T., Lu, Y., He, Y., and Tian, L. (2004). Regional homogeneity approach to fMRI data analysis. *Neuroimage* 22, 394–400. doi: 10.1016/j.neuroimage.2003.12.030

Conflict of Interest: The authors declare that the research was conducted in the absence of any commercial or financial relationships that could be construed as a potential conflict of interest.

Publisher's Note: All claims expressed in this article are solely those of the authors and do not necessarily represent those of their affiliated organizations, or those of the publisher, the editors and the reviewers. Any product that may be evaluated in this article, or claim that may be made by its manufacturer, is not guaranteed or endorsed by the publisher.

frontiers in Molecular Neuroscience

ORIGINAL RESEARCH
published: 28 February 2022
doi: 10.3389/fnmol.2022.829886

Quercetin Mitigates Methamphetamine-Induced Anxiety-Like Behavior Through Ameliorating Mitochondrial Dysfunction and Neuroinflammation

Fengrong Chen[1,2], Jiaxue Sun[2,3], Cheng Chen[2,3], Yongjin Zhang[2,4], Lei Zou[2,5], Zunyue Zhang[2,6], Minghui Chen[1,2], Hongjin Wu[2], Weiwei Tian[2], Yu Liu[7], Yu Xu[2,3], Huayou Luo[2,3], Mei Zhu[2], Juehua Yu[2,4], Qian Wang[8] and Kunhua Wang[2,6]**

[1] School of Medicine, Kunming University of Science and Technology, Kunming, China, [2] NHC Key Laboratory of Drug Addiction Medicine, Kunming Medical University, Kunming, China, [3] Yunnan Institute of Digestive Disease, The First Affiliated Hospital of Kunming Medical University, Kunming, China, [4] Center for Experimental Studies and Research, The First Affiliated Hospital of Kunming Medical University, Kunming, China, [5] Department of Organ Transplant, The First Affiliated Hospital of Kunming Medical University, Kunming, China, [6] Yunnan University, Kunming, China, [7] The School of Foreign Languages, University of Shanghai for Science and Technology, Shanghai, China, [8] Tianhua College, Shanghai Normal University, Shanghai, China

OPEN ACCESS

Edited by:
Qi Wang,
Southern Medical University, China

Reviewed by:
Huijie Huang,
Sanford Burnham Prebys Medical Discovery Institute, United States
Cheng-Liang Luo,
Soochow University, China

***Correspondence:**
Qian Wang
hi_wangqian@126.com
Kunhua Wang
kunhuawang1@163.com

Specialty section:
This article was submitted to Molecular Signaling and Pathways, a section of the journal Frontiers in Molecular Neuroscience

Received: *06 December 2021*
Accepted: *19 January 2022*
Published: *28 February 2022*

Citation:
Chen F, Sun J, Chen C, Zhang Y, Zou L, Zhang Z, Chen M, Wu H, Tian W, Liu Y, Xu Y, Luo H, Zhu M, Yu J, Wang Q and Wang K (2022) Quercetin Mitigates Methamphetamine-Induced Anxiety-Like Behavior Through Ameliorating Mitochondrial Dysfunction and Neuroinflammation. Front. Mol. Neurosci. 15:829886. doi: 10.3389/fnmol.2022.829886

Methamphetamine (MA) abuse results in neurotoxic outcomes, including increased anxiety and depression. Studies have reported an association between MA exposure and anxiety, nonetheless, the underlying mechanism remains elusive. In the present study, we developed a mouse model of anxiety-like behavior induced by MA administration. RNA-seq was then performed to profile the gene expression patterns of hippocampus (HIPP), and the differentially expressed genes (DEGs) were significantly enriched in signaling pathways related to psychiatric disorders and mitochondrial function. Based on these, mitochondria was hypothesized to be involved in MA-induced anxiety. Quercetin, as a mitochondrial protector, was used to investigate whether to be a potential treatment for MA-induced anxiety; accordingly, it alleviated anxiety-like behavior and improved mitochondrial impairment *in vivo*. Further experiments *in vitro* suggested that quercetin alleviated the dysfunction and morphological abnormalities of mitochondria induced by MA, *via* decreasing the levels of reactive oxygen species (ROS), mitochondrial membrane potential (MMP), and increasing the oxygen consumption rate (OCR) and ATP production. Moreover, the study examined the effect of quercetin on astrocytes activation and neuroinflammation, and the results indicated that it significantly attenuated the activation of astrocytes and reduced the levels of IL-1β, TNFα but not IL-6. In light of these findings, quantitative evidence is presented in the study supporting the view that MA can evoke anxiety-like behavior *via* the induction of mitochondrial dysfunction. Quercetin exerted antipsychotic activity through modulation of mitochondrial function and neuroinflammation, suggesting its potential for further therapeutic development in MA-induced anxiety.

Keywords: methamphetamine, anxiety, mitochondrial dysfunction, oxidative stress, quercetin, neuroinflammation

INTRODUCTION

As a highly addictive psychostimulant drug, methamphetamine (MA) abuse is an increasingly common worldwide phenomenon, resulting in significant physical, behavioral, cognitive, and psychiatric outcomes (Meredith et al., 2005; Homer et al., 2008; Glasner-Edwards and Mooney, 2014). Epidemiological studies have shown that amphetamine-type stimulants represent the most widely used illicit drugs in the world after cannabis, with $\leq$ 51 million global users between the ages of 15 and 64 years (Wearne and Cornish, 2018). Among abusers, 72–100% experience MA-induced psychotic reactions (Srisurapanont et al., 2003; Smith et al., 2009), and 30.2% of chronic MA users are diagnosed with anxiety (Hellem, 2016). In a recent cohort research in Australia, even more than half (60%) of the participants were classified as experiencing moderate to severe anxiety and/or depression (Duncan et al., 2021).

Human neuroimaging studies have suggested that MA users experience significant changes in multiple brain regions, including the orbitofrontal cortex, striatum, amygdala, hippocampus, and insula, which are involved in a variety of functional networks, including the salience network, limbic system, and frontostriatal circuit (Uhlmann et al., 2016; May et al., 2020; Nie et al., 2021). Further evidence has demonstrated that MA administration can evoke changes in behavior, synaptic transmission, and volume in the hippocampus (Uhlmann et al., 2016; Golsorkhdan et al., 2020), resulting in the dysregulation of neurotransmitters and their receptors in these regions (Uhlmann et al., 2016), often accompanied by oxidative stress, apoptosis, and autophagy (Huang et al., 2017). Hippocampal damage, particularly dentate gyrus (DG) and ventral hippocampus (vH), is associated with the pathogenesis of anxiety and depression (Satpute et al., 2012; Allsop et al., 2014; Baksh et al., 2021). The relation between anxiety and hippocampal activity has been subject to research for many years. Therefore, it is important to take the role of hippocampus into consideration to identify anxiety-related genes with MA treatment.

Previous studies have demonstrated that both oxidative stress and mitochondrial dysfunction may play significant affective roles in the pathology of anxiety (Chang et al., 2007; Kohno et al., 2018). Excessive dopamine induced by MA is thought to trigger the overproduction of reactive oxygen species (ROS) by the mitochondria and relevant enzymes, exacerbating neurodegenerative diseases (Shin et al., 2017), which suggested that mitochondrial functional processes may play major roles in the brain abnormalities in relation to MA-induced anxiety. Increasing experimental evidence has supported the existence of a link between mitochondrial dysfunction, brain dysfunction, and neuropsychiatric disorders (Wallace, 2017; Pei and Wallace, 2018; Filiou and Sandi, 2019). Suboptimal mitochondrial function would be vulnerable to the stress-associated depletion of the brain's energy resources, resulting in the development of psychiatric disorders (e.g., anxiety and depression) (Morava and Kozicz, 2013). However, the mechanisms underlying the etiology of MA-induced anxiety remain poorly understood.

Research has suggested that the treatment of co-occurring psychiatric disorders, including depression and anxiety, may also be important for preventing relapses (Glasner-Edwards et al., 2010; Su et al., 2017). A substantial amount of literature has demonstrated the efficacy of both first- and second-generation antipsychotic drugs for the treatment of psychotic symptoms associated with MA-induced depression and anxiety (Shoptaw et al., 2009; Wang et al., 2016; Chiang et al., 2019). However, adverse events are frequently reported in these studies. Quercetin, which is a flavonoid-type secondary metabolite found in foods and medicinal plants, is presumed to have antioxidant, anti-inflammatory, immunoprotective, and anti-carcinogenic effects and has been found to mitigate anxiety-like behaviors in mice by modulating oxidative stress and monoamine oxidase activity (Dhiman et al., 2019), preventing antioxidant enzyme impairment, regulating serotonergic and cholinergic neurotransmission, and decreasing neuroinflammation and neuronal apoptosis (Samad et al., 2018; Kosari-Nasab et al., 2019). Quercetin has been confirmed to be safe when used as a single compound in dietary supplements in both animal and human studies, and adverse effects following supplemental quercetin intake have rarely been reported (Andres et al., 2018). Despite evidence that quercetin serves as an oxidative stress and inflammatory modulator, no research has examined the effects of quercetin on anxiety-like behaviors induced by chronic MA.

In this study, we aimed to understand the gene profiling of hippocampus of MA-induced anxious mice and determine whether quercetin intervention could mitigate anxiety-like behaviors by exploring the underlying mechanisms. We first performed RNA-seq in HIPP to identify susceptibility genes in relation in anxiety induced by MA. Then the potential underlying pathways were analyzed by Kyoto Encyclopedia of Genes and Genomes (KEGG) analyses. Subsequently, in view of the functional enrichment, we assessed the anti-anxiety effects of quercetin as a mitochondrial protector *in vitro*. Finally, we performed experiments *in vivo* and *in vitro* to further explore the role of quercetin in mitochondria and neuro-inflammation. These findings will contribute to a better understanding of the role of mitochondria in anxiety and allow for the therapeutic potential of quercetin against MA-induced anxiety to be assessed.

MATERIALS AND METHODS

Animals and Treatment

Mice were housed with a 12-h light/dark cycle (lights on at 7:00 A.M). Behavioral testing is performed between 9:00 AM and 6:00 PM. The experimental mice were transferred to the behavioral testing room 30 min before the first trial to allow them to habituate to the room conditions. All procedures were approved by the Committee on Ethics in the Use of Animals from Kunming Medical University (CEUA no. kmmu2021227). MA was dissolved in sterile saline to a concentration of 1 mg/ml as a stock solution. Quercetin was purchased from Sigma-Aldrich Company (Sigma-Aldrich, MO, United States) and was first

dissolved in polyethylene glycol (PEG, Sigma-Aldrich), at a final concentration of 50 mg/kg in 20% PEG with 0.9% saline. Adult male C57BL/6 mice which weighed from 22 to 25 g were randomly divided into three groups ($n = 12$ each group): control, MA-treated, and MA + quercetin (Q)-treated. The control group received normal saline injection intraperitoneally; the MA group received escalating MA doses, as described in a previous study (Manning et al., 2016), at 5, 10, and 15 mg/kg during the first, second, and third weeks, respectively; and the MA + Q group received escalating MA doses and quercetin treatment, administered with one dose at 50 mg/kg daily for 4 days during the first week and 5 days in the second week, as described in a previous study (Zhang et al., 2019). On the 22nd day, the open field (OFT) and Elevated Plus Maze (EPM) tests were used to examine the motor activity and anxiety levels, respectively. After behavioral testing, the animals were sacrificed immediately, and subsequent experiments were conducted.

Conditioned Place Preference Test

The conditioned place preference test (CPP) apparatus consisted of two compartments: one had black and white striped walls, a white floor, and a black ceiling; the other had black and white checkered walls, a black floor, and a white ceiling. The two compartments were separated by a removable board. Behavioral subjects were habituated for 5 min and placed in the experimental environment for adaptation for 3 days before the CPP test.

Pre-test, conditioning, and a test were included in the MA CPP session. During the pre-test phase, the mice were placed in the middle of the conditioning apparatus and allowed to freely explore the full extent of the CPP apparatus for 15 min. The time spent in each chamber was measured. Mice that spent > 65% (> 585 s) or < 35% (< 315 s) of the total time (900 s) on one side were eliminated from subsequent CPP experiments (Zhou et al., 2019). Conditioning was conducted on mice confined to one chamber for 30 min, which was paired with an intraperitoneal (i.p.) MA injection on days 1, 3, 5, and 7, and on days 2, 4, and 6, the mice were confined to the other chamber for 30 min, which was paired with an i.p. saline injection. For the CPP test, mice were released from the middle part of the CPP apparatus and allowed to freely explore both chambers for 15 min. The CPP score was calculated by subtracting the time spent within the saline-paired side from that spent on the MA-paired side. Mouse behavior was analyzed using the ANY-maze video tracking system (Stoelting Co.).

Open Field Test

Each experimental animal was placed in the corner of the open field apparatus (50 × 50 × 40 cm^3, SANS Co., Jiangsu, China), which consisted of a white plastic floor and wall. The OFT performance was recorded using a video camera attached to a computer and controlled by a remote device. The total distance traveled (cm) and time spent in the center area (20 × 20 cm^2) were recorded during a 5−min test period. After each trial, the whole open field apparatus was cleaned with 75% ethyl alcohol to efficiently remove odor to prevent any bias based on olfactory cues. The mouse behavior was analyzed using the ANY-maze video tracking system (Stoelting Co.).

Elevated Plus Maze Test

The EPM consisted of two open arms (30 cm × 5 cm) and two enclosed arms of the same size, with 15 cm white plastic walls. The four arms were connected by a central square (5 cm × 5 cm) (SANS Co., Jiangsu, China). The arms were elevated 55 cm above the floor. Each experimental mouse was placed in the central square of the maze, facing one of the enclosed arms. The number of entries into each arm and the time spent in the open arms were recorded during a 5-min test period. When a mouse falls from the maze, the data were excluded. After each trial, all arms and the center area were cleaned with 75% ethyl alcohol, as previously described. All experimental data was collected and analyzed described.

RNA Preparation, Library Construction, and Sequencing

Total RNA was isolated using RNA-Bee reagent, following the manufacturer's protocol. RNA purity was determined using the NanoPhotometer spectrophotometer (IMPLEN, CA, United States), and the concentration was determined using the Qubit RNA Assay Kit (Life Technologies, CA, United States). Samples with RNA integrity values > 7.0 were used for the following experiments, which were assessed by the RNA Nano 6000 Assay Kit of the Bioanalyzer 2100 system (Agilent Technologies, CA, United States).

Sequencing libraries were prepared using the NEB Next Ultra RNA Library Prep Kit (Illumina, United States), according to the manufacturer's recommendations, which were described in our previous research (Sun et al., 2020). In brief, mRNA was purified using poly-T oligo-attached magnetic beads, fragmentation was performed using divalent cations, and library quality was assessed on the Agilent Bioanalyzer 2100 and qPCR. The clustering of the index-coded samples was performed on an acBot Cluster Generation System using TruSeq PE Cluster Kitv3-cBot-HS (Illumina, San Diego, CA, United States). The library preparations were then sequenced on an Illumina Hiseq platform, and paired-end reads were generated.

Quantification and Differential Expression Analysis of mRNA

As mentioned in Sun et al. (2020), the reference genome index was built, and paired-end clean reads were aligned to the reference genome using Hisat2 v2.0.5. Feature Counts v1.5.0-p3 was used to count the reads numbers. The expected number of fragments per kilobase of transcript sequence per millions (FPKM) of base pairs sequenced was calculated based on the gene length, and read counts were mapped to the gene.

Differential expression analysis ($n = 3$ per group) was performed using the DESeq2 R package (1.16.1). P-values were adjusted using the Benjamini and Hochberg approach for controlling the false discovery rate (FDR), and $p < 0.05$ and $\log_2$ fold-change > 1 were considered to be significant DEGs. DEGs enrichment in the KEGG pathways was assessed using the web tool Metascape[1].

[1]http://metascape.org

Immunofluorescence Staining and Imaging

Mice were deeply anesthetized and perfused with 25 ml ice-cold PBS, followed by 25 ml 4% ice-cold paraformaldehyde (PFA) in PBS. Brains were removed and dehydrated with 15% and 30% sucrose at 4°C. The fixed brains were sliced into 30-μm-thick sagittal slices using a Leica CM1950. Slices were permeabilized in 1.2% Triton X-100 in PBS for 15 min and subject to incubation in blocking solution. Slices were incubated with primary antibodies for NeuN (1:200, Abcam), glial fibrillary acidic protein (GFAP, 1:500, Abcam) for 24 h at 4°C, followed by incubation with species-matched and Alexa Fluor conjugated secondary antibodies raised in rabbit (1:5,000, Invitrogen) for 2 h at room temperature. 4′,6-Diamadino-2-phenylindole (DAPI, 1:1,000, Invitrogen) was incubated after secondary antibody incubation for 15 min at room temperature. Slices were mounted and coverslipped using VECTASHIELD H-1000 mounting medium and scanned on a Nikon C2 confocal microscope using NIS-Element software.

H&E Staining and Electron Microscope Imaging

The brain tissues were fixed in 4% paraformaldehyde (PFA) immediately after sacrifice. H&E staining was performed on 5 μm paraffin sections using standard H&E staining protocol which were described previously (Sun et al., 2020). The thin sections were made with an ultramicrotome, stained by OsO_4. Electron microscopy and ultrastructural studies were performed on a transmission electron microscope (JEM-1400Flash).

Cell Culture

Hippocampal astrocytes were prepared from C57BL/6 mouse pups under sterile conditions. Neonatal mouse pups were decapitated, after brain removal, hippocampus were separated and cut in small pieces, and incubated in trypsin solution (GIBICO) at 37°C for 20 min, DNase I (50 μl/ml) was added. Tissue pieces were washed with DMEM + 10%FBS. Cells were centrifuged at 1,000 rpm for 5 min and suspended with astrocytes medium (AM, Cell Sciences). Astrocytes were plated into poly-D-lysine (Byotime) coated 25 cm2 flasks at 1×10^6 cells/flask, and grown in astrocytes medium, maintained in a humidified 37°C incubator with 5% CO2 with media exchange next day. Cells were digested with trypsin, the 3rd passages were used in all experiments.

Measurement of ATP, Mitochondrial Membrane Potential, and Reactive Oxygen Species

Intracellular ATP was determined using a firefly luciferase-based ATP assay kit (Beyotime, Beijing, China) based on a fluorescence technique. In brief, astrocytes (1×10^4) were plated in 96-wells, and appropriate drug treatments were applied for 48 h. Opaque-walled 96-well plates with culture media (50 μL) were prepared. Luminescence test solution (50 μL) was added and incubated for 30 min and then measured using a luminescence microplate reader. Mitochondria-derived ATP was measured after treatment with 300 mM iodoacetic acid (IAA, Sigma-Aldrich, MO, United States). IAA was added to half of the wells and the cells were then incubated at 37°C and 5% CO_2 for 60 min. After 30 min, 1 mM oligomycin was added to half of the wells containing IAA and incubated for 30 min to abolish all ATP production and confirm that the ATP levels in the presence of IAA were produced by the mitochondrial ATP synthase. Subsequently, the media was removed from the wells and cellular ATP was measured using ATP assay kit (mentioned before).

JC-1 assay was conducted to analyze the MMP using the JC-1 mitochondrial membrane potential assay kit (Beyotime, Beijing, China). In brief, astrocytes (2×10^5) were plated in 6-well plates and, after appropriate drug treatments, stained with 10 μM JC-1 for 20 min. JC-1 exhibits double fluorescence staining, either as red fluorescent J-aggregates (530 nm excitation/590 nm emission, as P3) at high potentials or as green fluorescent J-monomers (490 nm excitation/530 nm emission, as P2) at low potentials; Flow cytometric analysis was performed by fluorescence-assisted cell sorting (FACS) after JC-1 staining detected changes in MMP and the value was calculated. The relative proportion of red and green fluorescence was used as an index of change in membrane potential.

For ROS generation measurements, primary astrocytes were plated in 96-wells, and appropriate drug treatments were applied for 48 h. Then, cells were loaded with the ROS probe 70-dichlorodihydrofluorescein diacetate (DCFDA, 2 μM) for 40 min at RT in the dark. The mROS assay was conducted using the MitoSOX red mitochondrial superoxide indicator (Mercury Drive, Sunnyvale, CA, United States). Cells were measured by FACS at 488 nM excitation.

Oxygen Consumption Rate Analysis

Astrocytes were plated at 7.5×10^4/well in seahorse assay plates and treated with their respective treatments at 37°C and 5% CO_2 and for 24 h. Mitochondrial oxygen consumption rate (OCR) was measured by extracellular flux (XF) assay (Seahorse XFp analyzer, Agilent Technologies, Santa Clara, CA, United States), according to manufacturer's procedures. Briefly, cells were incubated in a CO_2-free environment for 1 h, and OCR was measured every 3 min for the next 90 min. First, OCR was acquired in basal conditions (20 mM glucose), followed by in the presence of 1.5 μM oligomycin (ATP synthase inhibitor), with 3.5 μM carbonyl cyanide-p-trifluoromethoxy phenylhydrazone (FCCP), and finally, with 0.5 μM rotenone/antimycin A.

Quantification of Gene Expression Assay

Quantification of gene expression was performed by ABI 7500 Sequence Detection System (Applied Biosystems, Foster City, CA, United States). The qPCR assays were performed as described in our previous study (Chen et al., 2016). The primers used for qPCR are shown in **Supplementary Table 1**. The mRNA levels were determined by qPCR in triplicate for each of the independently prepared RNA samples, and mRNA levels

were normalized against the levels of glyceraldehyde 3-phosphate dehydrogenase (*GAPDH)* expression.

Western Blotting Analysis

Total protein was extracted from astrocytes or brain tissue and quantified by bicinchoninic acid (BCA) protein assay kit (Pierce, United States) and used for immunoblotting analysis, as described previously. Briefly, the blot was incubated with a specific primary antibody overnight (anti- GFAP, 1:1,000), followed by incubation with HRP-conjugated secondary antibody. The bands were detected with a chemiluminescence detection kit (Millipore Co., MA, United States) and scanned using the iBright FL1500 chemiluminescence imaging system (Thermo Fisher Scientific, United States).

Statistical Analysis

The results are presented as the mean ± standard error of the mean (SEM). For comparisons between two or multiple groups, the Student's *t*-test or one-way analysis of variance (ANOVA) analysis was conducted, respectively. Significance is indicated by asterisks: $^{*}p < 0.05$, $^{**}p < 0.01$, $^{***}p < 0.001$.

RESULTS

Repeated Methamphetamine Administrations Induce Anxiety-Like Behavior in Mice

Initially, to identify an optimal concentration for the generation of an MA-addicted mouse model, we tested three different MA concentrations (2.5, 5, and 10 mg/kg, i.p.). Mice were trained to associate the MA reward with the paired context during training for the MA CPP (**Figure 1A**). A preference for the MA-paired side indicates the expression of a reward–context associated memory, which was assessed by measuring the time that an animal spent on the MA-paired side in the CPP apparatus. After four sessions of MA CPP training, mice treated with 5 mg/kg MA as well as the 2.5 mg/kg MA-treated group (**Figure 1B**, $p < 0.05$), respectively, showed a significant preference for the MA-paired side. However, 6 of 8 mice died in the 10 mg/kg MA-treated group. We then adopted 5 mg/kg MA as the initial concentration to establish a subsequent mouse model (**Figure 1C**), due to 2.5 mg/kg MA-group failing to exhibited anxiety-like behaviors (data not shown).

After 3 weeks with escalating dose of MA treatment, mice demonstrated a fear of entering the open arms of the EPM test (**Figure 1D**) with fewer numbers of entries to open zone and less time ($p < 0.01$) and shorter distance ($p < 0.05$) spent in the open zone. Consistently, MA treatments also displayed decreased locomotor activity and spent significantly less time in the center of the OFT than control mice (**Figure 1E**, $p < 0.01$). This suggested we successfully generated an animal model with anxiety-like behaviors.

RNA-seq Revealed Differentially Expressed Genes in the Hippocampus in the Methamphetamine-Treated Mouse Model

To better elucidate the molecular features of MA-induced anxiety-like behaviors in mice, we performed RNA-seq to investigate DEGs between control and chronic MA-treated mice in HIPP. Hierarchical clustering analysis was performed and displayed in **Figure 2A**. Fourteen upregulated genes were identified between the control and MA-treated groups, which were displayed in **Supplementary Table 2**.

To further investigate the altered signaling pathways involved in mice presenting with MA-induced anxiety-like behavior, we then performed KEGG enrichment analyses. The results demonstrated that DEGs between the control and MA-treated groups were mainly enriched in following signaling pathways: protein folding (chaperone-mediated protein folding, response to unfolded protein, chaperone cofactor-dependent protein refolding, "*de novo*" posttranslational protein folding, "*de novo*" protein folding, cellular response to unfolded protein), synaptic plasticity and synaptic transmission (regulation of synaptic plasticity, positive regulation of synaptic transmission), rhythmic processes (regulation of synaptic plasticity, positive regulation of synaptic transmission), protein phosphorylation (negative regulation of phosphorylation, negative regulation of protein phosphorylation, peptidyl-threonine dephosphorylation), oxidative stress, and the intrinsic apoptotic signaling pathway (**Figure 2B**). The targeted genes related to the top 5 shared KEGG pathways are shown in **Figure 2C**. These pathways indicates mitochondria, which participated in protein folding, and synaptic plasticity and synaptic transmission, oxidative stress, and the intrinsic apoptotic (Cheng et al., 2015; Fang et al., 2015; Song et al., 2017; Saito and Imaizumi, 2018), plays an important role in MA-induced anxiety and might be promising therapeutic target.

Furthermore, as immediate early genes (IEGs) have been reported to be involved in MA use and the development of neuropsychiatric disorders (McCoy et al., 2011; Gallitano, 2020), we used three samples from each group to validate four selected DEGs which were classified as IEGs (*Fos, Egr1, Arc* and *Nr4a1*). The results revealed that, in general, MA upregulated all the four IEGs identified, in accordance with the RNA-seq results (**Figure 2D**).

Administration of Quercetin Ameliorates Anxiety-Like Behaviors in a Methamphetamine Mouse Model

Quercetin has been reported to mitigate anxiety-like symptoms in a lipopolysaccharide-induced mouse model of anxiety (Samad et al., 2018; Lee et al., 2020) and has been reported as a mediator of mitochondrial function and ER stress (Khan et al., 2016). Therefore, we evaluated the effects of quercetin on MA-induced behavioral phenotypes and the role played by quercetin in mitochondrial functional modifications in the present study (**Figure 3A**).

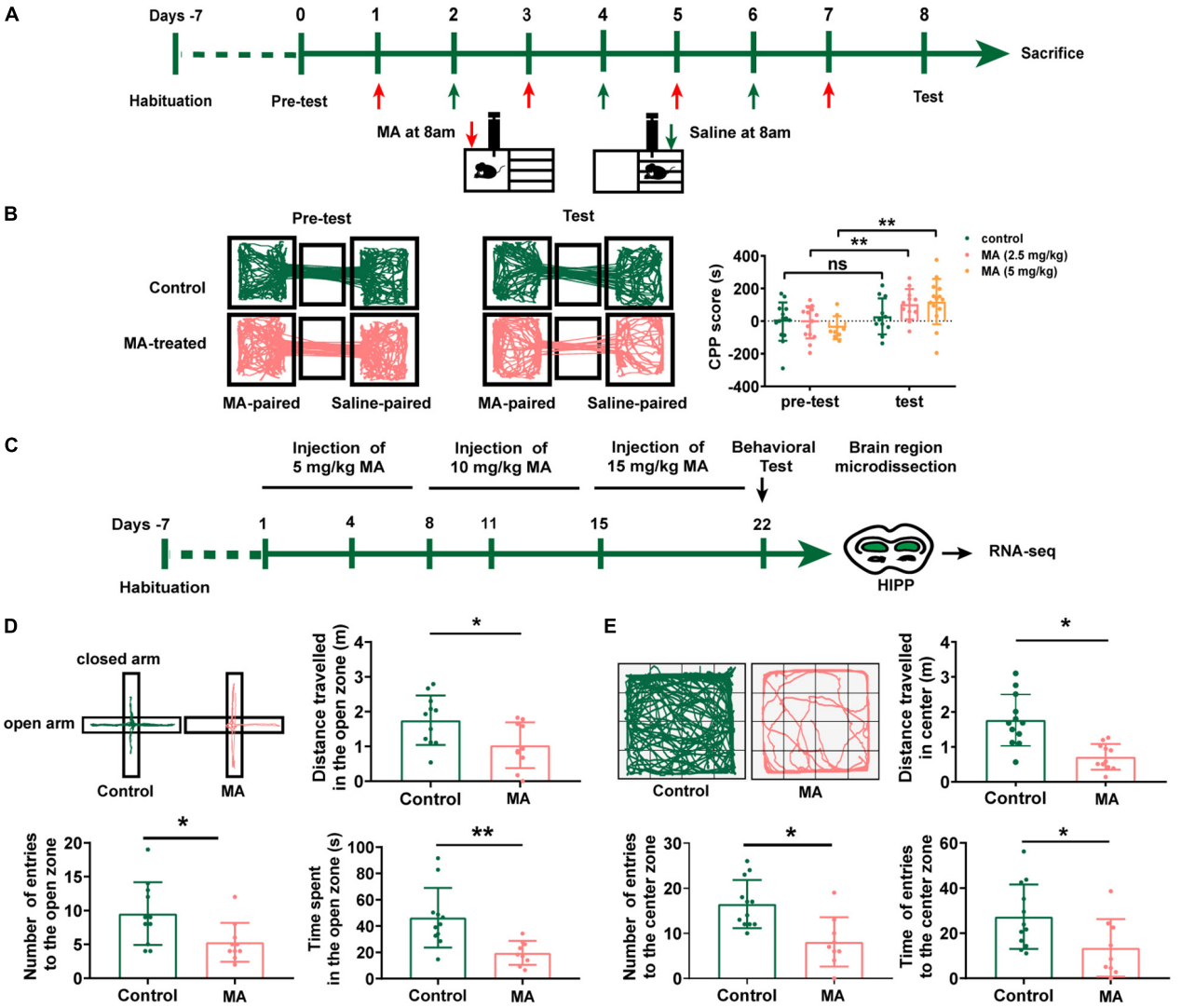

FIGURE 1 | Repeated MA administrations induce anxiety-like behavior in mice. **(A)** Timeline of the Conditional place preference (CPP) experimental procedure. **(B)** The movement trajectory of the two groups of mice across compartments (left); CPP scores were assessed as the difference of time spent in the drug-paired compartment between the post and pre-conditioning phases (right). Data collected from three independent experiments. **(C)** Timeline of the model establishment and sample collection. **(D,E)** Anxiety assessment with the elevated plus maze (EPM) and open field test (OFT). Student *t*-tests, $^{*}p < 0.05$ and $^{**}p < 0.05$. Data collected from three independent experiments.

In the EPM test, the time spent and the number of entries into the open arms were significantly reduced in the MA-treated group compared with those in the control group (**Figure 3B**, $p < 0.05$); in contrast, when compared with the control group, the time spent and number of entries into the closed arms were significantly elevated in the MA-treated group (Data not shown). However, mice treated with MA + Q showed the significant restoration of the time spent and the number of entries into the open arms compared with those for the single MA-treated group (**Figure 3B**, $p < 0.05$), with no significant differences observed between the control group and the MA + Q group (**Figure 3B**, $p > 0.05$).

The OFT results revealed that a single administration of MA significantly reduced the number of times MA-treated mice crossed in the central zone compared to the saline-treated group (**Figure 3C**, $p < 0.05$), while no significant difference in the number of crossings in the peripheral zone were observed (Data not shown). Quercetin combined with MA treatment significantly enhanced the number of central zone crossings compared with the single MA-treated group (**Figure 3C**, $p < 0.05$).

Quercetin Ameliorates Mitochondrial Dysfunction and Aberrant Morphology in Astrocytes

Astrocytes have been shown to participate in anxiety development through the synaptic pruning of neurons

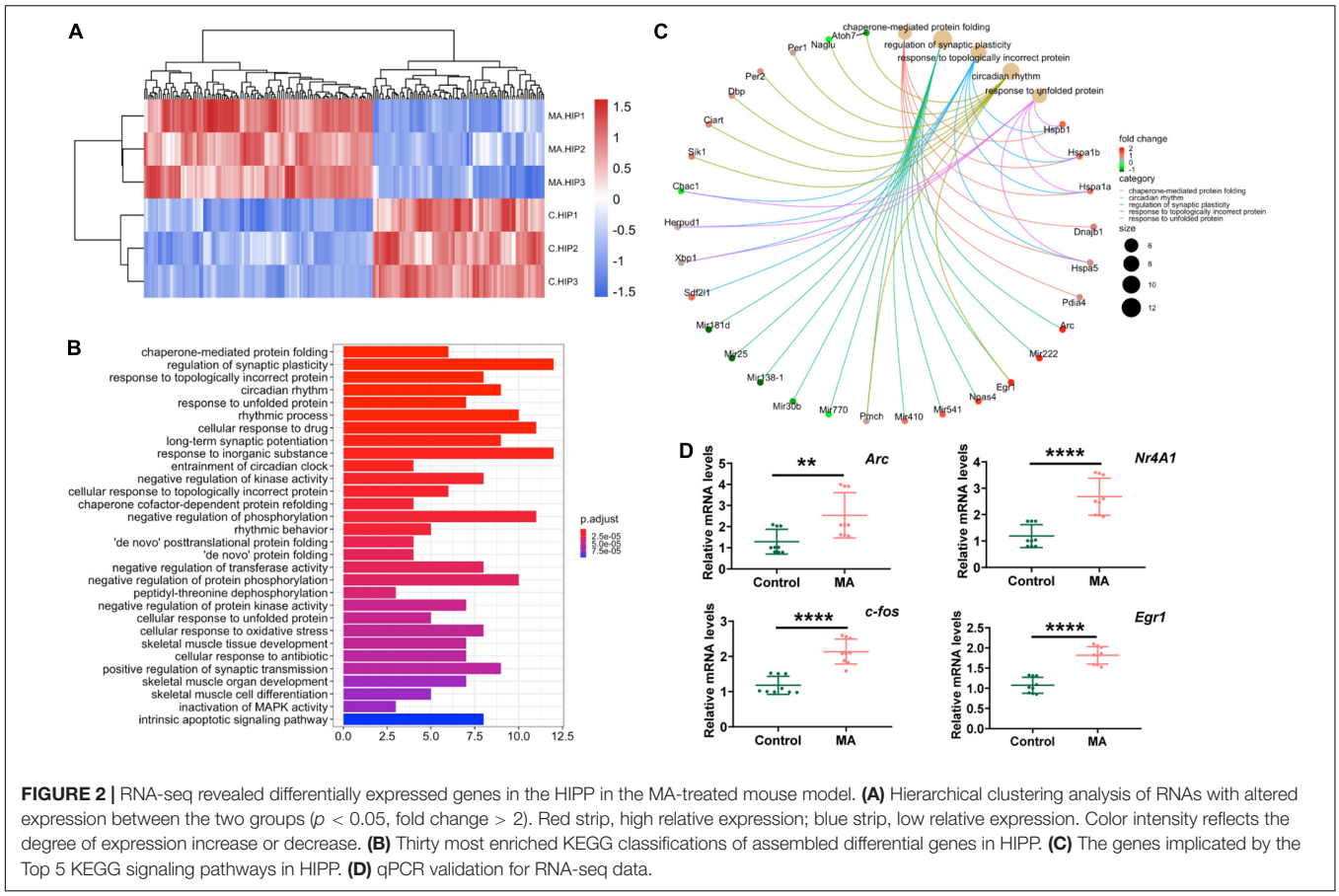

FIGURE 2 | RNA-seq revealed differentially expressed genes in the HIPP in the MA-treated mouse model. **(A)** Hierarchical clustering analysis of RNAs with altered expression between the two groups ($p < 0.05$, fold change > 2). Red strip, high relative expression; blue strip, low relative expression. Color intensity reflects the degree of expression increase or decrease. **(B)** Thirty most enriched KEGG classifications of assembled differential genes in HIPP. **(C)** The genes implicated by the Top 5 KEGG signaling pathways in HIPP. **(D)** qPCR validation for RNA-seq data.

(Çalışkan et al., 2020) and, although most of previous researches have focused on MA-induced neuronal injury. In this study, we performed experiments on astrocytes to explore its roles in MA-induced anxiety.

As signaling pathways linked to mitochondrial function have emerged as deregulated pathways forementioned, we also evaluated mitochondrial morphology of astrocytes in the HIPP using electron microscopy. The control group presented with relatively long, tubular mitochondria, whereas the mitochondria of MA-treated group were relatively more fragmented and swollen, with the loss of cristae (**Figure 4A**), indicating MA-induced damage to mitochondria of astrocytes in HIPP. Quercetin treatment was able to reinstate mitochondrial morphology toward long tubular mitochondria with intact cristae in MA-treated astrocytes (**Figure 4A**).

To further assess the effect of MA on mitochondria *in vitro*, we first evaluated mitochondrial morphology. The results demonstrated that tubular mitochondria in astrocytes shortened in length and swelled in width, forming large, spherical structures (**Figure 4B**), when exposed to MA. Similar morphological changes in mitochondria were viewed using mitotracker (**Figure 4C**). Quercetin treatment rescued abnormal mitochondrial morphology in astrocytes treated with MA (**Figures 4A–C**). The percentage of astrocytes with short/long mitochondria among different groups was analyzed and shown in **Figure 4D**.

Then, we test mitochondrial function in astrocytes. Mitochondria, as the intracellular source of ROS in animal cells, when confronting with oxidative stress, is the primary target attacked by ROS, and also produces excessive amounts of ROS due to the damage to enzymes in the electron transport chain. Therefore, we evaluated the total ROS by DCFDA and the mitochondrial ROS by MitoSOX staining respectively, and quantified the fluorescence intensity in MA-treated astrocytes with or without quercetin treatment. The results showed that both the total ROS (**Figure 4E** left, $p < 0.05$) and mitochondrial ROS (**Figure 4E** right, $p < 0.001$) were markedly increased in MA treated group, which were rescued by quercetin (**Figure 4E**, $p < 0.05$).

As we know, a series of redox reactions creates an electrochemical gradient through the mitochondrial electron transport chain, which drives the synthesis of ATP and generates the MMP. Therefore we measured the total and mitochondria-derived ATP, and MMP to evaluated mitochondrial function. The results revealed decreasing in MMP (**Figure 4F**, $p < 0.01$) and ATP (**Figure 4G**, $p < 0.001$) in MA-treated astrocytes, indicating mitochondria dysfunction after MA treatment. The quercetin supplementation of MA-treated astrocytes markedly elevated

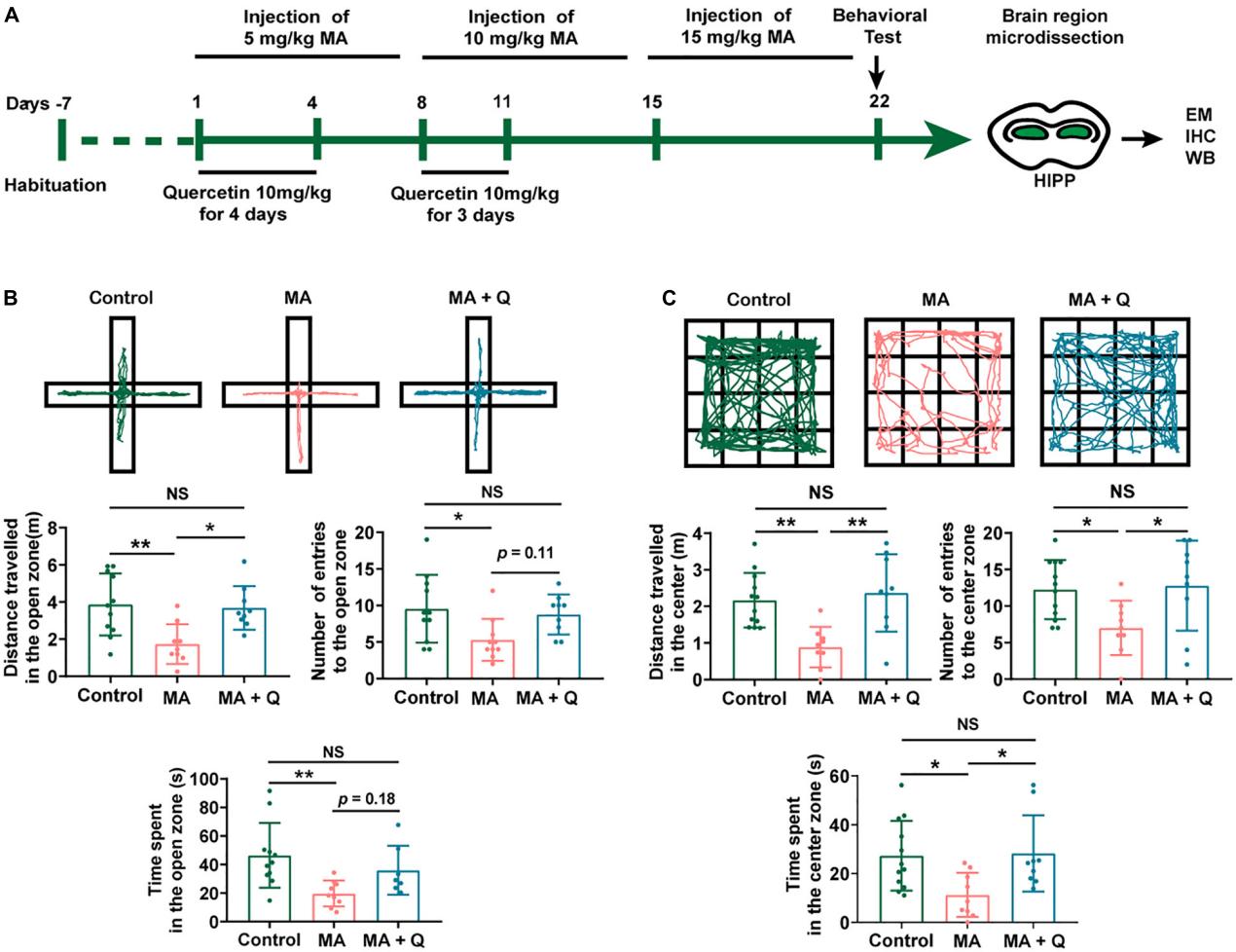

FIGURE 3 | Administration of quercetin ameliorates anxiety-like behaviors in an MA mouse model. **(A)** Timeline of the model establishment and sample collection. **(B,C)** Anxiety assessment with the elevated plus maze (EPM) and open field test (OFT). Student *t*-tests, $^{*}p < 0.05$ and $^{**}p < 0.05$. Data collected from three independent experiments.

both the total ATP (**Figure 4G** left, $p < 0.05$) and mitochondria-derived ATP levels (**Figure 4G** right, $p < 0.001$) and increased MMP in MA-treated astrocytes (**Figure 4F**, $p < 0.05$). We used an XF24 metabolic bioanalyzer to assess the effects of quercetin supplementation on OCR in MA-treated astrocytes; as a result, we found that quercetin markedly reinstated the decreasing in the OCR induced by MA (**Figure 4H**, $p < 0.001$).

Considering mitochondrial also play an important role in neurons, we also evaluated the effects of quercetin on mitochondrial morphology and function in PC12. The mitochondria in MA-treated PC12 exhibited short and fragmented morphology with a significant decrease in number of PC12 (**Supplementary Figures 1A,B**) as compared to the control group. The quercetin supplementation partially restores mitochondrial morphology and the number of PC12 when exposed to MA. The results of mitochondrial function revealed that MMP (**Supplementary Figure 1C**, $p < 0.05$) and ATP (**Supplementary Figure 1D**, $p < 0.05$) decreased in 2 mM MA-treated PC12, accompanying an increase in ROS (**Supplementary Figure 1E**, $p < 0.05$). Quercetin diminished total ROS production (**Supplementary Figure 1E**, $p < 0.05$), but failed to rescue the abnormality of ATP production and MMP induced by MA (**Supplementary Figures 1C,D**, $p > 0.05$).

Quercetin Mitigated Astrocytes Activation and Neuroinflammatory Induced by Methamphetamine

Research have reported that astrocytes were activated in an MA-treated animal model, resulting in morphological and phenotypic abnormality (Zhou et al., 2019), and fragmented and dysfunctional mitochondria trigger A1 astrocytic response and propagate inflammatory neurodegeneration (Joshi et al., 2019). We evaluate astrocytes activation by immunostaining and western blotting for GFAP. The results indicated GFAP expression increased after MA treatment (**Figure 5F**, $p < 0.05$) with a larger area of astrocytes (**Figures 5A–E**, $p < 0.05$). Quercetin alleviated the activation of astrocytes (**Figures 5A–F**,

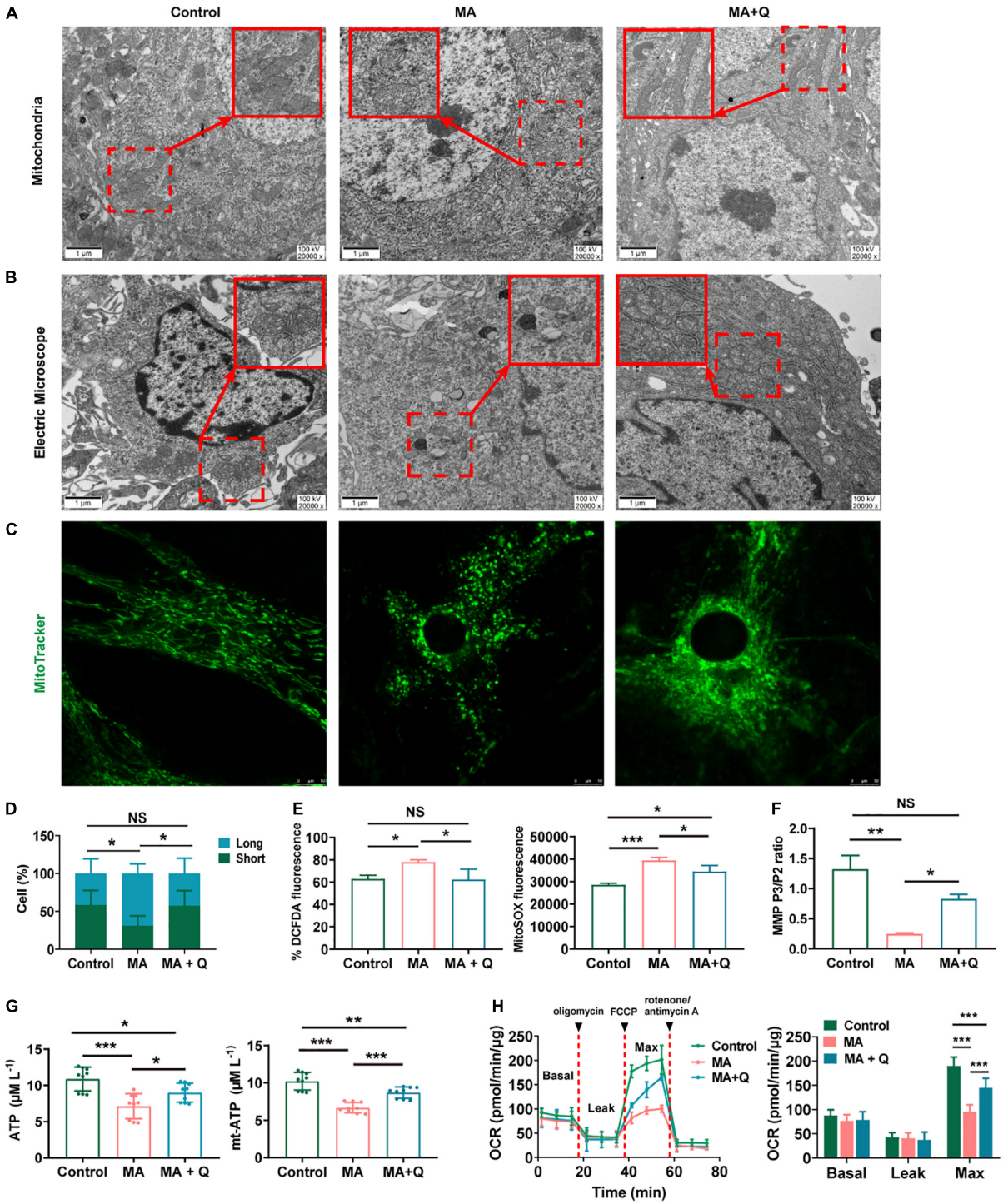

FIGURE 4 | Quercetin ameliorates mitochondrial dysfunction and aberrant morphology in astrocytes. **(A)** Electron microscopy analysis (magnification, × 20,000) of astrocytes in HIPP. Areas in red boxes are magnified (Insets). **(B)** Electron microscopy analysis (magnification, × 20,000) in astrocytes. Areas in red boxes are magnified (Insets). **(C)** Representative images of astrocytic mitochondria. Alive astrocytes were incubated with MitoTraker Green as a probe for mitochondria in each group. **(D)** The percentage of astrocytes for short-shape (blue) and long-shape (green) mitochondria in different group is presented as histograms in panel **(C)**. **(E)** Total ROS (left) and mitochondria-derived ROS (right) production quantification by flow cytometry in each group. **(F)** Quantification of the mitochondrial membrane potential (MMP). **(G)** Quantification of the total (left) and mitochondria-derived ATP (right) by using an ATP quantification kits. **(H)** An analysis of O2 consumption in astrocytes. The Agilent SeahorseXFe24 analyzer measures OCR at basal and after injection of oligomycin (3.5 μM), FCCP (4 μM), and antimycin A (1 μM)/rotenone (1 μM) for three measurement cycles at each step (left). Basal, ATP-linked, maximal, and reserve capacity OCR in each group. $^{*}p < 0.05$, $^{**}p < 0.01$, and $^{***}p < 0.001$ vs. control, as determined by Student's *t* test.

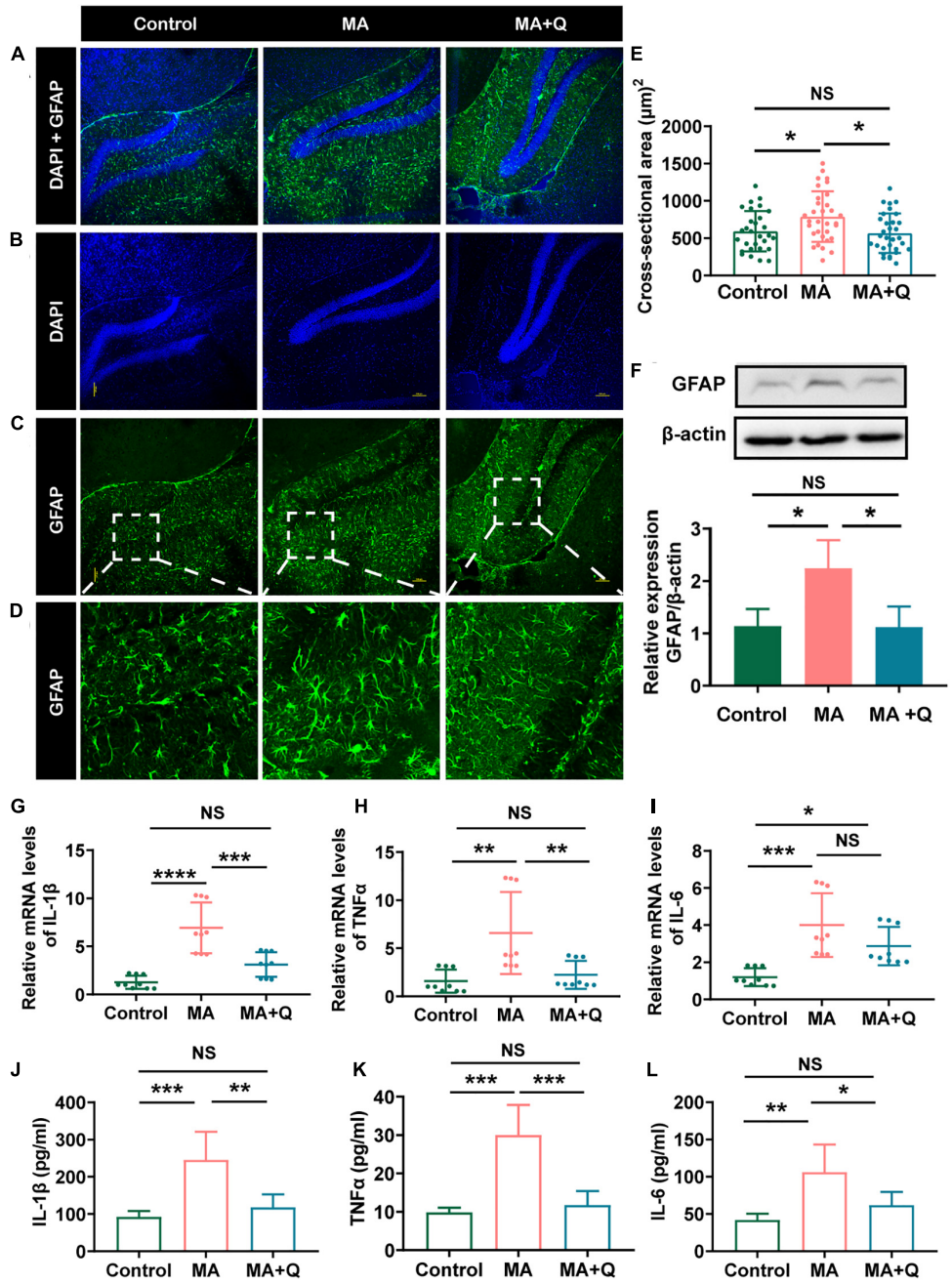

FIGURE 5 | Quercetin mitigated astrocytes activation and neuroinflammatory induced by MA. **(A)** Merged image of panels **(B,C)**; Immunofluorescence was performed with anti-GFAP [green, **(C)**] and DAPI [blue, **(B)**]; **(D)** Enlarged images of the areas marked in panel **(C)** with a white box; **(E)** Area of astrocytes (μm^2/cell) in each group, $^*p < 0.05$, $^{**}p < 0.01$. **(F)** Representative band pattern of the WB of different treatment of astrocytes using antibodies for GFAP and β-Actin (left); summary bar graphs of GFAP and β-Actin levels in different group (right). **(G–I)** Expression of proinflammatory factors by qPCR in the hippocampus (IL-1β, TNFα, IL-6). **(J–L)** The levels of the proinflammatory factors IL-1β were detected by ELISA. All experiments represent the average of 3 independent experiments.

$p < 0.01$), suggesting that MA treatment facilitated astrocytes activation, whereas quercetin reversed the cellular phenotypes.

Previous studies have shown that mitochondrial dysfunction in astrocytes, combining with neuroinflammation, impair the generation of reactive astrocytes and enhance neuronal cell death (Fiebig et al., 2019). Therefore, we assessed the change of neurons and microglia, which was considered as the main components innate neuroimmune cell, by immunostaining for NeuN and Iba-1. The results demonstrated MA administration markedly decreased the numbers of neurons (**Supplementary Figures 2A–C**) and promoted microglia proliferation (**Supplementary Figures 2D–F**).

Astrocytes and microglia, as key regulators of neuroinflammation in CNS, are activated during neuroinflammation to secrete inflammatory cytokines and chemokines (Kwon and Koh, 2020); consequently, we analyzed the expression of elevation of interleukin (IL)-1β, IL-6, and tumor necrosis factor (TNF)α, the pro-inflammatory cytokines which were triggered by drug abuse (Dang et al., 2021). As suspected, MA treatment accelerated astrocyte activation, accompanied by the elevation of IL-1β (**Figure 5G**, $p < 0.001$), TNFα (**Figure 5H**, $p < 0.01$), and IL-6 (**Figure 5I**, $p < 0.001$) in the HIPP and MA-treated astrocytes (**Figures 5J–L**). Quercetin, as an anti-inflammatory agent, decreases all the three cytokines *in vitro*, and attenuated the expression of IL-1β and TNFα, but not IL-6 in HIPP.

DISCUSSION

In the present study, we found mitochondrial morphological defects accompanied the dysfuntion in MA-treated mice with anxiety-like behavior. Quercetin attenuated anxious symptoms and pathology, and modified mitochondria and neuroinflammation in both a mouse model and cultured astrocytes treated with MA. These findings, for the first time, suggested that quercetin could inhibit the progression of MA-induced anxiety by modulating mitochondrial function and morphology and mitigating neuroinflammation in the central nervous system. The results indicated that quercetin represents a potential therapeutic medicine for future development and supported the hypothesis that changes in mitochondrial function mediate anxiety progression.

We found that MA-induced anxiety-like behavior in mice, as previously described (Ru et al., 2019; Jayanthi et al., 2021). Consistent with our findings, Iwazaki et al. (2008) have demonstrated synaptic plasticity- and synaptic transmission-, oxidative stress-, and intrinsic apoptotic-related signaling pathway were dysregulated in protein expression level in MA-treated rats. As an organelle generating secondary ROS, which can disturb protein folding and cause mitochondrial DNA mutations, mitochondria are regarded as both a source and a target of oxidative stress (Song et al., 2017), besides, they play an important role in apoptosis *via* the intrinsic apoptotic program which was identified to be dysregulated in frontal cortex in MA-treated rats (Iwazaki et al., 2008). Furthermore, ER-misfolded proteins have been reported to accumulate at ER-mitochondria contact regions, where they eventually imported into mitochondrial matrix and resulted in impaired mitochondrial function (Saito and Imaizumi, 2018; Cortés et al., 2021), and dysfunction mitochondria failed to maintain synaptic ion homeostasis and synaptic plasticity due to decreased ATP production and overloaded Ca^{2+} concentrations (Fang et al., 2015). In summary, MA exposure facilitated mitochondrial damage, intracellular ROS production (Cao et al., 2017), the depolarization of MMP and metabolic disturbance (Li et al., 2015), eventually leading to mitochondrial dysfunction (Xie et al., 2016) and intrinsic apoptotic program activation (Iwazaki et al., 2008). In this article, pathways related to mitochondria were markedly changed, and mitochondria were found to be short, fragmented with abnormal morphology after MA treatment *in vivo* and *in vitro*. Multiple parameters about mitochondria function were then displayed aberrant, such as ROS and ATP production, MMP, and OCR, implying that mitochondria as a target organelle in MA-treatment. Based on these, we speculate that mitochondria represent a primary target organelle of MA treatment in the HIPP.

Accumulating data has highlighted the contributions of brain mitochondria and bioenergetics to the development of psychiatric disorders and stress-related pathologies (Einat et al., 2005; Manji et al., 2012). The damaged mitochondria accumulation induced synaptic loss, and neuron apoptosis (de la Mata et al., 2017), underscoring the importance of mitochondria in the development of psychotic disorders. In addition, The fundamental role played by mitochondria in the synthesis of the primary excitatory neurotransmitter (glutamate) and the inhibitory neurotransmitter (γ-aminobutyric acid, GABA) suggest that the mitochondrial adaptations observed in the context of anxiety may contribute to an imbalance in neural excitation and inhibition, which is thought to underlie several neuropsychiatric disorders (Filiou and Sandi, 2019). Mitochondria-targeting drugs have been reported to show good outcomes in anxiety-related studies in both humans and rodents (Filiou and Sandi, 2019). In this article, we further demonstrated that modification of mitochondrial function and morphology might represent a potential strategy for alleviating anxiety-like behaviors induced by MA, since chronic MA exposure resulted in the dysregulation of mitochondrial morphology and mitochondrial dysfunction. Quercetin, as a bioactive compound with diverse pharmacologic effects, has been reported to exert several beneficial effects, including neuroprotective effects (Costa et al., 2016), the regulation of the sleep–wake cycle (Kambe et al., 2010), and the optimization of mitochondrial function (Houghton et al., 2018). In this study, quercetin supplementation significantly mitigated MA-induced anxiety-like behavior by improving mitochondrial morphology and function, alleviating neuronal injury, both *in vivo* and *in vitro*. Here, we also identified the novel pharmacological efficacy of quercetin in the treatment of anxiety induced by MA.

As a major source of glycogen and lactate, astrocytes provided neurons with additional energy and play key metabolic roles in the CNS (Shirakawa et al., 2010). Moreover, astrocytes can dispose of and recycle damaged mitochondria released by neurons, and release healthy extracellular mitochondrial particles to neuron (Hayakawa et al., 2016). Astrocyte dysfunction has been shown to facilitate the pathogenesis of neurological and psychiatric disorders (Tian et al., 2018). Hence, astrocytes and the mitochondria may represent an important target of neurological and psychiatric disorders. Thus, we intended to focus this study on astrocytes in subsequent experiments. Research has shown MA exposure facilitated dysfunction and morphological abnormalities of mitochondrial (Valian et al., 2019), which can trigger various innate immune signaling pathways in a cell-intrinsic or -extrinsic manner (Bader and Winklhofer, 2020), resulting in the release of inflammatory factors. In this work, we observed MA-induced morphological abnormalities of

mitochondria *in vivo* and *in vitro*, and mitochondrial dysfunction in astrocytes, and the phenotypes were rescued by quercetin. As we know, except for microglia, astrocytes also serve as crucial regulators of the innate and adaptive immune responses, and play critical roles in neuroinflammation (Colombo and Farina, 2016). In this study, we found that MA treatment accelerated astrocyte activation, accompanied by the elevation of interleukin (IL)-1β, IL-6, and tumor necrosis factor (TNF)α in the HIPP and MA-treated astrocytes (**Figure 5**). Quercetin, as a bioactive compound with antioxidant and anti-inflammatory properties (Khan et al., 2016), reduced the expression of IL-1β and TNFα *in vitro* and *in vivo*, and alleviated astrocytes activation when treated with MA in this work (**Figure 5**). These results suggested that MA treatment accelerated astrocytes activation and facilitated the release of inflammatory factors, which can trigger neuronal apoptosis and synaptic loss (Garwood et al., 2011; Çalışkan et al., 2020). Moreover, the excessive accumulation of damaged mitochondria, combined with astrocyte activation and the increase in inflammatory factors, induces neurotoxicity and promotes neuronal apoptosis (Nicholls, 2004), which initiates a vicious cycle that aggravates the anxiety process (Garwood et al., 2011; Çalışkan et al., 2020). These findings also confirmed the neuroprotective activity of quercetin, through modulating astrocytes and rebalancing neuroinflammation levels activation.

Nevertheless, the mechanisms by which quercetin exerts its anti-neuroinflammation activity and modulates mitochondrial function remain unclear. According to previous reports, Nr4a1 (also known as TR3 or NGFI-B), which was upregulated in our RNA-seq results, is an orphan member of the nuclear receptor superfamily. It migrates from the nucleus to the mitochondria, where it binds to Bcl-2 to induce apoptosis and cause the release of cytochrome c (Liu et al., 2008). Nr4a1 evoked cellular oxidative stress and disrupt ATP generation (Zhang and Yu, 2018), and the expression and activity of Nr4a1 are sustained by chronic stress in animal models and in human studies of neuropathologies sensitive to the buildup of chronic stress (Akiyama et al., 2008; Jeanneteau et al., 2018). Nr4a1 has also been shown to be important for regulating metabolic and morphological aspects of neuronal functions by modifying the expression of several mitochondrial regulatory genes, including *Mfn1*, *Mfn2, Fis1* and *OPA1* (Jeanneteau et al., 2018), which can result in mitochondrial dysfunction and behavioral phenotypes. Therefore, we speculated that quercetin might modulate genes associated with mitochondrial function *via* downregulating Nr4a1. Thus, we detected the expression of Nr4a1 in MA + quercetin and MA groups *in vivo*, the results verified the effects of quercetin in decreasing the Nr4a1 expression both in RNA and protein level (**Supplementary Figure 3**). Future work will explore the molecular mechanism extensively.

In conclusion, our study indicated that MA cause damage to brain cells, including neurons and astrocytes, by influencing mitochondrial metabolism, energy production, and morphology in astrocytes, which participated in the development of neuropsychiatric disorders, such as anxiety. The oral supplementation of quercetin neutralized the neuropsychiatric status of MA-treated mice; our findings indicated the potential of quercetin as a candidate agent for alleviating MA-induced anxiety and support the hypothesis that mitochondria mediate anxiety progression. Further study is necessary to illustrate the contributions and mechanisms of mitochondria in the progression of anxiety induced by MA.

DATA AVAILABILITY STATEMENT

The raw reads data from mRNA-seq are available at NCBI GEO with the accession number: GSE193829 and **Supplementary Material**, further inquiries can be directed to the corresponding authors.

ETHICS STATEMENT

The animal study was reviewed and approved by Committee on Ethics in the Use of Animals from Kunming Medical University.

AUTHOR CONTRIBUTIONS

FC and JY designed the experiments and participated in the data analysis. FC, JY, QW, and YL wrote the manuscript. JS and CC performed the sequence alignment and bioinformatics. MC, YZ, and WT performed the animal experiments. FC, LZ, and ZZ performed the cell experiments. HW, HL, YX, and MZ participated in data analysis. JY and KW conceived of the study and supervised the project. All authors read and approved the final manuscript.

FUNDING

This work was supported by grants from the National Natural Science Foundation of China (Grant Nos. 3171101074, 81860100, 31860306, and 81870458), the Central Public-Interest Scientific Institution Basal Research Fund (2019PT310003), the Science and Technology Department of Yunnan Province [Grant No. 2018DH006, 2018NS0086, 2019FE001 (-218), 2018FE001 (-144), 202001AS070004 and 202001AV070010], and Yunling Scholar (Grant No. YLXL20170002).

ACKNOWLEDGMENTS

We would like to thank Jie Bai and Xiangyang Kong for the technical support of behavioral test. We would also like to thank the technical support of Shaoyou Li for the Flow Cytometry test.

SUPPLEMENTARY MATERIAL

The Supplementary Material for this article can be found online at: https://www.frontiersin.org/articles/10.3389/fnmol.2022.829886/full#supplementary-material

Supplementary Figure 1 | The effect of quercetin on mitochondrial morphology and function in MA-treated in PC12. **(A)** Representative images of mitochondria in PC12. Alive cells were incubated with MitoTraker Green as a probe for mitochondria in each group. **(B)** Enlarged images of the areas marked in A with a white box. **(C)** Quantification of the mitochondrial membrane potential (MMP). **(D)** Quantification of the total ATP in PC12. **(E)** Total ROS production quantification by flow cytometry in each group. All experiments represent the average of 3 independent experiments. $*p < 0.05$, as determined by Student's *t* test.

Supplementary Figure 2 | Confocal microscopic analysis of neuron and astrocytes using immunofluorescence stainings. **(A–C)** Immunofluorescence was performed with anti-NeuN [green, **(C)**] and DAPI [blue, **(B)**], **(C)** Merged image of panels **(A,B)**. **(D–F)** Immunofluorescence was performed with anti-Iba [green, **(D)**] and DAPI [blue, **(E)**], **(F)** Merged image of panels **(D,E)**. All experiments represent the average of 3 independent experiments.

Supplementary Figure 3 | Quercetin rescued MA-induced Nr4a1 upregulation in gene and protein level. **(A)** Representative band pattern of the WB of different treatment of HIPP using antibodies for Nr4a1 and GAPDH. **(B)** Summary bar graphs of Nr4a1 and GAPDH levels in different groups in hippocampus. **(C)** Expression of Nr4a1 and GAPDH by qPCR in HIPP. $*p < 0.05$, $***p < 0.0005$, and $****p < 0.0001$. All experiments represent the average of 3 independent experiments.

REFERENCES

Akiyama, K., Isao, T., Ide, S., Ishikawa, M., and Saito, A. (2008). mRNA expression of the Nurr1 and NGFI-B nuclear receptor families following acute and chronic administration of methamphetamine. *Prog. Neuropsychopharmacol. Biol. Psychiatry* 32, 1957–1966. doi: 10.1016/j.pnpbp.2008.09.021

Allsop, S. A., Vander Weele, C. M., Wichmann, R., and Tye, K. M. (2014). Optogenetic insights on the relationship between anxiety-related behaviors and social deficits. *Front. Behav. Neurosci.* 8:241. doi: 10.3389/fnbeh.2014.00241

Andres, S., Pevny, S., Ziegenhagen, R., Bakhiya, N., Schäfer, B., Hirsch-Ernst, K. I., et al. (2018). Safety aspects of the use of quercetin as a dietary supplement. *Mol. Nutr. Food Res.* 62:1700447. doi: 10.1002/mnfr.201700447

Bader, V., and Winklhofer, K. F. (2020). Mitochondria at the interface between neurodegeneration and neuroinflammation. *Semin. Cell Dev. Biol.* 99, 163–171. doi: 10.1016/j.semcdb.2019.05.028

Baksh, R. A., Ritchie, C. W., Terrera, G. M., Norton, J., Raymont, V., and Ritchie, K. (2021). The association between anxiety disorders and hippocampal volume in older adults. *Psychol. Aging* 36, 288–297. doi: 10.1037/pag0000597

Çalışkan, G., Müller, A., and Albrecht, A. (2020). Long-Term impact of early-life stress on hippocampal plasticity: spotlight on astrocytes. *Int. J. Mol. Sci.* 21:4999. doi: 10.3390/ijms21144999

Cao, J. J., Tan, C. P., Chen, M. H., Wu, N., Yao, D. Y., Liu, X. G., et al. (2017). Targeting cancer cell metabolism with mitochondria-immobilized phosphorescent cyclometalated iridium(iii) complexes. *Chem. Sci.* 8, 631–640. doi: 10.1039/c6sc02901a

Chang, L., Alicata, D., Ernst, T., and Volkow, N. (2007). Structural and metabolic brain changes in the striatum associated with methamphetamine abuse. *Addiction (Abingdon, England)* 102(Suppl. 1), 16–32. doi: 10.1111/j.1360-0443.2006.01782.x

Chen, F., Zhu, L., Cai, L., Zhang, J., Zeng, X., Li, J., et al. (2016). A stromal interaction molecule 1 variant up-regulates matrix metalloproteinase-2 expression by strengthening nucleoplasmic Ca2+ signaling. *Biochim. Biophys. Acta* 1863, 617–629. doi: 10.1016/j.bbamcr.2016.01.007

Cheng, M. C., Hsu, S. H., and Chen, C. H. (2015). Chronic methamphetamine treatment reduces the expression of synaptic plasticity genes and changes their DNA methylation status in the mouse brain. *Brain Res.* 1629, 126–134. doi: 10.1016/j.brainres.2015.10.021

Chiang, M., Lombardi, D., Du, J., Makrum, U., Sitthichai, R., Harrington, A., et al. (2019). Methamphetamine-associated psychosis: clinical presentation, biological basis, and treatment options. *Hum. Psychopharmacol.* 34:e2710. doi: 10.1002/hup.2710

Colombo, E., and Farina, C. (2016). Astrocytes: key regulators of neuroinflammation. *Trends Immunol.* 37, 608–620. doi: 10.1016/j.it.2016.06.006

Cortés, S. A., Santhosh, K. H., Mantovani, M., Osinnii, I., Mateos, J. M., Kaech, A., et al. (2021). ER-misfolded proteins become sequestered with mitochondria and impair mitochondrial function. *Commun. Biol.* 4:1350. doi: 10.1038/s42003-021-02873-w

Costa, L. G., Garrick, J. M., Roquè, P. J., and Pellacani, C. (2016). Mechanisms of neuroprotection by quercetin: counteracting oxidative stress and more. *Oxid. Med. Cell. Longev.* 2016:2986796. doi: 10.1155/2016/2986796

Dang, J., Tiwari, S. K., Agrawal, K., Hui, H., Qin, Y., and Rana, T. M. (2021). Glial cell diversity and methamphetamine-induced neuroinflammation in human cerebral organoids. *Mol. Psychiatry* 26, 1194–1207. doi: 10.1038/s41380-020-0676-x

de la Mata, M., Cotán, D., Oropesa-Ávila, M., Villanueva-Paz, M., de Lavera, I., Álvarez-Córdoba, M., et al. (2017). Coenzyme Q10 partially restores pathological alterations in a macrophage model of Gaucher disease. *Orphanet J. Rare Dis.* 12:23. doi: 10.1186/s13023-017-0574-8

Dhiman, P., Malik, N., Sobarzo-Sánchez, E., Uriarte, E., and Khatkar, A. (2019). Quercetin and related chromenone derivatives as monoamine oxidase inhibitors: targeting neurological and mental disorders. *Molecules (Basel, Switzerland)* 24:418. doi: 10.3390/molecules24030418

Duncan, Z., Kippen, R., Sutton, K., Ward, B., Agius, P. A., Quinn, B., et al. (2021). Correlates of anxiety and depression in a community cohort of people who smoke methamphetamine. *Aust. N. Z. J. Psychiatry* 48674211048152. doi: 10.1177/00048674211048152

Einat, H., Yuan, P., and Manji, H. K. (2005). Increased anxiety-like behaviors and mitochondrial dysfunction in mice with targeted mutation of the Bcl-2 gene: further support for the involvement of mitochondrial function in anxiety disorders. *Behav. Brain Res.* 165, 172–180. doi: 10.1016/j.bbr.2005.06.012

Fang, D., Wang, Y., Zhang, Z., Du, H., Yan, S., Sun, Q., et al. (2015). Increased neuronal PreP activity reduces Aβ accumulation, attenuates neuroinflammation and improves mitochondrial and synaptic function in Alzheimer disease's mouse model. *Hum. Mol. Genet.* 24, 5198–5210. doi: 10.1093/hmg/ddv241

Fiebig, C., Keiner, S., Ebert, B., Schäffner, I., Jagasia, R., Lie, D. C., et al. (2019). Mitochondrial dysfunction in astrocytes impairs the generation of reactive astrocytes and enhances neuronal cell death in the cortex upon photothrombotic lesion. *Front. Mol. Neurosci.* 12:40. doi: 10.3389/fnmol.2019.00040

Filiou, M. D., and Sandi, C. (2019). Anxiety and brain mitochondria: a bidirectional crosstalk. *Trends Neurosci.* 42, 573–588. doi: 10.1016/j.tins.2019.07.002

Gallitano, A. L. (2020). Editorial: the role of immediate early genes in neuropsychiatric illness. *Front. Behav. Neurosci.* 14:16. doi: 10.3389/fnbeh.2020.00016

Garwood, C. J., Pooler, A. M., Atherton, J., Hanger, D. P., and Noble, W. (2011). Astrocytes are important mediators of Aβ-induced neurotoxicity and tau phosphorylation in primary culture. *Cell Death Dis.* 2:e167. doi: 10.1038/cddis.2011.50

Glasner-Edwards, S., and Mooney, L. J. (2014). Methamphetamine psychosis: epidemiology and management. *CNS Drugs* 28, 1115–1126. doi: 10.1007/s40263-014-0209-8

Glasner-Edwards, S., Mooney, L. J., Marinelli-Casey, P., Hillhouse, M., Ang, A., Rawson, R., et al. (2010). Anxiety disorders among methamphetamine dependent adults: association with post-treatment functioning. *Am. J. Addict.* 19, 385–390. doi: 10.1111/j.1521-0391.2010.00061.x

Golsorkhdan, S. A., Boroujeni, M. E., Aliaghaei, A., Abdollahifar, M. A., Ramezanpour, A., Nejatbakhsh, R., et al. (2020). Methamphetamine administration impairs behavior, memory and underlying signaling pathways in the hippocampus. *Behav. Brain Res.* 379:112300. doi: 10.1016/j.bbr.2019.112300

Hayakawa, K., Esposito, E., Wang, X., Terasaki, Y., Liu, Y., Xing, C., et al. (2016). Transfer of mitochondria from astrocytes to neurons after stroke. *Nature* 535, 551–555. doi: 10.1038/nature18928

Hellem, T. L. (2016). A review of methamphetamine dependence and withdrawal treatment: a focus on anxiety outcomes. *J. Subst. Abuse Treat.* 71, 16–22. doi: 10.1016/j.jsat.2016.08.011

Homer, B. D., Solomon, T. M., Moeller, R. W., Mascia, A., DeRaleau, L., and Halkitis, P. N. (2008). Methamphetamine abuse and impairment of social functioning: a review of the underlying neurophysiological causes and behavioral implications. *Psychol. Bull.* 134, 301–310. doi: 10.1037/0033-2909.134.2.301

Houghton, M. J., Kerimi, A., Tumova, S., Boyle, J. P., and Williamson, G. (2018). Quercetin preserves redox status and stimulates mitochondrial function in metabolically-stressed HepG2 cells. *Free Radic. Biol. Med.* 129, 296–309. doi: 10.1016/j.freeradbiomed.2018.09.037

Huang, R., Zhang, Y., Han, B., Bai, Y., Zhou, R., Gan, G., et al. (2017). Circular RNA HIPK2 regulates astrocyte activation via cooperation of autophagy and ER stress by targeting MIR124-2HG. *Autophagy* 13, 1722–1741. doi: 10.1080/15548627.2017.1356975

Iwazaki, T., McGregor, I. S., and Matsumoto, I. (2008). Protein expression profile in the amygdala of rats with methamphetamine-induced behavioral sensitization. *Neurosci. Lett.* 435, 113–119. doi: 10.1016/j.neulet.2008.02.025

Jayanthi, S., Daiwile, A. P., and Cadet, J. L. (2021). Neurotoxicity of methamphetamine: main effects and mechanisms. *Exp. Neurol.* 344:113795. doi: 10.1016/j.expneurol.2021.113795

Jeanneteau, F., Barrère, C., Vos, M., De Vries, C., Rouillard, C., Levesque, D., et al. (2018). The stress-induced transcription factor NR4A1 adjusts mitochondrial function and synapse number in prefrontal cortex. *J. Neurosci.* 38, 1335–1350. doi: 10.1523/JNEUROSCI.2793-17.2017

Joshi, A. U., Minhas, P. S., Liddelow, S. A., Haileselassie, B., Andreasson, K. I., Dorn, G. W., et al. (2019). Fragmented mitochondria released from microglia trigger A1 astrocytic response and propagate inflammatory neurodegeneration. *Nat. Neurosci.* 22, 1635–1648. doi: 10.1038/s41593-019-0486-0

Kambe, D., Kotani, M., Yoshimoto, M., Kaku, S., Chaki, S., and Honda, K. (2010). Effects of quercetin on the sleep-wake cycle in rats: involvement of gamma-aminobutyric acid receptor type A in regulation of rapid eye movement sleep. *Brain Res.* 1330, 83–88. doi: 10.1016/j.brainres.2010.03.033

Khan, I., Paul, S., Jakhar, R., Bhardwaj, M., Han, J., and Kang, S. C. (2016). Novel quercetin derivative TEF induces ER stress and mitochondria-mediated apoptosis in human colon cancer HCT-116 cells. *Biomed. Pharmacother.* 84, 789–799. doi: 10.1016/j.biopha.2016.09.094

Kohno, M., Loftis, J. M., Huckans, M., Dennis, L. E., McCready, H., and Hoffman, W. F. (2018). The relationship between interleukin-6 and functional connectivity in methamphetamine users. *Neurosci. Lett.* 677, 49–54. doi: 10.1016/j.neulet.2018.04.037

Kosari-Nasab, M., Shokouhi, G., Ghorbanihaghjo, A., Mesgari-Abbasi, M., and Salari, A. A. (2019). Quercetin mitigates anxiety-like behavior and normalizes hypothalamus-pituitary-adrenal axis function in a mouse model of mild traumatic brain injury. *Behav. Pharmacol.* 30, 282–289. doi: 10.1097/FBP.0000000000000480

Kwon, H. S., and Koh, S. H. (2020). Neuroinflammation in neurodegenerative disorders: the roles of microglia and astrocytes. *Transl. Neurodegener.* 9:42. doi: 10.1186/s40035-020-00221-2

Lee, B., Yeom, M., Shim, I., Lee, H., and Hahm, D. H. (2020). Protective effects of quercetin on anxiety-like symptoms and neuroinflammation induced by lipopolysaccharide in rats. *Evid. Based Complement. Alternat. Med. eCAM* 2020:4892415. doi: 10.1155/2020/4892415

Li, P., Wang, B., Sun, F., Li, Y., Li, Q., Lang, H., et al. (2015). Mitochondrial respiratory dysfunctions of blood mononuclear cells link with cardiac disturbance in patients with early-stage heart failure. *Sci. Rep.* 5:10229. doi: 10.1038/srep10229

Liu, J., Zhou, W., Li, S. S., Sun, Z., Lin, B., Lang, Y. Y., et al. (2008). Modulation of orphan nuclear receptor Nur77-mediated apoptotic pathway by acetylshikonin and analogues. *Cancer Res.* 68, 8871–8880. doi: 10.1158/0008-5472.CAN-08-1972

Manji, H., Kato, T., Di Prospero, N. A., Ness, S., Beal, M. F., Krams, M., et al. (2012). Impaired mitochondrial function in psychiatric disorders. *Nat. Rev. Neurosci.* 13, 293–307. doi: 10.1038/nrn3229

Manning, E. E., Halberstadt, A. L., and van den Buuse, M. (2016). BDNF-deficient mice show reduced psychosis-related behaviors following chronic methamphetamine. *Int. J. Neuropsychopharmacol.* 19:yv116. doi: 10.1093/ijnp/pyv116

May, A. C., Aupperle, R. L., and Stewart, J. L. (2020). Dark times: the role of negative reinforcement in methamphetamine addiction. *Front. Psychiatry* 11:114. doi: 10.3389/fpsyt.2020.00114

McCoy, M. T., Jayanthi, S., Wulu, J. A., Beauvais, G., Ladenheim, B., Martin, T. A., et al. (2011). Chronic methamphetamine exposure suppresses the striatal expression of members of multiple families of immediate early genes (IEGs) in the rat: normalization by an acute methamphetamine injection. *Psychopharmacology* 215, 353–365. doi: 10.1007/s00213-010-2146-7

Meredith, C. W., Jaffe, C., Ang-Lee, K., and Saxon, A. J. (2005). Implications of chronic methamphetamine use: a literature review. *Harv. Rev. Psychiatry* 13, 141–154. doi: 10.1080/10673220591003605

Morava, E., and Kozicz, T. (2013). Mitochondria and the economy of stress (mal)adaptation. *Neurosci. Biobehav. Rev.* 37, 668–680. doi: 10.1016/j.neubiorev.2013.02.005

Nicholls, D. G. (2004). Mitochondrial dysfunction and glutamate excitotoxicity studied in primary neuronal cultures. *Curr. Mol. Med.* 4, 149–177. doi: 10.2174/1566524043479239

Nie, L., Ghahremani, D. G., Mandelkern, M. A., Dean, A. C., Luo, W., Ren, A., et al. (2021). The relationship between duration of abstinence and gray-matter brain structure in chronic methamphetamine users. *Am. J. Drug Alcohol Abuse* 47, 65–73. doi: 10.1080/00952990.2020.1778712

Pei, L., and Wallace, D. C. (2018). Mitochondrial etiology of neuropsychiatric disorders. *Biol. Psychiatry* 83, 722–730. doi: 10.1016/j.biopsych.2017.11.018

Ru, Q., Xiong, Q., Zhou, M., Chen, L., Tian, X., Xiao, H., et al. (2019). Withdrawal from chronic treatment with methamphetamine induces anxiety and depression-like behavior in mice. *Psychiatry Res.* 271, 476–483. doi: 10.1016/j.psychres.2018.11.072

Saito, A., and Imaizumi, K. (2018). Unfolded protein response-dependent communication and contact among endoplasmic reticulum, mitochondria, and plasma membrane. *Int. J. Mol. Sci.* 19:3215. doi: 10.3390/ijms19103215

Samad, N., Saleem, A., Yasmin, F., and Shehzad, M. A. (2018). Quercetin protects against stress-induced anxiety- and depression-like behavior and improves memory in male mice. *Physiol. Res.* 67, 795–808. doi: 10.33549/physiolres.933776

Satpute, A. B., Mumford, J. A., Naliboff, B. D., and Poldrack, R. A. (2012). Human anterior and posterior hippocampus respond distinctly to state and trait anxiety. *Emotion* 12, 58–68. doi: 10.1037/a0026517

Shin, E. J., Dang, D. K., Tran, T. V., Tran, H. Q., Jeong, J. H., Nah, S. Y., et al. (2017). Current understanding of methamphetamine-associated dopaminergic neurodegeneration and psychotoxic behaviors. *Arch. Pharm. Res.* 40, 403–428. doi: 10.1007/s12272-017-0897-y

Shirakawa, H., Sakimoto, S., Nakao, K., Sugishita, A., Konno, M., Iida, S., et al. (2010). Transient receptor potential canonical 3 (TRPC3) mediates thrombin-induced astrocyte activation and upregulates its own expression in cortical astrocytes. *J. Neurosci.* 30, 13116–13129. doi: 10.1523/JNEUROSCI.1890-10.2010

Shoptaw, S. J., Kao, U., and Ling, W. (2009). Treatment for amphetamine psychosis. *Cochrane Database Syst. Rev.* 8:CD003026. doi: 10.1002/14651858.CD003026.pub3

Smith, M. J., Thirthalli, J., Abdallah, A. B., Murray, R. M., and Cottler, L. B. (2009). Prevalence of psychotic symptoms in substance users: a comparison across substances. *Compr. Psychiatry* 50, 245–250. doi: 10.1016/j.comppsych.2008.07.009

Song, X., Chen, Z., Jia, R., Cao, M., Zou, Y., Li, L., et al. (2017). Transcriptomics and proteomic studies reveal acaricidal mechanism of octadecanoic acid-3, 4 – tetrahydrofuran diester against *Sarcoptes scabiei* var. *cuniculi*. *Sci. Rep.* 7:45479. doi: 10.1038/srep45479

Srisurapanont, M., Ali, R., Marsden, J., Sunga, A., Wada, K., and Monteiro, M. (2003). Psychotic symptoms in methamphetamine psychotic in-patients. *Int. J. Neuropsychopharmacol.* 6, 347–352. doi: 10.1017/S1461145703003675

Su, H., Zhang, J., Ren, W., Xie, Y., Tao, J., Zhang, X., et al. (2017). Anxiety level and correlates in methamphetamine-dependent patients during acute withdrawal. *Medicine* 96:e6434. doi: 10.1097/MD.0000000000006434

Sun, J., Chen, F., Chen, C., Zhang, Z., Zhang, Z., Tian, W., et al. (2020). Intestinal mRNA expression profile and bioinformatics analysis in a methamphetamine-induced mouse model of inflammatory bowel disease. *Ann. Transl. Med.* 8:1669. doi: 10.21037/atm-20-7741

Tian, H., Li, X., Tang, Q., Zhang, W., Li, Q., Sun, X., et al. (2018). Yi-nao-jie-yu prescription exerts a positive effect on neurogenesis by regulating notch signals in the hippocampus of post-stroke depression rats. *Front. Psychiatry* 9:483. doi: 10.3389/fpsyt.2018.00483

Uhlmann, A., Fouche, J. P., Koen, N., Meintjes, E. M., Wilson, D., and Stein, D. J. (2016). Fronto-temporal alterations and affect regulation in methamphetamine dependence with and without a history of psychosis. *Psychiatry Res. Neuroimaging* 248, 30–38. doi: 10.1016/j.pscychresns.2016.01.010

Valian, N., Heravi, M., Ahmadiani, A., and Dargahi, L. (2019). Effect of methamphetamine on rat primary midbrain cells; mitochondrial biogenesis as a compensatory response. *Neuroscience* 406, 278–289. doi: 10.1016/j.neuroscience.2019.03.016

Wallace, D. C. (2017). A mitochondrial etiology of neuropsychiatric disorders. *JAMA Psychiatry* 74, 863–864. doi: 10.1001/jamapsychiatry.2017.0397

Wang, G., Zhang, Y., Zhang, S., Chen, H., Xu, Z., Schottenfeld, R. S., et al. (2016). Aripiprazole and risperidone for treatment of methamphetamine-associated psychosis in Chinese patients. *J. Subst. Abuse Treat.* 62, 84–88. doi: 10.1016/j.jsat.2015.11.009

Wearne, T. A., and Cornish, J. L. (2018). A comparison of methamphetamine-induced psychosis and schizophrenia: a review of positive, negative, and cognitive symptomatology. *Front. Psychiatry* 9:491. doi: 10.3389/fpsyt.2018.00491

Xie, N., Yuan, K., Zhou, L., Wang, K., Chen, H. N., Lei, Y., et al. (2016). PRKAA/AMPK restricts HBV replication through promotion of autophagic degradation. *Autophagy* 12, 1507–1520. doi: 10.1080/15548627.2016.1191857

Zhang, P., Kishimoto, Y., Grammatikakis, I., Gottimukkala, K., Cutler, R. G., Zhang, S., et al. (2019). Senolytic therapy alleviates Aβ-associated oligodendrocyte progenitor cell senescence and cognitive deficits in an Alzheimer's disease model. *Nat. Neurosci.* 22, 719–728. doi: 10.1038/s41593-019-0372-9

Zhang, Z., and Yu, J. (2018). NR4A1 promotes cerebral ischemia reperfusion injury by repressing Mfn2-Mediated mitophagy and inactivating the MAPK-ERK-CREB signaling pathway. *Neurochem. Res.* 43, 1963–1977. doi: 10.1007/s11064-018-2618-4

Zhou, Y., Zhu, H., Liu, Z., Chen, X., Su, X., Ma, C., et al. (2019). A ventral CA1 to nucleus accumbens core engram circuit mediates conditioned place preference for cocaine. *Nat. Neurosci.* 22, 1986–1999. doi: 10.1038/s41593-019-0524-y

Conflict of Interest: The authors declare that the research was conducted in the absence of any commercial or financial relationships that could be construed as a potential conflict of interest.

Publisher's Note: All claims expressed in this article are solely those of the authors and do not necessarily represent those of their affiliated organizations, or those of the publisher, the editors and the reviewers. Any product that may be evaluated in this article, or claim that may be made by its manufacturer, is not guaranteed or endorsed by the publisher.

frontiers in Molecular Neuroscience

ORIGINAL RESEARCH
published: 10 March 2022
doi: 10.3389/fnmol.2022.800406

Menthol Flavor in E-Cigarette Vapor Modulates Social Behavior Correlated With Central and Peripheral Changes of Immunometabolic Signalings

Zhibin Xu[1,2†], Ye Tian[1,3†], A.-Xiang Li[1,4†], Jiahang Tang[1], Xiao-Yuan Jing[1], Chunshan Deng[1], Zhizhun Mo[1], Jiaxuan Wang[1], Juan Lai[1], Xuemei Liu[1], Xuantong Guo[1], Tao Li[4], Shupeng Li[5,6,7], Liping Wang[1,2,3], Zhonghua Lu[1,2,3], Zuxin Chen[1,2,3,8] and Xin-an Liu[1,2,3]**

[1] Guangdong Provincial Key Laboratory of Brain Connectome and Behavior, CAS Key Laboratory of Brain Connectome and Manipulation, Brain Cognition and Brain Disease Institute (BCBDI), Shenzhen Institute of Advanced Technology, Chinese Academy of Sciences, Shenzhen, China, [2] Shenzhen-Hong Kong Institute of Brain Science-Shenzhen Fundamental Research Institutions, Shenzhen, China, [3] University of Chinese Academy of Sciences, Beijing, China, [4] Department of Forensic Medicine, School of Medicine, Xi'an Jiaotong University, Xi'an, China, [5] State Key Laboratory of Oncogenomics, School of Chemical Biology and Biotechnology, Peking University Shenzhen Graduate School, Shenzhen, China, [6] Department of Psychiatry, University of Toronto, Toronto, ON, Canada, [7] Key Laboratory of Modern Toxicology of Shenzhen, Shenzhen Center for Disease Control and Prevention, Shenzhen, China, [8] Shenzhen Key Laboratory of Drug Addiction, Shenzhen Neher Neural Plasticity Laboratory, The Brain Cognition and Brain Disease Institute, Shenzhen Institute of Advanced Technology, Chinese Academy of Sciences, Shenzhen, China

The use of electronic cigarette (e-cigarette) has been increasing dramatically worldwide. More than 8,000 flavors of e-cigarettes are currently marketed and menthol is one of the most popular flavor additives in the electronic nicotine delivery systems (ENDS). There is a controversy over the roles of e-cigarettes in social behavior, and little is known about the potential impacts of flavorings in the ENDS. In our study, we aimed to investigate the effects of menthol flavor in ENDS on the social behavior of long-term vapor-exposed mice with a daily intake limit, and the underlying immunometabolic changes in the central and peripheral systems. We found that the addition of menthol flavor in nicotine vapor enhanced the social activity compared with the nicotine alone. The dramatically reduced activation of cellular energy measured by adenosine 5′ monophosphate-activated protein kinase (AMPK) signaling in the hippocampus were observed after the chronic exposure of menthol-flavored ENDS. Multiple sera cytokines including C5, TIMP-1, and CXCL13 were decreased accordingly as per their peripheral immunometabolic responses to menthol flavor in the nicotine vapor. The serum level of C5 was positively correlated with the alteration activity of the AMPK-ERK signaling in the hippocampus. Our current findings provide evidence for the enhancement of

OPEN ACCESS

Edited by:
Jianfeng Liu,
Texas A&M University, United States

Reviewed by:
Qing Tian,
Huazhong University of Science and Technology, China
Wei Li,
Tongji University, China

***Correspondence:**
Zuxin Chen
zx.chen3@siat.ac.cn
Xin-an Liu
xa.liu@siat.ac.cn

[†] These authors have contributed equally to this work

Specialty section:
This article was submitted to Molecular Signalling and Pathways, a section of the journal Frontiers in Molecular Neuroscience

Received: 23 October 2021
Accepted: 21 January 2022
Published: 10 March 2022

Citation:
Xu Z, Tian Y, Li A-X, Tang J, Jing X-Y, Deng C, Mo Z, Wang J, Lai J, Liu X, Guo X, Li T, Li S, Wang L, Lu Z, Chen Z and Liu X-a (2022) Menthol Flavor in E-Cigarette Vapor Modulates Social Behavior Correlated With Central and Peripheral Changes of Immunometabolic Signalings. Front. Mol. Neurosci. 15:800406. doi: 10.3389/fnmol.2022.800406

menthol flavor in ENDS on social functioning, which is correlated with the central and peripheral immunometabolic disruptions; this raises the vigilance of the cautious addition of various flavorings in e-cigarettes and the urgency of further investigations on the complex interplay and health effects of flavoring additives with nicotine in e-cigarettes.

Keywords: e-cigarette, nicotine, menthol, social activity, electronic nicotine delivery systems (ENDS)

INTRODUCTION

The use of electronic nicotine delivery systems (ENDS), also known as electronic cigarettes (e-cigarettes) has been dramatically increasing in recent years, and it has become a serious public health issue. Despite the lack of either health data or the demonstrated efficacy in promoting smoking cessation, the e-cigarette is often advertised as a safer alternative or cessation aid to conventional tobacco cigarette smoke, mainly due to its much lower levels of toxic/carcinogenic chemicals (Arnold, 2014; Benowitz, 2014; Ramamurthi et al., 2016). Although the popularity of e-cigarette use continues to increase, research evidence based on scientific knowledge is lacking and the main focused aspect of e-cigarettes include their beneficial roles in tobacco smoking cessation or reduction, their health risks, and their environmental consequences (Rom et al., 2015; Hartmann-Boyce et al., 2020).

The major composition of e-cigarettes usually consists of propylene glycol and vegetable glycerol (PG/VG) as odorless liquid vehicles to generate vapor, nicotine which is the main addictive substance, and a wide variety of flavorings (Allen et al., 2016; Smith et al., 2020). As the number of users grows exponentially worldwide, liquids of e-cigarettes are available in a dramatically large combination of flavor additives, with more than 8,000 flavorings (Zhu et al., 2014; Hsu et al., 2018). A recent increase in the prevalence of e-cigarettes among young adults and adolescents may largely be due to their widely available flavors which appeal to the youth (Ambrose et al., 2015; Villanti et al., 2017; Cullen et al., 2019a,b). Epidemiological survey data have shown that the most common flavor categories include fruit, menthol, and tobacco. Menthol flavor was shown to be one of the most popular flavors among young users (Leventhal et al., 2019) and the extent of satisfaction with vaping varies among unique flavor users (Gravely et al., 2020; Rose et al., 2020). However, the incorporated effects of flavorings when added in the nicotine-containing vapor and the underlying mechanisms are largely unknown.

Many previous studies have confirmed the association between cigarette smoking and neurodegeneration (Deochand et al., 2016; Yu et al., 2016; Liu et al., 2020), cognition and memory (Ge et al., 2019; Wei et al., 2020; Martin Rios et al., 2021), and mental disorders, such as attentional deficits (Joo et al., 2017; Lawrence et al., 2021) and schizophrenia (Donde et al., 2020; King et al., 2020), considering the wide distribution of nicotinic acetylcholine receptors (nAChRs) throughout the brain (Levin et al., 2015). Based on the fact that nicotine is one of the main addictive components of an e-cigarette, there is increasing recognition that e-cigarettes impact brain functions, for instance, e-cigarettes impaired the integrity of the blood-brain barrier (BBB) and exacerbated the cognitive dysfunction (Chen et al., 2021), mental disorders (Pham et al., 2020), vascular inflammation (Kaisar et al., 2017), metabolic imbalance (Debarba et al., 2020), and neurotoxicity (Ruszkiewicz et al., 2020) in the brain of human and animal models, while the effects of ENDS with specific flavor on the behaviors need further disclosure. Furthermore, it is the utmost emergency to understand the molecular architectures sculptured in the brain and the peripheral system that synergistically respond to the ingredients of e-cigarettes.

The aim of the current study is to provide a comprehensive behavioral analysis of ENDS with menthol flavor in male mice (Leventhal et al., 2021). We sought to characterize the impacts of the immunometabolic signals on the key brain regions that may account for the behavioral changes. The proteomic cytokine array of the serum was also investigated to detect the circulating immunological signals that were influenced by menthol flavor in ENDS. The correlation analyses among the behavioral parameters and the central and peripheral immunometabolic indices were conducted to reveal the systemic responses mediated by menthol flavor in ENDS.

MATERIALS AND METHODS

Animals

Male C57BL/6J mice (Hunan SJA Laboratory Animal Co., Ltd., Hunan, China) aged 8 weeks old, were maintained in standard housing conditions on a 12/12 h day/night cycle (lights on at 7 a.m. and off at 7 p.m.) with *ad libitum* access to food and water. All behavioral tests were conducted at a fixed time period during the light cycle. All mice were handled for 15–20 min per day for 3 days before behavioral assays to reduce the stress introduced by contact with an experimenter. All animal experiments and procedures were carried out in accordance with the protocols approved by the Animal Care and Use Ethics Committee of the Shenzhen Institutes of Advanced Technology, Chinese Academy of Sciences.

E-Cigarette Exposure System

The inExpose e-cigarette device (SCIREQ Scientific Respiratory Equipment Inc.) was used in our experiments for vapor exposures of accurate amounts of nicotine between groups, as shown in **Figure 1**. During the experiments, 8 mice were treated in one single run, in a closed whole body exposure chamber with relatively spacious space. The action state of animals in the chamber was recorded in real-time by a camera connected to a computer. A supporting software (IX-2PD-4DIO-ECIG

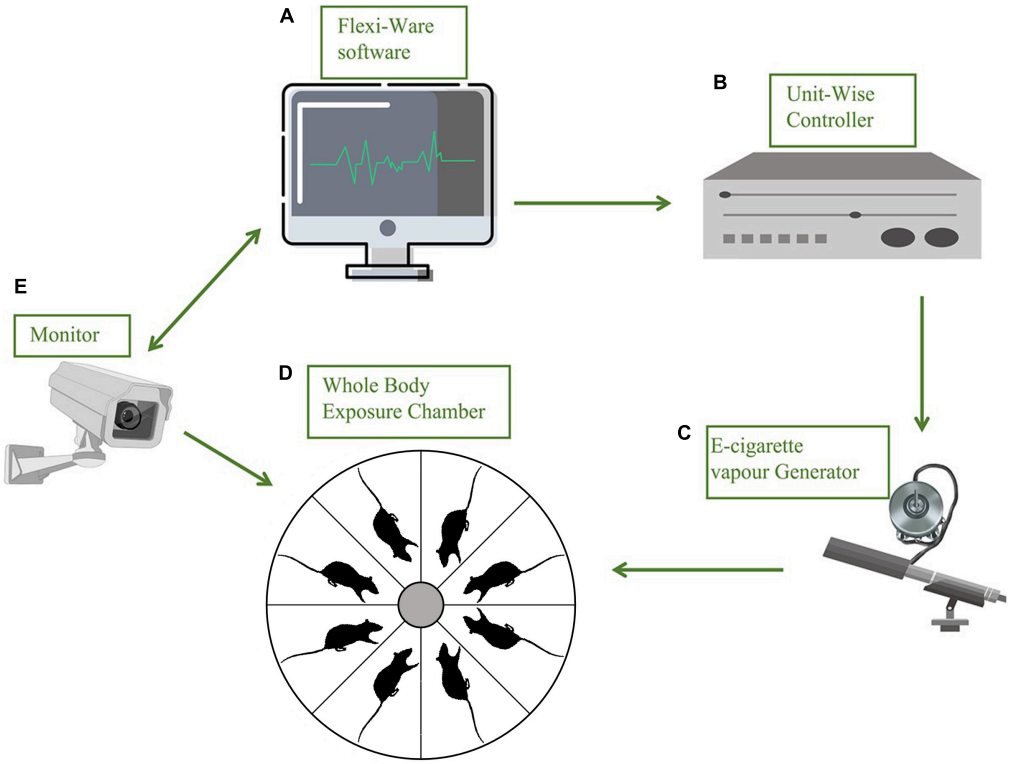

FIGURE 1 | Schematic diagram of a precise substance vapor device. Each part of the device is represented by a stick figure. **(A)** Flexiware software: the exposure temperature, patterns of smoking and humidity, and the exposure time and duration can be modified practically by the computerized exposure system; **(B)** a Uint-Wise controller connected with **(C)** e-cigarette vapor generator; **(D)** whole body exposure chamber with relatively spacious space, eight mice for every single run, and the action state of animals in the chamber was recorded in real-time by a camera **(E)** connected with **(A)**; a gas purifier before it is discharged.

inExpose) was applied for controlling the e-cigarette vapor generation and postprocessing. For details of the running program, the exposure duration was set as 30 min per run, one time per day. The gas flow rate was set as 2 L per min (**Supplementary Table 1**). The purified exhaust gas was expelled after the exposure. The e-cigarette vapor exposures were carried out for 7 days per week, for 43 days, and the following behavioral tests were performed with a continuous daily vapor exposure except that the elevated plus maze was assessed when the ENDS had been withdrawn for 48 h (**Figure 2**). The mice were randomly assigned to one of the three treatment groups and exposed daily as follows: (1) Veh cont: Vehicle control of 50% propylene glycol (PG) + 50% vegetable glycerin (VG); (2) Nico: 4% Nicotine + 46% PG + 50% VG; (3) Nico + ment: nicotine with menthol flavoring: 10% of menthol flavoring agent + 4% of Nicotine + 35% of PG + 51% of VG. All behavioral tests were conducted approximately around 15–16 h following the e-cigarette exposure to avoid its acute effects, except the Elevated plus maze test performed at the 48 h withdrawal period.

Behavioral Assessment

Three-Chamber Sociability and Social Novelty Test

The three-chamber test (TCT) is widely used to observe the sociability and social novelty of rodents. An opaque white box (42 cm length × 60 cm width × 25 cm height) was made of acrylic and each chamber measured 42 cm length × 20 cm width × 25 cm height. Before the test, the mice were placed in the corner of the center chamber to habituate to the 3 chambers and two empty cups for 10 min. In the TCT, a subject mouse is allowed to explore two opposing chambers containing another mouse (social stimulus) or empty cage in the sociability test; and to explore two opposing chambers containing the familiar mouse or the novel mouse in the test of preference for social novelty. In the first session (sociability test), the test mice were placed in the corner of the center chamber, a new male mice of the same age were placed into the cup in the left chamber, while no mice were placed in the right chamber. In the second session (social memory test), the mice in the left chamber remained unchanged, and another set of new male mice of the same age was placed into the cup in the right chamber. Each session was monitored for 10 min. Time around and the number of interactions with each wire cage, which either housed the mice or not, and the time spent in each chamber zone was recorded. The contact zone was considered to be at a 2-cm distance from each cup. The 3-chamber box and the cups were cleaned with 70% of ethanol between the sessions.

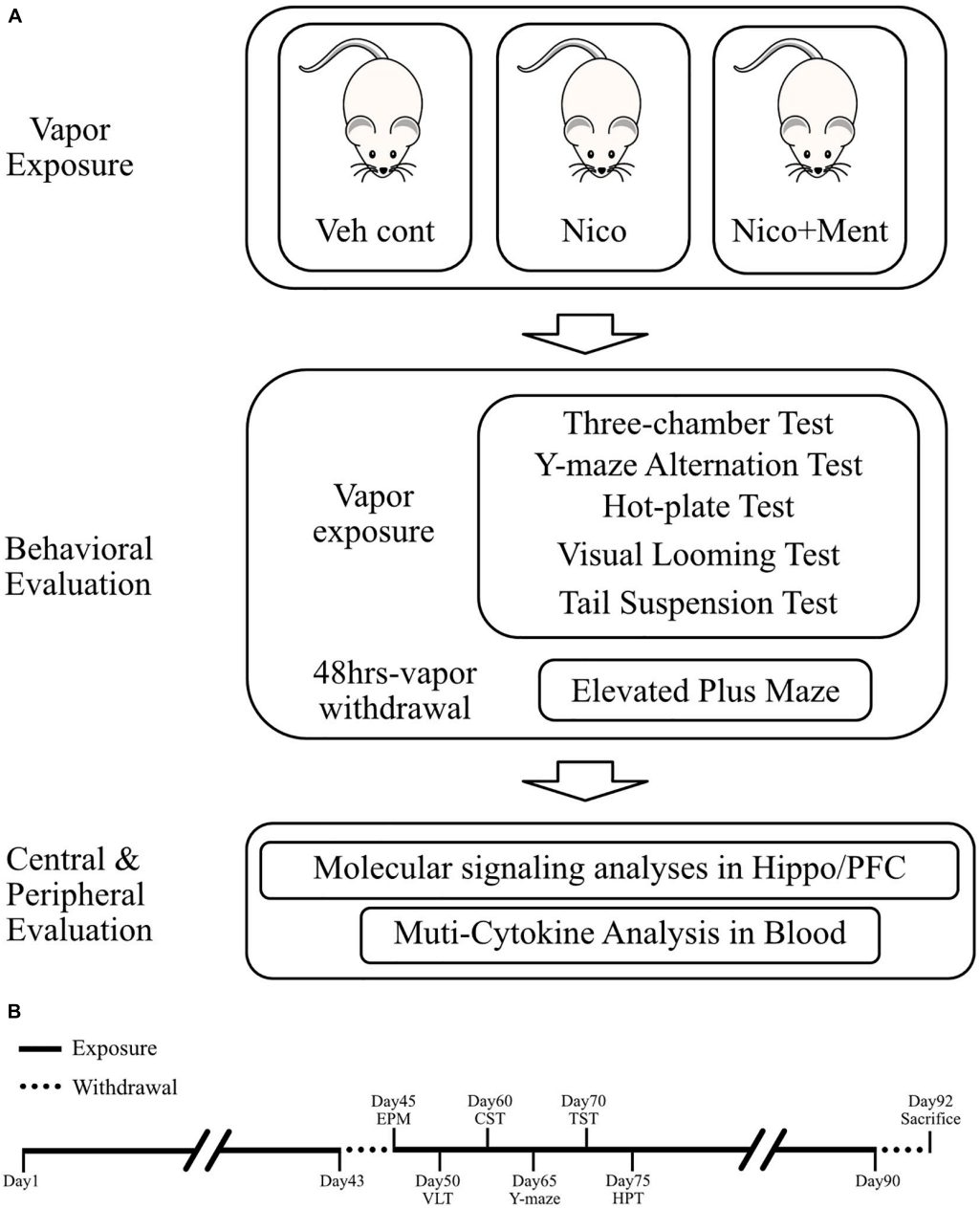

FIGURE 2 | Experimental design of this study. **(A)** Diagram of experimental procedures. The duration of vapor exposure is 30 min per day and 7 days a week. Veh cont, Vehicle control of propylene glycol/vegetable glycerin; Nico, Nicotine; Nico + ment, nicotine with menthol flavor. **(B)** Schematic workflow of this study. Veh cont, Vehicle control of 50% propylene glycol (PG) + 50% of vegetable glycerin (VG); Nico: 4% of Nicotine + 46% of PG + 50% of VG; Nico + ment: 10% of menthol flavoring agent + 4% of Nicotine + 35% of PG + 51% of VG.

For sociability sessions,

$$\text{Preference index} = \frac{\text{Time around stranger 1}}{\text{Time around stranger 1} + \text{Time around empty cage}}$$

$$\text{Preference of chamber} = \frac{\text{Time in stranger 1 chamber}}{\text{Time in stranger 1 chamber} + \text{Time in empty cage chamber}}.$$

For social novelty sessions,

$$\text{Preference index} = \frac{\text{Time around stranger 2}}{\text{Time around stranger 1} + \text{Time around stranger 2}}$$

$$\text{Preference of chamber} = \frac{\text{Time in stranger 2 chamber}}{\text{Time in stranger 1 chamber} + \text{Time in stranger 2 chamber}}.$$

Elevated Plus Maze

To measure the anxiety levels in e-cigarette withdrawn mice, the elevated plus maze (EPM) was assessed by using a plastic elevated plus maze constructed from two white open arms (25 cm length × 5 cm width) and two white enclosed arms (25 cm length × 5 cm width × 15 cm height) extending from a central platform (5 cm length × 5 cm width) at 90° which form a plus shape. The maze was placed 65 cm above the floor. A camera was set directly above the EPM apparatus for video recording. The mice were individually placed at the center, with their heads facing the open arms. The number of entries and the amount of time spent in the same type of arms were recorded during the 5-min sessions.

Tail Suspension Test

The tail suspension test (TST simulates the behavioral despair states similar to depression, and this behavioral test was performed as described before (Can et al., 2012; Liu et al., 2021). After 1 h of habituation in the experimental environment, each mouse was suspended on a metal bar 50 cm above the floor of the suspension box with an adhesive tape placed approximately 1 cm from the tip of the tail for 6 min. At the beginning of the test, the animals exhibited escape behaviors, which after a period of struggle, became more subtle. These subtle movements were considered as the immobility time. Immobility was defined as the absence of any limb or body movements, except those caused by respiration. The activities of the mice were recorded by a camera, and the immobility time during the 6-min testing period was calculated. During the test, the mice were recorded separately to prevent animals from observing or interacting with each other. After each animal had completed the test, the suspension box was thoroughly cleaned to eliminate olfactory effects.

Visual Looming Test

The visual looming test (VLT) was performed in a closed Plexiglas box (40 cm length × 40 cm width × 30 cm height) with a sheltered nest in the corner. For upper field looming stimulus (LS), an LCD monitor was placed on the ceiling to present multiple LS, which was a black disc expanding from a visual angle of 2° to 20° in 0.3 s, expanding the speed of 60° per second. The expanding disc stimulus was repeated 15 times in quick succession (totally 4.5 s). This together with a 0.066 s pause between each repeat forms the total upper visual field LS that lasts 5.5 s. Behavior was recorded using an HD digital camera (Sony, Shanghai, China). The latency between the placement and the first overt behavioral signs, such as escape behavior and time staying in the nest were recorded. Animals were handled and habituated for 10–15 min in the looming box 1 day before testing. During the looming test session, the mice were first allowed to freely explore the looming box for 5 min. No observable adaptation was observed in all our experiments.

Hot-Plate Test

To measure the basal responsiveness to nociceptive stimulation, the mice were placed on a hot-plate set at 55 ± 1°C. The antinociceptive response was the latency from the placement of the mouse on the heated surface until the first overt behavioral sign of nociception, such as licking a hind paw, vocalization, or jumping off the plate. The time between the placement and the first overt behavioral sign was recorded as a pain threshold in this test and the mouse was immediately removed from the hot plate immediately after responding or after a maximum of 30 s (cut-off), to prevent tissue damage.

Y Maze Spontaneous Alternation Test

The Y maze test was conducted to detect spatial memory and spontaneous alternation performance. The Y maze used in this study is composed of three arms (42 cm length × 4 cm width × 25 cm height) projecting from a central triangular area. The mice were placed in the central area and were allowed to explore freely for 8 min. The observer recorded an arm entry when the hind paws were completely within the arm. Spontaneous alternation was defined as successive entries into the three different arms (without returning to any arm). The percentage alternation was calculated as the ratio of actual to possible alternations (the total number of arm entries - 2) × 100. The arms were cleaned with 70% ethanol between sessions.

Tissue Processing and Western Blot

The mice were sacrificed immediately after behavioral experiments. They were anesthetized with isoflurane (0.3 ml per 25 g mouse) and euthanized by exsanguination. The brain regions of the frontal cortex and the hippocampus were dissected out on the ice and stored at -80°C for later use. The samples were homogenized in a Radioimmunoprecipitation (RIPA) lysis buffer with 1 time protease inhibitor cocktail and 1 time phenylmethylsulfonyl fluoride (PMSF). Homogenates were incubated on ice for 30 min and centrifuged at 12,000 × rpm for 10 min at 4°C. The concentration of total protein in each sample was measured using a bicinchoninic acid (BCA) kit. Then, the sample was mixed with 6 times loading buffer and boiled at 100°C for 10 min. The denatured samples containing 20 μg of total protein were separated by sodium dodecyl sulfate–polyacrylamide gel electrophoresis (SDS-PAGE), and then transferred to the nitrocellulose membrane. The membrane was blocked with 5% non-fat milk in Tris-buffered saline (TBST; 0.1% Tween 20) at room temperature for 1 h, then incubated in primary antibodies overnight at 4°C. The next day, the membrane was incubated with HRP-conjugated secondary antibodies for 1 h at room temperature. For detection, the ECL super signal chemiluminescence kit was used according to the manufacturer's protocol. The gray intensity analysis of the bands was performed using Image J software (NIH, United States).

Blood Collection and Proteome Profiler Mouse Cytokine Array

Orbital sinus blood samples were collected before sacrifice from the chronic ENDS-exposed mice. After collection, the blood samples were kept on ice and then centrifuged (3,000 rotations per minute for 10 min at 4°C), and the serum was separated. The serum samples were used fresh or kept at -80°C until further

processing. The Proteome Profiler Mouse Cytokine Array Kit (Panel A; R&D Systems) was used to profile cytokines in 50 μL of serum samples according to the manufacturer's protocol. The visualization of the array membranes was achieved using an enhanced chemiluminescence detection and exposure to X-ray film (Kodak, United States). Densitometry analysis was carried out using Quantity One.

Urine Collection

To confirm the exposure of nicotine e-cigarettes in the appropriate treatment group, urinary cotinine levels in all the groups were measured at random days after aerosol exposure by using ultraperformance liquid chromatography coupled with tandem mass spectrometry (UPLC-MS/MS) method. Urine was collected during aerosol exposure from the plastic film located at the bottom of the exposure chamber using a pipette and transferred to a microcentrifuge tube. Separate films were replaced between groups in the exposure trials.

Ultraperformance Liquid Chromatography Coupled With Tandem Mass Spectrometry Analysis

The UPLC–MS-MS analysis was performed on a Waters Acquity ultra-performance liquid chromatography (UPLC) system interfaced with a Waters Xevo TQ MS. Chromatographic separation of cotinine was achieved with an HSS T3 column (2.1 × 100 mm; 1.8 μm particle size). The temperature of the column was maintained at 40°C. A portion of 2.0 μL of the extracted sample was injected onto the column and the gradient elution was performed with 0.1% (v/v) formic acid in deionized water (mobile phase A) and (methanol mobile phase B) at a flow rate of 0.2 mL/min. The MS detection of cotinine was conducted by electrospray ionization (ESI) in the positive ion mode, using the multiple reaction monitoring (MRM) for analyte identification. The following ESI conditions were applied: capillary voltage of 1.5 kV; source temperature of 150°C; desolvation temperature of 400°C; and desolvation gas flow (nitrogen) of 800 L/h; The analysis time was approximately 5 min per sample. About 100 μL of the test urine sample was first diluted by 900 μL of ultrapure water in the centrifuge tube, and then eddied for 1 min and centrifuged at 10,000 rpm for 10 min. The supernatant was taken for testing.

Statistical Analyses

Experiment data are expressed as the mean ± SEM of the number of tests stated. Statistical comparisons were made using one-way ANOVA followed by Tukey's HSD test, as indicated in the figure legends. All the statistical tests were performed using the Prism 8.0 software (GraphPad Software Inc., San Diego, CA, United States). Spearman's correlation analysis was used to conduct the correlations among the behavioral parameters and the AMPK activation in the hippocampus, as well as the altered cytokine levels in the sera. A p-value of less than 0.05 was considered statistically significant.

RESULTS

Compensatory Enhanced Sociability in Mice Exposed to Electronic Nicotine Delivery Systems With Menthol Flavor

The e-cigarette products in the market usually offer a very wide variety of flavoring agents mixed with nicotine, which is one of the biggest health concerns of e-cigarettes (Rambaran et al., 2019; Malik et al., 2021). Here, we aim to evaluate whether the social functioning is modified by ENDS with a flavoring compound. Menthol is one of the most prevalent and common flavors used in e-cigarettes; so, we compared the behavioral responses in vapor-exposed mice between the nicotine alone group and nicotine group mixed with menthol flavoring. To do this, adult male C57BL/6J mice were randomly assigned to three treatment groups (n = 8 per group) which were exposed to the following: (1) propylene glycol and vegetable glycerol as vehicle control (50:50, PG/VG, Veh cont); (2) PG/VG with 4% (vol/vol) nicotine (Nico); (3) Vapor of 4% nicotine with 10% of menthol flavorings (Nico + ment). Here, we selected the inhalation model with a short duration (30 min) per day and long-term vapor exposure (>40 days) period. After a daily vapor exposure of 30 min and 7 days a week for 43 days, the three-chamber sociability and social novelty tests were evaluated between the above groups (**Figures 2A,B**). Since we focused to investigate the merged effects of menthol flavor in the nicotine vapor, here, we have only used the PG/VG as vehicle control in the following sets of behavioral assessments. To verify the exposure constituents, the levels of urine cotinine (i.e., nicotine metabolite) were assessed for the mice in all three vapor exposure groups. Mean cotinine levels averaged from multiple mice per exposure run on the random days were higher in urine from the mice exposed to vapors of nicotine alone (319.3 ± 33.99 ng/mL) or nicotine with menthol flavor (452.8 ± 92.71 ng/mL) compared to the Veh control (50.97 ± 13.36 ng/mL) [$F_{(2,6)}$ = 12.65, p = 0.0070, **Supplementary Figure 1**]. The body weight was measured weekly and no significant differences were observed in weight gain among all the treatment groups under our vapor exposure condition (**Supplementary Figure 2**).

Social interaction is a complex and highly conserved neuropsychiatric behavior that safeguards survival (Barak and Feng, 2016). Whether the additive of menthol flavor into e-cigarette would change the social interaction was unknown. We evaluated the social behaviors of mice *via* three-chamber social tests in this study. Sociability was investigated in the sociability session of the test (**Figure 3A**). Mice exposed to long-term ENDS with or without menthol flavor showed normal sociability as assessed by interaction time and time spent in the target chamber. Mice from the Nico group appeared normal while having slightly less contact and socialization with the stranger mouse 1 than in the empty arena compared with that in the Veh control group (No statistical significance, **Figures 3C–E**). Interestingly, the mice in the Nico + ment group prefer and spent more time (129.3 ± 21.01 s) to socialize with the stranger mouse 1 compared to the Nico group (83.67 ± 5.558 s, **Figures 3C,F**) while the time spent in the chamber of stranger mouse 1 and the

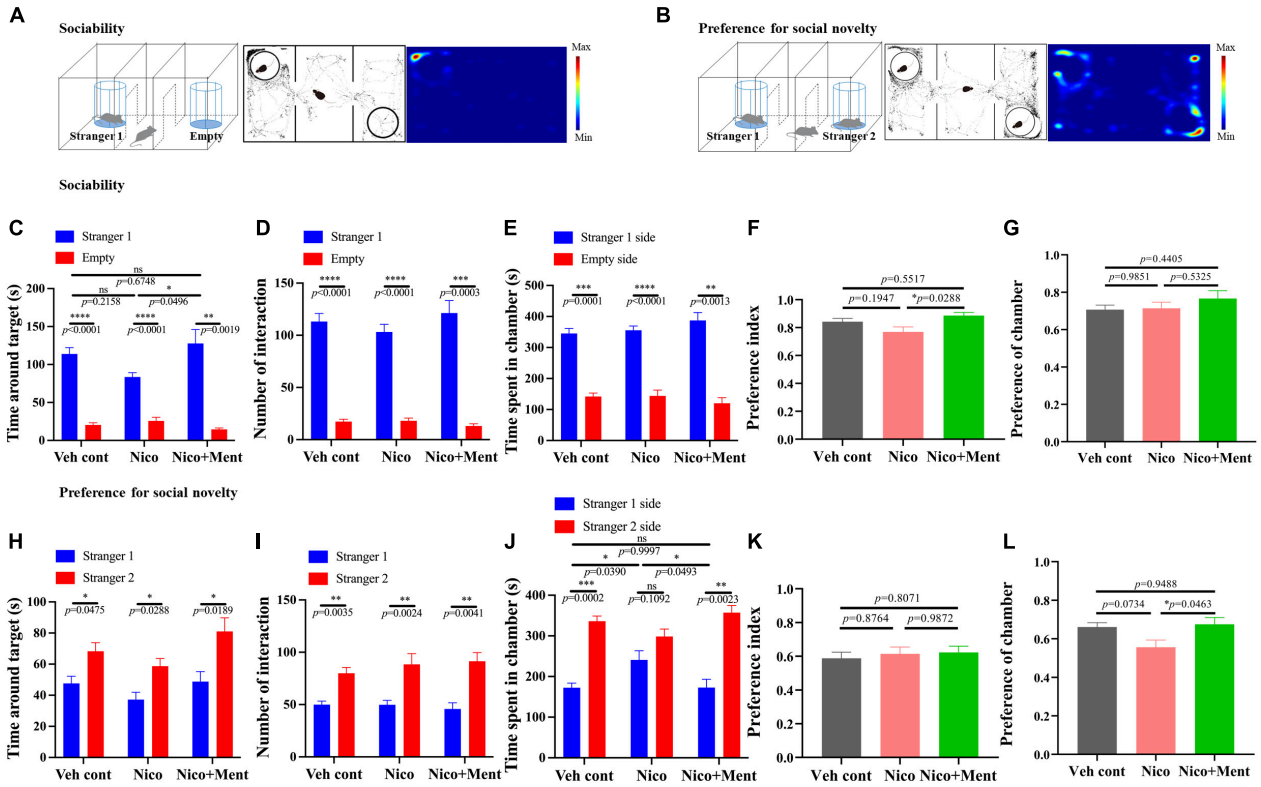

FIGURE 3 | Social behavioral assessments in mice after long-term vapor exposure. Schematic diagram of two parts of the Three-Chamber Test (TCT); stage one **(A)** and stage two **(B)**. **(A,B)** Left: the schematic diagram of the sociability session and the social novelty session of the TCT. Center: the trajectory graphs represent the movements of the tested mouse during the sociability session and the social novelty session, respectively. Right: the heatmaps represent the trajectory of motions in mice. **(C–G)** Social behavioral assessments of tested mice in the sociability session. Time around target mouse [$F_{(2,20)}$ = 3.383, p = 0.0543] **(C)** and the number of interactions with stranger 1 [$F_{(2,20)}$ = 0.9427, p = 0.4062] or empty cage **(D)**. Time spent in the chambers of stranger 1 side or the empty side **(E)**. **(F)** Preference index of stranger 1 among groups. $F_{(2,20)}$ = 4.040, p = 0.0336. **(G)** Preference of stranger 1 chamber against the empty side among the exposure groups [$F_{(2,20)}$ = 0.9022, p = 0.4216]. **(H–L)** Social behavioral assessments of tested mice in the social novelty session. Time around target mouse **(H)** and the number of interactions [$F_{(2,20)}$ = 0.5234, p = 0.6004] **(I)** with stranger 2 mouse or stranger 1 mouse. **(J)** Time spent in the chambers of stranger 2 sides or the stranger 1 side. **(K)** Preference index of stranger 2 among the groups [$F_{(2,20)}$ = 0.2197, p = 0.8047]. **(L)** Preference of stranger 2 chamber against stranger 1 side among the exposure groups [$F_{(2,20)}$ = 4.081, p = 0.0326]. The calculations of Preference index and Preference of chamber are presented in Methods. Data are shown as mean ± SEM. *$p < 0.05$, **$p < 0.01$, ***$p < 0.001$, and ****$p < 0.0001$ as determined by ordinary one-way ANOVA, within-group analyses using paired t-test, with the factors of test condition (sociability or social novelty), cages, and chamber sides (e.g., stranger 1 side or the opposite side). Veh cont, Vehicle control; Nico, Nicotine; Nico + ment, nicotine with menthol flavor.

preference of chamber was similar to the mice of all the groups [$F_{(2,20)}$ = 1.411, p = 0.2672, **Figures 3E,G**]. In the test session of preference for social novelty (**Figure 3B**), mice spent more time making contact and socializing with the newly introduced unfamiliar mouse (stranger 2) than stranger 1, as a normal manifestation of social memory and preference for social novelty [$F_{(2,20)}$ = 3.005, p = 0.0723, **Figure 3H**]. No significant difference were observed among the groups in their interacting time, the number of interaction, and the preference index with the novel mouse (**Figures 3H,I,K**), while mice exposed to nicotine alone spent less time in the chamber of the stranger 2 [$F_{(2,20)}$ = 4.542, p = 0.0236, **Figure 3J**], and mice of Nico + ment group also showed an increased preference for staying in the chamber of the newly introduced stranger 2 mice than with the familiar mouse, the stranger 1, compared to the mice in the group of nicotine vapor alone (**Figures 3J,L**). Our data suggested that long exposure to menthol-flavored ENDS may have compensatory enhancing effects on the sociability and preference for social novelty compared to the vapor exposure of nicotine alone.

Effects of Long-Term Electronic Nicotine Delivery Systems Exposure With Menthol Flavor on Anxiety, Depression-Like Behaviors

The previous study has demonstrated the interplay between social behaviors and anxiety status (Lupien et al., 2009; Yamamuro et al., 2020). Since social stress is one of the major risk factors for the progression of anxiety disorders (Gross and Hen, 2004) (Feder et al., 2009), and shared neuronal circuits between them has been confirmed (Mottolese et al., 2014; Jing et al., 2021), we assessed the anxiety and the depression-like behaviors of the mice after long-term vapor exposure. We compared the 48 h-withdrawal responses in vapor-exposed mice with nicotine or

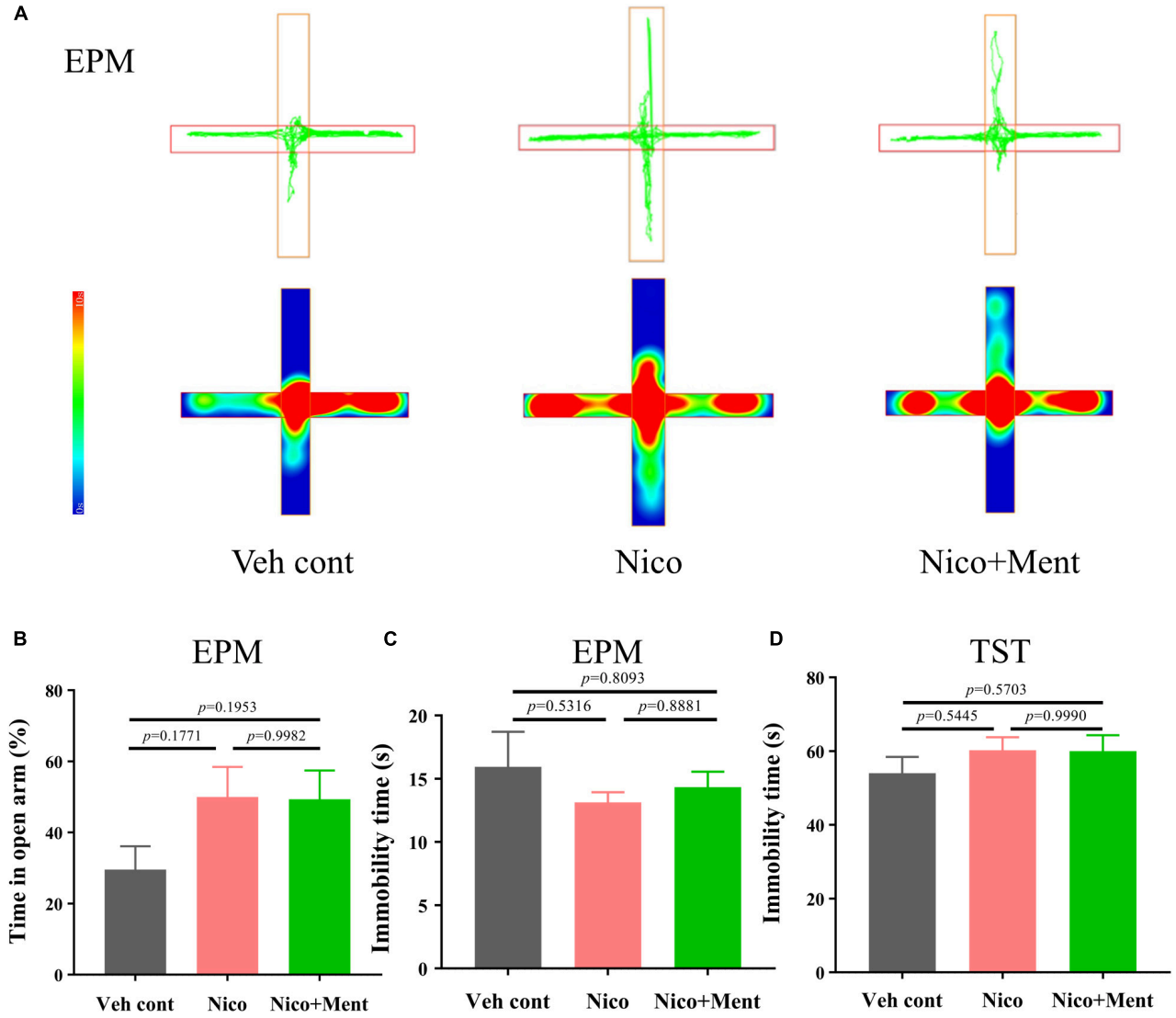

FIGURE 4 | Anxiety, depressive-like behavioral assessments in mice exposed to long-term vapor exposure. **(A)** The trajectory and heatmap of mice in the EPM. **(B)** The percentage of time of staying in the open arm to the time of one trial ratio (%) [$F_{(2,21)} = 2.222$, $p = 0.1333$]. **(C)** The immobility time of mice during the trial in EPM (s). **(D)** Immobility time of mice during Tail suspension test (s). The value of $^*p < 0.05$ as determined by ordinary one-way ANOVA and multiple comparisons with every other group. Bars represent marginal means ± SEM. $N = 8$ per group. Veh cont, Vehicle control; Nico, Nicotine; Nico + ment: nicotine with menthol flavor. EPM, Elevated plus maze. TST, Tail suspension test.

nicotine plus menthol. By performing the behavioral tests of EPM (after 48 h-withdrawal) in mice, we observed that long-term vapor exposure of daily half-hour ENDS with or without menthol flavor did not cause significant withdrawal responses evaluated by anxiety-like behaviors in EPM at the 48-h-ENDS withdrawal period (**Figures 4A,B**). Specifically, we analyzed the immobility time for all groups during the EPM test [$F_{(2,21)} = 0.5963$, $p = 0.5599$, **Figure 4C**; no significant differences were observed. Further, a tail hanging test was performed for the evaluation of depressive-like behaviors. No significant changes were observed on immobility time in the tail suspension test [$F_{(2,21)} = 0.7295$, $p = 0.4940$, **Figure 4D**]. Our current data suggested that long-term e-cigarette usage with short daily nicotine exposure time did not induce anxiety or depression-like behaviors in mice, even after adding the menthol flavor in the e-liquid. These data suggested that the enhancement of menthol flavor in ENDS on social functioning is independent of the emotional status.

No Innate Visual or Perceptual Behavioral Alterations in Mice After Long-Term Electronic Nicotine Delivery Systems Exposure With Menthol Flavor

We further evaluated whether the social functioning changes induced by the menthol flavor in ENDS are associated with any alternations on innate visual or perceptual behaviors

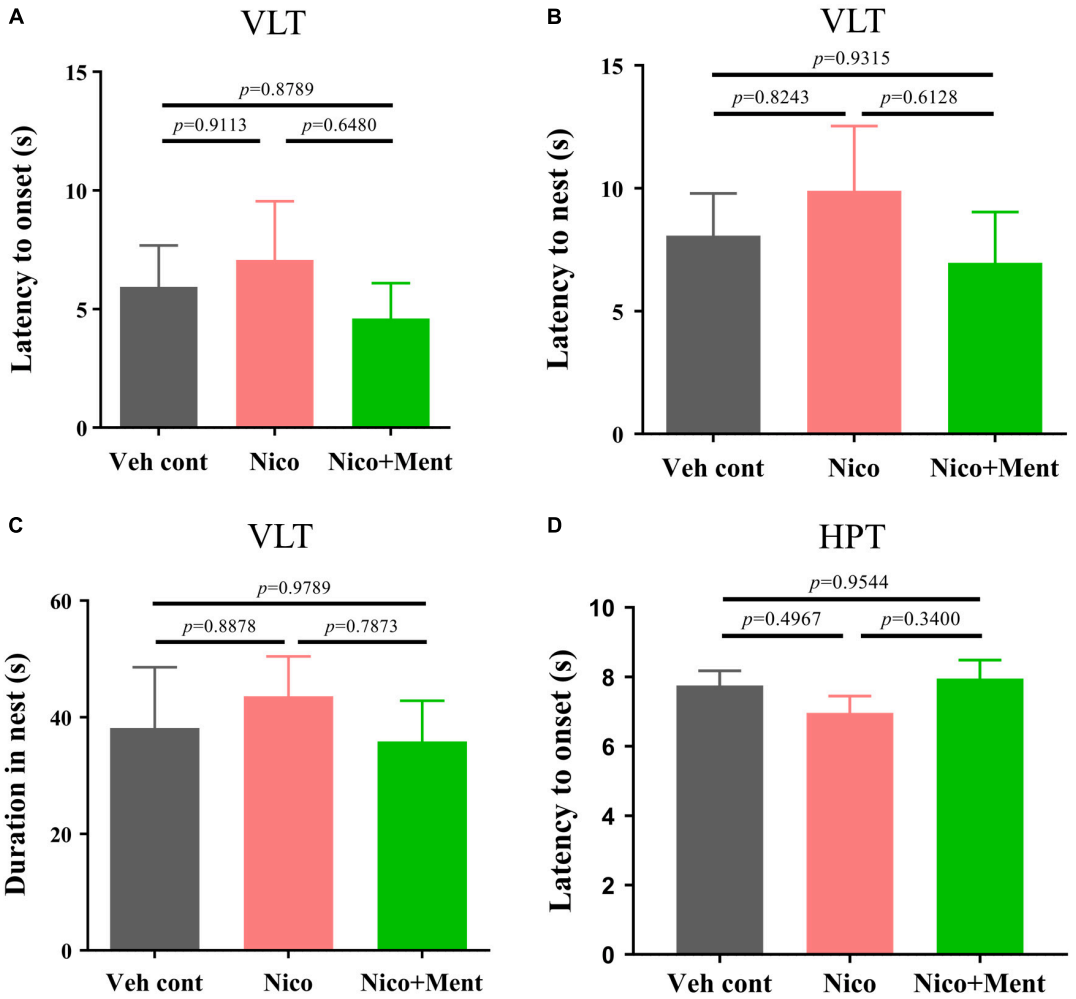

FIGURE 5 | The innate visual or perceptual behavioral assessment in mice after long-term ENDS exposure. The behavioral tests were performed in order during ENDS exposure as described in **Figure 2B**. **(A)** The latency to the onset behavior of mice during the Visual looming test (VLT; s) [$F_{(2,21)} = 0.4033$, $p = 0.6732$]. **(B)** The latency of flight to the nest behavior of mice during VLT (s) [$F_{(2,21)} = 0.4649$, $p = 0.6345$]. **(C)** Duration of mice hiding in the nest (s) [$F_{(2,21)} = 0.2317$, $p = 0.7952$]. **(D)** The latency to the onset behavior of mice during the Hot-plate test (s). The value of $^*p < 0.05$ as determined by ordinary one-way ANOVA and multiple comparisons with every other group. Bars represent marginal means ± SEM. $N = 8$ per group. Veh cont, Vehicle control; Nico, Nicotine; Nico + ment, nicotine with menthol flavor.

(Ferrara et al., 2021; Sakurai, 2021; Wei et al., 2021). Behavioral paradigms, such as innate fear and heat pain response were used in our experiments. In the VLT, innate fear responses were quantified. Unexpected salient visual cues stimulate the animal's defensive behaviors, such as shying away and hiding back in the nest (Zhou et al., 2019). We analyzed the onset latency of mice to such behaviors. There were no changes in the latency of flight to nest, the flight-to-nest latency, as well as the duration in the nest in the Nico group when compared to both Veh control and Nico + ment groups (**Figures 5A–C**). Chronic ENDS inhalation with daily limited-duration may not affect the innate fear responses in mice, and the same was also observed when menthol flavor was added. In the Hot-Plate Test (HPT), the pain response to a thermal stimulus was assessed by the onset of latency, and we found no differences among all groups [$F_{(2,21)} = 1.157$, $p = 0.3337$, **Figure 5D**]. These data suggested that chronic nicotine vapor with or without menthol under our exposure conditions did not affect the innate visual or perceptual behaviors.

Normal Spatial Learning and Memory in Mice With Long-Term Exposure of Electronic Nicotine Delivery Systems With or Without Menthol Flavor

Previous studies have suggested a potential relationship between social activity and the overall executive functioning, working memory, and visuospatial abilities in healthy older adults (Kelly et al., 2017; Kuiper et al., 2017; Perry et al., 2021). Here, we used the Y-maze test to measure the cognition and spatial memory of mice after exposure to e-cigarette vapor. The percentage of alternation in Y-maze arms was analyzed (**Figures 6A,B**). There

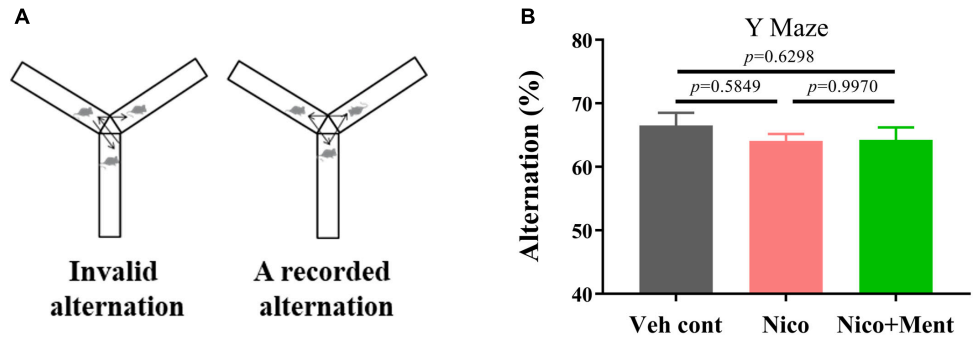

FIGURE 6 | Spatial memory assessment in mice exposed to long-term vapor exposure. **(A)** Schematic diagram of recorded alternation of one trial in Y-maze. Spontaneous alternation was defined as successive entries into the three different arms (without returning to any arm). **(B)** The percentage alternation was calculated as the ratio of actual to possible alternations (the total number of arm entries - 2) × 100. The value of $*p < 0.05$ as determined by ordinary one-way ANOVA and multiple comparisons with every other group. Bars represent marginal means ± SEM. $N = 8$ per group. Veh cont, Vehicle control; Nico, Nicotine; Nico + ment, nicotine with menthol flavor.

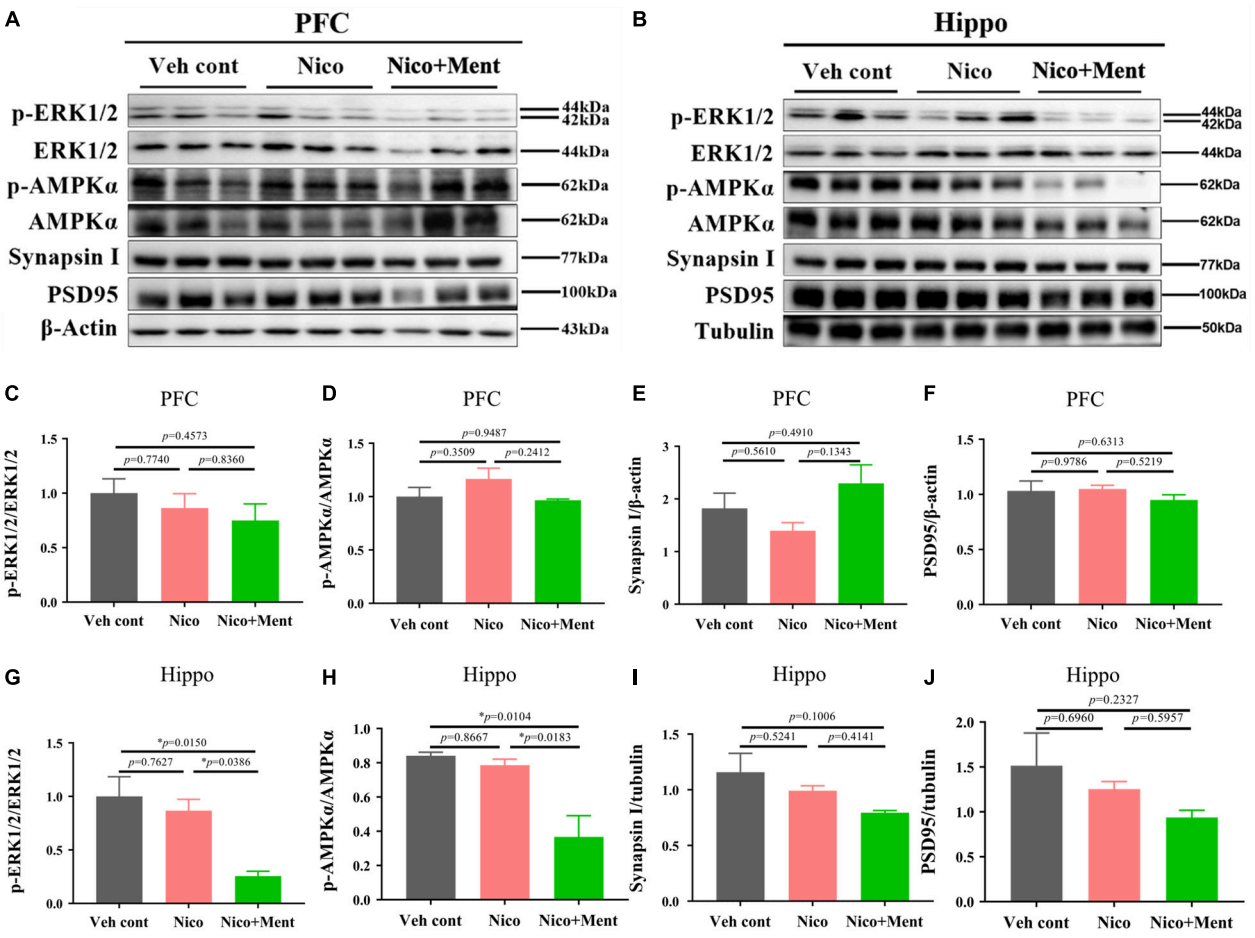

FIGURE 7 | The immunometabolic signals and synaptic protein analyses in the PFC/hippocampus of mice after long-term vapor exposure. Western blot analyses of the expressions of p/t-ERK1/2, p/t-AMPKα, synaptic proteins, such as Synapsin-1 and PSD95 in the PFC **(A)** and the hippocampus **(B)**. The quantification data of the above molecules are presented in **(C–J)**, respectively. Data are expressed as means ± SEM. The values of $*p < 0.05$ as determined by ordinary one-way ANOVA and multiple comparisons with every other group. Veh cont, Vehicle control; Nico, Nicotine; Nico + ment, nicotine with menthol flavor.

were no significant changes of alternation [$F_{(2,21)}$ = 0.6216, p = 0.5467] in the mice of either Nico group (64.07 ± 1.119 %) or Nico + ment group (64.25 ± 1.973 %) compared to the PG/VG group (66.53 ± 1.978 %). These data indicated that menthol flavor combined with nicotine in e-cigarette had no effect on spatial learning and memory.

The Reduced Adenosine 5′ Monophosphate-Activated Protein Kinase Activation in the Hippocampus by Chronic Electronic Nicotine Delivery Systems Exposure With Menthol Flavor

We further investigated the underlying mechanisms of the effects of chronic vapor on nicotine with or without menthol flavor. The prefrontal cortex and the hippocampus are the interconnected brain regions and hubs for modulating high brain functions and neuropsychiatric behaviors especially social behaviors (Padilla-Coreano et al., 2016; Eichenbaum, 2017). We here analyzed the AMPK/ERK signaling pathways which are involved in neuronal metabolism, neuroinflammation, and synaptic plasticity. By using Western blotting, we found that the hippocampal activation of ERK1/2 (as shown by phosphorylated/total ERK1/2) and AMPKα (as presented by phosphorylated/total AMPKα) in the hippocampus was decreased by menthol flavor when added into the nicotine vapor (**Figures 7B,G,H**). Further, we also evaluated the expression levels of presynaptic protein, synaptin-1, and the postsynaptic protein, PSD95 in the prefrontal cortex and the hippocampus to assess the alterations in synaptic plasticity. A slight reduction of synapsin-1 was observed in the hippocampal region without statistical significance (**Figure 7I**). The AMPK/ERK signaling in PFC (**Figures 7A,C,D**), and the expressions of Synapsin I and PSD95 in PFC and the hippocampus were not significantly changed under our vapor exposure condition (**Figures 7A,B,E,F,I,J**). These data suggested that the menthol flavor in ENDS might inactivate the AMPK-ERK signaling in the hippocampus.

Alterations of Peripheral Cytokine Levels Responded to Menthol Flavor in Electronic Nicotine Delivery Systems

Multiple cytokines and chemokines have been investigated regarding their roles in neuropsychiatric behaviors (Kronfol and Remick, 2000; Polacchini et al., 2018). No significant differences in weight gain among all the treatment groups were observed (**Supplementary Figure 2**). Here, we profiled multiple cytokines in the sera to assess the peripheral effects of chronic ENDS vapors which might respond to the social behavioral changes. Forty cytokines were measured in our experiment and we observed that the sera levels of CXCL12 and TIMP-1 were significantly reduced while that of the CXCL5 was dramatically increased after nicotine vapor exposure, and a further decline of TIMP-1 and CXCL13 were detected in the group of menthol-flavored ENDS compared to the Nicotine alone group. The serum expressions of CXCL12 were decreased in vapor groups with or without menthol flavor compared to the Veh control group, suggesting that the menthol flavor had no additional effects in ENDS on the serum level of CXCL12. The sera level of M-CSF was only reduced in Nico + ment group compared to the Vehicle control group. The C5 level in the sera was found dramatically decreased in the vapor group of nicotine with menthol flavor compared to either vehicle or ENDS exposure of nicotine only, suggesting a strong downregulation of C5 in the sera of menthol flavorings in ENDS (**Figures 8A,B**). These data suggested that menthol flavor may modulate the serum expressions of cytokines that responded to the alteration on the social activity by ENDS.

Linear Correlations Among the Central/Peripheral Immunometabolic Indices and the Response of Social Behaviors to Menthol Flavor in Electronic Nicotine Delivery Systems

To elucidate the correlation among the social activity and the immunometabolic indices in the hippocampus and in the sera which were affected by menthol flavor in ENDS, we conducted the Spearman's correlation analysis among social behavioral indices that activated the AMPK in the hippocampus and the cytokine levels in the sera ($p < 0.05$, **Figure 9**). The serum level of C5 was found to be negatively correlated with the preference for social novelty as measured by the target exploration time in Stage 2 (r = -0.7). The serum level of C5 was also positively correlated with the activation of ERK (p-ERK/ERK, r = 0.79) and AMPK (p-AMPK/AMPK, r = 0.87) in the hippocampus. The levels of M-CSF and TIMP-1 in the sera were also found to be correlated with the AMPK-ERK signaling in the hippocampus (**Figure 9**). This set of correlation data suggested that the menthol flavor in ENDS may induce comprehensive immunometabolic responses in the brain nuclei and in the sera corresponding to the social activity change.

DISCUSSION

The e-cigarette is among the focus of controversy since it may be harm-reducing for traditional smokers seeking to quit, while harm-initiating for former or never smokers, particularly among the youth (Kalkhoran and Glantz, 2016; Fairchild et al., 2018; Prochaska, 2019). The US FDA has been seeking to reduce nicotine concentrations in conventional tobacco cigarettes to non-addictive levels while emphasizing other nicotine delivery products, such as the role of e-cigarettes in attenuating the harmful effects of combustible tobacco (McCarthy, 2017). However, further scientific evidence is needed to convince the safety of e-cigarette and their aid on smoking cessation, given the widespread use of chemicals/artificial flavors to mimic natural flavors commonly used in the e-cigarettes.

A wide variety of flavor options of e-cigarettes on the market has grown in popularity and entices young generations to smoke (Zare et al., 2018). The menthol flavor is among the most commonly used flavorings in e-cigarettes, and an exception in which the flavored e-cigarettes have been banned by Federal regulations recently (Kaur et al., 2020). It has been well-documented that e-cigarettes cause systemic toxicity,

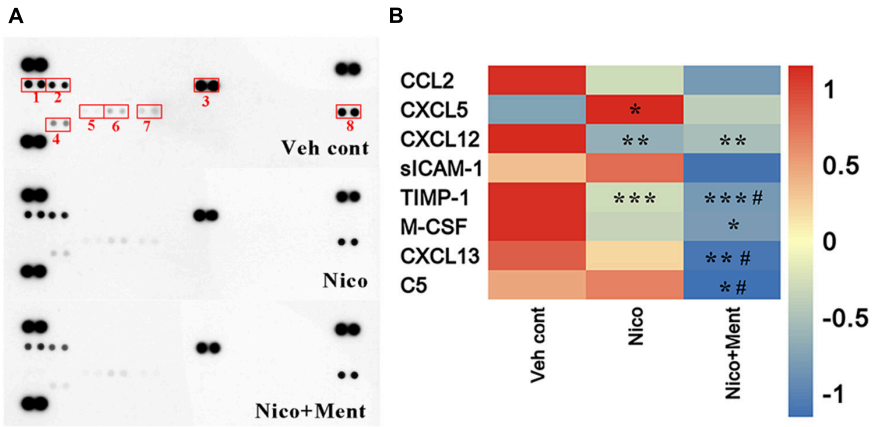

FIGURE 8 | The cytokine profile in the sera is altered by long-term vapor exposure. **(A)** Representative blots from serum samples of mice treated with long-term vapor exposures of vehicle control, ENDS, or ENDS with menthol flavor that presented levels of 40 known cytokines using the murine Proteome Profiler Cytokine Array. Spots showing differential expression are boxed. (1): CXCL13; (2): C5; (3): sICAM-1; (4): TIMP-1; (5): CXCL5; (6): M-CSF; (7): CCL2; (8): CXCL12. **(B)** Heatmap of quantification revealed significant changes greater than 1.2-fold, data were determined by ordinary one-way ANOVA and multiple comparisons with every other group. $^{*}p < 0.05$, $^{**}p < 0.01$, $^{***}p < 0.001$ compared to the Veh cont; $^{\#}p < 0.05$ compared to Nico group, accordingly. Veh cont, Vehicle control; Nico, Nicotine; Nico + ment, nicotine with menthol flavor.

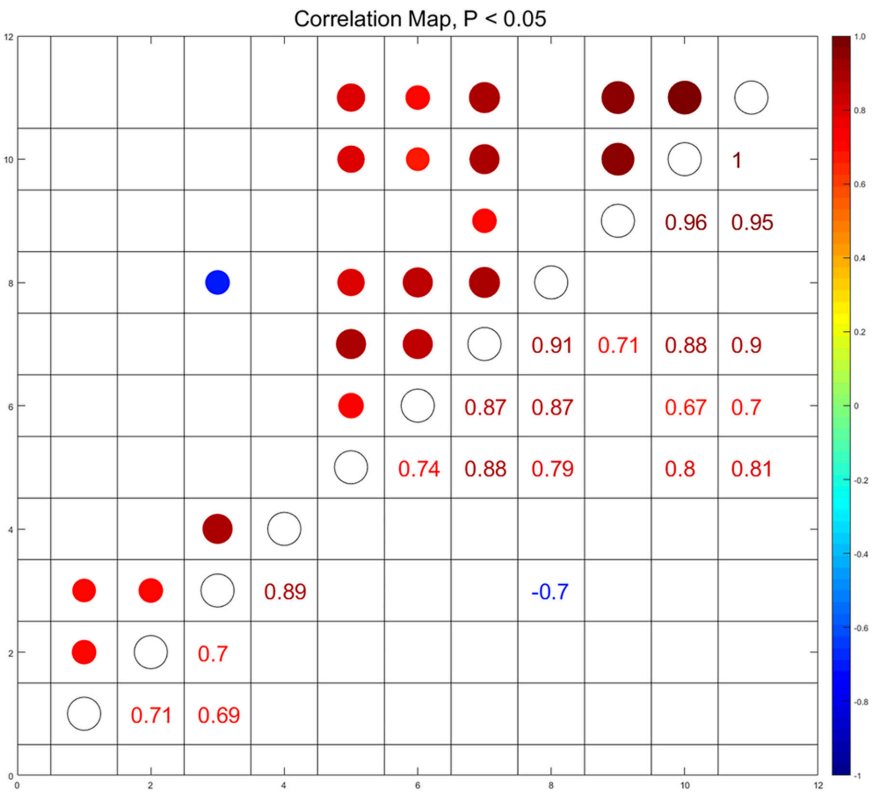

FIGURE 9 | Correlations among immunometabolic signals presented as the activation of AMPK-ERK in the PFC and the hippocampus, cytokines in the sera, and the social behavioral parameters ($p < 0.05$). Through pairwise comparison of the social behavioral index and biochemical indicators, we selected and displayed those with *p*-value less than 0.05, and used the area and color depth of the dot to represent the *r*-value. (1): Time around the target in the sociability session of Three-Chamber Test (TCT); (2): Preference index in the sociability session; (3): Time around the target in the test session of preference for social novelty; (4): Preference index in the test session of preference for social novelty; (5): the level of p-ERK/ERK in the hippocampus; (6): the level of p-AMPKα/AMPKα in the hippocampus; (7–11): the serum level of CXCL13 (7), C5 (8), CXCL12 (9), M-CSF (10), and TIMP-1 (11).

including lung and liver injuries; the cytotoxicity induced by e-cigarette flavoring chemicals has also been determined in cell lines and humans. Repeated exposure to menthol was found to significantly decrease cell viability (Rickard et al., 2021); therefore additional research is urged to understand the mechanisms of the toxicity of flavorings and the chemical combinations in ENDS.

Smoking may increase the risk of mental disorders and non-affective psychoses. A systematic review of literature from 1946 to 2017 followed by a meta-analysis suggested that chronic tobacco smoking was strongly associated with neuropsychological deficits and cognitive impulsivity (Conti et al., 2019). The e-cigarette products in the market are generally composed of nicotine with flavor. Menthol flavor was the top choice among teen vapers according to research in the US (Leventhal et al., 2019). In this case, it is necessary to understand the neuropsychiatric roles and their effects on the brain as well as the peripheral system of menthol-flavored e-cigarettes. However, there is limited evidence on the neuropsychiatric roles of menthol flavor in ENDS that was specifically evaluated *in vivo* in animal models or humans.

Social behaviors are fundamental for the survival of any vertebrate species. Epidemiological data indicated that smokers endorse socializing as a reason to smoke (Fidler and West, 2009) and social functioning was found enhanced in smokers which was supposed to be related to nicotine (Martin and Sayette, 2018). However, very limited work has been implemented to depict the effect of e-cigarettes on social functions in animal models to reveal the underlying molecular mechanisms. In our current work, we have used a standard and precise vapor device to mimic the exposure of ENDS, which avoided the restraint stress that might have been caused by the nose-only aerosol exposure, and evaluated the social behaviors after long-term exposure with daily 30-min inhalation. As shown in the previous study, the effects of nicotine on social behaviors are complex regarding the dose, the schedule of administration, housing, and individual differences; nicotine may increase the social interaction at low doses but reduce it at high doses (Blanco-Gandia et al., 2015); and it was also presented to improve the sociability and reduced repetitive behaviors in a mouse model of autism at certain doses while no effects were observed in the normal mice (Mahmood et al., 2020). Consistent with some of these literature, we found in our experiment that, although the slight decrease in the social activity (no statistical difference) was observed in nicotine-vapored mice, the long exposure to menthol flavored ENDS was found to have compensatory enhancing effects on the sociability and preference for social novelty compared to the vapor exposure of nicotine alone, suggesting the antagonistic effect on the social functioning of menthol flavoring as a combinational ingredient with nicotine in ENDS.

Since social behaviors are instinctive with flexibility (Wei et al., 2021), and influenced by other psychiatric behaviors, we further assessed the behaviors related to emotion, cognition, and innate state in the mice after ENDS exposure with or without menthol flavor. Interestingly, under our ENDS exposure condition, which was a short-term treatment per day and it lasted for the long term; the ENDS exposure with menthol flavor did not change the anxiety/depressive-like behaviors measured by the elevated plus maze and tail suspension test; the innate visual or perceptual behavioral responses measured by the VLT, HPT, and the spatial memory evaluated by Y-maze in mice. One limitation of this study was that only male mice were used with a limited sample size. It will be necessary to understand how female individuals cope with e-cigarettes and to further confirm the complex interplay of menthol flavoring with nicotine in ENDS.

Further, we characterized the central and peripheral changes induced by the vapors of nicotine alone or combined with menthol flavor that may be related to the alterations in social activities. The prefrontal cortex and hippocampus are hub regions that are dominant in many complex behaviors including social activities and social cognition (Preston and Eichenbaum, 2013; Li et al., 2020; Qi et al., 2021). Increasing attention has been paid to the role of the crosstalk between metabolic, inflammatory, and neuropsychiatric disorders (Culmsee et al., 2018), such as the activation of ERK and the AMPK levels (Camargo et al., 2021). The adenosine 5′ monophosphate-activated protein kinase (AMPK) is a heterotrimeric serine/threonine kinase that promotes ATP generation and is regarded as a key regulator of cellular energy metabolism and mitochondrial homeostasis (Chaube and Bhat, 2016; Herzig and Shaw, 2018). Therefore, we measured the immunometabolic molecular signals in the prefrontal cortex, hippocampus, and the cytokines in the sera altered by nicotine vapor with or without menthol flavor and investigated their correlations with social behavioral changes. Our results suggested a negative correlation of preference for social novelty and C5 level in the sera of mice. Further, the serum level of C5 was also found to positively correlate with the activation of AMPK-ERK signaling in the hippocampus, which may hint at a coordinated response in the central and peripheral system to ENDS which contribute to the social behavioral enhancement induced by the menthol flavor. Previous studies have shown that anxiety was associated with low levels of many cytokines in sera, such as CCL11, CCL2, CCL5, and IL-6; and lower peripheral levels of CXCL5 was observed in people with psychiatric disorders, such as schizophrenia and recurrent depressive disorder with suicidal ideation (Polacchini et al., 2018). The cytokine profile observed in our study indicated that the menthol flavor in ENDS may act to reverse the potentially reducing effects of nicotine on social activities.

In conclusion, our present study profiled the social behaviors modulated by menthol flavor in ENDS. We presented the compensatory enhanced social activity induced by menthol flavor in the nicotine-containing e-cigarette. The striking enhancement in social activity induced by menthol flavoring, in combination with nicotine in ENDS, may explain the increased severity of nicotine dependence in menthol-flavored e-cigarette vaporer and the popularity of menthol/mint-flavored e-cigarettes in the market. The ENDS induced the immunometabolic alternations in the hippocampus, as well as in the sera that correspond to social behavioral changes, suggesting the disruption of systemic homeostasis are only induced by nicotine but also by other flavorings in the e-cigarette. Although our current data indicated the mild influences of the neuropsychiatric behaviors in the mice due to long-term ENDS exposure with daily intake limit; the phenomenon of enhanced social functions induced by menthol flavor in ENDS highly alerts us with the information that e-cigarette flavoring additives may have complex interplay with nicotine and lead to increased addiction as well as

immunometabolic disruption among the e-cigarette users who definitely need further investigations.

DATA AVAILABILITY STATEMENT

The raw data supporting the conclusions of this article will be made available by the authors, without undue reservation.

ETHICS STATEMENT

All animal experiments and procedures were carried out in accordance with protocols approved by the Animal Care and Use Ethics Committee of the Shenzhen Institutes of Advanced Technology, Chinese Academy of Sciences.

AUTHOR CONTRIBUTIONS

X-AL designed the experiments. ZX, ZM, A-XL, JT, JL, and JW performed the experiments. ZX, YT, CD, ZC, A-XL, X-YJ, JT, and XL performed the data analyses. X-AL, ZC, YT, A-XL, JT, and XG contributed to the manuscript writing. TL, ZC, ZL, LW, and SL revised the manuscript. All authors have read and approved the manuscript.

FUNDING

This work was funded in part by the financial support from the National Natural Science Foundation of China (NSFC) (31900728 to XL, 32000710 to ZC, and U20A2016 to ZC), the CAS Youth Innovation Fund (Y9G022 to XL), the Guangdong Provincial Natural Science Foundation (2019A1515110190 to ZC), the Shenzhen Key Basic Research Project (JCYJ20200109115641762 to ZC), and the Shenzhen Governmental Grant (ZDSYS20190902093601675).

SUPPLEMENTARY MATERIAL

The Supplementary Material for this article can be found online at: https://www.frontiersin.org/articles/10.3389/fnmol.2022.800406/full#supplementary-material

Supplementary Figure 1 | Urine cotinine measured during vapor exposure. The urine samples from the mice of all exposure groups were collected immediately following the daily exposure period and assessed by Liquid chromatography-mass spectrometry (LC-MS/MS) for cotinine as a marker for the intake of nicotine-containing vapors. Data are expressed as group mean ± standard error. $^{*}p < 0.05$, $^{**}p < 0.001$ as determined by ordinary one-way ANOVA and multiple comparisons with every other group. Veh cont, Vehicle control; Nico, Nicotine; Nico + ment, nicotine with menthol flavor.

Supplementary Figure 2 | Weight measured weekly during vapor exposure. **(A)** Weight measured weekly from week 0 to week 12. **(B)** Delta weight gain corrected for physiological growth, as measured in the weight value of the following week minus the weight value of the first week. Data are shown as mean ± SEM. $^{*}p < 0.05$. Veh cont, Vehicle control; Nico, Nicotine; Nico + ment, nicotine with menthol flavor.

Supplementary Table 1 | Device parameters of e-cigarette vapor exposure program.

Supplementary Table 2 | Primary antibodies used for Western blot in this study.

REFERENCES

Allen, J. G., Flanigan, S. S., LeBlanc, M., Vallarino, J., MacNaughton, P., Stewart, J. H., et al. (2016). Flavoring Chemicals in E-Cigarettes: diacetyl, 2,3-pentanedione, and acetoin in a sample of 51 products, including fruit-, candy-, and cocktail-flavored E-Cigarettes. *Environ. Health Perspect.* 124, 733–739. doi: 10.1289/ehp.1510185

Ambrose, B. K., Day, H. R., Rostron, B., Conway, K. P., Borek, N., Hyland, A., et al. (2015). Flavored tobacco product use among US Youth Aged 12-17 Years, 2013-2014. *JAMA* 314, 1871–1873. doi: 10.1001/jama.2015.13802

Arnold, C. (2014). Vaping and health: what do we know about e-cigarettes? *Environ. Health Perspect.* 122, A244–A249. doi: 10.1289/ehp.122-A244

Barak, B., and Feng, G. (2016). Neurobiology of social behavior abnormalities in autism and Williams syndrome. *Nat. Neurosci.* 19, 647–655. doi: 10.1038/nn.4276

Benowitz, N. L. (2014). Emerging nicotine delivery products. Implications for public health. *Ann. Am. Thorac. Soc.* 11, 231–235. doi: 10.1513/AnnalsATS.201312-433PS

Blanco-Gandia, M. C., Mateos-Garcia, A., Garcia-Pardo, M. P., Montagud-Romero, S., Rodriguez-Arias, M., Minarro, J., et al. (2015). Effect of drugs of abuse on social behaviour: a review of animal models. *Behav. Pharmacol.* 26, 541–570. doi: 10.1097/FBP.0000000000000162

Camargo, A., Dalmagro, A. P., Wolin, I. A. V., Siteneski, A., Zeni, A. L. B., and Rodrigues, A. L. S. (2021). A low-dose combination of ketamine and guanosine counteracts corticosterone-induced depressive-like behavior and hippocampal synaptic impairments via mTORC1 signaling. *Prog. Neuropsychopharmacol. Biol. Psychiatry* 111:110371. doi: 10.1016/j.pnpbp.2021.110371

Can, A., Dao, D. T., Terrillion, C. E., Piantadosi, S. C., Bhat, S., and Gould, T. D. (2012). The tail suspension test. *J. Vis. Exp.* 2012:e3769. doi: 10.3791/3769

Chaube, B., and Bhat, M. K. (2016). AMPK, a key regulator of metabolic/energy homeostasis and mitochondrial biogenesis in cancer cells. *Cell Death Dis.* 7:e2044. doi: 10.1038/cddis.2015.404

Chen, H., Wang, B., Li, G., Steele, J. R., Stayte, S., Vissel, B., et al. (2021). Brain health is independently impaired by E-vaping and high-fat diet. *Brain Behav. Immun.* 92, 57–66. doi: 10.1016/j.bbi.2020.11.028

Conti, A. A., McLean, L., Tolomeo, S., Steele, J. D., and Baldacchino, A. (2019). Chronic tobacco smoking and neuropsychological impairments: A systematic review and meta-analysis. *Neurosci. Biobehav. Rev.* 96, 143–154. doi: 10.1016/j.neubiorev.2018.11.017

Cullen, K. A., Gentzke, A. S., Sawdey, M. D., Chang, J. T., Anic, G. M., Wang, T. W., et al. (2019a). e-Cigarette use among youth in the united states, 2019. *JAMA* 322, 2095–2103. doi: 10.1001/jama.2019.18387

Cullen, K. A., Liu, S. T., Bernat, J. K., Slavit, W. I., Tynan, M. A., King, B. A., et al. (2019b). Flavored tobacco product use among middle and high school students - united states, 2014-2018. *MMWR Morb. Mortal. Wkly Rep.* 68, 839–844. doi: 10.15585/mmwr.mm6839a2

Culmsee, C., Michels, S., Scheu, S., Arolt, V., Dannlowski, U., and Alferink, J. (2018). Mitochondria, microglia, and the immune system-how are they linked in affective disorders? *Front. Psychiatry* 9:739. doi: 10.3389/fpsyt.2018.00739

Debarba, L. K., Mulka, A., Lima, J. B. M., Didyuk, O., Fakhoury, P., Koshko, L., et al. (2020). Acarbose protects from central and peripheral metabolic imbalance induced by benzene exposure. *Brain Behav. Immun.* 89, 87–99. doi: 10.1016/j.bbi.2020.05.073

Deochand, C., Tong, M., Agarwal, A. R., Cadenas, E., and De la Monte, S. M. (2016). Tobacco smoke exposure impairs brain insulin/igf signaling: potential co-factor role in neurodegeneration. *J. Alzheimers Dis.* 50, 373–386. doi: 10.3233/JAD-150664

Donde, C., Brunelin, J., Mondino, M., Cellard, C., Rolland, B., and Haesebaert, F. (2020). The effects of acute nicotine administration on cognitive and early

sensory processes in schizophrenia: a systematic review. *Neurosci. Biobehav. Rev.* 118, 121–133. doi: 10.1016/j.neubiorev.2020.07.035

Eichenbaum, H. (2017). Prefrontal-hippocampal interactions in episodic memory. *Nat. Rev. Neurosci.* 18, 547–558. doi: 10.1038/nrn.2017.74

Fairchild, A. L., Lee, J. S., Bayer, R., and Curran, J. (2018). E-Cigarettes and the harm-reduction continuum. *N Engl. J. Med.* 378, 216–219. doi: 10.1056/NEJMp1711991

Feder, A., Nestler, E. J., and Charney, D. S. (2009). Psychobiology and molecular genetics of resilience. *Nat. Rev. Neurosci.* 10, 446–457. doi: 10.1038/nrn2649

Ferrara, N. C., Trask, S., and Rosenkranz, J. A. (2021). Maturation of amygdala inputs regulate shifts in social and fear behaviors: A substrate for developmental effects of stress. *Neurosci. Biobehav. Rev.* 125, 11–25. doi: 10.1016/j.neubiorev.2021.01.021

Fidler, J. A., and West, R. (2009). Self-perceived smoking motives and their correlates in a general population sample. *Nicotine Tob Res.* 11, 1182–1188. doi: 10.1093/ntr/ntp120

Ge, L., D'Souza, R. S., Oh, T., Vincent, A., Mohabbat, A. B., Eldrige, J., et al. (2019). Tobacco use in fibromyalgia is associated with cognitive dysfunction: a prospective questionnaire study. *Mayo Clin. Proc. Innov. Qual. Outcom.* 3, 78–85. doi: 10.1016/j.mayocpiqo.2018.12.002

Gravely, S., Cummings, K. M., Hammond, D., Lindblom, E., Smith, D. M., Martin, N., et al. (2020). The Association of E-cigarette flavors with satisfaction, enjoyment, and trying to quit or stay abstinent from smoking among regular adult vapers from canada and the united states: findings from the 2018 ITC Four Country Smoking and Vaping Survey. *Nicotine Tob Res.* 22, 1831–1841. doi: 10.1093/ntr/ntaa095

Gross, C., and Hen, R. (2004). The developmental origins of anxiety. *Nat. Rev. Neurosci.* 5, 545–552. doi: 10.1038/nrn1429

Hartmann-Boyce, J., McRobbie, H., Lindson, N., Bullen, C., Begh, R., Theodoulou, A., et al. (2020). Electronic cigarettes for smoking cessation. *Cochrane Database Syst. Rev.* 10:CD010216. doi: 10.1002/14651858.CD010216.pub4

Herzig, S., and Shaw, R. J. (2018). AMPK: guardian of metabolism and mitochondrial homeostasis. *Nat. Rev. Mol. Cell Biol.* 19, 121–135. doi: 10.1038/nrm.2017.95

Hsu, G., Sun, J. Y., and Zhu, S. H. (2018). Evolution of Electronic Cigarette Brands From 2013-2014 to 2016-2017: Analysis of Brand Websites. *J. Med. Internet. Res.* 20:e80. doi: 10.2196/jmir.8550

Jing, W., Zhang, T., Liu, J., Huang, X., Yu, Q., Yu, H., et al. (2021). A circuit of COCH neurons encodes social-stress-induced anxiety via MTF1 activation of Cacna1h. *Cell Rep.* 37:110177. doi: 10.1016/j.celrep.2021.110177

Joo, H., Lim, M. H., Ha, M., Kwon, H. J., Yoo, S. J., Choi, K. H., et al. (2017). Secondhand Smoke exposure and low blood lead levels in association with attention-deficit hyperactivity disorder and its symptom domain in children: a community-based case-control study. *Nicotine Tob Res.* 19, 94–101. doi: 10.1093/ntr/ntw152

Kaisar, M. A., Villalba, H., Prasad, S., Liles, T., Sifat, A. E., Sajja, R. K., et al. (2017). Offsetting the impact of smoking and e-cigarette vaping on the cerebrovascular system and stroke injury: Is Metformin a viable countermeasure? *Redox Biol.* 13, 353–362. doi: 10.1016/j.redox.2017.06.006

Kalkhoran, S., and Glantz, S. A. (2016). E-cigarettes and smoking cessation in real-world and clinical settings: a systematic review and meta-analysis. *Lancet Respir. Med.* 4, 116–128. doi: 10.1016/S2213-2600(15)00521-4

Kaur, G., Gaurav, A., Lamb, T., Perkins, M., Muthumalage, T., and Rahman, I. (2020). Current perspectives on characteristics, compositions, and toxicological effects of e-cigarettes containing tobacco and menthol/mint flavors. *Front. Physiol.* 11:613948. doi: 10.3389/fphys.2020.613948

Kelly, M. E., Duff, H., Kelly, S., McHugh Power, J. E., Brennan, S., Lawlor, B. A., et al. (2017). The impact of social activities, social networks, social support and social relationships on the cognitive functioning of healthy older adults: a systematic review. *Syst. Rev.* 6:259. doi: 10.1186/s13643-017-0632-2

King, M., Jones, R., Petersen, I., Hamilton, F., and Nazareth, I. (2020). Cigarette smoking as a risk factor for schizophrenia or all non-affective psychoses. *Psychol. Med.* 2020, 1–9. doi: 10.1017/S0033291720000136

Kronfol, Z., and Remick, D. G. (2000). Cytokines and the brain: implications for clinical psychiatry. *Am. J. Psychiatry* 157, 683–694. doi: 10.1176/appi.ajp.157.5.683

Kuiper, J. S., Oude Voshaar, R. C., Zuidema, S. U., Stolk, R. P., Zuidersma, M., and Smidt, N. (2017). The relationship between social functioning and subjective memory complaints in older persons: a population-based longitudinal cohort study. *Int. J. Geriatr. Psychiatry* 32, 1059–1071. doi: 10.1002/gps.4567

Lawrence, D., Johnson, S. E., Mitrou, F., Lawn, S., and Sawyer, M. (2021). Tobacco smoking and mental disorders in Australian adolescents. *Aust. NZ J. Psychiatry* 2021:9617. doi: 10.1177/00048674211009617

Leventhal, A., Dai, H., Barrington-Trimis, J., and Sussman, S. (2021). 'Ice' flavoured e-cigarette use among young adults. *Tob Control* 2021:56416. doi: 10.1136/tobaccocontrol-2020-056416

Leventhal, A. M., Miech, R., Barrington-Trimis, J., Johnston, L. D., O'Malley, P. M., and Patrick, M. E. (2019). Flavors of e-cigarettes used by youths in the United States. *JAMA* 322, 2132–2134. doi: 10.1001/jama.2019.17968

Levin, E. D., Hall, B. J., and Rezvani, A. H. (2015). Heterogeneity across brain regions and neurotransmitter interactions with nicotinic effects on memory function. *Curr. Top Behav. Neurosci.* 23, 87–101. doi: 10.1007/978-3-319-13665-3_4

Li, R., Zhang, J., Wu, X., Wen, X., and Han, B. (2020). Brain-wide resting-state connectivity regulation by the hippocampus and medial prefrontal cortex is associated with fluid intelligence. *Brain Struct. Funct.* 225, 1587–1600. doi: 10.1007/s00429-020-02077-8

Liu, S., Xiu, J., Zhu, C., Meng, K., Li, C., Han, R., et al. (2021). Fat mass and obesity-associated protein regulates RNA methylation associated with depression-like behavior in mice. *Nat. Commun.* 12:6937. doi: 10.1038/s41467-021-27044-7

Liu, Y., Li, H., Wang, J., Xue, Q., Yang, X., Kang, Y., et al. (2020). Association of cigarette smoking with cerebrospinal fluid biomarkers of neurodegeneration, neuroinflammation, and oxidation. *JAMA Netw. Open* 3:e2018777. doi: 10.1001/jamanetworkopen.2020.18777

Lupien, S. J., McEwen, B. S., Gunnar, M. R., and Heim, C. (2009). Effects of stress throughout the lifespan on the brain, behaviour and cognition. *Nat. Rev. Neurosci.* 10, 434–445. doi: 10.1038/nrn2639

Mahmood, H. M., Aldhalaan, H. M., Alshammari, T. K., Alqasem, M. A., Alshammari, M. A., Albekairi, N. A., et al. (2020). The role of nicotinic receptors in the attenuation of autism-related behaviors in a murine BTBR T + tf/J Autistic Model. *Autism Res.* 13, 1311–1334. doi: 10.1002/aur.2342

Malik, A., Khan, M. I., Karbasian, H., Nieminen, M., Ammad-Ud-Din, M., and Khan, S. (2021). Modelling public sentiments about juul flavors on twitter through machine learning. *Nicotine Tob Res.* 2021:98. doi: 10.1093/ntr/ntab098

Martin, L. M., and Sayette, M. A. (2018). A review of the effects of nicotine on social functioning. *Exp. Clin. Psychopharmacol.* 26, 425–439. doi: 10.1037/pha0000208

Martin Rios, R., Lopez-Torrecillas, F., and Martin Tamayo, I. (2021). Executive functions in tobacco use disorder: new challenges and opportunities. *Front. Psychiatry* 12:586520. doi: 10.3389/fpsyt.2021.586520

McCarthy, M. (2017). US plan gives greater role to electronic cigarettes in tobacco harm reduction. *BMJ* 358:j3689. doi: 10.1136/bmj.j3689

Mottolese, R., Redoute, J., Costes, N., Le Bars, D., and Sirigu, A. (2014). Switching brain serotonin with oxytocin. *Proc. Natl. Acad. Sci. USA* 111, 8637–8642. doi: 10.1073/pnas.1319810111

Padilla-Coreano, N., Bolkan, S. S., Pierce, G. M., Blackman, D. R., Hardin, W. D., Garcia-Garcia, A. L., et al. (2016). Direct ventral hippocampal-prefrontal input is required for anxiety-related neural activity and behavior. *Neuron* 89, 857–866. doi: 10.1016/j.neuron.2016.01.011

Perry, B. L., McConnell, W. R., Coleman, M. E., Roth, A. R., Peng, S., and Apostolova, L. G. (2021). Why the cognitive "fountain of youth" may be upstream: Pathways to dementia risk and resilience through social connectedness. *Alzheimers Dement.* 2021:12443. doi: 10.1002/alz.12443

Pham, T., Williams, J. V. A., Bhattarai, A., Dores, A. K., Isherwood, L. J., and Patten, S. B. (2020). Electronic cigarette use and mental health: A Canadian population-based study. *J. Affect. Disord.* 260, 646–652. doi: 10.1016/j.jad.2019.09.026

Polacchini, A., Girardi, D., Falco, A., Zanotta, N., Comar, M., De Carlo, N. A., et al. (2018). Distinct CCL2, CCL5, CCL11, CCL27, IL-17, IL-6, BDNF serum profiles correlate to different job-stress outcomes. *Neurobiol. Stress* 8, 82–91. doi: 10.1016/j.ynstr.2018.02.002

Preston, A. R., and Eichenbaum, H. (2013). Interplay of hippocampus and prefrontal cortex in memory. *Curr. Biol.* 23, R764–R773. doi: 10.1016/j.cub.2013.05.041

Prochaska, J. J. (2019). The public health consequences of e-cigarettes: a review by the National Academies of Sciences. A call for more research, a need for regulatory action. *Addiction* 114, 587–589. doi: 10.1111/add.14478

Qi, S., Schumann, G., Bustillo, J., Turner, J. A., Jiang, R., Zhi, D., et al. (2021). Reward processing in novelty seekers: a transdiagnostic psychiatric imaging biomarker. *Biol. Psychiatry* 2021:11. doi: 10.1016/j.biopsych.2021.01.011

Ramamurthi, D., Gall, P. A., Ayoub, N., and Jackler, R. K. (2016). Leading-Brand advertisement of quitting smoking benefits for E-Cigarettes. *Am. J. Public Health* 106, 2057–2063. doi: 10.2105/AJPH.2016.303437

Rambaran, K., Sakhamuri, S., and Pereira, L. P. (2019). E-cigarettes: banning flavours is better than an outright ban. *Lancet Respir. Med.* 7:e37. doi: 10.1016/S2213-2600(19)30359-5

Rickard, B. P., Ho, H., Tiley, J. B., Jaspers, I., and Brouwer, K. L. R. (2021). E-Cigarette flavoring chemicals induce cytotoxicity in HepG2 Cells. *ACS Omega* 6, 6708–6713. doi: 10.1021/acsomega.0c05639

Rom, O., Pecorelli, A., Valacchi, G., and Reznick, A. Z. (2015). Are E-cigarettes a safe and good alternative to cigarette smoking? *Ann. NY Acad. Sci.* 1340, 65–74. doi: 10.1111/nyas.12609

Rose, S. W., Johnson, A. L., Glasser, A. M., Villanti, A. C., Ambrose, B. K., Conway, K., et al. (2020). Flavour types used by youth and adult tobacco users in wave 2 of the Population Assessment of Tobacco and Health (PATH) Study 2014-2015. *Tob Control* 29, 432–446. doi: 10.1136/tobaccocontrol-2018-054852

Ruszkiewicz, J. A., Zhang, Z., Goncalves, F. M., Tizabi, Y., Zelikoff, J. T., and Aschner, M. (2020). Neurotoxicity of e-cigarettes. *Food Chem. Toxicol.* 138:111245. doi: 10.1016/j.fct.2020.111245

Sakurai, T. (2021). Social processes and social environment during development. *Semin Cell Dev. Biol.* 2021:16. doi: 10.1016/j.semcdb.2021.09.016

Smith, T. T., Heckman, B. W., Wahlquist, A. E., Cummings, K. M., and Carpenter, M. J. (2020). The Impact of E-liquid propylene glycol and vegetable glycerin ratio on ratings of subjective effects, reinforcement value, and use in current smokers. *Nicotine Tob Res.* 22, 791–797. doi: 10.1093/ntr/ntz130

Villanti, A. C., Johnson, A. L., Ambrose, B. K., Cummings, K. M., Stanton, C. A., Rose, S. W., et al. (2017). Flavored tobacco product use in youth and adults: findings from the first wave of the PATH Study (2013-2014). *Am. J. Prev. Med.* 53, 139–151. doi: 10.1016/j.amepre.2017.01.026

Wei, D., Talwar, V., and Lin, D. (2021). Neural circuits of social behaviors: Innate yet flexible. *Neuron* 109, 1600–1620. doi: 10.1016/j.neuron.2021.02.012

Wei, S., Wang, D., Wei, G., Wang, J., Zhou, H., Xu, H., et al. (2020). Association of cigarette smoking with cognitive impairment in male patients with chronic schizophrenia. *Psychopharmacology* 237, 3409–3416. doi: 10.1007/s00213-020-05621-w

Yamamuro, K., Bicks, L. K., Leventhal, M. B., Kato, D., Im, S., Flanigan, M. E., et al. (2020). A prefrontal-paraventricular thalamus circuit requires juvenile social experience to regulate adult sociability in mice. *Nat. Neurosci.* 23, 1240–1252. doi: 10.1038/s41593-020-0695-6

Yu, R., Deochand, C., Krotow, A., Leao, R., Tong, M., Agarwal, A. R., et al. (2016). Tobacco Smoke-induced brain white matter myelin dysfunction: potential co-factor role of smoking in neurodegeneration. *J. Alzheimers Dis.* 50, 133–148. doi: 10.3233/JAD-150751

Zare, S., Nemati, M., and Zheng, Y. (2018). A systematic review of consumer preference for e-cigarette attributes: Flavor, nicotine strength, and type. *PLoS One* 13:e0194145. doi: 10.1371/journal.pone.0194145

Zhou, Z., Liu, X., Chen, S., Zhang, Z., Liu, Y., Montardy, Q., et al. (2019). A VTA GABAergic neural circuit mediates visually evoked innate defensive responses. *Neuron* 47:e476. doi: 10.1016/j.neuron.2019.05.027

Zhu, S. H., Sun, J. Y., Bonnevie, E., Cummins, S. E., Gamst, A., Yin, L., et al. (2014). Four hundred and sixty brands of e-cigarettes and counting: implications for product regulation. *Tob Control* 23, 3–9. doi: 10.1136/tobaccocontrol-2014-051670

Conflict of Interest: The authors declare that the research was conducted in the absence of any commercial or financial relationships that could be construed as a potential conflict of interest.

Publisher's Note: All claims expressed in this article are solely those of the authors and do not necessarily represent those of their affiliated organizations, or those of the publisher, the editors and the reviewers. Any product that may be evaluated in this article, or claim that may be made by its manufacturer, is not guaranteed or endorsed by the publisher.

frontiers in Molecular Neuroscience

ORIGINAL RESEARCH
published: 29 March 2022
doi: 10.3389/fnmol.2022.874080

Candidate Chinese Herbal Medicine Alleviates Methamphetamine Addiction *via* Regulating Dopaminergic and Serotonergic Pathways

Qin Ru[1,2], Qi Xiong[1], Xiang Tian[1], Congyue Xu[1], Can Li[1], Lin Chen[2] and Yuxiang Wu[2]**

[1] Wuhan Institutes of Biomedical Sciences, School of Medicine, Jianghan University, Wuhan, China, [2] Department of Health and Physical Education, Jianghan University, Wuhan, China

OPEN ACCESS

Edited by:
Qi Wang,
Southern Medical University, China

Reviewed by:
Zeng Xiao Feng,
Kunming Medical University, China
Mia Ericson,
University of Gothenburg, Sweden
Genshen Zhong,
Xinxiang Medical University, China

***Correspondence:**
Lin Chen
hdycl@126.com
Yuxiang Wu
yxwu@jhun.edu.cn

Specialty section:
This article was submitted to Molecular Signalling and Pathways, a section of the journal Frontiers in Molecular Neuroscience

Received: *11 February 2022*
Accepted: *03 March 2022*
Published: *29 March 2022*

Citation:
Ru Q, Xiong Q, Tian X, Xu C, Li C, Chen L and Wu Y (2022) Candidate Chinese Herbal Medicine Alleviates Methamphetamine Addiction via Regulating Dopaminergic and Serotonergic Pathways. Front. Mol. Neurosci. 15:874080. doi: 10.3389/fnmol.2022.874080

Methamphetamine (METH) addiction and its induced mental disorders have become a severe worldwide problem. A candidate Chinese herbal medicine (CCHM) in our lab had therapeutic effects on METH-induced locomotor sensitization, however, its chemical and pharmacological profiles remain to be elucidated. The current study aimed to investigate the effect of CCHM on conditioned place preference (CPP) induced by METH and screen the main active ingredients and key targets by using network pharmacology and molecular docking methods. Kyoto Encyclopedia of Genes and Genomes (KEGG) enrichment, Gene ontology (GO) analysis and protein-protein interaction (PPI) network were performed to discover the potential mechanisms. Results showed that CCHM could significantly inhibit METH-induced CPP behaviors in mice. A total of 123 components and 43 targets were screened. According to the network pharmacology analysis, ten hub targets including D(2) dopamine receptor (DRD2) and 5-hydroxytryptamine receptor 3A (HTR3A) were screened. GO analysis and KEGG enrichment indicated that mechanisms of CCHM treatment of METH addiction were related to multiple pathways such as dopaminergic synapse and serotoninergic synapse. Western blot results showed that the protein expressions of DRD2 in nucleus accumbens and prefrontal cortex were significantly decreased in METH group, while the protein expressions of HTR3A were significantly increased. These changes caused by METH could be prevented by CCHM pretreatment. The results of molecular docking displayed that the five active ingredients such as (S)-Scoulerine, Hyndarin, and Beta-Sitosterol had good affinities with DRD2 and HTR3A. In conclusion, this study constructed the CCHM's pharmacologic network for treating METH addiction based on the method of network analysis and experimental verification, and analyzed its major active ingredients and potential targets, indicating a new direction for further revealing its mechanisms of effect on METH addiction.

Keywords: Chinese herbal medicine, methamphetamine, addiction, network pharmacology, dopamine, serotonin

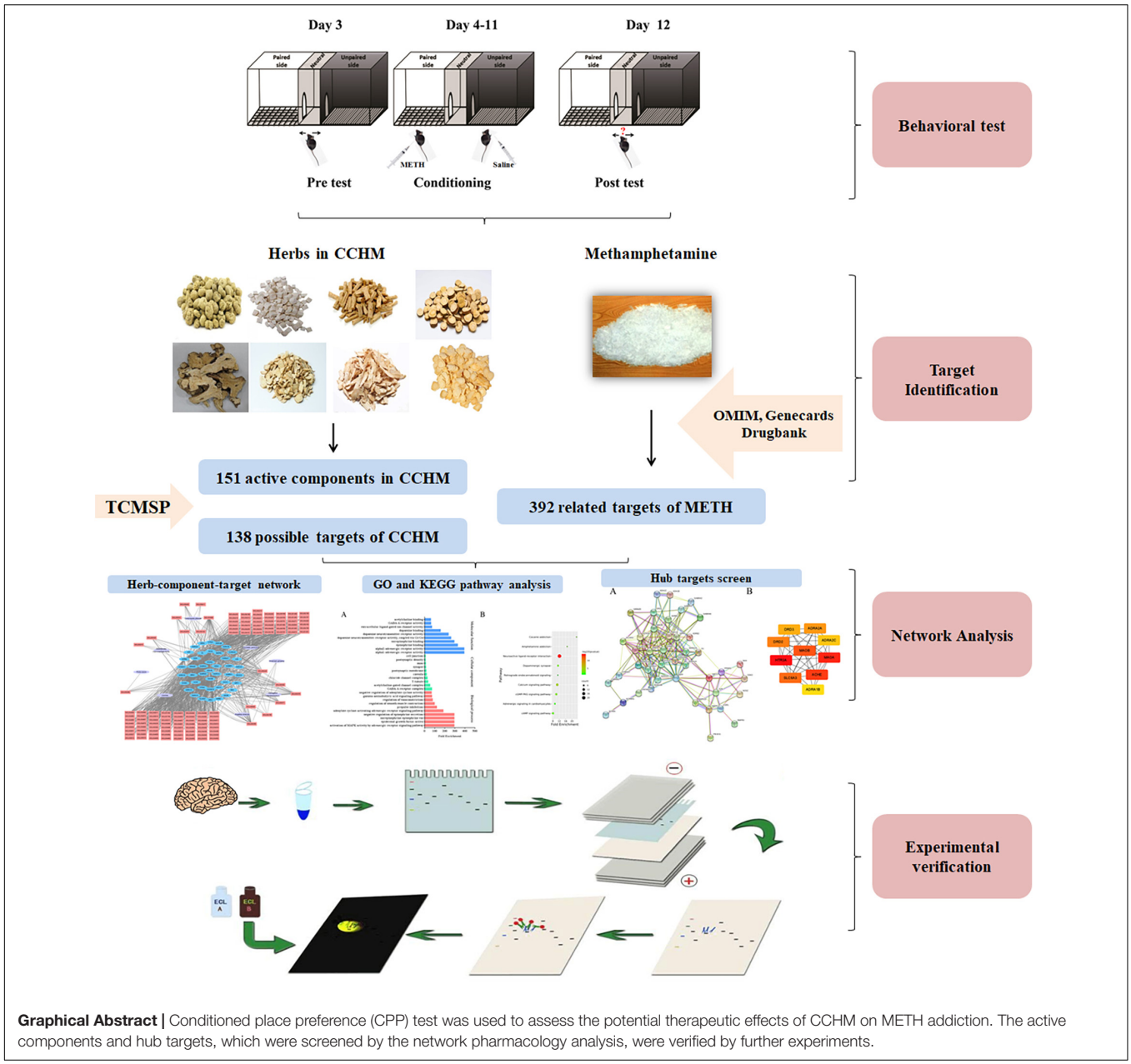

Graphical Abstract | Conditioned place preference (CPP) test was used to assess the potential therapeutic effects of CCHM on METH addiction. The active components and hub targets, which were screened by the network pharmacology analysis, were verified by further experiments.

INTRODUCTION

Drug addiction is a severe worldwide social problem, which has attracted great attention. Compared with drugs extracted from plants such as heroin and cocaine, the proportion of people who abuse amphetamine-type synthetic drugs is increasing year by year. According to reports released by United Nations Office on Drugs and Crime and the Ministry of Public Security of China, methamphetamine (METH) has become the most commonly abused amphetamine-type stimulant in Southeast Asia and North America. METH can easily enter the central nervous system through the blood-brain barrier, so its effect on brain is more evident than its peripheral effect (Paulus and Stewart, 2020). Studies have shown that METH abuse could seriously damage the structure and function of neurons and gliocyte in the prefrontal cortex, nucleus accumbens, hippocampus, and other brain regions of addicts, and cause a variety of central nervous system diseases, such as cognitive impairment, depression, and mental disorders (Zhang et al., 2018; Nie et al., 2020). The brain structure and function of most addicts cannot recover even after a prolonged period of abstinence, and the persistent mental disorders and negative emotions could also trigger the continuous drug-seeking behaviors, which led to relapse (Glasner-Edwards et al., 2009). METH addiction not only seriously affected the physical and mental health of abusers, but also led to crime, which has become a social problem endangering

public security. Although antipsychotic drugs have been used to control the psychiatric symptoms caused by addiction, there is still a lack of drugs with definite efficacy on METH addiction in clinic. Therefore, the research and development of drugs for the prevention and treatment of METH addiction with better efficacy and fewer side effects has become the focus in drug abuse field.

The mechanism of METH addiction remains unclear, and multiple brain regions such as the prefrontal cortex and nucleus accumbens are involved, therefore, traditional Chinese medicine has become the focus of development of anti-addiction drugs due to its multi-system and multi-target mechanism (Chen et al., 2021). Our previous work have shown that a candidate Chinese herbal medicine (CCHM), which was composed of 8 traditional Chinese medicines including *Corydalis yanhusuo* and Codonopsis, could significantly improve the learning and memory impairment induced by METH, and inhibit the acquisition and expression of METH-induced locomotor sensitization (Can et al., 2019; Jiaming et al., 2019). The results of acute and long-term toxicity tests showed that CCHM had no detectable toxic effects (Can, 2019). However, as a Chinese herbal compound, the composition of CCHM is complex. A large number of experiments are still needed to analyze its main active ingredients and possible mechanisms. Based on the theory of systems biology, network pharmacology has the characteristics of systematic and holistic, and it is similar to the mechanism of traditional Chinese medicine in treating diseases. Network pharmacology could reveal the complex biological network relationships between drugs, targets, and diseases, analyze and predict the pharmacological mechanism of candidate drugs (Guo et al., 2019). Therefore, this study aimed to analyze the main active ingredients and critical targets of CCHM in the treatment of METH addiction based on the network pharmacology and molecular docking, and to provide the evidence for the clinical application of CCHM.

MATERIALS AND METHODS

Animals

Male C57BL/6 mice (2 months old, weighing 18∼22 g) were purchased from Beijing Charles River Laboratories (Beijing, China). Mice were housed in a temperature-controlled room with a humidity of 45∼55% and subjected to a 12-h cycle of alternating light and dark. All mice had free access to food and water, and were pre-adapted to the environment for at least 3 days before the experiment. All experiment procedures were approved by the Ethics Committee of Jianghan University. As shown in **Figure 1A**, the mice were randomly divided into four groups: the control group, the METH group, CCHM low group, and CCHM high group. METH was offered by Hubei Public Security Bureau and was dissolved in saline, and CCHM was decocted and condensed into extract before use. Mice were intraperitoneally injected with METH (2 mg/kg) or saline following 1 h intragastric administration of CCHM (14.12, 56.48 g/kg) or saline. The dosage of CCHM was selected based on our published articles (Can et al., 2019).

The Conditioned Place Preference Apparatus and Procedure

The conditioned place preference (CPP) facility was brought from Shanghai Xinruan Information Technology Co., Ltd. (Shanghai, China) and comprised three compartments. One chamber had a grid floor and black walls (L × W × H: 35 cm × 35 cm × 35 cm). Another same-sized chamber had a mesh floor and white walls. The middle chamber had a flat, gray floor and gray walls (L × W × H: 15 cm × 35 cm × 35 cm) and is connected to the other two compartments by removable doors. The white and black chamber had a ceiling light and camera, respectively. The general activity in the facility was monitored by video, and the time spent in each chamber was recorded using XR-XT401 software.

The CPP procedure used in this experiment was performed as previously described (Yang G. et al., 2020). The pretreatment period lasted from day 1 to day 3. Mice were placed in the middle chamber and then moved freely between the black and white chambers for 15 min per day. The time spent in each chamber on the third day was used as pre-processing data. The most visited chamber (black chamber) was designated as the preferred compartment and the other compartment (white chamber) was defined as drug compartment. Each animal received individual CPP training. The CPP training period lasted for 8 days (day 4∼day 11) and included four METH sessions and four saline sessions. The saline- and drug-paired compartments were separated by closed doors. On day 4, 6, 8, and 10, mice in METH or CCHM group were pretreated with saline or CCHM for 1 h and then confined to a drug-paired chamber (white chamber) for 1 h after intraperitoneally injected with 2 mg/kg METH. On days 5, 7, 9, and 11, the mice in METH or CCHM group were given saline or CCHM respectively and confined to the saline paired chamber (black chamber) for 1 h after saline injection. After each session, the floor and walls of each chamber were wiped with 75% ethanol. On day 12, the post-adaptation test was conducted for 15 min, and each mouse was placed in the middle chamber and then moved freely between the black and white chambers. Preference (CPP score) was calculated by subtracting the time spent in the white chamber on day 3 from the time spent in the white chamber on day 12 (Yang C. et al., 2020). CPP score reflects the difference in the time spent in the post-conditioning and pre-conditioning phases of METH.

Identification of Candidate Components in Candidate Chinese Herbal Medicine

Candidate Chinese herbal medicine was composed of eight Chinese medicinal herbs, including *C. yanhusuo*, *Poria cocos*, *Codonopsis pilosula*, Licorice, *Atractylodes macrocephala* Koidz, *Astragalus membranaceus*, *Angelica sinensis,* and American ginseng. The components of CCHM were retrieved from Traditional Chinese medicine system pharmacology (TCMSP) database.[1] Oral Chinese medicine must overcome the obstacles of absorption, distribution, metabolism, and excretion (ADME) process in order to be effective, so oral bioavailability (OB) is one

[1]http://tcmspw.com/tcmsp.php

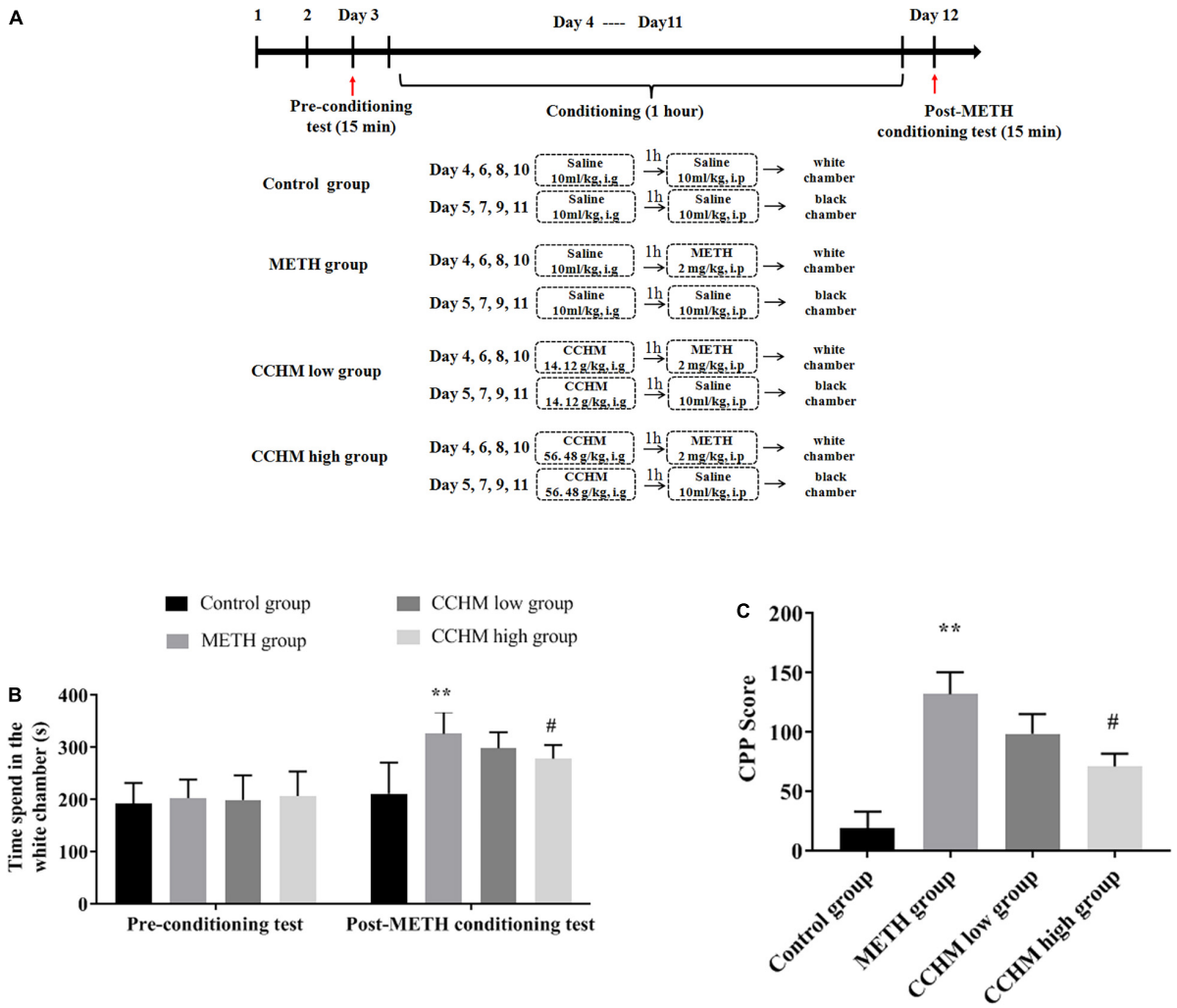

FIGURE 1 | Effect of candidate Chinese herbal medicine (CCHM) on Methamphetamine (METH)-induced conditioned place preference (CPP) in mice. **(A)** The experiment procedure of CPP test. Mice received METH (2 mg/kg, i.p) or saline (10 ml/kg, i.p) injections following 1 h pretreatments of CCHM (14.12, 56.48 g/kg, i.g) or saline (10 ml/kg, i.g) treatments. **(B)** Time spent in the white chamber was collected before and after METH abuse. **(C)** CPP score was calculated by subtracting the time spent in the drug-paired compartment in the pre-conditioning test from that after METH exposure. Data were presented as mean ± SE, $^{**}p < 0.01$, compared with control group; $^{\#}p < 0.05$, compared with METH group, $n = 10$.

of the most important pharmacokinetic parameters in ADME. High OB is usually an important index for determining drug similarity (DL) of active substances (Guo et al., 2019). Substances with OB no less than 30% are considered to have a higher OB. DL index, as a qualitative concept used to estimate the medicinal properties of molecules in drug design, can be used for rapid screening of active substances (Tao et al., 2013; He et al., 2019). In the Drugbank database, the average DL index is 0.18. Substances with a DL index no less than 0.18 have higher medicinal properties. Therefore, compounds with OB $\geq$ 30% and DL index $\geq$ 0.18 and blood brain barrier (BBB) ≥ -0.3 in CCHM were selected as active substances in this study. The possible targets of the active substances of CCHM were searched from TCMSP database. The Uniprot database[2] and the bioDBnet website[3] were used to verify the gene symbols corresponding to the possible targets.

Screening of Possible Targets of Methamphetamine Addiction

Potential targets involved in METH addiction were collected from OMIM,[4] Drugbank,[5] and Genecards[6] databases. Potential targets from different databases were combined and the duplicates has been deleted.

[2]http://www.Unitprot.org/

[3]https://biodbnet-abcc.ncifcrf.gov/

[4]https://www.omim.org/

[5]https://www.drugbank.ca/

[6]https://www.genecards.org/

Network Analysis of Active Compounds and Potential Targets

The potential targets of active compounds in CCHM were mapped with METH addiction-related targets on the Bioinformatics and Evolutionary Genomics website.[7] Cytoscape 3.8.0. software was used to construct the "herb-compound-target" network (Han et al., 2020). In these graphical networks, the compounds and proteins were expressed as nodes, whereas the compound-target interactions were expressed as edges.

Network Analysis of Protein-Protein Interaction

Potential targets of CCHM on METH addiction were analyzed by online STRING 11.0[8] to construct protein-protein interaction (PPI) network. The network was visualized with Cytoscape (3.8.0) and CytoHubba, a plug-in in Cytoscape, to filter the modules from the PPI network and to obtain the most important hub genes based on the degree score.

Gene Ontology and Kyoto Encyclopedia of Genes and Genomes Enrichment of Hub Genes

To further characterize the molecular mechanism of CCHM on METH addiction, the DAVID website[9] was used to conduct the GO analysis and KEGG enrichment of hub targets. Top terms of GO analysis and KEGG enrichment with thresholds of p-values ≤ 0.05 were chosen in functional annotation clustering.

Literature Verification

Literature retrieval was used to excavate and analyze the active components and possible mechanisms of CCHM in the treatment of METH addiction. This may provide literature verification for prediction results of the network pharmacology.

Western Blotting Analysis

Mice were sacrificed by cervical dislocation under anesthesia after behavioral testing. Protein extracts in nucleus accumbens and prefrontal cortex were isolated, lysed, and the supernatant was collected after centrifugation. BCA Protein Assay Kit was used to detect the concentration of protein extracts. Protein samples were separated and electroblotted onto the PVDF membrane. After blocking, membranes were incubated with primary antibodies followed by a horseradish peroxide conjugated secondary antibody. Enhanced chemiluminescence was used to visualize the band, and the intensity of each sample was determined quantitatively using Image J. Actin was used as loading control, and the results were normalized to the control group.

[7]http://bioinformatics.psb.ugent.be/webtools/Venn/

[8]https://string-db.org/

[9]https://david.ncifcrf.gov/

Molecule Docking of Main Active Compounds of Candidate Chinese Herbal Medicine With Hub Targets

The amino acid sequence of the two hub targets D(2) dopamine receptor (DRD2) and 5-hydroxytryptamine receptor 3A (HTR3A) were downloaded from the PDB protein structure database.[10] Furthermore, AutoDock v.4.2.6 was used to add the hydrogens, calculate charges, and merge the non-polar hydrogens of protein structure (Zulkipli et al., 2020). Next, the protein file was saved in PDBQT format. The three-dimensional (3D) structures of main active compounds were downloaded from the PubChem structure database.[11] The SDF format of main active compounds was converted to PDB format using OpenBabel 2.4.1 (Kumar et al., 2020). AutoDock v.4.2.6 was used to convert the PDB format of resveratrol to PDBQT format and for molecular docking of main active compounds with hub targets. PyMol software was used to conduct a visual analysis of docking results.

Statistical Analysis

Statistical analysis was processed with SPSS 23.0 and Prism 8 software. Data were shown as the mean ± SE and analyzed using one-way ANOVA and LSD *post-hoc* test. Differences between groups were considered to be statistically significant if values of $p < 0.05$.

RESULTS

Candidate Chinese Herbal Medicine Inhibited Methamphetamine-Induced Conditioned Place Preference Behavior in Mice

Conditioned place preference, a classic model widely used to assess drug-seeking behaviors, was used in this study to assess the preference for visual and tactile cues associated with METH after being administered with varying doses of CCHM. As shown in **Figure 1B**, mice in the control group did not produce motivational effects before or after place conditioning, which set the baseline measurement for the CPP test. METH administration at 2 mg/kg significantly increased preference of white chamber compared to the controls ($p < 0.01$). As shown in **Figure 1C**, compared to the METH group, pretreatment of CCHM reduced METH-induced motivational effects ($p < 0.05$), and CPP scores decreased with the increase of CCHM dose. Taken together, the results suggested that 2 mg/kg of METH was sufficient to induce CPP behaviors, and the co-administration of CCHM attenuated the acquisition of METH-induced CPP in mice.

[10]http://www.rcsb.org/

[11]https://pubchem.ncbi.nlm.nih.gov/

Identification of Bioactive Compounds and Possible Targets in Candidate Chinese Herbal Medicine

A total of 163 compounds in CCHM obtained from TCMSP database met the requirement of OB $\geq$ 30%, DL index $\geq$ 0.18 and BBB ≥ -0.3, and 48 of which belong to *C. yanhusuo*, six to *P. cocos*, 16 to *C. pilosula*, 69 to Licorice, four to *A. macrocephala* Koidz, 12 to *A. membranaceus*, two to *A. sinensis*, and six to American ginseng. After eliminating the overlaps, 151 compounds were chosen as candidate bioactive compounds for further analyses, and the detailed information was shown in **Table 1** and **Supplementary Material 1**. Among the 151 candidate bioactive components, 2,492 possible protein targets were retrieved from the TCMSP database. The detailed information was shown in **Supplementary Material 2**. After eliminating the overlaps, 138 protein targets were obtained for further analyses.

Targets Identification of Candidate Chinese Herbal Medicine on Methamphetamine Addiction

Sixty METH addiction-related targets were collected from OMIM, 356 targets were collected from the Genecards database, and 11 targets were obtained from Drugbank database. After eliminating the overlaps, 392 targets were obtained for further analyses. The detailed information was shown in **Supplementary Material 3**. Then, these protein targets of CCHM were mapped with METH addiction-related targets using the Bioinformatics and Evolutionary Genomics website. As a result, 43 proteins were selected, corresponding to 123 active ingredients of CCHM and the detailed information of 43 proteins was shown in **Supplementary Material 4**.

Construction of "Herb-Compound-Target" Network

Cytoscape software was used to construct the of "herb-compound-target" network, as shown in **Figure 2**. Among these bioactive compounds, the top 10 compounds were 7-*O*-Methylisomucronulatol, 7-Methoxy-2-Methylisoflavone, Formononetin, Beta- Sitosterol, *S*-Scoulerine, Isocorypalmine, Leonticine, Medicarpin, Licochalcone, and Hyndarin. The detailed information was shown in **Table 2**. These bioactive components may be the main active compounds of CCHM in treating METH addiction.

TABLE 1 | Information of "Herb-active component-predictive target" for candidate Chinese herbal medicine (CCHM).

Herb	Number of active components	Number of predictive target
Corydalis yanhusuo	48	942
Poria cocos	6	27
Codonopsis pilosula	16	139
Licorice	69	1276
Atractylodes macrocephala Koidz	4	22
Astragalus membranaceus	12	102
Angelica sinensis	2	69
American ginseng	6	65

Gene Ontology and Pathway Enrichment Analysis

To identify the biological characteristics of putative targets of CCHM on METH addiction in detail, the GO and KEGG enrichment of involved targets were conducted *via* the functional annotation tool of DAVID Bioinformatics Resources 6.8. There were 116 terms of biological process (BP), 20 terms of cellular component (CC), and 31 terms of molecular function (MF) in total, which met the requirements of Count $\geq$ 2 and p-value $\leq$ 0.05. The detailed information was shown in **Supplementary Material 5**. The top 10 significantly enriched terms in BP, CC, and MF categories were shown in **Figure 3A**, which indicated that CCHM may regulate neuron functions *via* adrenergic receptor signaling pathway, dopamine neurotransmitter receptor activity, dopamine binding to exert its therapeutic effects on METH addiction. To explore the underlying involved pathways of CCHM on METH addiction, KEGG pathway analysis of involved targets was conducted. The detailed pathway information of CCHM on METH addiction was shown in **Supplementary Material 6**. The top 15 significantly enriched pathways were shown in **Figure 3B**. The neuroactive ligand-receptor interaction pathways exhibited the largest number of involved targets (21 counts).

Screen of Hub Genes

The PPI network of possible targets involved in the treatment of CCHM on METH addiction was constructed using STRING (**Figure 4A**). There were 43 nodes and 200 edges, and the average node degree was 9.3. The average local clustering coefficient was 0.637, and the p-value of PPI enrichment was less than 1.0e-16. To obtain the hub genes in the PPI network, these node pairs were entered into the Cytoscape software. The scores of nodes were calculated by cytoHubba, and the top 10 hub genes were shown in **Figure 4B**.

The hub gene symbols, full names, and functions were shown in **Table 3**. These 10 key targets corresponded to 75 major active components of CCHM. The network diagram of "herb-major active component-hub target" constructed by Cytoscape software was shown in **Figure 5**.

Gene Ontology and Pathway Enrichment Analysis of Hub Genes

The GO analyses and KEGG enrichment of hub genes were conducted *via* DAVID 6.8. There were respectively 51 BP, 5 CC, and 10 MF terms in total, which met the requirements of Count $\geq$ 2 and p-value $\leq$ 0.05. The detailed information was shown in **Supplementary Material 7**. The top enriched terms in BP, CC, and MF categories were shown in **Figure 6**. Among them, the results of BP (**Figure 6A**) showed that the treatment of METH addiction by CCHM was mainly related to adenylate cyclase-activating adrenergic receptor signaling pathway, response to cocaine and dopamine catabolic process. The results of CC

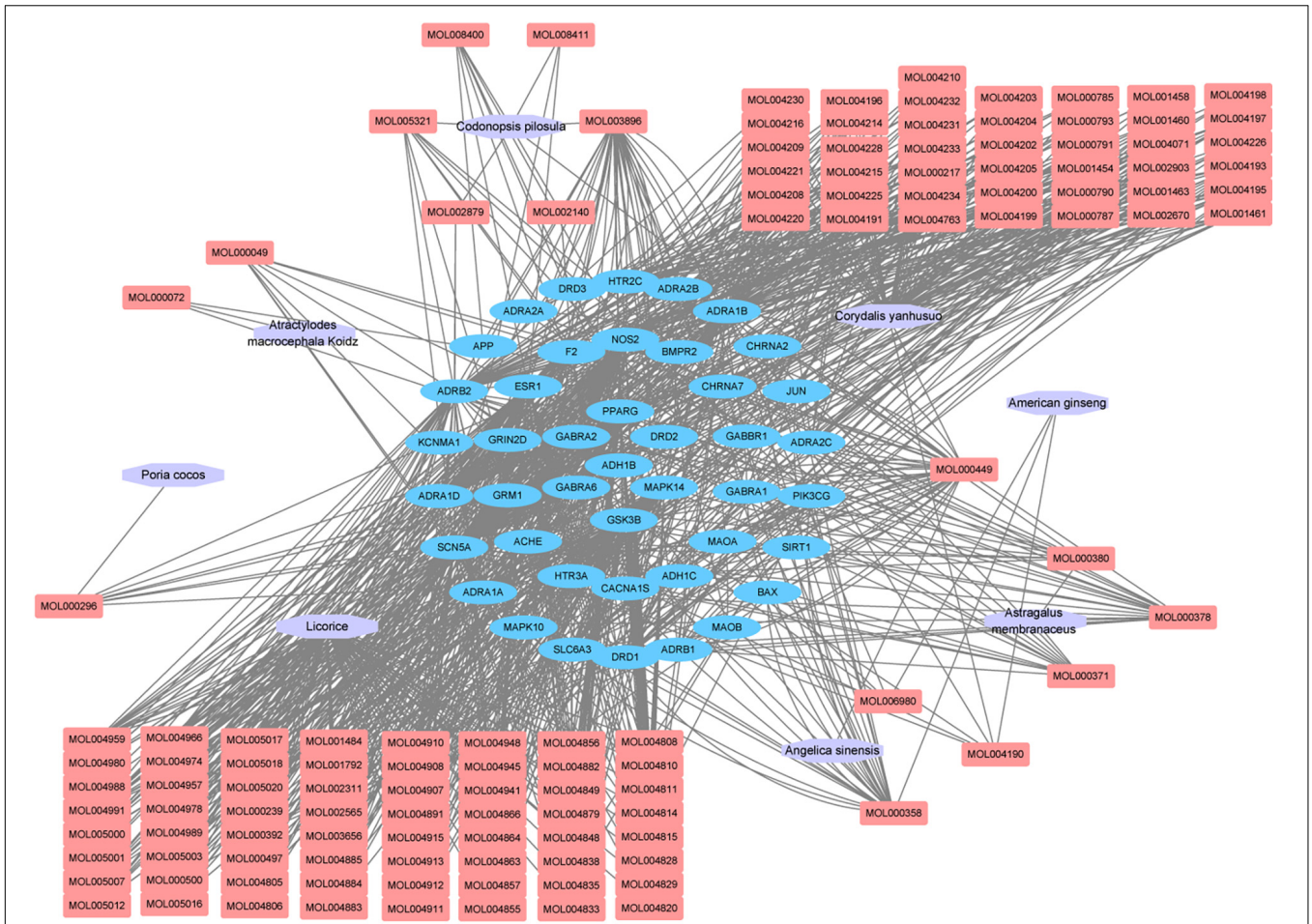

FIGURE 2 | "Herb-compound-target" network of candidate Chinese herbal medicine (CCHM) in the treatment of methamphetamine (METH) addiction. The purple polygons represented different herbs. The pink squares represented active compounds of herbs, and the blue circle represented potential protein targets. The edges represent the interactions between them.

TABLE 2 | Top ten components of candidate Chinese herbal medicine (CCHM) on methamphetamine (METH) addiction.

Molecule name	Number in TCMSP	Number of possible targets in TCMSP	Number of targets mapped with METH addiction	Herb
7-*O*-Methylisomucronulatol	MOL000378	45	17	*Astragalus membranaceus*
7-Methoxy-2-Methylisoflavone	MOL003896	43	17	*Codonopsis pilosula*/Licorice
Formononetin	MOL000392	39	13	Licorice
Beta-Sitosterol	MOL000358	38	12	American ginseng /*Angelica sinensis*
(S)-Scoulerine	MOL000217	36	12	*Corydalis yanhusuo*
Isocorypalmine	MOL000790	36	13	*Corydalis yanhusuo*
Leonticine	MOL004215	35	14	*Corydalis yanhusuo*
Medicarpin	MOL002565	34	12	Licorice
Licochalcone A	MOL000497	32	9	Licorice
Hyndarin	MOL004071	32	12	*Corydalis yanhusuo*

(**Figure 6B**) showed that its treatment was mainly related to plasma membrane, axon, axon terminus, and so on. The results of MF (**Figure 6C**) showed that items including dopamine binding, protein homodimerization activity, and dopamine neurotransmitter receptor activity had close relationship with the treatment of METH addiction by CCHM, and the genes involved were shown in **Table 4**. There were 11 KEGG pathways met the requirements of Count $\geq$ 2 and p-values $\leq$ 0.05. The detailed pathway information of hub genes was shown in **Supplementary Material 8** and **Figure 6D**, which indicated that CCHM may

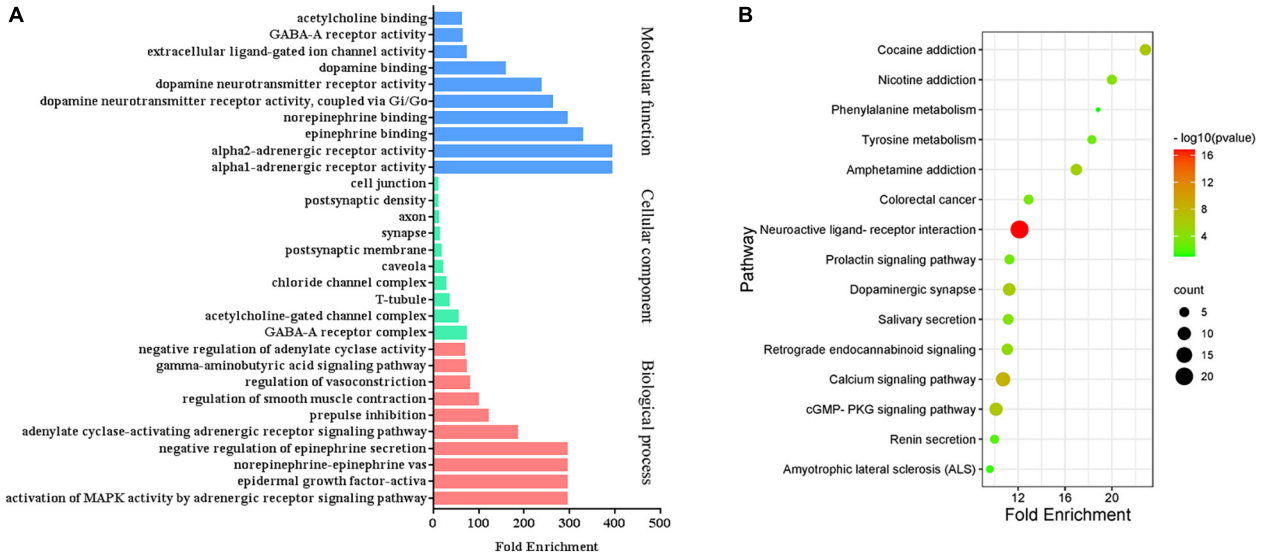

FIGURE 3 | Clustering analysis of possible targets of candidate Chinese herbal medicine (CCHM) in the treatment of methamphetamine (METH) addiction. **(A)** Gene ontology (GO) analysis of the possible targets. **(B)** Kyoto encyclopedia of genes and genomes (KEGG) enrichment analysis of the possible targets. Counts referred to the number of the enriched targets.

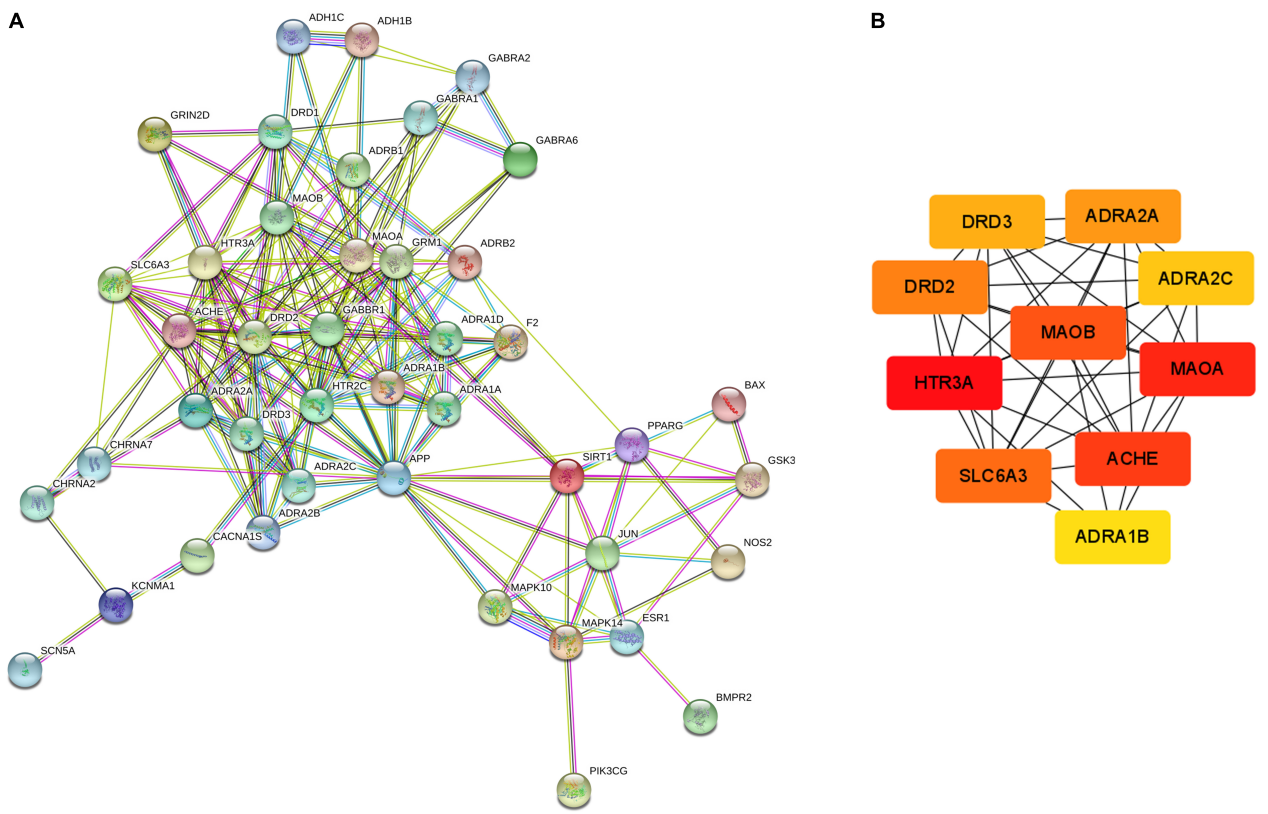

FIGURE 4 | Protein-protein interaction (PPI) network and Hub gene screening map of targets. **(A)** PPI network exported from STRING database. **(B)** Key subnetwork of top 10 nodes analysed by CytoHubba.

TABLE 3 | Detail information of ten hub genes of candidate Chinese herbal medicine (CCHM) on methamphetamine (METH) addiction.

Gene symbol	Full names	Functions
HTR3A	5-hydroxytryptamine receptor 3A	It is one of receptors for 5-hydroxytryptamine (serotonin), which when activated causes fast, depolarizing responses in neurons.
MAOA	Monoamine oxidase A	It catalyzes the oxidative deamination of biogenic and xenobiotic amines and has important functions in the metabolism of neuroactive and vasoactive amines. MAOA preferentially oxidizes biogenic amines such as 5-hydroxytryptamine (5-HT), norepinephrine and epinephrine. MAOB preferentially degrades benzylamine and phenylethylamine.
MAOB	Monoamine oxidase B	
ACHE	Acetylcholinesterase	It terminates signal transduction at the neuromuscular junction by rapid hydrolysis of the acetylcholine released into the synaptic cleft.
DRD2	D(2) dopamine receptor	Dopamine receptor whose activity is mediated by G proteins which inhibit adenylyl cyclase.
ADRA2A	Alpha-2A adrenergic receptor	It mediates the catecholamine-induced inhibition of adenylate cyclase through the action of G proteins.
SLC6A3	Sodium-dependent dopamine transport	It terminates the action of dopamine by its high affinity sodium-dependent reuptake into presynaptic terminals.
DRD3	D(3) dopamine receptor	Dopamine receptor whose activity is mediated by G proteins which inhibit adenylyl cyclase.
ADRA2C	Alpha-2C adrenergic receptor	It mediates the catecholamine-induced inhibition of adenylate cyclase through the action of G proteins.
ADRA1B	Alpha-1B adrenergic receptor	It mediates its action by association with G proteins that activate a phosphatidylinositol-calcium second messenger system.

regulate METH addiction *via* dopaminergic synapse, cocaine addiction, neuroactive ligand-receptor interaction, amphetamine addiction, and serotonergic synapse.

Literature Verification

It was found that Scoulerine could significantly inhibit the CPP behavior and alleviate the anxiety-like behavior caused by METH (Mi et al., 2016). Hyndarin, also known as *L*-tetrahydropalmatine, had significant inhibitory effects on locomotor sensitization, CPP behavior, self-administration behavior, and relapse behavior induced by METH (Zhao et al., 2014; Gong et al., 2016; Su et al., 2020), and hyndarin could also improve METH-induced learning and memory impairment (Cao et al., 2018). Studies have shown that hyndarin could improve METH-induced locomotor sensitization by regulating the activity of 5-HT neurons and the expression of dopamine D3 receptor (Yun, 2014b). These literature reports further validated the network pharmacological prediction results. The relationship between the other eight compounds and METH addiction has not been reported.

Protein Expression Validation of Predicted Target Genes

To further verify the effects of CCHM on the expressions of the potential targets identified *via* network pharmacology, the expression of DRD2 and HTR3A in nucleus accumbens and prefrontal cortex, which play important roles in the reward system, were examined using Western blotting. As shown in **Figures 7A,C**, compared with the control group, the protein level of DRD2 in nucleus accumbens was significantly decreased in the METH group, while the protein expression of HTR3A was greatly increased. Furthermore, pretreatment with CCHM could prevent METH-induced changes of DRD2 and HTR3A protein expressions in nucleus accumbens. Similar results were also found in the prefrontal cortex (**Figures 7B,D**). These results validated that CCHM may inhibit the METH induced abuse mainly through dopaminergic synapse and serotonergic synapse pathways.

Molecular Docking Main Active Compounds and Hub Targets

To screen the main active compounds in CCHM, the docking results of 10 major active components of CCHM acting on DRD2 and HTR3A were shown in **Table 5** and **Figure 8**. Results of molecular docking showed that eight of the 10 major active components had good binding abilities with the potential targets of methamphetamine treatment (DRD2 and HTR3A), and β-Sitosterol, scoulerine, isocorypalmine, medicarpin, and hyndarin had better binding activities with the two target proteins, and the molecular conformational binding was stable, which may affect the downstream signaling pathway to participate in the treatment of METH addiction by binding with the two targets.

DISCUSSION

Methamphetamine is widely abused worldwide, and effective clinical treatment strategy for METH abuse is still urgently needed. CCHM is a traditional Chinese medicine developed for the treatment of METH addiction, and our previous results showed that CCHM could significantly inhibit the acquisition and expression of METH-induced behavioral sensitization (Can et al., 2019), indicating that CCHM had the potential to ameliorate METH addiction. In this study, we found that pre-treatments of CCHM could significantly inhibit METH-induced conditional place preference, which further verified that CCHM had the potential to be developed as a candidate drug for the treatment of METH addiction. However, as a multi-component Chinese herbal compound, the pharmacodynamics basis and mechanism of CCHM are still unclear. In this study, GO and KEGG analysis revealed that CCHM could regulate dopaminergic synapse, serotonergic synapse, and neuroactive

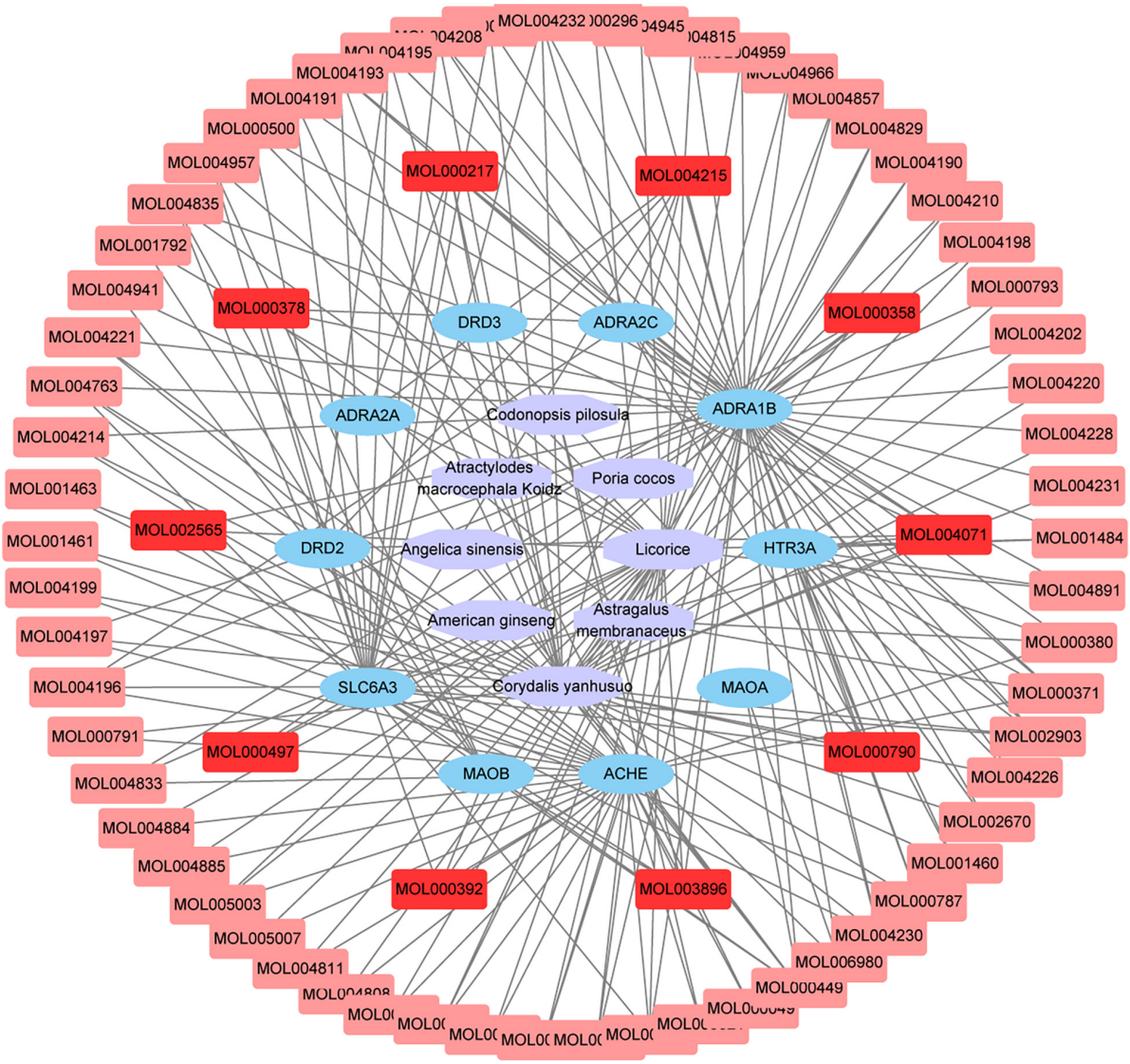

FIGURE 5 | Network chart of "Herb-Main active compounds-hub targets." The purple polygons represented different herbs. The blue circle represented potential protein targets. The pink squares represented active compounds of herbs, and the red squares represented main active compounds. The edges represent the interactions between them.

ligand-receptor interaction pathways. Among 10 hub targets out of 43 genes by PPI analyses, we focused on two most significant genes DRD2 and HTR3A, and performed molecular docking to verify interactions between active compounds of CCHM and DRD2 (or HTR3A). Our results demonstrated the effectiveness of CCHM in the treatment of METH addiction from bioinformatics and experimental perspectives, and provided more evidence for its clinical application.

Long-term abuse of METH would damage the nervous system, resulting in rapid cognitive decline, anxiety, mental disorders, hyperalgesia, depression, etc. (Prakash et al., 2017). At the same time, long-term use of METH also inhibited immune function and increased susceptibility to infection (Harms et al., 2012; Peerzada et al., 2013). CCHM consists of eight Chinese medicinal herbs. *C. yanhusuo* had the effect of promoting blood circulation and relieving pain (Ingram, 2014; Zhou et al., 2019). *A. macrocephala* Koidz, *P. cocos*, American ginseng, Licorice, and *C. pilosula* could improve the body immunity and reduce the damage of METH to the central nervous system (Fu et al., 2016; Tian et al., 2019; Bai et al., 2020). *A. sinensis* and *A. membranaceus* had good sedation and tranquilizing effects (Chen et al., 2004; Park et al., 2009). Therefore, it is reasonable to speculate that different herbs in CCHM may play an effective synergistic role in regulating METH addiction and its various complications, and the cooperation among different components could be achieved from the distinct mode of actions to achieve a complementary pharmacological synergy.

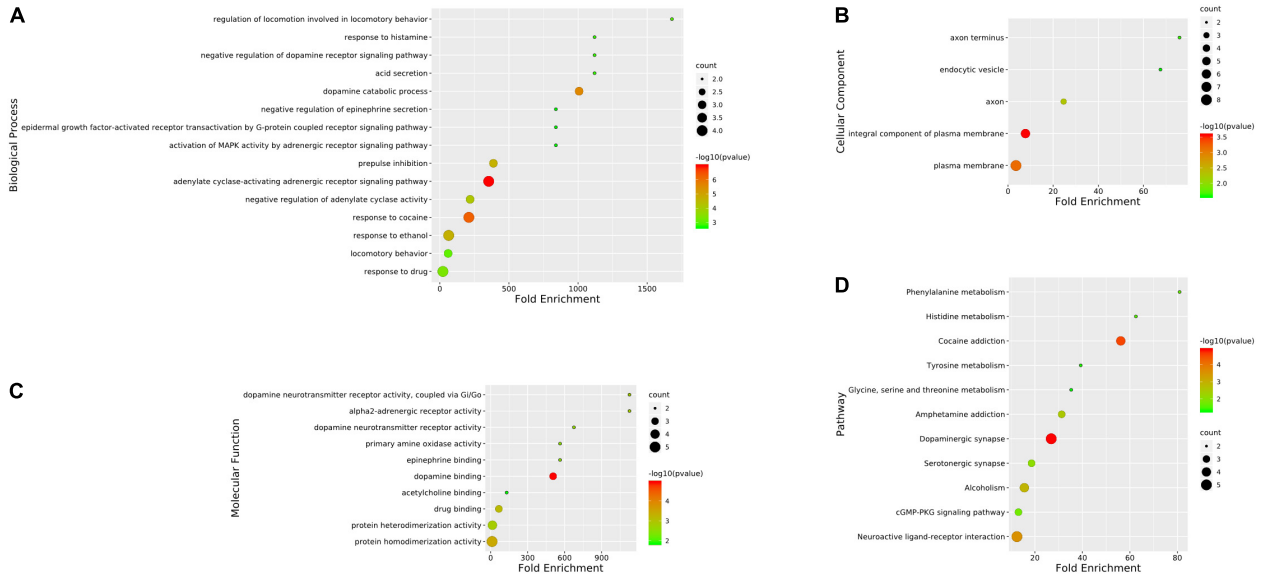

FIGURE 6 | Gene ontology (GO) analysis and kyoto encyclopedia of genes and genomes (KEGG) enrichment of hub targets of candidate Chinese herbal medicine (CCHM) in the treatment of methamphetamine (METH) addiction. **(A)** The top 15 significantly enriched terms in BP enrichment analysis of the hub genes. **(B)** The top five significantly enriched terms in CC enrichment analysis of the hub genes. **(C)** The top 10 significantly enriched terms in MF enrichment analysis of the hub genes. **(D)** The top 11 significantly enriched terms in KEGG enrichment analysis. Counts refer to the number of the enriched genes.

TABLE 4 | Results of kyoto encyclopedia of genes and genomes (KEGG) analysis on hub targets of candidate Chinese herbal medicine (CCHM) in the treatment of methamphetamine (METH) addiction.

Pathway	Counts	Genes
Dopaminergic synapse	5	DRD3, DRD2, SLC6A3, MAOA, MAOB
Cocaine addiction	4	DRD2, SLC6A3, MAOA, MAOB
Neuroactive ligand-receptor interaction	5	DRD3, DRD2, ADRA2A, ADRA1B, ADRA2C
Alcoholism	4	DRD2, SLC6A3, MAOA, MAOB
Amphetamine addiction	3	SLC6A3, MAOA, MAOB
Serotonergic synapse	3	MAOA, MAOB, HTR3A
cGMP-PKG signaling pathway	3	ADRA2A, ADRA1B, ADRA2C

In the current study, the components in CCHM with OB $\geq$ 30%, DL index $\geq$ 0.18 and BBB ≥ -0.3 were considered pharmacokinetically active as they are possibly absorbed and distributed in human brain. 123 components and 43 targets of CCHM for the treatment of METH addiction were screened by databases. Compounds with high-degree may account for the major therapeutic effects of CCHM on METH addiction. Ten major active components including Beta-Sitosterol, *S*-Scoulerine, Isocorypalmine, Leonticine, Hyndarin, and 10 hub targets including DRD2, HTR3A, and MAOA were screened out. Results of hub targets GO and KEGG enrichment analysis showed that dopaminergic synapses, cocaine addiction, neuroactive ligand-receptor interaction, alcoholism, and serotonergic synapse were the main possible pathways involved in the CCHM treatment of METH addiction.

The neural circuits that project from dopamine neurons in the ventral tegmental area to the nucleus accumbens and frontal cortex are called the mesolimbic dopamine system (MLDS). Numerous studies have identified the MLDS as a common reward circuit and main neuroanatomical basis for the rewarding or positive reinforcement of addictive drugs, involving in drug-induced reinforcement, pathological memory, craving, and relapse (Peters et al., 2021). Addictive substances affect the release of monoamine neurotransmitters such as dopamine, adrenaline and 5-hydroxytryptamine by acting on the reward system, and regulate the excitability of neurons. Under physiological conditions, the presynaptic release and reuptake of dopamine in dopaminergic neurons are in equilibrium (Volkow et al., 2017; Limanaqi et al., 2018). METH enters neurons through dopamine transporter, spurs presynaptic dopamine release and increases the concentration of dopamine in the synaptic cleft. Moreover, it could replace endogenous dopamine vesicles *via* combination of monoamine transporter in neurons, inhibit dopamine uptake, and promote the interaction of dopamine and receptors to produce neuroadaptive and addictive behaviors (Krasnova and Cadet, 2009; Shin et al., 2017). Michael et al. found that intravenous METH injection could significantly increase the levels of dopamine in the nucleus accumbens, and the locomotor

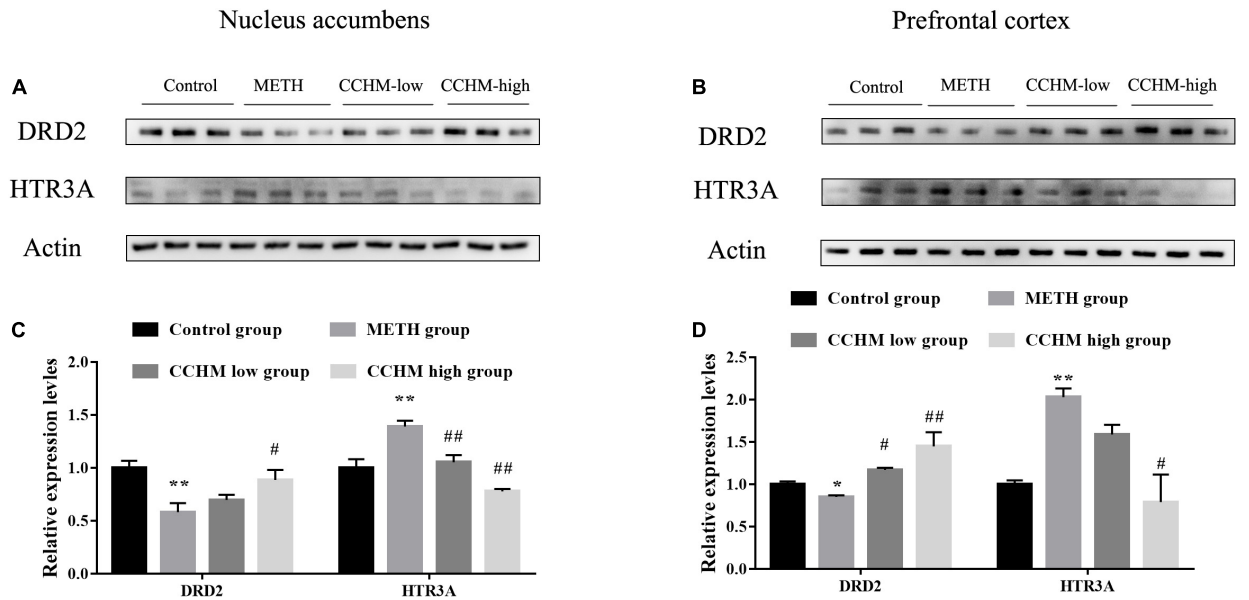

FIGURE 7 | Candidate Chinese herbal medicine (CCHM) administration inhibited methamphetamine (METH)-induced expression changes of D(2) dopamine receptor (DRD2) and 5-hydroxytryptamine receptor 3A (HTR3A) in the nucleus accumbens and prefrontal cortex. **(A)** Representative bands of DRD2 and HTR3A in the nucleus accumbens. **(B)** Representative bands of DRD2 and HTR3A in the prefrontal cortex. **(C)** METH significantly decreased expression of DRD2 and increased expression of HTR3A, while CCHM pretreatment could greatly upregulate DRD2 expression and downregulate HTR3A expression. **(D)** The expression of DRD2 notably decreased and the level of HTR3A increased in METH group, which could be reverse by CCHM pretreatment. $n = 3$ for per group, $^{*}p < 0.05$, $^{**}p < 0.01$ compared to the control group, $\#p < 0.05$, $\#\#p < 0.01$ compared to the METH group.

activities of rats was consistent with the change of dopamine levels in the nucleus accumbens (Baumann et al., 2011), and reducing dopamine levels in the nucleus accumbens could reduce the locomotor activities of addicted mice (Yun, 2014a). These studies suggested that dopaminergic system played important roles in METH-induced addictive behaviors. Among the 10 hub targets screened in this study, SLC6A3 is a dopamine transporter, which regulates the reuptake of dopamine, and plays a role in maintaining the homeostasis of dopamine in the synaptic cleft. The expression of SLC6A3 in the striatum of METH abusers was significantly decreased, accompanied with reduced learning and memory ability and motor ability (Volkow et al., 2001b,c). After 4 weeks of drug withdrawal, the expression of dopamine transporter in the striatum of abusers gradually recovered, but it was still significantly lower than that of healthy subjects (Yuan et al., 2014). Dopamine transporter inhibitors such as JHW007 and tetrabenazine significantly reduced relapse and locomoter sensitization in METH-addicted rats (Meyer et al., 2011; Ferragud et al., 2014). DRD2 and DRD3 belong to dopamine receptors. DRD3 antagonists could significantly inhibit the reinforcement of METH and relapse (Chen et al., 2014; Sun et al., 2016). METH abuse has been associated with DRD2 and DRD3 deficits in the caudate nucleus and nucleus accumbens, and DRD2 receptor availability was lower in the METH abusers and may mediate impulsive temperament and thereby influence addiction (Volkow et al., 2001a; Lee et al., 2009; Groman et al., 2012; Wang et al., 2012; Okita et al., 2018). Animal experiment also confirmed that mRNA expression of DRD2 was significantly decreased after METH administration (Landa et al., 2012), suggesting poor DRD2 function may be a biomarker that predicts a greater likelihood for relapse. Therefore, we focused on the expression of DRD2 in mesolimbic dopamine system to further verify the results of bioinformatics analysis. Consistent with previous literatures, our results also proved that DRD2 in nucleus accumbens and prefrontal cortex was significantly decreased in METH group, while CCHM treatment could increase the levels of DRD2. Our findings combined with previous reports further verified the vital role of dopamine system in the prevention and treatment of METH addiction.

TABLE 5 | Results of ligand-receptor protein molecular docking.

Molecule Name	Binding energy with DRD2/KJ mol^{-1}	Binding energy with HTR3A/KJ mol^{-1}
7-O-Methylisomucronulatol	−2.77	−2.92
Formononetin	−1.43	−3.52
Beta-Sitosterol	−2.94	−4.07
(S)-Scoulerine	−3.3	−3.96
Isocorypalmine	−3.42	−3.6
Leonticine	−1.87	−2.84
Medicarpin	−3.09	−4.28
Hyndarin	−3.54	−3.91

In addition to the dopamine system, 5-hydroxytryptamine, adrenaline system and their related metabolic enzymes are also the hub targets of CCHM in the prevention and treatment of METH addiction. MAOA and MAOB specifically

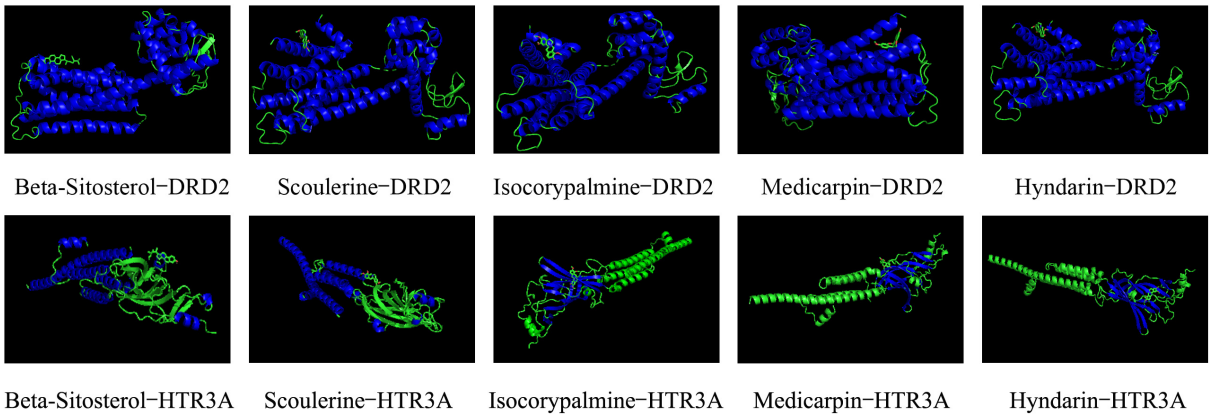

FIGURE 8 | Docking conformations of main active components with D(2) dopamine receptor (DRD2) and 5-hydroxytryptamine receptor 3A (HTR3A).

oxidize and inactivate monoamine transmitters, and MAOA gene polymorphisms were associated with susceptibility to METH-induced mental disorders (Nakamura et al., 2009). ADRA2A, ADRA2C, and ADRA1B are adrenergic receptors. METH could increase the expression of ADRA2A in the hippocampus (Nishio et al., 2002), and downregulation of ADRA2A inhibited METH-induced hyperactivity (Nishio et al., 2003), and knockdown of ADRA1B had a protective effect on METH-induced neurotoxicity (Battaglia et al., 2003). It was reported that karbalatin, an inhibitor of the acetylcholinesterase AChE could also reduce METH self-administration behavior (De La Garza et al., 2008), suggesting that acetylcholine may be involved in METH addiction. HTR3A is one of the 5-hydroxytryptamine receptors. Electrophysiological results showed 0.1 μM METH increased 5-HT-induced inward peak current (I_{5-HT}) in oocytes expressing HTR3A receptor, while high dose METH inhibited I_{5-HT}, and HTR3A receptor antagonist MDL72222 had an inhibitory effect on the acquisition and expression of METH locomoter sensitization (Yoo et al., 2006). HTR3A receptor antagonist ondansetron had a protective effect on the neurotoxicity caused by METH (Lafuente et al., 2018). Among all the hub genes, HTR3A has the highest degree score in the cytoHubba analysis, therefore, the expression of HTR3A in mesolimbic dopamine system was also detected. Our results demonstrated that METH addiction significantly increased HTR3A expression in nucleus accumbens and prefrontal cortex, while CCHM treatment decreased the levels of HTR3A while inhibiting METH addiction, which were consistent with results in previous literatures. These findings further validated that CCHM may inhibit the METH induced abuse mainly through regulating serotonergic system.

In this study, 10 major active compounds were molecularly docked with DRD2 and HTR3A, two receptors with higher degrees in the hub targets. The results showed that most active compounds could effectively bind to DRD2 and HTR3A receptors. Among them, β-Sitosterol, Scoulerine, Isocorypalmine, Medicarpin, and Hyndarin had lower binding energy with DRD2 and HTR3A. These results were consistent with previous studies which showed Scoulerine and Hyndarin had the potential to inhibit METH addiction, and Isocorypalmine could reduce the behavioral sensitization and reward of cocaine in mice by acting on dopamine receptors (Xu et al., 2013). To the best of our knowledge, there are no related literature reports on β-Sitosterol and Medicarpin and drug addiction, and our results suggested they might be novel potential molecules for the treatment of drug addiction. Based on literature verification and results of molecular docking, β-Sitosterol, Scoulerine, Isocorypalmine, Medicarpin, and Hyndarin may be potential active components for the treatment of CCHM on METH addiction, and the underlying mechanism of action may be through DRD2 and HTR3A signaling pathways.

CONCLUSION

To sum up, the pharmacological mechanism by which CCHM inhibited METH addiction was investigated based on the network pharmacology analysis, literature, and experimental validation. The results of the current study have shed light on further research on the pharmacodynamics and molecular mechanism of CCHM in the treatment of METH addiction and related mental disorders. In the future, *in vivo* and *in vitro* experiments are still needed to systematically verify the main active components and possible key targets in detail. The potential clinical therapeutic effects of CCHM may benefit from further studies.

DATA AVAILABILITY STATEMENT

The datasets presented in this study can be found in online repositories. The names of the repository/repositories and accession number(s) can be found in the article/**Supplementary Material**.

ETHICS STATEMENT

The animal study was reviewed and approved by the Ethics Committee of Jianghan University.

AUTHOR CONTRIBUTIONS

QR, LC, and YW designed the study, analyzed the data, and prepared the manuscript together. QR, XT, CL, and QX performed the experiments. All authors have read and approved the final version of the manuscript.

FUNDING

This study was supported by the National Natural Science Foundation of China (Grant Nos. 81971775 to LC and 82071970 to YW), the Wuhan Municipal Science and Technology Bureau (Grant No. 2019020701011499), and Innovation Research Project of Jianghan University (Grant No. 2021kjzx008). The Young Talents Project of Hubei Provincial Health Commission (Grant No. WJ2021Q053 to QR).

SUPPLEMENTARY MATERIAL

The Supplementary Material for this article can be found online at: https://www.frontiersin.org/articles/10.3389/fnmol.2022.874080/full#supplementary-material

REFERENCES

Bai, R. B., Zhang, Y. J., Fan, J. M., Jia, X. S., Li, D., Wang, Y. P., et al. (2020). Immune-enhancement effects of oligosaccharides from *Codonopsis pilosula* on cyclophosphamide induced immunosuppression in mice. *Food Funct.* 11, 3306–3315. doi: 10.1039/c9fo02969a

Battaglia, G., Fornai, F., Busceti, C. L., Lembo, G., Nicoletti, F., and De Blasi, A. (2003). Alpha-1B adrenergic receptor knockout mice are protected against methamphetamine toxicity. *J. Neurochem.* 86, 413–421.

Baumann, M. H., Clark, R. D., Woolverton, W. L., Wee, S., Blough, B. E., and Rothman, R. B. (2011). *In vivo* effects of amphetamine analogs reveal evidence for serotonergic inhibition of mesolimbic dopamine transmission in the rat. *J. Pharmacol. Exp. Ther.* 337, 218–225. doi: 10.1124/jpet.110.176271

Can, L. (2019). *Analysis of Jieduyihao Fingerprint And Its Effect On Behavioral Sensitization Induced By Methamphetamine In Mice*. Wuhan: Jianghan University.

Can, L., Lijun, T., Yuanren, S., Huaqiao, X., Qin, R., Mei, Z., et al. (2019). Effects of jieduyihao on methamphetamine-induced behavioral sensitization in mice. *J. Jianghan Univ. (Nat .Sci. Ed.)* 47, 57–65.

Cao, G., Zhang, Y., Zhu, L., Zhu, J., Zhao, N., Dong, N., et al. (2018). The inhibitory effect of levo-tetrahydropalmatine on the methamphetamine-induced spatial memory impairment in mice. *Neurosci. Lett.* 672, 34–39.

Chen, L., Ru, Q., Xiong, Q., Zhou, M., Yue, K., and Wu, Y. (2021). The role of chinese herbal therapy in methamphetamine abuse and its induced psychiatric symptoms. *Front. Pharmacol.* 12:679905. doi: 10.3389/fphar.2021.679905

Chen, S. W., Min, L., Li, W. J., Kong, W. X., Li, J. F., and Zhang, Y. J. (2004). The effects of angelica essential oil in three murine tests of anxiety. *Pharmacol. Biochem. Behav.* 79, 377–382. doi: 10.1016/j.pbb.2004.08.017

Chen, Y., Song, R., Yang, R. F., Wu, N., and Li, J. (2014). A novel dopamine D3 receptor antagonist YQA14 inhibits methamphetamine self-administration and relapse to drug-seeking behaviour in rats. *Eur. J. Pharmacol.* 743, 126–132.

De La Garza, R. II, Mahoney, J. J. III, Culbertson, C., Shoptaw, S., and Newton, T. F. (2008). The acetylcholinesterase inhibitor rivastigmine does not alter total choices for methamphetamine, but may reduce positive subjective effects, in a laboratory model of intravenous self-administration in human volunteers. *Pharmacol. Biochem. Behav.* 89, 200–208. doi: 10.1016/j.pbb.2007.12.010

Ferragud, A., Velazquez-Sanchez, C., and Canales, J. J. (2014). Modulation of methamphetamine's locomotor stimulation and self-administration by JHW 007, an atypical dopamine reuptake blocker. *Eur. J. Pharmacol.* 731, 73–79.

Fu, K., Lin, H., Miyamoto, Y., Wu, C., Yang, J., Uno, K., et al. (2016). Pseudoginsenoside-F11 inhibits methamphetamine-induced behaviors by regulating dopaminergic and GABAergic neurons in the nucleus accumbens. *Psychopharmacology* 233, 831–840. doi: 10.1007/s00213-015-4159-8

Glasner-Edwards, S., Marinelli-Casey, P., Hillhouse, M., Ang, A., Mooney, L. J., Rawson, R., et al. (2009). Depression among methamphetamine users: association with outcomes from the methamphetamine treatment project at 3-year follow-up. *J. Nerv. Ment. Dis.* 197, 225–231.

Gong, X., Yue, K., Ma, B., Xing, J., Gan, Y., Wang, D., et al. (2016). Levo-tetrahydropalmatine, a natural, mixed dopamine receptor antagonist, inhibits methamphetamine self-administration and methamphetamine-induced reinstatement. *Pharmacol. Biochem. Behav.* 144, 67–72. doi: 10.1016/j.pbb.2016.01.010

Groman, S. M., Lee, B., Seu, E., James, A. S., Feiler, K., Mandelkern, M. A., et al. (2012). Dysregulation of D(2)-mediated dopamine transmission in monkeys after chronic escalating methamphetamine exposure. *J. Neurosci.* 32, 5843–5852. doi: 10.1523/JNEUROSCI.0029-12.2012

Guo, W., Huang, J., Wang, N., Tan, H. Y., Cheung, F., Chen, F., et al. (2019). Integrating network pharmacology and pharmacological evaluation for deciphering the action mechanism of herbal formula zuojin pill in suppressing hepatocellular carcinoma. *Front. Pharmacol.* 10:1185. doi: 10.3389/fphar.2019.01185

Han, J., Wan, M., Ma, Z., Hu, C., and Yi, H. (2020). Prediction of targets of curculigoside a in osteoporosis and rheumatoid arthritis using network pharmacology and experimental verification. *Drug Design Dev. Therapy* 14, 5235–5250. doi: 10.2147/DDDT.S282112

Harms, R., Morsey, B., Boyer, C. W., Fox, H. S., and Sarvetnick, N. (2012). Methamphetamine administration targets multiple immune subsets and induces phenotypic alterations suggestive of immunosuppression. *PLoS One* 7:e49897. doi: 10.1371/journal.pone.0049897

He, D., Huang, J. H., Zhang, Z. Y., Du, Q., Peng, W. J., Yu, R., et al. (2019). A network pharmacology-based strategy for predicting active ingredients and potential targets of liuwei dihuang pill in treating type 2 diabetes mellitus. *Drug Design Dev. Therapy* 13, 3989–4005. doi: 10.2147/DDDT.S216644

Ingram, S. L. (2014). Pain: novel analgesics from traditional Chinese medicines. *Curr. Biol.* 24, R114–R116. doi: 10.1016/j.cub.2013.12.030

Jiaming, D., Mei, Z., and Chaoying, L. (2019). Improvement effects of jieduyihao on learning and memory impairment induced by methamphetamine in mice. *J. Jianghan Univ. (Nat. Sci. Ed.)* 47, 66–72.

Krasnova, I. N., and Cadet, J. L. (2009). Methamphetamine toxicity and messengers of death. *Brain Res. Rev.* 60, 379–407. doi: 10.1016/j.brainresrev.2009.03.002

Kumar, P., Kumar, M., Wisdom, K. S., Pathakota, G. B., Nayak, S. K., Reang, D., et al. (2020). Characterization, docking and molecular dynamics simulation of gonadotropin-inhibitory hormone receptor (gnihr2) in labeo catla. *Cell Physiol. Biochem.* 54, 825–841. doi: 10.33594/000000272

Lafuente, J. V., Sharma, A., Muresanu, D. F., Ozkizilcik, A., Tian, Z. R., Patnaik, R., et al. (2018). Repeated forced swim exacerbates methamphetamine-induced neurotoxicity: neuroprotective effects of nanowired delivery of 5-ht3-receptor antagonist ondansetron. *Mol. Neurobiol.* 55, 322–334. doi: 10.1007/s12035-017-0744-7

Landa, L., Jurajda, M., and Sulcova, A. (2012). Altered dopamine D1 and D2 receptor mRNA expression in mesencephalon from mice exposed to repeated treatments with methamphetamine and cannabinoid CB1 agonist methanandamide. *Neuro Endocrinol. Lett.* 33, 446–452.

Lee, B., London, E. D., Poldrack, R. A., Farahi, J., Nacca, A., Monterosso, J. R., et al. (2009). Striatal dopamine d2/d3 receptor availability is reduced in methamphetamine dependence and is linked to impulsivity. *J. Neurosci.* 29, 14734–14740. doi: 10.1523/JNEUROSCI.3765-09.2009

Limanaqi, F., Gambardella, S., Biagioni, F., Busceti, C. L., and Fornai, F. (2018). Epigenetic Effects Induced by Methamphetamine and Methamphetamine-Dependent Oxidative Stress. *Oxid. Med. Cell. Longev.* 2018:4982453. doi: 10.1155/2018/4982453

Meyer, A. C., Horton, D. B., Neugebauer, N. M., Wooters, T. E., Nickell, J. R., Dwoskin, L. P., et al. (2011). Tetrabenazine inhibition of monoamine

uptake and methamphetamine behavioral effects: locomotor activity, drug discrimination and self-administration. *Neuropharmacology* 61, 849–856. doi: 10.1016/j.neuropharm.2011.05.033

Mi, G., Gao, Y., Yan, H., Jin, X., Ye, E., Liu, S., et al. (2016). l-Scoulerine attenuates behavioural changes induced by methamphetamine in zebrafish and mice. *Behav. Brain Res.* 298(Pt A), 97–104. doi: 10.1016/j.bbr.2015.09.039

Nakamura, K., Sekine, Y., Takei, N., Iwata, Y., Suzuki, K., Anitha, A., et al. (2009). An association study of monoamine oxidase A (MAOA) gene polymorphism in methamphetamine psychosis. *Neurosci. Lett.* 455, 120–123. doi: 10.1016/j.neulet.2009.02.048

Nie, L., Zhao, Z., Wen, X., Luo, W., Ju, T., Ren, A., et al. (2020). Gray-matter structure in long-term abstinent methamphetamine users. *BMC Psychiatry* 20:158. doi: 10.1186/s12888-020-02567-3

Nishio, M., Kanda, Y., Mizuno, K., and Watanabe, Y. (2002). Methamphetamine increases the hippocampal alpha(2A)-adrenergic receptor and Galpha(o) in mice. *Neurosci. Lett.* 334, 145–148. doi: 10.1016/s0304-3940(02)01033-9

Nishio, M., Kuroki, Y., and Watanabe, Y. (2003). Role of hippocampal alpha(2A)-adrenergic receptor in methamphetamine-induced hyperlocomotion in the mouse. *Neurosci. Lett.* 341, 156–160. doi: 10.1016/s0304-3940(03)00171-x

Okita, K., Morales, A. M., Dean, A. C., Johnson, M. C., Lu, V., Farahi, J., et al. (2018). Striatal dopamine D1-type receptor availability: no difference from control but association with cortical thickness in methamphetamine users. *Mol. Psychiatry* 23, 1320–1327. doi: 10.1038/mp.2017.172

Park, H. J., Kim, H. Y., Yoon, K. H., Kim, K. S., and Shim, I. (2009). The effects of astragalus membranaceus on repeated restraint stress-induced biochemical and behavioral responses. *Korean J. Physiol. Pharmacol.* 13, 315–319. doi: 10.4196/kjpp.2009.13.4.315

Paulus, M. P., and Stewart, J. L. (2020). Neurobiology, clinical presentation, and treatment of methamphetamine use disorder: a review. *JAMA Psychiatry* 77, 959–966. doi: 10.1001/jamapsychiatry.2020.0246

Peerzada, H., Gandhi, J. A., Guimaraes, A. J., Nosanchuk, J. D., and Martinez, L. R. (2013). Methamphetamine administration modifies leukocyte proliferation and cytokine production in murine tissues. *Immunobiology* 218, 1063–1068. doi: 10.1016/j.imbio.2013.02.001

Peters, K. Z., Oleson, E. B., and Cheer, J. F. (2021). A brain on cannabinoids: the role of dopamine release in reward seeking and addiction. *Cold Spring Harbor Perspect. Med.* 11:a039305. doi: 10.1101/cshperspect.a039305

Prakash, M. D., Tangalakis, K., Antonipillai, J., Stojanovska, L., Nurgali, K., and Apostolopoulos, V. (2017). Methamphetamine: effects on the brain, gut and immune system. *Pharmacol. Res.* 120, 60–67. doi: 10.1016/j.phrs.2017.03.009

Shin, E. J., Dang, D. K., Tran, T. V., Tran, H. Q., Jeong, J. H., Nah, S. Y., et al. (2017). Current understanding of methamphetamine-associated dopaminergic neurodegeneration and psychotoxic behaviors. *Arch. Pharm. Res.* 40, 403–428. doi: 10.1007/s12272-017-0897-y

Su, H., Sun, T., Wang, X., Du, Y., Zhao, N., Zhu, J., et al. (2020). Levo-tetrahydropalmatine attenuates methamphetamine reward behavior and the accompanying activation of ERK phosphorylation in mice. *Neurosci. Lett.* 714:134416. doi: 10.1016/j.neulet.2019.134416

Sun, L., Song, R., Chen, Y., Yang, R. F., Wu, N., Su, R. B., et al. (2016). A selective D3 receptor antagonist YQA14 attenuates methamphetamine-induced behavioral sensitization and conditioned place preference in mice. *Acta Pharmacol. Sin.* 37, 157–165. doi: 10.1038/aps.2015.96

Tao, W., Xu, X., Wang, X., Li, B., Wang, Y., Li, Y., et al. (2013). Network pharmacology-based prediction of the active ingredients and potential targets of Chinese herbal Radix Curcumae formula for application to cardiovascular disease. *J. Ethnopharmacol.* 145, 1–10. doi: 10.1016/j.jep.2012.09.051

Tian, H., Liu, Z., Pu, Y., and Bao, Y. (2019). Immunomodulatory effects exerted by Poria Cocos polysaccharides *via* TLR4/TRAF6/NF-kappaB signaling *in vitro* and *in vivo*. *Biomed. Pharmacother.* 112:108709. doi: 10.1016/j.biopha.2019.108709

Volkow, N. D., Chang, L., Wang, G. J., Fowler, J. S., Ding, Y. S., Sedler, M., et al. (2001a). Low level of brain dopamine D2 receptors in methamphetamine abusers: association with metabolism in the orbitofrontal cortex. *Am. J. Psychiatry* 158, 2015–2021. doi: 10.1176/appi.ajp.158.12.2015

Volkow, N. D., Chang, L., Wang, G. J., Fowler, J. S., Franceschi, D., Sedler, M., et al. (2001b). Loss of dopamine transporters in methamphetamine abusers recovers with protracted abstinence. *J. Neurosci.* 21, 9414–9418. doi: 10.1523/JNEUROSCI.21-23-09414.2001

Volkow, N. D., Chang, L., Wang, G. J., Fowler, J. S., Leonido-Yee, M., Franceschi, D., et al. (2001c). Association of dopamine transporter reduction with psychomotor impairment in methamphetamine abusers. *Am. J. Psychiatry* 158, 377–382. doi: 10.1176/appi.ajp.158.3.377

Volkow, N. D., Wise, R. A., and Baler, R. (2017). The dopamine motive system: implications for drug and food addiction. *Nat. Rev. Neurosci.* 18, 741–752. doi: 10.1038/nrn.2017.130

Wang, G. J., Smith, L., Volkow, N. D., Telang, F., Logan, J., Tomasi, D., et al. (2012). Decreased dopamine activity predicts relapse in methamphetamine abusers. *Mol. Psychiatry* 17, 918–925. doi: 10.1038/mp.2011.86

Xu, W., Wang, Y., Ma, Z., Chiu, Y. T., Huang, P., Rasakham, K., et al. (2013). L-isocorypalmine reduces behavioral sensitization and rewarding effects of cocaine in mice by acting on dopamine receptors. *Drug Alcohol. Depend.* 133, 693–703. doi: 10.1016/j.drugalcdep.2013.08.021

Yang, C., Fu, X., Hao, W., Xiang, X., Liu, T., Yang, B. Z., et al. (2020). Gut dysbiosis associated with the rats' responses in methamphetamine-induced conditioned place preference. *Addict. Biol.* 26:e12975. doi: 10.1111/adb.12975

Yang, G., Liu, L., Zhang, R., Li, J., Leung, C. K., Huang, J., et al. (2020). Cannabidiol attenuates methamphetamine-induced conditioned place preference *via* the Sigma1R/AKT/GSK-3beta/CREB signaling pathway in rats. *Toxicol. Res.* 9, 202–211. doi: 10.1093/toxres/tfaa021

Yoo, J. H., Cho, J. H., Yu, H. S., Lee, K. W., Lee, B. H., Jeong, S. M., et al. (2006). Involvement of 5-HT receptors in the development and expression of methamphetamine-induced behavioral sensitization: 5-HT receptor channel and binding study. *J. Neurochem.* 99, 976–988. doi: 10.1111/j.1471-4159.2006.04137.x

Yuan, J., Lv, R., Robert Brasic, J., Han, M., Liu, X., Wang, Y., et al. (2014). Dopamine transporter dysfunction in Han Chinese people with chronic methamphetamine dependence after a short-term abstinence. *Psychiatry Res.* 221, 92–96. doi: 10.1016/j.pscychresns.2013.11.005

Yun, J. (2014a). Limonene inhibits methamphetamine-induced locomotor activity *via* regulation of 5-HT neuronal function and dopamine release. *Phytomedicine* 21, 883–887. doi: 10.1016/j.phymed.2013.12.004

Yun, J. (2014b). L-tetrahydropalmatine inhibits methamphetamine-induced locomotor activity *via* regulation of 5-HT neuronal activity and dopamine D3 receptor expression. *Phytomedicine* 21, 1287–1291. doi: 10.1016/j.phymed.2014.07.003

Zhang, Z., He, L., Huang, S., Fan, L., Li, Y., Li, P., et al. (2018). Alteration of brain structure with long-term abstinence of methamphetamine by voxel-based morphometry. *Front. Psychiatry* 9:722. doi: 10.3389/fpsyt.2018.00722

Zhao, N., Chen, Y., Zhu, J., Wang, L., Cao, G., Dang, Y., et al. (2014). Levo-tetrahydropalmatine attenuates the development and expression of methamphetamine-induced locomotor sensitization and the accompanying activation of ERK in the nucleus accumbens and caudate putamen in mice. *Neuroscience* 258, 101–110. doi: 10.1016/j.neuroscience.2013.11.025

Zhou, Z. Y., Zhao, W. R., Shi, W. T., Xiao, Y., Ma, Z. L., Xue, J. G., et al. (2019). Endothelial-dependent and independent vascular relaxation effect of tetrahydropalmatine on rat aorta. *Front. Pharmacol.* 10:336. doi: 10.3389/fphar.2019.00336

Zulkipli, N. N., Zakaria, R., Long, I., Abdullah, S. F., Muhammad, E. F., Wahab, H. A., et al. (2020). In silico analyses and cytotoxicity study of asiaticoside and asiatic acid from malaysian plant as potential mtor inhibitors. *Molecules* 25:3991. doi: 10.3390/molecules25173991

Conflict of Interest: The authors declare that the research was conducted in the absence of any commercial or financial relationships that could be construed as a potential conflict of interest.

Publisher's Note: All claims expressed in this article are solely those of the authors and do not necessarily represent those of their affiliated organizations, or those of the publisher, the editors and the reviewers. Any product that may be evaluated in this article, or claim that may be made by its manufacturer, is not guaranteed or endorsed by the publisher.

frontiers | Frontiers in Molecular Neuroscience

ORIGINAL RESEARCH
published: 01 April 2022
doi: 10.3389/fnmol.2022.861340

Inflammasome Inhibition Prevents Motor Deficit and Cerebellar Degeneration Induced by Chronic Methamphetamine Administration

*Jiuyang Ding[1,2†], Lingyi Shen[3†], Yuanliang Ye[4†], Shanshan Hu[5], Zheng Ren[1], Ting Liu[6], Jialin Dai[1], Zhu Li[1], Jiawen Wang[1], Ya Luo[1], Qiaojun Zhang[1], Xiali Zhang[1], Xiaolan Qi[2] and Jiang Huang[1]**

[1] School of Forensic Medicine, Guizhou Medical University, Guiyang, China, [2] Key Laboratory of Endemic and Ethnic Diseases, Ministry of Education, Guizhou Medical University, Guiyang, China, [3] School of Basic Medical Science, Guizhou Medical University, Guiyang, China, [4] Department of Neurosurgery, Liuzhou People's Hospital, Liuzhou, China, [5] Good Clinical Practice Center, Affiliated Hospital of Zunyi Medical University, Zunyi, China, [6] State Key Laboratory of Functions and Applications of Medicinal Plants, Key Laboratory of Pharmaceutics of Guizhou Province, Guizhou Medical University, Guiyang, China

OPEN ACCESS

Edited by:
Qi Wang,
Southern Medical University, China

Reviewed by:
Mingyang Zhang,
Soochow University, China
Lin Chen,
Jianghan University, China

***Correspondence:**
Jiang Huang
mmm_hj@126.com

[†] These authors have contributed equally to this work

Specialty section:
This article was submitted to Molecular Signalling and Pathways, a section of the journal Frontiers in Molecular Neuroscience

Received: 24 January 2022
Accepted: 03 March 2022
Published: 01 April 2022

Citation:
Ding J, Shen L, Ye Y, Hu S, Ren Z, Liu T, Dai J, Li Z, Wang J, Luo Y, Zhang Q, Zhang X, Qi X and Huang J (2022) Inflammasome Inhibition Prevents Motor Deficit and Cerebellar Degeneration Induced by Chronic Methamphetamine Administration. Front. Mol. Neurosci. 15:861340. doi: 10.3389/fnmol.2022.861340

Methamphetamine (METH), a psychostimulant, has the potential to cause neurodegeneration by targeting the cerebrum and cerebellum. It has been suggested that the NLRP3 inflammasome may be responsible for the neurotoxicity caused by METH. However, the role of NLRP3 in METH-induced cerebellar Purkinje cell (PC) degeneration and the underlying mechanism remain elusive. This study aims to determine the consequences of NLRP3 modulation and the underlying mechanism of chronic METH-induced cerebellar PC degeneration. In METH mice models, increased NLRP3 expression, PC degeneration, myelin sheath destruction, axon degeneration, glial cell activation, and motor coordination impairment were observed. Using the NLRP3 inhibitor MCC950, we found that inhibiting NLRP3 alleviated the above-mentioned motor deficits and cerebellar pathologies. Furthermore, decreased mature IL-1β expression mediated by Caspase 1 in the cerebellum may be associated with the neuroprotective effects of NLRP3 inflammasome inhibition. Collectively, these findings suggest that mature IL-1β secretion mediated by NLRP3-ASC-Caspase 1 may be a critical step in METH-induced cerebellar degeneration and highlight the neuroprotective properties of inflammasome inhibition in cerebellar degeneration.

Keywords: methamphetamine, inflammasome, cerebellum, degeneration, motor deficit

INTRODUCTION

Methamphetamine (METH), a potent psychostimulant, is widely used throughout the world and has the potential to cause serious injury to the central nervous system, heart and liver (Li et al., 2021). In the central nervous system, METH selectively targets dopaminergic neurons in the substantial nigral area (Ares-Santos et al., 2014; Ding et al., 2020a). METH induces dopaminergic

neuron degeneration through oxidative stress, inflammation and endoplasmic reticulum stress, to name a few (Ruan et al., 2020; Kohno et al., 2021). The cerebellum receives substantial signals from different neuronal types including serotoninergic, norepinephrinergic, dopaminergic and acetylcholinergic neurons (Wagner et al., 2021). Evidence suggests that METH could modulate neurotransmitter disorder, which leads to cerebellar dysfunction (Eskandarian Boroujeni et al., 2020). For instance, the serotonin transporter density in METH user cerebellum was lower than that in healthy subject (Sekine et al., 2006).

Methamphetamine may cause cerebellar degeneration, characterized by motor coordination deficits and a decrease in the number of PCs (Boroujeni et al., 2020; Ramshini et al., 2021). However, the precise mechanism by which METH causes cerebellar pathology is unknown.

Inflammasomes, which act as sensors in response to environmental stress insults, are multiprotein complexes (Rathinam and Fitzgerald, 2016; Qiu et al., 2021). Bacterial, viral, and protein aggregates such as neurofibril tangles and β-amyloid, as well as danger-associated molecular patterns such as ATP and oxygen deprivation, all contribute to the formation of the inflammasome (Schroder and Tschopp, 2010; Lamkanfi and Dixit, 2014). Three components comprise the canonical inflammasome complex: the nucleotide-binding domain and leucine-rich repeat-containing protein (NLRP), the apoptosis-associated speck-like protein containing a CARD (ASC), and pro-caspase-1 (Strowig et al., 2012; Nabar and Kehrl, 2019). These three components are referred to as the cytosolic sensor, adaptor protein, and effector, respectively (Song et al., 2017). The NLRP3 inflammasomes may promote the maturation of interleukin-1β (IL-1β) maturation, resulting in inflammation (Martinon et al., 2002). Recent research established that NLRP3 is activated *via* the P53-dependent apoptosis pathway in the hippocampal regions (Du et al., 2019). However, the role of NLRP3 in mice's cerebellar regions following METH intoxication remains unknown.

Our previous studies have shown that METH could increase α-synuclein (α-syn) and phosphorylated microtubule-associated protein Tau levels in METH mice models (Ding et al., 2020b). Moreover, α-syn could trigger NLRP3 activation in mice Parkinson's disease model. In addition, inhibiting NLRP3 alleviated α-syn phosphorylation and accumulation in the Parkinson's disease mice model (Gordon et al., 2018). Nevertheless, whether NLRP3 inhibition could affect α-syn and phosphorylated Tau (p-Tau) aggregation in mice cerebellums after METH administration has not been investigated to this date.

To gain a thorough understanding of the function of NLRP3 in the cerebellar region, we designed a METH-induced mouse model. Besides, the NLRP3 level, motor ability and cerebellar pathology of METH-induced mice were analyzed. Moreover, an NLRP3 inhibitor, MCC950, was utilized to observe the effect of NLRP3 inhibition on motor impairment and cerebellar neurodegeneration in our animal model.

MATERIALS AND METHODS

Animals

C57BL/6J mice (male 20∼24 g, 4∼8 weeks old) were purchased from the Laboratory Animal Center of Guizhou Medical University (Guizhou, China). Mice were kept under a controlled environment with a 12 h light-dark cycle. All mice were housed (four mice per cage) with *ad libitum* access to food and water. All animal experiments were preapproved by the Institutional Animal Care and Use Committee of Guizhou Medical University and were performed according to the National Institutes of Health guide.

Chronic Methamphetamine Exposure and Experimental Groups

Methamphetamine administration (purity >99%, National Institutes for Food and Drug Control, Guangzhou, China) followed the dosing schedule of **Table 1**. The chronic METH mouse models were initiated with low doses and concluded with a large challenge dose. The increasing dose and frequency could simulate the progressive use of METH observed in humans and was reported in previous studies (Danaceau et al., 2007).

The mice were divided into five groups as follows:

Con: Saline was administered intraperitoneally to WT mice, in place of METH;
Con + MCC950 (20 mg): Mice were intraperitoneally injected with MCC950 (20 mg body weight) once daily from day 1 to day 14 as shown in **Figure 1A**;
Methamphetamine: METH was administered intraperitoneally as shown in **Table 1**;
Methamphetamine + MCC950 (10 mg): Both METH (**Table 1**) and MCC950 (10 mg body weight, once daily) were intraperitoneally injected for a total of 14 days;
Methamphetamine + MCC950 (20 mg): Both METH (**Table 1**) and MCC950 (20 mg body weight, once daily) were intraperitoneally injected for a total of 14 days.

Rotarod Test

The rotarod tests were carried out to evaluate the body balance and motor coordinative abilities of experimental mice (Nobrega et al., 2013; Zhang C. et al., 2021). The rotarod test was conducted by placing the mice on an accelerating rod. The speed of the rod was set from 4 to 40 rpm. The trial was performed for 5 min. And the test lasted for 5 days (once a day). Animals were trained 3 days before the test. Each animal was tested three times, and an average latency to fall was recorded.

Footprint Analysis

The footprint analysis were carried out to evaluate the motor coordinative abilities of experimental mice (Nobrega et al., 2013). The testing apparatus is a wooden U-shaped runway that is 10 cm in width and 40 cm in length. A piece of white paper was placed on the bottom of the runway. Before the test, the mice had two forepaws, and two hind paws painted red and black, respectively. Mice were trained for 2 days before the tests. Mice were placed

TABLE 1 | Dosing schedule of Methamphetamine (METH) treatment (mg/kg).

Day	1	2	3	4	5	6	7	8	9	10	11	12	13	14
8:00	1.0	1.0	1.0	1.0	1.5	1.5	2.0	2.0	2.5	3.0	3.5	4.0	4.5	5.0
10:00				1.0	1.5	1.5	2.0	2.0	2.5	3.0	3.5	4.0	4.5	5.0
12:00				1.0	1.5	1.5	2.0	2.0	2.5	3.0	3.5	4.0	4.5	5.0
14:00		1.0	1.0	1.0	1.5	1.5	2.0	2.0	2.5	3.0	3.5	4.0	4.5	5.0

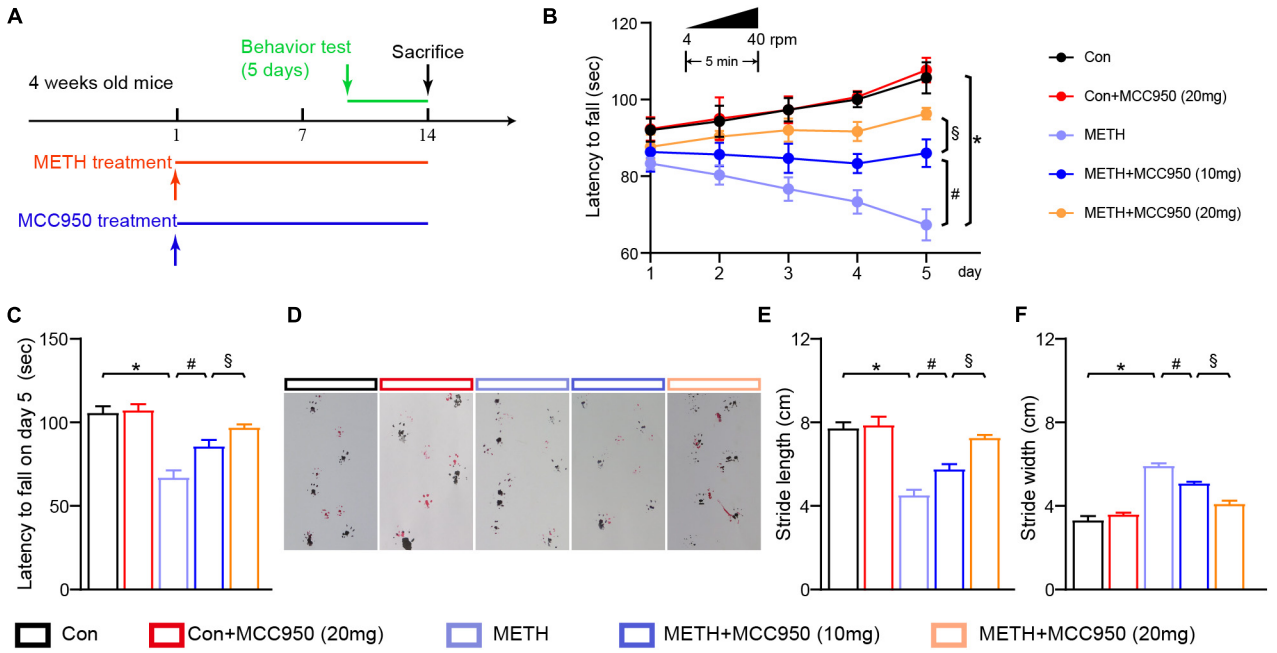

FIGURE 1 | MCC950 ameliorated motor coordination impairment in METH mice model. **(A)** Experimental design of METH and MCC 950 treatment regimen. **(B)** Rotarod test performance in each group mice from day 1 to day 5. **(C)** Latency to fall on day 5 in rotarod test. **(D)** Effect of MCC950 on footprint pattern of mice treated with METH. **(E)** Stride length analysis in footprint test. **(F)** Stride width analysis in footprint test. $n = 6$ per group by one-way ANOVA and Bonferroni's *post-hoc* analysis, $^{*}p < 0.05$, compared with the Con group; $^{\#}p < 0.05$, compared with the METH-treated group; §$p < 0.05$, compared with the METH + MCC950 (10 mg) group.

on the beginning of the runway and then allowed to move. The footprints were taken using a camera, and the stride length and width were measured for analysis.

Western Blot

Cerebellar tissues were homogenized in extraction buffer before centrifugation. The protein concentration in the supernatant was quantified. Then the samples were mixed with the loading buffer before boiling at 99°C for 10 min. The proteins were separated by SDS-PAGE and transferred onto PVDF membranes (Millipore, MA, United States). Targeted protein expression were assessed by using antibodies to rabbit monoclonal α-synuclein antibody (ab138501, 1:1,000 dilution, Abcam, United States), rabbit monoclonal phosphor-Tau antibody (ab32057, 1:800 dilution, Abcam, United States), rabbit monoclonal Tau antibody (ab254256, 1:1,000 dilution, Abcam, United States), rabbit polyclonal NF-200 antibody (18934-1-AP, 1:1,500 dilution, Proteintech, China), rabbit monoclonal MBP antibody (78896, 1:1,000 dilution, CST technology, United States), rabbit monoclonal CNP antibody (5664, 1:1,000 dilution, CST technology, United States), mouse monoclonal GFAP antibody (3670, 1:800 dilution, CST technology, United States), rabbit monoclonal Iba1 antibody (17198, 1:1,000 dilution, CST technology, United States), rabbit polyclonal IL-6 antibody (21865-1-AP, 1:2,000 dilution, Proteintech, China), mouse monoclonal TNF-α antibody (60291-1-Ig, 1:3,000 dilution, Proteintech, China), rabbit monoclonal NLRP3 antibody (ab263899, 1:1,000 dilution, Abcam, United States), rabbit monoclonal ASC antibody (ab155970, 1:5,000 dilution, Abcam, United States), rabbit monoclonal Cleaved Caspase-1 antibody (89332, 1:1,000 dilution, CST technology, United States), rabbit monoclonal Caspase-1 antibody (24232, 1:1,000 dilution, CST technology, United States), rabbit monoclonal Mature IL-1β antibody (A1112, 1:1,000 dilution, ABclonal, China), rabbit monoclonal IL-1β antibody (12507, 1:1,000 dilution, CST technology, United States), mouse monoclonal β-actin antibody (3700, 1:1,000 dilution, CST technology, United States). Membranes were incubated overnight at 4°C with primary antibodies before be blocked in 5% non-fat milk for 1 h. Then the membranes were incubated with adequate secondary antibodies

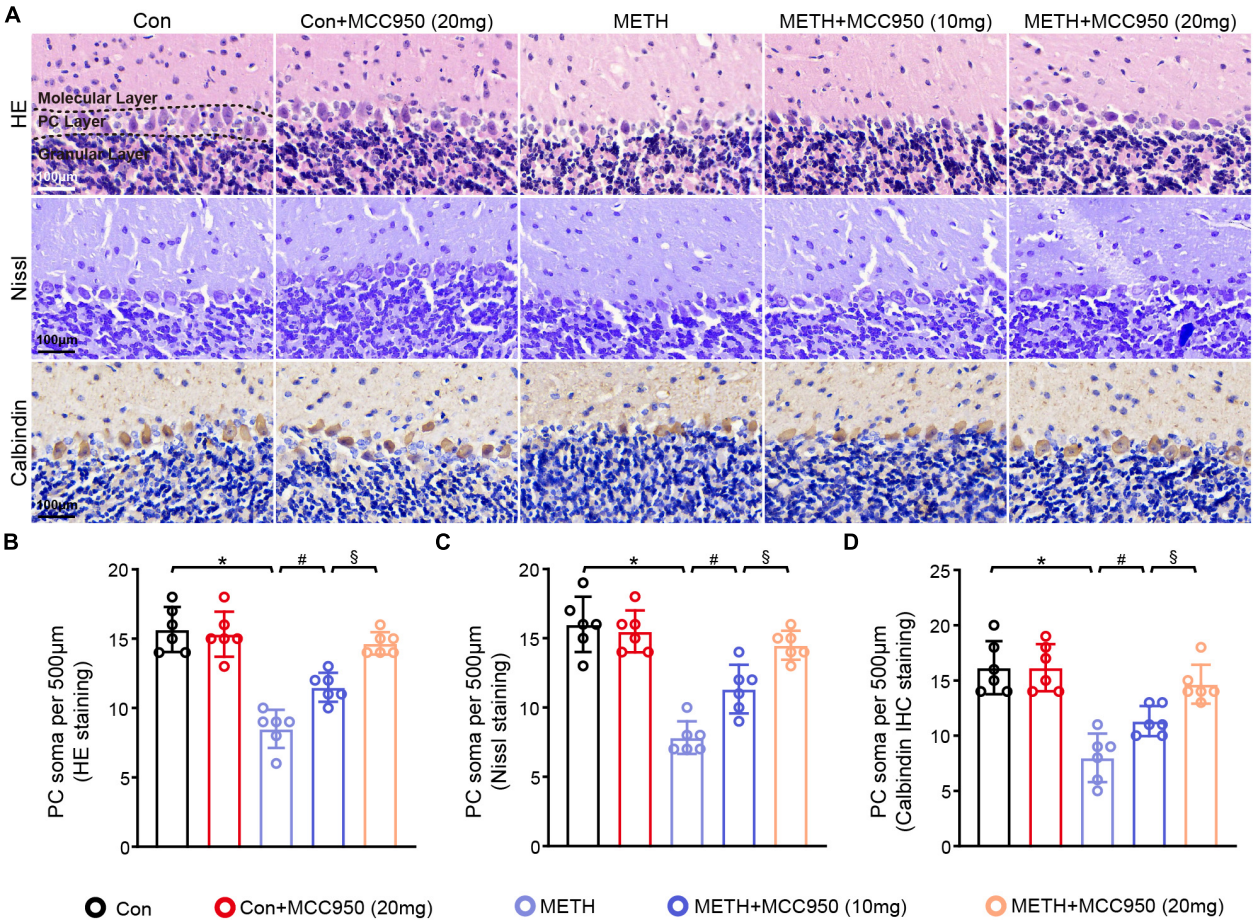

FIGURE 2 | MCC950 alleviated PC soma number loss in chronic METH mice model. **(A)** HE staining, Nissl staining and Calbindin IHC staining in the cerebellar area. **(B)** Comparison of PC soma number from HE staining results. **(C)** Comparison of PC soma number from Nissl staining results. **(D)** Comparison of PC soma number from Calbindin IHC staining results. $n = 6$ per group by one-way ANOVA and Bonferroni's *post-hoc* analysis, $^{*}p < 0.05$, compared with the Con group; $^{\#}p < 0.05$, compared with the METH-treated group; §$p < 0.05$, compared with the METH + MCC950 (10 mg) group.

HRP conjugated goat anti-mouse IgG antibody (91196, 1:10,000 dilution, CST technology, United States) or HRP conjugated goat anti-rabbit IgG antibody (ab6721, 1:10,000 dilution, Abcam, United States). Electrochemiluminescence reagents were used to visualize the blot signals. All protein expression levels were normalized to β-actin. Three animals per group were used for western blot analysis.

Immunohistochemistry and Immunofluorescence Staining

Cerebellar tissues were fixed in 4% PFA for 12 h. For IHC staining, the tissues were embedded in wax. The 3 μm sections were conducted using a microtome (RM2235, Leica, Germany). After antigen recovery and blocking, the sections were incubated with antibodies mouse monoclonal Calbindin antibody (66394-1-Ig, 1:200 dilution, Proteintech, China), rabbit monoclonal α-synuclein antibody (ab138501, 1:200 dilution, Abcam, United States), rabbit monoclonal phosphor-Tau antibody (ab32057, 1:500 dilution, Abcam, United States), rabbit monoclonal CNP antibody (5664, 1:300 dilution, CST technology, United States) and mouse monoclonal GFAP antibody (3670, 1:500 dilution, CST technology, United States) at 4°C overnight. Targeted proteins were visualized using 3, 3 - diaminobenzidine (DAB) kits (CW2069, CWBio, China). Images were acquired using a microscope (CX23, Olympus, Japan). When both the soma and the nuclei appeared, the PC was counted. Three mice per group and three serial sections per mouse were conducted in the experiment.

For immunofluorescence staining, the fixed cerebellar tissues were embedded in optimum cutting temperature compound before sectioning. The 20 μm thickness sections were cut using a microtome (CM 1950, Leica, Germany). Sections were incubated in solution containing 1% Triton X-100 and 5% BSA for 40 min. Then the sections were incubated in primary antibody rabbit monoclonal Iba1 antibody (ab220815, 1:200 dilution, Abcam, MA, United States) at 4°C overnight. Then the Alexa Fluor 488-conjugated secondary antibodies goat anti-rabbit IgG antibody (A-11034, 1:500 dilution, Thermo Fisher Scientific, MA, United States) were incubated for 1 h. Nuclei were stained by

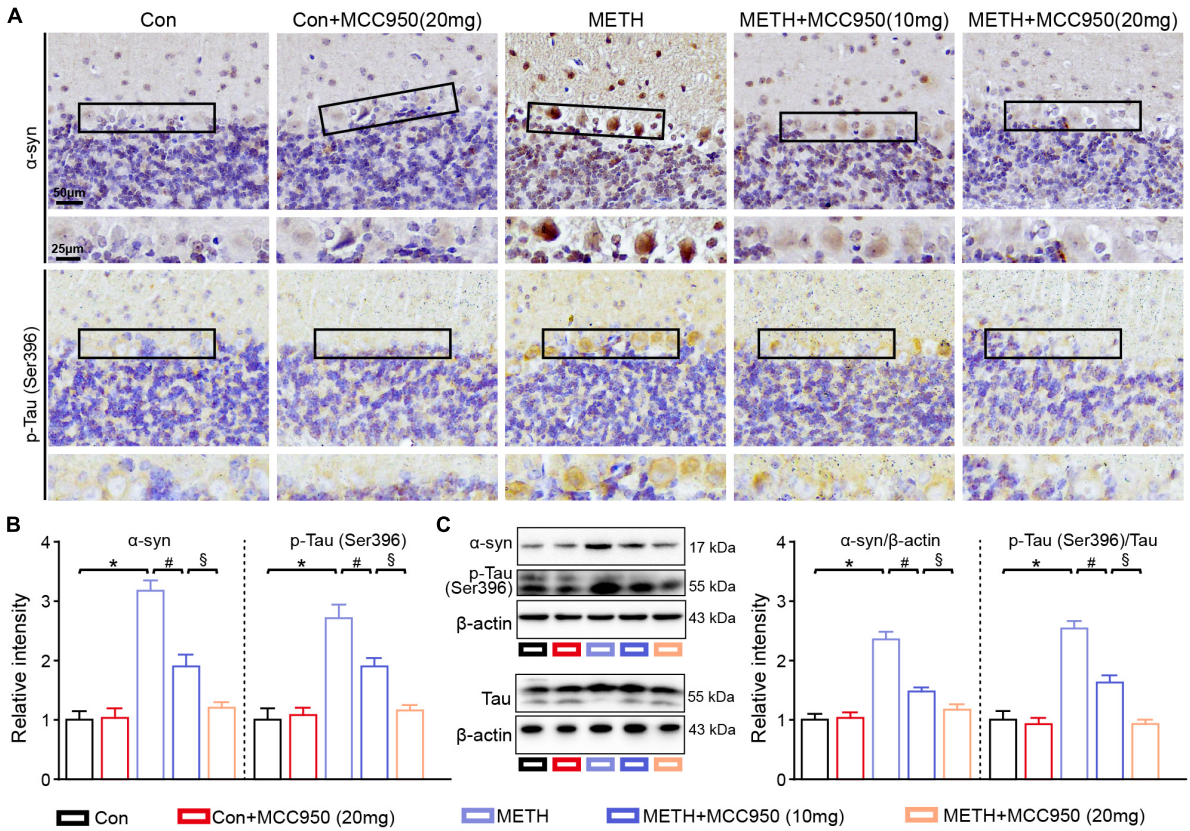

FIGURE 3 | MCC950 reversed α-syn and p-Tau level increasing. **(A)** Representative images of α-syn and pSer396-Tau IHC staining. **(B)** Relative intensity of α-syn and pSer396-Tau in cerebellar areas. **(C)** Western blot and quantification for α-syn and pSer396-Tau in cerebellum. $n = 6$ per group by one-way ANOVA and Bonferroni's *post-hoc* analysis, $^{*}p < 0.05$, compared with the Con group; $^{\#}p < 0.05$, compared with the METH-treated group; §$p < 0.05$, compared with the METH + MCC950 (10 mg) group.

mounting Medium (Cat# H-1020, Vector Lab, United States). And when the soma and the nuclei appeared, the glial cell was counted regardless of the projections. Images were captured using a confocal microscope (LSM 780Zeiss, Carl Zeiss, Germany).

Hematoxylin and Eosin Staining, Luxol Fast Blue Staining and Silver Staining

The 3 μm sections were acquired as described above. Then the sections were dewaxed and rinsed in water. For HE staining, the sections were stained with hematoxylin for 3 min before being rinsed in eosin for 2 min. For LFB staining, the sections were stained with LFB overnight before rinsing in PBS. Then the sections were stained with eosin for 2 min. For silver staining, the sections were rinsed in acid formaldehyde for 5 min, and the sections were then rinsed in 0.25% silver nitrate solution at 37°C for 3 min. After rinsing in gallic hydroxide, the sections were washed using water. All stained sections were dehydrated in gradient alcohol and rinsed in dimethylbenzene before being sealed with gum. Images were acquired using a microscope (CX23, Olympus, Japan). Three mice per group and three serial sections per mouse were conducted in each experiment.

Statistical Analysis

All data were expressed as mean ± standard deviation. All analyses were analyzed using SPSS 19.0, and charts were conducted using Graphpad prism 9.2. The one-way ANOVA with Bonferroni's multiple comparison *post-hoc* test was conducted for the statistical analysis. Randomization and blind analyses were used in behavioral test and pathological analysis. Statistical significance was set at $p < 0.05$. The number of different experimental groups is reported in the figure legends.

RESULTS

Restoration of Motor Performance in Chronic Methamphetamine Mice Treated With NLRP3 Inhibitor MCC950

The rotarod test was used to investigate motor deficits in mice following METH intoxication and determine whether the motor deficit was restored when the selective NLRP3 inhibitor MCC950 was used. The rotarod test revealed that the latency to fall was significantly reduced in METH-treated mice compared to control mice (**Figure 1B**). However, administration of MCC950 (10 and

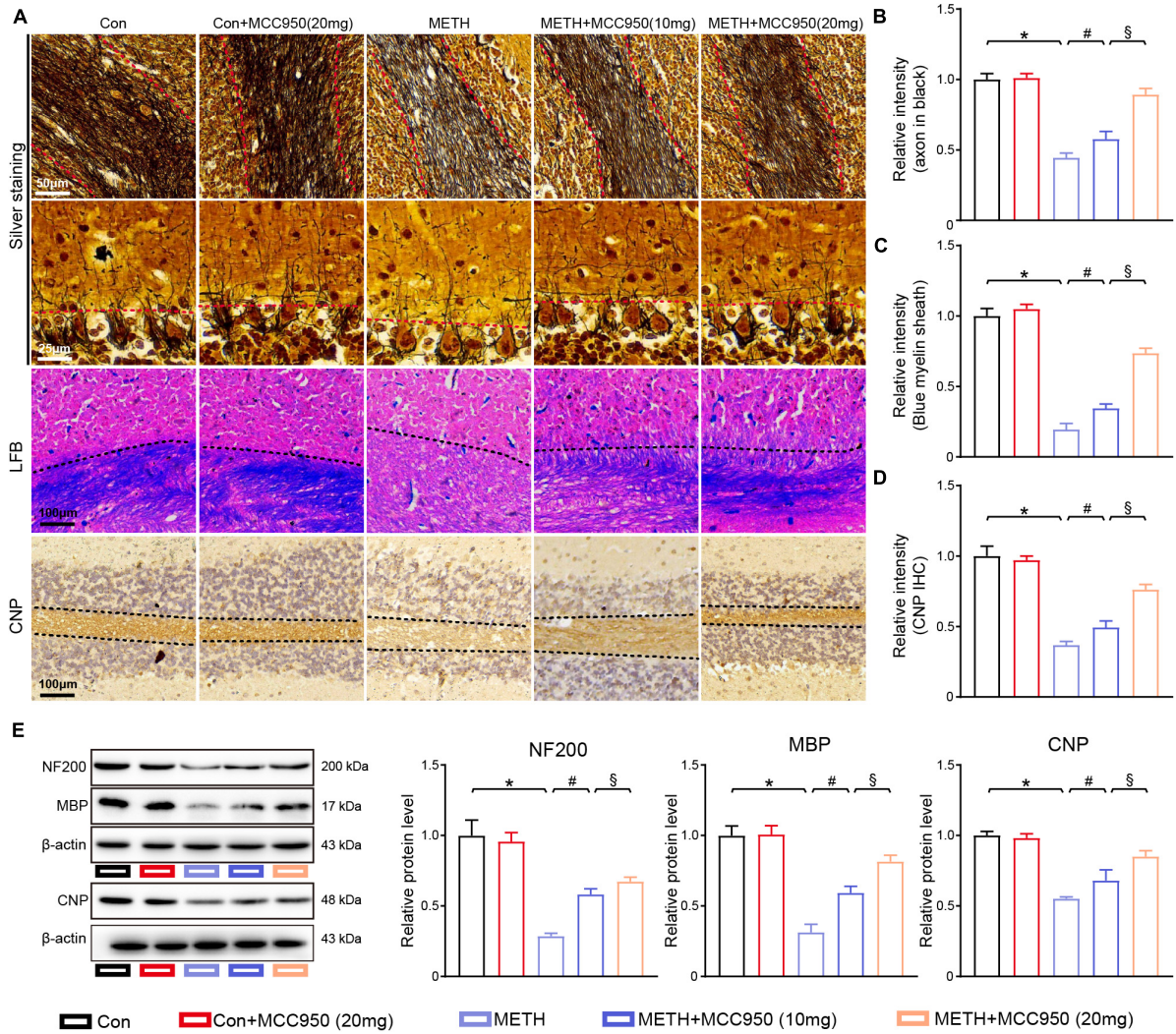

FIGURE 4 | MCC950 diminished the axon degeneration and myelin loss in cerebellum. **(A)** Representative images of silver staining, LFB staining, CNP IHC staining in cerebellar areas. **(B)** Intensity of axons analysis. **(C)** Myelin sheath intensity analysis. **(D)** Relative intensity of CNP in cerebellar areas. **(E)** Western blot and quantification for NF-200, MBP, and CNP in cerebellum. $n = 6$ per group by one-way ANOVA and Bonferroni's *post-hoc* analysis, $^{*}p < 0.05$, compared with the Con group; $^{\#}p < 0.05$, compared with the METH-treated group; §$p < 0.05$, compared with the METH + MCC950 (10 mg) group.

20 mg/kg) could reverse the decline in fall latency of METH-induced mice (**Figure 1B**). 20 mg/kg MCC950 normalized the fall latency in mice treated with METH when compared to control mice on day 5 (**Figure 1C**). METH-treated mice had a shorter stride length and a wider stride width during the gait test compared to the control mice. In contrast, the MCC950 intervention could reverse the effect of METH *in vivo* (**Figures 1D–F**).

Administration of MCC950 Protected Against Purkinje Cell Soma Loss in Methamphetamine Mice Model

Next we investigated the mechanism of action of the NLRP3 inhibitor MCC950 in METH-induced PC degeneration. HE staining, nissl staining, Calbindin (A PC marker) and IHC staining were used to assess the number of PC soma in cerebellar regions. The number of PC soma was smaller in the METH mice group than in the control group. However, MCC950 at 10 or 20 mg/kg could alleviate the loss of PC soma number caused by METH. In this regard, no significant difference in the PC soma number was found between the Con + MCC950 (20 mg/kg) group and control mice (**Figures 2A–D**).

Treatment With MCC950 Reduced α-Synuclein and Phosphorylated Tau Accumulation in the Cerebellar Purkinje Cell

Next, we assessed whether NLRP3 inhibition altered α-syn and p-Tau levels within the cerebellar regions by α-syn and p-Tau IHC staining. We found that α-syn and p-Tau mainly

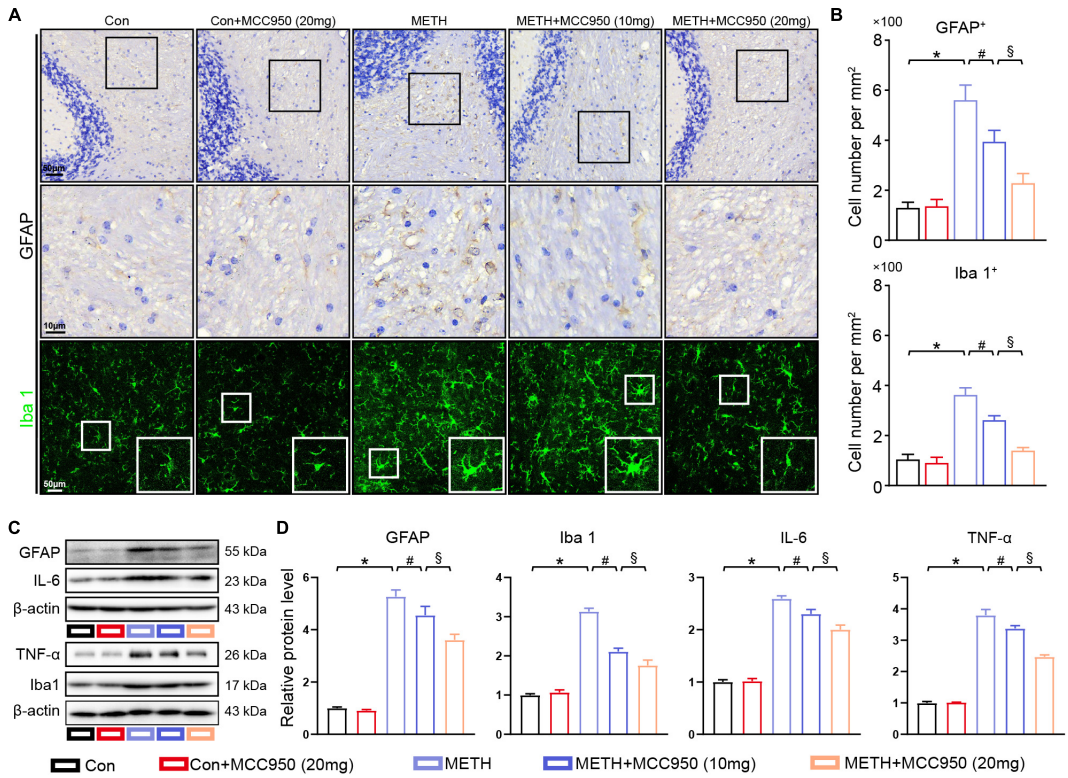

FIGURE 5 | MCC950 alleviated glial activation in cerebellar regions. **(A)** Representative images of GFAP IHC staining and Iba 1 IF staining in cerebellar regions. **(B)** Quantification of GFAP and Iba 1 positive cell number in cerebellar subregions. **(C,D)** Western blot and quantification for GFAP, Iba 1, IL-6, and TNF-α in cerebellum. $n = 6$ per group by one-way ANOVA and Bonferroni's *post-hoc* analysis, $^{*}p < 0.05$, compared with the Con group; $^{\#}p < 0.05$, compared with the METH-treated group; §$p < 0.05$, compared with the METH + MCC950 (10 mg) group.

accumulated in cerebellar PC soma after METH treatment from the high magnification images (Magnified black box in the lower panel). A decline in α-syn and p-Tau accumulation was found in the cerebellum of METH-treated mice after administration of MCC950. Moreover, the α-syn and p-Tau levels in the METH + MCC950 (20 mg/kg) group mice were lower than in METH + MCC950 (10 mg/kg) group mice (**Figures 3A,B**). Consistently, the protein levels of GFAP and Iba 1 were elevated in the METH group compared to the control group and reversed by MCC950 administration (**Figure 3C**).

Pharmacological Inhibition With MCC950 Prevents Axonal Degeneration and Myelin Sheath Destruction in the Cerebellum

To characterize cerebellar axonal degeneration after METH-induced injury, we conducted silver staining to examine the axons in the cerebellar white matter. Silver staining showed a decline in axon intensities in the white matter tracts of the METH mice, whereas both 10 and 20 mg/kg MCC950 treatment preserved axonal intensity assessed after METH intoxication (**Figures 4A,B**). Immunofluorescence of NF200 (an axon-specific protein) showed axonal degeneration in METH group mice. Consistent with the silver staining results, MCC950 attenuated the reduction in NF200 levels in the cerebellum of mice treated with METH (**Figure 4E**).

To assess the protective effect of MCC950 against METH-induced myelin loss, we conducted LFB staining and CNP immunostaining. Prophylactic treatment with MCC950 protected the myelin sheath loss in the cerebellum of METH-treated mice (**Figures 4A,C,D**). Consistent with the results of the staining sections, myelin-specific protein CNP and MBP immunoblotting showed that inflammasome modulation with MCC950 reversed the myelin-specific proteins loss induced by METH (**Figure 4E**).

MCC950 Attenuated Glial Cell Activation in Methamphetamine Mice Model

To investigate the effect of MCC950 on glial activation induced by METH, we employed GFAP and Iba 1 immunostaining to quantify the number of astrocytes and microglia. We found that METH increased the numbers of astrocytes and microglia within the cerebellum. METH-treated mice that received MCC950 exhibited significantly fewer astrocytes and microglia cells in the cerebellum than control mice (**Figures 5A,B**). Immunoblotting showed a significant increase in GFAP and Iba 1 levels in METH-treated mice compared with control mice. Inhibition of NLRP3

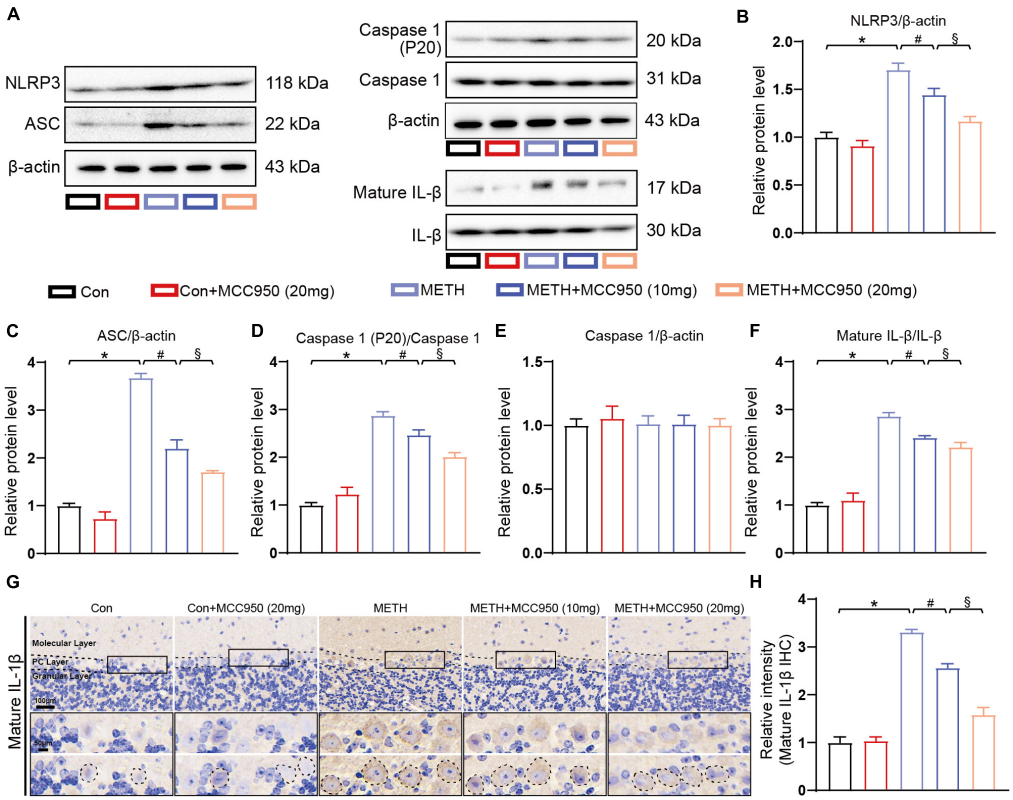

FIGURE 6 | Effect of MCC950 on NLRP3 pathway in METH mice model. **(A)** Representative western blot bands of NLRP3, ASC, Caspase-1, Cleaved Caspase-1, mature IL-1β, and IL-1β of mice cerebellar tissues in each group. **(B–F)** Quantification of NLRP3, ASC, Caspase-1, Cleaved Caspase-1, mature IL-1β, and IL-1β protein levels of mice cerebellar tissues from western blot bands. $n = 3$ per group. **(G)** Representative images of mature IL-1β IHC staining in cerebellar areas. **(H)** Relative intensity of mature IL-1β in cerebellar areas. One-way ANOVA and Bonferroni's *post-hoc* analysis, $^{*}p < 0.05$, compared with the Con group; $^{\#}p < 0.05$, compared with the METH-treated group; §$p < 0.05$, compared with the METH + MCC950 (10 mg) group.

by MCC950 enhanced IL-6 and TNF-α upregulation in the cerebellum of METH-treated mice (**Figures 5C,D**).

Modulating NLRP3 by MCC950 Decreased Interleukin-1β Secretion Through Caspase-1 Dependent Pathway in Methamphetamine Mice Model

To explore the mechanism underlying the protective effect of MCC950 in METH-induced cerebellar degeneration, we conducted an immunoblotting analysis of NLRP3 pathway proteins including NLRP3, ASC, Caspase-1, Cleaved Caspase-1 (P20), IL-1β and mature IL-1β. We found that NLRP3, ASC, Cleaved Caspase-1 and mature IL-1β protein expression were elevated in the cerebellum of METH-treated mice. Furthermore, MCC950 (at 10 and 20 mg/kg) suppressed METH-induced increases in protein levels of NLRP3, Cleaved Caspase-1 and mature IL-1β. Moreover, the cerebellar NLRP3, Cleaved Caspase-1 and mature IL-1β protein levels were significantly lower in the (METH + 20 mg/kg MCC950) group than in the (METH + 10 mg/kg MCC950) group (**Figures 6A–F**). Finally, IHC staining revealed that mature IL-1β intensity was significantly decreased in the (METH + MCC950) group mice compared to METH-treated mice (**Figures 6G,H**).

DISCUSSION

It has been established that the nigrostriatal dopaminergic system is vulnerable to METH exposure since METH can be transferred into the cytoplasm by dopamine transporters (Huang et al., 2020). A recent study indicated that METH might lead to electrophysiological and morphological alternations of cerebellar PC (Ramshini et al., 2021). In the present study, we demonstrated that chronic METH could influence behavioral performance and cerebellar neurodegeneration involving a decrease in the number of PC, α-syn and p-Tau accumulation, axon degeneration, myelin sheath destruction and glial activation.

Importantly, the NLRP3-ASC-Caspase 1 pathway is activated during this process. To the best of our knowledge, this is the first study to expound that modulation of NLRP3 by MCC950 exerts a protective effect against motor deficits and cerebellar degeneration in METH-treated mice. These results suggested that NLRP3 might be a therapeutic target, and the NLRP3 pathway is associated with METH-induced cerebellar degeneration.

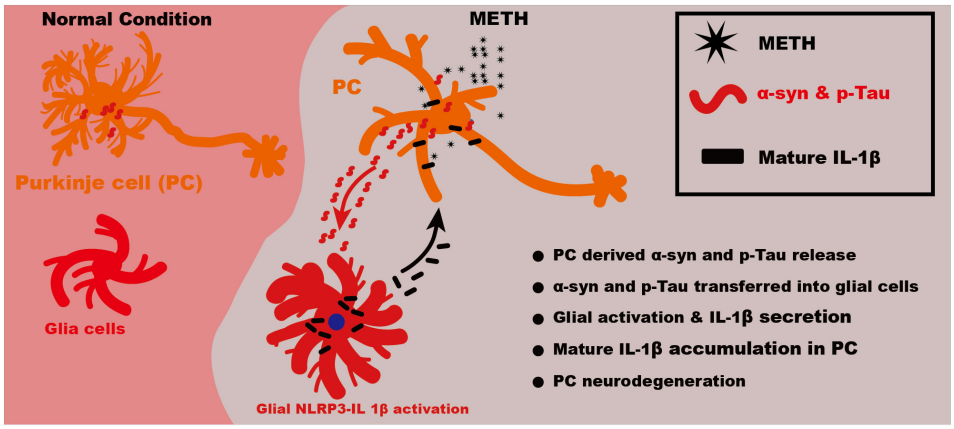

FIGURE 7 | Schematic illustration of mechanism of NLRP3–IL-1β mediating METH induced cerebellar neurodegeneration. Upon METH treatment, the α-syn and p-Tau level was increased in PCs. The increased α-syn and p-Tau might release from neurons and be uptaken by glia cells. The activated glia could secrete inflammatory factors IL-1β through NLRP3 activation. The excess IL-1β damage the neurons, which lead to α-syn and p-Tau level increasing. Thus the neuronal α-syn and p-Tau accumulation and microglial NLRP3 activation form a vicious cycle.

An increasing body of evidence suggests that NLRP3 participates in the formation of inflammasomes in several neurodegenerative diseases, such as Alzheimer's disease and Parkinson's disease (Yang et al., 2020). Moreover, targeting NLRP3 can alleviate learning and memory deficits in an Alzheimer's disease mice model (Lonnemann et al., 2020). To confirm that NLRP3 inhibition alleviates the behavioral impairment induced by METH, we conducted behavioral tests. Indeed, we found NLRP3 inhibition exerts protective effects on motor balance and coordination impairments induced by METH (**Figures 1B–F**). Importantly, we found that 20 mg/kg MCC950 was more effective than 10 mg/kg MCC950 in response to METH-induced behavior impairment.

It has been established that the PC is a unique kind of neuron that represents the only efferent neuron in the cerebellar cortex, essential for cerebellar function (Schonewille et al., 2021). It is well documented that the PC number is reduced in response to METH (Ramshini et al., 2021). Consistent with this study, we found a decline in PC number in mice cerebellum after METH intoxication, which could be alleviated by 10 and 20 mg/kg of MCC950. Previous studies showed the PC loss was sufficient to drive behavioral chanes such as the impaired coordination of limb movement (Zhang H. et al., 2021). Since cerebellar PC dysfunction or degeneration is frequently accompanied with cerebellar ataxia (Aoki et al., 2022). In our study, we showed a reduction of PC number in METH group mice, which was sufficient to drive motor coordination deficit in rotarod test and footprint analysis test.

The accumulation of α-syn and p-Tau are the hallmarks of Parkinson's disease and Alzheimer's disease, respectively (Vasili et al., 2019; Yin et al., 2021). It is widely acknowledged that α-syn and p-Tau are "teammates" in neurodegenerative disease (Moussaud et al., 2014). Our previous studies revealed that both α-syn and p-Tau are upregulated in several brain regions in response to METH (Ding et al., 2020b). The present study found increased cerebellar levels of α-syn and p-Tau in METH-treated mice, especially in the PCs (**Figure 3**). Furthermore, we found that MCC950 could restore cerebellar α-syn and p-Tau aggregation levels in chronic METH-treated mice. These findings suggested that therapeutic NLRP3 inhibition could alleviate pathological α-syn and p-Tau accumulations in METH-treated mice, consistent with findings of a recent study that showed that pharmacological inhibition of NLRP3 could protect against α-syn pathology in a Parkinson's disease mice model (Gordon et al., 2018). Importantly, α-syn can trigger NLRP3 activation in Parkinson's disease, leading to α-syn accumulation (Codolo et al., 2013; Zhang C. et al., 2021). We hypothesize that α-syn accumulation and NLRP3 activation form a vicious cycle, and disrupting this cycle by NLRP3 inhibition could alleviate α-syn pathologies in METH-treated mice.

The PC axons are the sole efferent neuron fiber in the cerebellum and are crucial to PC function (Falcon-Moya et al., 2018). Besides, the myelin sheaths, formed by oligodendrocytes, are vital for PC signal output (Bechet et al., 2020). In the present study, we observed the cerebellar axon and myelin sheath morphology in METH-treated mice. Silver and LFB stainings showed reduced axon intensity, myelin sheath destruction, respectively, and pharmacological inhibition of NLRP3 alleviated axon and myelin sheath pathologies induced by METH (**Figure 4**).

In addition to PC degeneration, glial cells activation participates in the neurodegenerative diseases process (Saijo et al., 2009). It has been suggested that activated glial cells act as phagocytic cells, which can clear the abnormal protein aggregates and cell debris and act as inflammatory factors secreting cells (Chen et al., 2021). Our previous study showed that METH triggered glial cell activation in the hippocampal and substantial nigral region (Ding et al., 2020a). Accordingly, we assessed whether METH would affect glial cell activation in the cerebellar region. The immunolabeling of GFAP (an astrocyte marker) and Iba 1 (a microglia marker) in mice

cerebellar sections revealed a significant increase in astrocyte and microglia number and inflammatory factors after 2 weeks of METH treatment. However, glial activation was suppressed in METH-treated mice after administration of MCC950, which was supported by reduced inflammatory factors such as TNF-α and IL-6 (**Figure 5**). Given that inflammatory factors may trigger neuronal dysfunction, we hypothesize that NLRP3 inhibition can alleviate cerebellar degeneration *via* modulation of inflammation.

To explore the mechanisms involved in the METH-induced cerebellar degeneration, we quantified NLRP3-ASC-Caspase 1-IL-1β pathway protein levels. Treatment with METH triggered the NLRP3 sensor, which led to the upregulation of downstream proteins including ASC, Caspase 1 and mature IL-1β. Furthermore, pharmacological inhibition of NLRP3 suppressed activation of the NLRP3-ASC-Caspase 1-IL-1β pathway. Given that mature IL-1β secretion has been shown to be a key mediator in inflammation-induced neuronal apoptosis in neurodegenerative disease (Rui et al., 2021), our mechanistic finding suggests that pharmacological inhibition of NLRP3 may alleviate inflammation through Caspase 1 dependent mature IL-1β secretion (**Figure 6**). Moreover, we found mature IL-1β accumulation in the cytoplasm of PC in METH-treated mice, indicating that glial-derived mature IL-1β was transferred into the PCs. In addition, the transfer could be blocked by MCC950 (**Figures 6G,H**). It has been reported that NLRP3 dependent mature IL-1β secretion can induce neurodegeneration in several mice models (Holbrook et al., 2021), consistent with our findings.

Taking together, our study showed that METH could upregulate the α-syn and p-Tau level in PCs. The increased α-syn and p-Tau might release from PCs and be uptaken by glial cells. The activated glial cells could secrete inflammatory factors IL-1β through NLRP3 activation. The excess IL-1β damage the neurons by inhibiting neuronal autophagy flux, which lead to α-syn and p-Tau level increasing. Thus the neuronal α-syn and p-Tau accumulation and microglial NLRP3 activation form a vicious cycle (**Figure 7**).

Overall, we demonstrated that METH could cause cerebellar neurodegeneration and motor coordination deficit through NLRP3 dependent mature IL-1β secretion-induced inflammation in METH-treated mice. Moreover, NLRP3 inhibition alleviated cerebellar pathologies and behavior abnormalities. Our study provided compelling evidence of the therapeutic effect of NLRP3 inhibitor in treating METH-induced cerebellar neurodegeneration. Nonetheless, further studies are warranted to better understand other inflammatory pathways involved in METH-induced cerebellar degeneration.

DATA AVAILABILITY STATEMENT

The original contributions presented in the study are included in the article/supplementary material, further inquiries can be directed to the corresponding author.

ETHICS STATEMENT

The animal study was reviewed and approved by the Institutional Animal Care and Use Committee of Guizhou Medical University.

AUTHOR CONTRIBUTIONS

JYD and JH conceived and designed the research. JYD, LS, YY, SH, ZR, JLD, ZL, JW, YL, QZ, and XZ performed the experiments. ZR, XQ, and TL contributed reagents, materials, analysis tools. JYD and LS wrote the manuscript. All authors edited and approved of the final manuscript.

FUNDING

This work was supported by the Research Foundation for Advanced Talents of Guizhou Medical University (Grant No. University Contract of Doctors J [2021] 014), Natural Science Foundation of Guizhou Medical University Incubation Program (Grant No. 20NSP084) (to JYD), Guizhou Province Engineering Technology Research Centre Project (Qian High-Tech of Development and Reform Commission No. [2016]1345), Guizhou Scientific Support Project (Qian Science Support [2019] 2825), Guizhou "Hundred" innovative talents project (Qian Science Talent Platform [2020] 6012), Guizhou Scientific Support Project (Qian Science Support [2020] 4Y057), and Guizhou Science Project (Qian Science Foundation [2020] 1Y353) (to JH).

REFERENCES

Aoki, H., Higashi, M., Okita, M., Ando, N., Murayama, S., Ishikawa, K., et al. (2022). Thymidine kinase 2 and mitochondrial protein COX I in the cerebellum of patients with spinocerebellar ataxia type 31 caused by penta-nucleotide repeats (TTCCA) n. *Cerebellum*. doi: 10.1007/s12311-021-01364-2

Ares-Santos, S., Granado, N., Espadas, I., Martinez-Murillo, R., and Moratalla, R. (2014). Methamphetamine causes degeneration of dopamine cell bodies and terminals of the nigrostriatal pathway evidenced by silver staining. *Neuropsychopharmacology* 39, 1066–1080. doi: 10.1038/npp.2013.307

Bechet, S., O'sullivan, S. A., Yssel, J., Fagan, S. G., and Dev, K. K. (2020). Fingolimod rescues demyelination in a mouse model of Krabbe's disease. *J. Neurosci.* 40, 3104–3118. doi: 10.1523/JNEUROSCI.2346-19.2020

Boroujeni, M. E., Nasrollahi, A., Boroujeni, P. B., Fadaeifathabadi, F., Farhadieh, M., Tehrani, A. M., et al. (2020). Exposure to methamphetamine exacerbates motor activities and alters circular RNA profile of cerebellum. *J. Pharmacol. Sci.* 144, 1–8. doi: 10.1016/j.jphs.2020.05.010

Chen, M., Lai, X., Wang, X., Ying, J., Zhang, L., Zhou, B., et al. (2021). Long Non-coding RNAs and circular RNAs: insights into microglia and astrocyte mediated neurological diseases. *Front. Mol. Neurosci.* 14:745066. doi: 10.3389/fnmol.2021.745066

Codolo, G., Plotegher, N., Pozzobon, T., Brucale, M., Tessari, I., Bubacco, L., et al. (2013). Triggering of inflammasome by aggregated alpha-synuclein, an inflammatory response in synucleinopathies. *PLoS One* 8:e55375. doi: 10.1371/journal.pone.0055375

Danaceau, J. P., Deering, C. E., Day, J. E., Smeal, S. J., Johnson-Davis, K. L., Fleckenstein, A. E., et al. (2007). Persistence of tolerance to methamphetamine-induced monoamine deficits. *Eur. J. Pharmacol.* 559, 46–54. doi: 10.1016/j.ejphar.2006.11.045

Ding, J., Hu, S., Meng, Y., Li, C., Huang, J., He, Y., et al. (2020a). Alpha-synuclein deficiency ameliorates chronic methamphetamine induced neurodegeneration in mice. *Toxicology* 438, 152461. doi: 10.1016/j.tox.2020.152461

Ding, J., Lian, Y., Meng, Y., He, Y., Fan, H., Li, C., et al. (2020b). The effect of alpha-synuclein and Tau in methamphetamine induced neurotoxicity *in vivo* and *in vitro*. *Toxicol. Lett.* 319, 213–224. doi: 10.1016/j.toxlet.2019.11.028

Du, L., Shen, K., Bai, Y., Chao, J., Hu, G., Zhang, Y., et al. (2019). Involvement of NLRP3 inflammasome in methamphetamine-induced microglial activation through miR-143/PUMA axis. *Toxicol. Lett.* 301, 53–63. doi: 10.1016/j.toxlet.2018.10.020

Eskandarian Boroujeni, M., Peirouvi, T., Shaerzadeh, F., Ahmadiani, A., Abdollahifar, M. A., and Aliaghaei, A. (2020). Differential gene expression and stereological analyses of the cerebellum following methamphetamine exposure. *Addict. Biol.* 25:e12707. doi: 10.1111/adb.12707

Falcon-Moya, R., Losada-Ruiz, P., Sihra, T. S., and Rodriguez-Moreno, A. (2018). Cerebellar kainate receptor-mediated facilitation of glutamate release requires Ca(2+)-calmodulin and PKA. *Front. Mol. Neurosci.* 11:195. doi: 10.3389/fnmol.2018.00195

Gordon, R., Albornoz, E. A., Christie, D. C., Langley, M. R., Kumar, V., Mantovani, S., et al. (2018). Inflammasome inhibition prevents alpha-synuclein pathology and dopaminergic neurodegeneration in mice. *Sci. Transl. Med.* 10:eaah4066. doi: 10.1126/scitranslmed.aah4066

Holbrook, J. A., Jarosz-Griffiths, H. H., Caseley, E., Lara-Reyna, S., Poulter, J. A., Williams-Gray, C. H., et al. (2021). Neurodegenerative disease and the NLRP3 inflammasome. *Front. Pharmacol.* 12:643254. doi: 10.3389/fphar.2021.643254

Huang, J., Yang, G., Li, Z., Leung, C. K., Wang, W., Li, Y., et al. (2020). Involvement of dopamine D3 receptor and dopamine transporter in methamphetamine-induced behavioral sensitization in tree shrews. *Brain Behav.* 10:e01533. doi: 10.1002/brb3.1533

Kohno, M., Dennis, L. E., Mccready, H., and Hoffman, W. F. (2021). Dopamine dysfunction in stimulant use disorders: mechanistic comparisons and implications for treatment. *Mol. Psychiatry*. doi: 10.1038/s41380-021-01180-4

Lamkanfi, M., and Dixit, V. M. (2014). Mechanisms and functions of inflammasomes. *Cell* 157, 1013–1022. doi: 10.1016/j.cell.2014.04.007

Li, J. H., Liu, J. L., Zhang, K. K., Chen, L. J., Xu, J. T., and Xie, X. L. (2021). The adverse effects of prenatal METH exposure on the offspring: a review. *Front. Pharmacol.* 12:715176. doi: 10.3389/fphar.2021.715176

Lonnemann, N., Hosseini, S., Marchetti, C., Skouras, D. B., Stefanoni, D., D'Alessandro, A., et al. (2020). The NLRP3 inflammasome inhibitor OLT1177 rescues cognitive impairment in a mouse model of Alzheimer's disease. *Proc. Natl. Acad. Sci. U.S.A.* 117, 32145–32154. doi: 10.1073/pnas.2009680117

Martinon, F., Burns, K., and Tschopp, J. (2002). The inflammasome: a molecular platform triggering activation of inflammatory caspases and processing of proIL-beta. *Mol. Cell* 10, 417–426. doi: 10.1016/s1097-2765(02)00599-3

Moussaud, S., Jones, D. R., Moussaud-Lamodiere, E. L., Delenclos, M., Ross, O. A., and Mclean, P. J. (2014). Alpha-synuclein and tau: teammates in neurodegeneration? *Mol. Neurodegener.* 9:43. doi: 10.1186/1750-1326-9-43

Nabar, N. R., and Kehrl, J. H. (2019). Inflammasome inhibition links IRGM to innate immunity. *Mol. Cell* 73, 391–392. doi: 10.1016/j.molcel.2019.01.029

Nobrega, C., Nascimento-Ferreira, I., Onofre, I., Albuquerque, D., Conceicao, M., Deglon, N., et al. (2013). Overexpression of mutant ataxin-3 in mouse cerebellum induces ataxia and cerebellar neuropathology. *Cerebellum* 12, 441–455. doi: 10.1007/s12311-012-0432-0

Qiu, X., Wang, Q., Hou, L., Zhang, C., Wang, Q., and Zhao, X. (2021). Inhibition of NLRP3 inflammasome by glibenclamide attenuated dopaminergic neurodegeneration and motor deficits in paraquat and maneb-induced mouse Parkinson's disease model. *Toxicol. Lett.* 349, 1–11. doi: 10.1016/j.toxlet.2021.05.008

Ramshini, E., Sheykhzade, M., Dabiri, S., and Shabani, M. (2021). Cannabinoid CB1 receptor mediates METH-induced electrophysiological and morphological alterations in cerebellum Purkinje cells. *Hum. Exp. Toxicol.* 40, 940–951. doi: 10.1177/0960327120975448

Rathinam, V. A., and Fitzgerald, K. A. (2016). Inflammasome complexes: emerging mechanisms and effector functions. *Cell* 165, 792–800. doi: 10.1016/j.cell.2016.03.046

Ruan, Q. T., Yazdani, N., Blum, B. C., Beierle, J. A., Lin, W., Coelho, M. A., et al. (2020). A mutation in Hnrnph1 that decreases methamphetamine-induced reinforcement, reward, and dopamine release and increases synaptosomal hnRNP H and mitochondrial proteins. *J. Neurosci.* 40, 107–130. doi: 10.1523/JNEUROSCI.1808-19.2019

Rui, W., Xiao, H., Fan, Y., Ma, Z., Xiao, M., Li, S., et al. (2021). Systemic inflammasome activation and pyroptosis associate with the progression of amnestic mild cognitive impairment and Alzheimer's disease. *J. Neuroinflammation* 18:280. doi: 10.1186/s12974-021-02329-2

Saijo, K., Winner, B., Carson, C. T., Collier, J. G., Boyer, L., Rosenfeld, M. G., et al. (2009). A Nurr1/CoREST pathway in microglia and astrocytes protects dopaminergic neurons from inflammation-induced death. *Cell* 137, 47–59. doi: 10.1016/j.cell.2009.01.038

Schonewille, M., Girasole, A. E., Rostaing, P., Mailhes-Hamon, C., Ayon, A., Nelson, A. B., et al. (2021). NMDARs in granule cells contribute to parallel fiber-Purkinje cell synaptic plasticity and motor learning. *Proc. Natl. Acad. Sci. U.S.A.* 118:e2102635118. doi: 10.1073/pnas.2102635118

Schroder, K., and Tschopp, J. (2010). The inflammasomes. *Cell* 140, 821–832.

Sekine, Y., Ouchi, Y., Takei, N., Yoshikawa, E., Nakamura, K., Futatsubashi, M., et al. (2006). Brain serotonin transporter density and aggression in abstinent methamphetamine abusers. *Arch. Gen. Psychiatry* 63, 90–100. doi: 10.1001/archpsyc.63.1.90

Song, L., Pei, L., Yao, S., Wu, Y., and Shang, Y. (2017). NLRP3 inflammasome in neurological diseases, from functions to therapies. *Front. Cell. Neurosci.* 11:63. doi: 10.3389/fncel.2017.00063

Strowig, T., Henao-Mejia, J., Elinav, E., and Flavell, R. (2012). Inflammasomes in health and disease. *Nature* 481, 278–286. doi: 10.1038/nature10759

Vasili, E., Dominguez-Meijide, A., and Outeiro, T. F. (2019). Spreading of alpha-Synuclein and Tau: a systematic comparison of the mechanisms involved. *Front. Mol. Neurosci.* 12:107. doi: 10.3389/fnmol.2019.00107

Wagner, M. J., Savall, J., Hernandez, O., Mel, G., Inan, H., Rumyantsev, O., et al. (2021). A neural circuit state change underlying skilled movements. *Cell* 184, 3731–3747.e21. doi: 10.1016/j.cell.2021.06.001

Yang, J., Wise, L., and Fukuchi, K. I. (2020). TLR4 cross-Talk With NLRP3 inflammasome and complement signaling pathways in Alzheimer's disease. *Front. Immunol.* 11:724. doi: 10.3389/fimmu.2020.00724

Yin, X., Zhao, C., Qiu, Y., Zhou, Z., Bao, J., and Qian, W. (2021). Dendritic/Post-synaptic Tau and early pathology of Alzheimer's disease. *Front. Mol. Neurosci.* 14:671779. doi: 10.3389/fnmol.2021.671779

Zhang, C., Zhao, M., Wang, B., Su, Z., Guo, B., Qin, L., et al. (2021). The Nrf2-NLRP3-caspase-1 axis mediates the neuroprotective effects of Celastrol in Parkinson's disease. *Redox Biol.* 47, 102134. doi: 10.1016/j.redox.2021.102134

Zhang, H., Hong, Y., Yang, W., Wang, R., Yao, T., Wang, J., et al. (2021). SNX14 deficiency-induced defective axonal mitochondrial transport in Purkinje cells underlies cerebellar ataxia and can be reversed by valproate. *Natl. Sci. Rev.* 8:nwab024. doi: 10.1093/nsr/nwab024

Conflict of Interest: The authors declare that the research was conducted in the absence of any commercial or financial relationships that could be construed as a potential conflict of interest.

Publisher's Note: All claims expressed in this article are solely those of the authors and do not necessarily represent those of their affiliated organizations, or those of the publisher, the editors and the reviewers. Any product that may be evaluated in this article, or claim that may be made by its manufacturer, is not guaranteed or endorsed by the publisher.

frontiers | Frontiers in Molecular Neuroscience

ORIGINAL RESEARCH
published: 14 April 2022
doi: 10.3389/fnmol.2022.839233

Identification of Functional CircRNA–miRNA–mRNA Regulatory Network in Dorsolateral Prefrontal Cortex Neurons of Patients With Cocaine Use Disorder

Yun Chen[1,2], Xianfeng Li[3], Shiqiu Meng[2], Shihao Huang[4], Suhua Chang[5] and Jie Shi[2,6]**

[1] Department of Pharmacology, School of Basic Medical Sciences, Peking University Health Science Center, Beijing, China, [2] Beijing Key Laboratory on Drug Dependence Research, National Institute on Drug Dependence, Peking University, Beijing, China, [3] Department of Gastroenterology of Dapping Hospital, Third Military Medical University, Chongqing, China, [4] Key Laboratory of Molecular Epidemiology of Hunan Province, School of Medicine, Hunan Normal University, Changsha, China, [5] Institute of Mental Health, National Clinical Research Center for Mental Disorders, Key Laboratory of Mental Health and Peking University Sixth Hospital, Peking University, Beijing, China, [6] Peking University, Shenzhen Hospital, Shenzhen, China

OPEN ACCESS

Edited by:
Jianfeng Liu,
Texas A&M University, United States

Reviewed by:
Min Zhao,
Shanghai Changning Mental Health Center, China
Biao Yan,
Fudan University, China

***Correspondence:**
Jie Shi
shijie@bjmu.edu.cn
Suhua Chang
changsh@bjmu.edu.cn

Specialty section:
This article was submitted to Molecular Signalling and Pathways, a section of the journal Frontiers in Molecular Neuroscience

Received: 19 December 2021
Accepted: 01 March 2022
Published: 14 April 2022

Citation:
Chen Y, Li X, Meng S, Huang S, Chang S and Shi J (2022) Identification of Functional CircRNA–miRNA–mRNA Regulatory Network in Dorsolateral Prefrontal Cortex Neurons of Patients With Cocaine Use Disorder. Front. Mol. Neurosci. 15:839233. doi: 10.3389/fnmol.2022.839233

Increasing evidence has indicated that circular RNAs (circRNAs) act as competing endogenous RNAs (ceRNAs) regulatory network to regulate the expression of target genes by sponging microRNAs (miRNAs), and therefore play an essential role in many neuropsychiatric disorders, including cocaine use disorder. However, the functional roles and regulatory mechanisms of circRNAs as ceRNAs in dorsolateral prefrontal cortex (dlPFC) of patients with cocaine use disorder remain to be determined. In this study, an expression profiling for dlPFC in 19 patients with cocaine use disorder and 17 controls from Gene Expression Omnibus datasets was used for the differentially expressed circRNAs analysis and the differentially expressed mRNAs analysis. Several tools were used to predict the miRNAs targeted by the circRNAs and the miRNAs targeted mRNAs, which then overlapped with the cocaine-associated differentially expressed mRNAs to determine the functional roles of circRNAs. Functional analysis for the obtained mRNAs was performed *via* Gene Ontology (GO) in Metascape database. Integrated bioinformatics analysis was conducted to further characterize the circRNA–miRNA–mRNA regulatory network and identify the functions of distinct circRNAs. We found a total of 41 differentially expressed circRNAs, and 98 miRNAs were targeted by these circRNAs. The overlapped mRNAs targeted by the miRNAs and the differentially expressed mRNAs constructed a circRNA–miRNA–mRNA regulation network including 24 circRNAs, 43 miRNAs, and 82 mRNAs in the dlPFC of patients with cocaine use disorder. Functional analysis indicated the regulation network mainly participated in cell response-related, receptor signaling-related, protein modification-related and axonogenesis-related pathways, which might be involved with cocaine use disorder. Additionally, we determined four hub genes (*HSP90AA1*, *HSPA1B*, *YWHAG*,

and *RAB8A*) from the protein–protein interaction network and constructed a circRNA–miRNA-hub gene subnetwork based on the four hub genes. In conclusion, our findings provide a deeper understanding of the circRNAs-related ceRNAs regulatory mechanisms in the pathogenesis of cocaine use disorder.

Keywords: cocaine use disorder, circRNAs, ceRNAs regulatory network, protein–protein interaction network, hub genes, integrated bioinformatics analysis

INTRODUCTION

Cocaine addiction inflicts enormous health and economic costs to individuals, families, and society (Reid et al., 2012; United Nations Office on Drugs and Crime, 2020). Recently, significantly increased studies have focused on the field of neuroscience of cocaine use disorder, but its neurobiological mechanism is still unclear, and there is no effective clinical treatment for cocaine use disorder (Gawin and Ellinwood, 1989; Majewska, 1996a,b; Heal et al., 2014).

Epigenetic mechanisms can integrate both genetic and diverse environmental stimuli to exert potent and often long-lasting changes in gene expression (Jaenisch and Bird, 2003). Accumulating research has found epigenetic mechanism plays an important role in the drug addiction (Robison and Nestler, 2011; Nestler, 2014; Nestler and Lüscher, 2019). Non-coding RNAs, specifically long non-coding RNAs, circular RNAs (circRNAs), and small non-coding RNAs, are one type of common epigenetic regulators that play a vital role in many biological processes associated with diseases (Amin et al., 2019; Mehta et al., 2020).

Circular RNAs are vastly conserved non-coding RNAs formed by back-splicing and covalent fusion of RNA free ends into natural circles (Vicens and Westhof, 2014; Szabo and Salzman, 2016; Greene et al., 2017; Li et al., 2018). Because circRNAs lack poly(A) tails and cap structure, they are not affected by RNA exonuclease (Vicens and Westhof, 2014; Szabo and Salzman, 2016; Greene et al., 2017; Li et al., 2018). CircRNAs usually exert their functions as transcriptional and post-transcriptional regulators through various functional mechanisms, such as RNA binding protein (RBP) "sponges" (Du et al., 2016; Holdt et al., 2016), translated proteins (Legnini et al., 2017; Pamudurti et al., 2017), and RNA–RNA interaction (Li et al., 2015). At present, circRNAs function mainly by absorbing microRNAs (miRNAs) as competing endogenous RNAs (ceRNAs) regulatory network to regulate their target genes expression, which construct a functional circRNA–miRNA–mRNA regulation network (Hansen et al., 2013; Vicens and Westhof, 2014; Rybak-Wolf et al., 2015; Du et al., 2017; Greene et al., 2017; Li et al., 2018; Mehta et al., 2020). For example, knockdown of circHIPK2 expression significantly inhibited astrocyte activation induced by methamphetamine through the targeting of miR124 and SIGMAR1 (Huang et al., 2017). Another study reported that circTmeff-1 promotes incubation of context-induced morphine craving by sponging miR-541/miR-6934 in the nucleus accumbens (Yu et al., 2021).

Although several circRNAs have been identified as participating in cocaine addiction, the regulatory networks in patients with cocaine use disorder are still unknown. It is necessary to conduct the circRNA–miRNA–mRNA regulatory networks in patients with cocaine use disorder to help to advance our understanding of the molecular mechanism of cocaine use disorder. Dorsolateral prefrontal cortex (dlPFC), similar role to medial PFC in rodents (Seamans et al., 2008), is a crucial component brain region of inhibitory control (Gass and Chandler, 2013; Moeller et al., 2014), which undergoes significant changes after long-term cocaine use (Matochik et al., 2003; Moreno-Lopez et al., 2012) and is involved in compulsive drug-seeking behaviors, increasing drug intake and addiction severity (Chen B. T. et al., 2013; Conti and Nakamura-Palacios, 2014; Terraneo et al., 2016). In this study, we aimed to investigate the functional circRNA–miRNA–mRNA regulatory networks in the dlPFC of patients with cocaine use disorder. Lastly, we constructed a circRNA–miRNA–mRNA regulation network including 24 circRNAs, 43 miRNAs, and 82 mRNAs, which may reveal a novel molecular mechanism in pathogenesis of patients with cocaine use disorder.

MATERIALS AND METHODS

Data Collection

The circRNAs expression data were obtained from GSE99349 in GEO database.[1] The data were generated using RNA sequencing (RNA-seq) of human postmortem dlPFC neuronal nuclei for 19 patients with cocaine use disorder and 17 unaffected controls. All patients who met criteria for cocaine use disorder were identified sudden deaths due to the toxic effects of chronic cocaine abuse (Ribeiro et al., 2017). Unaffected controls, who were selected from homicides, accidental or natural deaths, were drug-free age-matched subjects. Post-mortem interval (PMI), RNA integrity number (RIN), age, and race are provided in the original paper and do not significantly differ between cases and controls (Ribeiro et al., 2017). In the original study, the authors analyzed the differentially expressed genes and non-coding linear RNAs, but did not analyze the circRNAs. We further analyzed the circRNAs using the data of GSE99349 and used the differentially expressed genes in the original study to overlap predicted genes.

In addition, we collected some differentially expressed mRNAs from PFC RNA-seq data of different cocaine addiction animal models (GSE124952 and GSE89572) (Li et al., 2017; Bhattacherjee et al., 2019).

[1] http://www.ncbi.nlm.nih.gov/geo/

Identification of Differentially Expressed Circular RNAs

Cutadapt (Martin, 2011) was used to remove the reads that contained adaptor contamination, low-quality bases, and undetermined bases. Next, sequence quality was verified using FastQC (Andrews, 2010). Bowtie 2 was used to map reads to the human genome hg37 (Langmead and Salzberg, 2012). CIRI2 was initially used for *de novo* assembly of the mapped reads into circRNAs (Gao et al., 2018); subsequently, back-splicing reads were identified in unmapped reads using CIRI2. The total reads and the number of mapped reads per sample is shown in **Supplementary Table 1**. The differentially expressed of circRNAs were calculated using R package edgeR (Robinson et al., 2010). Only the comparisons with P-value < 0.05 and fold change ≥ 1.5 were regarded as differential expressed circRNAs.

Target MicroRNAs and mRNAs Prediction and Regulatory Network Establishment

MicroRNAs targeted by circRNAs were predicted using miRDB (target score >80) (Liu and Wang, 2019; Chen and Wang, 2020). Putative miRNAs were listed based on competitive binding ability, the top five miRNAs for each circRNA were mainly considered as circRNA target (Lv et al., 2018) and selected for further targeted mRNA predictions using TargetScan (score <−0.4) (Agarwal et al., 2015), DIANA-microT (score >0.8) (Paraskevopoulou et al., 2013), Tarbase (Vergoulis et al., 2012), and miRDB (score >80) (Liu and Wang, 2019). TargetScan, DIANA-microT, and TarBase are based on DIANA-miRPath v.3 platform (Fromm et al., 2015; Vlachos and Hatzigeorgiou, 2017). Only the target mRNAs presented in at least 3 out of 4 databases were considered as target genes of the given miRNAs. The targeted mRNAs were then overlapped with the differentially expressed mRNA data of the dlPFC neurons of patients with cocaine use disorder (Ribeiro et al., 2017). Last, a circRNA–miRNA–mRNA regulatory network was constructed. Cytoscape (Shannon et al., 2003) (version 3.6.0) was used to delineate the cocaine-related gene regulatory network.

Gene Set Enrichment Analysis for mRNAs in the Regulatory Network

To assess functional enrichment, Metascape Gene Ontology (GO) terms were used to perform gene set enrichment analysis for the mRNAs in the circRNA–miRNA–mRNA network (Zhou et al., 2019). The thresholds of enrichment analysis were set as GO terms with $P < 0.01$ and the count of genes involved in the GO terms ≥3.

Establishment of Protein–Protein Interaction Network and Identification of Hub Genes

The protein–protein interaction (PPI) network of the mRNAs in the circRNA–miRNA–mRNA network was established using the STRING database (Szklarczyk et al., 2017; Doncheva et al., 2019), and then visualized using Cytoscape software (Shannon et al., 2003). Subsequently, cytoHubba app (Chin et al., 2014) of Cytoscape was used to determine the hub genes. According to the degree ranks of cytoHubba app, the nodes degree ≥5 were considered as hub genes. The structure pattern of several vital circRNAs associated with hub genes were drawn using the database CSCD (Feng et al., 2021), which can be used for predicting miRNA response element, RBP, and open reading frame to better explore the potentially functional mechanisms of the selected circRNA.

RESULTS

Identification of Differentially Expressed Circular RNAs in Dorsolateral Prefrontal Cortex of Patients With Cocaine Use Disorder

A total 2,046 circRNAs were identified in the GSE99349 dataset, and exon-derived circRNA account for 77.4% (**Figure 1A**). Among these, 16 up-regulated circRNAs and 25 down-regulated circRNAs with fold changes ≥ 1.5 and P-values ≤ 0.05 were considered as significantly differentially expressed circRNAs (**Figure 1B**). Among the differentially expressed circRNAs, 65.9% had already existed in the circBase database (Glažar et al., 2014), 14 were *de novo* significantly differentially expressed circRNAs (**Tables 1**, **2**). Of the differentially expressed circRNAs, 90.24% were covered in the exon of the genome (**Figure 1C**), others aligned with intron or other sequences. Interestingly, non-coding RNA MALAT1 produced seven circRNAs (named circMALAT1-1 to circMALAT1-7 in **Tables 1**, **2**). Additionally, the chromosome distribution of the circRNAs showed no significant differences (**Figure 1D**).

Construction of the circRNA–miRNA–mRNA ceRNAs Network

Given the potential regulatory roles of circRNAs on recruiting miRNAs to regulate the expression of target genes, we predicted the miRNA "sponges" of circRNA using miRDB database, and 98 miRNAs were found to be closely targeted by the differentially expressed circRNAs. These 98 miRNAs further targeted 2,115 mRNA genes, among which, 82 mRNAs were overlapped with the differentially expressed mRNA of dlPFC neurons of patients with cocaine use disorder (Ribeiro et al., 2017), including 22 up-regulated mRNAs and 60 down-regulated mRNAs (**Figures 2A,B**). Ultimately, the 82 target mRNAs were targeted by 43 miRNAs, and the miRNAs were further targeted by 24 circRNAs, which formed a circRNA–miRNA–mRNA network for further study (**Figure 2C**).

Functional and Pathway Enrichment Analyses

Gene Ontology pathway enrichment analysis for the 82 genes aberrantly expressed in the patients with cocaine use disorder and indirectly regulated by circRNAs revealed that the 22

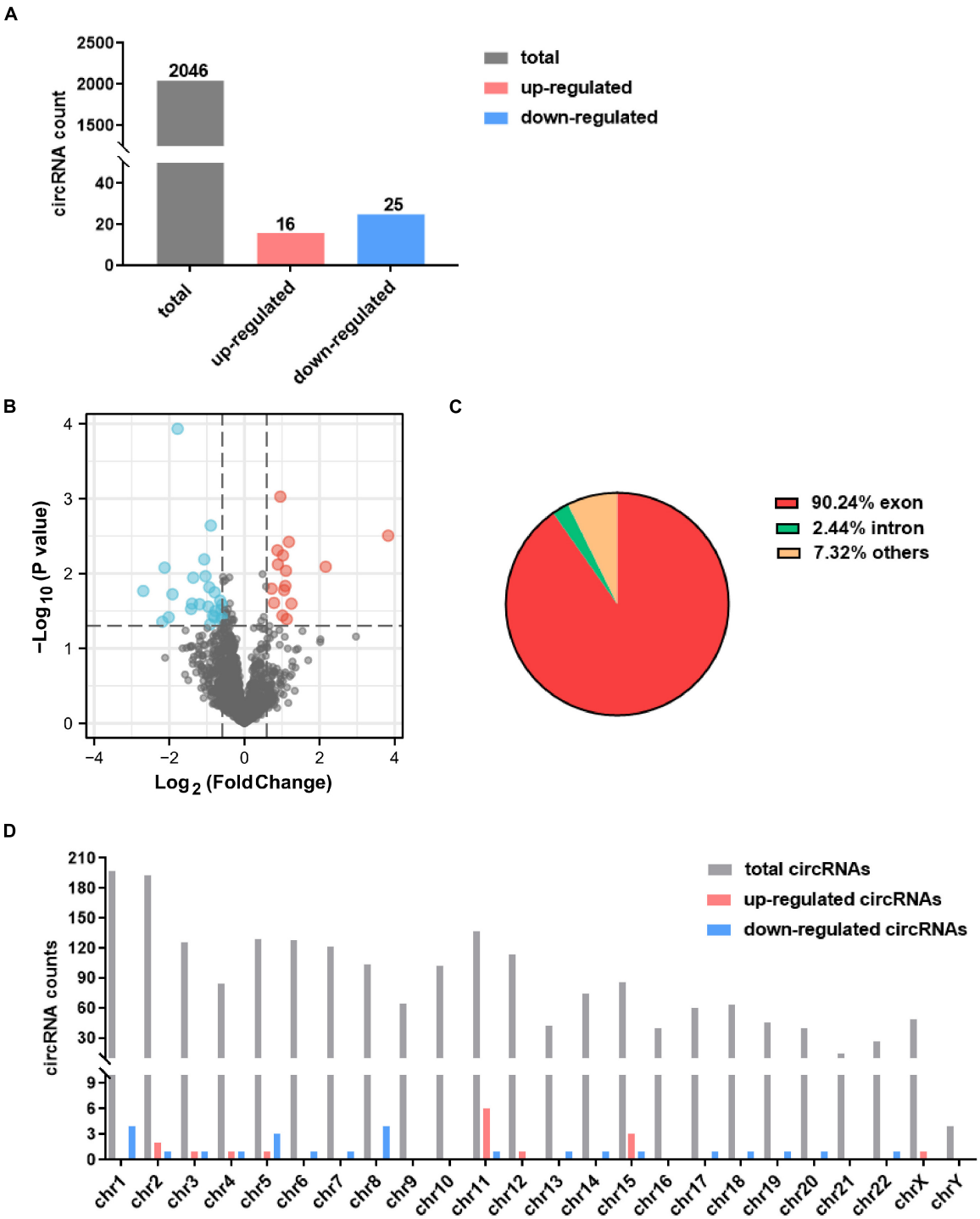

FIGURE 1 | Identification of differentially expressed circRNAs in dorsolateral prefrontal cortex neurons of patients with cocaine use disorder. **(A)** The count of identified circRNAs. **(B)** Volcano plot showing circRNAs expression in patients with cocaine use disorder and unaffected controls. The red and blue dots represent circRNAs with statistically significant differences in expression. **(C)** Pie chart showing the percentage of circRNAs derived from different genomic regions. **(D)** Distributions of identified circRNAs along the chromosomes.

up-regulated genes participated in vital biological processes including positive regulation of axonogenesis (GO: 0050772) and cell junction organization (GO: 0034330) (**Figure 3A**), which is consistent with current reports on the relationship between cocaine addiction and the synaptic transmission (Li et al., 2021; Wang et al., 2021; Zinsmaier et al., 2021).

TABLE 1 | Basic characteristics of the up-regulated circRNAs.

CircRNA_name	circBase_ID	Ensemble_ID	Log fold_change	*P*_value	Genome_location
circPAPSS1	hsa_circ_0005965	ENSG00000138801	3.826226	0.00312	chr4:108603171| 108615162
circEIF3J	–	ENSG00000104131	2.162914	0.008119	chr15:44843074| 44846865
circDBN1	–	ENSG00000113758	1.249996	0.025277	chr5:176887645| 176893833
circSLC30A6	hsa_circ_0005695	ENSG00000152683	1.126922	0.040697	chr2:32399132| 32409407
circERC2	hsa_circ_0124267	ENSG00000187672	1.105095	0.00919	chr3:55984453| 56026278
circSCAPER	hsa_circ_0000640	ENSG00000140386	1.088051	0.014667	chr15:77020936| 77025725
circGRIN2B	–	ENSG00000273079	1.024252	0.005729	chr12:13708789| 13708961
circMALAT1-1	–	ENSG00000251562	0.955983	0.000941	chr11:65267096| 65267394
circMALAT1-2	–	ENSG00000251562	1.182962	0.003779	chr11:65267060| 65267236
circMALAT1-3	–	ENSG00000251562	0.722058	0.015946	chr11:65267954| 65268132
circMALAT1-4	–	ENSG00000251562	1.056787	0.016663	chr11:65267237| 65267385
circMALAT1-5	–	ENSG00000251562	0.786989	0.024681	chr11:65266605| 65266756
circMALAT1-6	–	ENSG00000251562	1.014213	0.036447	chr11:65266720| 65266894
circSRBD1	hsa_circ_0120146	ENSG00000068784	0.89058	0.007569	chr2:45773871| 45812913
circMYO5A	hsa_circ_0103878	ENSG00000197535	0.877909	0.004901	chr15:52638558| 52646211
circIL1RAPL1	–	ENSG00000169306	0.666318	0.050085	chrX:28941541| 28943776

The symbol "–" indicating this circRNA was not existing in circBase database.

TABLE 2 | Basic characteristics of the down-regulated circRNAs.

CircRNA_name	circBase_ID	Ensemble_ID	Log fold_change	*P*_value	Genome_location
circMALAT1-7	–	ENSG00000251562	−0.59212	0.038581	chr11:65267160| 65267534
circEGLN1	hsa_circ_0000196	ENSG00000135766	−0.59753	0.026098	chr1:231506308| 231509845
circSATB1	hsa_circ_0064557	ENSG00000182568	−0.61692	0.041324	chr3:18456603| 18462483
circKHDRBS3	hsa_circ_0135838	ENSG00000131773	−0.61726	0.030379	chr8:136533480| 136569830
circLRCH1	hsa_circ_0002215	ENSG00000136141	−0.64777	0.023012	chr13:47297356| 47308133
circRGS7-1	hsa_circ_0112723	ENSG00000182901	−0.77351	0.031668	chr1:240990398| 241033419
circSATB2	hsa_circ_0003915	ENSG00000119042	−0.79387	0.017806	chr2:200233328| 200298237
circMNAT1	hsa_circ_0008215	ENSG00000020426	−0.79855	0.038421	chr14:61278705| 61346553
circRBM39	hsa_circ_0005848	ENSG00000131051	−0.83443	0.036584	chr20:34309662| 34320057
circHOOK3	hsa_circ_0005376	ENSG00000168172	−0.89529	0.002289	chr8:42780700| 42798588
circAKAP10	hsa_circ_0006256	ENSG00000108599	−0.9144	0.047896	chr17:19812494| 19813291
circSNTG1	–	ENSG00000147481	−0.93671	0.015294	chr8:51362228| 51503477
circATXN10	hsa_circ_0003054	ENSG00000130638	−0.96313	0.027635	chr22:46085592| 46114373
circESCO1	hsa_circ_0047071	ENSG00000141446	−1.03841	0.010851	chr18:19112434| 19112621
circSTXBP5-AS1	–	ENSG00000233452	−1.3646	0.011378	chr6:147394380| 147395983
circTJP1	hsa_circ_0034293	ENSG00000104067	−1.06956	0.006483	chr15:30053342| 30065560
circCAP1	hsa_circ_0009142	ENSG00000131236	−1.19278	0.0257077	chr1:40529899| 40530231
circMTHFD2L	hsa_circ_0069982	ENSG00000163738	−1.39497	0.025271	chr4:75040223| 75091111
circRGS7-2	hsa_circ_0007091	ENSG00000182901	−1.41979	0.029781	chr1:241094017| 241100006
circADAMTS19	hsa_circ_0073810	ENSG00000145808	−1.78036	0.000117	chr5:128861977| 128887600
circARHGAP26	hsa_circ_0074368	ENSG00000145819	−1.915	0.018909	chr5:142416761| 142437312
circRASA1	hsa_circ_0004317	ENSG00000145715	−2.01716	0.038434	chr5:86627165| 86649052
circLUC7L2	hsa_circ_0133534	ENSG00000146963	−2.12507	0.008356	chr7:139083345| 139097326
circCSPP1	hsa_circ_0084665	ENSG00000104218	−2.18439	0.044077	chr8:68007528| 68007967
*	–	Intergenic	−2.69379	0.017096	chr19:11977352| 12058122

The symbol "" indicating this circRNA was from intergenic region.*
The symbol "–" indicating this circRNA was not existing circBase database.

Moreover, the 62 down-regulated genes participated in vital biological processes including cellular response (GO:0032870, GO:0034605, and GO:0048511), protein modification and transport process (GO:0006986, GO:0046854, GO:0051258, GO:0031400, and GO:0017038), intracellular receptor and calcium-ion (GO:0030522, GO:0017156, and GO:0019722), cell and tissue morphogenesis (GO:0030099, GO:0001764, GO:0060538, GO:0048729, and GO:0030010), autophagy

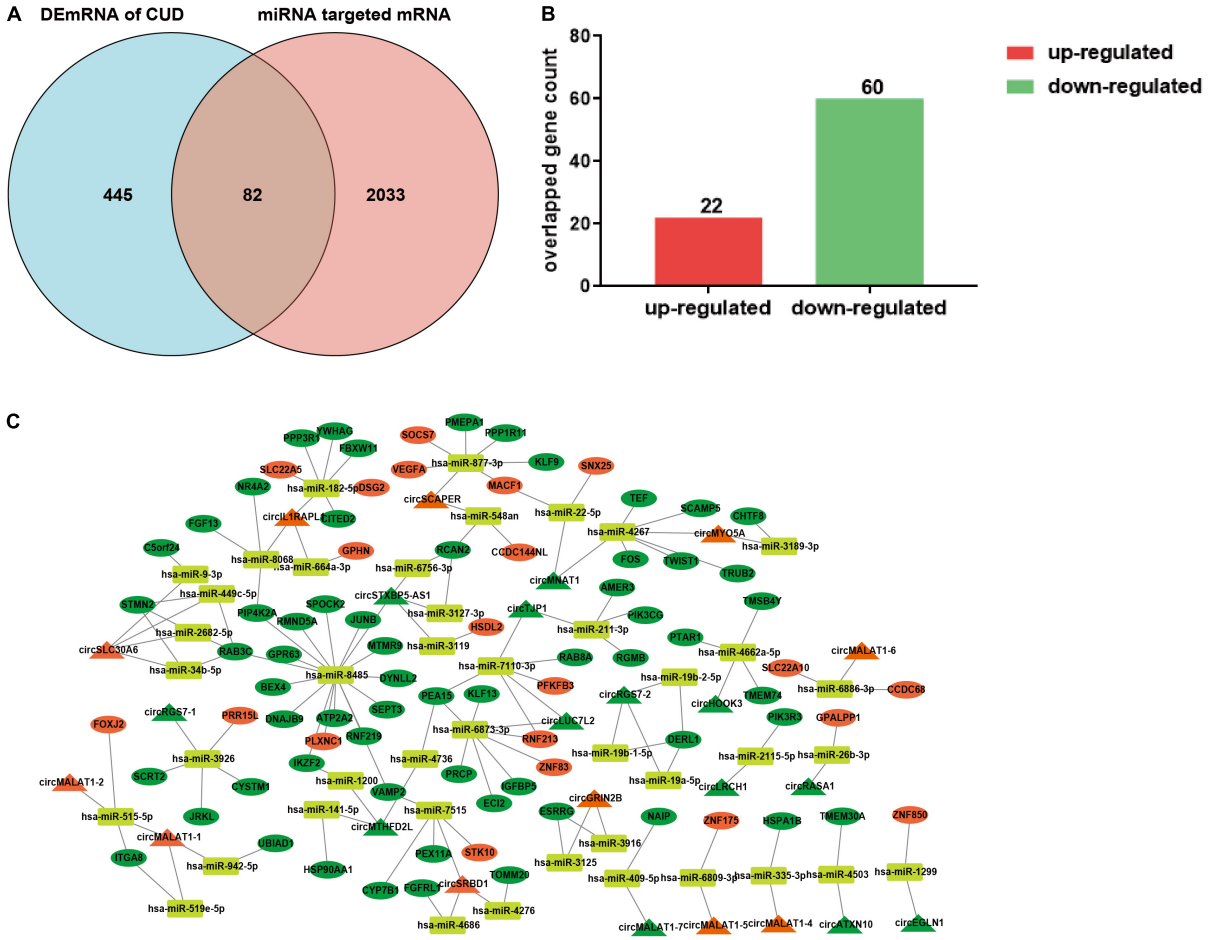

FIGURE 2 | Construction of the ceRNA network. **(A)** The shared genes between differentially expressed mRNAs in dlPFC neurons of patients with cocaine use disorder and predicted mRNAs using the miRNAs targeted by circRNAs. **(B)** Histogram showing the up-regulated mRNAs and down-regulated mRNAs in shared genes. **(C)** The circRNA–miRNA–mRNA regulatory network. The triangle, ellipse, rectangle, respectively presents circRNAs, mRNAs, and miRNAs. Orange triangle and ellipse represents up-regulated circRNAs and mRNAs, respectively; green triangle and ellipse represents down-regulated circRNAs and mRNAs, respectively. DEmRNAs, differentially expressed mRNAs; CUD, cocaine use disorder.

(GO:0006914), and positive regulation of cytokine production (GO:0001819) (**Figure 3B**), which implied that the etiology of cocaine use disorder may involve many biological processes.

Establishment of Protein–Protein Interaction Network and Identification of Hub Genes

Based on the STRING database, among the 82 genes aberrantly expressed in the patients with cocaine use disorder and indirectly regulated by circRNAs, 38 genes formed a PPI network, containing 38 nodes and 47 edges (**Figure 4A**). The highest-scoring nodes (degree $\geq$5) were screened as hub genes: *HSP90AA1*, *HSPA1B*, *YWHAG*, and *RAB8A* (**Figure 4B**). It is well known that hub nodes with high degrees of connectivity have vital functions in biological networks (Han et al., 2004; Wang et al., 2018). Hence, we used these genes to construct a circRNA–miRNA-hub gene subnetwork (**Figure 4C**): circMTHFD2L/hsa-miR-141-5p/*HSP90AA1*, circMALAT1-4/hsa-miR-335-3p/*HSPA1B*, circIL1RAPL1/hsa-miR-182-5p/*YWHAG*, circTJP1/hsa-miR-7110-3p/*RAB8A*, and circLUC7L2/hsa-miR-7110-3p/*RAB8A*. Based on the circRNA–miRNA-hub gene subnetwork, five circRNAs (circMTHFD2L, circMALAT1-4, circIL1RAPL1, circTJP1, and circLUC7L2) were likely to play important roles in cocaine use disorder. In order to further recover the function of the five vital circRNAs, the structural patterns of these vital circRNAs were shown in **Figure 5**.

Circular RNA–MicroRNA–mRNA Network Regulation in Different Cocaine Addiction Animal Model

To further verify the "sponge" function of circRNAs in cocaine addiction, we utilized the differentially expressed mRNAs from PFC RNA-seq data of different cocaine addiction models to overlap with the predicted mRNA indirectly regulated by circRNAs and differentially expressed mRNA in dlPFC of

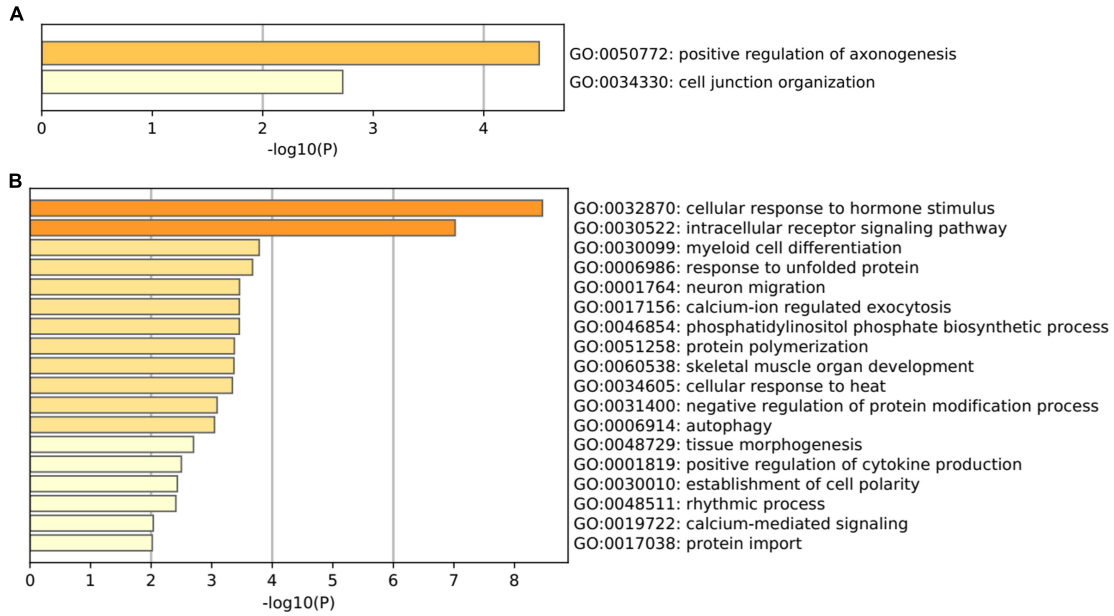

FIGURE 3 | Gene Ontology terms enriched by the shared genes between differentially expressed mRNAs in dlPFC neurons of patients with cocaine use disorder and predicted mRNAs using the miRNAs targeted by circRNAs. **(A)** GO terms enriched by the up-regulated mRNAs. **(B)** GO terms enriched by the down-regulated mRNAs.

patients with cocaine use disorder. Many genes participate in the circRNA–miRNA–mRNA network regulation (**Figure 6A**) in the chronic cocaine exposure models with different withdrawal time points. However, only one gene, *FOS*, was overlapped in all different withdrawal time points (**Table 3**). Similarly, there were many genes in the circRNAs–miRNA–mRNA network involving in cocaine self-administration model (**Figure 6B**). As shown in **Table 4**, hub gene *YWHAG* and *HSP90AA1* participated in cocaine maintains and withdrawal 15 days, respectively.

DISCUSSION

Most of previous research on the mechanism of addiction was based on animal models, or the peripheral blood of patients with substance use disorders; however, the studies do not truly portray the changes that occur in the brains of patients with substance use disorders, which may be an important obstruction to the study of drugs for the treatment of substance use disorders. The circRNA–miRNA–mRNA regulatory network we constructed will enhance the understanding of the addiction mechanism in the brain of patients with cocaine use disorder.

Through the functional enrichment analysis of the mRNAs in the network, we found that the up-regulated mRNAs were mainly involved in regulation of axonogenesis and cell junction, which suggests that our up-regulated mRNA may have a close connection with synaptic transmission, and previous studies have confirmed that abnormal synaptic transmission is a very critical factor for cocaine addiction (Khibnik et al., 2016; Martínez-Rivera et al., 2017; Li et al., 2021). Down-regulated mRNAs were found to be involved in many biological processes, including cellular response to hormone stimulus, response to unfolded protein, cellular response to heat, intracellular receptor signaling pathway, myeloid cell differentiation, calcium-ion regulated exocytosis, calcium-mediated signaling, and autophagy. All the biological processes related to down-regulated mRNAs in the circRNA–miRNA–mRNA regulatory network have been involved with cocaine addiction. For example, clinical trials have investigated that cocaine associated cues could significantly increase adrenocorticotropic hormone and cortisol (Berger et al., 1996). A single dose of cocaine can cause the accumulation of different heat shock proteins (Salminen et al., 1997), which leads to blood-brain barrier breakdown and brain edema formation thereby promoting cocaine intoxication (Sharma et al., 2009). Apart from this, Cocaine has the propensity to cause hyperthermia which increases the mortality rates to cocaine (Crandall et al., 2002). These are also evidences reported that various intracellular receptors, especially dopamine receptors and glutamate receptors, are all critical for cocaine addiction (Ellenbroek, 2013; Howell and Cunningham, 2015; Smaga et al., 2019). In addition, brain myeloid cells, particularly microglia, presented in the brain parenchyma, serve as a surveillance function for neuroinflammation and neurodegeneration in the central nervous system (Ransohoff and Cardona, 2010; Ajami et al., 2018; Jordão et al., 2019). Addictive drugs, especially cocaine, have been consistently shown to activate microglia both *in vitro* and *in vivo* (Guo et al., 2015; Liao et al., 2016). In rodents, inhibiting glial cell activation was shown to block cocaine-mediated behavioral changes (Chen et al., 2009). In humans, cocaine exposure can reduce microglial cells viability and inhibit the expression of extracellular vesicle-associated proteins

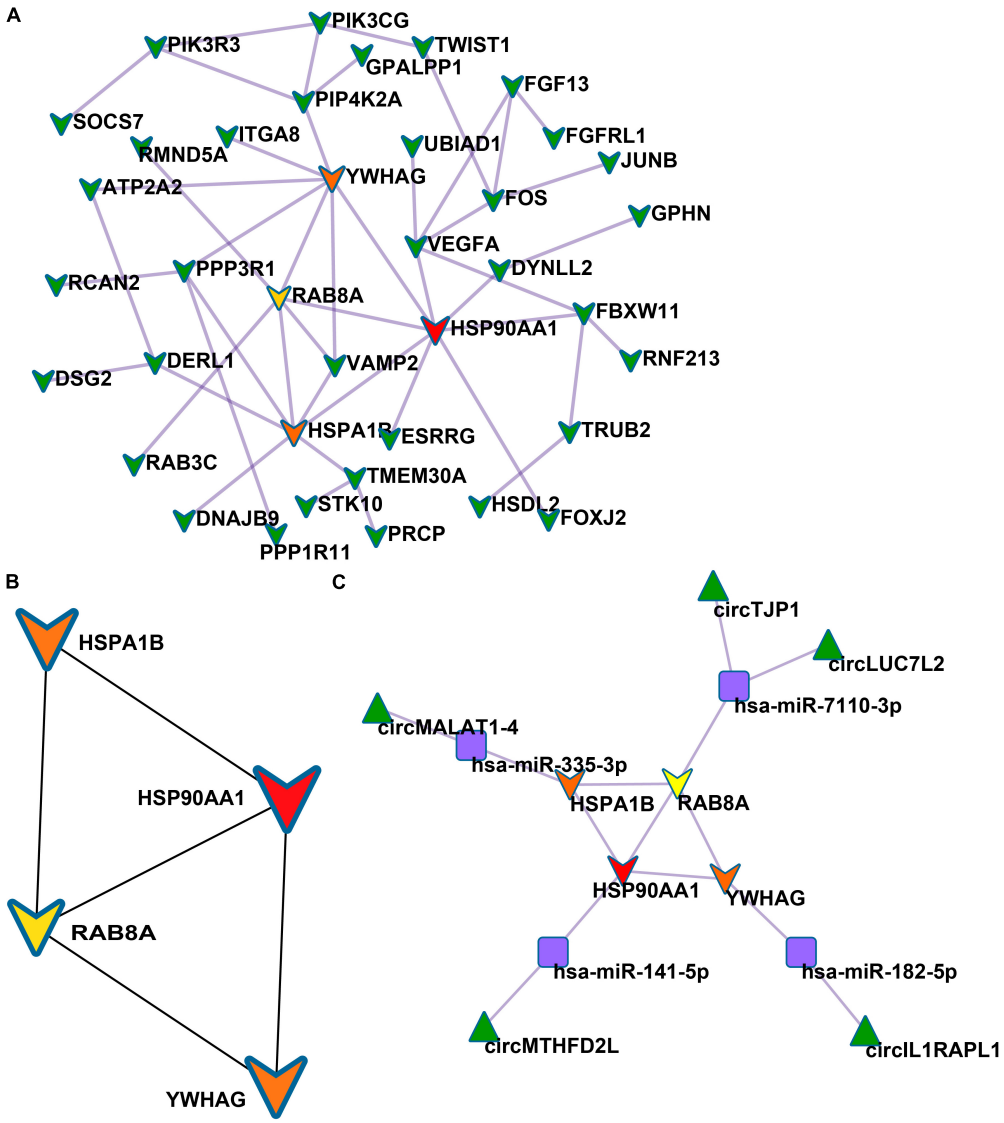

FIGURE 4 | Identification of hub genes from the PPI network. **(A)** PPI network containing 38 nodes and 47 edges. **(B)** PPI network of four hub genes that extracted from the PPI network. **(C)** The circRNA–miRNA-hub gene network.

disrupting cellular signaling and cell-to-cell communication (Kumar et al., 2020). Therefore, it can be considered that circRNAs were thought to play an important role in the multiple addiction-related networks in dlPFC of patients with cocaine use disorder.

Circular RNAs are endogenous non-coding RNAs with widespread distribution and various cellular function (Hansen et al., 2013; Vicens and Westhof, 2014; Rybak-Wolf et al., 2015; Du et al., 2017; Greene et al., 2017; Li et al., 2018; Mehta et al., 2020). Numerous studies have shown that circRNAs have an important influence on many complicated neuropsychiatric disorders (Cui et al., 2016; Zhang et al., 2018; An et al., 2019; Liu et al., 2019; Mahmoudi et al., 2019; Huang et al., 2020; Zhang Y. et al., 2020; Zimmerman et al., 2020), including drug addiction (Huang et al., 2017; Bu et al., 2019; Li et al., 2019, 2020; Zhang H. et al., 2020). Knockdown of circHomer1 ameliorates methamphetamine-induced neuronal injury through inhibiting Bbc3 expression (Li et al., 2020). The abnormal expression of mmu_circRNA_002381 in striatum was induced by cocaine self-administration and cocaine-induced locomotor activity model (Bu et al., 2019). Interestingly, siRNA-mediated mmu_circRNA_002381 down-regulation increased the expressions of *limk1* and *bdnf*, which are the targets of miR-138 associated with synaptic plasticity. Additionally, some studies predicted that circRNAs are involved in the progress and development of many addictive drug models by sponging miRNA to regulate downstream targets (Li et al., 2017, 2020; Bu et al., 2019; Zhang H. et al., 2020). In our study, 24 circRNAs were identified to be involved in the circRNA–miRNA–mRNA regulatory network. Among these, 15 were identified

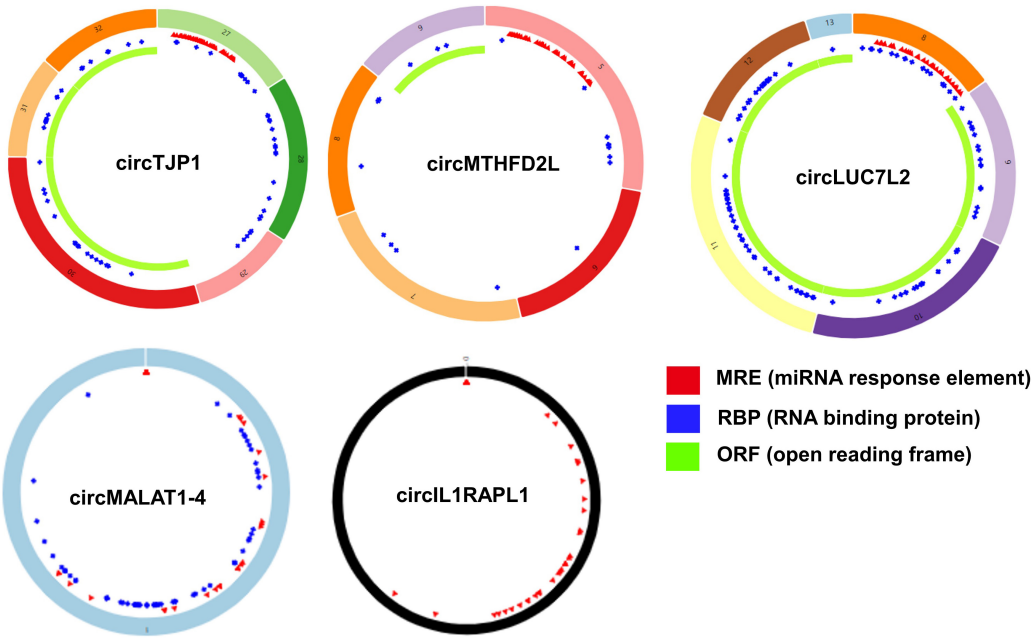

FIGURE 5 | Structural patterns of the five important circRNAs from circRNA–miRNA-hub gene network. Structural patterns of circTJP1, circMTHFD2L, circLUC7L2, circMALAT1-4, and circIL1RAPL1. The colored circle represents the circRNAs that consist of exons. The numbers on the circRNAs mean the exon number. The red, blue, and green regions inside the circRNA molecule, respectively represent MRE (microRNA response element), RBP (RNA binding protein), and ORF (open reading frame).

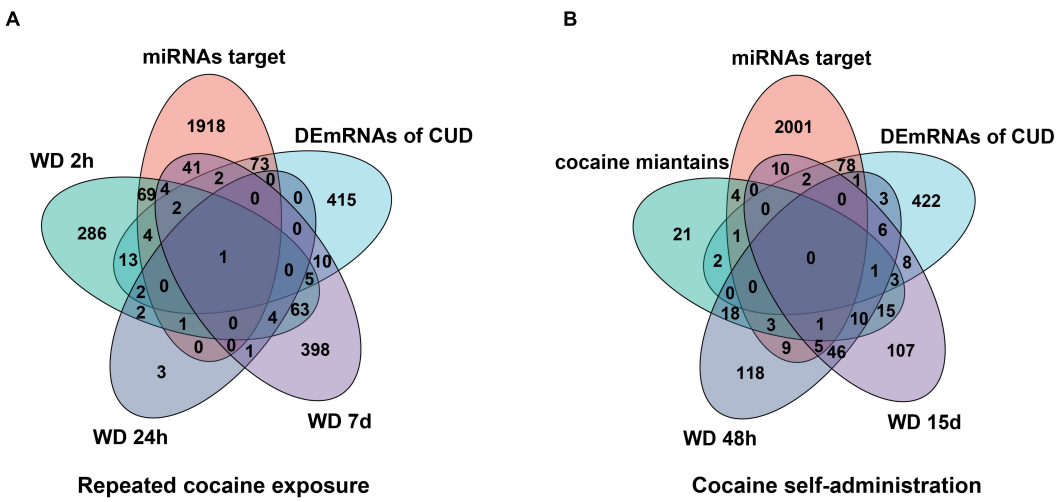

FIGURE 6 | Overlap analysis for the mRNAs from the circRNAs–miRNA–mRNA network with the differentially expressed genes in different cocaine addiction animal model. **(A)** The shared genes between mRNAs in ceRNA network and differentially expressed mRNAs in different withdrawal time points after repeated cocaine exposure. **(B)** The shared genes between mRNAs in ceRNA network and differentially expressed mRNAs in different withdrawal time points after cocaine self-administration. miRNA target, predicted mRNAs using miRNAs targeted by circRNAs; human mRNA, differentially expressed mRNAs in dlPFC neuron of human with cocaine use disorder; WD 2h, withdrawal 2 h; WD 24h, withdrawal 24h; WD 48 h, withdrawal 48h; WD 7d, withdrawal 7 days; WD 15d, withdrawal 15 days.

previously in the mammalian brain as being dysregulated during neuronal differentiation and highly enriched in synapses (Rybak-Wolf et al., 2015). It was suggested that circRNAs in the circRNA–miRNA–mRNA regulatory network may play their regulatory functions in the neurons or synapses of patients with cocaine use disorder.

Several studies have revealed that circRNAs contain multiple miRNA response elements and can bind to miRNAs, often termed as "miRNA sponges," decreasing cytoplasmic levels of miRNAs and liberating their respective downstream target mRNAs (Memczak et al., 2013; Piwecka et al., 2017; Kleaveland et al., 2018; Zhang Y. et al., 2020). Here, we constructed

TABLE 3 | The shared genes between mRNAs in ceRNA network and differentially expressed mRNAs in different withdrawal time points after repeated cocaine exposure.

mRNAs in ceRNA network overlapped with WD 2 h	mRNAs in ceRNA network overlapped with WD 24 h	mRNAs in ceRNA network overlapped with WD 7 days
PFKFB3	*FOS*	*SPOCK2*
KLF9		*STMN2*
KLF13		*KLF13*
SOCS7		*SOCS7*
NR4A2		*FOS*
JUNB		
FOS		

WD, withdrawal.

TABLE 4 | The shared genes between mRNAs in ceRNA network and differentially expressed mRNAs in different withdrawal time points after cocaine self-administration.

mRNAs in ceRNA network overlapped with cocaine maintains	mRNAs in ceRNA network overlapped with WD 48 h	mRNAs in ceRNA network overlapped with WD 15 days
YWHAG	*STMN2*	*TMEM30A*
		HSP90AA1

WD, withdrawal.

a circRNA–miRNA–mRNA regulation network involved in cocaine use disorder, including 24 circRNAs, 42 miRNAs, and 82 mRNAs. CircSLC30A6 was down-regulated in the dlPFC of patients with cocaine use disorder. Based on the analysis of circRNA–miRNA–mRNA network, we found that circSLC30A6 interacts with hsa-miR-9-3p. Interestingly, it has been known that hsa-miR-9-3p mediates the dynamic regulation of neural progenitor proliferation during neurogenesis (Pascale et al., 2020). Moreover, hsa-miR-9-3p is significantly increased in serums of patients with methamphetamine use disorder compared with normal controls (Gu et al., 2020). Therefore, we assume that circSLC30A6 up-regulation induced by the cocaine may be involved in cocaine effect through interacting with hsa-miR-9-3p. CircRASA1 and circMNAT1 were down-regulated in the dlPFC of patients with cocaine use disorder. Through the analysis of circRNA–miRNA–mRNA network, we found that circRASA1 interacts with hsa-miR-26b-3p and circMNAT1 interacts with hsa-miR-22-5p. miR-26b was found to be up-regulated in hippocampus following the acquisition and extinction but miR-22 was only up-regulated during extinction of cocaine-induced conditioned place preference in rats (Chen C. L. et al., 2013). Therefore, it is conceivable that circSLC30A6, circRASA1, and circMNAT1 might play an important role in cocaine use disorder through modulating their target miRNA.

To further identify the key circRNAs participating in the regulatory network, we established a PPI network and screened four hub genes, including *HSP90AA1*, *HSPA1B*, *YWHAG,* and *RAB8A*. Accordingly, we constructed a circRNA–miRNA-hub gene subnetwork. In the cocaine self-administration model, *HSP90AA1* had a significant decrease in PFC after withdrawal of 15 days (Bhattacherjee et al., 2019), however, the expression of *HSP90AA1* in posterior hippocampus increased significantly after 28 days of withdrawal (García-Fuster et al., 2012). These delayed neurobiological effects of *HSP90AA1* likely contribute to sustained vulnerability to cocaine relapse, which may be regulated by circMTHFD2L. *HSPA1B* gene is one of heat shock protein 70 (HSP70)-encoding transcripts, and it is reported that *HSPA1B* expression was increased in the postmortem brains of patients with cocaine use disorder exhibiting excited delirium in comparison with other (non-excited delirium) cocaine-related deaths and drug-free controls, concluding that elevated *HSPA1B* provides a reliable forensic biomarker for the identification of excited delirium (Mash et al., 2009; Johnson et al., 2012). The structure of circRNA makes them more stable and has a longer half-life, so it is considered to be a more ideal marker (Enuka et al., 2016). Previous studies reported that cocaine exposure dysregulated the expression of *YWHAG* (Bhattacherjee et al., 2019), and reduced *YWHAG* can lead to neuronal hyperexcitability, and normalization of hyperexcitability can rescue memory deficits (Roy et al., 2021). RAB8A is a member of the RAS superfamily, which are key regulators of intracellular membrane trafficking from the formation of transport vesicles to their fusion with membranes, and involve in polarized vesicular trafficking, and neurotransmitter release (Núñez et al., 2009; Esseltine et al., 2012; Sellier et al., 2016; Nüchel et al., 2018). Although no studies have shown that RAB8A has a direct effect on cocaine addiction, the biological process in which it participates is very important in cocaine addiction (Periyasamy et al., 2016; Harraz et al., 2021). Here, we identified five circRNA–miRNA-hub gene axes, indicating competitive regulatory relationships of five circRNAs with the four genes in cocaine use disorder. Nevertheless, the expression of downstream genes may be regulated by multiple circRNAs and miRNAs, the expression of the five key circRNAs may be not significantly correlated with its potential downstream gene targets in the sequencing data. Cocaine use disorder is a complex brain disease in which many factors, such as cell subtype specificity, synaptic plasticity, and neural circuit, can influence genes expression. The bioinformatics analysis, which integrated several datasets, could only provide a possible research direction, how the circRNAs contributes to the specific mechanism of cocaine use disorder requires more in-depth studies.

CONCLUSION

In conclusion, our research is the first to use dlPFC circRNAs and mRNA of patients with cocaine use disorder *via* bioinformatic tools to identify a circRNA–miRNA–mRNA regulatory network in the patients with cocaine use disorder. The circRNA–miRNA-hub genes regulatory sub-network uncovered five important circRNAs that might be involved in cocaine use disorder, providing new insight into the pathogenesis of cocaine use disorder and suggesting potential therapeutic targets that warrant further investigation.

DATA AVAILABILITY STATEMENT

Publicly available datasets were analyzed in this study. This data can be found here: http://www.ncbi.nlm.nih.gov/geo/, GSE99349, GSE124952, and GSE89572.

AUTHOR CONTRIBUTIONS

YC, JS, and SC contributed toward conception and design of research. YC and XL analyzed the data and wrote the manuscript together. YC, JS, SM, SC, XL, and SH interpreted the results and revised the manuscript. All authors have read and approved the final version of the manuscript.

FUNDING

This research was funded by the Ministry of Science and Technology of China (2021ZD0202100), National Natural Science Foundation of China (U1802283 and 82130040), and Beijing Municipal Science & Technology Commission (Z181100001518005).

SUPPLEMENTARY MATERIAL

The Supplementary Material for this article can be found online at: https://www.frontiersin.org/articles/10.3389/fnmol.2022.839233/full#supplementary-material

REFERENCES

Agarwal, V., Bell, G. W., Nam, J. W., and Bartel, D. P. (2015). Predicting effective microRNA target sites in mammalian mRNAs. *Elife* 4:e05005. doi: 10.7554/eLife.05005

Ajami, B., Samusik, N., Wieghofer, P., Ho, P. P., Crotti, A., Bjornson, Z., et al. (2018). Single-cell mass cytometry reveals distinct populations of brain myeloid cells in mouse neuroinflammation and neurodegeneration models. *Nat. Neurosci.* 21, 541–551. doi: 10.1038/s41593-018-0100-x

Amin, N., McGrath, A., and Chen, Y.-P. P. (2019). Evaluation of deep learning in non-coding RNA classification. *Nat. Mach. Intell.* 1, 246–256. doi: 10.1038/s42256-019-0051-2

An, T., He, Z. C., Zhang, X. Q., Li, J., Chen, A. L., Tan, F., et al. (2019). Baduanjin exerts anti-diabetic and anti-depression effects by regulating the expression of mRNA, lncRNA, and circRNA. *Chin. Med.* 14:3. doi: 10.1186/s13020-019-0225-1

Andrews, S. (2010). *FASTQC. A Quality Control Tool For High Throughput Sequence Data*.

Berger, S. P., Hall, S., Mickalian, J. D., Reid, M. S., Crawford, C. A., Delucchi, K., et al. (1996). Haloperidol antagonism of cue-elicited cocaine craving. *Lancet* 347, 504–508. doi: 10.1016/s0140-6736(96)91139-3

Bhattacherjee, A., Djekidel, M. N., Chen, R., Chen, W., Tuesta, L. M., and Zhang, Y. (2019). Cell type-specific transcriptional programs in mouse prefrontal cortex during adolescence and addiction. *Nat. Commun.* 10:4169. doi: 10.1038/s41467-019-12054-3

Bu, Q., Long, H., Shao, X., Gu, H., Kong, J., Luo, L., et al. (2019). Cocaine induces differential circular RNA expression in striatum. *Transl. Psychiatry* 9:199. doi: 10.1038/s41398-019-0527-1

Chen, B. T., Yau, H. J., Hatch, C., Kusumoto-Yoshida, I., Cho, S. L., Hopf, F. W., et al. (2013). Rescuing cocaine-induced prefrontal cortex hypoactivity prevents compulsive cocaine seeking. *Nature* 496, 359–362. doi: 10.1038/nature12024

Chen, C. L., Liu, H., and Guan, X. (2013). Changes in microRNA expression profile in hippocampus during the acquisition and extinction of cocaine-induced conditioned place preference in rats. *J. Biomed. Sci.* 20:96. doi: 10.1186/1423-0127-20-96

Chen, H., Uz, T., and Manev, H. (2009). Minocycline affects cocaine sensitization in mice. *Neurosci. Lett.* 452, 258–261. doi: 10.1016/j.neulet.2009.01.078

Chen, Y., and Wang, X. (2020). MIRDB: an online database for prediction of functional microRNA targets. *Nucleic Acids Res.* 48, D127–D131. doi: 10.1093/nar/gkz757

Chin, C. H., Chen, S. H., Wu, H. H., Ho, C. W., Ko, M. T., and Lin, C. Y. (2014). CytoHubba: identifying hub objects and sub-networks from complex interactome. *BMC Syst. Biol.* 8(Suppl. 4):S11. doi: 10.1186/1752-0509-8-S4-S11

Conti, C. L., and Nakamura-Palacios, E. M. (2014). Bilateral transcranial direct current stimulation over dorsolateral prefrontal cortex changes the drug-cued reactivity in the anterior cingulate cortex of crack-cocaine addicts. *Brain Stimul.* 7, 130–132. doi: 10.1016/j.brs.2013.09.007

Crandall, C. G., Vongpatanasin, W., and Victor, R. G. (2002). Mechanism of cocaine-induced hyperthermia in humans. *Ann. Intern. Med.* 136, 785–791. doi: 10.7326/0003-4819-136-11-200206040-00006

Cui, X., Niu, W., Kong, L., He, M., Jiang, K., Chen, S., et al. (2016). Hsa_circRNA_103636: potential novel diagnostic and therapeutic biomarker in Major depressive disorder. *Biomark Med.* 10, 943–952. doi: 10.2217/bmm-2016-0130

Doncheva, N. T., Morris, J. H., Gorodkin, J., and Jensen, L. J. (2019). Cytoscape stringapp: network analysis and visualization of proteomics data. *J. Proteome Res.* 18, 623–632. doi: 10.1021/acs.jproteome.8b00702

Du, W. W., Yang, W., Chen, Y., Wu, Z. K., Foster, F. S., Yang, Z., et al. (2017). Foxo3 circular RNA promotes cardiac senescence by modulating multiple factors associated with stress and senescence responses. *Eur. Heart J.* 38, 1402–1412. doi: 10.1093/eurheartj/ehw001

Du, W. W., Yang, W., Liu, E., Yang, Z., Dhaliwal, P., and Yang, B. B. (2016). Foxo3 circular RNA retards cell cycle progression *via* forming ternary complexes with p21 and CDK2. *Nucleic Acids Res.* 44, 2846–2858. doi: 10.1093/nar/gkw027

Ellenbroek, B. A. (2013). Histamine H(3) receptors, the complex interaction with dopamine and its implications for addiction. *Br. J. Pharmacol.* 170, 46–57. doi: 10.1111/bph.12221

Enuka, Y., Lauriola, M., Feldman, M. E., Sas-Chen, A., Ulitsky, I., and Yarden, Y. (2016). Circular RNAs are long-lived and display only minimal early alterations in response to a growth factor. *Nucleic Acids Res.* 44, 1370–1383. doi: 10.1093/nar/gkv1367

Esseltine, J. L., Ribeiro, F. M., and Ferguson, S. S. (2012). Rab8 modulates metabotropic glutamate receptor subtype 1 intracellular trafficking and signaling in a protein kinase C-dependent manner. *J. Neurosci.* 32, 16933a–16942a. doi: 10.1523/JNEUROSCI.0625-12.2012

Feng, J., Chen, W., Dong, X., Wang, J., Mei, X., Deng, J., et al. (2021). CSCD2: an integrated interactional database of cancer-specific circular RNAs. *Nucleic Acids Res.* 50, D1179–D1183. doi: 10.1093/nar/gkab830

Fromm, B., Billipp, T., Peck, L. E., Johansen, M., Tarver, J. E., King, B. L., et al. (2015). A uniform system for the annotation of vertebrate microRNA genes and the evolution of the human microRNAome. *Annu. Rev. Genet.* 49, 213–242. doi: 10.1146/annurev-genet-120213-092023

Gao, Y., Zhang, J., and Zhao, F. (2018). Circular RNA identification based on multiple seed matching. *Brief Bioinform.* 19, 803–810. doi: 10.1093/bib/bbx014

García-Fuster, M. J., Flagel, S. B., Mahmood, S. T., Watson, S. J., and Akil, H. (2012). Cocaine withdrawal causes delayed dysregulation of stress genes in the hippocampus. *PLoS One* 7:e42092. doi: 10.1371/journal.pone.0042092

Gass, J. T., and Chandler, L. J. (2013). The plasticity of extinction: contribution of the prefrontal cortex in treating addiction through inhibitory learning. *Front. Psychiatry* 4:46. doi: 10.3389/fpsyt.2013.00046

Gawin, F. H., and Ellinwood, E. H. Jr. (1989). Cocaine dependence. *Annu. Rev. Med.* 40, 149–161. doi: 10.1146/annurev.me.40.020189.001053

Glažar, P., Papavasileiou, P., and Rajewsky, N. (2014). Circbase: a database for circular RNAs. *RNA* 20, 1666–1670. doi: 10.1261/rna.043687.113

Greene, J., Baird, A. M., Brady, L., Lim, M., Gray, S. G., McDermott, R., et al. (2017). Circular RNAs: biogenesis, function and role in human diseases. *Front. Mol. Biosci.* 4:Artn38. doi: 10.3389/Fmolb.2017.00038

Gu, W. J., Zhang, C., Zhong, Y., Luo, J., Zhang, C. Y., Zhang, C., et al. (2020). Altered serum microRNA expression profile in subjects with heroin and methamphetamine use disorder. *Biomed. Pharmacother.* 125:109918. doi: 10.1016/j.biopha.2020.109918

Guo, M. L., Liao, K., Periyasamy, P., Yang, L., Cai, Y., Callen, S. E., et al. (2015). Cocaine-mediated microglial activation involves the ER stress-autophagy axis. *Autophagy* 11, 995–1009. doi: 10.1080/15548627.2015.1052205

Han, J. D., Bertin, N., Hao, T., Goldberg, D. S., Berriz, G. F., Zhang, L. V., et al. (2004). Evidence for dynamically organized modularity in the yeast protein-protein interaction network. *Nature* 430, 88–93. doi: 10.1038/nature02555

Hansen, T. B., Jensen, T. I., Clausen, B. H., Bramsen, J. B., Finsen, B., Damgaard, C. K., et al. (2013). Natural RNA circles function as efficient microRNA sponges. *Nature* 495, 384–388. doi: 10.1038/nature11993

Harraz, M. M., Guha, P., Kang, I. G., Semenza, E. R., Malla, A. P., Song, Y. J., et al. (2021). Cocaine-induced locomotor stimulation involves autophagic degradation of the dopamine transporter. *Mol. Psychiatry* 26, 370–382. doi: 10.1038/s41380-020-00978-y

Heal, D. J., Smith, S. L., and Henningfield, J. E. (2014). CNS stimulants. *Neuropharmacology* 87, 1–3. doi: 10.1016/j.neuropharm.2014.09.025

Holdt, L. M., Stahringer, A., Sass, K., Pichler, G., Kulak, N. A., Wilfert, W., et al. (2016). Circular non-coding RNA ANRIL modulates ribosomal RNA maturation and atherosclerosis in humans. *Nat. Commun.* 7:12429. doi: 10.1038/ncomms12429

Howell, L. L., and Cunningham, K. A. (2015). Serotonin 5-HT2 receptor interactions with dopamine function: implications for therapeutics in cocaine use disorder. *Pharmacol. Rev.* 67, 176–197. doi: 10.1124/pr.114.009514

Huang, R., Zhang, Y., Bai, Y., Han, B., Ju, M., Chen, B., et al. (2020). N(6)-methyladenosine modification of fatty acid amide hydrolase messenger RNA in circular RNA STAG1-Regulated astrocyte dysfunction and depressive-like behaviors. *Biol. Psychiatry* 88, 392–404. doi: 10.1016/j.biopsych.2020.02.018

Huang, R., Zhang, Y., Han, B., Bai, Y., Zhou, R., Gan, G., et al. (2017). Circular RNA HIPK2 regulates astrocyte activation *via* cooperation of autophagy and ER stress by targeting MIR124-2HG. *Autophagy* 13, 1722–1741. doi: 10.1080/15548627.2017.1356975

Jaenisch, R., and Bird, A. (2003). Epigenetic regulation of gene expression: how the genome integrates intrinsic and environmental signals. *Nat. Genet.* 33(Suppl.), 245–254. doi: 10.1038/ng1089

Johnson, M. M., David, J. A., Michelhaugh, S. K., Schmidt, C. J., and Bannon, M. J. (2012). Increased heat shock protein 70 gene expression in the brains of cocaine-related fatalities may be reflective of postdrug survival and intervention rather than excited delirium. *J. Forensic Sci.* 57, 1519–1523. doi: 10.1111/j.1556-4029.2012.02212.x

Jordão, M. J. C., Sankowski, R., Brendecke, S. M., Sagar, I., Locatelli, G., Tai, Y. H., et al. (2019). Single-cell profiling identifies myeloid cell subsets with distinct fates during neuroinflammation. *Science* 363:eaat7554. doi: 10.1126/science.aat7554

Khibnik, L. A., Beaumont, M., Doyle, M., Heshmati, M., Slesinger, P. A., Nestler, E. J., et al. (2016). Stress and cocaine trigger divergent and cell type-specific regulation of synaptic transmission at single spines in nucleus accumbens. *Biol. Psychiatry* 79, 898–905. doi: 10.1016/j.biopsych.2015.05.022

Kleaveland, B., Shi, C. Y., Stefano, J., and Bartel, D. P. (2018). A network of noncoding regulatory RNAs acts in the mammalian brain. *Cell* 174, 350.e–362.e. doi: 10.1016/j.cell.2018.05.022

Kumar, S., Matthews, Q. L., and Sims, B. (2020). Effects of cocaine on human glial-derived extracellular vesicles. *Front. Cell Dev. Biol.* 8:563441. doi: 10.3389/fcell.2020.563441

Langmead, B., and Salzberg, S. L. (2012). Fast gapped-read alignment with Bowtie 2. *Nat. Methods* 9, 357–359. doi: 10.1038/nmeth.1923

Legnini, I., Di Timoteo, G., Rossi, F., Morlando, M., Briganti, F., Sthandier, O., et al. (2017). Circ-ZNF609 is a circular RNA that can be translated and functions in myogenesis. *Mol. Cell* 66, 22.e9–39.e9. doi: 10.1016/j.molcel.2017.02.017

Li, J., Shi, Q., Wang, Q., Tan, X., Pang, K., Liu, X., et al. (2019). Profiling circular RNA in methamphetamine-treated primary cortical neurons identified novel circRNAs related to methamphetamine addiction. *Neurosci. Lett.* 701, 146–153. doi: 10.1016/j.neulet.2019.02.032

Li, J., Sun, Q., Zhu, S., Xi, K., Shi, Q., Pang, K., et al. (2020). Knockdown of circHomer1 ameliorates METH-induced neuronal injury through inhibiting Bbc3 expression. *Neurosci. Lett.* 732:135050. doi: 10.1016/j.neulet.2020.135050

Li, M., Xu, P., Xu, Y., Teng, H., Tian, W., Du, Q., et al. (2017). Dynamic expression changes in the transcriptome of the prefrontal cortex after repeated exposure to cocaine in mice. *Front. Pharmacol.* 8:142. doi: 10.3389/fphar.2017.00142

Li, X., Yang, L., and Chen, L. L. (2018). The biogenesis, functions, and challenges of circular RNAs. *Mol. Cell* 71, 428–442. doi: 10.1016/j.molcel.2018.06.034

Li, Y., Simmler, L. D., Van Zessen, R., Flakowski, J., Wan, J. X., Deng, F., et al. (2021). Synaptic mechanism underlying serotonin modulation of transition to cocaine addiction. *Science* 373, 1252–1256. doi: 10.1126/science.abi9086

Li, Z., Huang, C., Bao, C., Chen, L., Lin, M., Wang, X., et al. (2015). Exon-intron circular RNAs regulate transcription in the nucleus. *Nat. Struct .Mol. Biol.* 22, 256–264. doi: 10.1038/nsmb.2959

Liao, K., Guo, M., Niu, F., Yang, L., Callen, S. E., and Buch, S. (2016). Cocaine-mediated induction of microglial activation involves the ER stress-TLR2 axis. *J. Neuroinflammation* 13:33. doi: 10.1186/s12974-016-0501-2

Liu, W., and Wang, X. (2019). Prediction of functional microRNA targets by integrative modeling of microRNA binding and target expression data. *Genome Biol.* 20:18. doi: 10.1186/s13059-019-1629-z

Liu, Z., Ran, Y., Tao, C., Li, S., Chen, J., and Yang, E. (2019). Detection of circular RNA expression and related quantitative trait loci in the human dorsolateral prefrontal cortex. *Genome Biol.* 20:99. doi: 10.1186/s13059-019-1701-8

Lv, C., Sun, L., Guo, Z., Li, H., Kong, D., Xu, B., et al. (2018). Circular RNA regulatory network reveals cell-cell crosstalk in acute myeloid leukemia extramedullary infiltration. *J. Transl. Med.* 16:361. doi: 10.1186/s12967-018-1726-x

Mahmoudi, E., Fitzsimmons, C., Geaghan, M. P., Shannon Weickert, C., Atkins, J. R., Wang, X., et al. (2019). Circular RNA biogenesis is decreased in postmortem cortical gray matter in schizophrenia and may alter the bioavailability of associated miRNA. *Neuropsychopharmacology* 44, 1043–1054. doi: 10.1038/s41386-019-0348-1

Majewska, M. D. (1996b). Neurotoxicity and neuropathology associated with chronic cocaine abuse. *NIDA Res. Monogr.* 162, 70–72.

Majewska, M. D. (1996a). Cocaine addiction as a neurological disorder: implications for treatment. *NIDA Res. Monogr.* 163, 1–26.

Martin, M. (2011). Cutadapt removes adapter sequences from high-throughput sequencing reads. *Embnet J.* 17:3. doi: 10.14806/ej.17.1.200

Martínez-Rivera, A., Hao, J., Tropea, T. F., Giordano, T. P., Kosovsky, M., Rice, R. C., et al. (2017). Enhancing VTA Cav1.3 L-type Ca(2+) channel activity promotes cocaine and mood-related behaviors *via* overlapping AMPA receptor mechanisms in the nucleus accumbens. *Mol. Psychiatry* 22, 1735–1745. doi: 10.1038/mp.2017.9

Mash, D. C., Duque, L., Pablo, J., Qin, Y., Adi, N., Hearn, W. L., et al. (2009). Brain biomarkers for identifying excited delirium as a cause of sudden death. *Forensic Sci. Int.* 190, e13–e19. doi: 10.1016/j.forsciint.2009.05.012

Matochik, J. A., London, E. D., Eldreth, D. A., Cadet, J. L., and Bolla, K. I. (2003). Frontal cortical tissue composition in abstinent cocaine abusers: a magnetic resonance imaging study. *Neuroimage* 19, 1095–1102. doi: 10.1016/s1053-8119(03)00244-1

Mehta, S. L., Dempsey, R. J., and Vemuganti, R. (2020). Role of circular RNAs in brain development and CNS diseases. *Prog. Neurobiol.* 186:101746. doi: 10.1016/j.pneurobio.2020.101746

Memczak, S., Jens, M., Elefsinioti, A., Torti, F., Krueger, J., Rybak, A., et al. (2013). Circular RNAs are a large class of animal RNAs with regulatory potency. *Nature* 495, 333–338. doi: 10.1038/nature11928

Moeller, S. J., Frobose, M. I., Konova, A. B., Misyrlis, M., Parvaz, M. A., Goldstein, R. Z., et al. (2014). Common and distinct neural correlates of inhibitory dysregulation: stroop fMRI study of cocaine addiction and intermittent explosive disorder. *J. Psychiatr. Res.* 58, 55–62. doi: 10.1016/j.jpsychires.2014.07.016

Moreno-Lopez, L., Catena, A., Fernandez-Serrano, M. J., Delgado-Rico, E., Stamatakis, E. A., Perez-Garcia, M., et al. (2012). Trait impulsivity and prefrontal gray matter reductions in cocaine dependent individuals. *Drug Alcohol Depend.* 125, 208–214. doi: 10.1016/j.drugalcdep.2012.02.012

Nestler, E. J. (2014). Epigenetic mechanisms of drug addiction. *Neuropharmacology* 76 Pt B, 259–268. doi: 10.1016/j.neuropharm.2013.04.004

Nestler, E. J., and Lüscher, C. (2019). The molecular basis of drug addiction: linking epigenetic to synaptic and circuit mechanisms. *Neuron* 102, 48–59. doi: 10.1016/j.neuron.2019.01.016

Nüchel, J., Ghatak, S., Zuk, A. V., Illerhaus, A., Morgelin, M., Schonborn, K., et al. (2018). TGFB1 is secreted through an unconventional pathway dependent on the autophagic machinery and cytoskeletal regulators. *Autophagy* 14, 465–486. doi: 10.1080/15548627.2017.1422850

Núñez, E., Perez-Siles, G., Rodenstein, L., Alonso-Torres, P., Zafra, F., Jimenez, E., et al. (2009). Subcellular localization of the neuronal glycine transporter GLYT2 in brainstem. *Traffic* 10, 829–843. doi: 10.1111/j.1600-0854.2009.00911.x

Pamudurti, N. R., Bartok, O., Jens, M., Ashwal-Fluss, R., Stottmeister, C., Ruhe, L., et al. (2017). Translation of circRNAs. *Mol. Cell* 66, 9–21. doi: 10.1016/j.molcel.2017.02.021

Paraskevopoulou, M. D., Georgakilas, G., Kostoulas, N., Vlachos, I. S., Vergoulis, T., Reczko, M., et al. (2013). DIANA-microT web server v5.0: service integration into miRNA functional analysis workflows. *Nucleic Acids Res.* 41, W169–W173. doi: 10.1093/nar/gkt393

Pascale, E., Beclin, C., Fiorenzano, A., Andolfi, G., Erni, A., De Falco, S., et al. (2020). Long non-coding RNA T-UCstem1 controls progenitor proliferation and neurogenesis in the postnatal mouse olfactory bulb through interaction with miR-9. *Stem Cell Rep.* 15, 836–844. doi: 10.1016/j.stemcr.2020.08.009

Periyasamy, P., Guo, M. L., and Buch, S. (2016). Cocaine induces astrocytosis through ER stress-mediated activation of autophagy. *Autophagy* 12, 1310–1329. doi: 10.1080/15548627.2016.1183844

Piwecka, M., Glazar, P., Hernandez-Miranda, L. R., Memczak, S., Wolf, S. A., Rybak-Wolf, A., et al. (2017). Loss of a mammalian circular RNA locus causes miRNA deregulation and affects brain function. *Science* 357:eaam8526. doi: 10.1126/science.aam8526

Ransohoff, R. M., and Cardona, A. E. (2010). The myeloid cells of the central nervous system parenchyma. *Nature* 468, 253–262. doi: 10.1038/nature09615

Reid, A. G., Lingford-Hughes, A. R., Cancela, L. M., and Kalivas, P. W. (2012). Substance abuse disorders. *Handb. Clin. Neurol.* 106, 419–431. doi: 10.1016/B978-0-444-52002-9.00024-3

Ribeiro, E. A., Scarpa, J. R., Garamszegi, S. P., Kasarskis, A., Mash, D. C., and Nestler, E. J. (2017). Gene network dysregulation in dorsolateral prefrontal cortex neurons of humans with cocaine use disorder. *Sci. Rep.* 7:5412. doi: 10.1038/s41598-017-05720-3

Robinson, M. D., McCarthy, D. J., and Smyth, G. K. (2010). EdgeR: a Bioconductor package for differential expression analysis of digital gene expression data. *Bioinformatics* 26, 139–140. doi: 10.1093/bioinformatics/btp616

Robison, A. J., and Nestler, E. J. (2011). Transcriptional and epigenetic mechanisms of addiction. *Nat. Rev. Neurosci.* 12, 623–637. doi: 10.1038/nrn3111

Roy, D. S., Zhang, Y., Aida, T., Choi, S., Chen, Q., Hou, Y., et al. (2021). Anterior thalamic dysfunction underlies cognitive deficits in a subset of neuropsychiatric disease models. *Neuron* 109, 2590.e13–2603.e13. doi: 10.1016/j.neuron.2021.06.005

Rybak-Wolf, A., Stottmeister, C., Glazar, P., Jens, M., Pino, N., Giusti, S., et al. (2015). Circular RNAs in the mammalian brain are highly abundant, conserved, and dynamically expressed. *Mol. Cell* 58, 870–885. doi: 10.1016/j.molcel.2015.03.027

Salminen, W. F. Jr., Roberts, S. M., Fenna, M., and Voellmy, R. (1997). Heat shock protein induction in murine liver after acute treatment with cocaine. *Hepatology* 25, 1147–1153. doi: 10.1002/hep.510250517

Seamans, J. K., Lapish, C. C., and Durstewitz, D. (2008). Comparing the prefrontal cortex of rats and primates: insights from electrophysiology. *Neurotox. Res.* 14, 249–262. doi: 10.1007/BF03033814

Sellier, C., Campanari, M. L., Julie Corbier, C., Gaucherot, A., Kolb-Cheynel, I., Oulad-Abdelghani, M., et al. (2016). Loss of C9ORF72 impairs autophagy and synergizes with polyQ Ataxin-2 to induce motor neuron dysfunction and cell death. *EMBO J.* 35, 1276–1297. doi: 10.15252/embj.201593350

Shannon, P., Markiel, A., Ozier, O., Baliga, N. S., Wang, J. T., Ramage, D., et al. (2003). Cytoscape: a software environment for integrated models of biomolecular interaction networks. *Genome Res.* 13, 2498–2504. doi: 10.1101/gr.1239303

Sharma, H. S., Muresanu, D., Sharma, A., and Patnaik, R. (2009). Cocaine-induced breakdown of the blood-brain barrier and neurotoxicity. *Int. Rev. Neurobiol.* 88, 297–334. doi: 10.1016/S0074-7742(09)88011-2

Smaga, I., Sanak, M., and Filip, M. (2019). Cocaine-induced changes in the expression of NMDA receptor subunits. *Curr. Neuropharmacol.* 17, 1039–1055. doi: 10.2174/1570159X17666190617101726

Szabo, L., and Salzman, J. (2016). Detecting circular RNAs: bioinformatic and experimental challenges. *Nat. Rev. Genet.* 17, 679–692. doi: 10.1038/nrg.2016.114

Szklarczyk, D., Morris, J. H., Cook, H., Kuhn, M., Wyder, S., Simonovic, M., et al. (2017). The STRING database in 2017: quality-controlled protein-protein association networks, made broadly accessible. *Nucleic Acids Res.* 45, D362–D368. doi: 10.1093/nar/gkw937

Terraneo, A., Leggio, L., Saladini, M., Ermani, M., Bonci, A., and Gallimberti, L. (2016). Transcranial magnetic stimulation of dorsolateral prefrontal cortex reduces cocaine use: a pilot study. *Eur. Neuropsychopharmacol.* 26, 37–44. doi: 10.1016/j.euroneuro.2015.11.011

United Nations Office on Drugs and Crime (2020). *UNODC World Drug Report 2020: Global drug use rising; while COVID-19 has far reaching impact on global drug markets*. Vienna: United Nations Office on Drugs and Crime.

Vergoulis, T., Vlachos, I. S., Alexiou, P., Georgakilas, G., Maragkakis, M., Reczko, M., et al. (2012). TarBase 6.0: capturing the exponential growth of miRNA targets with experimental support. *Nucleic Acids Res.* 40, D222–D229. doi: 10.1093/nar/gkr1161

Vicens, Q., and Westhof, E. (2014). Biogenesis of circular RNAs. *Cell* 159, 13–14. doi: 10.1016/j.cell.2014.09.005

Vlachos, I. S., and Hatzigeorgiou, A. G. (2017). Functional analysis of miRNAs using the DIANA Tools online suite. *Methods Mol. Biol.* 1517, 25–50. doi: 10.1007/978-1-4939-6563-2_2

Wang, J., Li, K. L., Shukla, A., Beroun, A., Ishikawa, M., Huang, X., et al. (2021). Cocaine triggers astrocyte-mediated synaptogenesis. *Biol. Psychiatry* 89, 386–397. doi: 10.1016/j.biopsych.2020.08.012

Wang, Q., Cai, J., Fang, C., Yang, C., Zhou, J., Tan, Y., et al. (2018). Mesenchymal glioblastoma constitutes a major ceRNA signature in the TGF-beta pathway. *Theranostics* 8, 4733–4749. doi: 10.7150/thno.26550

Yu, H., Xie, B., Zhang, J., Luo, Y., Galaj, E., Zhang, X., et al. (2021). The role of circTmeff-1 in incubation of context-induced morphine craving. *Pharmacol. Res.* 170:105722. doi: 10.1016/j.phrs.2021.105722

Zhang, H., Chen, Z., Zhong, Z., Gong, W., and Li, J. (2018). Total saponins from the leaves of Panax notoginseng inhibit depression on mouse chronic unpredictable mild stress model by regulating circRNA expression. *Brain Behav.* 8:e01127. doi: 10.1002/brb3.1127

Zhang, H., Wang, Q., Wang, Q., Liu, A., Qin, F., Sun, Q., et al. (2020). Circular RNA expression profiling in the nucleus accumbens: effects of electroacupuncture treatment on morphine-induced conditioned place preference. *Addict Biol.* 25:e12794. doi: 10.1111/adb.12794

Zhang, Y., Du, L., Bai, Y., Han, B., He, C., Gong, L., et al. (2020). CircDYM ameliorates depressive-like behavior by targeting miR-9 to regulate microglial activation *via* HSP90 ubiquitination. *Mol. Psychiatry* 25, 1175–1190. doi: 10.1038/s41380-018-0285-0

Zhou, Y., Zhou, B., Pache, L., Chang, M., Khodabakhshi, A. H., Tanaseichuk, O., et al. (2019). Metascape provides a biologist-oriented resource for the analysis of systems-level datasets. *Nat. Commun.* 10:1523. doi: 10.1038/s41467-019-09234-6

Zimmerman, A. J., Hafez, A. K., Amoah, S. K., Rodriguez, B. A., Dell'Orco, M., Lozano, E., et al. (2020). A psychiatric disease-related circular RNA controls synaptic gene expression and cognition. *Mol. Psychiatry* 25, 2712–2727. doi: 10.1038/s41380-020-0653-4

Zinsmaier, A. K., Dong, Y., and Huang, Y. H. (2021). Cocaine-induced projection-specific and cell type-specific adaptations in the nucleus accumbens. *Mol. Psychiatry* doi: 10.1038/s41380-021-01112-2 [Epub ahead of print].

Conflict of Interest: The authors declare that the research was conducted in the absence of any commercial or financial relationships that could be construed as a potential conflict of interest.

Publisher's Note: All claims expressed in this article are solely those of the authors and do not necessarily represent those of their affiliated organizations, or those of the publisher, the editors and the reviewers. Any product that may be evaluated in this article, or claim that may be made by its manufacturer, is not guaranteed or endorsed by the publisher.

frontiers | Frontiers in Molecular Neuroscience

ORIGINAL RESEARCH
published: 02 May 2022
doi: 10.3389/fnmol.2022.884790

Aerobic Exercise Improves Methamphetamine-Induced Olfactory Dysfunction Through α-Synuclein Intervention in Male Mice

Zhuo Wang[1,3†], Rui Zheng[2†], Xiaohan Wang[3], Xuekun Huang[2], Jian Huang[3], Cihang Gu[3], Yitong He[3], Shuo Wu[2], Jingyuan Chen[2], Qintai Yang[2] and Pingming Qiu[3*]*

[1] Department of Infertility and Sexual Medicine, The Third Affiliated Hospital of Sun Yat-sen University, Guangzhou, China, [2] Department of Otorhinolaryngology-Head and Neck Surgery, Department of Allergy, The Third Affiliated Hospital of Sun Yat-sen University, Guangzhou, China, [3] Guangzhou Key Laboratory of Forensic Multi-Omics for Precision Identification, School of Forensic Medicine, Southern Medical University, Guangzhou, China

OPEN ACCESS

Edited by:
Qian Ren,
Hebei Medical University, China

Reviewed by:
Xuan (Anna) Li,
University of Maryland, College Park, United States
Jae-Ick Kim,
Ulsan National Institute of Science and Technology, South Korea

***Correspondence:**
Pingming Qiu
qiupmfy@126.com
Qintai Yang
yangqint@mail.sysu.edu.cn

[†] These authors have contributed equally to this work

Specialty section:
This article was submitted to Molecular Signalling and Pathways, a section of the journal Frontiers in Molecular Neuroscience

Received: 27 February 2022
Accepted: 04 April 2022
Published: 02 May 2022

Citation:
Wang Z, Zheng R, Wang X, Huang X, Huang J, Gu C, He Y, Wu S, Chen J, Yang Q and Qiu P (2022) Aerobic Exercise Improves Methamphetamine-Induced Olfactory Dysfunction Through α-Synuclein Intervention in Male Mice. Front. Mol. Neurosci. 15:884790. doi: 10.3389/fnmol.2022.884790

Methamphetamine (Meth) is a predominantly abused neurostimulant, and its abuse is often associated with multiple neurological symptoms. Olfaction, the sense of smell, is a highly neurotransmission-dependent physiological process; however, the effect of Meth on olfactory function and its underlying mechanisms remain largely unknown. This study aimed to explore the impact of Meth abuse on the olfactory system and the potential mechanisms. Chronic Meth abuse was induced by daily administration of Meth in male mice for 4 weeks, and we then systematically examined olfactory performance. Behavioral tests found that Meth-treated animals showed increased olfactory threshold, decreased olfactory sensitivity, reduced olfactory-dependent discrimination, and difficulty in seeking buried food. Notably, the increased deposition of α-synuclein (α-syn) in the olfactory bulb was detected. Adeno-associated virus (AAV)-mediated α-syn intervention therapy in the olfactory bulb significantly alleviated Meth-induced olfactory function impairment, and 8 weeks of aerobic exercise showed similar effects through the same principle of α-syn intervention. Notably, exercise-mediated reduction of α-syn inhibited abnormal firing activity and restored the inhibitory synaptic regulation of mitral cells in the olfactory bulb. These findings suggest the involvement of α-syn in the pathogenic mechanisms of Meth-induced olfactory dysfunction and shed light on the possible therapeutic applications of aerobic exercise in Meth-induced olfactory dysfunction.

Keywords: methamphetamine, α-synuclein, exercise, olfactory, mitral cells

INTRODUCTION

Methamphetamine (Meth) is a commonly abused psychoactive stimulant, and the related symptoms have been widely recognized, with a heavy social burden (Courtney and Ray, 2014). Chronic Meth administration leads to adverse effects on various types of neural cells across different brain regions and induces neuropsychiatric symptoms, such as addiction, emotional disorders,

cognitive impairment, and Parkinson's disease (PD) (Cruickshank and Dyer, 2009; Büttner, 2011). However, the effects of Meth on basic sensory systems, especially olfaction, are still less known and often overlooked.

Among the sensory systems, olfaction is one of the most evolutionarily conserved neural-processing senses and is crucial for survival across species. Olfaction is involved in multiple aspects of social behaviors, such as emotion control, reward activation, territory defense, social recognition, and mate selection (Kaupp, 2010; Pinto, 2011; Kavaliers et al., 2020). Notably, olfactory dysfunction is very common among populations with substance abuse, and more than 52% of substance abusers have reported abnormalities in olfactory performance (Podskarbi-Fayette et al., 2005). In Meth abusers, abnormalities of olfactory function, such as olfactory hallucinations, are common psychiatric complaints (Mahoney et al., 2010; McKetin et al., 2017). In animal studies, chronic Meth exposure has been found to induce alterations in the expression of proteins involved in processes such as neuroinflammation and neurodisability in the olfactory bulb (Zhu et al., 2016). In addition, acute Meth administration results in impaired socially/non-socially dependent olfactory discrimination in rodents (O'Dell et al., 2011; Ramkissoon and Wells, 2015). However, these studies could not distinguish whether the reduced olfactory recognition performance is caused by the impairment of olfactory cognitive function or olfaction alone, nor could they reveal the olfactory function and its underlying mechanism in drug abusers in chronic conditions.

Alpha-synuclein (α-syn, encoded by *SNCA*) is a soluble cytosolic neuronal protein belonging to the synuclein family (Sulzer and Edwards, 2019). Accumulating studies have revealed that α-syn is involved in maintaining normal synaptic transmission and is implicated in the pathogenesis of synucleinopathies (Burré et al., 2018), and the olfactory bulb is not only the brain region with high expression of α-syn (Hansen et al., 2013) but also the initial site of its propagation to multiple brain regions (Cersosimo, 2018). The accumulation of α-syn in the olfactory bulb is increased during aging and in neurodegenerative diseases (Bobela et al., 2015; Srinivasan et al., 2021), and artificial regulation of systemic/brain α-syn expression or direct overexpression of α-syn in the olfactory bulb has been shown to cause olfactory impairment (Hansen et al., 2013; Zhang et al., 2015; Chen et al., 2021). Notably, a definite association has been found between abnormal metabolism of α-syn and the occurrence of neuropsychiatric symptoms (Wu et al., 2021). However, whether and how Meth affects α-syn in the olfactory bulb remain unknown. According to anatomical and immunohistochemical results, α-syn is mainly distributed in the mitral/granulosa cell layer of the olfactory bulb (Hansen et al., 2013). In the olfactory system of information processing, the smell signal first activates olfactory sensory neurons in the nasal epithelium, and the activated olfactory sensory neurons can stimulate the olfactory bulb mitral cells. After processing and encoding olfactory information, mitral cells project olfactory information through axons to the higher olfactory cortex (Nunez-Parra et al., 2014). The fine regulation of mitral and granule cells in the olfactory bulb and their normal electrophysiological performance play an important role in the correct processing and transmission of olfactory information. However, when α-syn accumulates in the olfactory bulb, local olfactory bulb neural activity is perturbed (Kulkarni et al., 2020). These results imply the effect of Meth on olfactory function and its potential α-syn-involved mechanism.

Aerobic exercise, which has been widely used as rehabilitation therapy, has shown a protective role in brain functional recovery among Meth-dependent abusers (Zhang et al., 2018; Huang et al., 2020; Liu et al., 2021). In rodents, voluntary wheel running mimics long-term regular aerobic exercise with adequate oxygen supply (Manzanares et al., 2018). More intriguingly, aerobic exercise has been found to promote α-syn clearance and improve recovery of olfactory function (Koo and Cho, 2017; Tian et al., 2020). This finding has prompted our interest in exploring the effect of aerobic exercise on the potential impairment of olfactory function caused by chronic Meth administration. Accordingly, in this study, we investigated the effects of chronic Meth abuse on olfactory function and explored the potential mechanisms by which aerobic exercise improves Meth abuse-induced olfactory dysfunction.

MATERIALS AND METHODS

Animals

Male c57BL/6 mice aged 8–10 weeks and weighing 20–25 g were used in this study. The experimental animals were supplied by the Laboratory Animal Center of Southern Medical University (Guangzhou, Guangdong, China). Animals were raised in a standard specific pathogen-free experimental environment with free access to water and food, constant temperature (23 ± 1°C) and humidity (50–60%), and dark and light for 12 h each. All experimental procedures were carried out in accordance with the Principles of Laboratory Animal Care (NIH Publication no. 85–23, revised 1985) and supervised by the Animal Ethics Committee of The Third Affiliated Hospital of Sun Yat-sen University. The chronic administration route and dosage (10 mg/kg i. p. daily, National Institute Control of Pharmaceutical and Biological Products, Beijing, China) of Meth were chosen based on our previous chronic toxicity study (Wang et al., 2021a). Behavioral experiments were performed 1 week after the last Meth administration or 4 weeks after the virus injection. The exercise method utilized in this study was voluntary wheel-running and adapted from published procedures (Jang et al., 2017; El Hayek et al., 2019). Briefly, mice used for exercise training were housed individually and allowed free access to a steel running (rotatable/locked) wheel for 8 weeks. Upon completion of the behavioral experiments, the mice were deeply anesthetized with sodium pentobarbital for sample collection and electrophysiological recordings. Every possible effort was made to minimize animal pain or discomfort and reduce the number of animals used.

Behavioral Test

The assessment of mouse olfactory behavior was performed with a digital video recording device in the zenithal position

by an experienced double-blind researcher. Different experimental paradigms depict different perspectives on olfactory performance.

The olfactory threshold examination, which uses rodents' innate conditioned preference/aversion responses to odors, was performed and adapted as previously described by Breton-Provencher et al. (2009). The olfactory threshold and sensitivity of animals can be measured by observing their responses to different concentrations of odors. In this study, butyraldehyde was used as an aversive odor, and limonene was used as a preferred odor. During a 5 min period, each animal was allowed to explore different odorant solutions at different concentrations in three independent experiments with odorless solvent as a control, and the preference index was calculated (see **Figure 1A** for schematic diagram).

The olfactory discrimination habituation/dishabituation test was performed as described previously (Gheusi et al., 2000) to assess whether the animal could differentiate between different odors. Each session consisted of three repetitions of exploration with the same odor (Odor 1) as the familiar condition and a new odor (Odor 2) as a novel condition (see **Figure 1B** for schematic diagram).

Social odor discrimination was used to identify whether animals can discriminate between different social odors (Petit et al., 2013). The odorless blocks were placed for 24 h in cages with different animals (came from the tested animal or the conspecific stranger of the same sex). The time spent by the mouse sniffing exploration during a 5 min section with an 15 min interval of the block scented of its own and an exploration of novel social scent were matched and measured.

The non-social food buried test was adapted from a previous study (Wu et al., 2016). Mice were fasted for 48 h to ensure sufficient motivation to search for food. The experiment was divided into three 5-min stages, with an interval of 15 min.

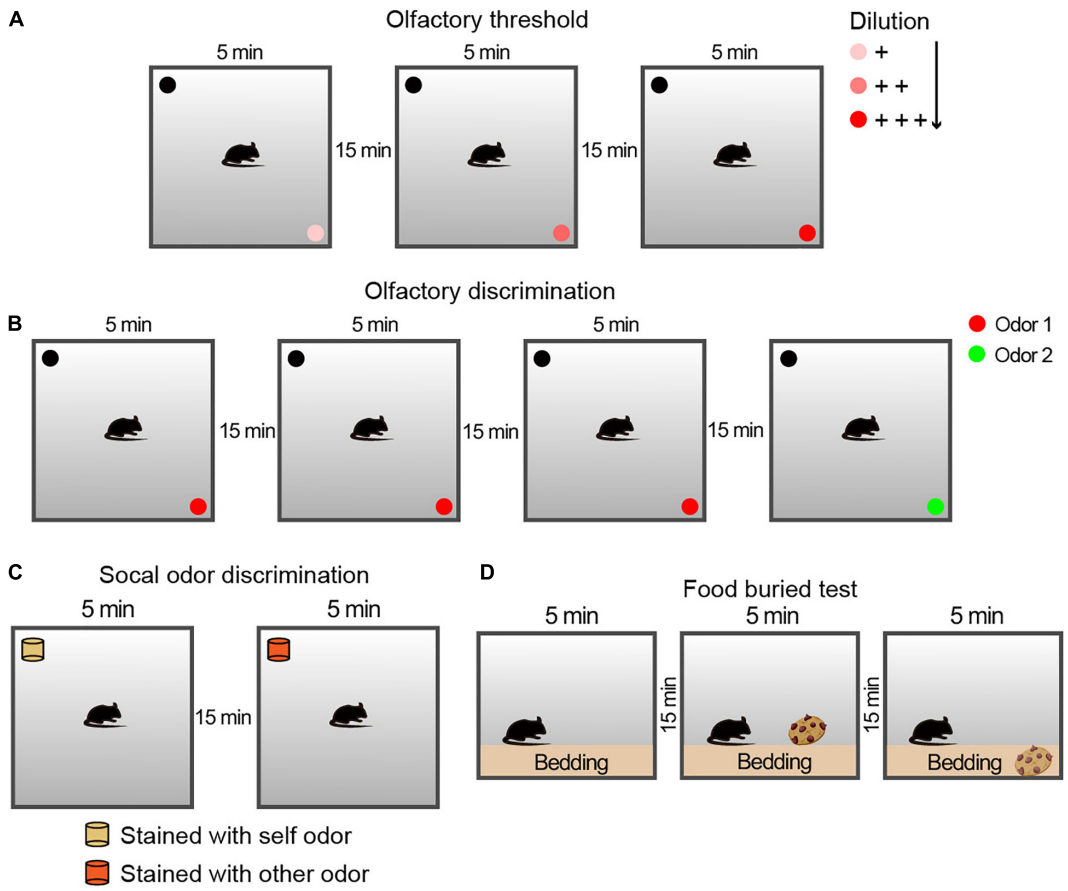

FIGURE 1 | Schematic diagram of the protocol of the behavioral experiment for the olfactory examination. **(A)** Experimental configuration for the olfactory threshold and sensitivity tests. Each trial lasted for 5 min, followed by a 15-min rest interval. For the avoidance and preference tests, three solutions of different concentrations were used. **(B)** Experimental configuration for the olfactory discrimination test. Each trial lasted 5 min, followed by a 15-min rest interval. For the olfactory discrimination test, two different odor solutions were used. **(C)** Schematic drawing of the experimental steps for the social olfactory discrimination test. Each trial lasted 5 min, followed by a 15-min rest interval. The blocks were placed consistently above the bedding between cages in the corresponding home cages. For social odor discrimination, mice were given a comparison between blocks with their own odor and those with the odor of an unfamiliar conspecific male. **(D)** Schematic drawing of the experimental steps for the buried food test for olfactory function examination. Each trial lasted 3 min, followed by a 15-min rest interval. The cookies were placed above or buried below the bedding in the corresponding two stages.

In the first stage, the animals were placed on the bedding and acclimatized to the environment. In the second stage (visible), a cookie was placed on the bedding of one corner, and the time the mice used to find the food and nibble it within 5 min was recorded. In the third stage (invisible), the food was buried 1.5 cm below the bedding in a randomly selected corner, and the time the animal used to find and nibble it was recorded.

Immunofluorescence

Immunohistochemistry assays were performed as previously described (Wang et al., 2021b), and mice were transcardially perfused with pre-cooled phosphate-buffered saline (PBS) and 4% paraformaldehyde. The brains were further fixed for 12 h at 4°C and dehydrated in 30% sucrose for cryoprotection. They were then cut into 20-mm-thick sections, and the sections were permeabilized with 0.3% Triton X-100 for 10 min and blocked with 5% bovine serum albumin (BSA) in PBS for 2 h. These brain sections were incubated with primary antibodies against α-syn (SC-7011, 1:1500, Santa Cruz Biotechnology, CA, United States) overnight at 4°C in PBS with 2% BSA. Thereafter, the brain sections were incubated with a secondary Alexa Fluor® 488-conjugated antibody (Invitrogen) for 1 h in the dark. After washing with PBS, 4′,6-diamidino-2-phenylindole (Vector Lab) was used to stain the nuclei, and images were then acquired using a Leica fluorescence microscope.

Western Blotting

Western blotting was performed after the behavioral experiment, and behavioral and expression data were analyzed for each animal individually. Total proteins were extracted from the olfactory bulb tissues using RIPA lysis buffer (Solarbio, Beijing, China), and the protein concentrations were measured using a Pierce™ BCA protein kit (23227, Thermo Fisher Scientific, Waltham, MA, United States). Equal amounts of protein lysates (approximately 40 μg) were separated using 12% sodium dodecyl sulfate polyacrylamide gel electrophoresis and subsequently transferred to polyvinylidene difluoride membranes (Millipore, Bedford, MA, United States). The membranes were incubated with 5% BSA to block non-specific binding. Next, the membranes were probed with specific primary monoclonal antibodies at 4°C overnight, including anti-α-syn (SC-7011, 1:3000, Santa Cruz Biotechnology) and glyceraldehyde 3-phosphate dehydrogenase (GAPDH, ab9485, 1:3000, Abcam). Subsequently, the membranes were incubated with HRP-labeled anti-rabbit IgG (ab288151, Abcam) at 37°C for 2 h. Finally, protein expression was visualized using enhanced chemiluminescence reagents (Thermo Fisher Scientific). GAPDH was used as an internal reference for normalization.

Viral Injection

Stereotaxic surgeries were performed as described previously (Wang et al., 2019). Under isoflurane gas anesthesia, mice were placed in a stereotaxic frame, and the skull was exposed and adjusted to ensure that the bregma and the lambda axis were horizontal. For α-syn (*Snca*) knockdown and overexpression, 1 μL of EGFP-tagged rAAV-α-syn (AAV-α-syn, 3.4E_12 V. g/L), rAAV-control (AAV-Con, 4.2E_12 V.G./ml), rAAV-α-synuclein-shRNA (α-syn-shRNA, 6.3E_12 V. g/mL), or rAAV-control-shRNA (Con-shRNA, 6.2E_12 V.G./ml) was bilaterally injected into the olfactory bulb (coordinates from bregma AP: 4.5 mm; ML: ± 0.75 mm; DV: −3.25 mm), and the needle was withdrawn gently 10 min after injection. Viral vectors were designed and constructed using a commercial packaging service (Brain Case Co., Ltd., Shenzhen, China). Mice with missed injections or EGFP expression outside the olfactory bulb were excluded from the analysis after *post-hoc* examination.

Electrophysiological Recording

The animals were euthanized by carbon dioxide asphyxiation and decapitated, and their brains were rapidly and gently removed. The olfactory bulb was then sliced into 300-μm-thick sections with a vibrating tissue slicer (World Precision Instruments Vibroslicer, Sarasota, FL, United States), and the sections were placed in a pre-cooled artificial cerebrospinal fluid (ACSF) circulating with 95% O_2 and 5% CO_2. The ACSF solution contains 124 mmol/L NaCl, 24 mmol/L $NaHCO_3$, 5 mmol/L KCl, 2.4 mmol/L $CaCl_2$, 1.3 mmol/L $MgSO_4$, 1.2 mmol/L $KH2PO_4$, and 10 mmol/L glucose (pH = 7. 4). Recordings began after at least 1 h of recovery. During recording, the olfactory bulb sections were transferred from the incubation tank to the recording tank and fixed with a brain slice fixator under light pressure. The recording tank was continuously filled with 95%O_2/5%CO_2-ventilated ACSF, which was prepared with ACSF in advance when certain drugs were applied, and the ACSF was replaced through the fluid inlet of the perfusion system. The irrigation rate was 2 mL/min, and the temperature of the recording tank was maintained at 29–30°C with a heating rod. Mitral cells in the olfactory bulb were identified by position, morphology, and electrical characteristics under a 60 × water-immersion objective microscope (Schoppa, 2006). For whole-cell action potential recording, pipettes were filled with a solution containing 130 mmol/L K-Gluconate, 20 mmol/L KCl, 10 mmol/L HEPES, 4 mmol/L MgATP, 10 mmol/L Na-Phosphocreatine, 0.3 mmol/L Na_2GTP, and 0.5 mmol/L EGTA, adjusted to pH 7.4 with KOH. The miniature inhibitory postsynaptic currents (mIPSCs) were monitored in the presence of tetrodotoxin to block action potentials. For mIPSC recordings, the intracellular solution contained 125 mmol/L KCl, 3 mmol/L Mg-ATP, 1 mmol/L $MgCl_2$, 10 mmol/L HEPES, 0.02 mmol/L EGTA, and 0.5 mmol/L Na_3-GTP. All data acquisition and analysis were performed using a Multiclamp 700 b amplifier (Cellular Devices, Sunnyvale, CA, United States), pClamp 10 (Molecular Devices, Sunnyvale, CA, United States), and Mini Analysis (Synaptosoft, Fort Lee, NJ, United States).

Statistical Analysis

GraphPad Prism 6.00 was used for data processing. All experimental results are expressed as mean ± SEM. Student's *t*-test was used to analyze the difference between two groups, one-way analysis of variance (ANOVA) among ≥three groups, and two-way ANOVA between factorial designed groups. A linear relation was analyzed by Spearman's correlation coefficient. The

sample size in each group is indicated in each figure legend. $P < 0.05$ represented a significant difference.

RESULTS

Chronic Methamphetamine Administration Induces Severe Olfactory Functional Deficits in Mice

To evaluate the effect of Meth on olfactory function, the overall olfactory performance was estimated using a series of statistical indicators, including olfactory threshold, olfactory discrimination, social odor discrimination, and food exploration. The behavioral research strategy is illustrated in **Figure 1**. Behavioral tests were conducted after 4 weeks of administration of Meth. Generally, animals display an inborn aversion or favorite to the conditioned odor. Thus, animals were tested for their avoidance or preference for a certain solution. Butyraldehyde and limonene were gradient-diluted to test the sensitivity of the animal to avoidance or preference. We found that chronic Meth administration significantly decreased olfactory sensitivity in both the avoidance and preference tests (**Figure 2A**); higher odor concentration was required to show preference/aversion, and the preference/aversion degree was lessened under the same odor concentration. In another olfactory test, which involved olfactory cognitive function, the animals were exposed to the same odor three times before being exposed to a novel odor in the fourth test (**Figure 2B**). With familiarity with the same smell, the mice in the control group showed a decrease in the desire to explore the familiar odor, while a significant increase was observed after giving new odors. This process was impaired in animals administered with chronic Meth. We also examined the social-related olfactory function (**Figure 2C**), and the control animals showed significant interest in exploring blocks that had been contaminated with the scent of a congeneric stranger,

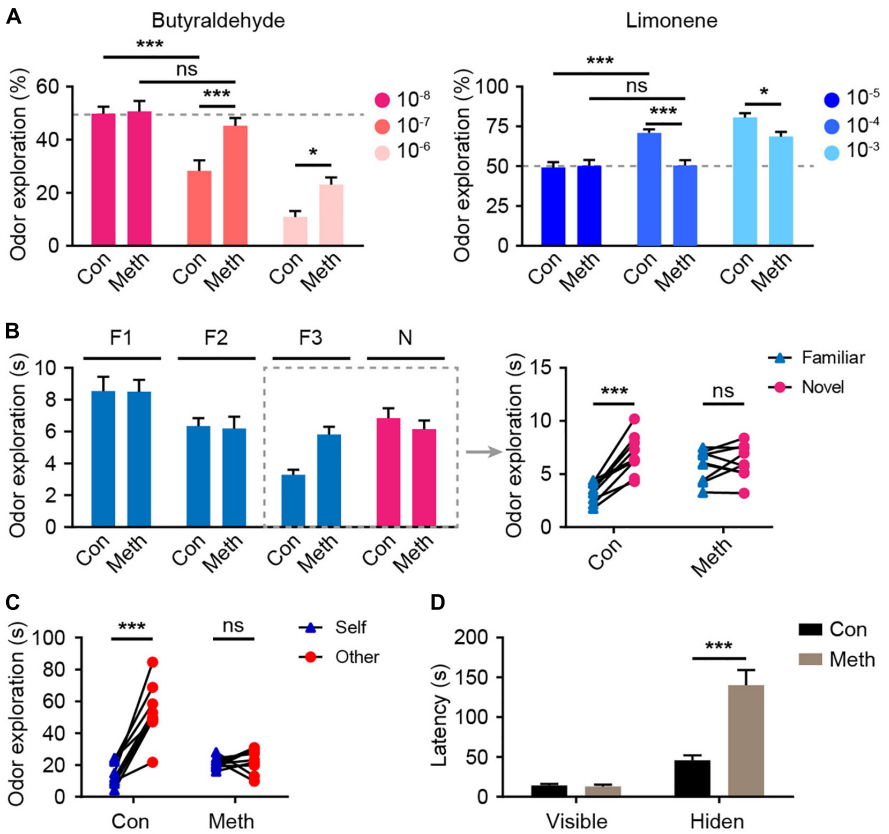

FIGURE 2 | Chronic methamphetamine administration induces impairment of olfactory performance. **(A)** Chronic Meth administration decreased olfactory sensitivity to both aversive and favorite odors. Left, olfactory avoidance performance for an aversive odor (butyraldehyde). The concentrations of the butyraldehyde solution ranged from 10^{-8} to 10^{-6} ($n = 9$). $F_{(2,32)} = 4.246$, $P = 0.0231$ by two-way RM ANOVA with Bonferroni's multiple comparisons test. Right, olfactory sensitivity to a favorite odor (Limonene). The concentrations of limonene solution ranged from 10^{-5} to 10^{-3} ($n = 9$). $F_{(2,32)} = 5.601$, $P = 0.0082$ by two-way RM ANOVA with Bonferroni's multiple comparisons test. **(B)** Chronic Meth administration impaired olfactory discrimination. Left, statistical analysis for the experiments that were performed independently four times. Right, the corresponding exploration time of each animal for different odors in the dashed rectangular line ($n = 9$). $F_{(1,16)} = 23.49$, $P = 0.0002$ by two-way RM ANOVA. **(C)** Chronic Meth administration impaired social olfactory discrimination. Scatter dots represent animals, and they were paired with the corresponding strangers ($n = 9$). $F_{(1,16)} = 37.13$, $P < 0.0001$ by two-way RM ANOVA. **(D)** Chronic Meth administration impaired olfactory function in locating food ($n = 9$). $F_{(1,16)} = 23.09$, $P = 0.0002$ by two-way RM ANOVA. F, familiar; N, novel; ns, not significant. Data are presented as mean ± SEM. $^{*}P < 0.05$; $^{***}P < 0.001$.

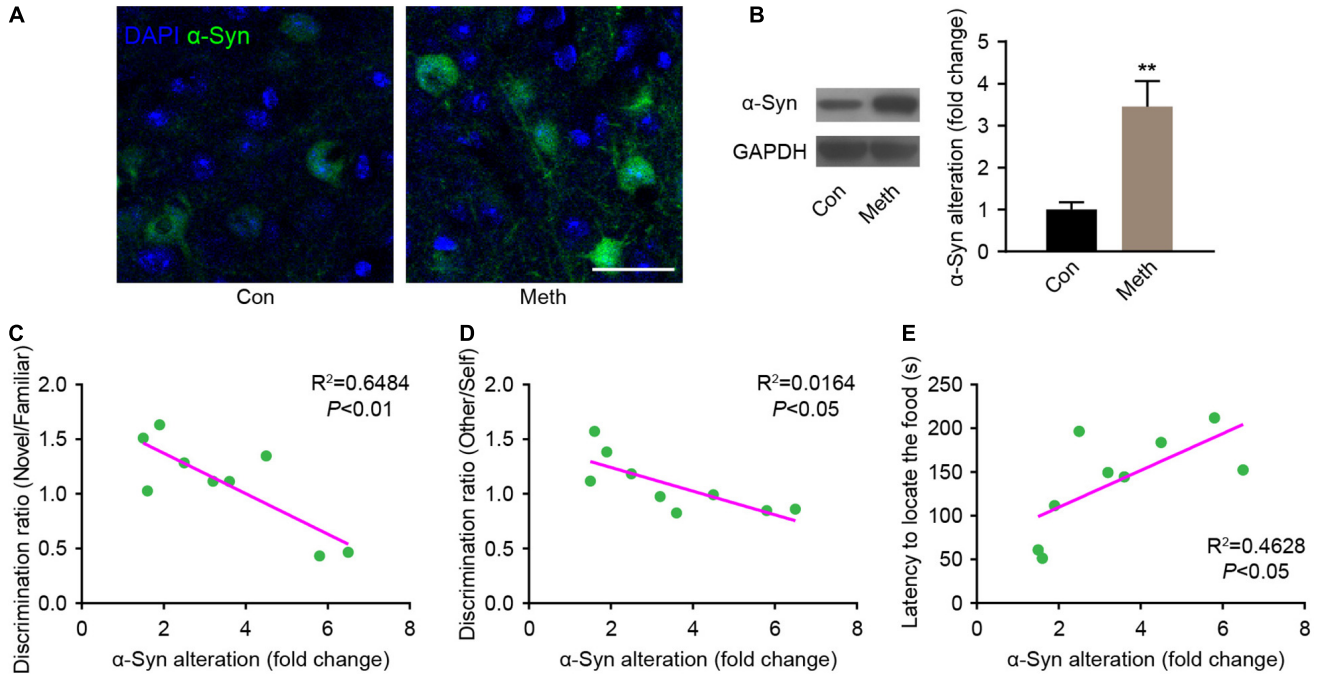

FIGURE 3 | Chronic methamphetamine administration increases the expression of α-syn in the olfactory bulb. **(A)** Representative confocal immunofluorescence images of the OB mitral cells stained for α-syn (Green) upon chronic methamphetamine administration. Scale bar, 20 μm. **(B)** The levels of α-syn were examined by western blotting (n = 9). t = 3.895 by unpaired t test. GAPDH served as a normalization control. The correlation between α-syn expression changes and olfactory discrimination **(C)**, social olfactory discrimination **(D)** and buried food test **(E)** results was analyzed in chronic methamphetamine-administered mice, and there was a significant association between α-syn changes and behavioral alterations (n = 9). Data are presented as mean ± SEM. $^{**}P < 0.01$.

while animals with chronic Meth administration showed obvious defects in this test. Finally, we assessed the ability of olfactory-dependent food acquisition (**Figure 2D**). When cookies were placed on the bedding, the two groups of animals could see food and showed a similar latency to eat. When the food was buried under the bedding, animals with chronic Meth administration took a longer time to find the food. These results indicate that chronic Meth administration induces olfactory dysfunction.

Chronic Methamphetamine Administration Increases the Expression of α-Synuclein in the Olfactory Bulb in Mice

Methamphetamine can promote the accumulation of α-syn, and the olfactory bulb is the core brain region of α-syn metabolism in the central nervous system (Rey et al., 2013, 2016; Zhu et al., 2018). Therefore, α-syn expression in the olfactory bulb was detected. Immunofluorescence staining showed that the presence of α-syn was remarkably increased after chronic Meth administration (**Figure 3A**), and western blot analysis confirmed the same effect (**Figure 3B**). Correlation analysis of the behavioral and western blotting results showed that the increase in α-syn was negatively correlated with the non-socially/socially odor discrimination ratio (**Figures 3C,D**), and positively correlated with the degree of olfactory function impairment (**Figure 3E**). This finding suggests a causal relationship between the increased expression of α-syn and the appearance of olfactory impairment.

Inhibition of α-Synuclein Prevents Methamphetamine-Induced Olfactory Deficits

To investigate the role of α-syn in the regulation of olfactory functional deficits following chronic Meth administration, olfactory bulb neurons were infected with rAAVs expressing shRNA against α-syn (α-syn-shRNA) or non-targeting scrambled sequence shRNA (Con-shRNA) as a control before the administration of Meth (**Figure 4A**). The injection accuracy and infection efficiency of rAAV were examined by immunofluorescence (**Figure 4B**), and a significant decrease in α-syn expression levels within olfactory bulb regions was successfully identified in α-syn-knockdown mice (**Figure 4C**). Knockdown of α-syn within the olfactory bulb significantly ameliorated Meth-induced olfactory deficits, as evidenced by increases in olfactory sensitivity in both the avoidance and preference tests (**Figure 4D**), novel odor discrimination (**Figure 4E**), social-related olfactory function (**Figure 4F**), and olfactory-dependent food acquisition (**Figure 4G**). These findings demonstrate that reducing the abnormal deposition of α-syn in the olfactory bulb ameliorates chronic Meth administration-induced olfactory dysfunction.

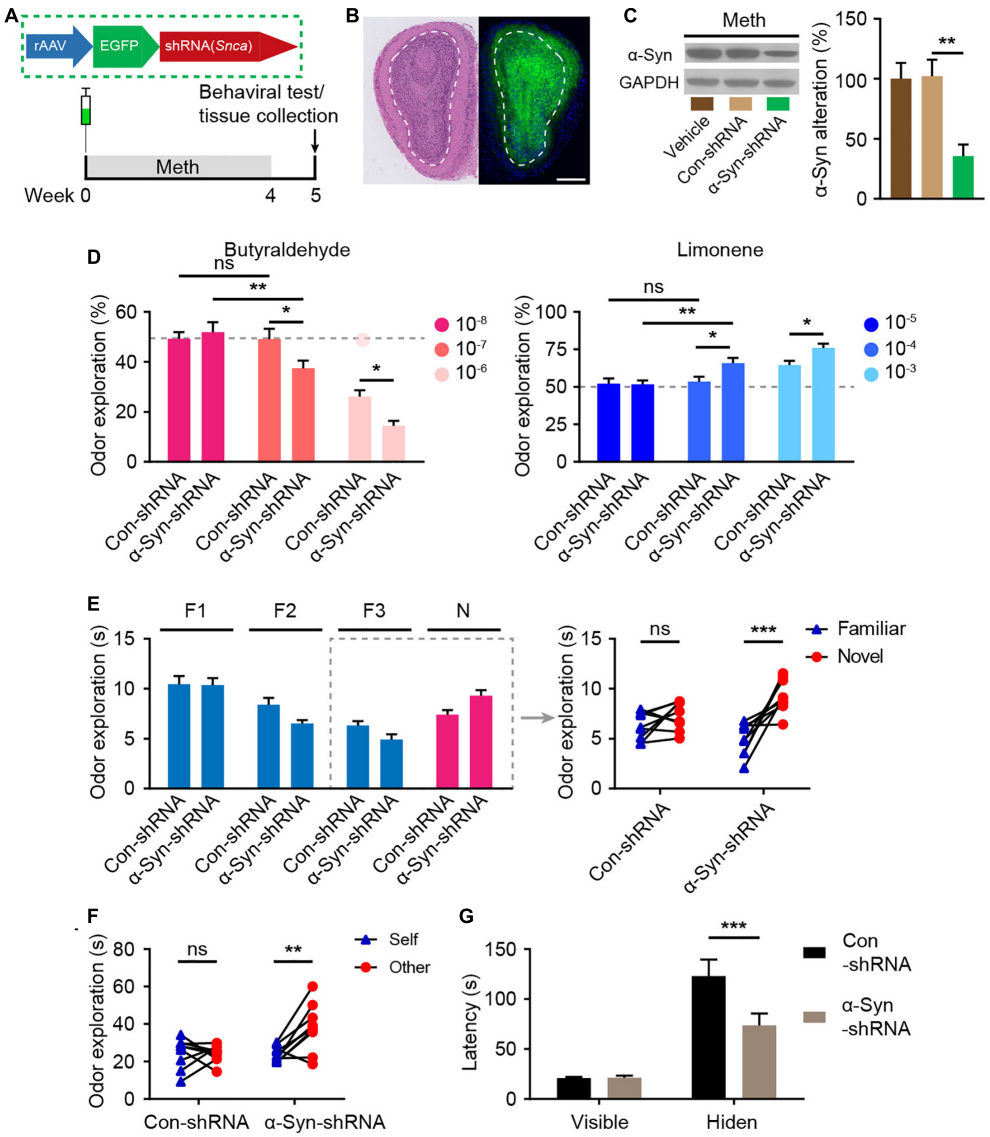

FIGURE 4 | Suppression of α-syn rescues methamphetamine-induced olfactory behavioral abnormalities. **(A)** Experimental scheme for injection of reconstructed adeno-associated virus (rAAV) containing α-syn-shRNA or control into the olfactory bulb and subsequent behavioral testing. **(B)** Schematic representation of the rAAV injection strategy and representative HE staining and immunofluorescence images of olfactory bulb sections of rAAV-injected mice (n = 3). Scale bar, 500 μm. **(C)** The efficiency of α-syn-shRNA was determined by western blot analysis (n = 6). F = 9.371, P = 0.0023 by One-way ANOVA with Bonferroni's multiple comparisons test. **(D)** Suppression of α-syn increased olfactory sensitivity to both aversive (butyraldehyde) and favorite (Limonene) odors (n = 9). Butyraldehyde: $F_{(2,32)}$ = 3.383, P = 0.0465 by two-way RM ANOVA with Bonferroni's multiple comparisons test. Limonene: $F_{(2,32)}$ = 2.926, P = 0.0681 by two-way RM ANOVA with Bonferroni's multiple comparisons test. **(E)** Suppression of α-syn improved olfactory discrimination (n = 9). $F_{(1,16)}$ = 8.432, P = 0.0104 by two-way RM ANOVA. **(F)** Suppression of α-syn improved social olfactory discrimination. Each scatter dot represents an animal, and it was paired with the corresponding stranger (n = 9). $F_{(1,16)}$ = 7.993, P = 0.0121 by two-way RM ANOVA. **(G)** Suppression of α-syn improved olfactory function to locate invisible food (n = 9). $F_{(1,16)}$ = 6.669, P = 0.0200 by two-way RM ANOVA. F, familiar; N, novel; ns, not significant. Data are presented as mean ± SEM. *P < 0.05; **P < 0.01; ***P < 0.001.

Exercise Alleviates Methamphetamine-Induced Olfactory Dysfunction Through α-Synuclein Intervention

Exercise has been recognized to combat the adverse effects of drug use and is closely associated with improved olfactory function as we have mentioned above. Here, we examined the effects of exercise on the olfactory dysfunction induced by chronic Meth. Furthermore, to test whether recovery of α-syn expression could block the effect of exercise, we generated rAAVs containing α-syn or GFP and injected them correspondingly during the exercise (**Figures 5A,B**). Eight weeks of aerobic exercise not only reduced the amount of α-syn deposited in the olfactory bulbs but also improved olfactory function (**Figures 5C–E**). However, overexpression of human α-syn

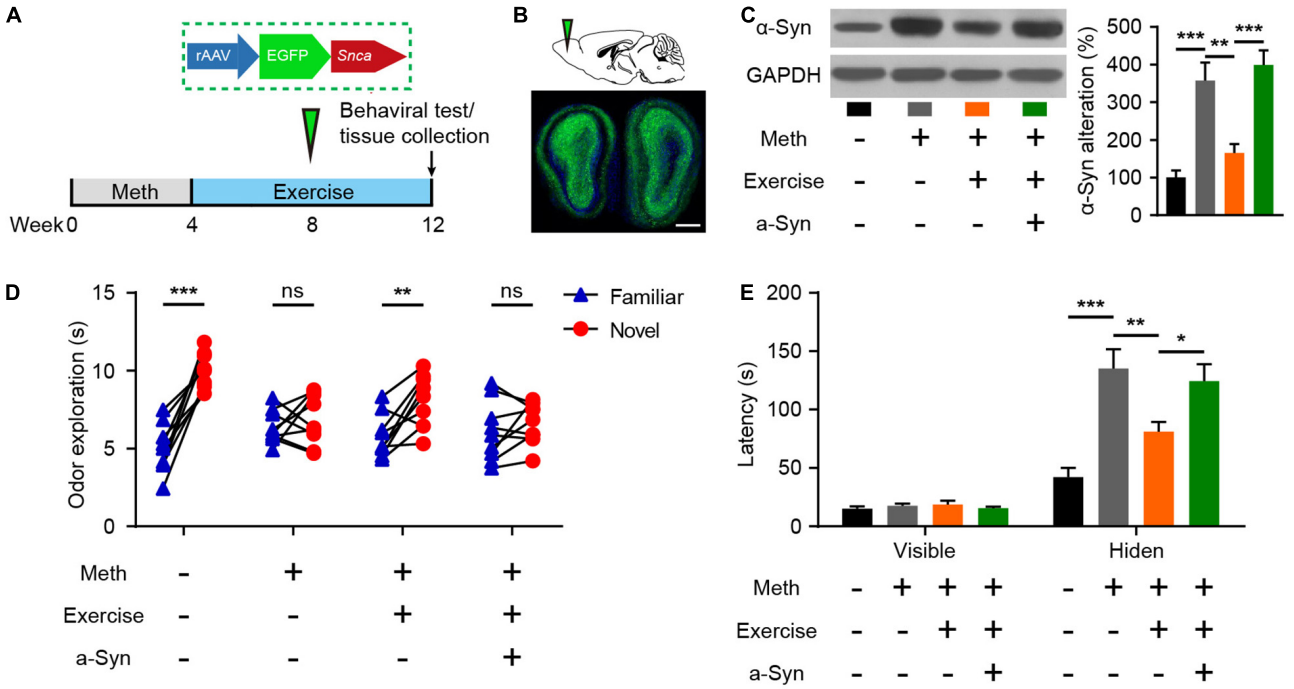

FIGURE 5 | Exercise improves methamphetamine-induced olfactory behavioral abnormalities through reduced α-syn expression. **(A)** Illustration of rAAV packed with human SNCA and experimental paradigm for methamphetamine administration, virus injection, and behavioral testing. **(B)** Schematic representation of rAAV-α-syn injection and GFP fluorescence in the infected region of the olfactory bulb. Scale bar, 500 μm. **(C)** Effects of exercise and olfactory bulb rAAV-α-syn injection on α-syn expression were determined by western blot analysis. $F = 17.98$, $P < 0.0001$ by One-way ANOVA with Bonferroni's multiple comparisons test. **(D)**: Effects of exercise and olfactory bulb rAAV-α-syn injection on olfactory discrimination ($n = 9$). $F_{(3,32)} = 11.47$, $P < 0.0001$ by two-way RM ANOVA with Bonferroni's multiple comparisons test. **(E)** Effects of exercise and olfactory bulb rAAV-α-syn injection on locating invisible food ($n = 9$). $F_{(3,48)} = 9.765$, $P < 0.0001$ by two-way RM ANOVA with Bonferroni's multiple comparisons test. Data are presented as mean ± SEM. $^*P < 0.05$; $^{**}P < 0.01$; $^{***}P < 0.001$; ns, non-significant.

blocked the alleviating effect of exercise on Meth-induced olfactory dysfunction (**Figures 5C–E**).

Exercise Improves Impaired Inhibitory Synaptic Transmission in the Olfactory Bulb

Normal neural activity and synaptic plasticity of mitral cells are required for the efficient performance of olfactory function, and the accumulation of α-syn is tightly coupled with abnormal electrical activity of olfactory neurons (Chen et al., 2021). According to the cell-attached recordings, Meth increased the spontaneous firing rate of mitral cells; this effect could be alleviated by exercise but blocked upon α-syn restoration (**Figures 6A,B**). The spontaneous firing activity of mitral cells is controlled by local inhibitory synaptic drive (Nai et al., 2009). Thus, we measured the level of mIPSCs in mitral neurons. We found that Meth administration caused a significant decrease in the frequency (but not in the amplitude) of mIPSCs (**Figures 6C–E**). As expected, exercise led to upregulation in the frequency of mIPSCs, and this effect was blocked by rAAV-α-syn injection; no significant changes were observed in the amplitude of mIPSCs (**Figures 6C–E**). These results suggest that exercise could reverses the impaired inhibitory synaptic transmission in the olfactory bulb through a α-syn-selective manner.

DISCUSSION

In this study, we systematically examined the effects of Meth on olfactory performance and demonstrated that Meth could impair olfactory function through upregulated α-syn levels in the olfactory bulb. Aerobic exercise could reverse this process by implementing α-syn intervention and restoring inhibitory synaptic transmission of mitral cells. These results deepen our understanding of Meth-induced neurotoxicity and provide new insights into the pathogenesis and treatment of meth-related encephalopathy.

Olfaction is the physiological basis of many biological behaviors (Mori and Sakano, 2021), and its dysfunction is a common symptom that occurs early in many neuropsychiatric diseases (Waldmann et al., 2020). In fact, many neuropsychiatric symptoms induced by Meth, such as aggressive behavior (Stowers et al., 2013), depressed mood (Athanassi et al., 2021), and olfactory hallucination (Mahoney et al., 2010), are all strongly linked to olfaction. Olfactory function is important but often neglected during physical examination in Meth users, and the damage to the nasal mucous membrane after long-term snorting/intranasal route administration may cause olfactory function damage naturally. However, the effects of Meth on the entire olfactory pathway have not been revealed. Thus, we employed intraperitoneal injection delivery methods, which

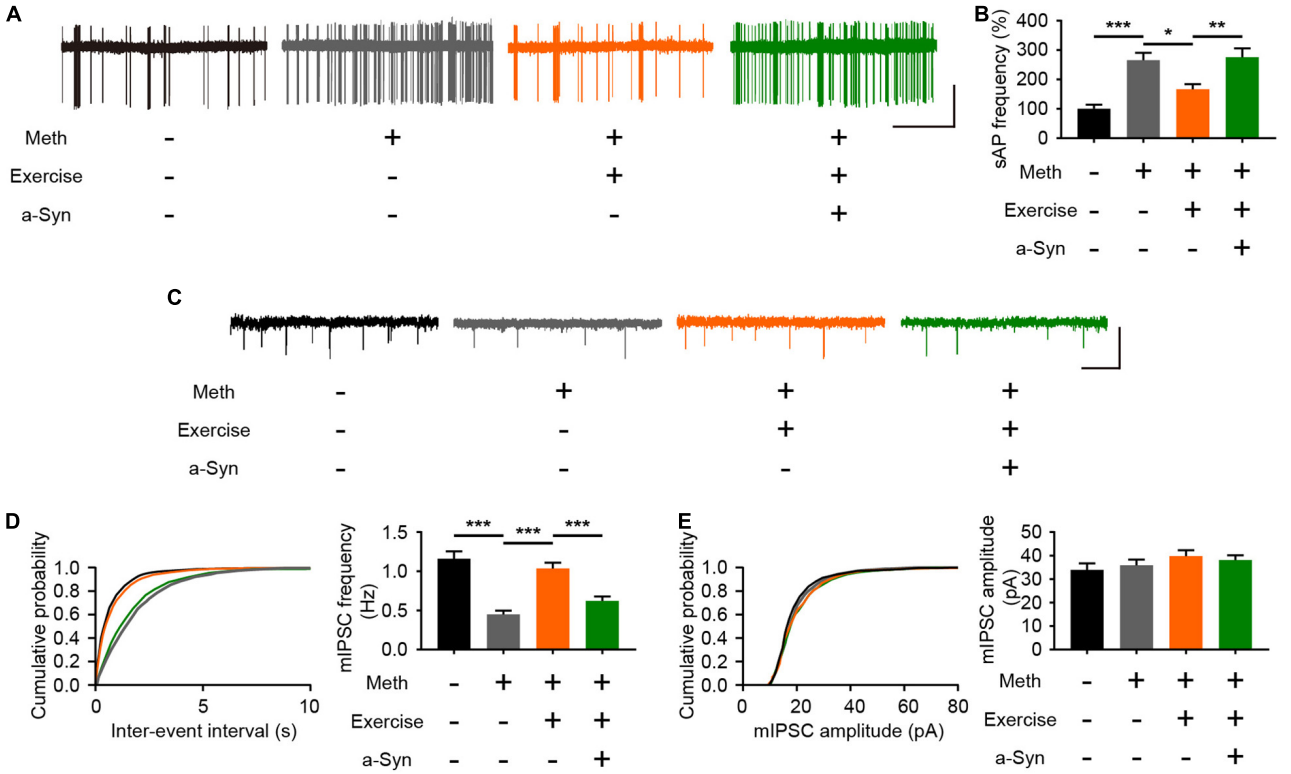

FIGURE 6 | Exercise improves methamphetamine-induced impaired inhibitory synaptic transmission in the olfactory bulb through α-syn intervention. **(A)** Representative traces of spontaneous action potential of mitral cells. Scale bar, 25 pA, 5 s. **(B)** Quantitative analysis of spontaneous firing rates of mitral cells in each group (a total of 12 cells from 3 to 4 mice were recorded in each group). $F = 13.87$, $P < 0.0001$ by One-way ANOVA with Bonferroni's multiple comparisons test. **(C)** Representative traces of whole-cell voltage-clamp recordings showing mIPSC events from mitral cells in olfactory bulb slices. Scale bar, 100 pA, 1 s. **(D)** Cumulative plots of the mIPSC interevent interval and quantitative analysis of mIPSC frequency in mitral cells (a total of 15 cells from four to five mice were recorded in each group). $F = 22.41$, $P < 0.0001$ by One-way ANOVA with Bonferroni's multiple comparisons test. **(E)** Cumulative plots of the mIPSC amplitude and quantitative analysis of mIPSC amplitude in mitral cells (a total of 15 cells from four to five mice were recorded in each group). $F = 1.078$, $P = 0.3659$ by One-way ANOVA with Bonferroni's multiple comparisons test. Data are presented as mean ± SEM. $^{*}P < 0.05$; $^{**}P < 0.01$; $^{***}P < 0.001$.

avoid direct adverse stimulation to the nasal mucosa and make it possible to explore the effects of Meth on the central olfactory system. Meth can cause severe cognitive dysfunction (Mizoguchi and Yamada, 2019); therefore, the influence of olfactory-related cognitive factors on olfactory behavior should be excluded when designing olfactory function examinations. Accordingly, we used the animals' instinctive aversion to malodorous odors and preference for fresh odors to rule out olfactory cognitive function as an intervening factor. We showed that chronic Meth administration significantly reduced the olfactory threshold and sensitivity of animals to averting and favoring smells, and olfactory cognitive function was also impaired, as manifested by impaired social/non-social odor discrimination and a decline in olfactory-dependent food exploration ability. These results suggest olfactory information processing abnormalities in Meth-abused animals.

Previous studies have demonstrated that Meth can induce significant changes in α-syn metabolism in the brain (Mauceli et al., 2006; Wu et al., 2021), and knockdown of α-syn could alleviate pathological brain injury caused by Meth (Ding et al., 2020). However, the behavioral manifestations remain unclear. We hypothesized that α-syn might also mediate the impairment of olfactory bulb function, and our results confirmed this hypothesis. Our findings indicate that the elevation of α-syn is implicated in Meth-induced olfactory dysfunction, and the dysfunction can be alleviated by knockdown of α-syn. Consistently, heterologous injection of α-syn into the olfactory bulb has also been shown to cause abnormalities in olfactory function (Niu et al., 2018; Chen et al., 2021); however, the artificial intervention could not mimic the natural process of disease progression. In this study, we demonstrated for the first time that Meth could impair olfactory function by increasing the levels of α-syn in the olfactory bulb; this is a potential pathophysiological mechanism by which Meth abuse influences olfactory function. An important question that remains to be explored is the exact source of increased α-syn. Meth abuse may not only promote the expression of α-syn in the olfactory bulb, and the increase in peripheral entry and the increased blood-brain barrier permeability may also contribute to the increased olfactory bulb α-syn levels induced by Meth. These hypotheses need to be further verified by subsequent experiments.

Normal synaptic transmission of olfactory bulb neurons plays an important role in olfactory information processing. Our electrophysiological results revealed that mitral cells with impaired inhibitory synaptic transmission exhibited higher cluster discharge activity. The increased firing activity of mitral cells induced by Meth is consistent with the result of direct injection of α-syn into the olfactory bulb (Chen et al., 2021), and similar damage to the inhibitory regulation of mitral cells has also been found in other neurodegenerative diseases, such as Alzheimer's disease (AD) (Hu et al., 2021). Parallel to the results, the inhibitory synaptic transmission manifested by inhibitory postsynaptic currents (IPSCs) was impaired, thus impairing local inhibitory circuits. α-syn is soluble and can be transported across brain regions in an axon-dependent manner (Li et al., 2004; Kuznetsov and Kuznetsov, 2016). Previous studies have confirmed the existence of α-syn transmission initiated from the olfactory bulb (Cersosimo, 2018). Mitral cells have axons, whereas granule cells are GABAergic interneurons without long projective axons. The spatiotemporal transfer of α-syn in mitral cells can be realized through axons, whereas in granulosa cells, α-syn cannot be translocated across brain regions, probably resulting in cytotoxicity, which may account for the damage of inhibitory synaptic transmissions. Moreover, increased mitral cell neuronal firing activity leads to more and faster transport of α-syn deposited in the olfactory bulb to other brain regions, increasing the risk of neural damage in downstream brain regions. This speculation is consistent with the clinical data and could explain, at least partially, the observed higher risk of early onset Meth-induced neurodegenerative diseases, such as PD (Lappin et al., 2018; Lappin and Darke, 2021). Whether α-syn intervention in the olfactory bulb can delay the development of subsequent neurodegeneration and alleviate related symptoms deserves further exploration.

Exercise is a natural intervention that has been widely implemented in recent years and has been proven to be effective in improving Meth-related neuropsychiatric symptoms. Based on the pathologically related mechanisms of α-syn revealed above, exercise strategies can refer to PD-related intervention training approaches. Indeed, both epidemiological and basic studies have found that aerobic exercise is an effective intervention for synucleinopathies, such as PD (Liu et al., 2020). Therefore, we chose running wheels, which is a widely accepted type of aerobic training. By locking the running wheel, the results of the experiment could eliminate the interference factors of the enriched environment to create a good contrast. This natural alternative therapy reduces the potential risks associated with prescription drugs. Notably, in this study, we revealed the protective effect of exercise on Meth-induced olfactory function impairment through α-synuclein intervention. The findings deepen the understanding of exercise against Meth-induced neurotoxicity.

CONCLUSION

In conclusion, our results indicate that Meth can impair olfactory function through the accumulation of α-syn in the olfactory bulb, leading to a state of "olfactory dementia." Moreover, the aggregation of α-syn induced by Meth affects the inhibitory synaptic input of mitral cells in the olfactory bulb, and exercise could improve olfactory function by rescuing these pathophysiological dysfunctions. The findings provide further evidence of olfactory abnormalities in the development of neurodegenerative diseases and confirm that α-syn in the olfactory bulb is an effective biomarker and therapeutic target for Meth-induced olfactory dysfunction. This study confirms the potential applications of aerobic exercise strategies in substance abusers.

DATA AVAILABILITY STATEMENT

The raw data supporting the conclusions of this article will be made available by the authors, without undue reservation.

ETHICS STATEMENT

The animal study was reviewed and approved by the Animal Ethics Committee of The Third Affiliated Hospital of Sun Yat-sen University.

AUTHOR CONTRIBUTIONS

PQ and QY designed and supervised the study. ZW, RZ, XW, XH, JH, CG, YH, SW, and JC collected, analyzed, and interpreted the data. ZW and RZ drafted the manuscript. PQ, QY, and XH revised the manuscript. All co-authors revised and approved the submitted version.

FUNDING

This work was supported by the National Natural Science Foundation of China (Grant Nos. 82171881, U20A20399, 82000958, 81870704, and 82001528) and Guangdong Basic and Applied Basic Research Foundation (Grant Nos. 2020A1515010133 and 2022A1515010922).

REFERENCES

Athanassi, A., Dorado Doncel, R., Bath, K. G., and Mandairon, N. (2021). Relationship between depression and olfactory sensory function: a review. *Chem. Senses* 46:bjab044. doi: 10.1093/chemse/bjab044

Bobela, W., Aebischer, P., and Schneider, B. L. (2015). Alpha-synuclein as a mediator in the interplay between aging and Parkinson's Disease. *Biomolecules* 5, 2675–2700. doi: 10.3390/biom5042675

Breton-Provencher, V., Lemasson, M., Peralta, M. R. III, and Saghatelyan, A. (2009). Interneurons produced in adulthood are required for the normal

functioning of the olfactory bulb network and for the execution of selected olfactory behaviors. *J. Neurosci.* 29, 15245–15257. doi: 10.1523/JNEUROSCI.3606-09.2009

Burré, J., Sharma, M., and Südhof, T. C. (2018). Cell biology and pathophysiology of α-synuclein. *Cold Spring Harb. Perspect. Med.* 8:a024091. doi: 10.1101/cshperspect.a024091

Büttner, A. (2011). Review: the neuropathology of drug abuse. *Neuropathol. Appl. Neurobiol.* 37, 118–134. doi: 10.1111/j.1365-2990.2010.01131.x

Cersosimo, M. G. (2018). Propagation of alpha-synuclein pathology from the olfactory bulb: possible role in the pathogenesis of dementia with Lewy bodies. *Cell Tissue Res.* 373, 233–243. doi: 10.1007/s00441-017-2733-6

Chen, F., Liu, W., Liu, P., Wang, Z., Zhou, Y., Liu, X., et al. (2021). α-Synuclein aggregation in the olfactory bulb induces olfactory deficits by perturbing granule cells and granular-mitral synaptic transmission. *NPJ Parkinsons Dis.* 7:114. doi: 10.1038/s41531-021-00259-7

Courtney, K. E., and Ray, L. A. (2014). Methamphetamine: an update on epidemiology, pharmacology, clinical phenomenology, and treatment literature. *Drug Alcohol Depend.* 143, 11–21. doi: 10.1016/j.drugalcdep.2014.08.003

Cruickshank, C. C., and Dyer, K. R. (2009). A review of the clinical pharmacology of methamphetamine. *Addiction* 104, 1085–1099. doi: 10.1111/j.1360-0443.2009.02564.x

Ding, J., Hu, S., Meng, Y., Li, C., Huang, J., He, Y., et al. (2020). Alpha-Synuclein deficiency ameliorates chronic methamphetamine induced neurodegeneration in mice. *Toxicology* 438:152461. doi: 10.1016/j.tox.2020.152461

El Hayek, L., Khalifeh, M., Zibara, V., Abi Assaad, R., Emmanuel, N., Karnib, N., et al. (2019). Lactate mediates the effects of exercise on learning and memory through SIRT1-dependent activation of hippocampal brain-derived neurotrophic factor (BDNF). *J. Neurosci.* 39, 2369–2382. doi: 10.1523/JNEUROSCI.1661-18.2019

Gheusi, G., Cremer, H., McLean, H., Chazal, G., Vincent, J. D., and Lledo, P. M. (2000). Importance of newly generated neurons in the adult olfactory bulb for odor discrimination. *Proc. Natl. Acad. Sci. U.S.A.* 97, 1823–1828. doi: 10.1073/pnas.97.4.1823

Hansen, C., Björklund, T., Petit, G. H., Lundblad, M., Murmu, R. P., Brundin, P., et al. (2013). A novel α-synuclein-GFP mouse model displays progressive motor impairment, olfactory dysfunction and accumulation of α-synuclein-GFP. *Neurobiol. Dis.* 56, 145–155. doi: 10.1016/j.nbd.2013.04.017

Hu, B., Geng, C., Guo, F., Liu, Y., Zong, Y. C., and Hou, X. Y. (2021). GABAA receptor agonist muscimol rescues inhibitory microcircuit defects in the olfactory bulb and improves olfactory function in APP/PS1 transgenic mice. *Neurobiol. Aging* 108, 47–57. doi: 10.1016/j.neurobiolaging.2021.08.003

Huang, J., Zheng, Y., Gao, D., Hu, M., and Yuan, T. (2020). Effects of exercise on depression, anxiety, cognitive control, craving, physical fitness and quality of life in methamphetamine-dependent patients. *Front. Psychiatry* 10:999. doi: 10.3389/fpsyt.2019.00999

Jang, Y., Koo, J. H., Kwon, I., Kang, E. B., Um, H. S., Soya, H., et al. (2017). Neuroprotective effects of endurance exercise against neuroinflammation in MPTP-induced Parkinson's disease mice. *Brain Res.* 1655, 186–193. doi: 10.1016/j.brainres.2016.10.029

Kaupp, U. B. (2010). Olfactory signalling in vertebrates and insects: differences and commonalities. *Nat. Rev. Neurosci.* 11, 188–200. doi: 10.1038/nrn2789

Kavaliers, M., Ossenkopp, K. P., and Choleris, E. (2020). Pathogens, odors, and disgust in rodents. *Neurosci. Biobehav. Rev.* 119, 281–293. doi: 10.1016/j.neubiorev.2020.09.037

Koo, J. H., and Cho, J. Y. (2017). Treadmill exercise attenuates α-synuclein levels by promoting mitochondrial function and autophagy possibly via SIRT1 in the chronic MPTP/P-induced mouse model of Parkinson's disease. *Neurotox. Res.* 32, 473–486. doi: 10.1007/s12640-017-9770-5

Kulkarni, A. S., Del Mar Cortijo, M., Roberts, E. R., Suggs, T. L., Stover, H. B., Pena-Bravo, J. I., et al. (2020). Perturbation of in vivo neural activity following α-synuclein seeding in the olfactory bulb. *J. Parkinsons Dis.* 10, 1411–1427. doi: 10.3233/JPD-202241

Kuznetsov, I. A., and Kuznetsov, A. V. (2016). Mathematical models of α-synuclein transport in axons. *Comput. Methods Biomech. Biomed. Engin.* 19, 515–526. doi: 10.1080/10255842.2015.1043628

Lappin, J. M., and Darke, S. (2021). Methamphetamine and heightened risk for early-onset stroke and Parkinson's disease: a review. *Exp. Neurol.* 343:113793. doi: 10.1016/j.expneurol.2021.113793

Lappin, J. M., Darke, S., and Farrell, M. (2018). Methamphetamine use and future risk for Parkinson's disease: evidence and clinical implications. *Drug Alcohol Depend.* 187, 134–140. doi: 10.1016/j.drugalcdep.2018.02.032

Li, W., Hoffman, P. N., Stirling, W., Price, D. L., and Lee, M. K. (2004). Axonal transport of human alpha-synuclein slows with aging but is not affected by familial Parkinson's disease-linked mutations. *J. Neurochem.* 88, 401–410. doi: 10.1046/j.1471-4159.2003.02166.x

Liu, J., Chen, C., Liu, M., and Zhuang, S. (2021). Effects of aerobic exercise on cognitive function in women with methamphetamine dependence in a detoxification program in Tianjin, China: a randomized controlled trial. *J. Nurs. Res.* 29:e164. doi: 10.1097/JNR.0000000000000440

Liu, W., Fu, R., Wang, Z., Liu, S., Tang, C., Li, L., et al. (2020). Regular aerobic exercise-alleviated dysregulation of CAMKIIα carbonylation to mitigate parkinsonism via homeostasis of apoptosis with autophagy. *J. Neuropathol. Exp. Neurol.* 79, 46–61. doi: 10.1093/jnen/nlz106

Mahoney, J. J. III, Hawkins, R. Y., De La Garza, R. II, Kalechstein, A. D., and Newton, T. F. (2010). Relationship between gender and psychotic symptoms in cocaine-dependent and methamphetamine-dependent participants. *Gend. Med.* 7, 414–421. doi: 10.1016/j.genm.2010.09.003

Manzanares, G., Brito-da-Silva, G., and Gandra, P. G. (2018). Voluntary wheel running: patterns and physiological effects in mice. *Braz. J. Med. Biol. Res.* 52:e7830. doi: 10.1590/1414-431X20187830

Mauceli, G., Busceti, C. I., Pellegrini, A., Soldani, P., Lenzi, P., Paparelli, A., et al. (2006). Overexpression of alpha-synuclein following methamphetamine: is it good or bad? *Ann. N. Y. Acad. Sci.* 1074, 191–197. doi: 10.1196/annals.1369.019

McKetin, R., Baker, A. L., Dawe, S., Voce, A., and Lubman, D. I. (2017). Differences in the symptom profile of methamphetamine-related psychosis and primary psychotic disorders. *Psychiatry Res.* 251, 349–354. doi: 10.1016/j.psychres.2017.02.028

Mizoguchi, H., and Yamada, K. (2019). Methamphetamine use causes cognitive impairment and altered decision-making. *Neurochem. Int.* 124, 106–113. doi: 10.1016/j.neuint.2018.12.019

Mori, K., and Sakano, H. (2021). Olfactory circuitry and behavioral decisions. *Annu. Rev. Physiol.* 83, 231–256. doi: 10.1146/annurev-physiol-031820-092824

Nai, Q., Dong, H. W., Hayar, A., Linster, C., and Ennis, M. (2009). Noradrenergic regulation of GABAergic inhibition of main olfactory bulb mitral cells varies as a function of concentration and receptor subtype. *J. Neurophysiol.* 101, 2472–2484. doi: 10.1152/jn.91187.2008

Niu, H., Shen, L., Li, T., Ren, C., Ding, S., Wang, L., et al. (2018). Alpha-synuclein overexpression in the olfactory bulb initiates prodromal symptoms and pathology of Parkinson's disease. *Transl. Neurodegener.* 7:25. doi: 10.1186/s40035-018-0128-6

Nunez-Parra, A., Li, A., and Restrepo, D. (2014). Coding odor identity and odor value in awake rodents. *Prog. Brain Res.* 208, 205–222. doi: 10.1016/B978-0-444-63350-7.00008-5

O'Dell, S. J., Feinberg, L. M., and Marshall, J. F. (2011). A neurotoxic regimen of methamphetamine impairs novelty recognition as measured by a social odor-based task. *Behav. Brain Res.* 216, 396–401. doi: 10.1016/j.bbr.2010.08.022

Petit, G. H., Berkovich, E., Hickery, M., Kallunki, P., Fog, K., Fitzer-Attas, C., et al. (2013). Rasagiline ameliorates olfactory deficits in an alpha-synuclein mouse model of Parkinson's disease. *PLoS One* 8:e60691. doi: 10.1371/journal.pone.0060691

Pinto, J. M. (2011). Olfaction. *Proc. Am. Thorac. Soc.* 8, 46–52. doi: 10.1513/pats.201005-035RN

Podskarbi-Fayette, R., Rydzewski, B., and Lipińska, M. (2005). [Smell and taste in drug addicts]. *Otolaryngol. Pol.* 59, 585–590.

Ramkissoon, A., and Wells, P. G. (2015). Methamphetamine oxidative stress, neurotoxicity, and functional deficits are modulated by nuclear factor-E2-related factor 2. *Free Radic. Biol. Med.* 89, 358–368. doi: 10.1016/j.freeradbiomed.2015.07.157

Rey, N. L., Petit, G. H., Bousset, L., Melki, R., and Brundin, P. (2013). Transfer of human α-synuclein from the olfactory bulb to interconnected brain regions in mice. *Acta Neuropathol.* 126, 555–573. doi: 10.1007/s00401-013-1160-3

Rey, N. L., Steiner, J. A., Maroof, N., Luk, K. C., Madaj, Z., Trojanowski, J. Q., et al. (2016). Widespread transneuronal propagation of α-synucleinopathy triggered

in olfactory bulb mimics prodromal Parkinson's disease. *J. Exp. Med.* 213, 1759–1778. doi: 10.1084/jem.20160368

Schoppa, N. E. (2006). Synchronization of olfactory bulb mitral cells by precisely timed inhibitory inputs. *Neuron* 49, 271–283. doi: 10.1016/j.neuron.2005.11.038

Srinivasan, E., Chandrasekhar, G., Chandrasekar, P., Anbarasu, K., Vickram, A. S., Karunakaran, R., et al. (2021). Alpha-synuclein aggregation in Parkinson's disease. *Front. Med. (Lausanne)* 8:736978. doi: 10.3389/fmed.2021.736978

Stowers, L., Cameron, P., and Keller, J. A. (2013). Ominous odors: olfactory control of instinctive fear and aggression in mice. *Curr. Opin. Neurobiol.* 23, 339–345. doi: 10.1016/j.conb.2013.01.007

Sulzer, D., and Edwards, R. H. (2019). The physiological role of α-synuclein and its relationship to Parkinson's disease. *J. Neurochem.* 150, 475–486. doi: 10.1111/jnc.14810

Tian, Y., Dong, J., and Shi, D. (2020). Protection of DAergic neurons mediates treadmill running attenuated olfactory deficits and olfactory neurogenesis promotion in depression model. *Biochem. Biophys. Res. Commun.* 521, 725–731. doi: 10.1016/j.bbrc.2019.10.158

Waldmann, S., Lübke, K. T., Pentzek, M., and Pause, B. M. (2020). [Olfactory dysfunctions: references to neuropsychiatric disorders and diagnostics]. *Fortschr. Neurol. Psychiatr.* 88, 184–193. German doi: 10.1055/a-1003-6798

Wang, Z., Li, C., Ding, J., Li, Y., Zhou, Z., Huang, Y., et al. (2021a). Basolateral amygdala serotonin 2C receptor regulates emotional disorder-related symptoms induced by chronic methamphetamine administration. *Front. Pharmacol.* 12:627307. doi: 10.3389/fphar.2021.627307

Wang, Z., Li, J., Wu, W., Qi, T., Huang, Z., Chen, J., et al. (2021b). Saikosaponin D rescues deficits in sexual behavior and ameliorates neurological dysfunction in mice exposed to chronic mild stress. *Front. Pharmacol.* 12:625074. doi: 10.3389/fphar.2021.625074

Wang, Z., Zeng, Y. N., Yang, P., Jin, L. Q., Xiong, W. C., Zhu, X. H., et al. (2019). Axonal iron transport in the brain modulates anxiety-related behaviors. *Nat. Chem. Biol.* 15, 1214–1222. doi: 10.1038/s41589-019-0371-x

Wu, M., Su, H., and Zhao, M. (2021). The role of α-synuclein in methamphetamine-induced neurotoxicity. *Neurotox. Res.* 39, 1007–1021. doi: 10.1007/s12640-021-00332-2

Wu, Q., Yang, X., Zhang, Y., Zhang, L., and Feng, L. (2016). Chronic mild stress accelerates the progression of Parkinson's disease in A53T α-synuclein transgenic mice. *Exp. Neurol.* 285(Pt. A), 61–71. doi: 10.1016/j.expneurol.2016.09.004

Zhang, K., Zhang, Q., Jiang, H., Du, J., Zhou, C., Yu, S., et al. (2018). Impact of aerobic exercise on cognitive impairment and oxidative stress markers in methamphetamine-dependent patients. *Psychiatry Res.* 266, 328–333. doi: 10.1016/j.psychres.2018.03.032

Zhang, S., Xiao, Q., and Le, W. (2015). Olfactory dysfunction and neurotransmitter disturbance in olfactory bulb of transgenic mice expressing human A53T mutant α-synuclein. *PLoS One* 10:e0119928. doi: 10.1371/journal.pone.0119928

Zhu, L. N., Qiao, H. H., Chen, L., Sun, L. P., Hui, J. L., Qiu, P. M., et al. (2018). SUMOylation of alpha-synuclein influences on alpha-synuclein aggregation induced by methamphetamine. *Front. Cell. Neurosci.* 12:262. doi: 10.3389/fncel.2018.00262

Zhu, R., Yang, T., Kobeissy, F., Mouhieddine, T. H., Raad, M., Nokkari, A., et al. (2016). The effect of chronic methamphetamine exposure on the hippocampal and olfactory bulb neuroproteomes of rats. *PLoS One* 11:e0151034. doi: 10.1371/journal.pone.0151034

Conflict of Interest: The authors declare that the research was conducted in the absence of any commercial or financial relationships that could be construed as a potential conflict of interest.

Publisher's Note: All claims expressed in this article are solely those of the authors and do not necessarily represent those of their affiliated organizations, or those of the publisher, the editors and the reviewers. Any product that may be evaluated in this article, or claim that may be made by its manufacturer, is not guaranteed or endorsed by the publisher.

frontiers | Frontiers in Molecular Neuroscience

ORIGINAL RESEARCH
published: 09 June 2022
doi: 10.3389/fnmol.2022.908948

Genetic Variability of Incretin Receptors and Alcohol Dependence: A Pilot Study

Evangelia Eirini Tsermpini[1], Katja Goričar[1], Blanka Kores Plesničar[2,3], Anja Plemenitaš Ilješ[4] and Vita Dolžan[1]**

[1] Pharmacogenetics Laboratory, Institute of Biochemistry and Molecular Genetics, Faculty of Medicine, University of Ljubljana, Ljubljana, Slovenia, [2] University Psychiatric Clinic, Ljubljana, Slovenia, [3] Faculty of Medicine, University of Ljubljana, Ljubljana, Slovenia, [4] Department of Psychiatry, University Clinical Centre Maribor, Maribor, Slovenia

Alcohol dependence is a chronic mental disorder that leads to decreased quality of life for patients and their relatives and presents a considerable burden to society. Incretin hormones, such as glucose-dependent insulinotropic polypeptide (GIP) and glucagon-like peptide 1 (GLP-1) are endogenous gut-brain peptides, which can travel across the blood-brain barrier and access the nervous system. Their respective receptors, GIPR and GLP-1R, are expressed in the reward-related brain areas and are involved in memory formation and neurogenesis, which results in behavioral changes in rodent models. The current study investigated the potential association of genetic variability of incretin receptors with alcohol dependence and alcohol-related psychosymptomatology. Alcohol dependence and comorbid psychosymptomatology were assessed in a cohort of Slovenian male participants, comprised of 89 hospitalized alcohol-dependent patients, 98 abstinent alcohol-dependent patients, and 93 healthy blood donors. All participants were genotyped for *GIPR* rs1800437 and *GLP1R* rs10305420 and rs6923761 polymorphisms. For the statistical analysis Kruskal–Wall and Mann–Whitney tests were used in additive and dominant genetic models. Our findings indicated that *GIPR* rs1800437 genotypes were associated with an increased risk of alcohol dependence. Statistically significant association between *GIPR* rs1800437 GG genotype and Brief Social Phobia Scale scores were observed in the abstinent alcohol-dependent patients, while *GLP1R* rs6923761 GG genotype was associated with Zung anxiety scores in healthy controls. Our pilot study indicates that *GIPR* rs1800437 may play some role in susceptibility to alcohol dependence, as well as in alcohol-related psychosymptomatology symptoms. To our knowledge, this is the first study that indicates the involvement of *GIPR* in alcohol dependence. However, studies with larger cohorts are needed to confirm these preliminary findings.

Keywords: alcohol dependence, alcohol-related psychosymptomatology, incretin receptors, GIPR, GLP-1R, polymorphism

OPEN ACCESS

Edited by:
Qian Ren,
Hebei Medical University, China

Reviewed by:
Laerke Smidt Gasbjerg,
University of Copenhagen, Denmark
Qiumin Le,
Fudan University, China

***Correspondence:**
Anja Plemenitaš Ilješ
anjaplemi@gmail.com
Vita Dolžan
vita.dolzan@mf.uni-lj.si

Specialty section:
This article was submitted to Molecular Signalling and Pathways, a section of the journal Frontiers in Molecular Neuroscience

Received: *31 March 2022*
Accepted: *09 May 2022*
Published: *09 June 2022*

Citation:
Tsermpini EE, Goričar K, Kores Plesničar B, Plemenitaš Ilješ A and Dolžan V (2022) Genetic Variability of Incretin Receptors and Alcohol Dependence: A Pilot Study. Front. Mol. Neurosci. 15:908948. doi: 10.3389/fnmol.2022.908948

INTRODUCTION

Alcohol dependence is a chronic mental disorder characterized by an intense craving for alcohol and the inability to control or stop alcohol consumption, usually accompanied by a history of excessive drinking (Carvalho et al., 2019; Domi et al., 2021). Regarding its epidemiology, alcohol dependence is one of the most prevalent mental disorders worldwide, and it is five times more

frequent in men than in women. In addition, alcohol dependence was found to be more frequent in high-income and upper - middle- income countries for both males and females (Carvalho et al., 2019). Alcohol dependence is also associated with high morbidity and mortality rates. Alcohol dependence is also related to other comorbid mental disorders, such as major depressive disorder, anxiety disorders, schizophrenia, bipolar disorder, and attention deficit hyperactivity disorder (Gandal et al., 2018; Kranzler and Soyka, 2018; Walters et al., 2018; Rudenstine et al., 2020; Zhou et al., 2020).

Alcohol dependence leads to decreased quality of life for patients and their relatives and presents a considerable burden to society (Carvalho et al., 2019; Klausen et al., 2022). Alcohol dependence and alcohol abuse used to be separate disorders in the Diagnostic and Statistical Manual of mental disorders (DSM-IV), whereas, in DSM-V, they are integrated into one broader category of alcohol use disorder (AUD) which includes sub-classifications, depending on the severity of the symptoms (Kathryn Mchugh and Weiss, 2019; Nutt et al., 2021). The stages of dependence can be divided into the acute and chronic state, followed by short-term and long-term abstinence. What sets them apart is the duration of each stage and the underlying molecular and cellular mechanisms involved (Nestler and Aghajanian, 1997; Koob and Volkow, 2016).

The emergence and perpetuation of AUD can be due to several factors, including genetic, environmental risk factors, and gene-environment interactions (Nestler and Aghajanian, 1997; Carvalho et al., 2019). Family, twin, and adoption studies (Cloninger et al., 1981; Heath et al., 1997; Verhulst et al., 2015) and a recent meta-analysis (Verhulst et al., 2015) indicated that heritability estimates are pretty high. Preclinical and clinical studies have shown that genetic variability is associated with susceptibility and development of AUD (Hiroi and Agatsuma, 2005; Jones et al., 2015; Bowen et al., 2022). A genome-wide meta-analysis on AUD and problematic alcohol use, which included 435,563 subjects of European ancestry, identified 29 independent risk variants, 19 of which were novel (Zhou et al., 2020).

Glucagon-like peptide 1 (GLP-1) and glucose-dependent insulinotropic polypeptide, also known as gastric inhibitory polypeptide (GIP), are endogenous gut-brain peptides that function both as a hormone and neuropeptide and are released from intestinal L-cells and K-cells, respectively, in response to food intake in humans and mice (Adner and Nygren, 1992; Dalgaard et al., 2004; Alvarez et al., 2005; Pannacciulli et al., 2007; Seino et al., 2010; Seino and Yabe, 2013; Abraham et al., 2015; Jerlhag, 2020; Marty et al., 2020; Eren-Yazicioglu et al., 2021). They stimulate glucose-induced insulin secretion, inhibit glucagon secretion, and decrease appetite in humans and mice (Adner and Nygren, 1992; Dalgaard et al., 2004; Seino et al., 2010; Underwood et al., 2010; Seino and Yabe, 2013; Abraham et al., 2015; Klausen et al., 2022). They have the ability to travel across the blood-brain barrier and access the nervous system in humans and rats (Isbil-Buyukcoskun et al., 2009; Eren-Yazicioglu et al., 2021). GLP-1 and GIP act by binding with their receptors GLP-1R and GIPR, respectively, which are members of the G-protein coupled receptors and are expressed in the peripheral and central nervous system (Seino et al., 2010; Seino and Yabe, 2013). GLP-1 and GIP and their receptors are involved in memory formation and neurogenesis in rats (Seino et al., 2010). GIPR is expressed in neurons, and GLP-1R can be found in several tissues, including human, rat and mice brain regions related to reward and addiction (Merchenthaler et al., 1999; Alvarez et al., 2005; Pannacciulli et al., 2007; Rinaman, 2010; Seino et al., 2010; Suchankova et al., 2015; Jensen et al., 2018; Eser et al., 2020; Eren-Yazicioglu et al., 2021). It can also modulate dopamine levels and glutamatergic neurotransmission, which results in behavioral changes in rats, and mice (Alhadeff et al., 2012; Reddy et al., 2016; Eren-Yazicioglu et al., 2021). Also, it displayed neuroprotective effects in male rats, mice, non-human primates (Klausen et al., 2022) and humans (Erbil et al., 2019). Furthermore, both preclinical and clinical studies indicated the crucial role of GLP-1R in reward function and addictive disorders, including alcohol-seeking and AUD (Egecioglu et al., 2013; Suchankova et al., 2015; Jayaram-Lindström et al., 2016; Marty et al., 2020; Eren-Yazicioglu et al., 2021). Animal model studies have suggested that peptides like GLP-1 regulate behavioral responses to alcohol consumption (Seino et al., 2010; Jerlhag, 2020), however, the role of GIP and its receptor has not been studied so well and the exact mechanism of action is not yet fully known.

GLP-1R also seems to have a neuroprotective role and, thus, has been investigated as a target in the cerebral infarction treatment (Seino and Yabe, 2013). There is also evidence that GLP-1R stimulation regulates alcohol-seeking and wanting behaviors (Suchankova et al., 2015; Eren-Yazicioglu et al., 2021). Nevertheless, based on the mechanism of action of FDA-approved GLP-1 receptor agonists, reduction in alcohol consumption can be due to the discomfort felt during alcohol use and abstinence and reduction in rewarding effects. GLP-1R agonists reduce the rewarding effects of alcohol, which leads to decreased alcohol intake. Exentin-4 is a well know example of GLP-1R agonist that affects the signal transmission, and according to studies, GLP-1R and GIPR have similar molecular mechanisms (Seino et al., 2010).

Genetic variability of GLP-1R and GIPR has been investigated in human pathologies, such as metabolic and cardiovascular diseases, and bone mineral density. According to the literature, genetic variability influences response to incretin peptides and their antagonists (Jensterle et al., 2015; Klen and Dolžan, 2022). More specifically, *GLP1R* rs10305420 has been associated with response to exenatide in overweight patients with type 2 diabetes (Yu et al., 2019) and liraglutide in obese women with polycystic ovary syndrome (Jensterle et al., 2015). Regarding *GLP1R* rs6923761, it has been shown to relate with metabolic and obesity parameters, such as body mass index, weight, fat mass, waist circumference, triglycerides, insulin, HOMA-IR, and HDL cholesterol (de Luis et al., 2013, 2014a,b,c,e, 2015b,d, 2018), weight loss (de Luis et al., 2014a,d), cardiovascular risk in patients with obesity (de Luis et al., 2018), type 2 diabetes (de Luis et al., 2015a). It has also been associated with gliptin therapies, like the DPP-4 inhibitor sitagliptin and vildagliptin (Javorský et al., 2016; Urgeová et al., 2020; Mashayekhi et al., 2021), liraglutide and exenatide (de Luis et al., 2015c; Chedid et al., 2018). *GIPR* rs1800437 has been associated with glucose homeostasis (Sauber et al., 2010), obesity (Vogel et al., 2009), heart failure prognosis

in obese patients (Agra et al., 2019), bone mineral density and fracture risk (Torekov et al., 2014).

Glucagon-like peptide 1 variability has been investigated in two preclinical studies with mice AUD models, one of which also included a cohort of AUD patients and controls (Koole et al., 2011; Suchankova et al., 2015). However, to our knowledge, there are no studies that focus on *GIPR* polymorphisms and alcohol.

The current study aimed to investigate the potential association of *GLP1R* rs10305420 and rs6923761 and *GIPR* rs1800437 with alcohol dependence, as well as alcohol-related comorbid psychosymptomatology.

MATERIALS AND METHODS

Study Population

The study cohort included three groups of participants: hospitalized alcohol-dependent patients, abstinent alcohol-dependent patients, and healthy controls with no alcohol dependence history. All participants were male of Slovenian origin, aged 18 to 66. Experienced psychiatrists recruited patients hospitalized for treatment of alcohol dependence at the University Clinical Center Maribor and the University Psychiatric Clinic Ljubljana. The inclusion criteria for the hospitalized alcohol-dependent patients were a diagnosis of alcohol-dependence, according to the DSM-IV (American Psychiatric Association, 2000), with no significant symptoms of abstinence, after hospitalization for at least 2 weeks. The abstinent alcohol-dependent patients were recruited from support group meetings, and the inclusion criterion was abstinence for at least 2 years. Exclusion criteria for these two groups of patients were: a medical history of mental or neurological disorders or significant medical conditions and a previous diagnosis of dependence (nicotine not included) according to DSM-IV. The healthy controls were blood donors with no DSM-IV axis I mental disorders or alcohol consumption problems. The study was approved by the Slovenian National Medical Ethics committee (approval No. 117/06/10 and 148/02/1011).

Written informed consent was obtained from all the participants after they were informed about the scope of the study. At the baseline, all the demographic and clinical data of each patient were also recorded. Demographic variables included age, residence, marital status, academic years, and smoking status. In addition, questionnaires that evaluate comorbid psychosymptomatology were employed in all groups of participants. More specifically, depression and anxiety symptoms were accessed using the Zung Depression (Zung, 1965) and Anxiety (Zung, 1971) scale, social anxiety symptoms, using the Brief Social Phobia Scale (BSPS) (Davidson et al., 1997), drinking habits, and severity of alcohol use and dependence using the Alcohol Use Disorders Identification Test (AUDIT) (Rush et al., 2008), obsessive-compulsive traits, using the Yale-Brown Obsessive-Compulsive Scale (YBOCS) (Goodman and Price, 1992) and Obsessive-Compulsive Drinking Scale (OCDS) (Anton, 2000), and symptoms of aggression and hostility, were evaluated using the and the Buss-Durkee Hostility Inventory (BDHI) (Buss and Durkee, 1957). More information about the cohorts can be found in our previous articles (Plemenitas et al., 2015; Ilješ et al., 2021).

Molecular Genetic Analysis

DNA was extracted from whole blood for hospitalized alcohol-dependent patients and healthy controls, whereas DNA was extracted from buccal swabs for the abstinent alcohol-dependent group of patients. QIAamp Blood Mini kit was used for the DNA extraction from whole blood, collected using ethylenediaminetetraacetic acid (EDTA) and QIAamp Mini kit for the DNA extraction from buccal swabs, according to the manufacturer's protocols (Qiagen GmbH, Hilden, Germany).

Genotyping was performed using fluorescence-based competitive allele-specific PCR (KASP) amplification combining KASP Master mix and custom validated KASP Genotyping Assays with a KASP reporting system, according to the manufacturer's instructions (LGC Genomics, United Kingdom). Thermal cycling conditions are presented in **Supplementary Table 1**.

Statistical Analysis

The statistical analyses were performed with IBM SPSS Statistics, version 27.0 (IBM Corporation, Armonk, NY, United States). The cut-off for the statistical significance was set at 0.05. Pearson's chi-square test was used to assess deviation from Hardy–Weinberg equilibrium (HWE) in healthy individuals for all studied polymorphisms. Additive and dominant genetic models were used in the analysis. To compare clinical characteristics between patient groups, we used Fisher's exact test for categorical variables and the Kruskal–Wallis test with 2 degrees of freedom for continuous variables. Fisher's exact test was also used to compare the frequencies of the rs10305420, rs6923761, and rs1800437 between the three studied groups. In logistic regression, odds ratios (ORs) and 95% confidence intervals (CIs) were determined. Age, residence place, marital status, academic years, and smoking status were considered as covariates and significant variables were used for adjustment in regression analysis. The association of genotypes with psychosymptomatology scores was evaluated using the Kruskal–Wallis and Mann–Whitney non-parametric tests for additive and dominant genetic models, respectively.

RESULTS

Our cohort comprised of 89 hospitalized alcohol-dependent patients, 98 abstinent alcohol-dependent patients, and 93 healthy controls with no alcohol dependence history (**Table 1**). Regarding the demographic characteristics, the median age of the hospitalized alcohol-dependent and abstinent alcohol-dependent patients was significantly higher compared to healthy controls ($p < 0.001$). The distribution of the years of education also differed among groups ($p < 0.001$), but there were no differences in residence place ($p = 0.265$). However, the majority of healthy controls and abstinent alcohol-dependent patients were smokers ($p < 0.001$) and had a partner ($p = 0.005$) in comparison with hospitalized alcohol-dependent patients (**Table 1**).

TABLE 1 | Cohort's characteristics.

Characteristic		Healthy controls (*N* = 93)	Abstinent alcohol-dependent (*N* = 98)	Hospitalized alcohol-dependent (*N* = 89)	*P**
Age	Years, median (25–75%)	36 (26–44.5)	49 (44–54.3)	47 (39–54)	<0.001
Education	Years, median (25–75%)	12 (12–12)	12 (11–12)	12 (11–12)	<0.001
Partnership	Single, *N* (%)	25 (26.9)	21 (21.4)	38 (42.7)	0.005
	Partnership, *N* (%)	68 (73.1)	77 (78.6)	51 (57.3)	
Environment	Rural, *N* (%)	37 (39.8)	46 (46.9)	46 (51.7)	0.265
	Urban, *N* (%)	56 (60.2)	52 (53.1)	43 (48.3)	
Smoking	No, *N* (%)	24 (25.8)	48 (49.0)	58 (65.2)	<0.001
	Yes, *N* (%)	69 (74.2)	50 (51.0)	31 (34.8)	

**Calculated using Fisher's exact test for categorical variables and Kruskal–Wallis test for continuous variables.*

TABLE 2 | Questionnaire scores.

Questionnaire		Healthy controls (*N* = 93)	Abstinent alcohol-dependent (*N* = 98)	Hospitalized alcohol-dependent (*N* = 89)	*P**
YBOCS obsession	Points, median (25–75%)	1 (1–1)	1 (1–1.3)	2 (1–7)	<0.001
YBOCS compulsion	Points, median (25–75%)	1 (1–1)	1 (1–1)	1 (1–3)	<0.001
BSPS	Points, median (25–75%)	9 (5.5–14)	10 (5–18.3)	10 (4–18.5)	0.623
AUDIT	Points, median (25–75%)	5 (4–7)	3 (3–5)	23 (19–28.5)	<0.001
OCDS	Points, median (25–75%)	3 (2–4)	2 (2–3)	18 (9–26.5)	<0.001
Zung depression	Points, median (25–75%)	22 (20–24)	29 (25–35)	34 (27–45)	<0.001
Zung anxiety	Points, median (25–75%)	22 (20–24)	28 (25–35)	34 (29–39)	<0.001
BDHI	Points, median (25–75%)	17 (10.5–23)	24 (15.8–31)	30 (22–40)	<0.001

**Calculated using Kruskal–Wallis test.*

TABLE 3 | Comparison of genotype frequencies between all alcohol-dependent patients and healthy controls.

Gene	SNP	Genotype	OR (95% CI)	*P*	OR (95% CI) adj	Padj
GIPR	rs1800437	GG	Reference		Reference	
		GC	1.77 (1.02–3.09)	**0.043**	1.71 (0.85–3.44)	0.135
		CC	1.41 (0.55–3.62)	0.477	1.79 (0.59–5.46)	0.303
		GC + CC	1.69 (1.01–2.84)	**0.045**	1.73 (0.90–3.31)	0.100
GLP1R	rs10305420	CC	Reference		Reference	
		CT	1.07 (0.63–1.82)	0.809	1.24 (0.62–2.47)	0.548
		TT	1.44 (0.64–3.23)	0.374	1.26 (0.46–3.47)	0.653
		CT + TT	1.15 (0.70–1.89)	0.583	1.24 (0.66–2.35)	0.505
GLP1R	rs6923761	GG	Reference		Reference	
		GA	0.96 (0.57–1.61)	0.866	1.13 (0.58–2.21)	0.721
		AA	0.65 (0.24–1.73)	0.389	0.38 (0.11–1.31)	0.124
		GA + AA	0.91 (0.55–1.49)	0.702	0.96 (0.51–1.82)	0.910

Adj: adjusted for age, education, smoking, and partnership. Statistically significant p values are printed in bold.

Regarding the questionnaires, differences were observed between the three groups in the scores of Zung Depression and Anxiety scale, YBOCS obsession and compulsion scale, AUDIT, OCDS, and BDHI questionnaires (all $p < 0.05$), but not for BSPS ($p = 0.623$) (**Table 2** and **Supplementary Table 2**).

The genotype distributions for all the studied polymorphisms were in HWE for the healthy controls (GG: 65.6%, GC: 26.9%, CC: 7.5%; $p = 0.068$ for rs1800437, CC: 51.1%, CT: 37.8%, TT: 11.1%; $p = 0.340$ for rs10305420 and GG: 46.2%, GA: 45.2%, AA: 8.6%; $p = 0.614$ for rs6923761).

When comparing all three groups, no differences in the distribution of genotype frequencies were observed for any of the studied polymorphisms ($p = 0.155$ for rs1800437; $p = 0.645$ for rs10305420 and $p = 0.632$ for rs6923761) (**Supplementary Table 3**).

Given that both the groups of hospitalized and abstinent patients had the diagnosis of alcohol dependence, we merged these two groups into one and we compared the genotype frequencies with those of the healthy controls, an association was observed for *GIPR* rs1800437 GC (OR = 1.77, 95% CI = 1.02–3.09, $p = 0.043$) and GC + CC genotypes (OR = 1.69, 95% CI = 1.01–2.84, $p = 0.045$), but it did not remain statistically significant after adjustment for age, education, smoking, and partnership. No associations were observed for *GLP1R* polymorphisms (**Table 3**).

We also compared each group of alcohol-dependent patients with the controls separately. When comparing genotype frequencies between abstinent alcohol-dependent patients and healthy controls, no statistically significant difference was observed for any of the three studied polymorphisms, neither before nor after adjustments for age, education and smoking (**Supplementary Table 4**).

However, *GIPR* rs1800437 GC + CC and GC genotypes were significantly more frequent in hospitalized alcohol-dependent patients than in healthy controls (OR = 2.13, 95% CI = 1.17–3.87, $p = 0.013$ and OR = 2.21, 95% CI = 1.16–4.19, $p = 0.015$, respectively). The association remained statistically significant for GC + CC genotypes in the dominant model after adjustment for age, education, smoking, residence, and partnership (OR = 2.42, 95% CI = 1.07–5.48, $p = 0.035$). No significant differences in *GLP1R* genotype frequencies' distribution were observed between these two groups (**Table 4**).

Regarding the potential relation between the studied polymorphisms and psychosymptomatology scores, we observed a statistically significant association between *GIPR* rs1800437 CC genotype and lower BSPS scores in the abstinent alcohol-dependent patients ($p = 0.033$) (**Figure 1A**). *GIPR* genotypes were not associated with any of the other psychosymptomatology scores (**Table 5**).

No statistically significant associations were observed between *GLP1R* rs10305420 and the assessed psychosymptomatology scores in any of the study groups (data not shown). However, *GLP1R* rs6923761 AA genotype was associated with lower Zung anxiety scores among healthy controls ($p = 0.021$) (**Figure 1B** and **Supplementary Table 5**).

DISCUSSION

We conducted a pilot study to investigate the role of *GLP1R* rs10305420 and rs6923761 and *GIPR* rs1800437 in alcohol dependence and related psychosymptomatology in a cohort of hospitalized alcohol-dependent patients, abstinent alcohol-dependent patients, and healthy individuals. To our knowledge, this is the first study that focuses on the role of *GIPR* on alcohol dependence and one of a few that investigated the relation of *GLP1R* with alcohol dependence in humans (Koole et al., 2011; Suchankova et al., 2015).

According to our results, *GIPR* rs1800437 genotypes were associated with an increased risk of alcohol dependence. No statistically significant associations were found for *GLP1R* rs10305420 and rs6923761 with alcohol dependence. We also observed statistically significant association between *GIPR* rs1800437 GG genotype and BSPS scores in the abstinent alcohol-dependent patients as well as the association between *GLP1R* rs6923761 GG genotype and Zung anxiety scores in healthy controls.

It is crucial to mention that this is the first study that indicates the involvement of GIPR in alcohol dependence and alcohol-related comorbid psychosymptomatology. The potential participation of GIP and its receptor in the etiology and pathophysiology of alcohol is limited. We know that GIPR is expressed in the adult rat hippocampus, a brain region related to memory (Nyberg et al., 2005). An animal model study has shown that mice with GIPR deficiency have synaptic plasticity deterioration, impaired neurogenesis, and learning disabilities (Faivre et al., 2011). Interestingly, GIP regulates progenitor cell proliferation (Nyberg et al., 2005) and neurotransmitter release and has a protective role on the synapses during synaptic plasticity (Gault and Hölscher, 2008). Alcohol use impacts the activity of the synapses, i.e., the points of contact between neurons, which affects the transmission of the information from one neuron to the next (Nestler and Aghajanian, 1997). Further studies are therefore needed to elucidate the role of GIPR genetic variability in AUD.

TABLE 4 | Comparison of genotype frequencies between hospitalized alcohol-dependent patients and healthy controls.

Gene	SNP	Genotype	OR (95% CI)	*P*	OR (95% CI) adj	Padj
GIPR	rs1800437	GG	Reference		Reference	
		GC	2.21 (1.16–4.19)	**0.015**	2.15 (0.90–5.15)	0.087
		CC	1.87 (0.65–5.41)	0.250	3.69 (0.93–14.70)	0.064
		GC + CC	2.13 (1.17–3.87)	**0.013**	2.42 (1.07–5.48)	**0.035**
GLP1R	rs10305420	CC	Reference		Reference	
		CT	1.08 (0.57–2.03)	0.818	1.20 (0.50–2.88)	0.680
		TT	1.88 (0.77–4.60)	0.167	1.50 (0.43–5.20)	0.524
		CT + TT	1.25 (0.70–2.24)	0.450	1.27 (0.57–2.85)	0.556
GLP1R	rs6923761	GG	Reference		Reference	
		GA	0.93 (0.51–1.70)	0.820	0.66 (0.29–1.55)	0.343
		AA	0.36 (0.09–1.44)	0.148	0.23 (0.04–1.41)	0.112
		GA + AA	0.84 (0.47–1.51)	0.560	0.58 (0.26–1.30)	0.186

Adj: adjusted for age, education, smoking, residence, and partnership. Statistically significant p values are printed in bold.

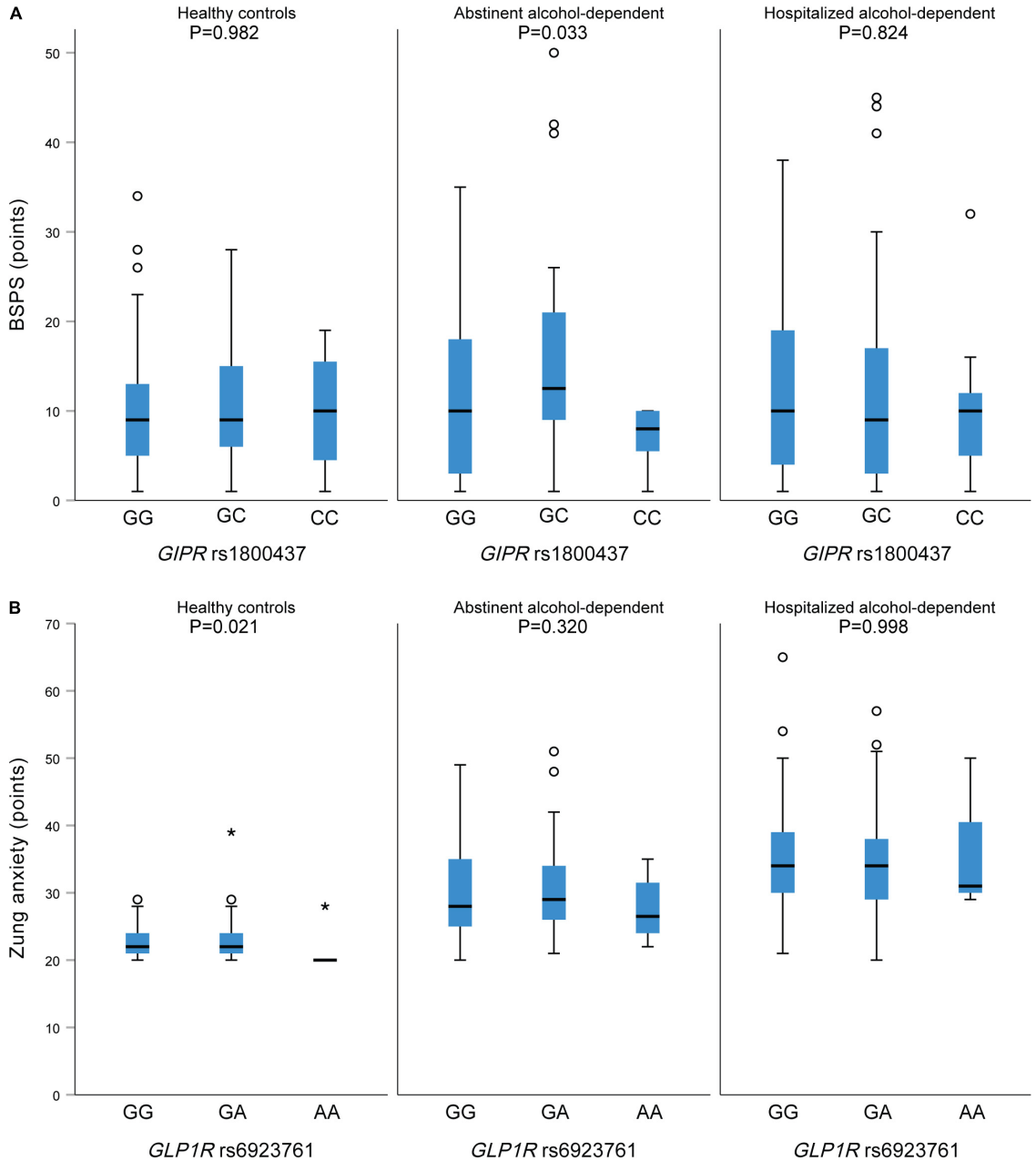

FIGURE 1 | (A) Association between GIPR rs1800437 and BSPS score in healthy controls (left), abstinent (middle) and hospitalized alcohol-dependent (right) patients. **(B)** Association between GLP1R rs6923761 and Zung anxiety score in healthy controls (left), abstinent (middle) and hospitalized alcohol-dependent (right) patients.

Regarding GLP-1, we observed an association between *GLP1R* rs6923761 GG genotype and Zung anxiety scores in healthy controls, but not between GLP1R rs10305420 and rs6923761 and alcohol dependence. Our results are in contrast with the findings of preclinical and clinical studies. An animal study indicated an interaction between alcohol use and the GLP-1 system, which might further elucidate the role of GLP-1R containing brain areas in reducing alcohol reinforcement through GLP-1R agonists and support the usage of GLP-1R as potential treatment targets for AUD. More specifically, the expression of the GLP-1 receptor in nucleus accumbens, which is the neural interface between motivation and action, was increased in high alcohol-consuming rodents compared to those under low alcohol consumption (Vallöf et al., 2019). In addition, Suchankova et al. (2015) investigated the impact of GLP-1R genetic variability on AUD in humans and a mouse model. Initially, they performed a case-control study that included 670 AUD patients and 238 controls with no current or

TABLE 5 | Associations between *GIPR* rs1800437 and the assessed psychosymptomatology scores.

Scale	*GIPR* rs1800437 genotype	Healthy controls (*N* = 93)		Abstinent alcohol-dependent (*N* = 98)		Hospitalized alcohol-dependent (*N* = 89)	
		Median (25–75%)	*P**	Median (25–75%)	*P**	Median (25–75%)	*P**
YBOCS obsession	GG	1 (1–1)	0.880	1 (1–2)	0.227	2 (1–7)	0.129
	GC	1 (1–1.5)		1 (1–1)		1 (1–8.3)	
	CC	1 (1–4)		1 (1–2)		1 (1–1.5)	
	GC + CC	1 (1–1.8)	0.991	1 (1–1)	0.118	1 (1–7)	0.228
YBOCS compulsion	GG	1 (1–1)	0.653	1 (1–1)	0.098	1 (1–6)	0.213
	GC	1 (1–1)		1 (1–1)		1 (1–2.3)	
	CC	1 (1–2)		1 (1–2)		1 (1–1)	
	GC + CC	1 (1–1)	0.677	1 (1–1)	0.315	1 (1–2)	0.356
BSPS	GG	9 (5–13.5)	0.982	10 (3–18)	**0.033**	10 (4–19)	0.824
	GC	9 (6–16)		12.5 (8.8–21.5)		9 (3–17.5)	
	CC	10 (3–18)		8 (3–10)		10 (3–14)	
	GC + CC	9 (6–16.5)	0.894	11 (8–20)	0.118	9 (3–17)	0.714
AUDIT	GG	5 (4–7)	0.194	3 (3–4)	0.999	23 (18.8–29.3)	0.208
	GC	4 (3–6)		3 (3–5)		23 (19.8–28)	
	CC	6 (5–8)		3 (3–5)		27 (22.5–32.5)	
	GC + CC	5 (3–6)	0.297	3 (3–5)	0.959	23 (20–28)	0.792
OCDS	GG	3 (2–4)	0.444	2 (2–3)	0.885	16 (9.8–26)	0.889
	GC	3 (2–4)		2 (2–3.3)		18 (8.8–29)	
	CC	4 (2–5)		2 (2–4)		19 (8–24.5)	
	GC + CC	3 (2–4)	0.535	2 (2–4)	0.792	18 (8–28)	0.736
Zung depression	GG	22 (20.5–24.5)	0.493	28 (24–34)	0.252	36 (25–49)	0.550
	GC	22 (20–22.5)		29.5 (27–35.3)		31.5 (27–40.5)	
	CC	21 (20–26)		32 (29–35)		35 (29–42)	
	GC + CC	22 (20–22.8)	0.251	31 (27–35)	0.106	32 (28–40)	0.300
Zung anxiety	GG	22 (20.5–25)	0.484	28 (25–32.5)	0.202	34.5 (29–42.5)	0.491
	GC	21 (20–23)		30 (26–37.3)		33.5 (29.8–37.3)	
	CC	21 (20–26)		30 (23–35)		32 (27–39.5)	
	GC + CC	21 (20–23)	0.238	30 (26–36.5)	0.078	33 (29–38)	0.319
BDHI	GG	17 (12–24.5)	0.483	24 (17–29)	0.420	33.5 (19.8–40)	0.080
	GC	13 (8–22.5)		25.5 (14.8–33)		33 (25.8–42.3)	
	CC	20 (11–22)		21 (14–25)		22 (15.5–29.5)	
	GC + CC	14.5 (8–22)	0.369	24 (14–31)	0.759	29 (24–42)	0.793

**Kruskal–Wall test for additive and Mann–Whitney test for the dominant model. Statistically significant p values are printed in bold.*

past alcohol abuse. Then, the emerged significant associations were examined on a genome-wide association cohort of 1,917 patients with alcohol dependence and 1,886 healthy individuals. For functional validation of the findings, they included 84 participants who underwent intravenous self-administration of alcohol. To evaluate brain activity changes, they performed functional magnetic resonance imaging (fMRI) in 22 patients with alcohol dependence. Finally, they investigated the impact of GLP-1R agonism on alcohol dependence in a mouse model. Overall, their results indicated that the rs6923761 A (Ser) allele was nominally associated with increased AUD. Also, rs6923761 heterozygotes had higher alcohol self-administration and higher Blood-oxygen-level-dependent imaging (BOLD) signal in the globus pallidus when participants received rewarding outcomes during the Monetary Incentive Delay task. Lastly, from the preclinical model emerged a significant reduction of alcohol use after pharmacological GLP-1R agonist (Suchankova et al., 2015). An earlier *in vitro* study has also shown that rs6923761 has a functional role, given that the A (Ser) allele is associated with reduced GLP-1R expression levels in the cell's surface (Koole et al., 2011). In our study, only potential association with psychosymptomatology was observed for rs6923761, while no differences in genotype frequencies were observed among different groups.

Regarding GLP-1 and its influences on reward processing through globus pallidus, ventral tegmental area and nucleus accumbens could explain detected association of *GIPR* rs1800437 and social anxiety scores, since neural activation in globus pallidus, among others, is associated with social phobia and anxiety disorders (Hattingh et al., 2013; Suchankova et al., 2015; Ashworth et al., 2021). Decreased connectivity between the nucleus accumbens and putamen was also reported in connection with social anxiety disorder. To the best of our knowledge, no human study explored the association of GLP-1

and GIP on the expression of anxiety symptoms. GLP-1 receptor gene polymorphism rs1042044 was associated with anhedonia, a symptom of major depressive disorder (Eser et al., 2020). Another human study reported about abnormal gene expression of GLP-1R in post-mortem brain of individuals with mood disorder (Mansur et al., 2019). The gut-brain axis with gastrointestinally derived neuropeptides like GLP-1, are emerging as potential key regulators of anxiety behavior. A study performed on rats reported chemogenetic activation of neurons and anxiolytic response. Another animal studies on rats reported anxiogenic and antidepressant effects of GLP-1 receptor stimulation and anti-anxiety effect of liraglutide which is GLP-1 agonist (Sharma et al., 2015; Anderberg et al., 2016). So further studies on this are warranted to elucidate this issue.

Nevertheless, our study has some limitations, such as the small sample size, and the lack of data on metabolic parameters of the participants. Given that age and the proportion of smokers differed between the three studied groups, differences in subjects' characteristics were considered as an adjustment in logistic regression analysis. Another limitation is the inclusion of a cohort comprised only of male participants. However, it should be noted that all animal model studies focus on male animals, and the innovative research of Suchankova mentioned above also indicated that the association between AUD and GLP-1R was more significant in men (Suchankova et al., 2015). In a mice AUD model, it has been shown that males and females are different in terms of alcohol consumption and response during the potential forced abstinence, which is known to affect interconnected networks of neural circuits that are associated with depression and anxiety symptoms. Female mice consumed more alcohol, but they could transit to an abstinence-induced depressive state more quickly than male mice (Dao et al., 2020). Murano et al. (2017) found a similar pattern of gene activity in the hippocampus and the prefrontal cortex of men with alcoholism and infants' developing brains, but not with women. These brain regions are associated with memory deficiency and cognitive problems, which are also symptoms of patients with alcoholism. They concluded that it is possible that these two brain region alterations are associated with the predisposition of patients to the alcohol abuse (Murano et al., 2017).

Concluding, our pilot study revealed a potential association between *GIPR* and alcohol dependence. Confirming this association in studies with bigger sample sizes and deciphering the role of genetic susceptibility may help with the identification of high-risk individuals and may also open the way to conceive novel treatment strategies.

DATA AVAILABILITY STATEMENT

The original contributions presented in the study are included in the article/**Supplementary Material**, further inquiries can be directed to the corresponding authors.

ETHICS STATEMENT

This study involving human participants was reviewed and approved by the Slovenian National Medical Ethics committee. The patients/participants provided their written informed consent to participate in this study.

AUTHOR CONTRIBUTIONS

EET, API, and VD: conceptualization. EET, KG, BKP, API, and VD: methodology and writing – review and editing. EET, KG, and API: formal analysis and visualization. KG: statistical analysis. EET and API: writing – original draft preparation. API and VD: supervision. VD: funding acquisition. All authors have read and agreed to the published version of the manuscript.

FUNDING

This study was financially supported by the Ministry of Education, Science and Sport of Slovenia (Grant No P1-0170).

ACKNOWLEDGMENTS

We kindly acknowledge Savica Soldat from the Pharmacogenetics Laboratory for her the expert technical assistance.

SUPPLEMENTARY MATERIAL

The Supplementary Material for this article can be found online at: https://www.frontiersin.org/articles/10.3389/fnmol.2022.908948/full#supplementary-material

REFERENCES

Abraham, K. A., Kearney, M. L., Reynolds, L. J., and Thyfault, J. P. (2015). Red wine enhances glucose-dependent insulinotropic peptide (GIP) and insulin responses in type 2 diabetes during an oral glucose tolerance test. *Diabetol. Int.* 7, 173–180. doi: 10.1007/s13340-015-0234-y

Adner, N., and Nygren, A. (1992). The influence of indomethacin, theophylline, and propranolol on ethanol augmentation of glucose-induced insulin secretion. *Metabolism* 41, 1165–1170. doi: 10.1016/0026-0495(92)90004-t

Agra, R. M., Gago-Dominguez, M., Paradela-Dobarro, B., Torres-Español, M., Alvarez, L., Fernandez-Trasancos, A., et al. (2019). Obesity-related genetic determinants of heart failure prognosis. *Cardiovasc. Drugs Ther.* 33, 415–424. doi: 10.1007/s10557-019-06888-8

Alhadeff, A. L., Rupprecht, L. E., and Hayes, M. R. (2012). GLP-1 neurons in the nucleus of the solitary tract project directly to the ventral tegmental area and nucleus accumbens to control for food intake. *Endocrinology* 153, 647–658. doi: 10.1210/en.2011-1443

Alvarez, E., Martínez, M. D., Roncero, I., Chowen, J. A., García-Cuartero, B., Gispert, J. D., et al. (2005). The expression of GLP-1 receptor mRNA and protein allows the effect of GLP-1 on glucose metabolism in the human hypothalamus and brainstem. *J. Neurochem.* 92, 798–806. doi: 10.1111/j.1471-4159.2004.02914.x

American Psychiatric Association (2000). *Diagnostic and Statistical Manual of Mental Disorders*, 4th Edn. Washington, DC: American Psychiatric Association. Text Revision (DSM-IV-TR).

Anderberg, R. H., Richard, J. E., Hansson, C., Nissbrandt, H., Bergquist, F., and Skibicka, K. P. (2016). GLP-1 is both anxiogenic and antidepressant; divergent effects of acute and chronic GLP-1 on emotionality. *Psychoneuroendocrinology* 65, 54–66. doi: 10.1016/j.psyneuen.2015.11.021

Anton, R. F. (2000). Obsessive-compulsive aspects of craving: development of the obsessive compulsive drinking scale. *Addiction* 95(Suppl. 2), S211–S217. doi: 10.1080/09652140050111771

Ashworth, E., Brooks, S. J., and Schiöth, H. B. (2021). Neural activation of anxiety and depression in children and young people: a systematic meta-analysis of fMRI studies. *Psychiatry Res. Neuroimaging* 311:111272. doi: 10.1016/j.pscychresns.2021.111272

Bowen, M. T., George, O., Muskiewicz, D. E., and Hall, F. S. (2022). Factors Contributing to the Escalation of Alcohol Consumption. *Neurosci. Biobehav. Rev.* 132, 730–756. doi: 10.1016/j.neubiorev.2021.11.017

Buss, A. H., and Durkee, A. (1957). An inventory for assessing different kinds of hostility. *J. Consult. Psychol.* 21, 343–349. doi: 10.1037/h0046900

Carvalho, A. F., Heilig, M., Perez, A., Probst, C., and Rehm, J. (2019). Alcohol use disorders. *Lancet* 394, 781–792.

Chedid, V., Vijayvargiya, P., Carlson, P., Van Malderen, K., Acosta, A., Zinsmeister, A., et al. (2018). Allelic variant in the glucagon-like peptide 1 receptor gene associated with greater effect of liraglutide and exenatide on gastric emptying: a pilot pharmacogenetics study. *Neurogastroenterol. Motil.* 30:e13313. doi: 10.1111/nmo.13313

Cloninger, C. R., Bohman, M., and Sigvardsson, S. (1981). Inheritance of alcohol abuse: cross-fostering analysis of adopted men. *Arch. Gen. Psychiatry* 38, 861–868. doi: 10.1001/archpsyc.1981.01780330019001

Dalgaard, M., Thomsen, C., Rasmussen, B. M., Holst, J. J., and Hermansen, K. (2004). Ethanol with a mixed meal decreases the incretin levels early postprandially and increases postprandial lipemia in type 2 diabetic patients. *Metabolism* 53, 77–83. doi: 10.1016/j.metabol.2003.08.011

Dao, N. C., Suresh Nair, M., Magee, S. N., Moyer, J. B., Sendao, V., Brockway, D. F., et al. (2020). Forced abstinence from alcohol induces sex-specific depression-like behavioral and neural adaptations in somatostatin neurons in cortical and amygdalar regions. *Front. Behav. Neurosci.* 14:86. doi: 10.3389/fnbeh.2020.00086

Davidson, J. R. T., Miner, C. M., De Veaugh-Geiss, J., Tupler, L. A., Colket, J. T., and Potts, N. L. S. (1997). The brief social phobia scale: a psychometric evaluation. *Psychol. Med.* 27, 161–166. doi: 10.1017/s0033291796004217

de Luis, D. A., Aller, R., de la Fuente, B., Primo, D., Conde, R., Izaola, O., et al. (2015d). Relation of the rs6923761 gene variant in glucagon-like peptide 1 receptor with weight, cardiovascular risk factor, and serum adipokine levels in obese female subjects. *J. Clin. Lab. Anal.* 29, 100–105. doi: 10.1002/jcla.21735

de Luis, D. A., Aller, R., Izaola, O., and Bachiller, R. (2015a). Role of rs6923761 gene variant in glucagon-like peptide 1 receptor in basal GLP-1 levels, cardiovascular risk factor and serum adipokine levels in naïve type 2 diabetic patients. *J. Endocrinol. Invest.* 38, 143–147. doi: 10.1007/s40618-014-0161-y

de Luis, D. A., Aller, R., Izaola, O., and Romero, E. (2015b). Effects of a high-protein/low-carbohydrate versus a standard hypocaloric diet on adipocytokine levels and cardiovascular risk factors during 9 months, role of rs6923761 gene variant of glucagon-like peptide 1 receptor. *J. Endocrinol. Invest.* 38, 1183–1189. doi: 10.1007/s40618-015-0304-9

de Luis, D. A., Diaz Soto, G., Izaola, O., and Romero, E. (2015c). Evaluation of weight loss and metabolic changes in diabetic patients treated with liraglutide, effect of RS 6923761 gene variant of glucagon-like peptide 1 receptor. *J. Diabetes Complications* 29, 595–598. doi: 10.1016/j.jdiacomp.2015.02.010

de Luis, D. A., Aller, R., Izaola, O., Bachiller, R., and Pacheco, D. (2014a). Cardiovascular risk factors and adipocytokines levels after two hypocaloric diets with different fat distribution in obese subjects and rs6923761 gene variant of glucagon-like peptide 1 receptor. *J. Endocrinol. Invest.* 37, 853–859. doi: 10.1007/s40618-014-0116-3

de Luis, D. A., Aller, R., Izaola, O., Lopez, J. J., Gomez, E., Torres, B., et al. (2014b). Effect of rs6923761 gene variant of glucagon-like peptide 1 receptor on metabolic response and weight loss after a 3-month intervention with a hypocaloric diet. *J. Endocrinol. Invest.* 37, 935–939. doi: 10.1007/s40618-014-0117-2

de Luis, D. A., Bachiller, R., Izaola, O., De La Fuente, B., and Aller, R. (2014c). Relation of the rs6923761 gene variant in glucagon-like peptide 1 receptor to metabolic syndrome in obese subjects. *Ann. Nutr. Metab.* 65, 253–258. doi: 10.1159/000365295

de Luis, D. A., Pacheco, D., Aller, R., Izaola, O., and Bachiller, R. (2014e). Roles of rs 6923761 gene variant in glucagon-like peptide 1 receptor on weight, cardiovascular risk factor and serum adipokine levels in morbid obese patients. *Nutr. Hosp.* 29, 889–893. doi: 10.3305/nh.2014.29.4.7218

de Luis, D. A., Pacheco, D., Aller, R., and Izaola, O. (2014d). Role of the rs6923761 gene variant in glucagon-like peptide 1 receptor gene on cardiovascular risk factors and weight loss after biliopancreatic diversion surgery. *Ann. Nutr. Metab.* 65, 259–263. doi: 10.1159/000365975

de Luis, D. A., Aller, R., Izaola, O., De La Fuente, B., Primo, D., Conde, R., et al. (2013). Evaluation of weight loss and adipocytokine levels after two hypocaloric diets with different macronutrient distribution in obese subjects with the rs6923761 gene variant of glucagon-like peptide 1 receptor. *Ann. Nutr. Metab.* 63, 277–282. doi: 10.1159/000356710

de Luis, D. A., Ballesteros, M., Lopez Guzman, A., Ruiz, E., Muñoz, C., Penacho, M. A., et al. (2018). rs6923761 gene variant in glucagon-like peptide 1 receptor: allelic frequencies and influence on cardiovascular risk factors in a multicenter study of Castilla-Leon. *Clin. Nutr.* 37, 2144–2148. doi: 10.1016/j.clnu.2017.10.013

Domi, E., Domi, A., Adermark, L., Heilig, M., and Augier, E. (2021). Neurobiology of alcohol seeking behavior. *J. Neurochem.* 157, 1585–1614. doi: 10.1111/jnc.15343

Egecioglu, E., Engel, J. A., and Jerlhag, E. (2013). The glucagon-like peptide 1 analogue, exendin-4, attenuates the rewarding properties of psychostimulant drugs in mice. *PLoS One* 8:e69010. doi: 10.1371/journal.pone.0069010

Erbil, D., Eren, C. Y., Demirel, C., Küçüker, M. U., Solaroğlu, I., and Eser, H. Y. (2019). GLP-1's role in neuroprotection: a systematic review. *Brain Inj.* 33, 734–819. doi: 10.1080/02699052.2019.1587000

Eren-Yazicioglu, C. Y., Yigit, A., Dogruoz, R. E., and Yapici-Eser, H. (2021). Can GLP-1 be a target for reward system related disorders? A qualitative synthesis and systematic review analysis of studies on palatable food, drugs of abuse, and alcohol. *Front. Behav. Neurosci.* 14:614884. doi: 10.3389/fnbeh.2020.614884

Eser, H. Y., Appadurai, V., Eren, C. Y., Yazici, D., Chen, C. Y., Ongur, D., et al. (2020). Association between GLP-1 receptor gene polymorphisms with reward learning, anhedonia and depression diagnosis. *Acta Neuropsychiatr.* 32, 218–225. doi: 10.1017/neu.2020.14

Faivre, E., Gault, V. A., Thorens, B., and Hölscher, C. (2011). Glucose-dependent insulinotropic polypeptide receptor knockout mice are impaired in learning, synaptic plasticity, and neurogenesis. *J. Neurophysiol.* 105, 1574–1580. doi: 10.1152/jn.00866.2010

Gandal, M. J., Haney, J. R., Parikshak, N. N., Leppa, V., Ramaswami, G., Hartl, C., et al. (2018). Shared molecular neuropathology across major psychiatric disorders parallels polygenic overlap. *Science* 359, 693–697.

Gault, V. A., and Hölscher, C. (2008). Protease-resistant glucose-dependent insulinotropic polypeptide agonists facilitate hippocampal LTP and reverse the impairment of LTP induced by beta-amyloid. *J. Neurophysiol.* 99, 1590–1595. doi: 10.1152/jn.01161.2007

Goodman, W. K., and Price, L. H. (1992). Assessment of severity and change in obsessive compulsive disorder. *Psychiatr. Clin. North Am.* 15, 861–869.

Hattingh, C. J., Ipser, J., Tromp, S. A., Syal, S., Lochner, C., Brooks, S. J., et al. (2013). Functional magnetic resonance imaging during emotion recognition in social anxiety disorder: an activation likelihood meta-analysis. *Front. Hum. Neurosci.* 6:347. doi: 10.3389/fnhum.2012.00347

Heath, A. C., Bucholz, K. K., Madden, P. A. F., Dinwiddie, S. H., Slutske, W. S., Bierut, L. J., et al. (1997). Genetic and environmental contributions to alcohol dependence risk in a national twin sample: consistency of findings in women and men. *Psychol. Med.* 27, 1381–1396. doi: 10.1017/s0033291797005643

Hiroi, N., and Agatsuma, S. (2005). Genetic susceptibility to substance dependence. *Mol. Psychiatry* 10, 336–344.

Ilješ, A. P., Plesnièar, B. K., and Dolžan, V. (2021). Associations of NLRP3 and CARD8 gene polymorphisms with alcohol dependence and commonly related psychiatric disorders: a preliminary study. *Arh. Hig. Rada Toksikol.* 72, 191–197. doi: 10.2478/aiht-2021-72-3432

Isbil-Buyukcoskun, N., Cam-Etoz, B., Gulec, G., and Ozluk, K. (2009). Effect of peripherally-injected glucagon-like peptide-1 on gastric mucosal blood flow. *Regul. Pept.* 157, 72–75. doi: 10.1016/j.regpep.2009.04.013

Javorský, M., Gotthardová, I., Klimčáková, L., Kvapil, M., Židzik, J., Schroner, Z., et al. (2016). A missense variant in GLP1R gene is associated with the glycaemic response to treatment with gliptins. *Diabetes. Obes. Metab.* 18, 941–944. doi: 10.1111/dom.12682

Jayaram-Lindström, N., Ericson, M., Steensland, P., and Jerlhag, E. (2016)."Dopamine and alcohol dependence: from bench to clinic," in *Recent Advances in Drug Addiction Research and Clinical Applications*, eds W. Meil and C. Ruby (Norderstedt: Books on Demand).

Jensen, C. B., Pyke, C., Rasch, M. G., Dahl, A. B., Knudsen, L. B., and Secher, A. (2018). Characterization of the glucagonlike peptide-1 receptor in male mouse brain using a novel antibody and in situ hybridization. *Endocrinology* 159, 665–675. doi: 10.1210/en.2017-00812

Jensterle, M., Pirš, B., Goričar, K., Dolžan, V., and Janež, A. (2015). Genetic variability in GLP-1 receptor is associated with inter-individual differences in weight lowering potential of liraglutide in obese women with PCOS: a pilot study. *Eur. J. Clin. Pharmacol.* 71, 817–824. doi: 10.1007/s00228-015-1868-1

Jerlhag, E. (2020). Alcohol-mediated behaviours and the gut-brain axis; with focus on glucagon-like peptide-1. *Brain Res* 1727:146562. doi: 10.1016/j.brainres.2019.146562

Jones, J. D., Comer, S. D., and Kranzler, H. R. (2015). The Pharmacogenetics of alcohol use disorder. *Alcohol. Clin. Exp. Res.* 39, 391–402.

Kathryn Mchugh, R., and Weiss, R. D. (2019). Alcohol use disorder and depressive disorders. *Alcohol Res.* 40, e1–e8.

Klausen, M. K., Thomsen, M., Wortwein, G., and Fink-Jensen, A. (2022). The role of glucagon-like peptide 1 (GLP-1) in addictive disorders. *Br. J. Pharmacol* 179, 625–641. doi: 10.1111/bph.15677

Klen, J., and Dolžan, V. (2022). Glucagon-like peptide-1 receptor agonists in the management of type 2 diabetes mellitus and obesity: the impact of pharmacological properties and genetic factors. *Int. J. Mol. Sci.* 23:3451. doi: 10.3390/ijms23073451

Koob, G. F., and Volkow, N. D. (2016). Neurobiology of addiction: a neurocircuitry analysis. *The lancet. Psychiatry* 3, 760–773.

Koole, C., Wootten, D., Simms, J., Valant, C., Miller, L. J., Christopoulos, A., et al. (2011). Polymorphism and ligand dependent changes in human glucagon-like peptide-1 receptor (GLP-1R) function: allosteric rescue of loss of function mutation. *Mol. Pharmacol.* 80, 486–497. doi: 10.1124/mol.111.072884

Kranzler, H. R., and Soyka, M. (2018). Diagnosis and pharmacotherapy of alcohol use disorder: a review. *JAMA* 320, 815–824. doi: 10.1001/jama.2018.11406

Mansur, R. B., Fries, G. R., Trevizol, A. P., Subramaniapillai, M., Lovshin, J., Lin, K., et al. (2019). The effect of body mass index on glucagon-like peptide receptor gene expression in the post mortem brain from individuals with mood and psychotic disorders. *Eur. Neuropsychopharmacol.* 29, 137–146. doi: 10.1016/j.euroneuro.2018.10.007

Marty, V. N., Farokhnia, M., Munier, J. J., Mulpuri, Y., Leggio, L., and Spigelman, I. (2020). Long-acting glucagon-like peptide-1 receptor agonists suppress voluntary alcohol intake in male wistar rats. *Front. Neurosci.* 14:599646. doi: 10.3389/fnins.2020.599646

Mashayekhi, M., Wilson, J. R., Jafarian-Kerman, S., Nian, H., Yu, C., Shuey, M. M., et al. (2021). Association of a glucagon-like peptide-1 receptor gene variant with glucose response to a mixed meal. *Diabetes. Obes. Metab.* 23, 281–286. doi: 10.1111/dom.14216

Merchenthaler, I., Lane, M., and Shughrue, P. (1999). Distribution of pre-pro-glucagon and glucagon-like peptide-1 receptor messenger RNAs in the rat central nervous system. *J. Comp. Neurol.* 403, 261–280. doi: 10.1002/(sici)1096-9861(19990111)403:2<261::aid-cne8>3.0.co;2-5

Murano, T., Koshimizu, H., Hagihara, H., and Miyakawa, T. (2017). Transcriptomic immaturity of the hippocampus and prefrontal cortex in patients with alcoholism. *Sci. Reports* 7:44531. doi: 10.1038/srep44531

Nestler, E. J., and Aghajanian, G. K. (1997). Molecular and cellular basis of addiction. *Science* 278, 58–63.

Nutt, D., Hayes, A., Fonville, L., Zafar, R., Palmer, E. O. C., Paterson, L., et al. (2021). Alcohol and the Brain. *Nutrients* 13:3938.

Nyberg, J., Anderson, M. F., Meister, B., Alborn, A. M., Ström, A. K., Brederlau, A., et al. (2005). Glucose-dependent insulinotropic polypeptide is expressed in adult hippocampus and induces progenitor cell proliferation. *J. Neurosci.* 25, 1816–1825. doi: 10.1523/JNEUROSCI.4920-04.2005

Pannacciulli, N., Le, D. S. N. T., Salbe, A. D., Chen, K., Reiman, E. M., Tataranni, P. A., et al. (2007). Postprandial glucagon-like peptide-1 (GLP-1) response is positively associated with changes in neuronal activity of brain areas implicated in satiety and food intake regulation in humans. *Neuroimage* 35, 511–517. doi: 10.1016/j.neuroimage.2006.12.035

Plemenitas, A., Kastelic, M., Porcelli, S., Serretti, A., Rus Makovec, M., Kores Plesnicar, B., et al. (2015). Genetic variability in CYP2E1 and catalase gene among currently and formerly alcohol-dependent male subjects. *Alcohol Alcohol* 50, 140–145. doi: 10.1093/alcalc/agu088

Reddy, I. A., Pino, J. A., Weikop, P., Osses, N., Sørensen, G., Bering, T., et al. (2016). Glucagon-like peptide 1 receptor activation regulates cocaine actions and dopamine homeostasis in the lateral septum by decreasing arachidonic acid levels. *Transl. Psychiatry* 6:e809. doi: 10.1038/tp.2016.86

Rinaman, L. (2010). Ascending projections from the caudal visceral nucleus of the solitary tract to brain regions involved in food intake and energy expenditure. *Brain Res.* 1350, 18–34. doi: 10.1016/j.brainres.2010.03.059

Rudenstine, S., Espinosa, A., and Kumar, A. (2020). Depression and anxiety subgroups across alcohol use disorder and substance use in a national epidemiologic study. *J. Dual Diagn.* 16, 299–311. doi: 10.1080/15504263.2020.1784498

Rush, A. J., First, M. B., and Blacker, D. (2008). "Task force for the handbook of psychiatric measures," in *Handbook of Psychiatric Measures*, ed. American Psychiatric Association (Washington, DC: American Psychiatric Association), 828. doi: 10.1002/14651858.CD012081.pub2

Sauber, J., Grothe, J., Behm, M., Scherag, A., Grallert, H., Illig, T., et al. (2010). Association of variants in gastric inhibitory polypeptide receptor gene with impaired glucose homeostasis in obese children and adolescents from Berlin. *Eur. J. Endocrinol.* 163, 259–264. doi: 10.1530/EJE-10-0444

Seino, Y., Fukushima, M., and Yabe, D. (2010). GIP and GLP-1, the two incretin hormones: similarities and differences. *J. Diabetes Investig.* 1, 8–23. doi: 10.1111/j.2040-1124.2010.00022.x

Seino, Y., and Yabe, D. (2013). Glucose-dependent insulinotropic polypeptide and glucagon-like peptide-1: incretin actions beyond the pancreas. *J. Diabetes Investig.* 4, 108–130. doi: 10.1111/jdi.12065

Sharma, A. N., Pise, A., Sharma, J. N., and Shukla, P. (2015). Glucagon-like peptide-1 (GLP-1) receptor agonist prevents development of tolerance to anti-anxiety effect of ethanol and withdrawal-induced anxiety in rats. *Metab. Brain Dis.* 30, 719–730. doi: 10.1007/s11011-014-9627-z

Suchankova, P., Yan, J., Schwandt, M. L., Stangl, B. L., Caparelli, E. C., Momenan, R., et al. (2015). The glucagon-like peptide-1 receptor as a potential treatment target in alcohol use disorder: evidence from human genetic association studies and a mouse model of alcohol dependence. *Transl. Psychiatry* 5:e583. doi: 10.1038/tp.2015.68

Torekov, S. S., Harsløf, T., Rejnmark, L., Eiken, P., Jensen, J. B., Herman, A. P., et al. (2014). A functional amino acid substitution in the glucose-dependent insulinotropic polypeptide receptor (GIPR) gene is associated with lower bone mineral density and increased fracture risk. *J. Clin. Endocrinol. Metab.* 99, E729–E733. doi: 10.1210/jc.2013-3766

Underwood, C. R., Garibay, P., Knudsen, L. B., Hastrup, S., Peters, G. H., Rudolph, R., et al. (2010). Crystal structure of glucagon-like peptide-1 in complex with the extracellular domain of the glucagon-like peptide-1 receptor. *J. Biol. Chem.* 285, 723–730. doi: 10.1074/jbc.M109.033829

Urgeová, A., Javorský, M., Klimčáková, L., Zidzik, J., Šalagovič, J., Hubáček, J. A., et al. (2020). Genetic variants associated with glycemic response to treatment with dipeptidylpeptidase 4 inhibitors. *Pharmacogenomics* 21, 317–323. doi: 10.2217/pgs-2019-0147

Vallöf, D., Vestlund, J., and Jerlhag, E. (2019). Glucagon-like peptide-1 receptors within the nucleus of the solitary tract regulate alcohol-mediated behaviors in rodents. *Neuropharmacology* 149, 124–132.

Verhulst, B., Neale, M. C., and Kendler, K. S. (2015). The heritability of alcohol use disorders: a meta-analysis of twin and adoption studies. *Psychol. Med.* 45, 1061–1072. doi: 10.1017/S0033291714002165

Vogel, C. I. G., Scherag, A., Brönner, G., Nguyen, T. T., Wang, H. J., Grallert, H., et al. (2009). Gastric inhibitory polypeptide receptor: association analyses for

obesity of several polymorphisms in large study groups. *BMC Med. Genet.* 10:19. doi: 10.1186/1471-2350-10-19

Walters, R. K., Polimanti, R., Johnson, E. C., McClintick, J. N., Adams, M. J., Adkins, A. E., et al. (2018). Transancestral GWAS of alcohol dependence reveals common genetic underpinnings with psychiatric disorders. *Nat. Neurosci.* 21, 1656–1669. doi: 10.1038/s41593-018-0275-1

Yu, M., Wang, K., Liu, H., and Cao, R. (2019). GLP1R variant is associated with response to exenatide in overweight Chinese Type 2 diabetes patients. *Pharmacogenomics* 20, 273–277. doi: 10.2217/pgs-2018-0159

Zhou, H., Sealock, J. M., Sanchez-Roige, S., Clarke, T. K., Levey, D. F., Cheng, Z., et al. (2020). Genome-wide meta-analysis of problematic alcohol use in 435,563 individuals yields insights into biology and relationships with other traits. *Nat. Neurosci.* 23, 809–818. doi: 10.1038/s41593-020-0643-5

Zung, W. W. K. (1965). A self-rating depression scale. *Arch. Gen. Psychiatry* 12, 63–70.

Zung, W. W. K. (1971). A rating instrument for anxiety disorders. *Psychosomatics* 12, 371–379. doi: 10.1016/S0033-3182(71)71479-0

Conflict of Interest: The authors declare that the research was conducted in the absence of any commercial or financial relationships that could be construed as a potential conflict of interest.

Publisher's Note: All claims expressed in this article are solely those of the authors and do not necessarily represent those of their affiliated organizations, or those of the publisher, the editors and the reviewers. Any product that may be evaluated in this article, or claim that may be made by its manufacturer, is not guaranteed or endorsed by the publisher.

frontiers | Frontiers in Molecular Neuroscience

ORIGINAL RESEARCH
published: 27 June 2022
doi: 10.3389/fnmol.2022.925272

Harmane Potentiates Nicotine Reinforcement Through MAO-A Inhibition at the Dose Related to Cigarette Smoking

Zheng Ding[1,2,3], Xiangyu Li[1,2,3], Huan Chen[1,2,3], Hongwei Hou[1,2,3] and Qingyuan Hu[1,2,3]**

[1] China National Tobacco Quality Supervision & Test Center, Zhengzhou, China, [2] Key Laboratory of Tobacco Biological Effects, Zhengzhou, China, [3] Joint Laboratory of Translational Neurobiology, Zhengzhou, China

Nicotine is the primary addictive component in cigarette smoke, and dopamine release induced by nicotine is considered a significant cause of persistent smoking and nicotine dependence. However, the effects of nicotine replacement therapy on smoking cessation were less effective than expected, suggesting that other non-nicotine constituents may potentiate the reinforcing effects of nicotine. Harmane is a potent, selective monoamine oxidase A (MAO-A) inhibitor found in cigarette smoke, but showed no effect on nicotine self-administration in previous studies, possibly due to the surprisingly high doses used. In the present study, we found that harmane potentiated nicotine self-administration on the fixed ration schedule at the dose related to human cigarette smoking by the synergistic effects in up-regulating genes in addiction-related pathways, and the effect was reduced at doses 10 times higher or lower than the smoking-related dose. The smoking-related dose of harmane also enhanced the increase of locomotor activity induced by nicotine, accompanied by increased dopamine basal level and dopamine release in the nucleus accumbens through MAO-A inhibition. Our findings provided new evidence for the important role of non-nicotine ingredients of tobacco products in smoking addiction.

Keywords: harmane, nicotine, monoamine oxidase (MAO), dopamine, cigarette smoking, substance abuse

OPEN ACCESS

Edited by:
Jie Yan,
Central South University, China

Reviewed by:
Lucia Carvelli,
Florida Atlantic University, United States
Jie Shi,
Peking University, China

****Correspondence:***
Hongwei Hou
qsfctc@163.com
Qingyuan Hu
huqy1965@163.com

Specialty section:
This article was submitted to Molecular Signalling and Pathways, a section of the journal Frontiers in Molecular Neuroscience

Received: *21 April 2022*
Accepted: *07 June 2022*
Published: *27 June 2022*

Citation:
Ding Z, Li X, Chen H, Hou H and Hu Q (2022) Harmane Potentiates Nicotine Reinforcement Through MAO-A Inhibition at the Dose Related to Cigarette Smoking. Front. Mol. Neurosci. 15:925272. doi: 10.3389/fnmol.2022.925272

INTRODUCTION

According to the Federal Trade Commission Cigarette Report, cigarette sales went up for the first time in 20 years (Ma et al., 2022). High cigarette smoking rates are attributed to nicotine, the main component of tobacco products (Benowitz, 1992, 2010). However, nicotine is only one of more than 8,000 chemical constituents in tobacco products (Rodgman and Perfetti, 2008). Nicotine replacement therapy is not enough to relieve withdrawal symptoms in smokers (Rose et al., 2000). Other non-nicotine components in tobacco products contribute to smoking addiction, but underlying mechanisms are unclear (Rose, 2006). Nicotine stimulates dopamine release by activating dopamine neurons, which induces the rewarding effects (Rice and Cragg, 2004; De Biasi and Dani, 2011). Monoamine oxidase is responsible for dopamine metabolism, and brain monoamine oxidase activity in smokers is significantly lower than that of non-smokers (Fowler et al., 1996a,b). Inhibition of monoamine oxidase increases nicotine-induced dopamine release and reinforces the rewarding effects of nicotine (Meyer et al., 2006; Lewis et al., 2007).

MAO has two isoenzymes: MAO-A and MAO-B (Weyler et al., 1990). Although MAO-A and MAO-B have been shown to metabolize dopamine *in vitro*, MAO-B is absent in dopaminergic neurons and does not affect baseline dopamine levels, whereas MAO-A is primarily responsible for dopamine metabolism in the brain (Butcher et al., 1990; Cho et al., 2021). Previous work focused only on the effects of medicinal or clinical MAO inhibitors (Guillem et al., 2005, 2006; Villégier et al., 2006; Smith et al., 2016). Little evidence is available about the potentiating effect of MAO inhibitors in tobacco products. Among the monoamine oxidase inhibitory components in cigarette smoke components, two potent inhibitors were found in cigarette smoke to affect monoamine oxidase, harmane and norharmane (Poindexter and Carpenter, 1962; Ho et al., 1968; Rommelspacher et al., 2002; Herraiz and Chaparro, 2005). Norharmane was shown to enhance low-dose nicotine self-administration possibly through the MAO-A inhibition (Arnold et al., 2014). The inhibitory ability of harmane to MAO-A is about 20 times that of norharmane (Herraiz and Chaparro, 2005). During short-term smoking cessation in smokers, the plasma levels of harmane instead of norharmane were significantly correlated with the brain MAO-A activity (Bacher et al., 2011). Therefore, it was speculated that harmane might also potentiate the reinforcing effects of nicotine, but harmane did not affect nicotine self-administration in previous studies. However, it is worth noting that harmane was used at doses much higher than those found in tobacco smoke (equivalent to smoking 100–5000 cigarettes a day) and was pre-injected rather than co-administered with nicotine in these studies (Villégier et al., 2006; Hall et al., 2014). On the one hand, the activity of neurons in the nucleus accumbens were inhibited by excessive doses of harmane (Ergene and Schoener, 1993). On the other hand, the monoamine oxidase inhibition of harmane might resulted in the loss of the potentiation of nicotine reinforcing effect (Smith et al., 2016). New findings might have emerged if harmane doses were designed according to human smoking levels.

In addition to the MAO-A inhibition, harmane has various other properties, including psychoactive and pharmacological effects (Adell and Myers, 1994; Aricioglu and Altunbas, 2003; Aricioglu and Utkan, 2003; Aricioglu-Kartal et al., 2003; Khan et al., 2017). Since the potential effects of harmane may enhance or reducenicotine reinforcement, we performed an RNA-seq study to explore the synergistic effects of harmane and nicotine in regulating the expression of addiction related genes.

Therefore, this study focused on the potentiation mechanism of harmane on the reinforcing effects of nicotine. Firstly, the effect of harmane on nicotine reinforcement was investigated. Secondly, the effects of harmane and nicotine on the basal levels and dopamine release were determined. Thirdly, the potentiation mechanisms of harmane on the reinforcing effects of nicotine were investigated. Finally, the potential synergistic effects of harmane and nicotine in regulating the expression of addiction-related genes were explored. Our results demonstrate that at the dose related to human smoking, harmane potentiates the reinforcing effects of nicotine through MAO-A inhibition and the synergistic effects of harmane and nicotine up-regulated genes in addiction-related pathways.

MATERIALS AND METHODS

Animals

Male Sprague Dawley rats (7 weeks, 200–250 g) were purchased from Beijing Vital River Laboratory Animal Technology Co., Ltd. When arrived in the laboratory, rats were placed in temperature, humidity, and pressure-controlled cages (light on from 8:00 p.m. to 8:00 a.m., test during dark time) and acclimated for a week before experiments. Rats were housed individually in cages with steel lids (for food storage) and filter tops and allowed free access to adequate water and food before the experiment. After starting the experiment, the rats were given ∼10 g (2∼3 pills) of food per day to keep weight. The experimental procedures were conducted according to the National Institutes of Health Guide for the Care and Use of Laboratory Animals. The procedures were approved by the Laboratory Animal Management and Ethics Committee of China National Tobacco Quality Supervision and Test Center (Approval Number: CTQTC-SYXK-2021002).

Drugs

Nicotine bi-L-(+)-tartrate dihydrate was purchased from TCI (N0080). Harmane was purchased from MCE (HY-101392). Drugs were dissolved in 0.9% sterile saline (pH 7.0–7.4). Since harmane cannot be directly dissolved in 0.9% sterile saline, harmane was pre-dissolved with tartaric acid (TCI, T0025) solution consistent with nicotine bi-L-(+)-tartrate dihydrate. The drug solution was prepared freshly and stored at 4°C immediately after use. The doses of harmane in this study were selected according to the ratio of harmane and nicotine in the cigarette smoke based on the human daily smoking levels. Moreover, the harmane in our research was self-administered with nicotine rather than pre-injected in our study to simulate the situation of human smoking.

Self-Administration Procedures

Before the experiment, the surgical instruments were sterilized with 70% ethanol and irradiated under ultraviolet light for 30 min. Rats were anesthetized with isoflurane and injected intramuscularly with Zoletil^{TM} 50 (Virbac). An electric shaver was used to remove hair from the right chest and part of the back of the rat. The pulsating jugular vein was found in the rat's right chest, and a pre-sterilized silicone tube was inserted. After the silicone tube is fixed, connect the other end of the silicone tube to the self-administration button (Instech, VABR1B/22) on the back. Silicone tubes were ventilated with saline containing heparin sodium and penicillin per day after the surgery. Rats were allowed to recover for at least 7 days before self-administration.

Self-administration program started without food training since food training enhances self-administration in rats (Valentine et al., 1997; Donny et al., 1998; Clemens et al., 2010; Garcia et al., 2014). Fixed ratio (FR) self-administration programs were used in this study (Weiss, 2013), where the number following FR represents the number of responses required to obtain a single drug injection. In FR1, FR2, and FR3 schedule, 1, 2, and 3 responses must be produced in order to obtain injections (Cooper et al., 2007). Rats were placed in the

operant chambers for 1 h with FR1, FR2, FR3 self-administration schedule on days 1–4, 5–12, and 13–27, allowing rats to learn longer at higher FR. When an infusion is triggered, the chamber's light will be turned off for 20 s, accompanied by a beeping sound for 1 s. During the light-off period, the nosepoke is invalid but still recorded.

Open-Field Experiments

A total of 24 rats (6 in each of 4 groups) were used for subcutaneous injection, including 14 day saline (S), 14 day 10 μg/kg harmane (H), 14 day 300 μg/kg nicotine (N), and 14 day 300 μg/kg nicotine + 10 μg/kg harmane (N + H) (equivalent to the harmane smoked by a smoker with 20 cigarettes/day). Rats were given 10 ± 0.5 g of food per day to reduce the effects of the diet and weight. Open field experiments refer to the method in JOVE (Seibenhener and Wooten, 2015). For the locomotor activity test, rats were free to move around in the open field for 10 min. The central area of the open field was defined as 60 cm × 60 cm. The total distance represented the locomotor activity and correlated with nucleus accumbens dopamine release in rats. Before testing, rats were adapted to the testing room for 30 min. Rats were placed in the open field before the first injection and 5 min after the last injection. The background was snapshotted before the experiment as a reference value.

MAO-A Level, MAO-A Activity, and Dopamine Level Determination

Rats were anesthetized with Zoletil 1 h after the last injection (refer to blood harmane return to baseline levels within 1 h after smoking a cigarette) and decapitated. The rat brains were washed and taken out with PBS in an ice-water mixture. Nucleus accumbens was extracted referred to the method of Jacobs et al. (2004). Pre-sterilized 0.5 mm iron bead was added to each ep tube and shook 20 times at 60 Hz for 30 s by Tissuelyser (Shanghai Jingxin, JXFSTPRP).

The homogenized samples were first centrifuged at 2000 rpm for 20 min, and 200 μL of the supernatant was taken to determine MAO-A activity and MAO-A level. The remaining samples were centrifuged at 5,000 rpm for 10 min (according to the recommended centrifugation speed of kits). The supernatants were filtered with a 0.22 μm membrane before determination. MAO-A activity was determined by the MAO-Glo™ Assay Systems kit (Promega, v1402). 10 nM (1.7 ng/mL) rasagiline in DMSO (Shanghai yuanye, S24846) was added to each well to reduce the influence of MAO-B. MAO-A and dopamine levels were detected using the Rat MAO-A ELISA kit (Laibio, JL39022) and Rat Dopamine ELISA kit (Laibio, JL12965). Fluorescence and luminescence were measured using the multimode microplate reader (Spark®, TECAN).

Microdialysis and Dopamine Detection

A total of 17 rats were used for microdialysis after subcutaneous injection, 10 μg/kg harmane (n = 4), 300 μg/kg nicotine (n = 7), and 300 μg/kg nicotine + 10 μg/kg harmane (n = 6) (equivalent to the nicotine and harmane smoked by a smoker with 20 cigarettes/day). Rats were anesthetized with isoflurane and injected intramuscularly with Zoletil™ 50 (Virbac). An electric shaver was used to remove hair on the top of the head. Microdialysis probes and cannulas (CMA/12, cat No. 8010432) were sterilized with UV light before use. Anesthetized rats were head-fixed on the stereotaxic apparatus (RWD, 68025). According to the rat brain stereotaxic reference book (Paxinos and Watson, 2006), the position of the nucleus accumbens shell was set as AP: +2.5 mm, ML: +1.4 mm, and DV: -7.0 mm. The microdialysis experiment was performed 3–5 days after the recovery of the rat after the cannula implantation surgery. The rats were kept for 2 h after connecting to the microdialysis device to keep the baseline stable. The flow rate of microdialysis was set at 2.5 μl per minute, and samples were collected every 10 min. Each rat was measured with 10 time points, the first 4 points were the baseline values, and the drug was injected from the 4th point. The detection of dopamine uses high-performance liquid chromatography combined with an electrochemical detector (HPLC-ECD).

RNA-Seq Study

Rats were anesthetized, decapitated, and brains removed within 2 h of the last self-administration. The nucleus accumbens of the rat was taken out for RNA-seq. After taking out the rat brain, blood and impurities were washed out with pre-chilled PBS. Nucleus accumbens was taken using a brain mold in an ice-water mixture and were immediately put into a liquid nitrogen box for storage. The samples were sent to Beijing Genomics Institute (BGI), where the RNA extraction and library construction were performed. High-throughput sequencing was completed using the BGISEQ-500 sequencing platform (Drmanac et al., 2010).

Statistical Analysis

Data analysis was mainly based on ANOVA of repeated measures, multiple comparisons, and t-tests when appropriate through Graph pad prism 8.0. Data were represented in the figure as the mean ± SEM. The RNA-seq data were analyzed using the online analysis system Dr. Tom provided by BGI,[1] and the visualization tool provided by Dr. Tom includes the drawing of bubble diagrams and Venn diagrams. Significance levels were set as $^{*}p < 0.05$, $^{**}p < 0.01$, $^{***}p < 0.001$ and the screening conditions for differential genes were set as $|\log2FoldChange| > 0.5$ and Q-value < 0.05.

RESULTS

Harmane Potentiated Nicotine Self-Administration at the Dose Related to Human Smoking

A total of 49 rats (7 in each of 7 groups) were used for self-administration. In 3R4F cigarette smoke, the content ratio of harmane and nicotine is about 1:30 (Jaccard et al., 2019; van der Toorn et al., 2019). Therefore, groups in the rat self-administration experiment were set as: Saline (S), Nicotine

[1] https://biosys.bgi.com/

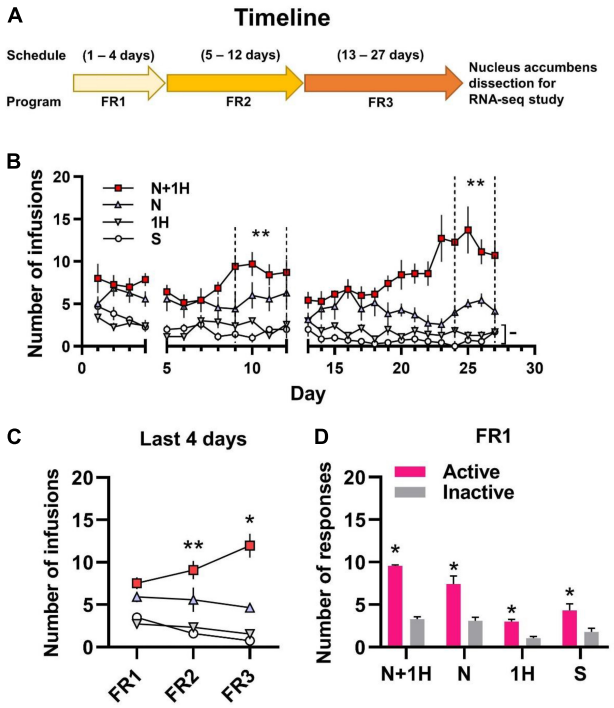

FIGURE 1 | Self-administration of smoking-related doses of nicotine and harmane in rats. **(A)** Timeline of 1 h/day self-administration. **(B)** Number of infusions in FR1-FR3 self-administration. White circle, saline group (S); gray inverted triangle, 1 μg/kg/inf harmane group (1H); blue triangle, 30 μg/kg/inf nicotine group (N); red square, 30 μg/kg/inf nicotine + 1 μg/kg/inf harmane group (N + 1H). The number of infusions in FR2-FR3 was significantly increased in the N + 1H group compared to the N group (**$p < 0.01$), while there was no significant difference from FR1 to FR3 in the H and S groups ($^{-}p > 0.05$). **(C)** Average infusions in the FR1-FR3 last 4 days in each group. The number of infusions increased significantly from FR1 to FR3 in the N + 1 group (**$p < 0.01$ from FR1 to FR2 and *$p < 0.05$ from FR2 to FR3), while other groups did not increase. **(D)** Histograms of the response data in FR1. Active responses were significantly higher in all groups than inactive responses (*$p < 0.05$). Data are presented in the figure using mean ± SEM.

(30 μg/kg/inj) (N), Harmane (1 μg/kg/inj) (1H), Nicotine (30 μg/kg/inj) + Harmane (1 μg/kg/inj) (N + 1H). The timeline of self-administration in rats is shown in **Figure 1A**, starting with FR1 for 4 days, followed by conversion to FR2 for 8 days, and finally FR3 for 15 days. The doses administered in each group of rats remained the same from FR1 to FR3, thus requiring more responses in FR2 and FR3 to maintain drug intake. FR1 was to allow rats learn self-administration (Chen et al., 2007), and FR2 to FR3 were used to investigate the maintenance and reinforcement of drugs (Sorge et al., 2009; De La Peña et al., 2015).

Rats in the nicotine group (N) actively self-administered nicotine compared to the S group in the last 4 days of FR2 and FR3 (*$p < 0.05$) but not in FR1 ($^{-}p = 0.0725$). Rats in the N group maintained stable self-administration ($p > 0.05$ between FR1, FR2, and FR3) (**Figures 1B,C**). Rats in the harmane + nicotine group (N + 1H) showed active self-administration in the last 4 days of each FR (*$p < 0.05$) compared to the S group and FR2-FR3 to those of N group ($^{-}p = 0.1142$, **$p = 0.0048$ and **$p = 0.0023$ for FR1-FR3) (**Figures 1B,C**). Comparing the last 4 days of each FR, harmane + nicotine further potentiated the number of infusions from FR1 to FR3 (FR2 vs. FR1 **$p = 0.0181$ and FR3 vs. FR2 *$p = 0.0343$) (**Figure 1C**). No significant difference ($^{-}p = 0.7465$, 0.6168, and 0.4508) was found between the S and H groups ($p > 0.05$) in the last 4 days of FR1-FR3 (**Figures 1B,C**). Rats in all groups learned to self-administer ($p < 0.05$ between active and inactive nosepokes) through the nature of nosepoke without food training in the FR1 program (**Figure 1D**). The results indicated that harmane potentiated nicotine self-administration but showed no reinforcing effects alone.

Reduced Potentiating Effect of Harmane on Nicotine Self-administration at Doses Not Related to Human Smoking.

To further examine the effects of harmane at different doses on nicotine reinforcement, nicotine (30 μg/kg/inj) + harmane (10 μg/kg/inj) (N + 10H) and nicotine (30 μg/kg/inj) + harmane (0.1 μg/kg/inj) (N + 0.1H) were also designed. The timeline of self-administration in rats was referred to the timeline in **Figure 1A** without RNA-seq study. As expected, no significant potentiating effects were shown in harmane at 10 times doses on nicotine self-administration in each FR ($^{-}p = 0.4378$, 0.7720, and 0.7423) (**Figures 2A,B**). Nicotine self-administration were not affected by 0.1 μg/kg/inj harmane in the last 4 days of FR1 and FR2 ($^{-}p = 0.9946$ and 0.9531), but a significant increase was found in the last 4 days of FR3 (*$p = 0.0150$) compared to those of N group (**Figures 2A,B**). The reinforcing effect of harmane at 1 μg/kg/inj (N + 1H) was significantly higher than at 10 and 0.1 μg/kg/inj in the last 4 days of FR3 [one-way ANOVA, $F_{(3.000,7.544)} = 66.00$, N + 1H vs. N + 10H **$p = 0.0018$ and N + 1H vs. N + 0.1H **$p = 0.0085$] (**Figure 2B**). A main effect of harmane doses was revealed by 3 × 4 two-way ANOVA [$F_{(2.174,13.04)} = 15.42$, $p = 0.0003$] but not FR [$F_{(1.834,11.00)} = 1.636$, $p = 0.2383$], and no significant interaction between harmane dose and FR [$F_{(2.299,13.79)} = 2.493$, $p = 0.1138$] (**Figure 2C**). Both N + 10H and N + 0.1H groups learned to self-administer in FR1 ($p < 0.05$ between active and inactive nosepokes) (**Figure 2D**). The results indicated that harmane potentiated nicotine self-administration within a range of doses and the potentiating effect was reduced at doses beyond this dose range. The results of the number of responses were consistent with the results of the number of infusions (**Supplementary Figure 3**).

Harmane Increased Basal Levels of Dopamine by Inhibiting MAO-A and Synergized With Nicotine to Potentiate Locomotor Activity in Rats

One of the striking differences between nicotine and other addictive drugs concerns its locomotor effects. Unlike other addictive drugs enhance locomotor activity, nicotine showed weak or no effect in animals (Villégier et al., 2006). Unlike other addictive drugs enhance locomotor activity, nicotine showed weak or no effect in animals (Marks et al., 1983; Freeman et al., 1987; Whiteaker et al., 1995), but the synergistic effects of nicotine with MAO inhibitors resulted in increased locomotor

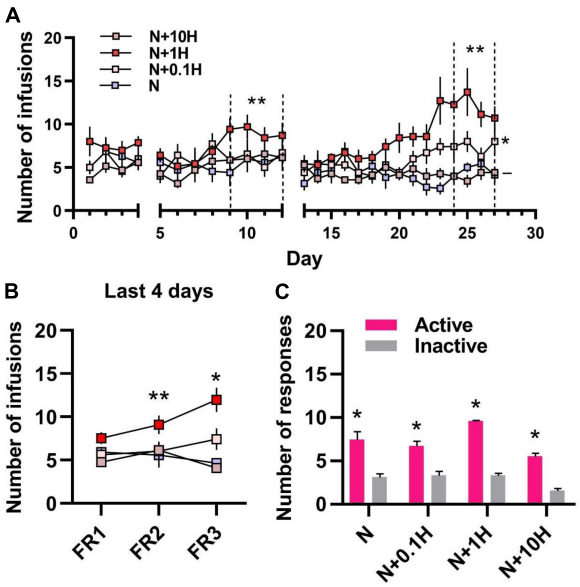

FIGURE 2 | Self-administration of nicotine with different doses of harmane in rats. **(A)** Number of infusions in FR1-FR3 self-administration. Blue square, 30 μg/kg/inf nicotine group (N); pink square 30 μg/kg/inf nicotine + harmane (0.1 μg/kg/inf, N + 0.1H), red square, nicotine + harmane (1 μg/kg/inf, N + 1H) and brown square, nicotine + harmane (10 μg/kg/inf, N + 10H). The number of infusions in FR2-FR3 was significantly increased in the N + 1H group compared to the N group (**$p < 0.01$), while the N + 0.1H group was only significantly higher in FR3 (*$p < 0.05$), and the N + 10H group had no significant difference compared to the N group ($^{-}p > 0.05$). **(B)** Infusions in the FR1-FR3 last 4 days in each group. The number of infusions increased significantly from FR1 to FR3 in the N + 1 group (**$p < 0.01$ from FR1 to FR2 and *$p < 0.05$ from FR2 to FR3), while other groups did not increase. **(C)** Histograms of the response data in FR1. Active responses were significantly higher in all groups than inactive responses (*$p < 0.05$). Data are presented in the figure using mean ± SEM.

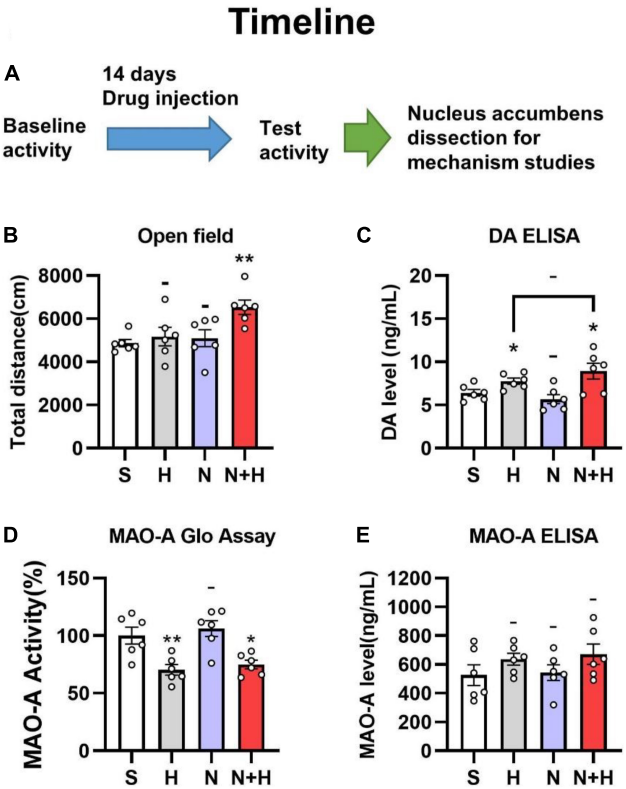

FIGURE 3 | (A) Timeline of subcutaneous administration in rats. **(B)** Effects of nicotine and harmane on the open field total distance of the rats in S, H, N, and N + H groups after drug injection. Rats in the N + H group significantly increased the open field total distance (**$p < 0.01$), while no significant difference were found in the other groups. **(C)** Effects of nicotine and harmane on the basal level of dopamine in the nucleus accumbens. Compared to the S group, the dopamine level in the H and N + H groups increased significantly (*$p < 0.05$), but there was no significant change in the N group. **(D)** Effects of nicotine and harmane on the activity of MAO-A in the nucleus accumbens (NAc) of rats. Compared to the S group, the MAO-A activity in the H and N + H groups decreased significantly (*$p < 0.05$), but there was no significant change in the N group. **(E)** Effects of nicotine and harmane on levels of MAO-A in the nucleus accumbens (NAc) of rats. No significant difference was found in the all four groups. Data are presented in the figure using mean ± SEM.

activity (Villégier et al., 2003, 2006). Since harmane is a potential monoamine oxidase inhibitor, we used open field tests to examine whether the synergistic effects of harmane and nicotine cause locomotor activity changes in rats. The injection dose of nicotine and harmane was set at 300 μg/kg/day and 10 μg/kg/day (30:1) (**Figure 3A**), equivalent to the nicotine and harmane intake through 20 cigarettes by a smoker a day (Matta et al., 2007).

Rats in each group showed similar locomotor activity before subcutaneous injection of the drug (**Supplementary Figure 1**). A significantly increased locomotor activity were shown in the harmane and nicotine (N + H) groups than in the saline (S) group (**$p = 0.0025$) after 14 days of co-administration (**Figure 3B**). Harmane and nicotine alone did not induce significant change in locomotor activity ($p > 0.05$ compared to the S group). These findings indicated that the synergistic effects of harmane and nicotine rather than alone caused the increase in locomotor activity.

MAO-A inhibition proved to increase basal levels of dopamine by inhibiting dopamine metabolism, which increases dopamine release upon stimulation of neuronal signaling (Cho et al., 2021). Although harmane is a MAO-A inhibitor *in vitro* studies (Herraiz and Chaparro, 2005), whether harmane can cause MAO-A inhibition and increase basal dopamine levels have not been investigated. Therefore, immunoassays (ELISA kits for dopamine determination) were used to examine whether harmane potentiates nicotine reinforcement by increasing basal dopamine levels. Since the nucleus accumbens is the main brain area for dopamine release, metabolism and recycling in the drug reward pathway (Di Chiara et al., 2004), the samples used were the nucleus accumbens of rats that completed the open-field experiments. A significant increase in the dopamine basal level of in the nucleus accumbens was found in the H and N + H groups (*$p = 0.0240$ and 0.0402) (**Figure 3C**). Nicotine alone or in combination with harmane did not significantly affect dopamine levels (*$p = 0.2868$ and 0.2771) (**Figure 3C**). Elevated baseline dopamine levels induced by harmane provided

a basis for harmane to increase nicotine-induced dopamine release (Cho et al., 2021).

In addition to examining basal dopamine levels, we asked whether these changes are induced by harmane-induced MAO-A inhibition. The inhibition of MAO-A is not only related to the inhibition of MAO-A activity but also associated with the expression levels of MAO-A also contribute to MAO-A activity. Therefore, the effects of nicotine and harmane on MAO-A in the nucleus accumbens were examined. The samples used to determine MAO-A levels, and MAO-A activity was the nucleus accumbens of rats that completed the open field experiment. Instead of causing changes in MAO-A levels in nucleus accumbens (**Figure 3E**), harmane inhibited MAO-A activity ($^{**}p = 0.0078$) (**Figure 3D**). Nicotine alone did not cause changes in MAO-A activity ($^{-}p > 0.05$), nor did it synergize with harmane ($^{-}p > 0.05$ compared H group to the NH group) (**Figure 3D**).

Harmane Potentiated and Prolonged Nicotine-Induced Dopamine Release

Smoking-related doses of harmane induced MAO-A inhibition in nucleus accumbens and increased dopamine basal levels. To verify whether harmane increased nicotine-induced dopamine release, a microdialysis study was performed (**Figure 4A**). The injection dose of nicotine and harmane was set at 300 μg/kg and 10 μg/kg (consistent with behavioral experiments). Nicotine-induced dopamine release within 20 min of drug injection ($^{**}p = 0.0014$), and dopamine returned to basal levels after 30 min ($^{-}p > 0.05$ compared to basal levels) (**Figure 4B**). The synergistic effects of harmane with nicotine increased the release of dopamine ($^{*}p = 0.0263$ compared to N group) in the first 20 min, and maintained high levels of extracellular dopamine in 40 min after injection ($^{*}p = 0.0375$ comparing the N + H group with the N group) and returned to basal levels after 50 min (**Figure 4C**). No significant effects were found on baseline extracellular dopamine levels of the H group ($^{-}p > 0.05$ compared to baseline, not shown in the figure). Results indicated that harmane may potentiate nicotine reinforcement through a mechanism of increasing the dopamine release induced by nicotine.

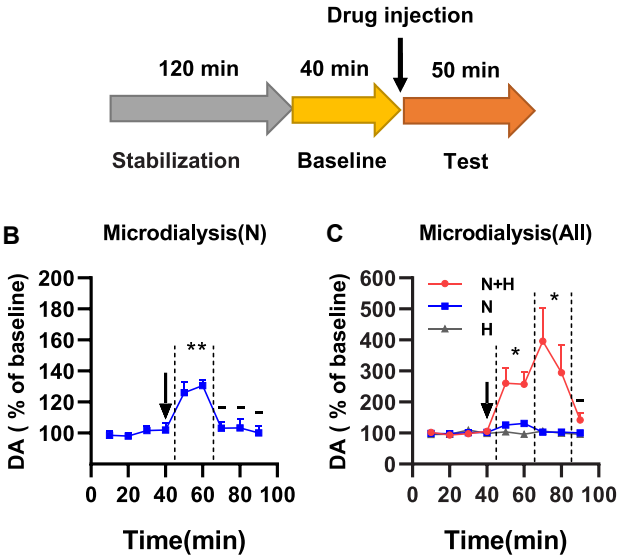

FIGURE 4 | (A) Timeline of microdialysis study. **(B)** Effects of nicotine alone on dopamine release in nucleus accumbens. Significant dopamine release was showed in N group within 20 min of drug injection ($^{**}p < 0.01$). **(C)** Effects of harmane and nicotine on dopamine release in nucleus accumbens. N + H group showed significantly increased release of dopamine compared to N group ($^{*}p < 0.05$) in the first 20 min, and maintained high levels of extracellular dopamine in 40 min after injection compared to N group ($^{*}p < 0.05$). Data are presented in the figure using mean ± SEM.

The Synergistic Effects of Harmane and Nicotine Increased the Number of Genes Affected in Addiction-Related Pathways

In addition to being an MAO-A inhibitor, harmane has other psychoactive and pharmacological effects that may contribute to nicotine reinforcement. To further reveal these potential effects, transcriptomic analysis of the nucleus accumbens of rats in the S, 1H, N, and N + 1H groups were performed by RNA sequencing (RNA-Seq) after self-administration studies. The N + 1H group was chosen because it has a higher potentiating effect than the N + 0.1H and N + 10H groups. Considering that 1H group hardly self-administered harmane, we injected the rats in group H with the dose of harmane equivalent to the N + H group in the last 4 days of FR2 (10 inf × 1 μg/kg/inf = 10 μg/kg) to hold the 30:1 ration. Injecting harmane did not alter harmane infusions ($^{-}p = 0.1152$) between the last 4 days of FR2 and FR3 of the 1H group. Nucleus accumbens samples from the 4 groups of rats were renamed SAL, HAR, NIC, and NH, such that SAL_NAC_1 refers to the nucleus accumbens of the first rat in the saline group.

The transcriptomes of the HAR, NIC, and NH groups were compared with those of the S group, and the resulting differentially expressed genes (DEGs) ($|\log2FC| > 0.5$ and Q-value < 0.05) were represented by Venn diagrams (**Figure 5A**. We focused on the DEGs in NH groups, as the synergistic effect of harmane and nicotine showed the strongest self-administration. For the DEGs in the NH group, 290 + 376 DEGs were induced by the administration of nicotine (section named NIC), 380 + 376 DEGs were induced by the administration of harmane (section named HAR), and the other 1271 DEGs were induced by the synergistic effects of harmane and nicotine (section named NH).

Next, the Kyoto Encyclopedia of Genes and Genomes (KEGG) pathway enrichment analysis was performed according to the genes of each section (NIC, HAR, and NH sections) and found that addiction-related pathways were significantly enriched (**Figure 5B**). Not only the nicotine reinforcement and the dopaminergic neuron pathways have a significant response under the combined action of harmane and nicotine, but also the addiction pathways of other drug addiction (cocaine, morphine, amphetamine addiction, and alcoholism) and various other neurotransmitters (serotonin, glutamate, GABA, and choline) pathways all exhibit the responses that harmane and nicotine

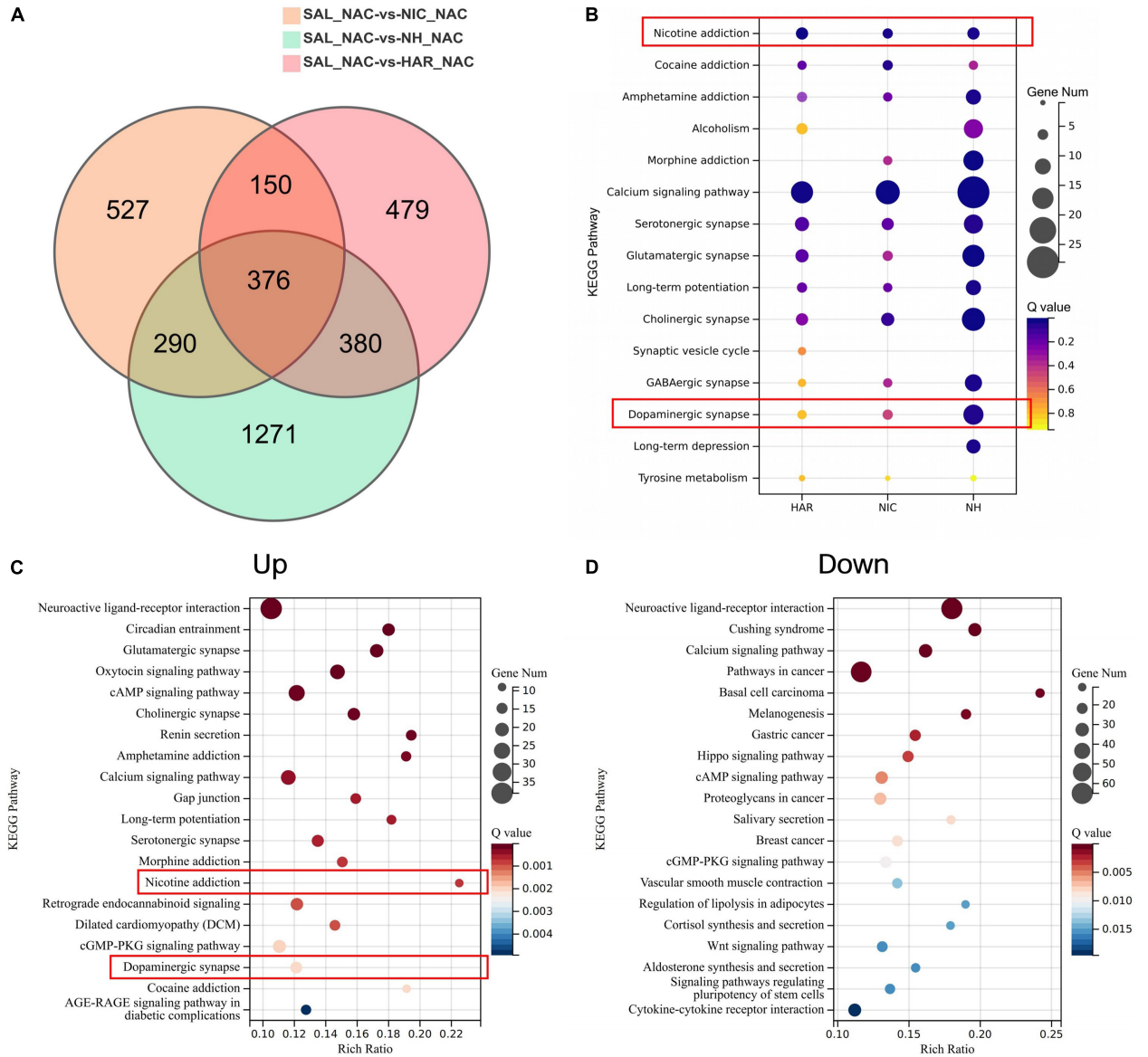

FIGURE 5 | Analysis of differential genes and pathways in the nucleus accumbens transcriptome of self-administered rats. **(A)** Venn diagram of differential genes in three-group alignment. SAL, HAR, NAC, and NH refer to the S, 1H, N, and N + 1H groups. NAC refers to the nucleus accumbens. **(B)** Bubble plot of addiction-related pathways enriched for differential genes in the NH group. HAR, NIC, and NH refer to the intersection of HAR and NH (290 + 376), the intersection of NIC and NH (380 + 376), and the non-intersection of NH (1271). Bubble plot of pathways enriched by up-regulated **(C)** and down-regulated **(D)** genes in nucleus accumbens of NH group.

alone do not. In addition, the synergistic effect of harmane and nicotine also produced responses related to memory in the calcium signaling pathway, long-term potentiation, and long-term depression. It can be seen from the bubble chart responses induced by harmane and nicotine alone contributed only part of the effect, and more response genes were observed only in the co-administration of harmane and nicotine (**Figure 5B**).

To better understand the synergistic effects of harmane and nicotine on the nucleus accumbens, KEGG pathway enrichment analysis was performed for the DEGs that were up-regulated (Up) and down-regulated (Down) in the NH group (**Figures 5C,D**). We were surprised to find that the genes of the nicotine addiction and dopaminergic pathways were significantly up-regulated in the top 20 most significant pathways. The activation of the addiction-related pathways facilitated the reinforcement of self-administration and locomotor behaviors in rats. In addition, possibly due to increased dopamine release, the dopamine D2 receptor gene Drd2 was up-regulated, and the tyrosine hydroxylase gene Th was down-regulated (**Supplementary Figure 2** and **Supplementary Table 1**), which might lead to a block in dopamine synthesis (El Mestikawy et al., 1986; Lindgren et al., 2001), and these effects might reflect the loss of potentiation

at high doses of harmane. The genes of the top 20 most significant pathways downregulated by the synergistic effects of harmane and nicotine were not directly associated with addiction but were primarily associated with cancer and disease, reflecting the pharmacological functions of harmane and nicotine. Similar to the findings in self-administration and dopamine release, the synergistic effects of harmane and nicotine produced profound responses in the nucleus accumbens, including nicotine reinforcement and the dopaminergic pathways. Taken together, it can be speculated that with the increase of the dopamine release induced by the synergistic effects of harmane and nicotine, the addiction-related pathways are activated, and self-administration is potentiated (Dayan, 2009; Subramaniyan and Dani, 2015).

DISCUSSION

Our study demonstrated that, at the dose related to human cigarette smoking, (1) nicotine self-administration was potentiated by harmane and reduced at 10× or 0.1× doses; (2) locomotor activity was increased by the synergistic effects of nicotine and harmane; (3) dopamine basal levels and nicotine-induced dopamine release were increased by harmane through MAO-A inhibition; (4) the pathways related to nicotine reinforcement were reinforced by the synergistic effects of nicotine and harmane. These findings suggest that harmane, a non-nicotine component in tobacco products, plays a role in smoking addiction through MAO-A inhibition.

It is worth noting that appropriate doses and approaches were performed compared to previous studies of harmane and other MAO inhibitors-using the dose related to human cigarette smoking and co-injection with nicotine. Excessive doses of harmane inhibited the activity of nucleus accumbens neurons in a previous study (Ergene and Schoener, 1993). The level of harmane to activate neurons in the nucleus accumbens is comparable to the level achieved by cigarette smoke (Talhout et al., 2007). Our study suggests that there exists a dose range of harmane to show strengthening effects. Previous studies used harmane beyond this dose range, where harmane exhibited no effects. Similar to an earlier study of acetaldehyde strengthening nicotine self-administration, the three doses used in the study were only twofold different, causing acetaldehyde to lose its reinforcement. Interestingly, harmane is related to acetaldehyde since acetaldehyde reacts with tryptamine and 5-HT to produce harmane (Talhout et al., 2007). The intake of ethanol also increases harmane. The primary metabolite of ethanol is acetaldehyde (Collins, 1988), indicating that the conversion of ethanol and acetaldehyde into harmane may also be important factors to reinforce nicotine reinforcement.

The effect of MAO-A inhibition may not only directly inhibit MAO-A but can also affect the MAO-A through gene and protein alteration. Previous studies on harmane inhibition of MAO-A were conducted *in vitro*, which were inappropriate since another factor was overlooked - the level of MAO-A. This study demonstrated that subcutaneous injection of smoking-related doses of harmane inhibited rat brain MAO-A activity rather than affected the expressions. Therefore, we not only examined the inhibition of MAO-A by harmane but also examined the effect of harmane on MAO-A levels and proved that harmane only inhibited MAO-A but not the expression of MAO-A. Similar to the inhibition of human brain MAO-A by smoking, the inhibition of harmane on MAO-A at a dose related to smoking is also partial. With the assistance of harmane, nicotine-induced dopamine release increased, and thus nicotine reward was reinforced. Other drugs may become more addictive when combined with harmane as well, since inhibition of MAO-A and drugs involved in the dopaminergic reward pathway may be affected and become an addiction-susceptible state. Future research should provide greater insight into the properties of other substances in cigarette smoke that may significantly affect nicotine reinforcement, even if they are weak or non-addictive.

Interestingly, the combination of harmane and nicotine also affected other pathways. The pathways with neurotransmitters and other addictive substances are enhanced, possibly because harmane inhibiting MAO-A may cause changes in other neurotransmitters, as MAO-A metabolizes dopamine and participates in the metabolism of different neurotransmitters (Shih et al., 1999). Changes in these neurotransmitters may contribute to reinforcing addictive pathways, including nicotine. Glutamatergic (Tzschentke and Schmidt, 2003; Chen et al., 2021), cholinergic (Mansvelder et al., 2003), serotonergic (Dhonnchadha and Cunningham, 2008), and GABAergic (Xi and Stein, 2002) are potentially linked to drug addiction, revealing a reinforcing pathway for co-use of smoking and other addictive drugs. Harmane may inhibit addiction to these substances at high doses, as we found that harmane inhibit the expression of tyrosine hydroxylase (Th). Genes in some disease- and cancer-related pathways are down-regulated, which suggests pharmacological effects of nicotine and harmane.

There are several limitations exist in our studies. Firstly, we do not have a positive control for MAO-A inhibition, as these substances may affect nicotine addiction through other mechanisms and are not present in tobacco products (Lotfipour et al., 2011; Villégier et al., 2011). There are technical barriers to stable regulation of MAO-A activity by gene knockout and knock-in and may affect normal activities in rats (Bortolato et al., 2013; Singh et al., 2013). Secondly, due to the difficulty of *in vivo* detection of MAO-A and basal dopamine levels, these indicators are all detected *in vitro* and cannot reflect the changes of each rat before and after drug injection. Thirdly, the doses we used were based on 3R4F cigarette smoke, which might be different in other tobacco products. Fourthly, although subcutaneous nicotine injection is a common and convenient method of administration, the rate of nicotine uptake is relatively rapid compared with smoking. However, when nicotine is administered by injection, peak brain nicotine levels are significantly lower than those achieved by intravenous injection or smoking (Turner, 1975; Benowitz and Iii, 1984), so higher doses of nicotine were used in rats due to differences in metabolic rates between humans and rats (Gorrod and Jenner, 1975; Clarke and Kumar, 1983; Shoaib et al., 1994; Hukkanen et al., 2005; Matta et al., 2007). Finally, our study demonstrates the potentiation of harmane at the smoking dose, but revealing a maximum effect is time consuming. Despite these limitations, our findings underscore

the importance of examining potential addiction-potentiating substances in tobacco products.

In conclusion, this study demonstrated that harmane, a monoamine oxidase inhibitor of tobacco smoke components, potentiated nicotine self-administration at human smoking-related doses. The involving mechanism of harmane is MAO-A inhibition which increases dopamine level nicotine-induced dopamine release. The nicotine pathway was strengthened by the synergistic effects of harmane and nicotine, which provided evidence of pathway changes contributing to nicotine reinforcement. Taken together, other non-nicotinic ingredients in tobacco products and their underlying mechanisms remain a need for further research, which helps to reveal the mechanism of smoking addiction and the factors that contribute to smoking.

DATA AVAILABILITY STATEMENT

Publicly available datasets were analyzed in this study. This data can be found here: https://ngdc.cncb.ac.cn/gsub/ and the accession number is PRJCA009953 (https://ngdc.cncb.ac.cn/search/?dbId=&q=%20PRJCA009953).

ETHICS STATEMENT

The animal study was reviewed and approved by the Laboratory Animal Management and Ethics Committee of China National Tobacco Quality Supervision and Test Center (Approval Number: CTQTC-SYXK-2021002).

AUTHOR CONTRIBUTIONS

ZD, XL, HC, HH, and QH conceived and designed the experiments. ZD, XL, and HC performed the experiments. ZD performed the data analyses and drafted the manuscript writing. ZD and XL revised the manuscript. All authors have read and approved the manuscript.

FUNDING

This work was supported by grants from the State Bureau Key Projects [Nos. 110202001006 (XX-02), 110202001021 (JY-14), and 110202101018 (XX-04)] and the Young Elite Scientist Sponsorship Program (NO. 502020CR0120).

ACKNOWLEDGMENTS

We thank all the professors and teachers at China National Tobacco Quality Supervision and Test Center. We thank Ping Wu of the National Institute on Drug Dependence for her assistance in our research.

SUPPLEMENTARY MATERIAL

The Supplementary Material for this article can be found online at: https://www.frontiersin.org/articles/10.3389/fnmol.2022.925272/full#supplementary-material

REFERENCES

Adell, A., and Myers, R. D. (1994). Increased alcohol intake in low alcohol drinking rats after chronic infusion of the β-carboline harman into the hippocampus. *Pharmacol. Biochem. Behav.* 49, 949–953. doi: 10.1016/0091-3057(94)90248-8

Arici oglu, F., and Altunbas, H. (2003). Harmane induces anxiolysis and antidepressant-like effects in rats. *Ann. N.Y. Acad. Sci.* 1009, 196–201. doi: 10.1196/annals.1304.024

Arici oglu, F., and Utkan, T. (2003). Inhibitory effect of harmane on morphine-dependent guinea pig ileum. *Ann. N.Y. Acad. Sci.* 1009, 185–189. doi: 10.1196/annals.1304.022

Arici oglu-Kartal, F., Kayır, H., and Uzbay, I. T. (2003). Effects of harman and harmine on naloxone-precipitated withdrawal syndrome in morphine-dependent rats. *Life Sci.* 73, 2363–2371. doi: 10.1016/S0024-3205(03)00647-7

Arnold, M. M., Loughlin, S. E., Belluzzi, J. D., and Leslie, F. M. (2014). Reinforcing and neural activating effects of norharmane, a non-nicotine tobacco constituent, alone and in combination with nicotine. *Neuropharmacology* 85, 293–304. doi: 10.1016/j.neuropharm.2014.05.035

Bacher, I., Houle, S., Xu, X., Zawertailo, L., Soliman, A., Wilson, A. A., et al. (2011). Monoamine oxidase a binding in the prefrontal and anterior cingulate cortices during acute withdrawal from heavy cigarette smoking. *Arch. General Psychiatry* 68, 817–826. doi: 10.1001/archgenpsychiatry.2011.82

Benowitz, N. L. (1992). Cigarette smoking and nicotine addiction. *Med. Clin. Am.* 76, 415–437. doi: 10.1016/S0025-7125(16)30360-1

Benowitz, N. L. (2010). Nicotine addiction. *New Eng. J. Med.* 362, 2295–2303. doi: 10.1056/nejmra0809890

Benowitz, N. L., and Iii, P. J. (1984). Daily intake of nicotine during cigarette smoking. *Clin. Pharmacol. Ther.* 35, 499–504.

Bortolato, M., Godar, S. C., Alzghoul, L., Zhang, J., Darling, R. D., Simpson, K. L., et al. (2013). Monoamine oxidase A and A/B knockout mice display autistic-like features. *Int. J. Neuropsychopharmacol.* 16, 869–888. doi: 10.1017/S1461145712000715

Butcher, S. P., Fairbrother, I. S., Kelly, J. S., and Arbuthnott, G. W. (1990). Effects of selective monoamine oxidase inhibitors on the in vivo release and metabolism of dopamine in the rat striatum. *J. Neurochem.* 55, 981–988. doi: 10.1111/j.1471-4159.1990.tb04587.x

Chen, H., Matta, S. G., and Sharp, B. M. (2007). Acquisition of nicotine self-administration in adolescent rats given prolonged access to the drug. *Neuropsychopharmacology* 32, 700–709. doi: 10.1038/sj.npp.1301135

Chen, L., Yan, H., Wang, Y., He, Z., Leng, Q., Huang, S., et al. (2021). The mechanisms and boundary conditions of drug memory reconsolidation. *Front. Neurosci.* 15, 1–10.

Cho, H.-U., Kim, S., Sim, J., Yang, S., An, H., Nam, M.-H., et al. (2021). Redefining differential roles of MAO-A in dopamine degradation and MAO-B in tonic GABA synthesis. *Exp. Mol. Med.* 53, 1148–1158. doi: 10.1038/s12276-021-00646-3

Clarke, P. B. S., and Kumar, R. (1983). The effects of nicotine on locomotor activity in non-tolerant and tolerant rats. *Br. J. Pharmacol.* 78, 329–337. doi: 10.1111/j.1476-5381.1983.tb09398.x

Clemens, K. J., Caillé, S., and Cador, M. (2010). The effects of response operandum and prior food training on intravenous nicotine self-administration in rats. *Psychopharmacology* 211, 43–54. doi: 10.1007/s00213-010-1866-z

Collins, M. A. (1988). Acetaldehyde and its condensation products as markers in alcoholism. *Recent Dev. Alcoholism* 1988, 387–403. doi: 10.1007/978-1-4615-7718-8_22

Cooper, J. O., Heron, T. E., and Heward, W. L. (2007). *Applied Behavior Analysis*. London: Pearson Education.

Dayan, P. (2009). Dopamine, reinforcement learning, and addiction. *Pharmacopsychiatry* 42, S56–S65. doi: 10.1055/s-0028-1124107

De Biasi, M., and Dani, J. A. (2011). Reward, addiction, withdrawal to nicotine. *Ann. Rev. Neurosci.* 34, 105–130. doi: 10.1146/annurev-neuro-061010-113734

De La Peña, J. B., Ahsan, H. M., Tampus, R., Botanas, C. J., dela Peña, I. J., Kim, H. J., et al. (2015). Cigarette smoke exposure during adolescence enhances sensitivity to the rewarding effects of nicotine in adulthood, even after a long period of abstinence. *Neuropharmacology* 99, 9–14. doi: 10.1016/j.neuropharm.2015.06.014

Dhonnchadha, B. ÁN., and Cunningham, K. A. (2008). Serotonergic mechanisms in addiction-related memories. *Behav. Brain Res.* 195, 39–53. doi: 10.1016/j.bbr.2008.06.026

Di Chiara, G., Bassareo, V., Fenu, S., De Luca, M. A., Spina, L., Cadoni, C., et al. (2004). Dopamine and drug addiction: the nucleus accumbens shell connection. *Neuropharmacology* 47, 227–241. doi: 10.1016/j.neuropharm.2004.06.032

Donny, E. C., Caggiula, A. R., Mielke, M. M., Jacobs, K. S., Rose, C., and Sved, A. F. (1998). Acquisition of nicotine self-administration in rats: the effects of dose, feeding schedule, and drug contingency. *Psychopharmacology* 136, 83–90. doi: 10.1007/s002130050542

Drmanac, R., Sparks, A. B., Callow, M. J., Halpern, A. L., Burns, N. L., Kermani, B. G., et al. (2010). Human genome sequencing using unchained base reads on self-assembling DNA nanoarrays. *Science* 327, 78–81. doi: 10.1126/science.1181498

El Mestikawy, S., Glowinski, J., and Hamon, M. (1986). Presynaptic dopamine autoreceptors control tyrosine hydroxylase activation in depolarized striatal dopaminergic terminals. *J. Neurochem.* 46, 12–22. doi: 10.1111/j.1471-4159.1986.tb12919.x

Ergene, E., and Schoener, E. P. (1993). Effects of harmane (1-methyl-β-carboline) on neurons in the nucleus accumbens of the rat. *Pharmacol. Biochem. Behav.* 44, 951–957. doi: 10.1016/0091-3057(93)90030-W

Fowler, J. S., Volkow, N. D., Wang, G.-J., Pappas, N., Logan, J., Shea, C., et al. (1996a). Brain monoamine oxidase a inhibition in cigarette smokers. *Proc. Natl. Acad. Sci.* 93, 14065–14069. doi: 10.1073/pnas.93.24.14065

Fowler, J. S., Volkow, N. D., Wang, G. J., Pappas, N., Logan, J., MacGregor, R., et al. (1996b). Inhibition of monoamine oxidase B in the brains of smokers. *Nature* 379, 733–736. doi: 10.1038/379733a0

Freeman, G. B., Sherman, K. A., and Gibson, G. E. (1987). Locomotor activity as a predictor of times and dosages for studies of nicotine's neurochemical actions. *Pharmacol. Biochem. Behav.* 26, 305–312. doi: 10.1016/0091-3057(87)90123-7

Garcia, K. L. P., Lê, A. D., and Tyndale, R. F. (2014). Effect of food training and training dose on nicotine self-administration in rats. *Behav. Brain Res.* 274, 10–18. doi: 10.1016/j.bbr.2014.07.043

Gorrod, J. W., and Jenner, P. (1975). The metabolism of tobacco alkaloids. *Essays Toxicol.* 1975, 35–78.

Guillem, K., Vouillac, C., Azar, M. R., Parsons, L. H., Koob, G. F., Cador, M., et al. (2005). Monoamine oxidase inhibition dramatically increases the motivation to self-administer nicotine in rats. *J. Neurosci.* 25, 8593–8600. doi: 10.1523/JNEUROSCI.2139-05.2005

Guillem, K., Vouillac, C., Azar, M. R., Parsons, L. H., Koob, G. F., Cador, M., et al. (2006). Monoamine oxidase a rather than monoamine oxidase B inhibition increases nicotine reinforcement in rats. *Eur. J. Neurosci.* 24, 3532–3540. doi: 10.1111/j.1460-9568.2006.05217.x

Hall, B. J., Wells, C., Allenby, C., Lin, M. Y., Hao, I., Marshall, L., et al. (2014). Differential effects of non-nicotine tobacco constituent compounds on nicotine self-administration in rats. *Pharmacol. Biochem. Behav.* 120, 103–108. doi: 10.1016/j.pbb.2014.02.011

Herraiz, T., and Chaparro, C. (2005). Human monoamine oxidase is inhibited by tobacco smoke: β-carboline alkaloids act as potent and reversible inhibitors. *Biochem. Biophys. Res. Commun.* 326, 378–386. doi: 10.1016/j.bbrc.2004.11.033

Ho, B. T., McIsaac, W. M., Walker, K. E., and Estevez, V. (1968). Inhibitors of monoamine oxidase. influence of methyl substitution on the inhibitory activity of β−carbolines. *J. Pharmaceut. Sci.* 57, 269–274. doi: 10.1002/jps.2600570205

Hukkanen, J., Jacob, P., and Benowitz, N. L. (2005). Metabolism and disposition kinetics of nicotine. *Pharmacol. Rev.* 57, 79–115.

Jaccard, G., Djoko, D. T., Korneliou, A., Stabbert, R., Belushkin, M., and Esposito, M. (2019). Mainstream smoke constituents and in vitro toxicity comparative analysis of 3R4F and 1R6F reference cigarettes. *Toxicol. Rep.* 6, 222–231. doi: 10.1016/j.toxrep.2019.02.009

Jacobs, E. H., De Vries, T. J., Smit, A. B., and Schoffelmeer, A. N. M. (2004). Gene transcripts selectively down-regulated in the shell of the nucleus accumbens long after heroin self-administration are up-regulated in the core independent of response contingency. *FASEB J.* 18, 200–202. doi: 10.1096/fj.03-0317fje

Khan, H., Patel, S., and Kamal, A. (2017). Pharmacological and toxicological profile of harmane-β-carboline alkaloid: friend or foe. *Curr. Drug Metab.* 18, 853–857. doi: 10.2174/1389200218666170607100947

Lewis, A., Miller, J. H., and Lea, R. A. (2007). Monoamine oxidase and tobacco dependence. *Neurotoxicology* 28, 182–195. doi: 10.1016/j.neuro.2006.05.019

Lindgren, N., Xu, Z. Q. D., Herrera-Marschitz, M., Haycock, J., Hökfelt, T., and Fisone, G. (2001). Dopamine D2 receptors regulate tyrosine hydroxylase activity and phosphorylation at Ser40 in rat striatum. *Eur. J. Neurosci.* 13, 773–780.

Lotfipour, S., Arnold, M. M., Hogenkamp, D. J., Gee, K. W., Belluzzi, J. D., and Leslie, F. M. (2011). The monoamine oxidase (MAO) inhibitor tranylcypromine enhances nicotine self-administration in rats through a mechanism independent of MAO inhibition. *Neuropharmacology* 61, 95–104. doi: 10.1016/j.neuropharm.2011.03.007

Ma, H., Reimold, A. E., and Ribisl, K. M. (2022). Trends in cigarette marketing expenditures, 1975-2019: an analysis of federal trade commission cigarette reports. *Nicot. Tobacco Res.* 2022:272. doi: 10.1093/ntr/ntab272

Mansvelder, H. D., De Rover, M., McGehee, D. S., and Brussaard, A. B. (2003). Cholinergic modulation of dopaminergic reward areas: upstream and downstream targets of nicotine addiction. *Eur. J. Pharmacol.* 480, 117–123. doi: 10.1016/j.ejphar.2003.08.099

Marks, M. J., Burch, J. B., and Collins, A. C. (1983). Genetics of nicotine response in four inbred strains of mice. *J. Pharmacol. Exp. Ther.* 226, 291–302.

Matta, S. G., Balfour, D. J., Benowitz, N. L., Boyd, R. T., Buccafusco, J. J., Caggiula, A. R., et al. (2007). Guidelines on nicotine dose selection for in vivo research. *Psychopharmacology* 190, 269–319. doi: 10.1007/s00213-006-0441-0

Meyer, J. H., Ginovart, N., Boovariwala, A., Sagrati, S., Hussey, D., Garcia, A., et al. (2006). Elevated monoamine oxidase a levels in the brain: an explanation for the monoamine imbalance of major depression. *Arch. Gen. Psychiatry* 63, 1209–1216. doi: 10.1001/archpsyc.63.11.1209

Paxinos, G., and Watson, C. (2006). *The Rat Brain In Stereotaxic Coordinates: Hard Cover Edition*. Amsterdam: Elsevier.

Poindexter, E. H. Jr., and Carpenter, R. D. (1962). The isolation of harmane and norharmane from tobacco and cigarette smoke. *Phytochemistry* 1, 215–221. doi: 10.1016/S0031-9422(00)82825-3

Rice, M. E., and Cragg, S. J. (2004). Nicotine amplifies reward-related dopamine signals in striatum. *Nat. Neurosci.* 7, 583–584. doi: 10.1038/nn1244

Rodgman, A., and Perfetti, T. A. (2008). *The Chemical Components Of Tobacco And Tobacco Smoke*. Boca Raton: CRC press.

Rommelspacher, H., Meier-Henco, M., Smolka, M., and Kloft, C. (2002). The levels of norharman are high enough after smoking to affect monoamineoxidase B in platelets. *Eur. J. Pharmacol.* 441, 115–125. doi: 10.1016/s0014-2999(02)01452-8

Rose, J. E. (2006). Nicotine and nonnicotine factors in cigarette addiction. *Psychopharmacology* 184, 274–285. doi: 10.1007/s00213-005-0250-x

Rose, J. E., Behm, F. M., Westman, E. C., and Johnson, M. (2000). Dissociating nicotine and nonnicotine components of cigarette smoking. *Pharmacol. Biochem. Behav.* 67, 71–81. doi: 10.1016/S0091-3057(00)00301-4

Seibenhener, M. L., and Wooten, M. C. (2015). Use of the open field maze to measure locomotor and anxiety-like behavior in mice. *J. Vis. Exp.* 96:e52434. doi: 10.3791/52434

Shih, J. C., Chen, K., and Ridd, M. J. (1999). Role of MAO A and B in neurotransmitter metabolism and behavior. *Polish J. Pharmacol.* 51, 25–29.

Shoaib, M., Stolerman, I. P., and Kumar, R. C. (1994). Nicotine-induced place preferences following prior nicotine exposure in rats. *Psychopharmacology* 113, 445–452. doi: 10.1007/BF02245221

Singh, C., Bortolato, M., Bali, N., Godar, S. C., Scott, A. L., Chen, K., et al. (2013). Cognitive abnormalities and hippocampal alterations in monoamine oxidase

A and B knockout mice. *Proc. Natl. Acad. Sci. U.S.A.* 110, 12816–12821. doi: 10.1073/pnas.1308037110

Smith, T. T., Rupprecht, L. E., Cwalina, S. N., Onimus, M. J., Murphy, S. E., Donny, E. C., et al. (2016). Effects of monoamine oxidase inhibition on the reinforcing properties of low-dose nicotine. *Neuropsychopharmacology* 41, 2335–2343. doi: 10.1038/npp.2016.36

Sorge, R. E., Pierre, V. J., and Clarke, P. (2009). Facilitation of intravenous nicotine self-administration in rats by a motivationally neutral sensory stimulus. *Psychopharmacology* 207, 191–200. doi: 10.1007/s00213-009-1647-8

Subramaniyan, M., and Dani, J. A. (2015). Dopaminergic and cholinergic learning mechanisms in nicotine addiction. *Ann. N.Y. Acad. Sci.* 1349, 46–63. doi: 10.1111/nyas.12871

Talhout, R., Opperhuizen, A., and van Amsterdam, J. G. C. (2007). Role of acetaldehyde in tobacco smoke addiction. *Eur. Neuropsychopharmacol.* 17, 627–636. doi: 10.1016/j.euroneuro.2007.02.013

Turner, D. M. (1975). Influence of route of administration on metabolism of [14C] nicotine in four species. *Xenobiotica* 5, 553–561. doi: 10.3109/00498257509056125

Tzschentke, T. M., and Schmidt, W. J. (2003). Glutamatergic mechanisms in addiction. *Mol. Psychiatry* 8, 373–382. doi: 10.1038/sj.mp.4001269

Valentine, J. D., Hokanson, J. S., Matta, S. G., and Sharp, B. M. (1997). Self-administration in rats allowed unlimited access to nicotine. *Psychopharmacology* 133, 300–304. doi: 10.1007/s002130050405

van der Toorn, M., Koshibu, K., Schlage, W. K., Majeed, S., Pospisil, P., Hoeng, J., et al. (2019). Comparison of monoamine oxidase inhibition by cigarettes and modified risk tobacco products. *Toxicol. Rep.* 6, 1206–1215. doi: 10.1016/j.toxrep.2019.11.008

Villégier, A. S., Belluzzi, J. D., and Leslie, F. M. (2011). Serotonergic mechanism underlying tranylcypromine enhancement of nicotine self-administration. *Synapse* 65, 479–489. doi: 10.1002/syn.20864

Villégier, A.-S., Blanc, G., Glowinski, J., and Tassin, J.-P. (2003). Transient behavioral sensitization to nicotine becomes long-lasting with monoamine oxidases inhibitors. *Pharmacol. Biochem. Behav.* 76, 267–274. doi: 10.1016/s0091-3057(03)00223-5

Villégier, A.-S., Salomon, L., Granon, S., Changeux, J.-P., Belluzzi, J. D., Leslie, F. M., et al. (2006). Monoamine oxidase inhibitors allow locomotor and rewarding responses to nicotine. *Neuropsychopharmacology* 31, 1704–1713. doi: 10.1038/sj.npp.1300987

Weiss, M. J. (2013). "Fixed ratio," in *Encyclopedia of Autism Spectrum Disorders*, ed. F. R. Volkmar (New York, NY: Springer New York), 1298–1299.

Weyler, W., Hsu, Y.-P. P., and Breakafield, X. O. (1990). Biochemistry and genetics of monoamine oxidase. *Pharmacol. Ther.* 47, 391–417. doi: 10.1016/0163-7258(90)90064-9

Whiteaker, P., Garcha, H. S., Wonnacott, S., and Stolerman, I. P. (1995). Locomotor activation and dopamine release produced by nicotine and isoarecolone in rats. *Br. J. Pharmacol.* 116:2097. doi: 10.1111/j.1476-5381.1995.tb16417.x

Xi, Z.-X., and Stein, E. A. (2002). GABAergic mechanisms of opiate reinforcement. *Alcoholism* 37, 485–494. doi: 10.1093/alcalc/37.5.485

Conflict of Interest: The authors declare that the research was conducted in the absence of any commercial or financial relationships that could be construed as a potential conflict of interest.

Publisher's Note: All claims expressed in this article are solely those of the authors and do not necessarily represent those of their affiliated organizations, or those of the publisher, the editors and the reviewers. Any product that may be evaluated in this article, or claim that may be made by its manufacturer, is not guaranteed or endorsed by the publisher.

frontiers | Frontiers in Molecular Neuroscience

ORIGINAL RESEARCH
published: 27 June 2022
doi: 10.3389/fnmol.2022.932939

Inhibition of Glycogen Synthase Kinase 3β Activity in the Basolateral Amygdala Disrupts Reconsolidation and Attenuates Heroin Relapse

*Yuanyang Xie[1,2], Yingfan Zhang[3], Ting Hu[1,2], Zijin Zhao[1,2], Qing Liu[1,2] and Haoyu Li[1,2]**

[1] Department of Neurosurgery, Xiangya Hospital, Central South University, Changsha, China, [2] The Institute of Skull Base Surgery and Neurooncology at Hunan Province, Changsha, China, [3] Teaching and Research Section of Clinical Nursing, Xiangya Hospital, Central South University, Changsha, China

OPEN ACCESS

Edited by:
Jianfeng Liu,
Texas A&M University, United States

Reviewed by:
Yingjie Zhu,
Shenzhen Institutes of Advanced Technology (CAS), China
Yixiao Luo,
Hunan Normal University, China

***Correspondence:**
Haoyu Li
haoyu.li@csu.edu.cn

Specialty section:
This article was submitted to Molecular Signalling and Pathways, a section of the journal Frontiers in Molecular Neuroscience

Received: 30 April 2022
Accepted: 06 June 2022
Published: 27 June 2022

Citation:
Xie Y, Zhang Y, Hu T, Zhao Z, Liu Q and Li H (2022) Inhibition of Glycogen Synthase Kinase 3β Activity in the Basolateral Amygdala Disrupts Reconsolidation and Attenuates Heroin Relapse. Front. Mol. Neurosci. 15:932939. doi: 10.3389/fnmol.2022.932939

Exposure to a heroin-associated conditioned stimulus can reactivate drug reward memory, trigger drug cravings, and induce relapse in heroin addicts. The amygdala, a brain region related to emotions and motivation, is involved in processing rewarding stimulus. Recent evidence demonstrated that disrupting the reconsolidation of the heroin drug memories attenuated heroin seeking which was associated with the basolateral amygdala (BLA). Meanwhile, neural functions associated with learning and memory, like synaptic plasticity, are regulated by glycogen synthase kinase 3 beta (GSK-3β). In addition, GSK-3β regulated memory processes, like retrieval and reconsolidation of cocaine-induced memory. Here, we used a heroin intravenous self-administration (SA) paradigm to illustrate the potential role of GSK-3β in the reconsolidation of drug memory. Therefore, we used SB216763 as a selective inhibitor of GSK-3β. We found that injecting the selective inhibitor SB216763 into the BLA, but not the central amygdala (CeA), immediately after heroin-induced memory retrieval disrupted reconsolidation of heroin drug memory and significantly attenuated heroin-seeking behavior in subsequent drug-primed reinstatement, suggesting that GSK-3β is critical for reconsolidation of heroin drug memories and inhibiting the activity of GSK-3β in BLA disrupted heroin drug memory and reduced relapse. However, no retrieval or 6 h after retrieval, administration of SB216763 into the BLA did not alter heroin-seeking behavior in subsequent heroin-primed reinstatement, suggesting that GSK-3β activity is retrieval-dependent and time-specific. More importantly, a long-term effect of SB216763 treatment was observed in a detectable decrease in heroin-seeking behavior, which lasted at least 28 days. All in all, this present study demonstrates that the activity of GSK-3β in BLA is required for reconsolidation of heroin drug memory, and inhibiting GSK-3β activity of BLA disrupts reconsolidation and attenuates heroin relapse.

Keywords: addiction, heroin, amygdala, reconsolidation, GSK-3β, self-administration

INTRODUCTION

Opioid use disorder is a chronic recurrent brain disease caused by abnormal learning and memory patterns. And the symptom is the loss of substance use control. Drug-associated cues are important factors to promote the relapse to drug use. In addiction animal models, cues related to drug abuse can promote relapse (Davis and Smith, 1976; Dymshitz and Lieblich, 1987; Di Ciano and Everitt, 2004; Anker and Carroll, 2010). Once drug use occurs, it is possible to form the association between cues and reward-related memory that is not easily disrupted.

Same as other types of memories (Nader et al., 2000; Milekic and Alberini, 2002; Morris et al., 2006; Piva et al., 2019), drug reward memory experiences the process of acquisition, consolidation, retrieval, and reconsolidation. Once a consolidated drug memory is reactivated, it becomes unstable, allowing for modification or destruction by different treatments (Miller and Marshall, 2005; Lee et al., 2006; Wang et al., 2008; Lee, 2009; Li et al., 2010). The role of reconsolidation is critical in stabilizing the reactivated memory, involving de novo protein synthesis (Nader et al., 2000). Reconsolidation provides a time window, during which is expected to modify or even eliminate drug memory. Thus, disrupting reconsolidation of addiction memory is considered to be an effective measure of preventing relapse and drug seeking.

A large amount of evidence shows that pharmacological interventions disrupting reconsolidation of drug-reward memory are effective in relapse prevention. Using a conditioned place preference (CPP) or self-administration (SA) animal model, propranolol or rapamycin has been shown to effectively interfere with reconsolidation of drug memory and attenuate drug-seeking behavior (Lin et al., 2014; Xue et al., 2017; Chen et al., 2021; Zhang et al., 2021).

Glycogen synthase kinase-3 (GSK-3), a serine/threonine-protein kinase expressed widely in the mammalian brain, has essential roles in physiological activities like development, cell cycle, or apoptosis (Jope and Johnson, 2004; Medina et al., 2011). GSK-3β is a isoform of GSK-3, extensively involved in memory processing. The regulation of GSK-3β can affect neural functions like synaptic plasticity, which is the foundation of learning and memory (Banach et al., 2022; Li et al., 2022; Marosi et al., 2022). Also, GSK-3β regulates the structural and functional synaptic plasticity. GSK-3β deficient mice marked that memory reconsolidation and their ability to form long-term memories were impaired, suggesting that GSK-3β is important for normal brain function (O'Brien et al., 2004; Kimura et al., 2008; Kaidanovich-Beilin et al., 2009; Maurin et al., 2013). It has been detected that GSK-3β Ser21/9 phosphorylation levels changed during long-term potentiation (LTP) or long-term depression (LTD), which were essential for memory (Hooper et al., 2007; Peineau et al., 2007). For example, GSK-3β affects long-term memory formation as it promotes LTD by inhibitory phosphorylation of Serine-9 in inhibitory avoidance and novel object recognition test (Dewachter et al., 2009). The removal of GSK-3β in excitatory neurons of dentate gyrus reduced the synaptic transmission of hippocampus and decreased the expression of synaptic proteins like N-methyl-D-aspartate receptor (NMDAR) and anti-alpha-amino-3-hydroxy-5-methyl-4-isoxazolepropinoic receptor (AMPAR), impairing the formation of spatial and fear memories (Liu et al., 2017). Cocaine administration for 14 days could obviously reduce the phosphorylation of GSK-3β in the amygdala (Perrine et al., 2008). Hippocampal GSK-3β was activated during memory retrieval progress in the passive avoidance task (Hong et al., 2012). Memory retrieval activates hippocampal GSK-3β, and memory reconsolidation is impaired by a GSK-3 inhibitor systemically administration before memory retrieval (Kimura et al., 2008; Hong et al., 2012). Knockdown GSK-3β of ventral hippocampal displays a developmental reduction in cocaine-CPP, while not in morphine-CPP (Barr et al., 2020). Wu et al. (2011) directionally inhibited GSK-3β in the BLA immediately after the retrieval of drug cue memories to reduce the subsequent cocaine-seeking behavior (Wu et al., 2011). It has been shown that GSK-3β signaling pathway participated in the reconsolidation of cocaine-induced CPP.

However, whether the inhibition of GSK-3β in BLA could disrupt reconsolidation and prevent drug seeking and relapse in heroin SA animal model remains unknown. In our present study, we inhibited the activity of GSK-3β in the BLA to identify the effects of GSK-3β on reconsolidation of heroin cue memory in SA animal model. Amygdala plays a critical role in both cue-associated learning and the expression of cue-induced relapse of drug-seeking behavior (Luo et al., 2013), and also mediates the reconsolidation of aversive or appetitive memories (McGaugh, 2004; Díaz-Mataix et al., 2013; Nader, 2015; Björkstrand et al., 2016; Haubrich et al., 2020; Higginbotham et al., 2021; Yan et al., 2021). So we chose it as a targeted brain region to deliver SB216763. The role of GSK-3β activity in amygdala on reconsolidation of heroin cue memory was assessed by the heroin self-administration paradigm. More importantly, the long-term inhibitory effects of GSK-3β activity inhibition on reconsolidation of heroin cue memory were also tested.

MATERIALS AND METHODS

Subjects

We housed the Sprague Dawley rats (male, 7-8 weeks of age on arrival) five-per-cage in a 26°C and 60% humidity room and the cycle was 12-h- light/dark (8 a.m.–8 p.m.). Food and water were provided ad libitum. For the animal better adapted to operator, we performed a 5-day grasp-stroking adaptation procedure 3 min per day on experimental animals before the surgeries. All animal procedures and operations were carried out with the approval of the Xiangya Hospital Ethics Committee, Xiangya Hospital (Changsha, China). At the dark phase (8 a.m.–8 p.m.), the experiments were performed.

Intravenous Surgery

Surgery was performed when the rats' weight reaches 300–320 g. We used the sodium pentobarbital (60 mg/kg, i.p.) to anesthetize rats. The right jugular was exposed by surgery, then inserted an aseptic catheter into it (Lu et al., 2005; Ambroggi et al., 2008).

The catheter passed under the skin of the neck and through the skin of the head and was fixed to the rat's skull with dental acrylic. Heparinized saline (30 USP heparin/saline; Hospira) was infused into the intravenous catheters per 2 days to prevent clogging. After surgery, rats undergo a 7-day recovery period and their weight should remain constant.

Cannulae Implantation

Guide cannulae was implanted 1 mm above the BLA or CeA bilaterally after the rats (300–320 g) were anesthetized by using the sodium pentobarbital (60 mg/kg, i.p.). And the coordinate of BLA (Wu et al., 2011) were the following: anterior/posterior: –2.9 mm and medial/lateral: ± 5.0 mm from bregma, dorsal/ventral: –8.5 mm from the surface of the skull. The coordinates for the CeA were the following: anterior/posterior: –2.9 mm and medial/lateral: ± 4.2 mm from bregma, dorsal/ventral: –7.8 mm from the surface of the skull. And the guide cannulae was anchored by the stainless steel screws and dental cement. After surgery, rats undergo a 5–7 days' recovery period.

Intracranial Injections

The injection of SB216763 was based on a previous report by some minor changes (Xu et al., 2009). The BLA or CeA (0.5 μL/side) was received drug delivery by a microinjection pump with a rat of 0.5 μL/min. The injection time was no more than one minute. To ensure that the drug is fully administered and fully diffused, wait for more than 1 min to withdraw the needle after administration. Nissl staining was used to verify the cannula placements. A schematic diagram of the injection site in the BLA or CeA is shown in **Figure 1**.

Behavioral Procedures

Intravenous Heroin Self-Administration (SA) Training

Following the study of Ye et al. (2017), we established an intravenous SA training session experimental conditions were slightly modified. The operant chambers (AniLab Scientific Instruments Co., Ltd., China) used in this experiment were equipped with two nosepoke sensors, which were 5 cm high from the installation floor. The nosepoke sensors could record the number of animals' nosepokes. The number of nosepoke recorded by the sensor in the left side operandum was defined as "active." Nosepokes in "active" would lead to intravenous heroin administration with a 5 s tone-light cue synchronization. Corresponding to "active," the sensor operandum recorded the number of "inactive" nosepoke in the right side. "Inactive" nosepokes had no programmed consequences.

We trained rats to adapt the intravenous heroin self-administration (0.05 mg/kg/infusion) for 10 days. In the training sessions, rats have been trained for three 1-h daily training sessions and every training session was separated by 5 min. The training of rats using a fixed ratio 1 (FR1) reinforcement program up to 40 s. In 10-day training program, rats were received three 1-h heroin infusions intravenously (0.05 mg/kg/infusion) per day, each infusion separated 5 min. All heroin infusions were completed by an injection pump loading a 10 ml syringe. Each training companied a house light illuminated until the end. When rats were at the left nosepoke (active), the maneuver results in an intravenous heroin infusion with a 5 s tone-light cue synchronization. However, the inactive nosepokes had no consequences. To prevent animals' from death due to overdose, the drug infusions degree was restricted to 20 times/h (Xue et al., 2012; Luo et al., 2015). Some rats (n = 11) were excluded from the experiments: five rats died in intravenous surgery and six rats can't form a stable heroin self-administration.

Nosepoke Extinction

After the drug self-administration session, a 3-h daily nosepoke extinction training was followed. In extinction training (Experiments 1–4), the nosepoke behavior of rats to the sensor resulted in no programmed consequences like heroin intravenous delivery, tone-light cues. When at the last three self-administration sessions, the number of active nosepoke responding decreased at least 80% compared with the self-administration, the nosepoke extinction session was ended.

Heroin Memory Retrieval Trial

In Experiments 1, 2, and 4, the heroin-associated memories were reacted by performing a 15 min retrieval trial. The conditions of the retrieval session were the same as the SA training session, except that when rats got the "active" sensor, no reward heroin was infusion.

Cue Extinction

In Experiments 1, 3, and 4, a cue extinction session, which 3-h per day, was performed on rats. The conditions of the cue extinction session were the same as that SA training session. But after the cue (tone/light) rendering, there was no heroin intravenous delivery.

Cue-Induced Reinstatement of Drug-Seeking (Experiments 1–4)

After the SB216763 or vehicle administration (intracranial injections into BLA or CeA), rats got rest for 24 h and then returned to the SA training context and the reinstatement test was performed. In this session, the number of active and inactive nosepokes was recorded for 1 hr. The test condition was the same as the heroin memory retrieval trial.

Heroin-Induced Reinstatement Test (Experiments 1, 3, and 4)

A low dose of heroin (0.25 mg/kg, s.c.) was delivered to rats 5 min earlier before the session started, then put rats in the SA training context. Through the two sensors, the number of two type nosepokes ("active" and "inactive") was recorded during the test. The reinstatement test lasted for 1 h. The test condition was the same as the heroin memory retrieval trial.

Spontaneous Recovery Test (Experiment 2)

In this test, after 28 days of the withdrawal phase, two types of nosepokes ("active" and "inactive") were recorded for 1 h. The test condition was the same as the heroin memory retrieval trial.

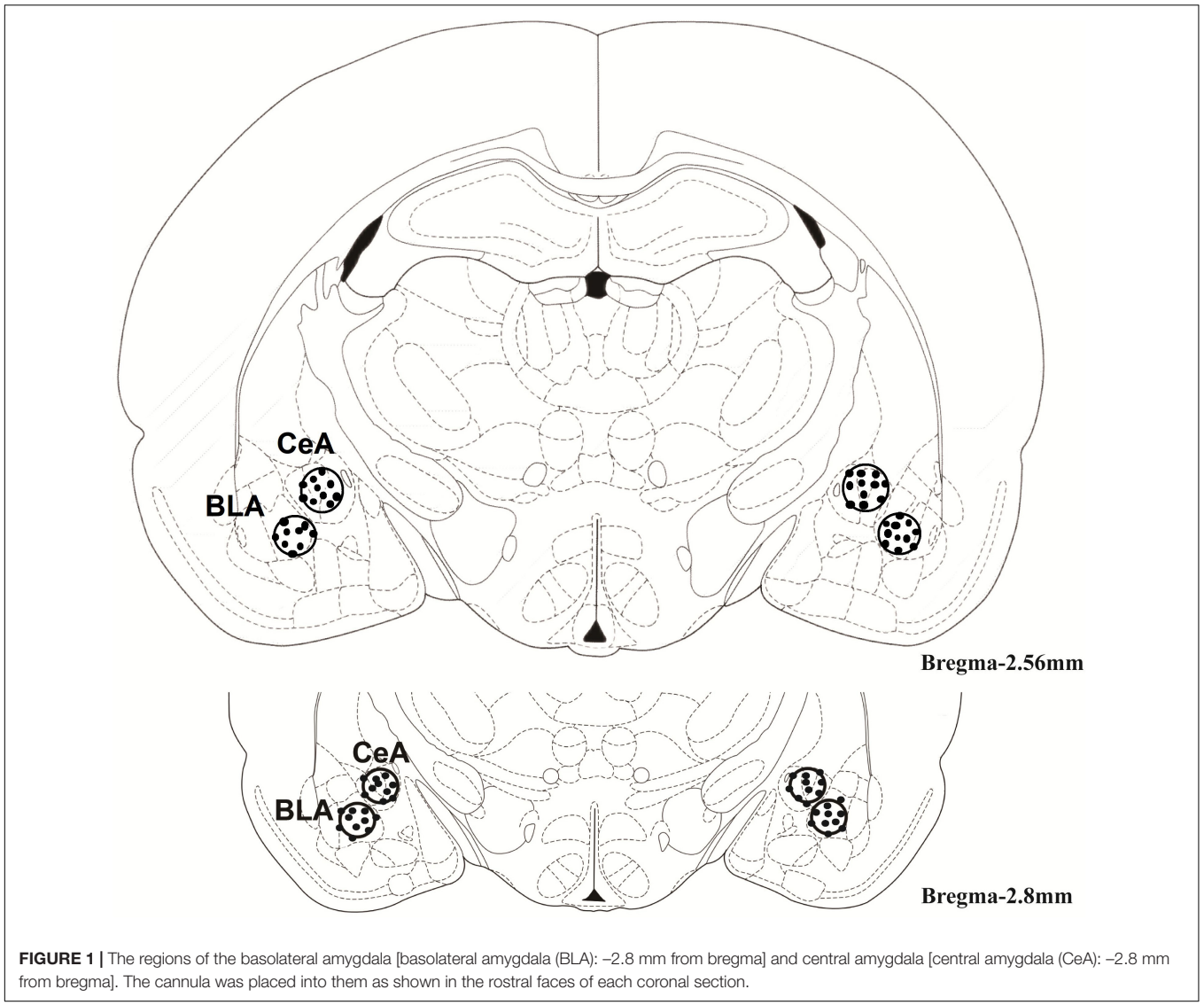

FIGURE 1 | The regions of the basolateral amygdala [basolateral amygdala (BLA): –2.8 mm from bregma] and central amygdala [central amygdala (CeA): –2.8 mm from bregma]. The cannula was placed into them as shown in the rostral faces of each coronal section.

Experimental Design

Experiment 1: The Effect of Immediate Post-CS Retrieval SB216763 Treatment on Subsequent Heroin-Seeking Behavior

Through 10 days of heroin SA training, nosepoke extinction training was followed in the same apparatus for 10 consecutive days. After nosepoke extinction training, rats were allowed a rest for 24 h, then rats were received a 15-min conditioned stimulus (CS) retrieval session. After CS exposure, the rats were divided into four groups: (1) Intracranial injection of vehicle into BLA (0.5 μL/side) immediate after the retrieval trial (BLA+vehicle); (2) Intracranial injection of SB216763 into BLA (0.5 μL/side) immediate after a 15 min retrieval test (BLA+SB216763); (3) Intracranial injection of vehicle into CeA (0.5 μL/side) immediate after a 15 min retrieval test (CeA+vehicle); (4) Intracranial injection of SB216763 into CeA (0.5 μL/side) immediate after a 15 min retrieval test (CeA+SB216763). On Day 23, the rats were performed a cue-induced reinstatement test to explore the effect of SB216763 on heroin drug memory. Subsequently, the two-day cue extinction session was carried out. On Day 26, heroin priming-induced reinstatement was tested in rats (**Figure 2A**).

Experiment 2: The Lasting and Long-Term Effect of Immediate Post-CS Retrieval SB216763 Treatment on Cue-Induced Reinstatement Test and Spontaneous Recovery 28 Days Later

After CS exposure, the rats were divided into four groups: (1) Intracranial administration of vehicle into BLA (0.5 μL/side) immediate after a 15 min retrieval trial (BLA+vehicle); (2) Intracranial injection of SB216763 into BLA (0.5 μL/side) immediate after a 15 min retrieval trial (BLA+SB216763); (3) Intracranial injection of the

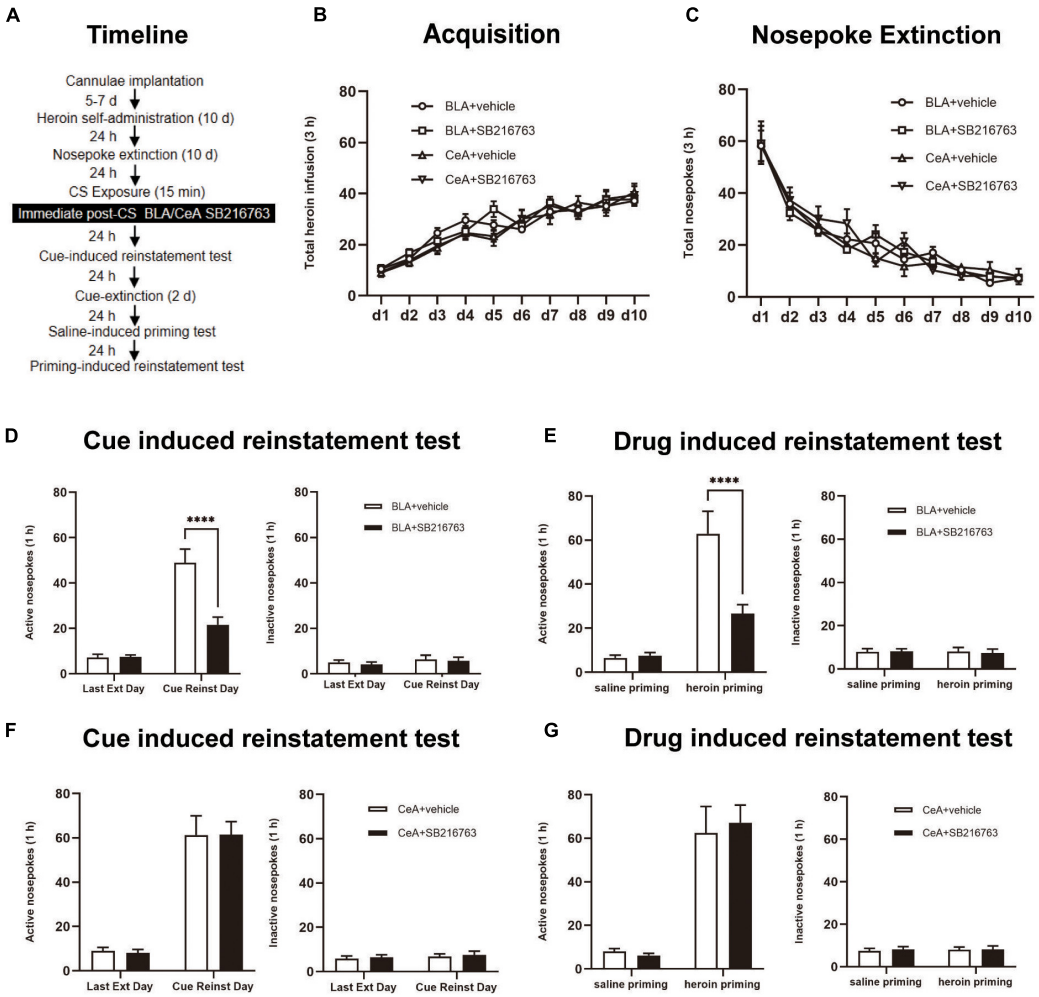

FIGURE 2 | Immediate post-CS SB216763 treatment in BLA rather than CeA can reduce subsequent cue-induced and heroin-primed reinstatement of heroin seeking. **(A)** Timeline of heroin self-administration, nosepoke extinction, cue-induced reinstatement test and drug-induced reinstatement test. **(B)** Total number of heroin infusions during acquisition of heroin self-administration. **(C)** Total number of active nosepoke responses during extinction training sessions. **(D,F)** Active (left) and inactive (right) nosepoke responses during the last extinction training session and the cue-induced reinstatement test. **(D)** Nosepoke responses of rats with BLA drug injection. **(F)** Nosepoke responses of rats with CeA drug injection. **(E,G)** Active (left) and inactive (right) nosepoke responses across the saline- or heroin-primed reinstatement test. **(E)** Nosepoke responses of rats with BLA drug injection. **(G)** Nosepoke responses of rats with CeA drug injection. n = 10–11 mice per group. Data are means ± SEM, ****$p < 0.0001$, compared with the vehicle group. CS, conditioned stimulus; Ext, extinction; Reinst, reinstatement.

vehicle into CeA (0.5 μL/side) immediate after a 15 min retrieval trial (CeA+vehicle); (4) Intracranial injection of SB216763 into CeA(0.5 μL/side) immediate after a 15 min retrieval (CeA+SB216763). Rats were received a cue-induced reinstatement test after a 24 h rest. After 28 days of abstinence, to access the long-term effect of SB216763 on heroin-seeking behavior, a spontaneous recovery test was carried out (**Figure 3A**).

Experiments 3 A and B: The Effect of SB216763 Treatment on Subsequent Heroin-Seeking Behavior Without CS Exposure

The experimental procedure was the same as Experiment 1, except that no CS exposure session to reactivate heroin cue memories (**Figure 4A**).

Experiment 4: The Effect of Delayed Post-CS Retrieval SB216763 Treatment

The rats were received treatment of SB216763 delayed for 6 h after the retrieval session, and other parts of the experiment were the same as Experiment 1 (**Figure 5A**).

Statistical Analysis

We used the repeated-measures ANOVAs to analyze the data with the between-subjects factor of treatment condition and within-subjects factor of test condition, followed by Tukey's *post-hoc test* in each experiment (see Results). All values of experiments were presented as mean ± SEM and data analysis was done on GraphPad, v.9.0. p values < 0.05 were considered statistically significant.

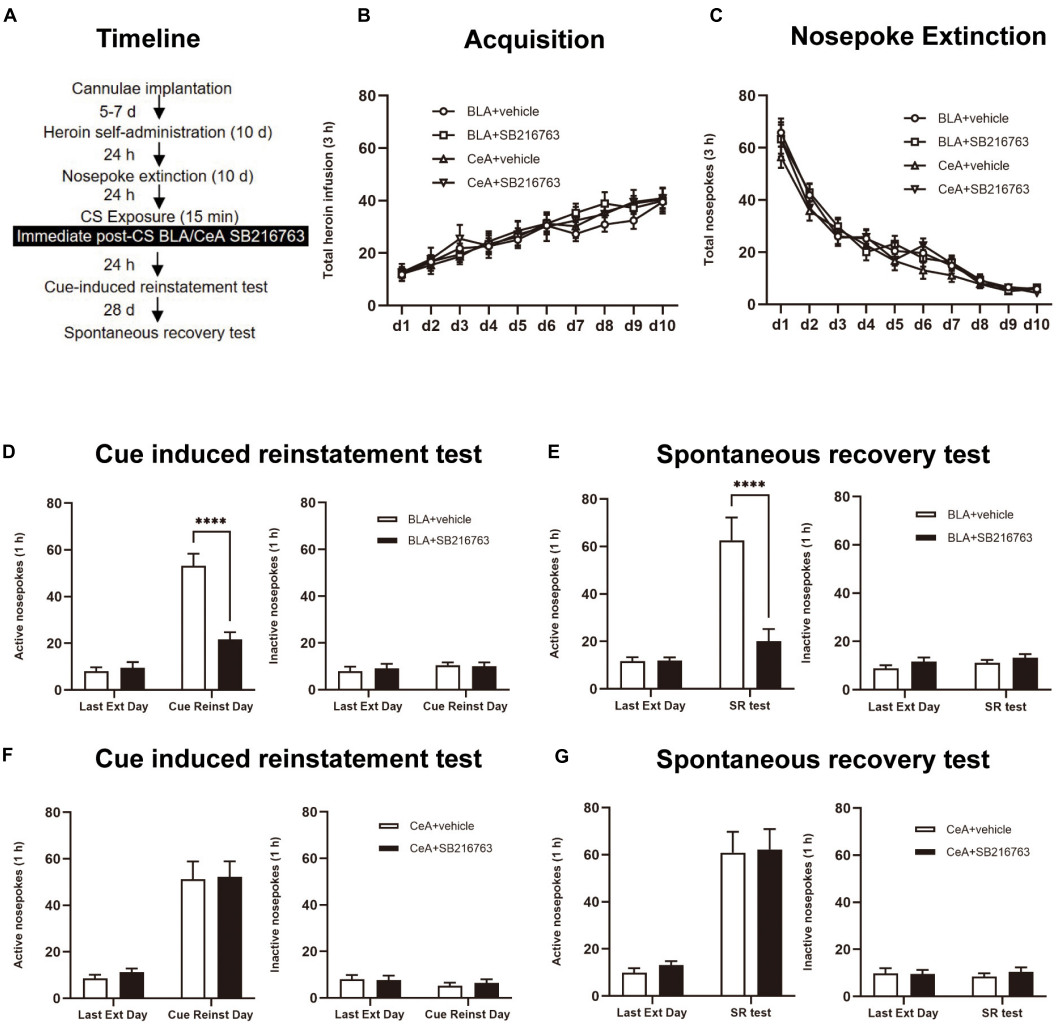

FIGURE 3 | Immediate post-CS SB216763 treatment in BLA rather than CeA can reduce subsequent cue-induced heroin seeking and the spontaneous recovery of heroin seeking. **(A)** Timeline of heroin self-administration, nosepoke extinction, cue-induced reinstatement test and spontaneous recovery test. **(B)** Total number of heroin infusions during acquisition of heroin self-administration. **(C)** Total number of active nosepoke responses during extinction training sessions. **(D,F)** Active (left) and inactive (right) nosepoke responses during the last extinction training session and the cue-induced reinstatement test. **(D)** Nosepoke responses of rats with BLA drug injection. **(F)** Nosepoke responses of rats with CeA drug injection. **(E,G)** Active (left) and inactive (right) nosepoke responses across the last extinction training session and spontaneous recovery test. **(E)** Nosepoke responses of rats with BLA drug injection. **(G)** Nosepoke responses of rats with CeA drug injection. $n = 10$ mice per group. Data are means ± SEM, $^{****}p < 0.0001$, compared with the vehicle group. CS, conditioned stimulus; Ext, extinction; Reinst, reinstatement; SR, spontaneous recovery.

RESULTS

Experiment 1: Immediate Post-CS SB216763 Treatment in BLA Rather Than CeA Can Reduce Subsequent Cue-Induced and Heroin-Primed Reinstatement of Heroin Seeking

We tested the influences of post-retrieval BLA and CeA SB216763 injection on reinstatement of heroin seeking which was cue-induced or heroin-induced by using four groups of rats (**Figure 2A**). In the acquisition session, there were no significant differences between groups of BLA injected with vehicle ($N = 10$) or SB216763 ($N = 11$) and groups of CeA treated with vehicle ($N = 10$) or SB216763 ($N = 11$) which were shown by the heroin infusion numbers [main effect of acquisition time: $F_{(9,342)} = 81.35$, $p < 0.0001$; administration condition: $F_{(3,38)} = 0.2803$, $p = 0.8393$; acquisition time × administration condition interaction: $F_{(27,342)} = 1.443$, $p = 0.0744$; **Figure 2B**]. As the numbers of nosepokes showed, groups did not significantly differ from each other in the extinction session [main effect of extinction time: $F_{(9,342)} = 95.68$, $p < 0.0001$; administration condition: $F_{(3,38)} = 0.092$, $p = 0.9640$; extinction time × administration condition interaction: $F_{(27,342)} = 0.8897$, $p = 0.6274$; **Figure 2C**].

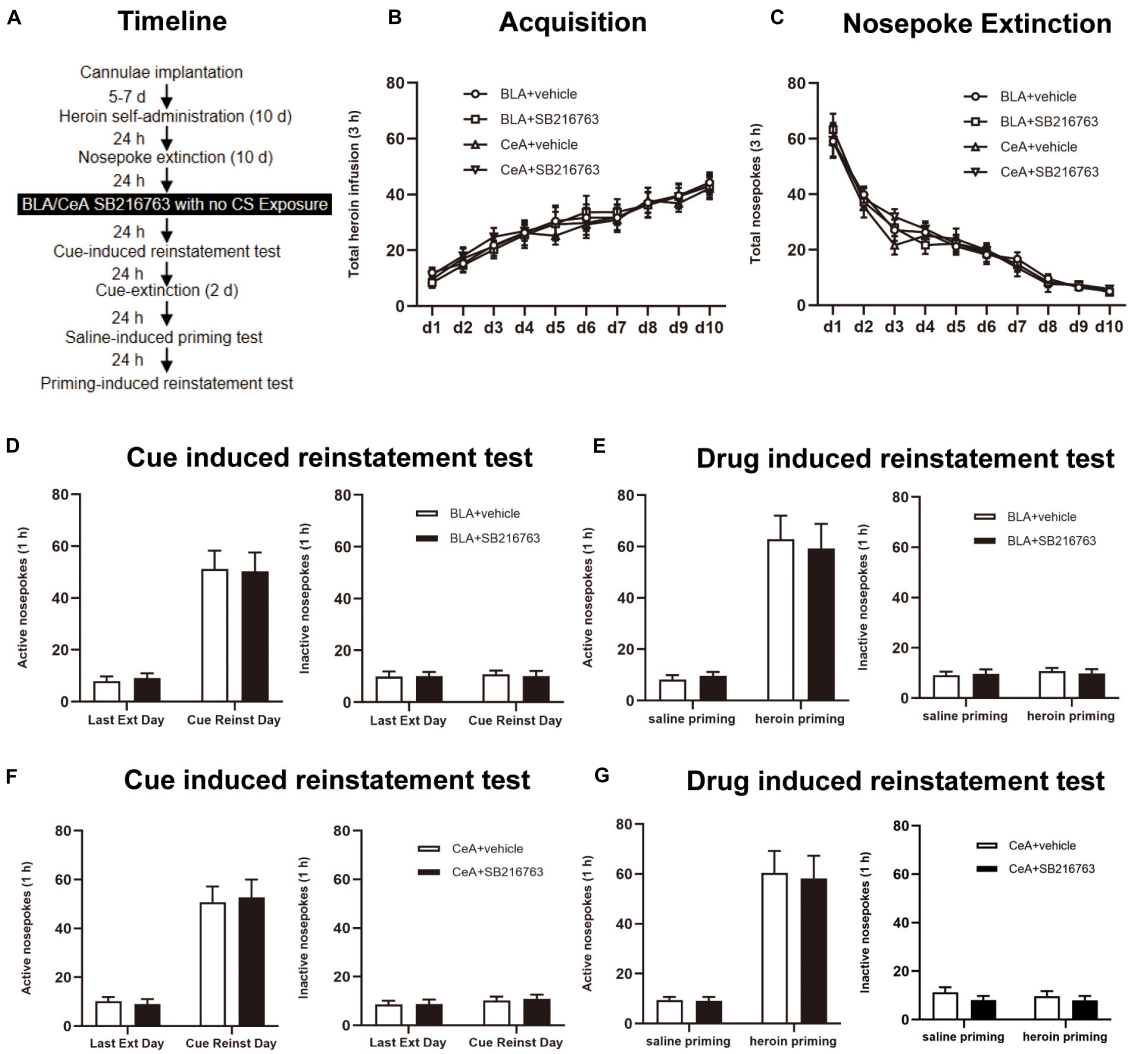

FIGURE 4 | SB216763 treatment without CS retrieval does not affect subsequent cue-induced and heroin-primed reinstatement of heroin seeking. **(A)** Timeline of heroin self-administration, nosepoke extinction, cue-induced reinstatement test and drug-induced reinstatement test. **(B)** Total number of heroin infusions during acquisition of heroin self-administration. **(C)** Total number of active nosepoke responses during extinction training sessions. **(D,F)** Active (left) and inactive (right) nosepoke responses during the last extinction training session and the cue-induced reinstatement test. **(D)** Nosepoke responses of rats with BLA drug injection. **(F)** Nosepoke responses of rats with CeA drug injection. **(E,G)** Active (left) and inactive (right) nosepoke responses across the saline- or heroin- primed reinstatement test. **(E)** Nosepoke responses of rats with BLA drug injection. **(G)** Nosepoke responses of rats with CeA drug injection. *n* = 10 mice per group. Data are means ± SEM. CS, conditioned stimulus; Ext, extinction; Reinst, reinstatement.

In active nosepokes, BLA+vehicle and BLA+SB216763 groups were significantly different in cue-induced reinstatement test [main effect of trial condition: $F_{(1,37)} = 65.71$, $p < 0.0001$; administration condition: $F_{(1,37)} = 15.47$, $p = 0.0004$; trial condition × administration condition interaction: $F_{(1,37)} = 16.05$, $p = 0.0003$]. In cue-induced reinstatement test, the *post-hoc* test revealed a reduction significantly in active side nosepokes of BLA+SB216763 group compared to that BLA+vehicle ($p < 0.001$) (**Figure 2D** left), while there was no obvious difference in the inactive side [main effect of trial condition: $F_{(1,19)} = 1.187$, $p = 0.2895$; administration condition: $F_{(1,19)} = 0.2169$, $p = 0.6467$; trial condition × administration condition interaction: $F_{(1,19)} = 0.0156$, $p = 0.9020$; **Figure 2D** right]. While in the cue-induced reinstatement test of the CeA+vehicle and CeA+SB216763 groups, no significant differences were found in active side [main effect of trial condition: $F_{(1,38)} = 101.4$, $p < 0.0001$; administration condition: $F_{(1,38)} = 0.0052$, $p = 0.9432$; trial condition × administration condition interaction: $F_{(1,38)} = 0.0140$, $p = 0.9063$; **Figure 2F** left] and the inactive side [main effect of trial condition: $F_{(1,19)} = 0.7022$, $p = 0.4125$; administration condition: $F_{(1,19)} = 0.1727$, $p = 0.6824$; trial condition × administration condition interaction: $F_{(1,19)} = 0.0065$, $p = 0.9368$; **Figure 2F** right]. In addition, in drug-induced reinstatement test, active nosepokes significantly differed in BLA+vehicle and BLA+SB216763 groups [main effect of trial condition:

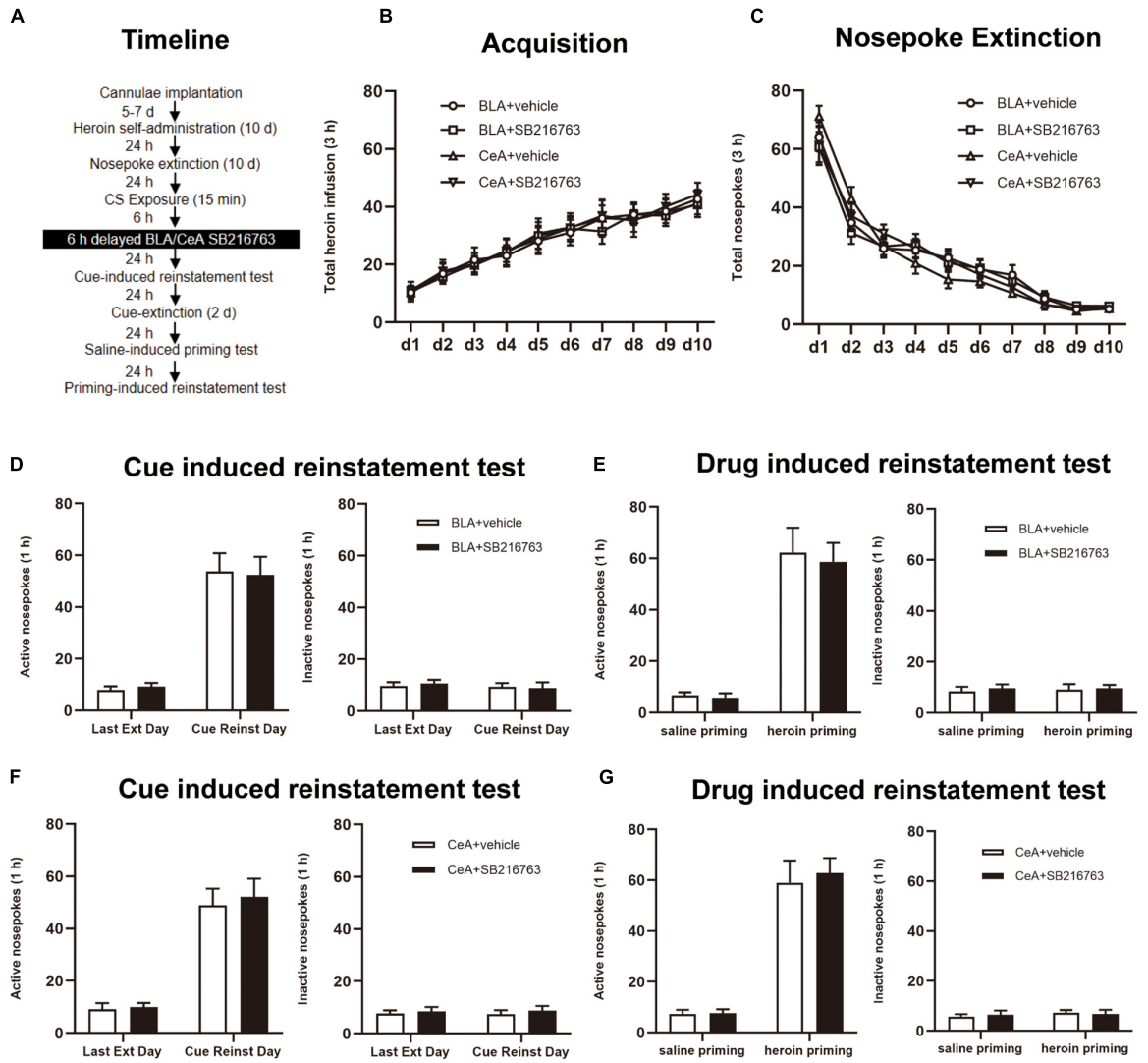

FIGURE 5 | SB216763 treatment 6 h after retrieval does not affect the heroin seeking in the following cue-induced and heroin-primed reinstatement. **(A)** Timeline of heroin self-administration, nosepoke extinction, cue-induced reinstatement test and drug-induced reinstatement test. **(B)** Total number of heroin infusions during acquisition of heroin self-administration. **(C)** Total number of active nosepoke responses during extinction training sessions. **(D,F)** Active (left) and inactive (right) nosepoke responses during the last extinction training session and the cue-induced reinstatement test. **(D)** Nosepoke responses of rats with BLA drug injection. **(F)** Nosepoke responses of rats with CeA drug injection. **(E,G)** Active (left) and inactive (right) nosepoke responses across the saline- or heroin- primed reinstatement test. **(E)** Nosepoke responses of rats with BLA drug injection. **(G)** Nosepoke responses of rats with CeA drug injection. *n* = 9–10 mice per group. Data are means ± SEM. CS, conditioned stimulus; Ext, extinction; Reinst, reinstatement.

$F_{(1,19)}$ = 51.16, p < 0.0001; administration condition: $F_{(1,19)}$ = 9.702, p = 0.0057; trial condition × administration condition interaction: $F_{(1,19)}$ = 12.55, p = 0.0022]; the *post-hoc* test showed a significant reduction of BLA+SB216763 group in drug-seeking compared with BLA+vehicle group in heroin priming-induced reinstatement test (p < 0.0001) (**Figure 2E** left), but did not differ in the inactive side [main effect of trial condition: $F_{(1,19)}$ = 0.0450, p = 0.8342; administration condition: $F_{(1,19)}$ = 0.0123, p = 0.9130; trial condition × administration condition interaction: $F_{(1,19)}$ = 0.0736, p = 0.7891; **Figure 2E** right]. Moreover, no significant differences were found in active side of CeA+vehicle and CeA+SB216763 groups in drug-induced reinstatement test [main effect of trial condition: $F_{(1,19)}$ = 67.29, p < 0.0001; administration condition: $F_{(1,19)}$ = 0.0369, p = 0.8498; trial condition × administration condition interaction: $F_{(1,19)}$ = 0.2259, p = 0.6400; **Figure 2G** left column] or the inactive side [main effect of trial condition: $F_{(1,19)}$ = 0.0218, p = 0.8841; administration condition: $F_{(1,19)}$ = 0.1738, p = 0.6814; trial condition × administration condition interaction: $F_{(1,19)}$ = 0.0218, p = 0.8841; **Figure 2G** right].

The results suggest that injecting SB216763 in BLA but not the CeA reduced cue-induced and heroin-primed heroin seeking reinstatement immediately after heroin cue retrieval.

Experiment 2: Immediate Post-CS SB216763 Treatment in BLA Rather Than CeA Can Reduce Subsequent Cue-Induced Heroin Seeking and the Spontaneous Recovery of Heroin Seeking

We tested the influences of immediate post-retrieval SB216763 injection in BLA and CeA on heroin seeking reinstatement which was cue-induced or heroin-induced besides the influences of long-term by using four rats groups (**Figure 3A**). In the heroin self-administration acquisition session, groups of BLA administrated vehicle (N = 10) or SB216763 (N = 10) and of CeA administrated vehicle (N = 10) or SB216763 (N = 10) had no significant differences that were shown by the similar heroin infusion numbers [main effect of acquisition time: $F_{(9,324)} = 48.79$, $p < 0.0001$; administration condition: $F_{(3,36)} = 0.1662$, $p = 0.9185$; acquisition time × administration condition interaction: $F_{(27,324)} = 0.5552$, $p = 0.9663$; **Figure 3B**]. Analogously, no significant differences of group were found in 10-day extinction training [main effect of extinction time: $F_{(9,324)} = 207.2$, $p < 0.0001$; administration condition: $F_{(3,36)} = 0.5019$, $p = 0.6833$; extinction time × administration condition interaction: $F_{(27,324)} = 0.9528$, $p = 0.5354$; **Figure 3C**].

Consistent with the results of Experiment 1, in the cue-induced reinstatement test, we found that nosepokes of groups differed from each other significantly in active side of BLA+vehicle and BLA+SB216763 groups [main effect of trial condition: $F_{(1,18)} = 67.92$, $p < 0.0001$; administration condition: $F_{(1,18)} = 21.07$, $p = 0.0002$; trial condition × administration condition interaction: $F_{(1,18)} = 22.67$, $p = 0.0002$]. In the cue-induced reinstatement test, the *post-hoc* test shown a significant reduction in active side nosepokes of BLA+SB216763 group compared to that BLA+vehicle ($p < 0.001$) (**Figure 3D** left), but not in the inactive side [main effect of trial condition: $F_{(1,18)} = 1.212$, $p = 0.2854$; administration condition: $F_{(1,18)} = 0.0327$, $p = 0.8585$; trial condition × administration condition interaction: $F_{(1,18)} = 0.2860$, $p = 0.5993$; **Figure 3D** right]. And in the cue-induced reinstatement test, there were no significant differences between CeA+vehicle and CeA+SB216763 groups of the active side [main effect of trial condition: $F_{(1,18)} = 53.73$, $p < 0.0001$; administration condition: $F_{(1,18)} = 0.1503$, $p = 0.7028$; trial condition × administration condition interaction: $F_{(1,18)} = 0.0223$, $p = 0.8830$; **Figure 3F** left column; **Figure 3F** left] and the inactive side [main effect of trial condition: $F_{(1,18)} = 1.683$, $p = 0.2110$; administration condition: $F_{(1,18)} = 0.0485$, $p = 0.8281$; trial condition × administration condition interaction: $F_{(1,18)} = 0.3407$, $p = 0.5666$; **Figure 3F** right]. Furthermore, during the spontaneous recovery test, active nosepokes significantly differed in BLA+vehicle and BLA+SB216763 groups [main effect of trial condition: $F_{(1,18)} = 29.44$, $p < 0.0001$; administration condition: $F_{(1,18)} = 13.79$, $p = 0.0016$; trial condition × administration condition interaction: $F_{(1,18)} = 15.39$, $p = 0.0010$]. During the spontaneous recovery test, a *post-hoc* test showed a significant reduction of BLA+SB216763 group in drug-seeking compared with BLA+vehicle group ($p < 0.0001$) (**Figure 3E** left) but not in the inactive side [main effect of trial condition: $F_{(1,18)} = 1.688$, $p = 0.2103$; administration condition: $F_{(1,18)} = 2.840$, $p = 0.1092$; trial condition × administration condition interaction: $F_{(1,18)} = 0.0604$, $p = 0.8086$; **Figure 3E** right]. While, in spontaneous recovery test, no significant differences of CeA+vehicle and CeA+SB216763 groups were found in active side [main effect of trial condition: $F_{(1,18)} = 74.83$, $p < 0.0001$; administration condition: $F_{(1,18)} = 0.1074$, $p = 0.7469$; trial condition × administration condition interaction: $F_{(1,18)} = 0.027$,$p = 0.8714$; **Figure 3G** left] and the inactive side [main effect of trial condition: $F_{(1,18)} = 0.0110$, $p = 0.9176$; administration condition: $F_{(1,18)} = 0.1554$, $p = 0.6981$; trial condition × administration condition interaction: $F_{(1,18)} = 0.6468$, $p = 0.4318$; **Figure 3G** right].

Thus, the results suggest that immediate post-CS BLA SB216763 treatment rather than CeA can reduce subsequent cue-induced heroin seeking and last at least 28 days.

Experiment 3: SB216763 Treatment Without CS Retrieval Does Not Affect Subsequent Cue-Induced and Heroin-Primed Reinstatement of Heroin Seeking

We tested whether SB216763 affecting subsequent heroin seeking depends on CS retrieval by using four rats groups. When heroin acquisition and extinction training were finished, rats were received BLA or CeA SB216763 treatment with no CS exposure (**Figure 4A**). During the training sessions of heroin self-administration, groups of BLA administrated vehicle (N = 10) or SB216763 (N = 10) and of CeA administrated vehicle (N = 10) or SB216763 (N = 10) had no differences in acquisition session [main effect of acquisition time: $F_{(9,324)} = 37.72$, $p < 0.0001$; administration condition: $F_{(3,36)} = 0.0764$, $p = 0.9724$; acquisition time × administration condition interaction: $F_{(27,324)} = 0.1869$, $p > 0.9999$; **Figure 4B**] and in 10-day extinction training [main effect of extinction time: $F_{(9,324)} = 127.0$, $p < 0.0001$; administration condition: $F_{(3,36)} = 0.1659$, $p = 0.9187$; extinction time × administration condition interaction: $F_{(27,324)} = 0.4249$, $p = 0.9953$; **Figure 4C**] as suggested by the similar heroin infusions.

Cue-induced reinstatement test was shown that no significant differences were found in nosepokes of active side [main effect of trial condition: $F_{(1,18)} = 67.15$, $p < 0.0001$; administration condition: $F_{(1,18)} = 0.0008$, $p = 0.9778$; trial condition × administration condition interaction: $F_{(1,18)} = 0.0415$, $p = 0.8409$; **Figure 4D, left**] and **inactive** side [main effect of trial condition: $F_{(1,18)} = 0.0816$, $p = 0.7784$; administration condition: $F_{(1,18)} = 0.0184$, $p = 0.8937$; trial condition × administration condition interaction: $F_{(1,18)} = 0.0816$, $p = 0.7784$; **Figure 4D**, right] between the BLA+vehicle and BLA+SB216763 groups. Similarly, no significant differences of nosepokes were found in active side [main effect of trial condition: $F_{(1,18)} = 78.74$, $p < 0.0001$; administration condition: $F_{(1,18)} = 0.0068$, $p = 0.9353$; trial condition × administration condition

interaction: $F_{(1,18)} = 0.1212$, $p = 0.7317$; **Figure 4F**, left] or in inactive side [main effect of trial condition: $F_{(1,18)} = 1.561$, $p = 0.2275$; administration condition: $F_{(1,18)} = 0.0312$, $p = 0.8618$; trial condition × administration condition interaction: $F_{(1,18)} = 0.0285$, $p = 0.8678$; **Figure 4F**, right] of CeA+vehicle and CeA+SB216763 groups. In drug-induced reinstatement test, no significant differences of nosepokes were found in active side [main effect of trial condition: $F_{(1,18)} = 61.05$, $p < 0.0001$; administration condition: $F_{(1,18)} = 0.0232$, $p = 0.8806$; trial condition × administration condition interaction: $F_{(1,18)} = 0.1465$, $p = 0.7064$; **Figure 4E, left**] and **in** inactive side [main effect of trial condition: $F_{(1,18)} = 0.3709$, $p = 0.5501$; administration condition: $F_{(1,18)} = 0.0075$, $p = 0.9318$; trial condition × administration condition interaction: $F_{(1,18)} = 0.2887$, $p = 0.5976$; **Figure 4E**, right] in BLA+vehicle and BLA+SB216763 groups. Besides, it was not significantly different in nosepokes of active side [main effect of trial condition: $F_{(1,18)} = 58.06$, $p < 0.0001$; administration condition: $F_{(1,18)} = 0.0397$, $p = 0.8444$; trial condition × administration condition interaction: $F_{(1,18)} = 0.0209$, $p = 0.8866$; **Figure 4G**, left] or inactive side [main effect of trial condition: $F_{(1,18)} = 0.1848$, $p = 0.6724$; administration condition: $F_{(1,18)} = 2.064$, $p = 0.1679$; trial condition × administration condition interaction: $F_{(1,18)} = 0.1118$, $p = 0.7420$; **Figure 4G**, right] between the CeA+vehicle and CeA+SB216763 groups.

Thus, the results indicate that the CS retrieval of drug-associated memory determines the effect of SB216763 on subsequent heroin seeking and when SB216763 is used alone, there will be no influence on the heroin seeking of the subsequent cue-induced and heroin-primed reinstatement test.

Experiment 4: SB216763 Treatment 6 h After Retrieval Does Not Affect the Heroin Seeking in the Following Cue-Induced and Heroin-Primed Reinstatement

Finally, we employed whether SB216763 treated out of the reconsolidation time window would suppress the following heroin seeking (**Figure 5A**). During the training sessions, groups of BLA administrated vehicle ($N = 10$) or SB216763 ($N = 10$) and of CeA administrated vehicle ($N = 10$) or SB216763 ($N = 10$) had no differences in heroin self-administration acquisition [main effect of acquisition time: $F_{(9,315)} = 32.37$, $p < 0.0001$; administration condition: $F_{(3,35)} = 0.0423$, $p = 0.9882$; acquisition time × administration condition interaction: $F_{(27,315)} = 0.1182$, $p > 0.9999$; **Figure 5B**] and in 10-day extinction sessions [main effect of extinction time: $F_{(9,315)} = 155.5$, $p < 0.0001$; administration condition: $F_{(3,35)} = 0.0613$, $p = 0.9798$; extinction time × administration condition interaction: $F_{(27,315)} = 1.120$, $p = 0.3139$; **Figure 5C**] which were shown by the similar heroin injections numbers.

In cue-induced reinstatement test, the nosepokes did not significantly differ in the active side [main effect of trial condition: $F_{(1,18)} = 73.20$, $p < 0.0001$; administration condition: $F_{(1,18)} = 0.0001$, $p = 0.9922$; trial condition × administration condition interaction: $F_{(1,18)} = 0.0675$, $p = 0.7979$; **Figure 5D**, left] or in the inactive side [main effect of trial condition: $F_{(1,18)} = 0.3240$, $p = 0.5763$; administration condition: $F_{(1,18)} = 0.0135$, $p = 0.9088$; trial condition × administration condition interaction: $F_{(1,18)} = 0.2073$, $p = 0.6543$; **Figure 5D**, right] of BLA+vehicle and BLA+SB216763 groups. Similarly, no significant differences in nosepokes were found in active side [main effect of trial condition: $F_{(1,17)} = 67.32$, $p < 0.0001$; administration condition: $F_{(1,18)} = 0.1421$, $p = 0.7106$; trial condition × administration condition interaction: $F_{(1,17)} = 0.0610$, $p = 0.8079$; **Figure 5F**, left] or in the inactive side [main effect of trial condition: $F_{(1,17)} = 0.0001$, $p = 0.9944$; administration condition: $F_{(1,17)} = 0.3902$, $p = 0.5405$; trial condition × administration condition interaction: $F_{(1,17)} = 0.0182$, $p = 0.8943$; **Figure 5F**, right] of CeA+vehicle and CeA+SB216763 groups. As for the drug-induced reinstatement test, the nosepokes did not significantly differ in the active side [main effect of trial condition: $F_{(1,18)} = 77.38$, $p < 0.0001$; administration condition: $F_{(1,18)} = 0.1286$, $p = 0.7241$; trial condition × administration condition interaction: $F_{(1,18)} = 0.0481$, $p = 0.8289$; **Figure 5E**, left] or in the inactive side [main effect of trial condition: $F_{(1,18)} = 0.0473$, $p = 0.8304$; administration condition: $F_{(1,18)} = 0.2022$, $p = 0.6583$; trial condition × administration condition interaction: $F_{(1,18)} = 0.0241$, $p = 0.8783$; **Figure 5E**, right] between the BLA+vehicle and BLA+SB216763 groups. Besides, the nosepokes did not significantly differ in the active side [main effect of trial condition: $F_{(1,17)} = 94.30$, $p < 0.0001$; administration condition: $F_{(1,18)} = 0.1377$, $p = 0.7149$; trial condition × administration condition interaction: $F_{(1,17)} = 0.0955$, $p = 0.7611$; **Figure 5G**, left] or in the inactive side [main effect of trial condition: $F_{(1,17)} = 0.3672$, $p = 0.5525$; administration condition: $F_{(1,17)} = 0.0108$, $p = 0.9184$; trial condition × treatment condition interaction: $F_{(1,17)} = 0.2189$, $p = 0.6458$; **Figure 5G**, right] in the CeA+vehicle and CeA+SB216763 groups.

The results suggest that the effect of SB216763 on the heroin seeking of the following cue-induced and heroin-primed reinstatement test is time-specific.

DISCUSSION

In our present study, we examined the effects of SB216763, a GSK-3β inhibitor, on heroin-seeking behavior and relapse *via* an intravenous heroin SA procedure. The main findings are following: (1) Immediate post-CS SB216763 treatment in BLA rather than CeA can reduce subsequent cue-induced and heroin-primed reinstatement of heroin seeking. (2) The effect of SB216763 (intracranial injection into BLA) immediately after retrieval session, which reactivated the heroin cue memory, on cocaine-seeking behavior continued for at least twenty-eight days; (3) SB216763 administration into BLA delayed 6 h or without the retrieval have no effect on the cue-induced and heroin priming-induced reinstatement test, suggesting that the effects of SB216763 on drug-seeking behavior are retrieval-dependent and time-specific. The

results demonstrated that the activity of GSK-3β in BLA is required for reconsolidation and intra-BLA injection of SB216763 disrupts memory reconsolidation, suggested that inhibiting GSK-3β activity of BLA disrupts reconsolidation and attenuates heroin relapse.

Existing evidence has shown that consolidated drug-induced memory could be unstable after retrieval by conditioned stimulus (drug-associated cues) or unconditioned stimulus (the drugs). Disrupting the reconsolidation after drug memory retrieval effectively blocks the association between drug-related cues and drugs, thus producing a forgetting effect and reducing drug-seeking behavior. Memory retrieval activates GSK-3β in the BLA, and reconsolidation was impaired by systemical administration of a GSK-3 inhibitor before memory retrieval in rats (Wu et al., 2011). We have demonstrated that SB216763, as a GSK-3β inhibitor, reduced heroin seeking and relapse by disrupting reconsolidation of heroin drug memory. Nevertheless, without CS exposure or with a 6h delay administration of SB216763 has no effect on heroin seeking behavior, which is consistent with the "reconsolidation theory" that allowing for modifications during reconsolidation in a putative time window. Indeed, GSK-3β expressed in multiple brain regions (e.g., NAc, PFC, amygdala) (Winder et al., 2002; Morgane et al., 2005; Robbins et al., 2008), regulates the dopamine-associated behaviors (Beaulieu et al., 2007a). The role of GSK-3β in drug addiction has also been confirmed by several studies. For example, in a cocaine-induced CPP model, the reconsolidation of cocaine-cue memories was impaired by systemic injection of lithium chloride (a GSK-3β inhibitor) after memory retrieval, and SB216763 administration into BLA can result in a long-term effect on cocaine cue memories *via* disrupting reconsolidation (Wu et al., 2011).

Our present study complements the role of GSK-3β in heroin self-administration model. We show that inhibiting GSK-3β activity by injection of SB216763 into the BLA, but not the CeA, immediately after the retrieval reduced the drug-seeking behavior. In addition, some studies have shown that the GSK-3β in the hippocampus regulates learning and memory ability. Targeted downregulation of GSK-3β in the ventral hippocampus disrupting the formation of cocaine CPP and the spatial memory (Barr et al., 2020). Overexpression of GSK-3β in the hippocampus impaired the spatial memory (Liu et al., 2020). And both the amygdala, hippocampus, are the important brain regions in drug addiction (Alizamini et al., 2022). Previous study found that inhibited the activity of GSK-3β in the BLA immediately after the retrieval could disrupte cocaine context memory (Wu et al., 2011). Our findings are consistent with these results and showed that inhibiting GSK-3β in the BLA in the reconsolidation time window decreased drug seeking and relapse in heroin SA rats.

The amygdala, associated with emotion and motivation, plays roles in processing rewarding environmental stimulus (Janak and Tye, 2015). Recent evidence demonstrates that disrupting the reconsolidation of the cocaine drug memories attenuates cocaine seeking which was associated with the BLA (Wu et al., 2011). In our present study, we discussed the role of GSK-3β in a heroin self-administration rat model. Inhibiting activity of GSK-3β in the BLA, but not the CeA, effectively disrupted reconsolidation of heroin cue memory and blocked subsequent drug-seeking behaviors. Many studies have demonstrated that BLA is involved in memory reconsolidation (Wells et al., 2013; Yuan et al., 2020). However, the spcefic mechanism of GSK-3β in drug memory reconsolidation remains to be elucidated.

GSK-3β is widely expressed in the brain and involved in fundamental brain functions like neurogenesis, neurotransmitter signaling (Beaulieu et al., 2004, 2007b; Li et al., 2004), circadian rhythms (Yin et al., 2006), and memory process (Hooper et al., 2007; Kimura et al., 2008; Hong et al., 2012). GSK-3β has been shown to regulate many transcription factors (e.g., β-catenin, NF-κB, activator protein-1), and memory-associated proteins which have been implicated in fundamental brain functions (Frame and Cohen, 2001). Specifically, in Liu et al.'s study, the role of GSK-3β/β-catenin signaling pathway on memory consolidation in rats trained in a Morris water maze task was proved (Liu et al., 2014) and the consolidation of fear memory need the β-catenin in the amygdala (Maguschak and Ressler, 2008). As a study revealed, the Akt/GSK-3/mTORC1 signaling pathway, which has been found in the hippocampus and nucleus accumbens, participates in the reconsolidation progress of cocaine memory (Shi et al., 2014). Psychostimulant activates GSK-3β by inactivating protein kinase B (Akt) and reducing its inhibition of serine-phosphorylation (Miller et al., 2014). These findings indicate that during the reconsolidation process, GSK-3β may be required to be activated, but the role of GSK-3β on reconsolidation of heroin-SA and the possible molecular mechanisms involved in this process have not yet known. Our present study showed that intra-BLA infusion of the GSK-3β inhibitor SB216763 disrupted the reconsolidation of heroin reward memory and the reduction of heroin seeking behaviors lasted for a long time (28 days). And these effects were BLA- specific and time-specific. Studies have reported that the activity of GSK-3β was involved in the LTP and LTD which both depended on the NMDA receptor and also regulated the interreaction between them (Peineau et al., 2007, 2008, 2009). But there is less study that reported the relationship between GSK-3β and NMDA in addiction. Furthermore, reconsolidation is associated with de novo protein synthesis and synaptic plasticity alteration (Nader et al., 2000). Thus, our future study will focus on the relationship between GSK-3β and NMDA in reconsolidation of heroin reward memory and investigate the synaptic plasticity alteration during this process by electrophysiological methods. Compared with Wu et al. (2011) study, our present study is the extension of previous studies, and we used a drug self-administration paradigm, which can simulate craving and relapse in addicts and is more suitable for studying craving and relapse (Spealman and Goldberg, 1978; Schindler et al., 2002).

In summary, the present study demonstrated the effects of GSK-3β on the reconsolidation of drug reward memory *via* a rats heroin SA paradigm. After heroin cue memory retrieval, injection of SB216763 into BLA impairs reconsolidation of the heroin cue memory, effectively reduces the heroin seeking behavior in rats, and these effects lasted at least 28 days. Moreover, the reconsolidation window may be an important determinant to reduce heroin seeking and relapse. Our present study identifies

that GSK-3β inhibitors may have the potential therapeutic value in the treatment of heroin addiction.

DATA AVAILABILITY STATEMENT

The raw data supporting the conclusions of this article will be made available by the authors, without undue reservation.

ETHICS STATEMENT

The animal study was reviewed and approved by the Xiangya Hospital Ethics Committee, Xiangya Hospital (Changsha, China).

AUTHOR CONTRIBUTIONS

HL and YX: conceptualization. YZ and YX: data curation. TH and ZZ: writing – original draft preparation. YX and QL: writing – review and editing. HL: supervision and funding acquisition. All authors have read and agreed to the published version of the manuscript.

FUNDING

This work was financially supported by National Natural Science Foundation of China (Grant No. 82101247) and the Natural Science Foundation of Hunan Province, China (Grant Nos. 2021JJ40999 and 2021JJ31112).

REFERENCES

Alizamini, M. M., Li, Y., Zhang, J. J., Liang, J., and Haghparast, A. (2022). Endocannabinoids and addiction memory: relevance to methamphetamine/morphine abuse. *World J. Biol. Psychiatry* 2022, 1–21. doi: 10.1080/15622975.2022.2039408

Ambroggi, F., Ishikawa, A., Fields, H. L., and Nicola, S. M. (2008). Basolateral amygdala neurons facilitate reward-seeking behavior by exciting nucleus accumbens neurons. *Neuron* 59, 648–661. doi: 10.1016/j.neuron.2008.07.004

Anker, J. J., and Carroll, M. E. (2010). Reinstatement of cocaine seeking induced by drugs, cues, and stress in adolescent and adult rats. *Psychopharmacology (Berl)* 208, 211–222. doi: 10.1007/s00213-009-1721-2

Banach, E., Szczepankiewicz, A., Kaczmarek, L., Jaworski, T., and Urban-Ciecko, J. (2022). Dysregulation of miRNAs levels in glycogen synthase kinase-3beta overexpressing mice and the role of miR-221-5p in synaptic function. *Neuroscience* 490, 287–295. doi: 10.1016/j.neuroscience.2022.03.024

Barr, J. L., Shi, X., Zaykaner, M., and Unterwald, E. M. (2020). Glycogen synthase kinase 3β in the ventral hippocampus is important for cocaine reward and object location memory. *Neuroscience* 425, 101–111. doi: 10.1016/j.neuroscience.2019.10.055

Beaulieu, J. M., Gainetdinov, R. R., and Caron, M. G. (2007a). The Akt-GSK-3 signaling cascade in the actions of dopamine. *Trends Pharmacol. Sci.* 28, 166–172. doi: 10.1016/j.tips.2007.02.006

Beaulieu, J. M., Tirotta, E., Sotnikova, T. D., Masri, B., Salahpour, A., Gainetdinov, R. R., et al. (2007b). Regulation of Akt signaling by D2 and D3 dopamine receptors *in vivo*. *J. Neurosci.* 27, 881–885. doi: 10.1523/jneurosci.5074-06.2007

Beaulieu, J. M., Sotnikova, T. D., Yao, W. D., Kockeritz, L., Woodgett, J. R., Gainetdinov, R. R., et al. (2004). Lithium antagonizes dopamine-dependent behaviors mediated by an AKT/glycogen synthase kinase 3 signaling cascade. *Proc. Natl. Acad. Sci. U.S.A.* 101, 5099–5104. doi: 10.1073/pnas.0307921101

Björkstrand, J., Agren, T., Åhs, F., Frick, A., Larsson, E. M., Hjorth, O., et al. (2016). Disrupting reconsolidation attenuates long-term fear memory in the human amygdala and facilitates approach behavior. *Curr. Biol.* 26, 2690–2695. doi: 10.1016/j.cub.2016.08.022

Chen, L., Huang, S., Yang, C., Wu, F., Zheng, Q., Yan, H., et al. (2021). Blockade of β-adrenergic receptors by propranolol disrupts reconsolidation of drug memory and attenuates heroin seeking. *Front. Pharmacol.* 12:686845. doi: 10.3389/fphar.2021.686845

Davis, W. M., and Smith, S. G. (1976). Role of conditioned reinforcers in the initiation, maintenance and extinction of drug-seeking behavior. *Pavlov J. Biol. Sci.* 11, 222–236. doi: 10.1007/bf03000316

Dewachter, I., Ris, L., Jaworski, T., Seymour, C. M., Kremer, A., Borghgraef, P., et al. (2009). GSK3beta, a centre-staged kinase in neuropsychiatric disorders, modulates long term memory by inhibitory phosphorylation at serine-9. *Neurobiol. Dis.* 35, 193–200. doi: 10.1016/j.nbd.2009.04.003

Di Ciano, P., and Everitt, B. J. (2004). Conditioned reinforcing properties of stimuli paired with self-administered cocaine, heroin or sucrose: implications for the persistence of addictive behaviour. *Neuropharmacology* 47, 202–213. doi: 10.1016/j.neuropharm.2004.06.005

Díaz-Mataix, L., Ruiz Martinez, R. C., Schafe, G. E., LeDoux, J. E., and Doyère, V. (2013). Detection of a temporal error triggers reconsolidation of amygdala-dependent memories. *Curr. Biol.* 23, 467–472. doi: 10.1016/j.cub.2013.01.053

Dymshitz, J., and Lieblich, I. (1987). Opiate reinforcement and naloxone aversion, as revealed by place preference paradigm, in two strains of rats. *Psychopharmacology (Berl)* 92, 473–477. doi: 10.1007/bf00176481

Frame, S., and Cohen, P. (2001). GSK3 takes centre stage more than 20 years after its discovery. *Biochem. J.* 359, 1–16. doi: 10.1042/0264-6021:3590001

Haubrich, J., Bernabo, M., and Nader, K. (2020). Noradrenergic projections from the locus coeruleus to the amygdala constrain fear memory reconsolidation. *Elife* 9:e57010. doi: 10.7554/eLife.57010

Higginbotham, J. A., Jones, N. M., Wang, R., Christian, R. J., Ritchie, J. L., McLaughlin, R. J., et al. (2021). Basolateral amygdala CB1 receptors gate HPA axis activation and context-cocaine memory strength during reconsolidation. *Neuropsychopharmacology* 46, 1554–1564. doi: 10.1038/s41386-020-00919-x

Hong, J. G., Kim, D. H., Lee, C. H., Park, S. J., Kim, J. M., Cai, M., et al. (2012). GSK-3β activity in the hippocampus is required for memory retrieval. *Neurobiol. Learn. Mem.* 98, 122–129. doi: 10.1016/j.nlm.2012.07.003

Hooper, C., Markevich, V., Plattner, F., Killick, R., Schofield, E., Engel, T., et al. (2007). Glycogen synthase kinase-3 inhibition is integral to long-term potentiation. *Eur. J. Neurosci.* 25, 81–86. doi: 10.1111/j.1460-9568.2006.05245.x

Janak, P. H., and Tye, K. M. (2015). From circuits to behaviour in the amygdala. *Nature* 517, 284–292. doi: 10.1038/nature14188

Jope, R. S., and Johnson, G. V. (2004). The glamour and gloom of glycogen synthase kinase-3. *Trends Biochem. Sci.* 29, 95–102. doi: 10.1016/j.tibs.2003.12.004

Kaidanovich-Beilin, O., Lipina, T. V., Takao, K., van Eede, M., Hattori, S., Laliberté, C., et al. (2009). Abnormalities in brain structure and behavior in GSK-3alpha mutant mice. *Mol. Brain* 2:35. doi: 10.1186/1756-6606-2-35

Kimura, T., Yamashita, S., Nakao, S., Park, J. M., Murayama, M., Mizoroki, T., et al. (2008). GSK-3beta is required for memory reconsolidation in adult brain. *PLoS One* 3:e3540. doi: 10.1371/journal.pone.0003540

Lee, J. L. (2009). Reconsolidation: maintaining memory relevance. *Trends Neurosci.* 32, 413–420. doi: 10.1016/j.tins.2009.05.002

Lee, J. L., Milton, A. L., and Everitt, B. J. (2006). Cue-induced cocaine seeking and relapse are reduced by disruption of drug memory reconsolidation. *J. Neurosci.* 26, 5881–5887. doi: 10.1523/jneurosci.0323-06.2006

Li, F. Q., Xue, Y. X., Wang, J. S., Fang, Q., Li, Y. Q., Zhu, W. L., et al. (2010). Basolateral amygdala cdk5 activity mediates consolidation and reconsolidation of memories for cocaine cues. *J. Neurosci.* 30, 10351–10359. doi: 10.1523/jneurosci.2112-10.2010

Li, N., Xiao, K., Mi, X., Li, N., Guo, L., Wang, X., et al. (2022). Ghrelin signaling in dCA1 suppresses neuronal excitability and impairs memory acquisition *via* PI3K/Akt/GSK-3beta cascades. *Neuropharmacology* 203:108871. doi: 10.1016/j.neuropharm.2021.108871

Li, X., Zhu, W., Roh, M. S., Friedman, A. B., Rosborough, K., and Jope, R. S. (2004). *In vivo* regulation of glycogen synthase kinase-3beta (GSK3beta) by

serotonergic activity in mouse brain. *Neuropsychopharmacology* 29, 1426–1431. doi: 10.1038/sj.npp.1300439

Lin, J., Liu, L., Wen, Q., Zheng, C., Gao, Y., Peng, S., et al. (2014). Rapamycin prevents drug seeking *via* disrupting reconsolidation of reward memory in rats. *Int. J. Neuropsychopharmacol.* 17, 127–136. doi: 10.1017/s1461145713001156

Liu, E., Xie, A. J., Zhou, Q., Li, M., Zhang, S., Li, S., et al. (2017). GSK-3β deletion in dentate gyrus excitatory neuron impairs synaptic plasticity and memory. *Sci. Rep.* 7:5781. doi: 10.1038/s41598-017-06173-4

Liu, G., Yin, F., Zhang, C., Zhang, Y., Li, X., and Ling, Y. (2020). Effects of regulating miR-132 mediated GSK-3β on learning and memory function in mice. *Exp. Ther. Med.* 20, 1191–1197. doi: 10.3892/etm.2020.8768

Liu, H., Xu, G. H., Wang, K., Cao, J. L., Gu, E. W., Li, Y. H., et al. (2014). Involvement of GSK3β/β-catenin signaling in the impairment effect of ketamine on spatial memory consolidation in rats. *Neurobiol. Learn. Mem.* 111, 26–34. doi: 10.1016/j.nlm.2014.02.012

Lu, L., Hope, B. T., Dempsey, J., Liu, S. Y., Bossert, J. M., and Shaham, Y. (2005). Central amygdala ERK signaling pathway is critical to incubation of cocaine craving. *Nat. Neurosci.* 8, 212–219. doi: 10.1038/nn1383

Luo, Y. X., Xue, Y. X., Liu, J. F., Shi, H. S., Jian, M., Han, Y., et al. (2015). A novel UCS memory retrieval-extinction procedure to inhibit relapse to drug seeking. *Nat. Commun.* 6:7675. doi: 10.1038/ncomms8675

Luo, Y. X., Xue, Y. X., Shen, H. W., and Lu, L. (2013). Role of amygdala in drug memory. *Neurobiol. Learn. Mem.* 105, 159–173. doi: 10.1016/j.nlm.2013.06.017

Maguschak, K. A., and Ressler, K. J. (2008). Beta-catenin is required for memory consolidation. *Nat. Neurosci.* 11, 1319–1326. doi: 10.1038/nn.2198

Marosi, M., Arman, P., Aceto, G., D'Ascenzo, M., and Laezza, F. (2022). Glycogen synthase kinase 3: ion channels, plasticity, and diseases. *Int. J. Mol. Sci.* 23:413. doi: 10.3390/ijms23084413

Maurin, H., Lechat, B., Dewachter, I., Ris, L., Louis, J. V., Borghgraef, P., et al. (2013). Neurological characterization of mice deficient in GSK3α highlight pleiotropic physiological functions in cognition and pathological activity as tau kinase. *Mol. Brain* 6:27. doi: 10.1186/1756-6606-6-27

McGaugh, J. L. (2004). The amygdala modulates the consolidation of memories of emotionally arousing experiences. *Ann. Rev. Neurosci.* 27, 1–28. doi: 10.1146/annurev.neuro.27.070203.144157

Medina, M., Garrido, J. J., and Wandosell, F. G. (2011). Modulation of GSK-3 as a therapeutic strategy on tau pathologies. *Front. Mol. Neurosci.* 4:24. doi: 10.3389/fnmol.2011.00024

Milekic, M. H., and Alberini, C. M. (2002). Temporally graded requirement for protein synthesis following memory reactivation. *Neuron* 36, 521–525. doi: 10.1016/s0896-6273(02)00976-5

Miller, C. A., and Marshall, J. F. (2005). Molecular substrates for retrieval and reconsolidation of cocaine-associated contextual memory. *Neuron* 47, 873–884. doi: 10.1016/j.neuron.2005.08.006

Miller, J. S., Barr, J. L., Harper, L. J., Poole, R. L., Gould, T. J., and Unterwald, E. M. (2014). The GSK3 signaling pathway is activated by cocaine and is critical for cocaine conditioned reward in mice. *PLoS One* 9:e88026. doi: 10.1371/journal.pone.0088026

Morgane, P. J., Galler, J. R., and Mokler, D. J. (2005). A review of systems and networks of the limbic forebrain/limbic midbrain. *Prog. Neurobiol.* 75, 143–160. doi: 10.1016/j.pneurobio.2005.01.001

Morris, R. G., Inglis, J., Ainge, J. A., Olverman, H. J., Tulloch, J., Dudai, Y., et al. (2006). Memory reconsolidation: sensitivity of spatial memory to inhibition of protein synthesis in dorsal hippocampus during encoding and retrieval. *Neuron* 50, 479–489. doi: 10.1016/j.neuron.2006.04.012

Nader, K. (2015). Reconsolidation and the dynamic nature of memory. *Cold Spring Harb Perspect Biol.* 7:a021782. doi: 10.1101/cshperspect.a021782

Nader, K., Schafe, G. E., and Le Doux, J. E. (2000). Fear memories require protein synthesis in the amygdala for reconsolidation after retrieval. *Nature* 406, 722–726. doi: 10.1038/35021052

O'Brien, W. T., Harper, A. D., Jové, F., Woodgett, J. R., Maretto, S., Piccolo, S., et al. (2004). Glycogen synthase kinase-3beta haploinsufficiency mimics the behavioral and molecular effects of lithium. *J. Neurosci.* 24, 6791–6798. doi: 10.1523/jneurosci.4753-03.2004

Peineau, S., Bradley, C., Taghibiglou, C., Doherty, A., Bortolotto, Z. A., Wang, Y. T., et al. (2008). The role of GSK-3 in synaptic plasticity. *Br. J. Pharmacol.* 153, S428–S437. doi: 10.1038/bjp.2008.2

Peineau, S., Nicolas, C. S., Bortolotto, Z. A., Bhat, R. V., Ryves, W. J., Harwood, A. J., et al. (2009). A systematic investigation of the protein kinases involved in NMDA receptor-dependent LTD: evidence for a role of GSK-3 but not other serine/threonine kinases. *Mol. Brain* 2:22. doi: 10.1186/1756-6606-2-22

Peineau, S., Taghibiglou, C., Bradley, C., Wong, T. P., Liu, L., Lu, J., et al. (2007). LTP inhibits LTD in the hippocampus *via* regulation of GSK3beta. *Neuron* 53, 703–717. doi: 10.1016/j.neuron.2007.01.029

Perrine, S. A., Miller, J. S., and Unterwald, E. M. (2008). Cocaine regulates protein kinase B and glycogen synthase kinase-3 activity in selective regions of rat brain. *J. Neurochem.* 107, 570–577. doi: 10.1111/j.1471-4159.2008.05632.x

Piva, A., Gerace, E., Di Chio, M., Padovani, L., Paolone, G., Pellegrini-Giampietro, D. E., et al. (2019). Reconsolidation of sucrose instrumental memory in rats: the role of retrieval context. *Brain Res.* 1714, 193–201. doi: 10.1016/j.brainres.2019.03.006

Robbins, T. W., Ersche, K. D., and Everitt, B. J. (2008). Drug addiction and the memory systems of the brain. *Ann. N.Y.Acad. Sci.* 1141, 1–21. doi: 10.1196/annals.1441.020

Schindler, C. W., Panlilio, L. V., and Goldberg, S. R. (2002). Second-order schedules of drug self-administration in animals. *Psychopharmacology (Berl)* 163, 327–344. doi: 10.1007/s00213-002-1157-4

Shi, X., Miller, J. S., Harper, L. J., Poole, R. L., Gould, T. J., and Unterwald, E. M. (2014). Reactivation of cocaine reward memory engages the Akt/GSK3/mTOR signaling pathway and can be disrupted by GSK3 inhibition. *Psychopharmacology (Berl)* 231, 3109–3118. doi: 10.1007/s00213-014-3491-8

Spealman, R. D., and Goldberg, S. R. (1978). Drug self-administration by laboratory animals: control by schedules of reinforcement. *Ann. Rev. Pharmacol. Toxicol.* 18, 313–339. doi: 10.1146/annurev.pa.18.040178.001525

Wang, X. Y., Zhao, M., Ghitza, U. E., Li, Y. Q., and Lu, L. (2008). Stress impairs reconsolidation of drug memory *via* glucocorticoid receptors in the basolateral amygdala. *J. Neurosci.* 28, 5602–5610. doi: 10.1523/jneurosci.0750-08.2008

Wells, A. M., Arguello, A. A., Xie, X., Blanton, M. A., Lasseter, H. C., Reittinger, A. M., et al. (2013). Extracellular signal-regulated kinase in the basolateral amygdala, but not the nucleus accumbens core, is critical for context-response-cocaine memory reconsolidation in rats. *Neuropsychopharmacology* 38, 753–762. doi: 10.1038/npp.2012.238

Winder, D. G., Egli, R. E., Schramm, N. L., and Matthews, R. T. (2002). Synaptic plasticity in drug reward circuitry. *Curr. Mol. Med.* 2, 667–676. doi: 10.2174/1566524023361961

Wu, P., Xue, Y. X., Ding, Z. B., Xue, L. F., Xu, C. M., and Lu, L. (2011). Glycogen synthase kinase 3β in the basolateral amygdala is critical for the reconsolidation of cocaine reward memory. *J. Neurochem.* 118, 113–125. doi: 10.1111/j.1471-4159.2011.07277.x

Xu, C. M., Wang, J., Wu, P., Zhu, W. L., Li, Q. Q., Xue, Y. X., et al. (2009). Glycogen synthase kinase 3beta in the nucleus accumbens core mediates cocaine-induced behavioral sensitization. *J. Neurochem.* 111, 1357–1368. doi: 10.1111/j.1471-4159.2009.06414.x

Xue, Y. X., Deng, J. H., Chen, Y. Y., Zhang, L. B., Wu, P., Huang, G. D., et al. (2017). Effect of selective inhibition of reactivated nicotine-associated memories with propranolol on nicotine craving. *JAMA Psychiatry* 74, 224–232. doi: 10.1001/jamapsychiatry.2016.3907

Xue, Y. X., Luo, Y. X., Wu, P., Shi, H. S., Xue, L. F., Chen, C., et al. (2012). A memory retrieval-extinction procedure to prevent drug craving and relapse. *Science* 336, 241–245. doi: 10.1126/science.1215070

Yan, Y., Zhang, L., Zhu, T., Deng, S., Ma, B., Lv, H., et al. (2021). Reconsolidation of a post-ingestive nutrient memory requires mTOR in the central amygdala. *Mol. Psychiatry* 26, 2820–2836. doi: 10.1038/s41380-020-00874-5

Ye, X., Kapeller-Libermann, D., Travaglia, A., Inda, M. C., and Alberini, C. M. (2017). Direct dorsal hippocampal-prelimbic cortex connections strengthen fear memories. *Nat. Neurosci.* 20, 52–61. doi: 10.1038/nn.4443

Yin, L., Wang, J., Klein, P. S., and Lazar, M. A. (2006). Nuclear receptor rev-erbalpha is a critical lithium-sensitive component of the circadian clock. *Science* 311, 1002–1005. doi: 10.1126/science.1121613

Yuan, K., Cao, L., Xue, Y. X., Luo, Y. X., Liu, X. X., Kong, F. N., et al. (2020). Basolateral amygdala is required for reconsolidation updating of heroin-associated memory after prolonged withdrawal. *Addict. Biol.* 25:e12793. doi: 10.1111/adb.12793

Zhang, F., Huang, S., Bu, H., Zhou, Y., Chen, L., Kang, Z., et al. (2021). Disrupting reconsolidation by systemic inhibition of mtor kinase *via* rapamycin reduces cocaine-seeking behavior. *Front. Pharmacol.* 12:652865. doi: 10.3389/fphar.2021.652865

Conflict of Interest: The authors declare that the research was conducted in the absence of any commercial or financial relationships that could be construed as a potential conflict of interest.

Publisher's Note: All claims expressed in this article are solely those of the authors and do not necessarily represent those of their affiliated organizations, or those of the publisher, the editors and the reviewers. Any product that may be evaluated in this article, or claim that may be made by its manufacturer, is not guaranteed or endorsed by the publisher.

frontiers | Frontiers in Molecular Neuroscience

ORIGINAL RESEARCH
published: 01 July 2022
doi: 10.3389/fnmol.2022.885701

A Scientometric Visualization Analysis for Molecular Mechanisms of Substance Abuse and Its Neurotoxicity From 1997 to 2021

*Aijia Zhang†, Zilong Liu† and Man Liang**

Department of Forensic Medicine, Tongji Medical College, Huazhong University of Science and Technology, Wuhan, China

Substance abuse has become a global problem due to drug-induced addiction and neurotoxicity, which causes a huge physical, social, and financial burden. Various kinds of drugs can hijack the users'/abusers' behavior and associated neurocircuitry. To summarize recent scientific advances on drug abuse, we reviewed relevant publications to analyze research progress and such trends through bibliometric ways. Based on retrieval strategies, a total of 681 scientific records published from 1997 to 2021 were screened and included in the Web of Science (WoS) database. Further scientometric analysis revealed that annual publication output increased across this period, with the United States of America (USA) contributing a significant number of reasons. Research has focused on neurotransmitter, oxidative stress, mitochondrial system injury, and other neurotoxic mechanisms. Neuroimmune, neurotoxic targets, and new psychoactive substances have been hot topics in recent years, which deserve continued research in the future. Specific research on molecular mechanisms has progressed across this period, with an emphasis on the root cause of toxicity and molecular targets for therapy. Moreover, collaborations of international multi-disciplinary research teams have been efficient and need to be encouraged for addiction research and the development of appropriate therapeutic processes.

Keywords: scientometric analysis, visualization, molecular mechanism, substance abuse, neurotoxicity

OPEN ACCESS

Edited by:
Jie Yan,
Central South University, China

Reviewed by:
Xiaofeng Zeng,
Kunming Medical University, China
Richard Lowell Bell,
Indiana University Bloomington, United States

***Correspondence:**
Man Liang
liangman@hust.edu.cn

†These authors have contributed equally to this work and share first authorship

Specialty section:
This article was submitted to Molecular Signalling and Pathways, a section of the journal Frontiers in Molecular Neuroscience

Received: *28 February 2022*
Accepted: *03 May 2022*
Published: *01 July 2022*

Citation:
Zhang A, Liu Z and Liang M (2022) A Scientometric Visualization Analysis for Molecular Mechanisms of Substance Abuse and Its Neurotoxicity From 1997 to 2021. Front. Mol. Neurosci. 15:885701. doi: 10.3389/fnmol.2022.885701

INTRODUCTION

Substance abuse, including relapse, refers to excessive consumption of stimulants, cannabis, amphetamines, cocaine, and hallucinogens, according to ICD-11 (WHO, 2021) and DSM-5 (Quinn et al., 1997; Büttner and Weis, 2004; Cassel and Bernstein, 2008; American Psychiatric Association [APA], 2013), which induces physical and/or psychological harm, deteriorating cognition and motivation, as well as impulsive and aggressive behavior (Majewska, 1996; Pau et al., 2002). Addicts suffer from complex neurological impairments that are often associated with neurodegenerative diseases, such as Parkinson's disease (Cadet and Krasnova, 2009; Graves et al., 2021). According to the report of the European Monitoring Centre for Drugs and Drug Addiction (EMCDDA) in 2020, both the number of drug-related deaths and the number of addicts, across the European Union (EU), are increasing, which aggravates the global burden on public health systems, resulting in huge worldwide economic costs, including law enforcement resources (Rehm et al., 2009; EMCDDA, 2020).

Studies have shown that abused drugs activate the mesolimbic dopaminergic system, orbitofrontal cortex, and extended amygdala (Cunha-Oliveira et al., 2008; Koob and Volkow, 2010; Chen et al., 2021a,b). Specifically, substance abuse alters intracellular signaling pathways, transcription factors, and levels of gene expression in these reward circuits (Nestler, 2004; Hyman et al., 2006; Cunha-Oliveira et al., 2008; Koob and Volkow, 2010; Liao et al., 2021). In addition, recent advances have highlighted psychoactive substance-induced neuroinflammation, blood–brain barrier (BBB) dysfunction, and neurogenesis deficits (Gonçalves et al., 2014; Crews et al., 2021).

To provide an international description of scientific activities examining substance abuse, a bibliometric analysis is needed to quantify the influences of scientific literature sets, academic characteristics (e.g., journals), institutions, highly cited literature, high-frequency identifiers, and the relevant clustering of the above. The visible technology that provides an overview of programmatic research and its developmental trends will provide researchers with a clearer understanding of relative research breakthroughs and their expected future dynamics (Kamdem et al., 2019). With this in mind, we review the research on the neurotoxicity of substance abuse and relapse with the goal of deepening our understanding of this progress as well as trends for future research, and molecular targets for therapeutic development.

MATERIALS AND METHODS

The Medical Subject Headings (MeSH) listed in PubMed were applied to obtain synonyms and the following search strategy: [Topic#3 = (Topic#1) OR (Topic#2)], {Topic#1 = [("Substance Abuse") OR ("Substance Dependence") OR ("Substance Addiction") OR ("Substance Habituation") OR ("Drug Abuse") OR ("Drug Dependence") OR ("Drug Addiction") OR ("Drug Habituation")] AND [("Neurotoxicity") OR ("Neurotoxic Effect")]}, {Topic#2 = [("Relapse of Substance Abuse") OR ("Relapse of Substance Dependence") OR ("Relapse of Substance Addiction") OR ("Relapse of Substance Habituation") OR ("Relapse of Drug Abuse") OR ("Relapse of Drug Dependence") OR ("Relapse of Drug Addiction") OR ("Relapse of Drug Habituation")] AND [("Neurotoxicity") OR ("Neurotoxic Effect")]}. The Web of Science (WoS) Core Collection database is a global academic database indexing more than 20,000 authoritative and high-impact academic journals, covering natural science, engineering technology, biomedicine, social science, and arts and humanities. We retrieved 1,321 records published between January 1997 and December 2021, and excluded 25 non-English records, narrowing the list to 1,296 English manuscripts for further analysis. A total of 1,045 original articles were identified, and studies, including review, meeting abstract, letter, proceedings paper, editorial materials, early access, notes, book chapters, news items, and corrections, were excluded. Two investigators screened all of the original data, eliminated noise, respectively, and reached a consensus *via* discussion and re-evaluation by a third investigator when discrepancies were observed. Finally, 681 articles were assembled for scientometric mining (**Figure 1**). We used CiteSpace 5.8.R3 for statistical analysis and developed visual charts, including publication output flows, cooperation agreements between countries, co-occurrent observations, and keyword/identifier bursts for mapping research trends and frontiers (Chen, 2004, 2006; Chen et al., 2010, 2014).

RESULTS

Publication Trends

Overall, annual publication outputs had a generally positive growth rate, except for a few fluctuations, since 1997; for this period, the peak annual publication count was 45 in 2016 (**Figure 2**). In line with an increasing number of annual publications, substance abuse and its neurotoxicity remained an important research topic across this time period. Using the Mann–Kendall (MK) test, the statistical results ($Z = 4.2099 > 2.32 > 0$) indicated a significant increasing trend of annual publication outputs related to neurotoxicity of substance abuse with a 0.001 level of significance. Remarkably, according to the categorization of the topics, 487 publications were focused on molecular mechanisms, while the rest were almost all on behavior or neuropsychology. Accordingly, the proportion of articles on molecular mechanisms also increased year by year, with its highest level in 2013 at 87.88% (29/33, **Figure 2**).

Contributing Countries and Institutions

Overall, 44 countries/regions contributed scientific outputs with intensive bilateral cooperation during this period. The United States (50.81%, 346/681) was the most productive country, exhibiting a marked excess in volume of research output, followed closely by the People's Republic of China (9.25%, 63/681), Spain (7.93%, 54/681), and Japan (4.85%, 33/681) (**Table 1** and **Figure 3**). Besides this, other Asian (20.26%, 138/681) and European (23.49%, 160/681) countries have also published more in recent years. Among these top 10 productive countries, United States had the greatest number of publications devoted to studies on molecular mechanisms of neurotoxicity and substance abuse (67.05%, 232/346), followed by Portugal (83.33%, 25/30).

Figure 3 also depicts bilateral cooperation between contributing countries; the United States cooperated with 22 countries, making it the most collaborative country, followed by Germany and Canada, each, respectively, cooperating with 6 other countries. This indicates that the countries/regions shared and facilitated greater increase in the research field of substance abuse by exponential collaborations.

Highly Cited Publications

The 681 articles received a total of 22,625 citations according to the WoS, giving an average citation of 33.22 per article (22,625/681). Without a defined conservative cutoff of time limit for citation, Germany (45.17, 1355/30), the United States (43.42, 15023/346), and England (38.78, 698/18) were the top 3 leaders in citations per article. Other than this, the average H-index of the retrieved papers queried

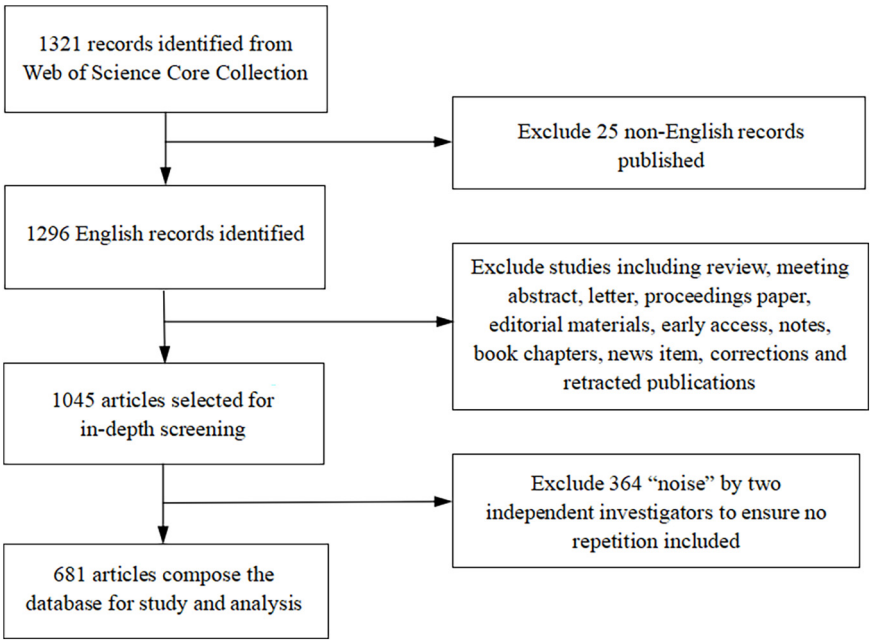

FIGURE 1 | The flowchart of methodology.

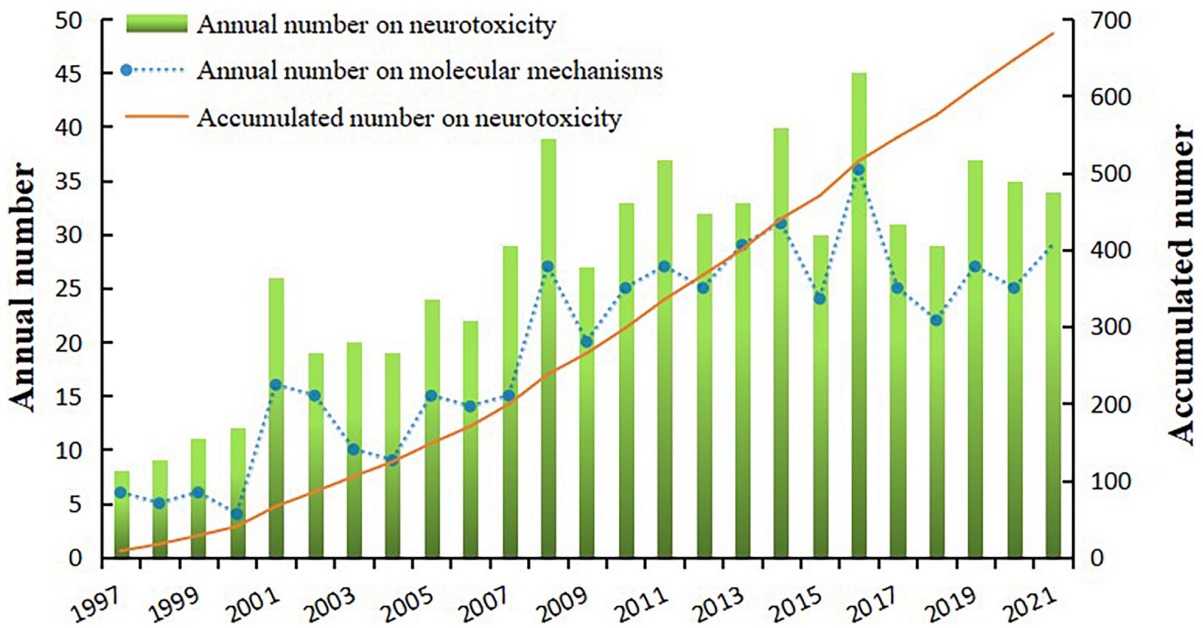

FIGURE 2 | Annual number and accumulated number of articles on neurotoxicity of substance abuse, and number of publications on molecular mechanisms from 1997 to 2021.

on the WoS was 71; and the top 3 countries were the United States with the highest H-index of 61, followed by Spain (24) and Germany (20). Furthermore, the core institutions in the countries, such as Portugal (90.00%), South Korea (38.89%), and Iran (33.33%), had other national achievements (**Table 1**).

Table 2 lists the top 10 most-cited articles, which were regarded as high-quality scientific research published in authoritative journals categorized in psychiatry (No. 1, 9), neuroscience (No. 2, 3, 7, 10), nature medicine (No. 4), neurology (No. 5, 6), and preventive medicine (No. 8). These most cited papers examined the mechanisms of psychomotor

TABLE 1 | The top 10 productive countries and institutions.

Country or region	Articles (%)	Citations	H-index	Citations per article	Top country institution	Top institution articles (%)
United States	346 (50.81%)	15023	61	43.42	National Institutes of Health Nih United States	52 (15.03%)
Peoples R China	63 (9.25%)	861	18	13.67	Southern Medical University China	9 (14.29%)
Spain	54 (7.93%)	1436	24	27.09	University of Barcelona	16 (29.63%)
Japan	33 (4.85%)	1062	16	32.18	Chiba University	5 (15.15%)
Germany	30 (4.41%)	1355	20	45.17	Humboldt University of Berlin	9 (30.00%)
Portugal	30 (4.41%)	984	18	32.80	Universidade Do Porto	27 (90.00%)
Italy	28 (4.11%)	759	14	27.11	University of Cagliari	7 (25.00%)
Iran	24 (3.52%)	173	8	7.21	Shahid Beheshti University Medical Sciences	8 (33.33%)
England	18 (2.64%)	698	13	38.78	University of London	4 (22.22%)
South Korea	18 (2.64%)	353	8	19.61	Kangwon National University	7 (38.89%)

impairment and neurotoxicity, and eight of the top 10 papers examined neurotoxic molecular mechanisms, like a role of the dopamine transporter (Volkow et al., 2001; Munro et al., 2006). Impressively, nine of the top 10 articles were contributed by the United States, and another one was contributed by England; correspondingly, IF5 and SJR of these top two countries were the United States (IF5: 17.825, SJR: 5.477) and England (IF5: 49.248, SJR: 19.536), respectively.

Active Journals

More than 200 authoritative journals published articles on the neurotoxicity of substance abuse. Among these, the top 10 of these active journals contained 28.93% of the manuscripts, such as Neurotoxicity Research (3.82%, 26/681), Neuroscience (3.67%, 25/681), and Psychopharmacology (3.52%, 24/681) (refer to **Table 3**); fields of research included neuroscience, biochemistry, pharmacology, as well as toxicology and pharmaceutics.

Hotspots of Research

After excluding irrelevant and repeated keywords, we analyzed, merged, and visualized the network maps of keyword co-occurrence by CiteSpace (**Figure 4**), which illustrated the relevance and frequency of keywords using circle link and size. High-frequency keywords, including "neurotoxicity" (frequency: 188, centrality: 0.23), "brain" (frequency: 117, centrality: 0.13), "oxidative stress" (frequency: 79, centrality: 0.09), "rat" (frequency: 77, centrality: 0.11), and "mdma" (frequency: 75, centrality: 0.11), represented by larger circles. Other keywords, such as "amphetamine" (frequency: 71, centrality: 0.10), "dopamine" (frequency: 62, centrality: 0.09), "nucleus accumbens (NAc)" (frequency: 57, centrality: 0.13), "activation" (frequency: 53, centrality: 0.08), and "apoptosis" (frequency: 42, centrality: 0.05) showed moderate frequencies.

Scientific Landscapes and Trends

After clustering and mapping co-cited literatures (**Figure 5**), we analyzed the timeline of developing trends of specific research fields, the observed shift of research focus, and the formal professional structures of these research systems (Niazi and Hussain, 2011). According to an in-depth analysis of the top ten clusters, we identified that most were distributed in the period from 1997 to 2010. The earlier studies have focused on methamphetamine (#3), drug abuse (#1), and dopamine (#5); then, the research hotspots shifted to heat shock protein (#7), synaptic plasticity (#8), NMDA receptor (#6), oxidative stress (#0), and neurotoxicity (#2), which are all involved in neurotoxic molecular mechanisms of substance abuse. As for alcohol therapy (#4), a therapeutic implication of drug abuse has maintained researchers' attention for several years.

We found that keywords could reveal research topics and contents, which play an apparent and updated role in tracking the transition of research hotspots. We obtained a keyword burst map to visualize shifts in focus and emergence across time on the basis of the strongest burst of keywords in scientific research articles (**Figure 6**). In addition, burst keywords could summarize outstanding research topics over any period of time by indicating the duration and intensity of these hot issues (Kleinberg, 2003; Chen, 2004, 2006; Chen et al., 2010, 2014). According to the top 24 keywords with the strongest citation bursts, the earlier research hotspots were neurotoxic target-organs and animal models (dismutase transgenic mice, rat brain, and central serotonergic neuron), examination (positron emission tomography), and commonly abused drugs (cocaine). Then, the burst keywords shifted to molecular mechanism-related items (e.g., messenger RNA, serotonin, microglial activation, oxidative stress, autophagy) and new psychoactive substances (e.g., bath salt and psychoactive substance). Besides these, the relationship between substance abuse and Alzheimer's disease and some comorbid models were examined.

DISCUSSION

Our study performed a visualized bibliometric analysis of substance abuse and its neurotoxicity from 1997 to 2021 using

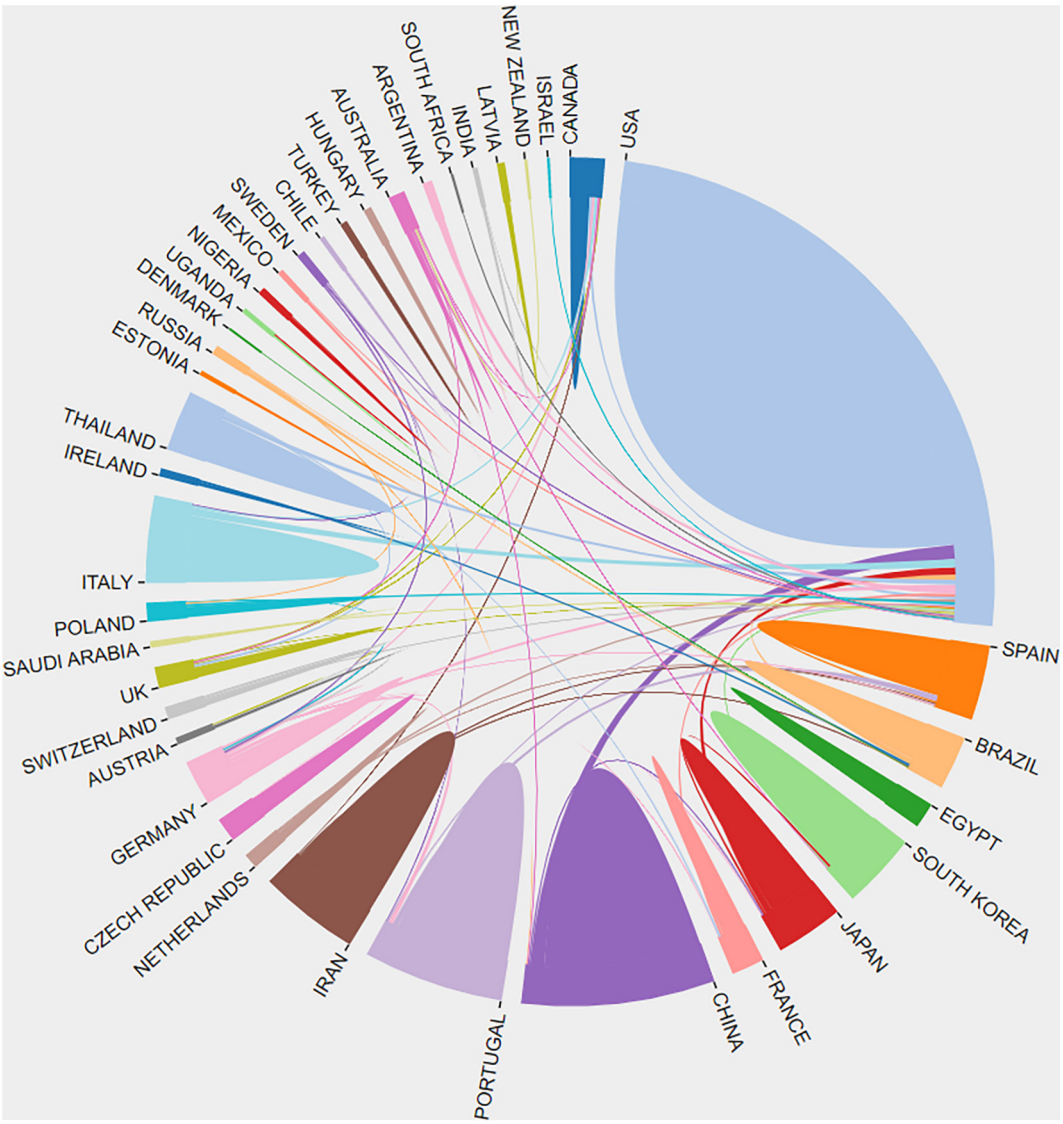

FIGURE 3 | Cooperation between contributed countries.

CiteSpace. Substance abuse has caused increasing global harm by impairing the nervous system and the development of psychiatric symptoms (Şenel and Demir, 2018; EMCDDA, 2020; da Silva et al., 2021). More and more research has focused on the neurotoxic progression of substance abuse, especially the complexities of molecular mechanisms. These fields of research have needed a review to map the publications providing new ideas for the treatment and prevention of drug abuse and relapse (i.e., hot topics).

Drug abuse has brought a tremendous socioeconomic burden to the whole world, especially in recent decades (Hagemeier, 2018); this dreadful situation needs more research to expose the severity of drug addiction and drug-induced neurological disorders. Encouragingly, from 1997 to 2021, the total amount of related publications reached a total of 681, with an average of 27 per year; and an annual number of publications had a generally rising trend with a peak in 2016.

Over the past 25 years, the United States, contributing more than half of the total publications, has played a leading significant role in productivity in this field, and Asian and European countries came followed with far less production. Regarding the reason for this status, in the United States, various types of smuggled drugs have flooded its streets; meanwhile, classic opiates, cocaine, and amphetamines were pursued by a large number of substance abusers. Except for such a severe social landscape, the United States government offered abundant research funds to support high-level research activity, which resulted in a high academic reputation and characteristic H-index value in scientific research (e.g., Substance Abuse and Mental Health Services Administration, 2002). Among the European

countries, Germany published a medium amount of research and had the highest number of citations per article, which indicated significant researchers' close attention.

Considering its global harm, there has been a significant increased hot topic research and collaborative projects in countries, such as the United States, Germany, and Canada (Fujáková-Lipski et al., 2017; Costa et al., 2021; Sogos et al., 2021). Based on legalized marijuana policies in the United States and Canada, similar domestic and international situations and potential cooperative opportunities increased exponentially; additionally, the United States provides attractive financial grants to facilitate efficient cooperation and productivity (Goundar et al., 2021; Isfandyari-Moghaddam et al., 2021). Under a shared global concern of drug abuse, worldwide scientific cooperation should be further strengthened to highlight research quality, and the outcomes should be noted to more deeply illustrate the harm of substance abuse and drug-induced toxicity (Rahim et al., 2012).

The 10 most active journals, as shown in **Table 3**, were of high quality and rational JCR quartile on neuroscience and neuropsychiatry, published nearly one-third of the total publications. Of the molecular mechanisms of neurotoxicity of substance abuse, the understanding has reached unprecedented depth, and significant advances are laudable over the past few decades. The neurotoxic effects of drug abuse are associated with oxidative stress, mitochondrial dysfunction, apoptosis, and neurogenesis inhibition, directly or indirectly affecting neurotransmitter systems, including but not limited to dopaminergic and glutamatergic neurons, and causing irreversible neuronal damage (Cunha-Oliveira et al., 2008; da Silva et al., 2021).

The bibliometric indicators, including publication numbers, citations per article, journal impact factors, crown indicators, H-index, and its variants, can manifest high-quality scientific results (Joshi, 2014). Our results indicated that the average citation per article on the neurotoxicity of substance abuse was 33.22, higher than on other subjects, implying that the topic has

TABLE 2 | The characteristics of highly cited articles.

Rank	Total citations	Article title	Journal	Published year	Country	IF 2020	IF 5- years	SJR 2020
1	688	Association of dopamine transporter reduction with psychomotor impairment in methamphetamine abusers	American Journal of Psychiatry	2001	United States	18.112	17.825	5.477
2	459	Reduced striatal dopamine transporter density in abstinent methamphetamine and methcathinone users: Evidence from positron emission tomography studies with [C-11]WIN-35,428	Journal of Neuroscience	1998	United States	6.167	6.993	3.483
3	437	Loss of dopamine transporters in methamphetamine abusers recovers with protracted abstinence	Journal of Neuroscience	2001	United States	6.167	6.993	3.483
4	423	Nitrous oxide (laughing gas) is an NMDA antagonist, neuroprotectant and neurotoxin	Nature Medicine	1998	England	53.440	49.248	19.536
5	277	Memory impairment in abstinent MDMA ("Ecstasy") users	Neurology	1998	United States	9.910	10.664	2.910
6	275	Evidence for long-term neurotoxicity associated with methamphetamine abuse–A H-1 MRS study	Neurology	2000	United States	9.910	10.664	2.910
7	275	Small changes in ambient temperature cause large changes in 3,4-methylenedioxymethamphetamine (MDMA)-induced serotonin neurotoxicity and core body temperature in the rat	Journal of Neuroscience	1998	United States	6.167	6.993	3.483
8	249	Sex differences in striatal dopamine release in healthy adults	Biological Psychiatry	2006	United States	13.382	14.103	5.335
9	245	Methamphetamine causes microglial activation in the brains of human abusers	Journal of Neuroscience	2008	United States	6.167	6.993	3.483
10	210	Neuronal apoptosis associated with morphine tolerance: Evidence for an opioid-induced neurotoxic mechanism	Journal of Neuroscience	2002	United States	6.167	6.993	3.483

TABLE 3 | The 10 most active journals that published articles on substance abuse and its neurotoxicity research.

Journal	Published numbers (%)	IF 2020	SJR 2020	JCR quartile	Categories
Neurotoxicity Research	26 (3.82%)	3.911	0.923	Q2	Neuroscience; pharmacology, toxicology and pharmaceutics
Neuroscience	25 (3.67%)	3.590	1.297	Q3	Neuroscience
Psychopharmacology	24 (3.52%)	4.530	1.378	Q2	Pharmacology; toxicology and pharmaceutics
Brain Research	20 (2.94%)	3.252	1.037	Q3	Biochemistry, genetics and molecular biology; medicine; neuroscience
Neuroscience Letters	19 (2.79%)	3.046	0.944	Q3	Neuroscience
Neuropharmacology	18 (2.64%)	5.251	1.760	Q2	Neuroscience; pharmacology, toxicology and pharmaceutics
Neuropsychopharmacology	18 (2.64%)	7.855	2.704	Q1	Medicine; pharmacology, toxicology and pharmaceutics
Neurotoxicology	16 (2.35%)	4.294	1.060	Q2	Neuroscience; pharmacology, toxicology and pharmaceutics
Journal of Neurochemistry	16 (2.35%)	5.372	1.750	Q2	Biochemistry, genetics and molecular biology; neuroscience
Pharmacology Biochemistry and Behavior	15 (2.20%)	3.533	1.184	Q2	Biochemistry, genetics and molecular biology; neuroscience; pharmacology, toxicology and pharmaceutics

kept a strong research interest. In general, highly cited articles are published in journals with high SJR or IF (Falagas and Alexiou, 2008). Notably, four of the top 10 most-cited articles have garnered more than 400 citations, and nine articles were published in journals with IF >5 or higher. From the angle of contributing countries, nine literatures were ascribed to the United States, which constituted a major force in this field; and the other one, published in Nature Medicine, the only journal with IF >50, was authored by researchers from England.

Furthermore, six of these articles focused on studies related to methamphetamine, while the remaining four articles analyzed the neurotoxicity mechanisms of 3,4-methylenedioxymethamphetamine (MDMA), nitrous oxide (laughing gas), and neuronal apoptosis associated with morphine tolerance. This could be interpreted that methamphetamine, as one of the most widely abused drugs, has attracted more researchers' interests than others; and the mainstream views show that significant alterations in dopamine and serotonin by dopamine transporter dysfunction in the striatum led to long-term neuronal damage and ultimately motor and cognitive impairment (Volkow et al., 2001). Among the methamphetamine abusers, the aforementioned neurotoxicity is significantly more severe in men than in women; nevertheless, no significant molecular differences were observed between the sexes (Munro et al., 2006). Moreover, the 10 most-cited articles were all published from 1998 through 2008, which suggest that these results have primarily progressed and verified the mechanisms of neurotoxicity of substance abuse in this decade and enlightened more research afterward.

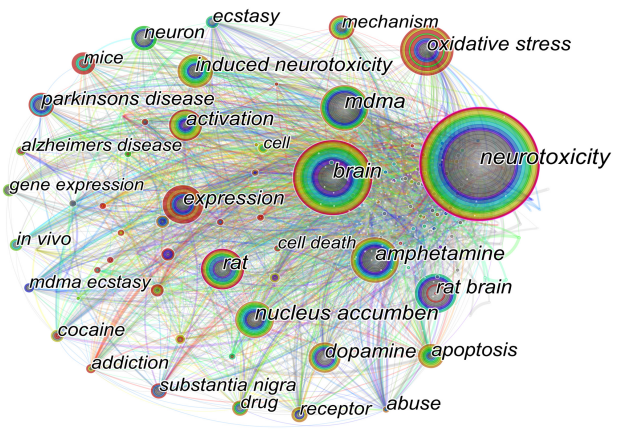

FIGURE 4 | Network of keywords co-occurrence. The circle size and the link illustrated the frequency and relevance of keywords, respectively.

According to the presented keyword co-occurrence network, the core direction of the specific research topics was examined. In **Figure 4**, the clustered topics, such as neurotoxicity, brain, oxidative stress, dopamine, MDMA (ecstasy), amphetamine, Parkinson's disease, and Alzheimer's disease, can be categorized as "neuroscience," "molecular biology," "epidemiology," or "psychoneuropathology"; and these interdisciplinary aspects represent the evolutionary process of more concerning issues in this field.

The neurotoxic effects of abused substances could be described as inhibiting (e.g., opioids, cannabinoids, nicotine) or stimulating (e.g., cocaine and amphetamines) neurotransmitters, decreasing dopamine and serotonin reserves by inactivating their transporters, reducing vesicular monoamine transporters, and activating alpha-(2)-adrenergic receptors (Volkow et al., 2001; Cozzi and Foley, 2003; Garrido et al., 2005; Jîtcã et al., 2021). Besides, studies also proved that tachykinins, especially substance P (SP), are linked to the terminal degeneration of dopamine through NK-1 receptor activity in substantia nigra for chronic methamphetamine abusers (Yu et al., 2002). The neurotoxicity and senescence induced by methamphetamine resulted from the upregulation and aggregation of presynaptic

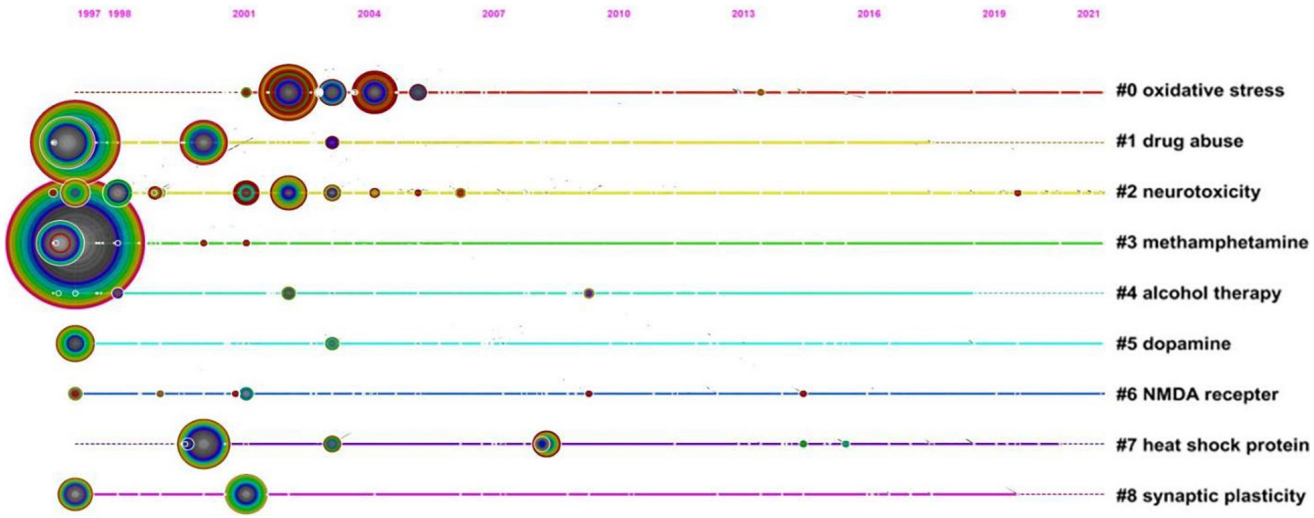

FIGURE 5 | Co-cited references timeline map of neurotoxicity of substance abuse. Nodes represent referenced documents. The size of nodes represents the frequencies of cited references, and the location reflects the present time. Years are arranged horizontally at the top. The clusters are performed based on the themes of co-cited references and the label of each cluster is shown at the end of the timeline.

protein α-synuclein (Fornai et al., 2005; Wu et al., 2021). Of note, drug participatory induced the release of monoamines from neuronal storage vesicles, metabolism by monoamine oxidase or catechol-O-methyltransferase (COMT), and reactive oxygen species (ROS) generation (da Silva et al., 2021); meanwhile, hydrogen peroxide, as a by-product of these activities interacting with transition metal ions, generates toxic hydroxyl radicals, which indicate that drug-induced excessive neurotransmitter release has a strong correlation with oxidative stress (Barbosa et al., 2012; Graves et al., 2021). It is worth noting that drug-induced mitochondrial metabolism dysfunction promotes oxidative stress by inhibiting oxidative phosphorylation and ATP production, triggering apoptotic signaling pathways, and then causing neuronal damage (Burrows et al., 2000; Huang et al., 2019). It has been shown that methamphetamine and cocaine, interfering with all electron transport chain (ETC) complexes, producing excess ROS, further aggravate mitochondrial disintegration, while mephedrone affects the activity of mitochondrial complex II and IV (Yang et al., 2018; Naserzadeh et al., 2019; Thornton et al., 2021).

Besides the above, the highly cited articles demonstrated that abused drugs could increase microglial reactivity and lead to neuroinflammation, which has shown a strong link to neurotoxicity (Lacagnina et al., 2017). Amphetamine compounds, acting on dopamine D1-like receptors, microglia, and relevant signaling proteins, exacerbated neuroinflammation responses and promoted macrophage polarization from M0 to M1, which provides a potential basis of long-term neurotoxicity (Li et al., 2018; Wang et al., 2019). Cocaine activated microglia in NAc, increasing the production and release of tumor necrosis factor-alpha (TNF-α) (Lewitus et al., 2016). Cannabis could impair the activation of Toll-like receptors 4 (TLR4) by inhibiting cytokine production and interfering with TLR-induced immune responses (Sexton, 2020). Moreover, synthetic cathinone and ketamine have been confirmed to induce the release of pro-inflammatory cytokines and microglial activation (Li et al., 2017; Oliver et al., 2018; Erickson et al., 2019). Regarding methamphetamine abuse, melatonin could reduce the expression of pro-inflammatory cytokines, inhibit the expression of inflammation-mediated enzymes, such as TNF-α and iNOS, and suppress neuroinflammation (Deng et al., 2006; Olcese et al., 2009; Veneroso et al., 2009). These referenced molecular mechanisms may provide valid and reliable therapy potential for substance abuse and relapse in the future.

As a prominent feature of bibliometrics, the research topic clustering technology categorizes all retrieved records with similar topics and generates a timeline map (Waltman et al., 2010). According to the clustering of the co-cited literatures, NMDA receptor (#6, *N*-methyl-D-aspartic acid receptor) has been a significant focus for a long time. Based on glutamatergic neurotransmission involved in several substances of abuse, activated NMDA receptors would increase intracellular calcium concentration, which increases extracellular glutamate with positive feedback (Rego and Oliveira, 2003; Tzschentke and Schmidt, 2003). Methamphetamine increased glutamate by exocytosis of astrocytes through TNF production and calcium mobilization, which thereby promoted microglial reactivity to neuroinflammation, and neuronal death (Canedo et al., 2021). In addition, other psychoactive substances (e.g., morphine, cocaine, and heroin) could increase extracellular glutamate concentrations in the ventral tegmental area (VTA), NAc, prefrontal cortex, and striatum (Siggins et al., 2003; Williams and Steketee,

Top 24 Keywords with the Strongest Citation Bursts

Keywords	Year	Strength	Begin	End	1997 - 2021
rat brain	1997	6.64	1997	2004	
dismutase transgenic mice	1997	3.99	1997	2002	
central serotonergic neuron	1997	4.24	1998	2001	
binding	1997	3.75	1998	2003	
positron emission tomography	1997	5.13	2001	2006	
cocaine	1997	3.55	2003	2005	
messenger rna	1997	3.78	2006	2011	
serotonin	1997	4.93	2009	2014	
microglial activation	1997	3.65	2009	2013	
involvement	1997	3.29	2009	2015	
mice	1997	9.31	2014	2017	
bath salt	1997	5.07	2014	2021	
inhibition	1997	4.25	2014	2019	
conditioned place preference	1997	5.81	2015	2018	
oxidative stress	1997	4.6	2016	2018	
alzheimers disease	1997	3.52	2016	2019	
psychoactive substance	1997	4.51	2017	2021	
dependence	1997	3.55	2017	2021	
exposure	1997	5.59	2018	2021	
up regulation	1997	3.81	2018	2021	
toxicity	1997	3.61	2018	2021	
expression	1997	6.06	2019	2021	
autophagy	1997	4.3	2019	2021	
stress	1997	3.68	2019	2021	

FIGURE 6 | Top 24 keywords with the strongest citation bursts. Each blue or red short line represents a year, and a red line stands for a burst detected year.

2004; Domingues et al., 2006; You et al., 2007). Otherwise, NMDA receptor antagonists, memantine and MK-801, may inhibit physical dependence and tolerance (Tzschentke and Schmidt, 1995; Trujillo, 2000; Ribeiro Do Couto et al., 2004). Therefore, further research on NMDA receptor activities may provide new strategies to treat substance abuse.

By CiteSpace algorithm-dependent keyword citation burst detection (Chen, 2006), compared with traditional drugs, new designer substances, such as "bath salt" from 2014, containing one or more synthetic cathinone derivatives, such as the most popular components of 4-methylcathinone (mephedrone), 3,4-methylenedioxymethcathinone (methylone), and 3,4-methylenedioxypyrovalerone (MDPV) (Baumann et al., 2013), have become popular particularly among adolescents since the mid-2000s (Altun and Çok, 2020). Similar to traditional drugs, synthetic cathinones also act on monoaminergic terminal functional markers, increasing ROS, activating apoptotic signaling pathways, and causing cytotoxicity (Leyrer-Jackson et al., 2019).

According to the bibliometrics analysis, we found that research on poly drug abuse often co-occurred recently. As quite a few drug abusers may prefer multi-substances of abuse (Gerostamoulos et al., 2001; Preti et al., 2002; Coffin et al., 2003; Darke, 2003; Steentoft et al., 2006), more studies focused on synergistic effects of alcohol and psychoactive substances; e.g., recreational co-abuse of alcohol and ketamine could aggravate characteristic apoptosis in morphologically sub-G1 phase and lead to intra-neuronal Ca^{2+} overload, down-regulation of p-Akt, p-CREB, PKA, CaMK-IV, Bcl-2, and BDNF, and up-regulation of cleaved caspase-3 and Bax (Moore et al., 1997; Wu et al., 2006; Quek et al., 2013; Zuo et al., 2017).

Other proportionately interesting findings on the neurotoxicity of substance abuse were also retrieved. Curcumin, a natural polyphenol extracted from the rhizome of *Curcuma longa* L, and *Melissa officinalis*, an antioxidant plant, both scavenge oxygen free radicals and inhibit monoamine oxidase to antagonize drug-induced neuronal apoptosis (Hassanzadeh et al., 2011; Ryskalin et al., 2021). This suggests a potential neuroprotective role of natural plant extracts for the treatment of substance abuse. A number of pharmacological interventions for drug-related memory deficits have shown significant benefits in preventing relapse at the preclinical level, such as propranolol interfering with heroin memory consolidation and reducing subsequent drug-seeking, making it an attractive treatment candidate for opioid addiction and relapse prevention (Chen et al., 2021a,b). Moreover, mTOR (mammalian target of rapamycin) interferes with cocaine-related memory consolidation, reduces cocaine-seeking behavior, and prevents relapse, and these effects are extract-dependent and time-specific (Zhang et al., 2021). Besides, 5-hydroxytryptamine receptor 1F (5-HT1F) receptor agonist, LY 344864, and cannabidiol showed a therapeutic

prevention of relapse to drug addiction (Shahidi et al., 2018; Metz et al., 2021).

CONCLUSION

While there has been an exponential increase in substance abuse harm and corresponding research, there is still a paucity of studies examining systematic bibliometric progress. With the included visualized illustration, we constructed this assessment to elucidate interdisciplinary information of research on psychoactive substances. Based on the studies of neurotoxicity, pharmacological effects, and epidemiology, this update on research evidence suggests greater scientific therapeutic predictability to combat addiction to psychoactive substances. The overall findings of this study suggest that research hotspots have focused on molecular mechanisms, and more scientific priority should be given to allocate research resources for these studies with the greatest potential to investigate therapeutic applications.

LIMITATIONS

There were inevitable limitations to our study. First, since the scientific literature database (WoS) keeps dynamic publishing, the interval lag between the publication and the retrieval would affect the time sensitivity of studies. Second, to comply with the software condition of CiteSpace, only English studies were analyzed for the function of co-occurrence and co-citation analysis methods (incompatibility of multiple languages).

DATA AVAILABILITY STATEMENT

The original contributions presented in this study are included in the article/supplementary material, further inquiries can be directed to the corresponding author.

AUTHOR CONTRIBUTIONS

ML and ZL contributed to the conception, design of the study, reviewed, and edited the manuscript. AZ organized the database and performed the statistical analysis. AZ and ML wrote the first draft of the manuscript. All authors contributed to the manuscript revision, read, and approved the submitted version.

FUNDING

This study was financially supported by the "National Engineering Laboratory for Forensic Science" (Grant No. 2019NELKFKT11) and National Engineering Laboratory for Forensic Science and Key Laboratory of Forensic Toxicology, Ministry of Public Security, People's Republic of China (Beijing Municipal Public Security Bureau).

ACKNOWLEDGMENTS

We thank the reviewers for their insightful comments on the manuscript, as their remarks led to an improvement of the work.

REFERENCES

Altun, B., and Çok, Ý (2020). Psychoactive bath salts and neurotoxicity risk. *Turk. J. Pharm. Sci.* 17, 235–241. doi: 10.4274/tjps.galenos.2018.40820

American Psychiatric Association [APA] (2013). *Diagnostic and Statistical Manual of Mental Disorders (DSM-5®)*. Washington, DC: American Psychiatric Publishing. doi: 10.1176/appi.books.9780890425596

Barbosa, D. J., Capela, J. P., Oliveira, J. M., Silva, R., Ferreira, L. M., Siopa, F., et al. (2012). Pro-oxidant effects of ecstasy and its metabolites in mouse brain synaptosomes. *Br. J. Pharmacol.* 165, 1017–1033. doi: 10.1111/j.1476-5381.2011.01453.x

Baumann, M. H., Partilla, J. S., and Lehner, K. R. (2013). Psychoactive "bath salts": not so soothing. *Eur. J. Pharmacol.* 698, 1–5. doi: 10.1016/j.ejphar.2012.11.020

Burrows, K. B., Gudelsky, G., and Yamamoto, B. K. (2000). Rapid and transient inhibition of mitochondrial function following methamphetamine or 3,4-methylenedioxymethamphetamine administration. *Eur. J. Pharmacol.* 398, 11–18. doi: 10.1016/s0014-2999(00)00264-8

Büttner, A., and Weis, S. (2004). "Central nervous system alterations in drug abuse," in *Forensic Pathology Reviews. Forensic Pathology Reviews*. 1, ed. M. Tsokos (Totowa, NJ: Humana Press). 330. doi: 10.1007/978-1-59259-786-4_4

Cadet, J. L., and Krasnova, I. N. (2009). Molecular bases of methamphetamine-induced neurodegeneration. *Int. Rev. Neurobiol.* 88, 101–119. doi: 10.1016/S0074-7742(09)88005-7

Canedo, T., Portugal, C. C., Socodato, R., Almeida, T. O., Terceiro, A. F., Bravo, J., et al. (2021). Astrocyte-derived TNF and glutamate critically modulate microglia activation by methamphetamine. *Neuropsychopharmacology* 46, 2358–2370. doi: 10.1038/s41386-021-01139-7

Cassel, E., and Bernstein, D. A. (2008). *Karch's Pathology of Drug Abuse*. 4th Edn. Boca Raton, FL: CRC Press. doi: 10.1201/9780849378812

Chen, C. M. (2004). Searching for intellectual turning points: progressive knowledge domain visualization. *Proc. Natl. Acad. Sci. U.S.A* 101, 5303–5310. doi: 10.1073/pnas.0307513100

Chen, C. M. (2006). CiteSpace II: detecting and visualizing emerging trends and transient patterns in scientific literature. *J. Am. Soc. Inf. Sci. Technol.* 57, 359–377. doi: 10.1002/asi.20317

Chen, C. M., Dubin, R., and Kim, M. C. (2014). Orphan drugs and rare diseases: a scientometric review (2000-2014). *Expert Opin. Orphan Drugs* 2, 709–724. doi: 10.1517/21678707.2014.920251

Chen, C. M., Ibekwe-SanJuan, F., and Hou, J. (2010). The structure and dynamics of cocitation clusters: a multiple-perspective cocitation analysis. *J. Am. Soc. Inf. Sci. Technol.* 61, 1386–1409. doi: 10.1002/asi.21309

Chen, L., Huang, S., Yang, C., Wu, F., Zheng, Q., Yan, H., et al. (2021a). Blockade of β-Adrenergic receptors by propranolol disrupts reconsolidation of drug memory and attenuates heroin seeking. *Front. Pharmacol.* 12:686845. doi: 10.3389/fphar.2021.686845

Chen, L., Yan, H., Wang, Y., He, Z., Leng, Q., Huang, S., et al. (2021b). The mechanisms and boundary conditions of drug memory reconsolidation. *Front. Neurosci.* 15:717956. doi: 10.3389/fnins.2021.717956

Coffin, P. O., Galea, S., Ahern, J., Leon, A. C., Vlahov, D., and Tardiff, K. (2003). Opiates, cocaineand alcohol combinations in accidental drug overdose deaths in New York City, 1990-98. *Addiction* 98, 739–747. doi: 10.1046/j.1360-0443.2003.00376.x

Costa, G., Caputi, F. F., Serra, M., Simola, N., Rullo, L., Stamatakos, S., et al. (2021). Activation of antioxidant and proteolytic pathways in the nigrostriatal dopaminergic system after 3,4-methylenedioxymethamphetamine

administration: sex-related differences. *Front. Pharmacol.* 12:713486. doi: 10.3389/fphar.2021.713486

Cozzi, N. V., and Foley, K. F. (2003). Methcathinone is a substrate for the serotonin uptake transporter. *Pharmacol. Toxicol.* 93, 219–225. doi: 10.1046/j.1600-0773.2003.pto930504.x

Crews, F. T., Zou, J., and Coleman, L. G. Jr. (2021). Extracellular microvesicles promote microglia-mediated pro-inflammatory responses to ethanol. *J. Neurosci. Res.* 99, 1940–1956. doi: 10.1002/jnr.24813

Cunha-Oliveira, T., Rego, A. C., and Oliveira, C. R. (2008). Cellular and molecular mechanisms involved in the neurotoxicity of opioid and psychostimulant drugs. *Brain Res. Rev.* 58, 192–208. doi: 10.1016/j.brainresrev.2008.03.002

da Silva, D. D., Silva, J. P., Carmo, H., and Carvalho, F. (2021). Neurotoxicity of psychoactive substances: a mechanistic overview. *Curr. Opin. Toxicol.* 28, 76–83. doi: 10.1016/j.cotox.2021.10.002

Darke, S. (2003). Polydrug use and overdose: overthrowing old myths. *Addiction* 98:711. doi: 10.1046/j.1360-0443.2003.00416.x

Deng, W. G., Tang, S. T., Tseng, H. P., and Wu, K. K. (2006). Melatonin suppresses macrophage cyclooxygenase-2 and inducible nitric oxide synthase expression by inhibiting p52 acetylation and binding. *Blood* 108, 518–524. doi: 10.1182/blood-2005-09-3691

Domingues, A., Cunha Oliveira, T., Laço, M. L., Macedo, T. R., Oliveira, C. R., and Rego, A. C. (2006). Expression of NR1/NR2B N-methyl-D-aspartate receptors enhances heroin toxicity in HEK293 cells. *Ann. N.Y. Acad. Sci.* 1074, 458–465. doi: 10.1196/annals.1369.046

EMCDDA (2020). *European Drug Report 2020: Trends and Developments*. Luxembourg: Publications Office of the European Union.

Erickson, E. K., Grantham, E. K., Warden, A. S., and Harris, R. A. (2019). Neuroimmune signaling in alcohol use disorder. *Pharmacol. Biochem. Behav.* 177, 34–60. doi: 10.1016/j.pbb.2018.12.007

Falagas, M. E., and Alexiou, V. G. (2008). An analysis of trends in globalisation of origin of research published in major general medical journals. *Int. J. Clin. Pract.* 62, 71–75. doi: 10.1111/j.1742-1241.2007.01590.x

Fornai, F., Lenzi, P., Ferrucci, M., Lazzeri, G., di Poggio, A. B., Natale, G., et al. (2005). Occurrence of neuronal inclusions combined with increased nigral expression of alpha-synuclein within dopaminergic neurons following treatment with amphetamine derivatives in mice. *Brain Res. Bull.* 65, 405–413. doi: 10.1016/j.brainresbull.2005.02.022

Fujáková-Lipski, M., Kaping, D., Šírová, J., Horáèek, J., Páleníèek, T., Zach, P., et al. (2017). Trans-generational neurochemical modulation of methamphetamine in the adult brain of the Wistar rat. *Arch. Toxicol.* 91, 3373–3384. doi: 10.1007/s00204-017-1969-y

Garrido, E., P é rez-Garcí a, C., Alguacil, L. F., and D í ez-Fern á ndez, C. (2005). The alpha2-adrenoceptor antagonist yohimbine reduces glial fibrillary acidic protein upregulation induced by chronic morphine administration. *Neurosci. Lett.* 383, 141–144. doi: 10.1016/j.neulet.2005.04.002

Gerostamoulos, J., Staikos, V., and Drummer, O. H. (2001). Heroin-related deaths in Victoria: a review of cases for 1997 and 1998. *Drug Alcohol Depend.* 61, 123–127. doi: 10.1016/s0376-8716(00)00128-9

Gonçalves, J., Baptista, S., and Silva, A. P. (2014). Psychostimulants and brain dysfunction: a review of the relevant neurotoxic effects. *Neuropharmacology* 87, 135–149. doi: 10.1016/j.neuropharm.2014.01.006

Goundar, P., Macaulay, T., and Szafron, M. (2021). A comparative analysis of laws on recreational cannabis edibles between Canada and the United States of America. *Int. J. Drug Policy* 94:103191. doi: 10.1016/j.drugpo.2021.103191

Graves, S. M., Schwarzschild, S. E., Tai, R. A., Chen, Y., and Surmeier, D. J. (2021). Mitochondrial oxidant stress mediates methamphetamine neurotoxicity in substantia nigra dopaminergic neurons. *Neurobiol. Dis.* 156:105409. doi: 10.1016/j.nbd.2021.105409

Hagemeier, N. E. (2018). Introduction to the opioid epidemic: the economic burden on the healthcare system and impact on quality of life. *Am. J. Managed Care* 24, S200–S206.

Hassanzadeh, G., Pasbakhsh, P., Akbari, M., Shokri, S., Ghahremani, M., Amin, G., et al. (2011). Neuroprotective properties of melissa officinalis L. extract against ecstasy-induced neurotoxicity. *Cell J.* 13, 25–30.

Huang, E., Huang, H., Guan, T., Liu, C., Qu, D., Xu, Y., et al. (2019). Involvement of C/EBPβ-related signaling pathway in methamphetamine-induced neuronal autophagy and apoptosis. *Toxicol. Lett.* 312, 11–21. doi: 10.1016/j.toxlet.2019.05.003

Hyman, S. E., Malenka, R. C., and Nestler, E. J. (2006). Neural mechanisms of addiction: the role of reward-related learning and memory. *Ann. Rev. Neurosci.* 29, 565–598. doi: 10.1146/annurev.neuro.29.051605.113009

Isfandyari-Moghaddam, A., Saberi, M. K., Tahmasebi-Limoni, S., Mohammadian, S., and Naderbeigi, F. (2021). Global scientific collaboration: a social network analysis and data mining of the co-authorship networks. *J. Inf. Sci.* doi: 10.1177/01655515211040655

Jîtcă, G., Ősz, B. E., Tero-Vescan, A., and Vari, C. E. (2021). Psychoactive drugs-from chemical structure to oxidative stress related to dopaminergic neurotransmission. *Rev. Antioxidants (Basel)* 10:381. doi: 10.3390/antiox10030381

Joshi, M. A. (2014). Bibliometric indicators for evaluating the quality of scientifc publications. *J. Contemp. Dent Pract.* 15, 258–262. doi: 10.5005/jp-journals-10024-1525

Kamdem, J. P., Duarte, A. E., Lima, K., Rocha, J., Hassan, W., Barros, L. M., et al. (2019). Research trends in food chemistry: a bibliometric review of its 40 years anniversary (1976-2016). *Food Chem.* 294, 448–457. doi: 10.1016/j.foodchem.2019.05.021

Kleinberg, J. (2003). Bursty and hierarchical structure in streams. *Data Min. Knowl. Discov.* 7, 373–397. doi: 10.1038/s41598-020-80059-w10.1023/a:1024940629314

Koob, G. F., and Volkow, N. D. (2010). Neurocircuitry of addiction. *Neuropsychopharmacology* 35, 217–238. doi: 10.1038/npp.2009.110

Lacagnina, M. J., Rivera, P. D., and Bilbo, S. D. (2017). Glial and neuroimmune mechanisms as critical modulators of drug use and abuse. *Neuropsychopharmacology* 42, 156–177. doi: 10.1038/npp.2016.121

Lewitus, G. M., Konefal, S. C., Greenhalgh, A. D., Pribiag, H., Augereau, K., and Stellwagen, D. (2016). Microglial TNF-α suppresses cocaine-induced plasticity and behavioral sensitization. *Neuron* 90, 483–491. doi: 10.1016/j.neuron.2016.03.030

Leyrer-Jackson, J. M., Nagy, E. K., and Olive, M. F. (2019). Cognitive deficits and neurotoxicity induced by synthetic cathinones: is there a role for neuroinflammation? *Psychopharmacology* 236, 1079–1095. doi: 10.1007/s00213-018-5067-5

Li, X., Wu, F., Xue, L., Wang, B., Li, J., Chen, Y., et al. (2018). Methamphetamine causes neurotoxicity by promoting polarization of macrophages and inflammatory response. *Hum. Exp. Toxicol.* 37, 486–495. doi: 10.1177/0960327117714039

Li, Y., Shen, R., Wen, G., Ding, R., Du, A., Zhou, J., et al. (2017). Effects of ketamine on levels of inflammatory cytokines IL-6, IL-1β, and TNF-α in the hippocampus of mice following acute or chronic administration. *Front. Pharmacol.* 8:139. doi: 10.3389/fphar.2017.00139

Liao, L. S., Lu, S., Yan, W. T., Wang, S. C., Guo, L. M., Yang, Y. D., et al. (2021). The Role of HSP90α in Methamphetamine/Hyperthermia-induced necroptosis in rat striatal neurons. *Front. Pharmacol.* 12:716394. doi: 10.3389/fphar.2021.716394

Majewska, M. D. (1996). Cocaine addiction as a neurological disorder: implications for treatment. *NIDA Res. Monogr.* 163, 1–26.

Metz, V. G., da Rosa, J., Rossato, D. R., Milanesi, L. H., Burger, M. E., and Pase, C. S. (2021). Cannabidiol prevents amphetamine relapse and modulates D1- and D2-receptor levels in mesocorticolimbic brain areas of rats. *Eur. Neuropsychopharmacol.* 50, 23–33. doi: 10.1016/j.euroneuro.2021.04.008

Moore, K. A., Kilbane, E. M., Jones, R., Kunsman, G. W., Levine, B., and Smith, M. (1997). Tissue distribution of ketamine in a mixed drug fatality. *J. Forensic Sci.* 42, 1183–1185.

Munro, C. A., McCaul, M. E., Wong, D. F., Oswald, L. M., Zhou, Y., Brasic, J., et al. (2006). Sex differences in striatal dopamine release in healthy adults. *Biol. Psychiatry* 59, 966–974. doi: 10.1016/j.biopsych.2006.01.008

Naserzadeh, P., Taghizadeh, G., Atabaki, B., Seydi, E., and Pourahmad, J. (2019). A comparison of mitochondrial toxicity of mephedrone on three separate parts of brain including hippocampus, cortex and cerebellum. *Neurotoxicology* 73, 40–49. doi: 10.1016/j.neuro.2019.02.014

Nestler, E. J. (2004). Molecular mechanisms of drug addiction. *Neuropharmacology* 47(Suppl. 1), 24–32. doi: 10.1016/j.neuropharm.2004.06.031

Niazi, M., and Hussain, A. (2011). Agent-based computing from multi-agentsystems to agent-based models: a visual survey. *Scientometrics* 89, 479–499. doi: 10.1007/s11192-011-0468-9

Olcese, J. M., Cao, C., Mori, T., Mamcarz, M. B., Maxwell, A., Runfeldt, M. J., et al. (2009). Protection against cognitive deficits and markers of neurodegeneration by long-term oral administration of melatonin in a transgenic model of Alzheimer disease. *J. Pineal Res.* 47, 82–96. doi: 10.1111/j.1600-079X.2009.00692.x

Oliver, C. F., Simmons, S. J., Nayak, S. U., Smith, G. R., Reitz, A. B., and Rawls, S. M. (2018). Chemokines and 'bath salts': CXCR4 receptor antagonist reduces rewarding and locomotor-stimulant effects of the designer cathinone MDPV in rats. *Drug Alcohol Depend.* 186, 75–79. doi: 10.1016/j.drugalcdep.2018.01.013

Pau, C. W., Lee, T. M., and Chan, S. F. (2002). The impact of heroin on frontal executive functions. *Arch. Clin. Neuropsychol.* 17, 663–670.

Preti, A., Miotto, P., and De Coppi, M. (2002). Deaths by unintentional illicit drug overdose in Italy, 566 1984-2000. *Drug Alcohol Depend.* 66, 275–282. doi: 10.1016/s0376-8716(01)00207-1

Quek, L. H., Chan, G. C., White, A., Connor, J. P., Baker, P. J., Saunders, J. B., et al. (2013). Concurrent and simultaneous polydrug use: latent class analysis of an Australian nationally representative sample of young adults. *Front. Public Health* 1:61. doi: 10.3389/fpubh.2013.00061

Quinn, D. I., Wodak, A., and Day, R. O. (1997). Pharmacokinetic and pharmacodynamic principles of illicit drug use and treatment of illicit drug users. *Clin. Pharmacokinet.* 33, 344–400. doi: 10.2165/00003088-199733050-00003

Rahim, B. E. A., Yagoub, U., Mahfouz, M. S., Solan, Y. M. H., and Alsanosi, R. (2012). Abuse of selected psychoactive stimulants: overview and future research trends. *Life Sci. J.* 9, 2295–2308.

Rego, A. C., and Oliveira, C. R. (2003). Mitochondrial dysfunction and reactive oxygen species in excitotoxicity and apoptosis: implications for the pathogenesis of neurodegenerative diseases. *Neurochem. Res.* 28, 1563–1574. doi: 10.1023/a:1025682611389

Rehm, J., Mathers, C., Popova, S., Thavorncharoensap, M., Teerawattananon, Y., and Patra, J. (2009). Global burden of disease and injury and economic cost attributable to alcohol use and alcohol-use disorders. *Lancet* 373, 2223–2233. doi: 10.1016/S0140-6736(09)60746-7

Ribeiro Do Couto, B., Aguilar, M. A., Manzanedo, C., Rodríguez-Arias, M., and Miñarro, J. (2004). Effects of NMDA receptor antagonists (MK-801 and memantine) on the acquisition of morphine-induced conditioned place preference in mice. *Prog. Neuropsychopharmacol. Biol. Psychiatry* 28, 1035–1043. doi: 10.1016/j.pnpbp.2004.05.038

Ryskalin, L., Puglisi-Allegra, S., Lazzeri, G., Biagioni, F., Busceti, C. L., Balestrini, L., et al. (2021). Neuroprotective effects of curcumin in Methamphetamine-induced toxicity. *Molecules* 26:2493. doi: 10.3390/molecules26092493

Şenel, E., and Demir, E. (2018). Bibliometric analysis of apitherapy in complementary medicine literature between 1980 and 2016. *Complement. Ther. Clin. Pract.* 31, 47–52. doi: 10.1016/j.ctcp.2018.02.003

Sexton, M. (2020). Cannabis in the time of coronavirus disease 2019: the yin and yang of the endocannabinoid system in immunocompetence. *J. Altern. Complement. Med.* 26, 444–448. doi: 10.1089/acm.2020.0144

Shahidi, S., Sadeghian, R., Komaki, A., and Asl, S. S. (2018). Intracerebroventricular microinjection of the 5-HT1F receptor agonist LY 344864 inhibits methamphetamine conditioned place preference reinstatement in rats. *Pharmacol. Biochem. Behav.* 173, 27–35. doi: 10.1016/j.pbb.2018.08.001Abuse

Siggins, G. R., Martin, G., Roberto, M., Nie, Z., Madamba, S., and De Lecea, L. (2003). Glutamatergic transmission in opiate and alcohol dependence. *Ann. N Y. Acad. Sci.* 1003, 196–211. doi: 10.1196/annals.1300.012

Sogos, V., Caria, P., Porcedda, C., Mostallino, R., Piras, F., Miliano, C., et al. (2021). Human neuronal cell lines as an in vitro toxicological tool for the evaluation of novel psychoactive substances. *Int. J. Mol. Sci.* 22:6785. doi: 10.3390/ijms22136785

Steentoft, A., Teige, B., Holmgren, P., Vuori, E., Kristinsson, J., Hansen, A. C., et al. (2006). Fatal poisoning in nordic drug addicts in 2002. *Forensic Sci. Int.* 160, 148–156. doi: 10.1016/j.forsciint.2005.09.004

Substance Abuse and Mental Health Services Administration (2002). *National Household Survey on Drug Abuse: Main Findings, Rockville, MDUS Department of Health and Human Services*. Rockville, MD: Substance Abuse and Mental Health Services Administration.

Thornton, C., Grad, E., and Yaka, R. (2021). The role of mitochondria in cocaine addiction. *Biochem. J.* 478, 749–764. doi: 10.1042/BCJ20200615

Trujillo, K. A. (2000). Are NMDA receptors involved in opiate-induced neural and behavioral plasticity? Areview of preclinical studies. *Psychopharmacology* 151, 121–141. doi: 10.1007/s002130000416

Tzschentke, T. M., and Schmidt, W. J. (1995). N-methyl-D-aspartic acid-receptor antagonists block morphine-induced conditioned place preference in rats. *Neurosci. Lett.* 193, 37–40. doi: 10.1016/0304-3940(95)11662-g

Tzschentke, T. M., and Schmidt, W. J. (2003). Glutamatergic mechanisms in addiction. *Mol. Psychiatry* 8, 373–382. doi: 10.1038/sj.mp.4001269

Veneroso, C., Tuñón, M. J., González-Gallego, J., and Collado, P. S. (2009). Melatonin reduces cardiac inflammatory injury induced by acute exercise. *J. Pineal Res.* 47, 184–191. doi: 10.1111/j.1600-079X.2009.00699.x

Volkow, N. D., Chang, L., Wang, G. J., Fowler, J. S., Leonido-Yee, M., Franceschi, D., et al. (2001). Association of dopamine transporter reduction with psychomotor impairment in methamphetamine abusers. *Am. J. Psychiatry* 158, 377–382. doi: 10.1176/appi.ajp.158.3.377

Waltman, L., van Eck, N. J., and Noyons, E. C. M. (2010). A unified approach to mapping and clustering of bibliometric networks. *J. Informetr.* 4, 629–635. doi: 10.1016/j.joi.2010.07.002

Wang, B., Chen, T., Xue, L., Wang, J., Jia, Y., Li, G., et al. (2019). Methamphetamine exacerbates neuroinflammatory response to lipopolysaccharide by activating dopamine D1-like receptors. *Int. Immunopharmacol.* 73, 1–9. doi: 10.1016/j.intimp.2019.04.053

WHO (2021). *WHO: Revision of ICD-11 (Mental Health) – Questions and Answers (Q&A)*. Available online at: https://www.who.int/multi-media/details/who-revision-oficd-11-(mental-health)-questions-and-answers-(q-a)

Williams, J. M., and Steketee, J. D. (2004). Cocaine increases medial prefrontal cortical glutamate overflow in cocaine-sensitized rats: a time course study. *Eur. J. Neurosci.* 20, 1639–1646. doi: 10.1111/j.1460-9568.2004.03618.x

Wu, L. T., Schlenger, W. E., and Galvin, D. M. (2006). Concurrent use of methamphetamine, MDMA, LSD, ketamine, GHB, and flunitrazepam among American youths. *Drug Alcohol Depend.* 84, 102–113. doi: 10.1016/j.drugalcdep.2006.01.002

Wu, M., Su, H., and Zhao, M. (2021). The Role of α-Synuclein in Methamphetamine-Induced Neurotoxicity. *Neurotox. Res.* 39, 1007–1021. doi: 10.1007/s12640-021-00332-2

Yang, X., Wang, Y., Li, Q., Zhong, Y., Chen, L., Du, Y., et al. (2018). The main molecular mechanisms underlying methamphetamine-induced neurotoxicity and implications for pharmacological treatment. *Front. Mol. Neurosci.* 11:186. doi: 10.3389/fnmol.2018.00186

You, Z. B., Wang, B., Zitzman, D., Azari, S., and Wise, R. A. (2007). A role for conditioned ventral tegmental glutamate release in cocaine seeking. *J. Neurosci.* 27, 10546–10555. doi: 10.1523/JNEUROSCI.2967-07.2007

Yu, J., Cadet, J. L., and Angulo, J. A. (2002). Neurokinin-1 (NK-1) receptor antagonists abrogate methamphetamine-induced striatal dopaminergic neurotoxicity in the murine brain. *J. Neurochem.* 83, 613–622. doi: 10.1046/j.1471-4159.2002.01155.x

Zhang, F., Huang, S., Bu, H., Zhou, Y., Chen, L., Kang, Z., et al. (2021). Disrupting reconsolidation by systemic inhibition of mtor kinase via rapamycin reduces cocaine-seeking behavior. *Front. Pharmacol.* 12:652865. doi: 10.3389/fphar.2021.652865

Zuo, D., Sun, F., Cui, J., Liu, Y., Liu, Z., Zhou, X., et al. (2017). Alcohol amplifies ketamine-induced apoptosis in primary cultured cortical neurons and PC12 cells through down-regulating CREB-related signaling pathways. *Sci. Rep.* 7:10523. doi: 10.1038/s41598-017-10868-z

Conflict of Interest: The authors declare that the research was conducted in the absence of any commercial or financial relationships that could be construed as a potential conflict of interest.

Publisher's Note: All claims expressed in this article are solely those of the authors and do not necessarily represent those of their affiliated organizations, or those of the publisher, the editors and the reviewers. Any product that may be evaluated in this article, or claim that may be made by its manufacturer, is not guaranteed or endorsed by the publisher.

frontiers | Frontiers in Molecular Neuroscience

ORIGINAL RESEARCH
published: 11 July 2022
doi: 10.3389/fnmol.2022.934167

Chloral Hydrate Alters Brain Activation Induced by Methamphetamine-Associated Cue and Prevents Relapse

Chenyu Jiang[1,2], Yunlong Xu[1,2], Jiafeng Zhong[1,2], Junyan Wu[1,3,4], Jian He[1,5], Wei Xu[1,2] and Yingjie Zhu[1,2,6,7,8]**

[1] Shenzhen Key Laboratory of Drug Addiction, Shenzhen Neher Neural Plasticity Laboratory, The Brain Cognition and Brain Disease Institute, Shenzhen Institute of Advanced Technology, Shenzhen-Hong Kong Institute of Brain Science-Shenzhen Fundamental Research Institutions, Chinese Academy of Sciences, Shenzhen, China, [2] College of Life Science, University of Chinese Academy of Sciences, Beijing, China, [3] The First Affiliated Hospital, Sun Yat-sen University, Guangzhou, China, [4] Medical College of Acupuncture-Moxibustion and Rehabilitation, Guangzhou University of Chinese Medicine, Guangzhou, China, [5] Department of Anesthesiology, The First People's Hospital of Foshan, Foshan, China, [6] Faculty of Life and Health Sciences, Shenzhen Institute of Advanced Technology, Chinese Academy of Sciences, Shenzhen, China, [7] CAS Center for Excellence in Brain Science and Intelligence Technology, Chinese Academy of Sciences, Shanghai, China, [8] CAS Key Laboratory of Brain Connectome and Manipulation, Brain Cognition and Brain Disease Institute (BCBDI), Shenzhen Institute of Advanced Technology (SIAT), Chinese Academy of Sciences, Shenzhen, China*

OPEN ACCESS

Edited by:
Jie Yan,
Central South University, China

Reviewed by:
Yixiao Luo,
Hunan Normal University, China
Yan-Xue Xue,
Peking University, China

***Correspondence:**
Wei Xu
xjy005349@siat.ac.cn
Yingjie Zhu
yj.zhu1@siat.ac.cn

Specialty section:
This article was submitted to Molecular Signaling and Pathways, a section of the journal Frontiers in Molecular Neuroscience

Received: *02 May 2022*
Accepted: *10 June 2022*
Published: *11 July 2022*

Citation:
Jiang C, Xu Y, Zhong J, Wu J, He J, Xu W and Zhu Y (2022) Chloral Hydrate Alters Brain Activation Induced by Methamphetamine-Associated Cue and Prevents Relapse. Front. Mol. Neurosci. 15:934167. doi: 10.3389/fnmol.2022.934167

Methamphetamine is a highly addictive drug and its abuse leads to serious health and social problems. Until now, no effective medications are yet available for the treatment of methamphetamine addiction. Our study reveals that chloral hydrate, a clinical sedative drug, suppresses the seeking desire for methamphetamine. After 5 days of continuous administration (subanesthetic dose 50 mg/kg and 100 mg/kg), methamphetamine-seeking behavior of rats was inhibited in the condition place preference and intravenous self-administration tests. Furthermore, chloral hydrate treatment robustly suppressed cue-induced methamphetamine relapse. The whole brain c-fos immunostaining revealed that chloral hydrate treatment suppressed neuronal activity in the rhomboid thalamic nucleus (Rh), dorsal endopiriform nucleus (dEn), and claustrum (Cl) while enhanced zona incerta (ZI) activity during cue-induced methamphetamine relapse. Therefore, chloral hydrate could remodel neural network activity and serve as a potential medicine to treat methamphetamine addiction.

Keywords: chloral hydrate (CH), methamphetamine, brain activation, cue-induced relapse, addiction

INTRODUCTION

Drug addiction is a chronic brain disease that is characterized by compulsive drug-seeking and unavoidable relapse. Relapse would be triggered by drugs, stress, and cues even after long-term abstinence. The changes in neuroplasticity are the biological basis of drug relapse. Multiple neurocircuits involve in the development of drug relapse. Thus, it is important to identify the activation of the neural network in drug relapse and develop therapeutic targets.

Methamphetamine (Meth) abuse is gradually increasing worldwide (Ballester et al., 2017). Chronic methamphetamine abuse can lead to malnutrition, psychosis, mania, aggression, and

other medical and psychiatric symptoms such as cardiovascular complications, especially during withdrawal (Scott et al., 2007). The addictive properties of Meth are believed to be mediated by elevating the synaptic cleft dopamine concentration in the mesolimbic area (Sulzer et al., 2005). Although several behavioral therapies have been used to treat Meth use disorders, the effects are limited in clinics (Ballester et al., 2017). There are no FDA-approved drug treatments for Meth addiction to date, and clinical trials have not identified compounds with clear efficacy. Thus, it is urgent to develop effective drugs to treat Meth addiction.

Chloral hydrate (CH) is one of the most commonly used sedatives for non-invasive procedure in clinic. It slows the activity of the whole central nervous system without a clear mechanism. Although CH has been used as a sedative for decades, it is almost unknown about its other applications. CH is able to enhance GABAa receptor function, thus it is potential to modulate the progression of drug addiction (Lu et al., 2008). In one retrospective study (Esmaeili et al., 2010), chloral hydrate was co-administered with clonidine to ameliorate opiate withdrawal symptoms and neonatal narcotic abstinence syndrome in neonates delivered by addicted mothers. In morphine-dependent rats, preceding treatment with a single injection of chloral hydrate decreased the withdrawal symptoms induced by naloxone (Streel et al., 2000). At the anesthetic dose, CH was potential to inhibit dopamine transporter function in the dorsal striatum as measured by high-speed chronoamperometry (Sabeti et al., 2003). In another study, CH did not affect the basal and cocaine-induced increases of dopamine levels, but decreased glutamatergic transmission in the striatum (Kreuter et al., 2004). In addition, the active metabolite of chloral hydrate-trichloroethanol (TCE) was able to increase the firing frequency of dopamine neurons in the ventral tegmental area (VTA) (Appel et al., 2006).

Considering the effects on dopamine system, we try to explore that the role of CH plays in Meth addiction. We comprehensively employed the conditioned place preference paradigm and self-administration paradigm to evaluate its role in drug addiction. We further observed the alteration in neural network activity by CH during cue-induced Meth reinstatement.

MATERIALS AND METHODS

Animals

Male Sprague–Dawley (SD) rats were purchased from Charles River (Beijing, China) at 6 weeks of age. Rats were pair-housed in a constant temperature (22 ± 1) and humidity-controlled (45 ± 5%) environment *ad libitum*. Lighting was maintained under a 12-h light–dark cycle (lights on from 8:00 am to 8:00 pm). The rats were habituated at least 14 days prior to conditioned place preference (CPP) and Meth self-administration (SA) experiments. The experimental procedures were performed in accordance with the guidelines for the National Care and Use of Animals, and the experiments were approved by the Institutional Animal Care and Use Committee (IACUC) of Shenzhen Institute of Advanced Technology. All efforts were made to minimize animal suffering.

Drugs

Chloral hydrate (Sigma, Shanghai, China) was dissolved in sterile saline as 100 and 200 mg/ml. Methamphetamine hydrochloride supplied by the National Institutes for Food and Drug Control/NIFDC (171212-201605) was dissolved in sterile saline as 0.25 mg/ml solution. The volume of intraperitoneal injection at 2.0 ml/kg.

Apparatus (CPP)

For place conditioning (a total of 24 male SD rats were used), we employed four identical polypropylene (PE) boxes with two equal-sized compartments (30 cm × 25 cm × 30 cm) separated by a black central area (10 cm × 25 cm × 30 cm). The compartments had different pattern walls (black and white column vs. black and white square) and distinct floor textures (fine grid in the column compartment and sandpaper in the square one). An industrial wide-angle camera was used to record the experiment video (LRCP, trade ID:3206). Anymaze software was adopted to analyze videos, and Deeplabcut software (from Harvard University) was used to trace the animal exercise trajectory.

Apparatus (Meth SA)

Operant chambers (AES-DSA6, Anilab) situated in sound-attenuating boxes (Anilab) were used for operant tasks. Self-administration chambers were equipped with two illuminated nose pokes ("active" and "inactive"), a house light, and infusion pump. The two nose poke operands were set on the front wall of the chamber. The stimulus light and sound cue were positioned directly above the active nose poke hole. The house light was set on the rear wall of the chamber and, except for 20 s timeout periods, the house light remained on when rats were inside the operant chamber. The apparatus was controlled and data were captured by Anilab Ver 6.40 software (Anilab).

Apparatus (OFT)

The open field test (a total of 15 male SD rats were used) was comprised of two identical PE equal-sized boxes (50 cm × 50 cm × 50 cm). The central area was defined as a 30 cm × 30 cm square. An industrial wide-angle camera (LRCP, trade ID:3206) was used for recording. The Anymaze software was used to analyze the video data, and Deeplabcut software (from Harvard University) was used to trace the trajectory.

Intravenous Catheterization

Rats were anesthetized with isoflurane (RWD; cat. no. R510-22-10). A silicon catheter (Dow, cat. no. 508-003) with rounded tip and double suture beads (one secured internally and other externally) was implanted into the right external jugular vein. The distal end of the catheter was subcutaneously placed around the shoulder and exited below the scapula *via* polycarbonate back-mount access port (PlasticsOne; C313G-5UP). Immediately after the surgery, catheters were flushed with 0.2 ml of (2 mg/ml; Sigma) diluted in sterile heparinized saline (10

U/ml; Tocris; cat. no. 2812/100). Atipamezole hydrochloride (0.5 mg/kg; IM; Sigma), diluted in saline was used to terminate anesthesia. Rats were given 5 days to recover from surgery before starting the experiment. During recovery, rats had *ad libitum* access to food for the first 4 days and then gradually food restricted to 90%. Catheters were daily flushed with heparinized saline (10 U/ml). Catheter patency was assessed with a 0.05 ml IV infusion of xylazine (20 mg/ml) at the end of methamphetamine self-administration phase or when patency loss was suspected. Only rats with patent catheters were adopted in the following experiments.

Conditioned Place Preference

Place conditioning consisted of three phases. In the first phase (or preconditioning, briefly named Pre-C), rats were allowed access to both compartments of the apparatus for 900 s per day on the first day. On day 2, the time spent in each compartment was recorded (test 0). The chamber in which mice spent less time will be selected as drug-paired compartment.

In the second phase (conditioning), which lasted 8 days, saline was paired with the preferred compartment and Meth was paired with the other compartment. Rats received 0.5 mg/kg Meth (*i.p.*) and saline injection alternately during this phase. Immediately after the injection, rats were restricted to the appropriate compartment with closed guillotine door for 45 min.

In the third phase (or postconditioning, briefly named Post-C, day 11, test 1), the CPP was measured. The CPP score was calculated as the time spent in the drug-paired compartment during the Post-C session minus the time spent in this compartment during the Pre-C session.

After the acquisition of CPP, rats received chloral hydrate (50 and 100 mg/kg) or saline (similar volume to chloral hydrate solution) injection (*i.p.*) during the maintenance stage. At this stage, rats stayed at home cage and received CH injection for 5 consecutive days. Then 24 h after the last injection, CPP was measured (test 2) to observe the effects of CH on the maintenance of CPP.

Self-Administration

The rats were subjected to the protocol after recovery from the surgery.

Acquisition

Experiments were conducted as previously described with slight modifications (Wakabayashi et al., 2010). The rats were trained for 12 daily fixed ratio 1 sessions (2 h/day). During the acquisition sessions, active nose pokes (termed fixed-ratio one, or FR1) triggered the infusion pump (0.2 mg/kg/infusion), 5-s continuous voice from the buzzer and the illuminated the nose poke. A 20-s time-out was signaled by the dimming of the house light. We set 50 infusions as the maximum per session to avoid drug overdoses. The rats with stable infusion (less than 20% variance over the final 3 days of self-administration training) were selected for subsequent experiments.

Maintenance

In the maintenance phase, the rats were randomly divided into two groups: saline group and CH group. The rats continued daily self-administration training, and received chloral hydrate (100 mg/kg, 2 ml/kg) or saline (2 ml/kg) injection (*i.p.*) immediately after they finished daily training session of 5 consecutive days (day 16–20). Then, we tested the effects of CH on the Meth self-administration on days 21, 22, 23, 27, 34, and 42.

Extinction and Cue-Induced Reinstatement

The experiment is designed according to the previous literatures with slightly modifications (Allain et al., 2021; Everett et al., 2021). During extinction, rats underwent 60 min training sessions, in which nose poke resulted in no scheduled consequences, but poke data were recorded. After the first extinction session, rats were subjected to the maintenance injection protocol. The extinction phase comprised 10 consecutive sessions. After the extinction phase, rats with active poke no more than 10 for 3 consecutive sessions were chosen for the reinstatement test.

During the reinstatement phase, a conditional cue (same as the acquisition phase) was given at the test beginning with 10 s. The active poke (termed fixed-ratio one, or FR1) resulted in the delivery of the same cue as the acquisition phase except no drug infusion. Reinstatement sessions lasted 1 h.

Treatment of Chloral Hydrate

Chloral hydrate was dissolved in sterile saline. In the rat's Meth CPP experiments, after CPP was established, chloral hydrate was given daily at doses of 50 or 100 mg/kg for continuous 5 days. In the rat's Meth self-administration experiments, chloral hydrate was given (*i.p.*) daily at doses of 100 mg/kg immediately after the training sessions for continuous 5 days. In the SA extinction experiments, chloral hydrate was given (*i.p.*) daily at doses of 100 mg/kg immediately after the extinction training sessions for continuous 5 days.

Sucrose Self-Administration

The rats were trained for 12 daily fixed ratio 1 sessions (2 h/day). During the acquisition sessions, active nose pokes (termed fixed-ratio one, or FR1) triggered the infusion pump (0.04 mg/infusion, 200 μl/infusion), 5-s continuous voice from the buzzer and the illuminated the nose poke. A 20-s time-out was signaled by the dimming of the house light. We set 100 infusions as the maximum per session. The rats with stable infusion (less than 20% variance over the final 3 days of self-administration training) were selected for subsequent CH or saline treatments.

Open Field Test

After the sucrose self-administration test, rats received 100 mg/kg chloral hydrate treatment for continuous 5 days. The open-field test was conducted 24 h after the last chloral hydrate injection. The rats were put in the OFT chamber central area and explored freely for 15 min. The traveling distance and staying in central time will be recorded and analyzed by Anymaze software.

c-fos Immunostaining

Then, 1 h after the cue-induced reinstatement test, rats were deeply anesthetized by pentobarbital sodium (80 mg/kg, *i.p.*) and perfused with phosphate buffered saline followed by 4% paraformaldehyde (PFA). Brains were postfixed overnight in 4% PFA and were sliced on a microtome at 45 μm. The slices were washed with 3 times TBST for 10 min and blocked with 5% goat serum dissolved in 0.3% TritonX-100 for 2 h at room temperature. Slices were incubated with primary antibodies dissolved in blocking buffer overnight at 4°C, followed by 3 times 10 min wash with TBST at room temperature. After that, slices were incubated with fluorescent-conjugated secondary antibodies dissolved in blocking buffer for 2 h at room temperature and washed 3 times with TBST. Then, slices were incubated with DAPI in PBS for 10 min at room temperature followed by 3 times 10-min wash with PBS. Finally, slices were mounted using mounting medium containing DAPI (Fluoroshiel, sigma). Primary and secondary antibodies are listed below:

Rabbit anti c-fos (1:2,000, Synaptic Systems Cat# 226 008, RRID:AB_2891278); goat anti-Rabbit IgG 647 (1:1,000, Thermo Fisher Scientific Cat# A-21245, RRID:AB_2535813). Data analysis used the OLYMPUS cellSens Dimension (Ver 3.2, Build 23706). The c-fos immunostaining of each brain region was averaged by the c-fos of two adjacent brain slices and the Student's *t*-test was used for statistical analysis.

Clustering Analysis

Clustering analysis was performed with MATLAB (Mathworks). Prior to the clustering, the variables during the maintenance phase (baseline to day 42) of each rat were normalized to the average time during the baseline sessions (days 13–15). The variables used from the Meth self-administration were the number of active pokes, useless pokes, inactive pokes, and infusions. Useless pokes were defined as the poke to active pokes during the 20-s time-out period after Meth infusions. A dimension reduction (MATLAB toolbox UAMP with option n_neighbors = 10, min_dist = 0.5, metric = euclidean, n_components = 3) was applied to the variables followed by a hierarchical clustering method (MATLAB functions "pdist," "linkage," and "cluster" with a metric = s-euclidean and linkage = ward). Since the UMAP is a stochastic method, the dimension reduction and clustering were run 500 times and choose the best result to hierarchical clustering. Finally, other relevant variables were sorted according to the obtained clustering (treatment).

Statistics

One-way ANOVA was applied to evaluate the effects of chloral hydrate dose (0, 50, and 100 mg/kg) using SPSS (version 25, General Linear Model Procedure). Student's *t*-test was used to determine the effects on maintenance and relapse across CH treatment and after treatment in self-administration, and

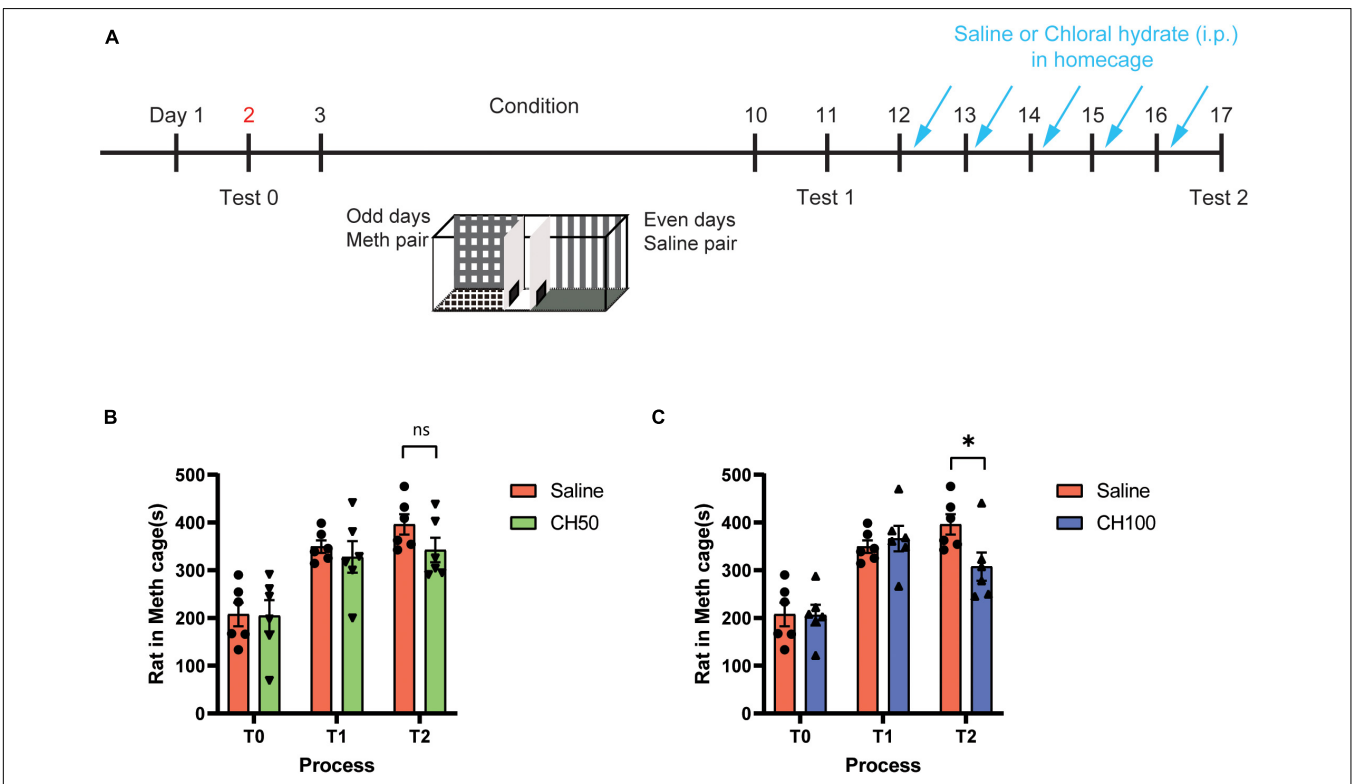

FIGURE 1 | Chloral hydrate reduces Meth-induced CPP maintenance. **(A)** Representation of rat CPP schedule. Three-chamber system was adopted. **(B)** The effect of 50 mg/kg CH treatment ($N = 6$) on the maintenance of Meth-associated CPP memory. **(C)** The effect of 100 mg/kg CH treatment ($N = 6$) on the maintenance of Meth-associated CPP memory. $^*p < 0.05$, ns: no significant difference. T0: test 0, T1: test 1, T2: test 2.

condition preference across CPP test using GraphPad Prism 8.4.7. Clustering analysis was conducted by MATLAB 2020b (MathWorks) for Windows. The minimum level of significance was set at $p < 0.05$. Data are presented as the mean ± SEM.

RESULTS

Chloral Hydrate Treatment Attenuates the Maintenance of Methamphetamine-Induced Conditioned Place Preference

The conditioned place preference **paradigm** is a standard preclinical behavioral model used to evaluate the rewarding effects of the drugs. We first employed CPP paradigm to assess the impact of CH treatment on the rewarding property of Meth (**Figure 1A**). Rats were habituated to 3-chambers CPP apparatus on day 1, and the baseline was assessed on day 2 (test 0). After 8 days of alternating saline and Meth pairing, a CPP expression test (test 1) was performed on day 11 to evaluate the Meth-associated memory. Then, rats were subjected to successive 5 days of saline or chloral hydrate treatment (50 and 100 mg/kg, *i.p.*). A second CPP test was performed to examine the impact of CH treatment on the CPP maintenance (test 2).

After 8 days CPP training, rats increased their time spent on Meth-paired side on test 1, suggesting the formation of Meth-associated CPP [$F_{(1,10)} = 26.58$, $p < 0.001$, **Figures 1B,C**]. After 5 days of CH injection, the 50 mg/kg CH treatment group showed slight decrease in the time spent on Meth-paired side compared to saline-treated group, but did not reach significant level ($p = 0.14$, **Figure 1B**). However, 100 mg/kg CH treatment significantly decreased the time spent on Meth-paired side ($p < 0.05$, **Figure 1C**). These results indicated that 100 mg/kg of CH treatment for 5 days is sufficient to attenuate Meth-associated CPP memories. Based on these results, we chose to use a dose of 100 mg/kg for subsequent studies.

Chloral Hydrate Treatment Reduces Methamphetamine-Seeking Behavior in Drug Self-Administration Model

We next examined the effect of chloral hydrate treatment on the Meth-seeking behavior with classical intravenous drug self-administration (SA) paradigm (**Figure 2A**). Then 7 days after jugular vein cannulation surgery, rats were subjected to 12 days of SA acquisition training. Rats that met the requirements of the successful self-administration were selected and randomly assigned to saline and CH groups. After 12 days of training, the saline group and CH group showed similar level of nose poking and Meth infusion (**Figures 2B,C**, left). During the maintenance phase, rats were treated with saline or CH (100 mg/kg) immediately after SA session and 22 h before the next SA session for successive 5 days. CH treatment reduced the nose pokes and the drug infusions [Infusion count: $F_{(1,8)} = 11.09$, $p < 0.05$, active poke count: $F_{(1,8)} = 10.03$, $p < 0.05$, **Figures 2B,C**, middle].

To examine how long the effect could last after the cessation of CH treatment, the rats were returned to apparatus to perform SA task 1 day, 2 days, 3 days, 1 week, 2 weeks, and 3 weeks after the last CH treatment. The Meth infusion and nose pokes in CH treatment group remained low [infusion count: $F_{(1,8)} = 26.35$, $p < 0.001$, active poke count: $F_{(1,8)} = 15.02$, $p < 0.01$, **Figures 2B,C** right], and the effect was still significant 3 weeks after the last CH treatment.

Parallel to the statistical analysis of *a priori* labeling of animal groups, a dimensionality reduction hierarchical clustering analysis based on the UMAP algorithm was performed. An unbiased clustering analysis integrating four self-administration behavioral parameters over the chloral hydrate delivery sessions yielded two clusters: decreasers (means drug-seeking behavior reduces) and perseveres (means drug-seeking behavior remains unchanged or increases, refer to **Figures 2D,E**). Out of 6 decreaser rats, 5 (83.3%) were classified into the CH100 treatment group. Correspondingly, 4 of the 5 rats in the control group were the perseveres. These results indicated that chloral hydrate had a positive effect on the control of methamphetamine drug-seeking behavior during the maintenance phase and the effect was kept for a long time after the cessation of chloral hydrate.

Chloral Hydrate Treatment Prevents Cue-Induced Relapse Without Affecting the Extinction of Methamphetamine-Seeking Behavior

We further explored the effect of CH on the relapse of Meth-seeking behavior. We subjected animals to extinction training after they acquired stable Meth self-administration (**Figure 3A**). Rats were given either saline or CH treatment (100 mg/kg, *i.p.*) immediately after extinction training sessions for successive 5 days. After 10 days of extinction training (at this stage, nose poke does not trigger drug injection), the rats met that the extinction criteria would accept the cue-induced relapse test. Rats gradually decreased their nose pokes and reach successful extinction criteria (< 10 active pokes/hour) after 10 days of extinction training in the saline-treated group. At this stage, rats in the CH-treated group were indistinguishable in nose pokes from that of saline group [$F_{(1,24)} = 0.0085$, $p = 0.93$, **Figure 3B**], indicating that CH is ineffective in facilitating drug extinction.

Then, the rats underwent cue-induced relapse test. The presentation of Meth-associated sensory cues induced robust active nose pokes in the saline control group, indicating successful reinstatement of Meth-seeking behavior ($p < 0.01$, **Figure 3C**). The CH-treated rats exhibited a significant lower number of nose pokes, suggesting CH treatment during extinction phase prevented cue-induced methamphetamine relapse [$F_{(1,14)} = 9.391$, $p < 0.01$, **Figure 3C**].

Chloral Hydrate Treatment Altered Whole Brain Neural Activation Induced by Methamphetamine-Associated Cue

The robust effect of CH on preventing cue-induced Meth relapse leads us to hypothesize that brain activation following cue presentation might be different between CH-treated and saline-treated group. We thus performed immunostaining of c-fos, a proxy of neural activity, to assess whole-brain activation induced by Meth-associated cues during relapse test. In the

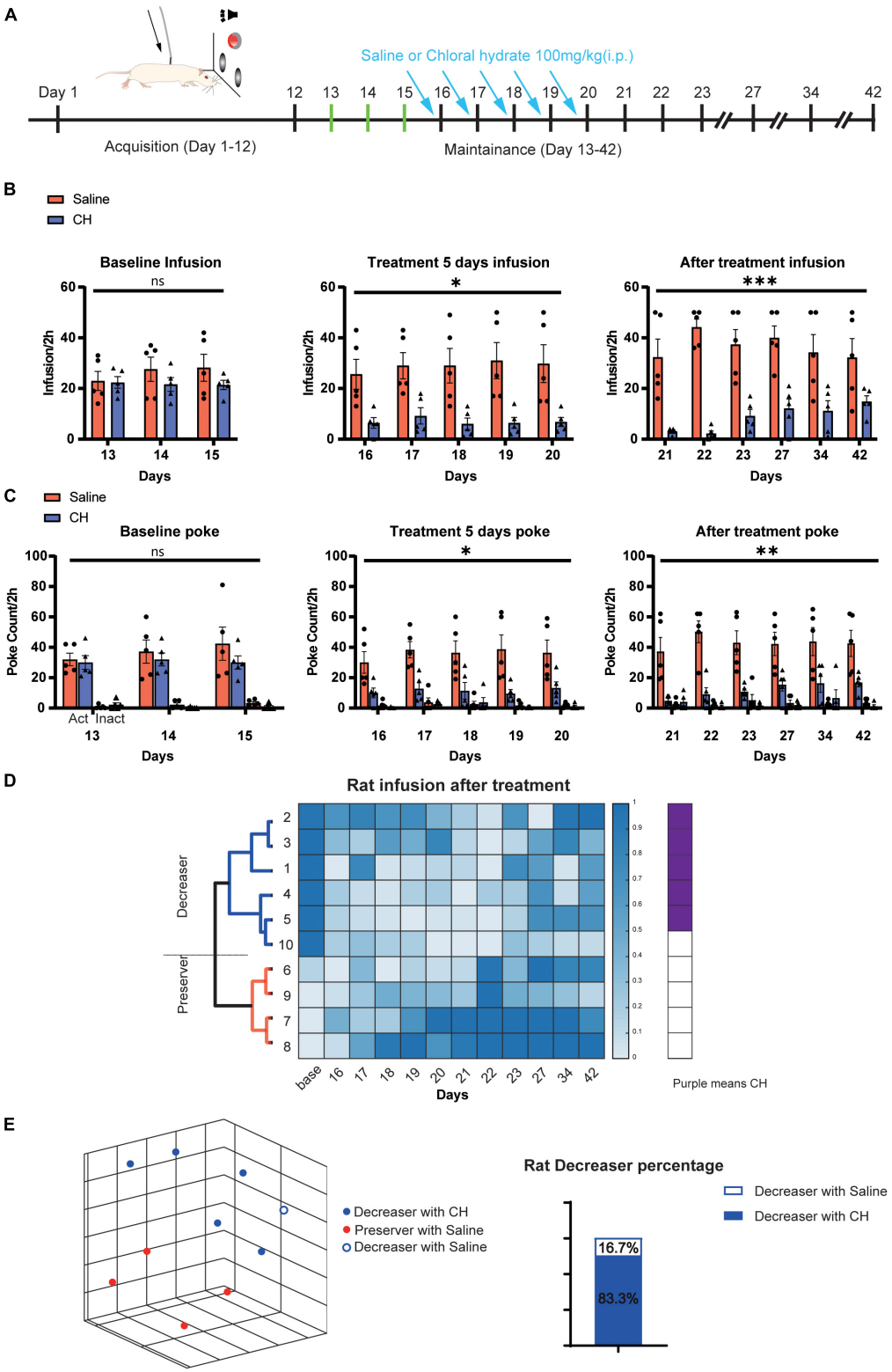

FIGURE 2 | Chloral hydrate reduces drug-seeking behavior in Meth self-administration. **(A)** Representation of rat self-administration schedule. **(B,C)** Chloral hydrate reduced drug-seeking behaviors ($N = 5$ in the CH100 group, $N = 5$ in the saline group). **(D)** Hierarchical cluster based on uniform manifold approximation and projection (UMAP) of different parameters of maintenance session of Meth SA. Purple means CH100 treatment rats. The dark and light blue colors represent the normalized number of the infusion count. **(E)** The representation of three-dimensional UMAP clusters of decreaser (cluster blue) and preserver (cluster red) after treatment in Meth SA. $^{*}p < 0.05$, $^{**}p < 0.01$, $^{***}p < 0.001$; two-way ANOVA.

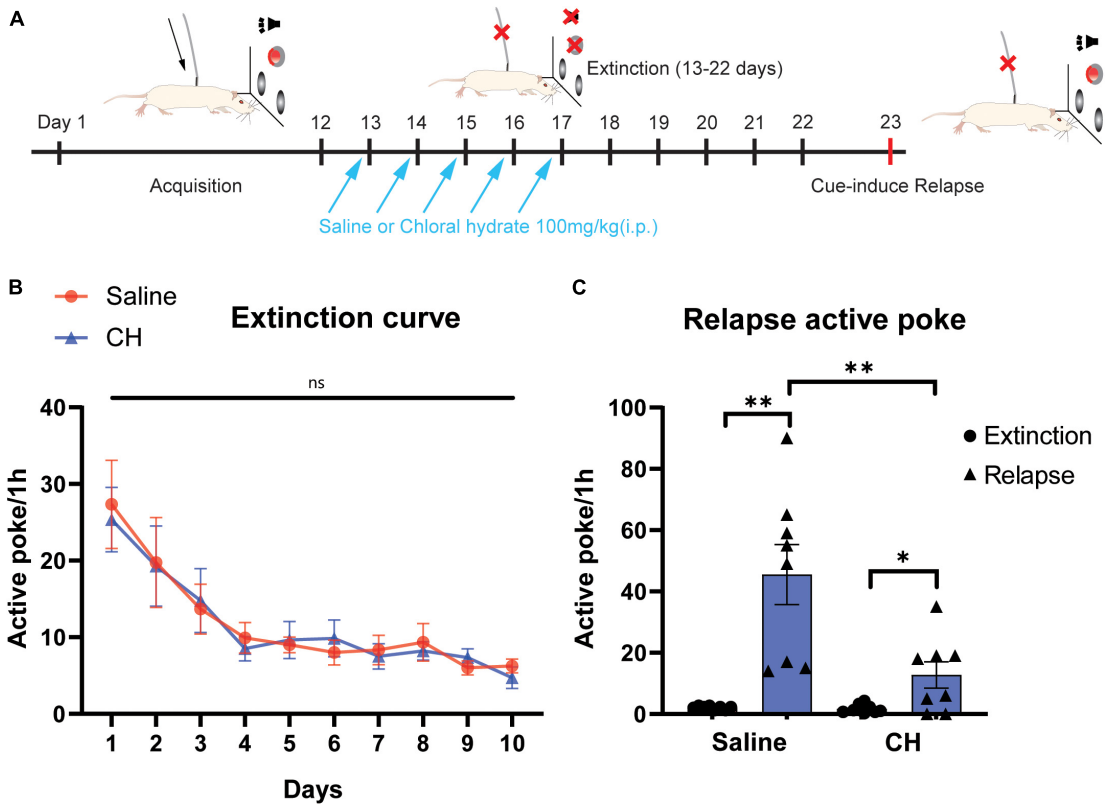

FIGURE 3 | Chloral hydrate reduced cue-induced relapse without affecting extinction in Meth self-administration model **(A)** Representation of extinction and relapse schedule. **(B)** Chloral hydrate treatment (N = 12) has no effect on drug extinction, compared with saline control (N = 12). **(C)** Chloral hydrate treatment (N = 8) prevents cue-induced Meth relapse (N = 8 for CH group and N = 8 for saline group). *$p < 0.05$, **$p < 0.01$, ns: no significant difference, Student's t-test.

saline control group, cue-induced Meth relapse resulted in robust c-fos activation in many brain regions, including some brain regions that have previously been reported to be important for drug addiction, such as the medial prefrontal cortex (PFC), nucleus accumbens (NAc), and VTA (**Figure 4A**). Meth-treated animals showed some overlapping but distinct brain activation patterns (**Figure 4A**). By carefully comparing brain activation between the two groups of animals, we identified 4 brain regions with significant difference (**Figure 4B**). Among them, claustrum (Cl), dorsal endopiriform nucleus (dEn), and rhomboid thalamic nucleus (Rh) showed significant reduction in c-fos numbers in CH-treated animals, whereas zona incerta (ZI) showed significant increase in c-fos activation. In addition, PFC showed enhanced c-fos activation and NAc showed reduced activation in the CH group, but both did not reach significant level. These changes in brain activation might contribute to the suppression effect of CH on cue-induced Meth relapse.

The Impact of Chloral Hydrate Treatment on Sucrose-Seeking, Locomotion, and Anxiety

We next examined the potential side effects of CH on the behavior and locomotor ability of rats. Sucrose self-administration test was adopted to evaluate the effect of chloral hydrate on the seeking of natural reward (**Figure 5A**). The open field experiment was used to evaluate the effect of chloral hydrate on the locomotor activity and anxiety level. The results showed that CH has no effect sucrose seeking and taking [treatment effect, $F_{1,13} = 1.483$, $p = 0.25$, **Figure 5B**], indicating that it does not affect seeking of natural reward. There was no difference in the body weights between the two groups [treatment effect, $F_{(1,13)} = 0.7355$, $p = 0.41$, **Figure 5C**]. The open field test showed that CH did not change the locomotor activity and anxiety level of rats (**Figure 5D**, central time, $p = 0.40$, moving distance, $p = 0.80$).

DISCUSSION

In this study, we discovered that CH dose-dependently ameliorated Meth-induced conditioned place preference, as well as Meth self-administration behavior. Single dose (100 mg/kg) treatment of chloral hydrate was able to reduce rat self-administration behavior. Furthermore, CH also effectively prevented cue-induced Meth reinstatement in rats. With 5 consecutive days of CH administrations during the withdrawal period, the rats exhibited reduced drug-seeking and drug-taking behavior in self-administration paradigm. This indicates that chloral hydrate may play an anti-addictive role at the whole stages of Meth self-administration in rats.

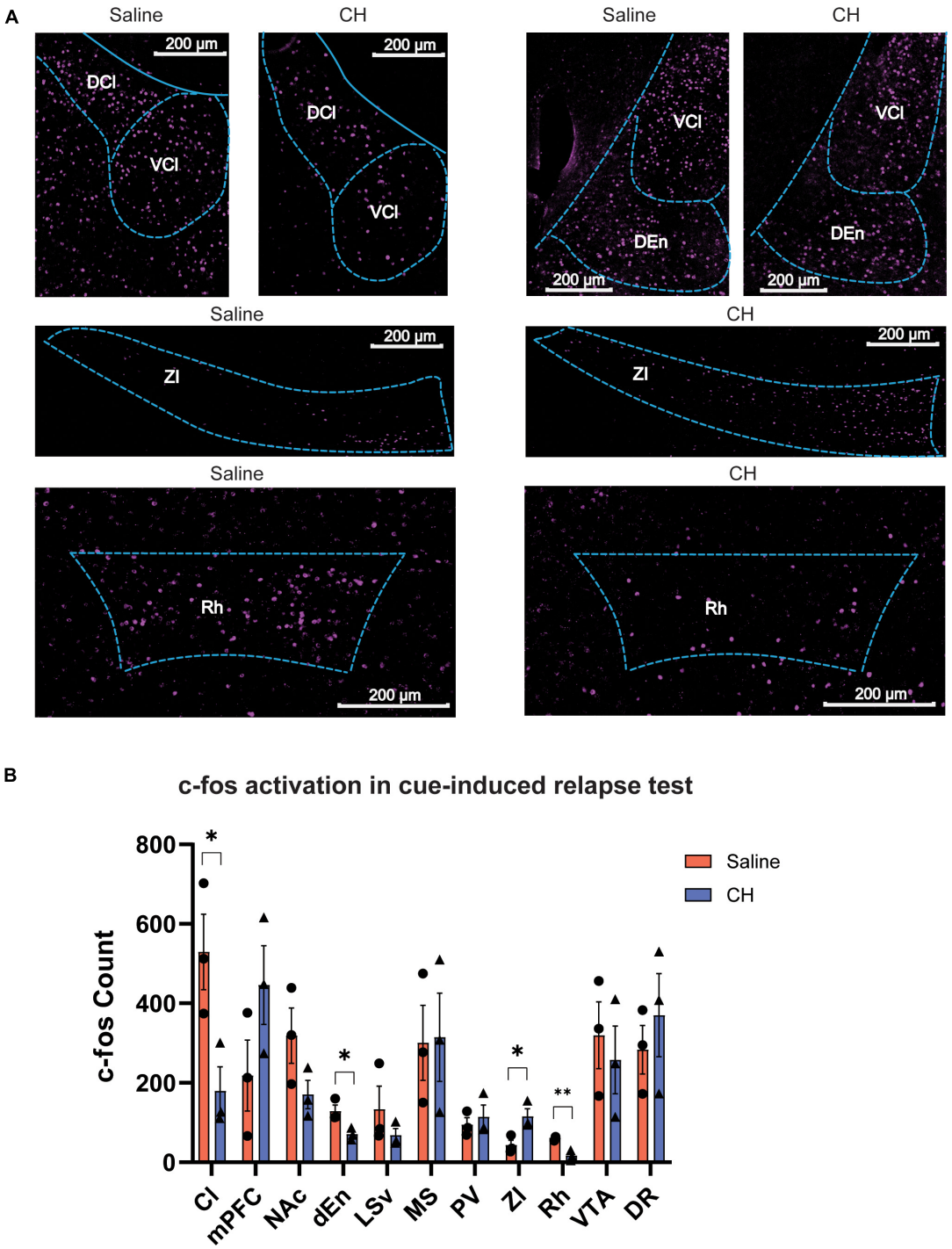

FIGURE 4 | C-fos brain activation after cue-induced Meth relapse in saline- and CH-treated groups. **(A)** Example images showing c-fos expression of multiple brain regions after relapse test ($N = 3$ for both groups). **(B)** Quantification of brain regions with significant differences in c-fos expression between saline (red) and CH (blue) rats. *p*-values are presented in **Supplementary Table 1**. Abbreviations: rhomboid thalamic nucleus (Rh), dorsal endopiriform nucleus (dEn), zona incerta (ZI), claustrum (Cl), medial prefrontal cortex (mPFC), nucleus accumbens (NAc), lateral septal nucleus, ventral part (LSv), dorsal raphe (DR), medial septal nucleus (MS), paraventricular thalamic nucleus (PV), and ventral tegmental area (VTA). Student's *t*-tests. $*p < 0.05$, $**p < 0.01$.

Chloral hydrate is a clinically used sedative drug. To discriminate its anti-addiction effect from its sedative effect, we administrated rats with CH 22 h before behavior test. In addition, we examined the effects of chloral hydrate treatment on the natural reward, locomotor activity, and the level of anxiety in rats. The results showed that chloral hydrate treatment only slightly

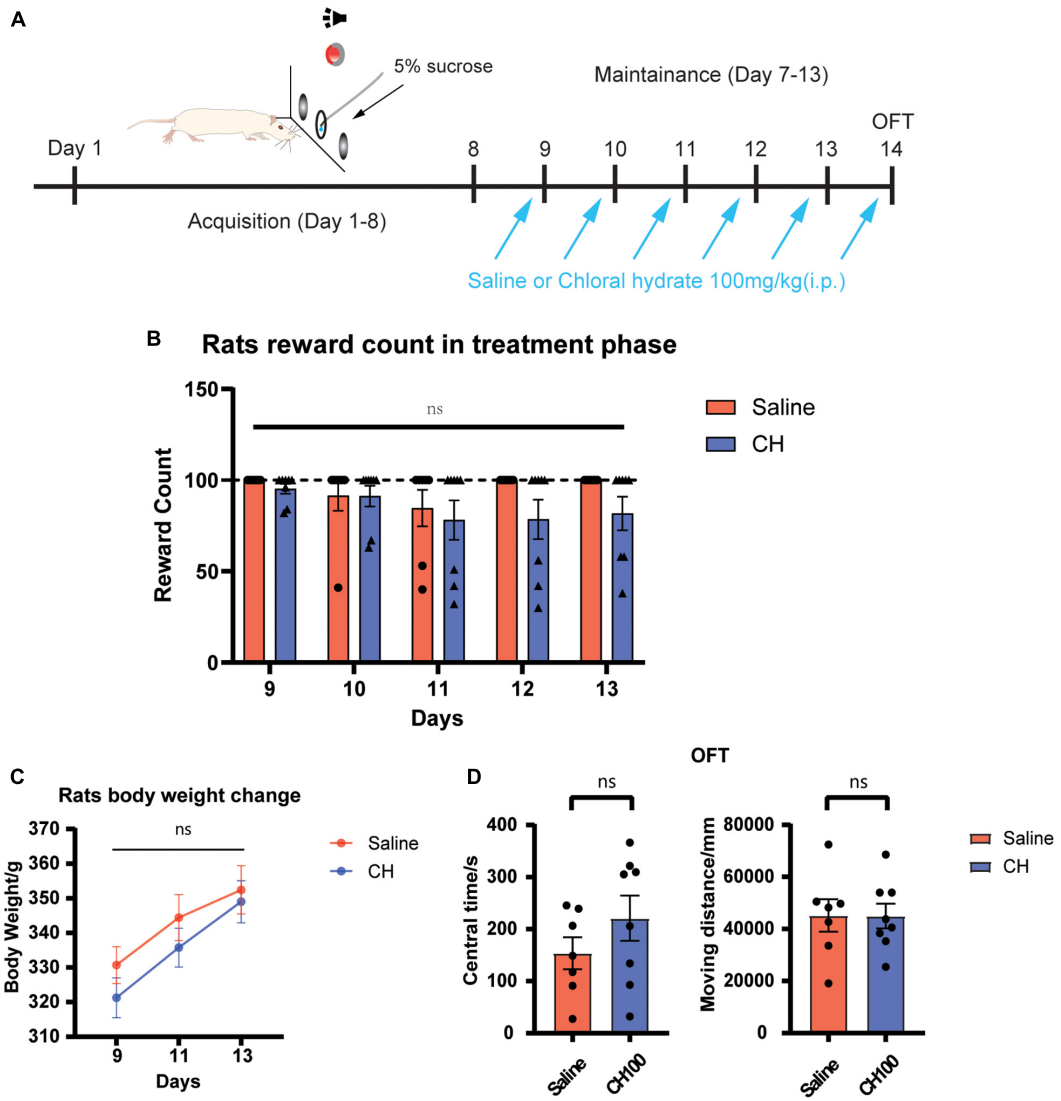

FIGURE 5 | Chloral hydrate had no obvious side effects (*N* = 7 in Saline group and N = 8 in CH100 groups). **(A)**Timeline for sucrose self-administration. **(B)** Chloral hydrate did not affect sucrose self-administration behavior. **(C)** Chloral hydrate had no significant effect on the weight in rats. **(D)** Chloral hydrate did not change locomotor activity and anxiety mood.

affected the driving force of the rats toward natural reward acquisition, whereas it had less effect on the locomotor activity. In addition, CH didn't affect the body weights and anxiety levels of the rats, indicating that chloral hydrate treatment is safe in general.

The whole-brain c-fos immunostaining revealed that CH treatment reduced the activities of the claustrum, the dorsal endopiriform nucleus and the rhomboid thalamic nucleus, while enhanced the activity of the zona incerta. The changes in claustrum were the most obvious. Claustrum projects to the PFC and inhibiting the activity of this projection could control the Meth-induced rat's impulsive behavior (Liu et al., 2019). A significant decrease in the availability of D2/3 receptors in the claustrum of methamphetamine-dependent patients has also been reported in human studies, and genetic studies have shown that genes involved in cocaine and nicotine addiction are specifically expressed in the claustrum (Lee et al., 2009; Liu et al., 2019).

Besides claustrum, the other brain regions with obvious c-fos alterations, such as dorsal endopiriform nucleus and rhomboid thalamic nucleus, also have close relation to drug addiction and dorsal endopiriform nucleus, which has large associations with the function of claustrum, in the brain paralleling information related to the regulation of the limbic system and motor function, both with some functional homogeneity (Watson et al., 2017; Smith et al., 2019). The rhomboid thalamic nucleus undertakes the function of information transmission between mPFC and hippocampus, and spatial memories, working memory, and advanced cognitive ability are related to this brain area (Vertes et al., 2007; Hembrook and Mair, 2011).

Because the activity of the rhomboid thalamic nucleus decreased in the CH treatment group, it is speculated that the rhomboid thalamic nucleus may affect the stability and recurrence of addictive memory. Zona incerta is widely connected to other regions. Its activation and inhibition may be related to the control of stereotyped behavior caused by amphetamines (Supko and Wallace, 1992) and also have the potential to participate in the process of drug addiction. In addition, the traditional addiction-related brain regions, such as the nucleus accumbens and the medial prefrontal cortex, showed a trend of changes without statistical significance. These results suggest that CH exerts its anti-addiction effect might be not through these classical addiction-related brain regions.

In conclusion, 100 mg/kg chloral hydrate significantly reduced methamphetamine self-administration and cue-induced relapse in rats. These effects do not appear to be the result of sedation or dyskinesia. Although the pharmacological mechanism of chloral hydrate is complex and not fully understood, the current results support further testing the potential of these compounds for the treatment of Meth use disorders. Chloral hydrate is a classic drug with a long history of use in the clinic, especially in pediatric testing, The dose we used in the study is the range of clinically permissible dose (Wilson et al., 2014; Mataftsi et al., 2017; Fong et al., 2021), so its safety can be certified and it is possible to conduct clinical testing, to develop the value of new use of its old drugs. In addition, this study further suggests that some sedative drugs previously used in the clinic may be anti-amphetamines with development potential for controlling the harm of synthetic drugs, especially Meth and other psychostimulants. It is of great significance to guide the development of drugs to treat addiction in the future.

DATA AVAILABILITY STATEMENT

The original contributions presented in this study are included in the article/**Supplementary Material**, further inquiries can be directed to the corresponding author/s.

ETHICS STATEMENT

The animal study was reviewed and approved by the Institutional Animal Care and Use Committee (IACUC) of Shenzhen Institute of Advanced Technology, Chinese Academy of Sciences.

AUTHOR CONTRIBUTIONS

CJ conducted behavior experiments. CJ, YX, JZ, JW, and JH performed histological experiments. CJ, WX, and YZ analyzed the data. CJ, WX, and YZ wrote the manuscript. All authors contributed to the article and approved the submitted version.

FUNDING

This work was supported by Science and Technology Innovation 2030—Major Project (2021ZD0202103), National Natural Science Foundation of China (81922024 and 82171492), Guangdong Provincial Key Laboratory of Brain Connectome and Behavior (2017B030301017), and Science, Technology, and Innovation Commission of Shenzhen Municipality (RCJC20200714114556103 and ZDSYS20190902093601675).

ACKNOWLEDGMENTS

We would like to thank Y. Sun for initial experiments and members of Zhu laboratory for helpful discussions.

SUPPLEMENTARY MATERIAL

The Supplementary Material for this article can be found online at: https://www.frontiersin.org/articles/10.3389/fnmol.2022.934167/full#supplementary-material

REFERENCES

Allain, F., Delignat-Lavaud, B., Beaudoin, M. P., Jacquemet, V., Robinson, T. E., Trudeau, L. E., et al. (2021). Amphetamine maintenance therapy during intermittent cocaine self-administration in rats attenuates psychomotor and dopamine sensitization and reduces addiction-like behavior. *Neuropsychopharmacology* 46, 305–315. doi: 10.1038/s41386-020-0773-1

Appel, S. B., Wise, L., McDaid, J., Koyama, S., McElvain, M. A., and Brodie, M. S. (2006). The effects of long chain-length n-alcohols on the firing frequency of dopaminergic neurons of the ventral tegmental area. *J. Pharmacol. Exp. Ther.* 318, 1137–1145.

Ballester, J., Valentine, G., and Sofuoglu, M. (2017). Pharmacological treatments for methamphetamine addiction: current status and future directions. *Expert Rev. Clin. Pharmacol.* 10, 305–314. doi: 10.1080/17512433.2017.1268916

Esmaeili, A., Keinhorst, A. K., Schuster, T., Beske, F., Schlösser, R., and Bastanier, C. (2010). Treatment of neonatal abstinence syndrome with clonidine and chloral hydrate. *Acta. Paediatr.* 99, 209–214. doi: 10.1111/j.1651-2227.2009.01547.x

Everett, N. A., Turner, A. J., Costa, P. A., Baracz, S. J., and Cornish, J. L. (2021). The vagus nerve mediates the suppressing effects of peripherally administered oxytocin on methamphetamine self-administration and seeking in rats. *Neuropsychopharmacology* 46, 297–304. doi: 10.1038/s41386-020-0719-7

Fong, C. Y., Lim, W. K., Li, L., and Lai, N. M. (2021). Chloral hydrate as a sedating agent for neurodiagnostic procedures in children. *Cochrane Database Syst. Rev.* 8:Cd011786. doi: 10.1002/14651858.CD011786.pub3

Hembrook, J. R., and Mair, R. G. (2011). Lesions of reuniens and rhomboid thalamic nuclei impair radial maze win-shift performance. *Hippocampus* 21, 815–826. doi: 10.1002/hipo.20797

Kreuter, J. D., Mattson, B. J., Wang, B., You, Z. B., and Hope, B. T. (2004). Cocaine-induced fos expression in rat striatum is blocked by chloral hydrate or urethane. *Neuroscience* 127, 233–242.

Lee, B., London, E. D., Poldrack, R. A., Farahi, J., Nacca, A., Monterosso, J. R., et al. (2009). Striatal dopamine d2/d3 receptor availability is reduced in methamphetamine dependence and is linked to impulsivity. *J. Neurosci.* 29, 14734–14740. doi: 10.1523/jneurosci.3765-09.2009

Liu, J., Wu, R., Johnson, B., Vu, J., Bass, C., and Li, J. X. (2019). The claustrum-prefrontal cortex pathway regulates impulsive-like behavior. *J. Neurosci.* 39, 10071–10080. doi: 10.1523/jneurosci.1005-19.2019

Lu, J., Nelson, L. E., Franks, N., Maze, M., Chamberlin, N. L., and Saper, C. B. (2008). Role of endogenous sleep-wake and analgesic systems in anesthesia. *J. Comp. Neurol.* 508, 648–662. doi: 10.1002/cne.21685

Mataftsi, A., Malamaki, P., Prousali, E., Riga, P., Lathyris, D., Chalvatzis, N. T., et al. (2017). Safety and efficacy of chloral hydrate for procedural sedation in paediatric ophthalmology: a systematic review and meta-analysis. *Br. J. Ophthalmol.* 101, 1423–1430. doi: 10.1136/bjophthalmol-2016-309449

Sabeti, J., Gerhardt, G. A., and Zahniser, N. R. (2003). Chloral hydrate and ethanol, but not urethane, alter the clearance of exogenous dopamine recorded by chronoamperometry in striatum of unrestrained rats. *Neurosci. Lett.* 343, 9–12.

Scott, J. C., Woods, S. P., Matt, G. E., Meyer, R. A., Heaton, R. K., Atkinson, J. H., et al. (2007). Neurocognitive effects of methamphetamine: a critical review and meta-analysis. *Neuropsychol. Rev.* 17, 275–297. doi: 10.1007/s11065-007-9031-0

Smith, J. B., Alloway, K. D., Hof, P. R., Orman, R., Reser, D. H., Watakabe, A., et al. (2019). The relationship between the claustrum and endopiriform nucleus: a perspective towards consensus on cross-species homology. *J. Comp. Neurol.* 527, 476–499. doi: 10.1002/cne.24537

Streel, E., Bredas, P., Dan, B., Hanak, C., Pelc, I., and Verbanck, P. (2000). Previous anesthesia can temporarily overshadow the expression of a withdrawal syndrome in opiate dependent rats. *Life Sci.* 67, 2883–2887. doi: 10.1016/s0024-3205(00)00867-5

Sulzer, D., Sonders, M. S., Poulsen, N. W., and Galli, A. (2005). Mechanisms of neurotransmitter release by amphetamines: a review. *Prog. Neurobiol.* 75, 406–433. doi: 10.1016/j.pneurobio.2005.04.003

Supko, D. E., and Wallace, L. J. (1992). AMPA glutamate receptor activation in the posterior zona incerta inhibits amphetamine- and apomorphine-induced stereotypy. *Brain Res.* 584, 213–218. doi: 10.1016/0006-8993(92)90897-i

Vertes, R. P., Hoover, W. B., Szigeti-Buck, K., and Leranth, C. (2007). Nucleus reuniens of the midline thalamus: link between the medial prefrontal cortex and the hippocampus. *Brain Res. Bull.* 71, 601–609. doi: 10.1016/j.brainresbull.2006.12.002

Wakabayashi, K. T., Weiss, M. J., Pickup, K. N., and Robinson, T. E. (2010). Rats markedly escalate their intake and show a persistent susceptibility to reinstatement only when cocaine is injected rapidly. *J. Neurosci.* 30, 11346–11355. doi: 10.1523/jneurosci.2524-10.2010

Watson, G. D. R., Smith, J. B., and Alloway, K. D. (2017). Interhemispheric connections between the infralimbic and entorhinal cortices: the endopiriform nucleus has limbic connections that parallel the sensory and motor connections of the claustrum. *J. Comp. Neurol.* 525, 1363–1380. doi: 10.1002/cne.23981

Wilson, M. E., Karaoui, M., Al Djasim, L., Edward, D. P., Al Shamrani, M., and Friedman, D. S. (2014). The safety and efficacy of chloral hydrate sedation for pediatric ophthalmic procedures: a retrospective review. *J. Pediatr. Ophthalmol. Strab.* 51, 154–159. doi: 10.3928/01913913-20140311-01

Conflict of Interest: The authors declare that the research was conducted in the absence of any commercial or financial relationships that could be construed as a potential conflict of interest.

frontiers | Frontiers in Molecular Neuroscience

TYPE Original Research
PUBLISHED 22 July 2022
DOI 10.3389/fnmol.2022.975820

OPEN ACCESS

EDITED BY
Jianfeng Liu,
Wuhan University of Science and Technology, China

REVIEWED BY
Qi Wang,
Southern Medical University, China
Tengfei Ma,
Nanjing Medical University, China
Swarup Mitra,
Marshall University, United States

*CORRESPONDENCE
Guibin Wang
guibinwang@imm.ac.cn
Jie Shi
shijie@bjmu.edu.cn

SPECIALTY SECTION
This article was submitted to Molecular Signalling and Pathways, a section of the journal Frontiers in Molecular Neuroscience

RECEIVED 22 June 2022
ACCEPTED 30 June 2022
PUBLISHED 22 July 2022

CITATION
Chen Y, Zhang L, Ding Z, Wu X, Wang G and Shi J (2022) Effects of 3-methylmethcathinone on conditioned place preference and anxiety-like behavior: Comparison with methamphetamine. *Front. Mol. Neurosci.* 15:975820. doi: 10.3389/fnmol.2022.975820

Effects of 3-methylmethcathinone on conditioned place preference and anxiety-like behavior: Comparison with methamphetamine

Yang Chen[1,2], Libo Zhang[1,3], Zengbo Ding[1], Xianwen Wu[4], Guibin Wang[5]* and Jie Shi[1,6,7]*

[1]National Institute on Drug Dependence and Beijing Key Laboratory of Drug Dependence, Peking University, Beijing, China, [2]Department of Pharmacology, School of Basic Medical Sciences, Peking University Health Science Center, Beijing, China, [3]Shenzhen Public Service Platform for Clinical Application of Medical Imaging, Shenzhen Key Laboratory for Drug Addiction and Medication Safety, Department of Ultrasound, Peking University Shenzhen Hospital, Shenzhen, China, [4]Department of Laboratory Animal Sciences, Peking University Health Sciences Center, Beijing, China, [5]Institute of Materia Medica, Chinese Academy of Medical Sciences and Peking Union Medical College, Beijing, China, [6]The State Key Laboratory of Natural and Biomimetic Drugs, Peking University, Beijing, China, [7]The Key Laboratory for Neuroscience of the Ministry of Education and Health, Peking University, Beijing, China

3-Methylmethcathinone (3-MMC), a drug belonging to synthetic cathinones family, raised public attention due to its harmful health effects and abuse potential. Although it has similar properties to other cathinone derivatives, the behavioral effects of 3-MMC remain largely unknown. In the present research, we evaluated the rewarding effect of 3-MMC using conditioned place preference (CPP) paradigm and its effect on anxiety-like behavior using elevated plus maze (EPM) and compared with methamphetamine (METH). Then, we performed a whole-brain c-Fos mapping to identify the specific brain regions in response to 3-MMC exposure and explored the changes of synaptic transmission in nucleus accumbens (NAc) using patch-clamp recording after chronic 3-MMC and METH exposure. 3-MMC induced CPP at higher doses of 3 or 10 mg/kg in rats and acute exposure of 3 mg/kg 3-MMC to rats produced anxiolytic-like effect, while anxiety-like behavior was increased after 7 days of injection with 3-MMC. Whole-brain immunostaining revealed increased c-Fos expression in anterior cingulate cortex (ACC), NAc and ventral tegmental area (VTA) after chronic 3-MMC injection compared with saline, which was similar to METH. Especially, 3-MMC induced more neural activation of VTA compared with METH. Finally, we found that amplitude of spontaneous inhibitory postsynaptic currents (sIPSCs) in NAc was decreased after chronic 3-MMC injection, while frequency of sIPSCs and spontaneous excitatory postsynaptic currents (sEPSCs) were not affected. Taken together, our results revealed the addictive potential of 3-MMC and

its effect on anxiety-like behavior, which warn the risks of 3-MMC abuse and justify the control of synthetic cathinones. And 3-MMC selectively inhibit inhibitory but not excitatory transmission onto neurons in NAc, which may contribute to its effects.

KEYWORDS

3-methylmethcathinone, conditioned place preference, elevated plus maze, nucleus accumbens, synaptic transmission

Introduction

As a type of novel psychoactive substance (NPS), synthetic cathinones first appeared in early 21st century and have become increasingly popular in smuggling and illicit drug markets (Assi et al., 2017; Pieprzyca et al., 2020). At the end of 2020, synthetic cathinones were the second largest group among over 830 NPSs detected by the European Monitoring Centre for Drugs and Drug Addiction including 3-Methylmethcathinone (EMCDDA, 2021). 3-methylmethcathinone, also known as 3-MMC or metaphedrone, was a designer drug from the synthetic cathinones family (Ferreira et al., 2019) which first appeared in Sweden in 2012 (Bäckberg et al., 2015) and is currently illegal in majority of nations including France, Poland and China (CFDA, 2015; Pieprzyca et al., 2020; EMCDDA, 2021). There is no known or medical use of 3-MMC, and such drug has attracted public attention around the world because of its harmful health effects and risks of abuse (Adamowicz et al., 2016; Jamey et al., 2016; Dias da Silva et al., 2019; Ferreira et al., 2019; Margasinska-Olejak et al., 2019). To date, there is relatively little literature concerning 3-MMC and it is important to explore its effects to provide sufficient scientific evidence to justify NPSs control.

As one of the NPSs, 3-MMC shares some biological effects with 4-methylmethcathinone (4-MMC), 3,4-methylenedioxy-methamphetamine (MDMA), and methamphetamine (METH) including euphoria, excitement, happiness, increased physical energy, alertness and enhanced awareness (Ferreira et al., 2019). Recently, some researches mentioned that 3-MMC had been related with addiction, several intoxications and even fatalities (Marusich et al., 2012; Ferreira et al., 2019; Margasinska-Olejak et al., 2019; Drevin et al., 2021). Pharmacological study showed that 3-MMC was a monoamine transporter substrate and displayed pronounced dopaminergic and serotonergic activity by inhibition of dopamine (DA) and norepinephrine (NE) uptake (Luethi et al., 2018). The brain dopaminergic system, which plays essential roles in reward, learning and memory, and decision making, is one of the most fundamental theoretical frameworks for drug addiction (Volkow et al., 2011). However, the alternations of neurotransmission remained elusive following 3-MMC administration, particularly in nucleus accumbens (NAc), a crucial downstream target of dopaminergic system and also played a key role in drug addiction (Volkow et al., 2011).

The aim of our research was to investigate the behavioral changes after acute and chronic 3-MMC exposure and its related neural mechanisms. Concretely, we assessed the effects of 3-MMC exposure on conditioned place preference (CPP), locomotor activity and the elevated plus maze (EPM), and compared these with METH. We also evaluated the expression of c-Fos, a marker of stimulus-induced neural activation, in various brain regions linked to addiction, as well as the electrophysiological alternations of NAc neurons after repeated 3-MMC injection.

Materials and methods

Animals

Adult male Sprague-Dawley (SD) rats (280–300 g) were purchased from Beijing Vital River Laboratory Animal Technology Co., Ltd. The rats were housed in groups of 4 per cage after arrival with appropriate temperature (22 ± 2°C) and humidity (50 ± 5%), as well as freely accessible water and food. The lighting time was controlled, under a 12-h light/dark cycle. All behavioral experiments were performed during the animal's dark period. Animal care and experimentation were performed in accordance with the National Institutes of Health Guide for the Care and Use of Laboratory Animals and were approved by the Biomedical Ethics Committee for Animal Use and Protection of Peking University (No: LA2019067).

Drugs

The METH and 3-MMC were provided by Drug Intelligence and Forensic Center of Ministry of Public Security, China. Both drugs were dissolved in 0.9% saline and ready for intraperitoneal injection.

Conditioned place preference

The conditioned place preference (CPP) procedure was performed using an unbiased, counterbalanced protocol that has

been described previously (Liang et al., 2017). The apparatus for CPP conditioning consisted of 10 identical three-chamber polyvinyl chloride (PVC) boxes. The boxes had two larger chambers (27.9 cm length × 21.0 cm width × 20.9 cm height) that differed in their floor texture (bar or grid, respectively) and the houselights on the walls. The two larger chambers were separated by a smaller chamber (12.1 cm length × 21.0 cm width × 20.9 cm height, with a smooth PVC floor). Baseline preference was assessed by placing the rats in the center chamber of the CPP apparatus and allowing them to explore all three chambers freely for 15 min. Rats that showed a strong unconditioned preference for either side chamber (i.e., >500 s) were excluded from the experiments. On the following 1, 3, 5, and 7 days, the rats received saline, 3-MMC (1, 3, or 10 mg/kg, i.p.), or METH (1 mg/kg, i.p.). Based on the dose of 3-MMC at 0.3 mg/kg for pigs (as 2 mg/kg for rats) in a pharmacological study (Shimshoni et al., 2015; Nair and Jacob, 2016) and intraperitoneal injection of 4-methylethcathinone at 1, 3, or 10 mg/kg in another study (Xu et al., 2016), we chose the dose above for CPP training. All rats received saline injection on the 2, 4, 6, and 8 days. After each injection, rats were immediately confined to the drug-paired or saline-paired conditioning chamber for 45 min before being returned to their home cages. On days 9, rats were placed in the central compartment without receiving any injection and were allowed to explore the entire apparatus freely for 15 min. The CPP score was calculated by the time (in seconds) spent in the drug-paired chamber minus the time spent in the saline-paired chamber during the CPP tests.

Locomotor activity

Locomotor Activity Test was conducted based on previous study (Deng et al., 2017). All rats were habituated to the locomotor chambers (40 cm × 40 cm × 65 cm) for 3 days (120 min/day) before locomotor activity test. In test day, we first recorded locomotor activity for 30 min, then rats were injected with a single of saline, 3-MMC (1, 3, or 10 mg/kg) or METH (1 mg/kg) and continued to record for 120 min. All locomotor activities were recorded and analyzed with an automated video tracking system (DigBehv-LM4; Shanghai Jiliang Software Technology, Shanghai, China). Locomotor activity is expressed as the total distance traveled in centimeters during a predetermined period of time.

Elevated plus maze

The elevated plus maze (EPM) was utilized to evaluate anxiety-like behavior based on the rats' natural fear of open, unprotected, and elevated spaces (Pellow et al., 1985). The EPM consisted of four crossed narrow arms elevated 70 cm from the floor, with two open arms and two closed arms (50 cm long and 10 cm wide). 10 min after acute injection (saline, 3-MMC [1, 3 or 10 mg/kg], or METH [1 mg/kg]) or the last injection of chronic drug administration, each rat was placed in the central zone of the EPM with its head facing an open arm and was allowed to freely explore the maze for 5 min. The time spent in each arm and the traces of rats were analyzed with the EthoVision XT (Noldus IT, Netherlands).

Immunostaining

Brains were fixed with 4% paraformaldehyde (PFA) for at least 24 h and transferred into phosphate-buffered saline (PBS, pH 7.2) containing 10, 20, and 30% sucrose until they sank. Coronal sections of the brain were cut into 20 μm slice at −20°C in the cryostat (Leica, CM3050 S). Slices were washed with three times of PBS for 5 min, blocked with 5% bovine serum albumin (BSA) dissolved in 0.2% Triton X-100 for 1 h at room temperature and incubated with Rabbit anti-c-Fos (1:500, Abcam, ab190289) primary antibodies dissolved in blocking buffer overnight at 4°C, followed by four times of 15-min wash with PBS at room temperature. After that, slices were incubated with Goat anti-Rabbit Secondary Antibody (Alexa Fluor 488, 1:500, Invitrogen, A-11008) dissolved in blocking buffer for 2 h at room temperature followed by four times of 15-min wash with PBS. Lastly, the slices were mounted by DAPI (Abcam, ab285390) and stored at 4°C for analysis.

Fluorescent images were acquired using a fluorescence microscope (Olympus, Tokyo, Japan) with a 20× objective lens and analyzed according to our previous study (Liang et al., 2017), in which at least three sections were selected from each brain region for each rat. The size of sampled areas for cell quantifications of each brain region from each section was 0.39 mm × 0.39 mm. Brightness and contrast adjustments were applied to the whole image. The number of c-Fos-positive cells were identified and counted in IMARIS software (Oxford Instruments, United Kingdom). An investigator blinded to the experimental conditions performed the image analyses.

Slice electrophysiology

The experiments were performed as previously described (Yu et al., 2022). Whole-cell patch-clamp recordings of NAc neurons were performed 24 h after the last injection of chronic administration with saline, 1 mg/kg METH or 3 mg/kg 3-MMC. The brains were rapidly removed after anesthetization and 250 μm coronal slices were prepared with a vibratome (Leica VT1200S) in ice-cold solution containing (in mM): 80 NaCl, 26 $NaHCO_3$, 3.0 KCl, 1.0 NaH_2PO_4, 1.3 $MgCl_2$, 1.0 $CaCl_2$, 20 D-glucose, and 75 sucrose, saturated with 95% O_2 and 5% CO_2.

The slices were moved to an incubation chamber containing artificial cerebrospinal fluid (ACSF) consisted of the following (in mM): 124 NaCl, 26 $NaHCO_3$, 3.0 KCl, 1.0 NaH_2PO_4, 1.3 $MgCl_2$, 1.5 $CaCl_2$, 20 D-glucose, saturated with 95% O_2 and 5% CO_2 at 34°C for 30 min and then at room temperature until used for recording.

For sIPSC recording, the pipette solution contained the following (in mm): 120 CsCl, 20 TEA-Cl, 4 ATP-Mg, 0.3 GTP, 0.5 EGTA, 10 HEPES, and 4.0 QX-314 (pH 7.2, 270–280 mOsm with sucrose). For sEPSC recording, the pipette solution contained the following (in mm): 110 Cs methylsulfate, 15 CsCl, 20 TEA-Cl, 4 ATP-Mg, 0.3 GTP, 0.5 EGTA, 10 HEPES, and 4.0 QX-314 (pH 7.2, 270–280 mOsm with sucrose).

All signals were amplified (Multiclamp 700B, Axon Instruments), filtered at 5 kHz and digitized at 20 kHz (National Instruments Board PCI-MIO-16E4, Igor, Wave Metrics). Data were recorded within Axon pClamp 10 (Molecular Devices, CA, United States). Data analysis referred to our previous research (Yu et al., 2022).

Statistical analysis

Statistical analyses were performed with GraphPad Prism 9. One-way analysis of variance (ANOVA), two-way ANOVA, or paired *t*-test was used to analyze data when applicable. Bonferroni test was used for *post hoc* analysis after ANOVA. Data were presented as mean ± standard errors of the mean (SEM). Significance was defined as $^{*}P < 0.05$, $^{**}P < 0.01$, and $^{***}P < 0.001$.

Results

3-Methylmethcathinone induced conditioned place preference dose-dependently and increased locomotor activity

Conditioned place preference and locomotor activity are paradigms commonly employed to determine the rewarding and psychomotor properties of psychoactive drugs, respectively (Tzschentke, 2007). To study the rewarding effect of 3-MMC, the rats underwent CPP training (1, 3, 10 mg/kg of 3-MMC; or 1 mg/kg of METH) for 8 days and received CPP test on day 9. Rats with 3 mg/kg 3-MMC, 10 mg/kg 3-MMC and 1 mg/kg METH displayed increased CPP score (paired *t*-test: $t_9 = 3.46$, $^{**}P = 0.0072$ for 1 mg/kg METH; $t_9 = 2.99$, $^{*}P = 0.0152$ for 3 mg/kg 3-MMC; $t_9 = 2.76$, $^{*}P = 0.0222$ for 10 mg/kg 3-MMC), implying that 3-MMC induced CPP dose-dependently (**Figure 1A**).

Because 3 mg/kg 3-MMC could effectively induce CPP, we next assessed its effect on locomotor activity of rats after acute exposure. A two-way ANOVA of moving distance revealed a main effect of drugs [$F_{(2,22)} = 97.94$, $P < 0.0001$], implying the psychomotor properties of 3-MMC. As shown in **Figure 1B**, rats treated with 3-MMC exhibited an enhanced locomotor activity from 5 to 30 min and 95–100 min (*post hoc* test: $^{*}P < 0.05$ for 3-MMC versus saline), while rats with METH injection showed increased activity from 5 to 120 min (*post hoc* test: $^{\#}P < 0.05$ for METH versus saline).

Acute 3-methylmethcathinone injection reduced anxiety-like behavior, while chronic use of 3-methylmethcathinone increased this behavior

To investigate the effect of acute 3-MMC exposure on anxiety-like behavior, we tested the performance of rats in EMP after acute 3-MMC (1, 3, and 10 mg/kg) injection. EMP test showed that rats with 3 mg/kg 3-MMC spent more time in the open arms (paired *t*-test: $t_6 = 2.45$, $^{*}P = 0.0497$), implying the rapid anxiolytic-like effect of 3-MMC (**Figure 2A**). However, the anxiolytic-like effect of 3-MMC instead decreased when the concentration was increased to 10 mg/kg (paired *t*-test: $t_6 = 2.00$, $P = 0.092$). In addition, there was no change of performance in EMP before and after acute METH exposure (paired *t*-test: $t_6 = 1.20$, $P = 0.2763$).

We next tested the effect of repeated 3-MMC (3 mg/kg for seven consecutive days) and METH (1 mg/kg for seven consecutive days) exposure on anxiety-like behavior in rats. Result showed that rats administered with chronic 3-MMC spent less time in the open arms (paired *t*-test: $t_8 = 3.223$, $^{*}P = 0.0122$), implying that prolonged use of 3-MMC could increase anxiety-like behavior (**Figure 2C**). And there was no change of performance in EMP before and after chronic METH exposure (paired *t*-test: $t_8 = 0.95$, $P = 0.3698$). All travel traces of rats in EMP test were presented in **Figures 2B,D**.

Region-specific expression of c-Fos after repeated 3-methylmethcathinone injection

Because results above showed that the behavioral changes caused by 3 mg/kg 3-MMC were more significant, we investigated the alternations of neuronal activity after chronic exposure to 3-MMC under this dose. Rats received injection of drugs for 7 days and were sacrificed 90 min after the last injection without any behavioral test. Next, we examined c-Fos expression in brain regions which had been reported to be involved in drug addiction (Piazza and Deroche-Gamonet, 2013; Apaydin et al., 2018) to identify the specific regions in response to chronic 3-MMC exposure.

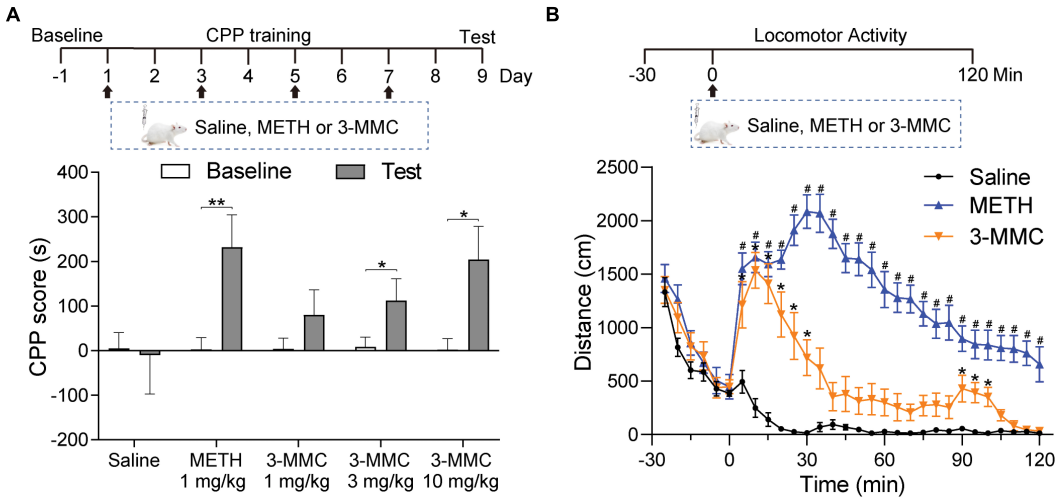

FIGURE 1
The effects of 3-MMC on CPP and locomotor activity. **(A)** Experimental timeline showing the CPP training. The rats trained with saline, METH (1 mg/kg) or 3-MMC (1, 3, or 10 mg/kg) for 8 days and tested in day 9, paired *t*-test, $^{*}P < 0.05$, $^{**}P < 0.01$ significant differences for each drug in CPP test, $n = 10$ for each group. **(B)** A single injection of 3-MMC (3 mg/kg) or METH (1 mg/kg) increased locomotor activity. Each point represents the average distance traveled in 5-min bins. Saline, Meth and 3-MMC group, *post hoc* test, $^{*}P < 0.05$ significant differences in distance for 3-MMC vs saline, $^{\#}P < 0.05$ significant differences for METH vs saline, $n = 8$, 9, and 8, respectively. Data are presented as mean values ± SEM.

As shown in Figures 3A,B, rats with repeated 3-MMC injection presented increased number of c-Fos labeled neurons in anterior cingulate cortex (ACC), NAc, and ventral tegmental area (VTA) compared with saline group [two-way ANOVA revealed a significant interaction effect: $F_{(18,81)} = 8.35$, $P < 0.0001$, *post hoc* test: $^{*}P < 0.05$ or $^{**}P < 0.01$ for 3-MMC versus saline group in brain regions above]. Noteworthy, 3-MMC exposure induced more significant activation of VTA than METH (*post hoc* test: $^{\#}P < 0.05$ for 3-MMC versus METH), which presented increased expression of c-Fos in ACC, anterior insular cortex (aIC), NAc, central amygdala (CeA) and VTA (*post hoc* test: $^{*}P < 0.05$ or $^{**}P < 0.01$ for METH versus saline group in brain regions above). The data of statistics results were shown in Table 1.

Effects of repeated 3-methylmethcathinone injection on synaptic transmission of nucleus accumbens neurons

As psychoactive substance, both 3-MMC and METH induced activation of NAc neurons after chronic exposure. However, there is no research about the effect of 3-MMC on NAc yet, a key structure in rewarding, motivation, and incentivized learning (Volkow et al., 2011). To determine the effects of 3-MMC on synaptic activity, we recorded spontaneous excitatory and inhibitory postsynaptic currents (sEPSCs and sIPSCs) in NAc. As shown in Figures 4E,F, the amplitude of sIPSCs was decreased after repeated 3-MMC exposure [one-way ANOVA, $F_{(2,81)} = 7.97$, $P = 0.0007$, *post hoc* test: $^{*}P < 0.05$ for saline versus 3-MMC, $^{***}P < 0.001$ for saline versus METH, $P = 0.7895$ for 3-MMC vs METH], while frequency of sIPSCs remained unchanged [one-way ANOVA, $F_{(2,81)} = 3.02$; $P = 0.0541$]. Neither the frequency [one-way ANOVA, $F_{(2,81)} = 2.17$; $P = 0.1207$] nor the amplitude of sEPSCs [one-way ANOVA, $F_{(2,81)} = 2.97$; $P = 0.0569$] was affected by repeated 3-MMC exposure (Figures 4B,C). The representative sEPSCs and sIPSCs traces of NAc neurons were presented in Figures 4A,D.

Discussion

3-Methylmethcathinone is a recently emerged cathinone derivative which is introduced initially to replace 4-MMC, and is legally controlled in many countries, but is still easily available for purchase from websites or entertainment venues (Ferreira et al., 2019). Most 3-MMC consumption concerns abuse, and its related mortality has alarmingly increased in recent years (Ferreira et al., 2019; Margasinska-Olejak et al., 2019; Drevin et al., 2021). Previous information on biological effects of 3-MMC was scarce, and most derived from humans, including case reports of intoxicated individuals that were admitted to the emergency, online questionnaires and self-reports of consumers. Our study evaluated the abuse potential of 3-MMC in rats using representative addictive model of CPP (Tzschentke, 2007) for the first time, and clearly demonstrated

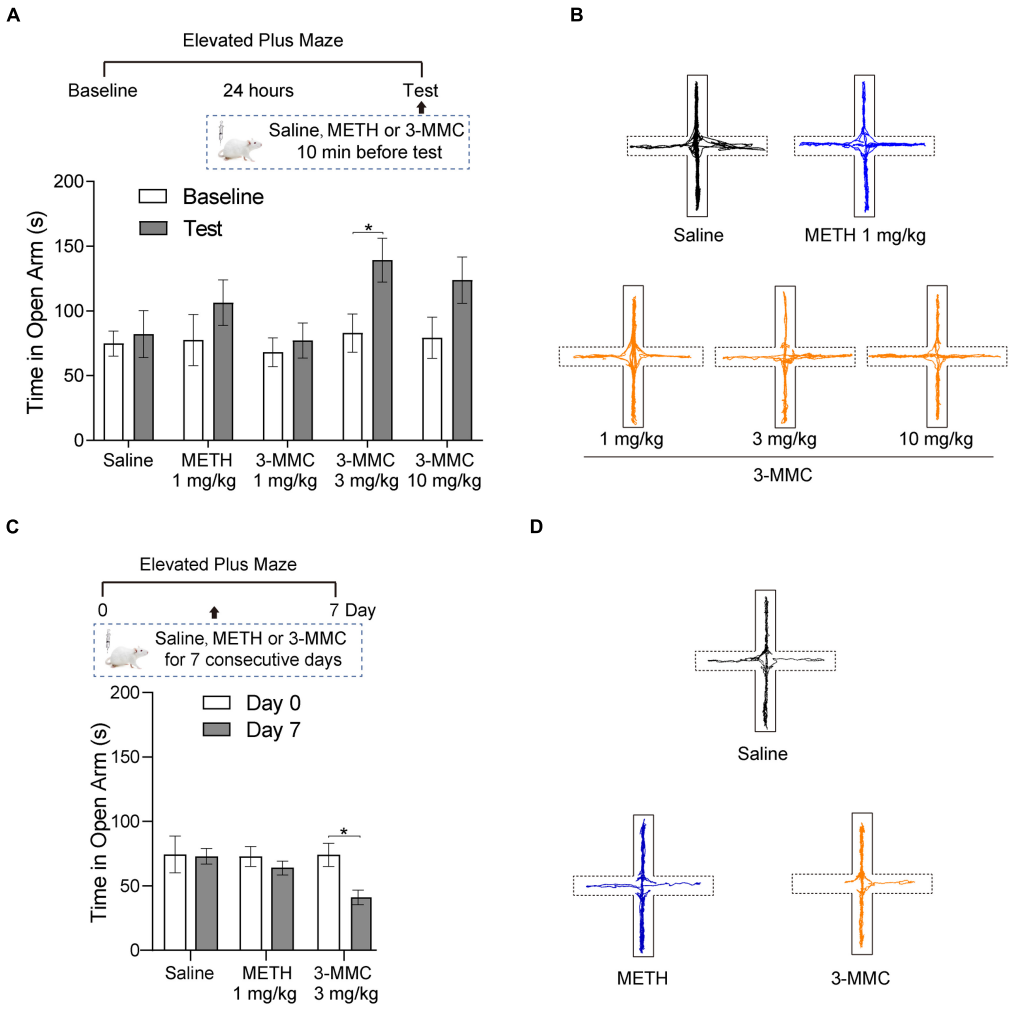

FIGURE 2
The effects of acute and chronic injection of 3-MMC on EPM. **(A)** A single injection of 3-MMC (3 mg/kg) increased the time in open arms, paired *t*-test, $^*P < 0.05$ significant differences for each drug in EPM test, $n = 7$ for each group. **(B)** Representative diagrams of travel trace in EPM after acute 3-MMC exposure. **(C)** 7 consecutive days of 3-MMC (3 mg/kg) injection decreased the time in open arms, paired *t*-test, $^*P < 0.05$ significant differences for each drug in EPM test, $n = 9$ for each group. **(D)** Representative diagrams of travel trace in EPM after chronic 3-MMC exposure. Data are presented as mean values ± SEM.

that 3-MMC induced CPP in a dose-dependent manner, indicating the rewarding effect of 3-MMC. In addition, rats with acute 3 mg/kg 3-MMC exposure increased locomotor activity, which lasted shorter than METH and reappeared after the first increase. It may be associated with the different effects of their metabolites. Within 30–45 min of METH injection, it reached maximum concentration in brain dialysate (El-Sherbeni et al., 2020) and was metabolized to amphetamine with similar psychoactive property as METH and para-hydroxymethamphetamine (p-OHMA) without psychoactive activity (Shima et al., 2008). Metabolism of METH explained its long-lasting psychoactive effects, which was consistent with the time-locomotor activity curve in present study. Within 5–10 min of 3-MMC oral ingestion, it reached peak concentration in plasma (Shimshoni et al., 2015) displayed its pharmacological characteristics of rapid absorption. Although 3-methylephedrine and 3-methylnorephedrine were identified as mainly metabolites of 3-MMC (Frison et al., 2016), their effects on locomotor activity have not been investigated yet. Further study of these metabolites may provide clear explanation for the effects of 3-MMC.

The desired effects of 3-MMC are euphoria, excitement, improved social skills and feelings of empathy, while chronic abuse may trigger deterioration of relationships with others, tachycardia, agitation, depression, and anxiety (Shimshoni et al., 2015; Sande, 2016; Ferreira et al., 2019; Drevin et al., 2021). We observed acute exposure of 3 mg/kg 3-MMC decreased anxiety-like behavior of rats, which has been reported for other

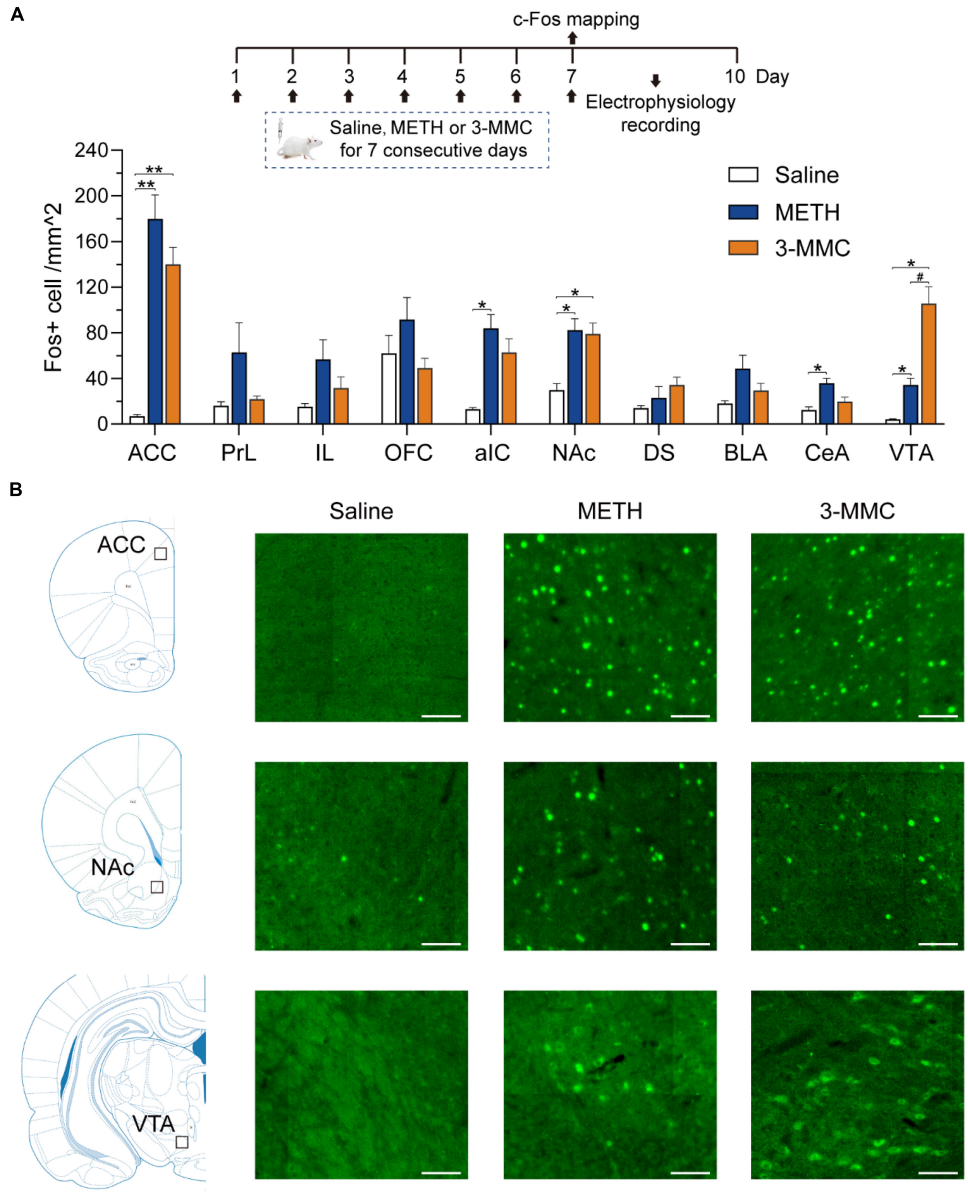

FIGURE 3
Specific brain regions response to chronic 3-MMC exposure. **(A)** The c-Fos expression of rats 90 min after last injection of drugs, *post hoc* test, $^{*}P < 0.05$, $^{**}P < 0.01$ significant differences for 3-MMC vs saline or METH vs saline, $^{\#}P < 0.05$ significant differences for 3-MMC vs METH, $n = 4$ for each group. **(B)** Representative immunofluorescent images of c-Fos expression in ACC, NAc, and VTA. Scale bar, 100 μm. ACC, anterior cingulate cortex; PrL, prelimbic cortex; IL, infralimbic cortex; OFC, orbitofrontal cortex; aIC, anterior insular cortex; NAc, nucleus accumbens; DS, dorsal striatum; BLA, basolateral amygdala; CeA, central amygdala; VTA, ventral tegmental area. Data are presented as mean values ± SEM.

synthetic cathinones such as mephedrone (Pail et al., 2015) and *N*-ethyl-pentedrone (Sande, 2016). This anxiolytic-like effect may be subjectively interpreted as a positive and euphoria experience by the consumers and influence on the further abuse. Interestingly, it seemed that the acute anxiolytic ability of 3-MMC decreased after exposure to 10 mg/kg of 3-MMC, implying the complex interaction between use of synthetic cathinones and adverse psychiatric sequelae. However, chronic administration of 3-MMC increased anxiety-like behavior, which was consistent with the problems users experienced (Sande, 2016).

Whole brain c-Fos mapping of present study showed that ACC, VTA, and NAc were significantly activated after chronic use of 3-MMC, which was consistent with its amphetamine-like stimulant properties (Ferreira et al., 2019; Espinosa-Velasco et al., 2022). Dopamine-releasing neurons of the VTA have central roles in reward-related and goal-directed behaviors (Morales and Margolis, 2017), and a major reward-related

TABLE 1 The c-Fos expression patterns in each brain region after chronic injection of saline, methamphetamine (METH) and 3-MMC.

Region	c-Fos + cells/mm^2 (mean ± SEM)			*post hoc* test: *P*		
	Saline	METH	3-MMC	Saline VS METH	Saline VS 3-MMC	METH VS 3-MMC
ACC	7.1 ± 1.2	179.7 ± 18.3	139.9 ± 13.0	0.0077**	0.0059**	0.3482
PrL	16.1 ± 3.0	62.6 ± 22.6	21.8 ± 2.6	0.3162	0.4770	0.3850
IL	15.2 ± 2.4	56.6 ± 15.0	31.6 ± 8.5	0.1827	0.3534	0.4768
OFC	61.9 ± 13.8	91.5 ± 16.7	49.0 ± 7.4	0.5063	0.7685	0.2224
aIC	13.0 ± 1.3	83.9 ± 10.6	62.6 ± 10.4	0.0197*	0.0505	0.4758
NAc	29.7 ± 4.9	82.2 ± 8.8	79.0 ± 8.3	0.0167*	0.0169*	0.9707
DS	13.8 ± 2.0	22.9 ± 8.7	34.3 ± 6.0	0.6883	0.1086	0.6423
BLA	18.1 ± 2.1	48.5 ± 10.2	29.4 ± 5.5	0.1534	0.3219	0.4010
CeA	12.3 ± 2.5	35.9 ± 3.7	19.6 ± 3.5	0.0114*	0.3765	0.0712
VTA	4.2 ± 0.3	34.3 ± 5.1	105.6 ± 12.9	0.0285*	0.0130*	0.0251$^{\#}$

post hoc test, *$P < 0.05$, **$P < 0.01$ significant differences for 3-MMC vs saline or METH vs saline, $^{\#}P < 0.05$ significant differences for 3-MMC vs METH.

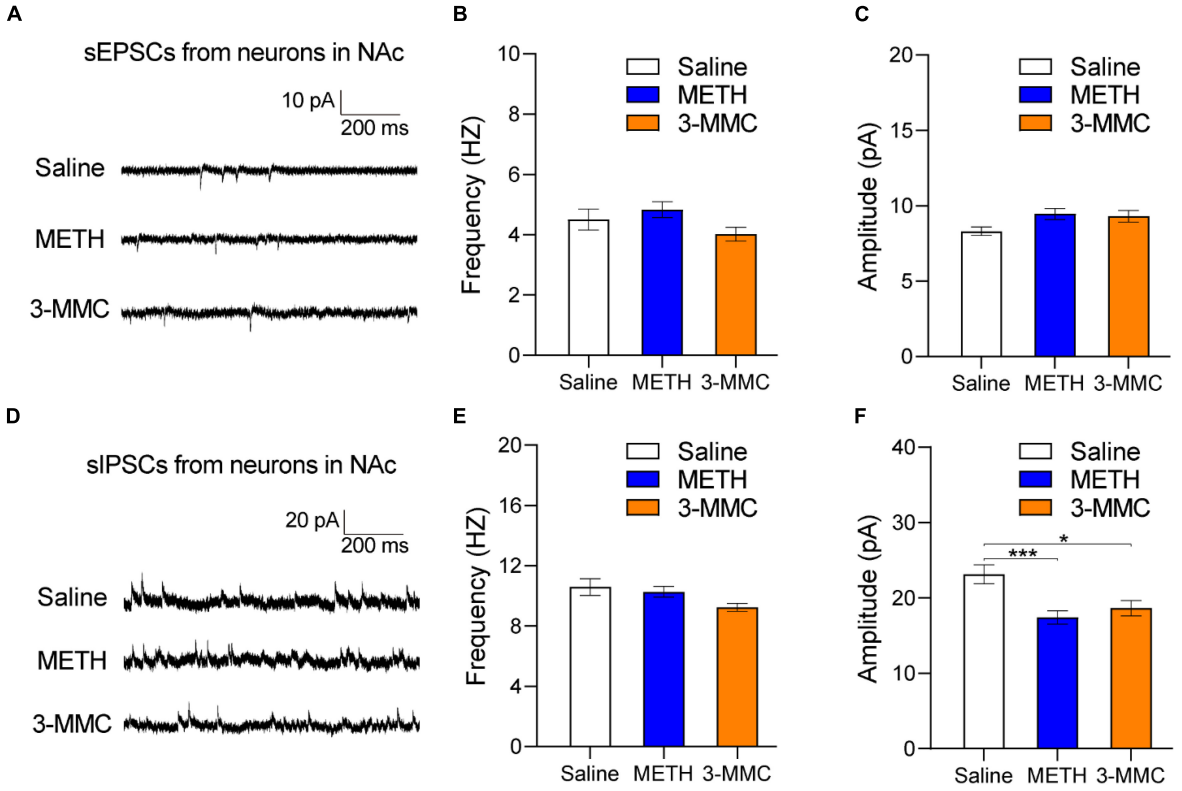

FIGURE 4
Changes of synaptic transmission in nucleus accumbens (NAc) after chronic 3-MMC injection. **(A)** Representative sEPSCs traces recorded in NAC 24 h after the last injection of drugs. **(B,C)** No difference in the frequency and the amplitude of sEPSCs in NAc after chronic 3-MMC injection. **(D)** Representative sIPSCs traces recorded in NAC 24 h after the last injection of drugs. **(E,F)** The amplitude of sIPSCs was decreased after chronic 3-MMC injection without change of frequency of sIPSCs, *post hoc* test, *$P < 0.05$, ***$P < 0.001$ significant differences for 3-MMC vs saline and METH vs saline respectively. For slice electrophysiology: 25 neurons from three rats with saline injection, 32 neurons from three rats with METH injection and 27 neurons from three rats with 3-MMC injection. Data are presented as mean values ± SEM.

output of VTA neurons is NAc (Cooper et al., 2017). Craving and impulsive behavior are related to increased neural activity in ACC (Zhao et al., 2020). Previous studies reported that 3-MMC could induce release of NE, serotonin (5-HT) and DA by inhibition of the reuptake of monoamines *via* DA, NE, and 5-HT transporters (Luethi et al., 2018; Zwartsen et al.,

2020), which may be the mechanism of 3-MMC addiction. Considering the enhancing effect on neuronal activity and rewarding of monoamines (Waterhouse and Navarra, 2019; Liu et al., 2020), 3-MMC may produce rewarding effect *via* increasing monoamines to activate ACC, VTA, and NAc, and demonstrated abuse liability. Compared with METH, rats treated with 3-MMC produced more activation of VTA, a region plays a role in both addiction and anxiety (Tovote et al., 2015; Salamone et al., 2016). Previous study reported that chemogenetic activation of VTA dopaminergic neurons directly triggered anxiety-like behavior (Qi et al., 2022), which explained that increased anxiety-like behavior after chronic 3-MMC exposure, implying pronounced effect of 3-MMC on dopaminergic neurons.

Nucleus accumbens plays a crucial role in addiction because it participates in the motivation, incentive salience, positive reinforcement, reward and reinforcement learning (Carlezon and Thomas, 2009; Salamone et al., 2016). Present and previous study found that chronic exposure of both 3-MMC and METH (Miliano et al., 2016) could activate NAc neurons. However, alterations of these neurons after chronic 3-MMC exposure are largely unknown. To the best of our knowledge, this is the first report of functional alterations of NAc neurons after chronic 3-MMC exposure in rats. Our results showed that sIPSCs of NAc neurons were decreased by chronic 3-MMC exposure without a change of sEPSCs, suggesting that 3-MMC inhibited inhibitory but not affecting excitatory neurotransmission. Rats with 7 days of 3-MMC injection exhibited reduced amplitude of sIPSCs, while the frequency of sIPSCs was not changed for NAc neurons, implying decreased postsynaptic neurotransmission by 3-MMC, without affecting presynaptic GABAergic transmitter release at the synapse of NAc (Gantz et al., 2013). Due to the complex neuron types in NAc, the precise neuronal mechanisms of 3-MMC addiction and its relationship with mental disorders need to be further studied.

There were two limitations in our study. One was that we performed the c-Fos mapping after chronic injection of 3-MMC without any behavioral test, which weakened the linking between 3-MMC induced neuronal activity and its effects on behavior of rats. The other was that the higher dose of 3-MMC should be introduced, such as 50 or 150 mg/kg. Because clinical study found that over half of the respondents consumed more than 0.5 g of 3-MMC (as 50 mg/kg for rats) in a single evening and 26.2% of those users reported more than 1.5 g of 3-MMC (as 150 mg/kg for rats) per day (Nair and Jacob, 2016; Sande, 2016).

In summary, our results revealed that 3-MMC has addictive potential due to its rewarding effects, which was related to activation of ACC, NAc and VTA after chronic exposure. Acute administration of 3 mg/kg 3-MMC produced anxiolytic-like effects, while chronic use of 3-MMC increased anxiety-like behavior, which may be related with hyperactivation of VTA. Moreover, the post-synaptic transmission of inhibitory neurons in the NAc might be involved in the mechanisms of chronic use of 3-MMC. Overall, all these findings are warning about the risks of 3-MMC consumption and encourage scientists to carry out further studies to fully elucidate the addictive potential, the neurochemical changes in the whole brain and other effects of this novel synthetic cathinone.

Data availability statement

The original contributions presented in this study are included in the article/supplementary material, further inquiries can be directed to the corresponding authors.

Ethics statement

The animal study was reviewed and approved by Biomedical Ethics Committee for Animal Use and Protection of Peking University.

Author contributions

YC and JS conceived the project. YC and LZ provided experimental design. YC and ZD performed the experiments. YC and XW contributed to analysis of the data. YC and GW wrote the manuscript with input from all authors. All authors contributed to the article and approved the submitted version.

Funding

This study was funded by the Ministry of Science and Technology of China (2021ZD0202100), National Natural Science Foundation of China (U1802283), and Beijing Municipal Science and Technology Commission (Z181100001518005).

Conflict of interest

The authors declare that the research was conducted in the absence of any commercial or financial relationships that could be construed as a potential conflict of interest.

Publisher's note

All claims expressed in this article are solely those of the authors and do not necessarily represent those of their affiliated organizations, or those of the publisher, the editors and the reviewers. Any product that may be evaluated in this article, or claim that may be made by its manufacturer, is not guaranteed or endorsed by the publisher.

References

Adamowicz, P., Gieron, J., Gil, D., Lechowicz, W., Skulska, A., and Tokarczyk, B. (2016). 3-Methylmethcathinone–interpretation of blood concentrations based on analysis of 95 cases. *J. Anal. Toxicol.* 40, 272–276. doi: 10.1093/jat/bkw018

Apaydin, N., Ustun, S., Kale, E. H., Celikag, I., Ozguven, H. D., Baskak, B., et al. (2018). Neural mechanisms underlying time perception and reward anticipation. *Front. Hum. Neurosci.* 12:115. doi: 10.3389/fnhum.2018.00115

Assi, S., Gulyamova, N., Kneller, P., and Osselton, D. (2017). The effects and toxicity of cathinones from the users' perspectives: a qualitative study. *Hum. Psychopharmacol.* 32:e2610. doi: 10.1002/hup.2610

Bäckberg, M., Lindeman, E., Beck, O., and Helander, A. (2015). Characteristics of analytically confirmed 3-MMC-related intoxications from the Swedish STRIDA project. *Clin. Toxicol.* 53, 46–53. doi: 10.3109/15563650.2014.981823

Carlezon, W. A. Jr., and Thomas, M. J. (2009). Biological substrates of reward and aversion: a nucleus accumbens activity hypothesis. *Neuropharmacology* 56(Suppl. 1), 122–132. doi: 10.1016/j.neuropharm.2008.06.075

CFDA (2015). *Measures for the List of Non-Medicinal Narcotic Drugs and Psychotropic Substances*. Beijing: China Food and Drug Administration.

Cooper, S., Robison, A. J., and Mazei-Robison, M. S. (2017). Reward circuitry in addiction. *Neurotherapeutics* 14, 687–697. doi: 10.1007/s13311-017-0525-z

Deng, J. H., Yan, W., Han, Y., Chen, C., Meng, S. Q., Sun, C. Y., et al. (2017). Predictable chronic mild stress during adolescence promotes fear memory extinction in adulthood. *Sci. Rep.* 7:7857. doi: 10.1038/s41598-017-08017-7

Dias da Silva, D., Ferreira, B., Roque Bravo, R., Rebelo, R., Duarte de Almeida, T., Valente, M. J., et al. (2019). The new psychoactive substance 3-methylmethcathinone (3-MMC or metaphedrone) induces oxidative stress, apoptosis, and autophagy in primary rat hepatocytes at human-relevant concentrations. *Arch. Toxicol.* 93, 2617–2634. doi: 10.1007/s00204-019-02539-x

Drevin, G., Rossi, L. H., Ferec, S., Briet, M., and Abbara, C. (2021). Chemsex/slamsex-related intoxications: a case report involving gamma-hydroxybutyrate (GHB) and 3-methylmethcathinone (3-MMC) and a review of the literature. *Forensic Sci. Int.* 321:110743. doi: 10.1016/j.forsciint.2021.110743

El-Sherbeni, A. A., Stocco, M. R., Wadji, F. B., and Tyndale, R. F. (2020). Addressing the instability issue of dopamine during microdialysis: the determination of dopamine, serotonin, methamphetamine and its metabolites in rat brain. *J. Chromatogr. A* 1627, 461403. doi: 10.1016/j.chroma.2020.461403

EMCDDA (2021). *European Drug Report 2021: Trends and Developments*. Lisbon: European Monitoring Centre for Drugs and Drug Addiction.

Espinosa-Velasco, M., Reguilón, M. D., Bellot, M., Nadal-Gratacós, N., Berzosa, X., Gómez-Canela, C., et al. (2022). Repeated administration of N-ethyl-pentedrone induces increased aggression and impairs social exploration after withdrawal in mice. *Prog. Neuropsychopharmacol. Biol. Psychiatry* 117:110562. doi: 10.1016/j.pnpbp.2022.110562

Ferreira, B., Dias da Silva, D., Carvalho, F., de Lourdes Bastos, M., and Carmo, H. (2019). The novel psychoactive substance 3-methylmethcathinone (3-MMC or metaphedrone): a review. *Forensic Sci. Int.* 295, 54–63. doi: 10.1016/j.forsciint.2018.11.024

Frison, G., Frasson, S., Zancanaro, F., Tedeschi, G., and Zamengo, L. (2016). Detection of 3-methylmethcathinone and its metabolites 3-methylephedrine and 3-methylnorephedrine in pubic hair samples by liquid chromatography-high resolution/high accuracy Orbitrap mass spectrometry. *Forensic Sci. Int.* 265, 131–137. doi: 10.1016/j.forsciint.2016.01.039

Gantz, S. C., Bunzow, J. R., and Williams, J. T. (2013). Spontaneous inhibitory synaptic currents mediated by a G protein-coupled receptor. *Neuron* 78, 807–812. doi: 10.1016/j.neuron.2013.04.013

Jamey, C., Kintz, P., Martrille, L., and Raul, J. S. (2016). Fatal Combination with 3-Methylmethcathinone (3-MMC) and Gamma-Hydroxybutyric Acid (GHB). *J. Anal. Toxicol.* 40, 546–552. doi: 10.1093/jat/bkw058

Liang, J., Li, J. L., Han, Y., Luo, Y. X., Xue, Y. X., Zhang, Y., et al. (2017). Calpain-GRIP signaling in nucleus accumbens core mediates the reconsolidation of drug reward memory. *J. Neurosci.* 37, 8938–8951. doi: 10.1523/jneurosci.0703-17.2017

Liu, Z., Lin, R., and Luo, M. (2020). Reward contributions to serotonergic functions. *Annu. Rev. Neurosci.* 43, 141–162. doi: 10.1146/annurev-neuro-093019-112252

Luethi, D., Kolaczynska, K. E., Docci, L., Krahenbuhl, S., Hoener, M. C., and Liechti, M. E. (2018). Pharmacological profile of mephedrone analogs and related new psychoactive substances. *Neuropharmacology* 134(Pt A), 4–12. doi: 10.1016/j.neuropharm.2017.07.026

Margasinska-Olejak, J., Celinski, R., Fischer, A., and Stojko, J. (2019). A fatal case of poisoning of a 19-year-old after taking 3-MMC. *Forensic Sci. Int.* 300, e34–e37. doi: 10.1016/j.forsciint.2019.02.040

Marusich, J. A., Grant, K. R., Blough, B. E., and Wiley, J. L. (2012). Effects of synthetic cathinones contained in "bath salts" on motor behavior and a functional observational battery in mice. *Neurotoxicology* 33, 1305–1313. doi: 10.1016/j.neuro.2012.08.003

Miliano, C., Serpelloni, G., Rimondo, C., Mereu, M., Marti, M., and De Luca, M. A. (2016). Neuropharmacology of new psychoactive substances (NPS): focus on the rewarding and reinforcing properties of cannabimimetics and amphetamine-like stimulants. *Front. Neurosci.* 10:153. doi: 10.3389/fnins.2016.00153

Morales, M., and Margolis, E. B. (2017). Ventral tegmental area: cellular heterogeneity, connectivity and behaviour. *Nat. Rev. Neurosci.* 18, 73–85. doi: 10.1038/nrn.2016.165

Nair, A. B., and Jacob, S. (2016). A simple practice guide for dose conversion between animals and human. *J. Basic Clin. Pharm.* 7, 27–31. doi: 10.4103/0976-0105.177703

Pail, P. B., Costa, K. M., Leite, C. E., and Campos, M. M. (2015). Comparative pharmacological evaluation of the cathinone derivatives, mephedrone and methedrone, in mice. *Neurotoxicology* 50, 71–80. doi: 10.1016/j.neuro.2015.08.004

Pellow, S., Chopin, P., File, S. E., and Briley, M. (1985). Validation of open:closed arm entries in an elevated plus-maze as a measure of anxiety in the rat. *J. Neurosci. Methods* 14, 149–167. doi: 10.1016/0165-027090031-7

Piazza, P. V., and Deroche-Gamonet, V. (2013). A multistep general theory of transition to addiction. *Psychopharmacology* 229, 387–413. doi: 10.1007/s00213-013-3224-4

Pieprzyca, E., Skowronek, R., Nižnanský, Ľ., and Czekaj, P. (2020).). Synthetic cathinones - From natural plant stimulant to new drug of abuse. *Eur. J. Pharmacol.* 875:173012. doi: 10.1016/j.ejphar.2020.173012

Qi, G., Zhang, P., Li, T., Li, M., Zhang, Q., He, F., et al. (2022). NAc-VTA circuit underlies emotional stress-induced anxiety-like behavior in the three-chamber vicarious social defeat stress mouse model. *Nat. Commun.* 13:577. doi: 10.1038/s41467-022-28190-2

Salamone, J. D., Pardo, M., Yohn, S. E., López-Cruz, L., SanMiguel, N., and Correa, M. (2016). Mesolimbic dopamine and the regulation of motivated behavior. *Curr. Top. Behav. Neurosci.* 27, 231–257. doi: 10.1007/7854_2015_383

Sande, M. (2016). Characteristics of the use of 3-MMC and other new psychoactive drugs in Slovenia, and the perceived problems experienced by users. *Int. J. Drug Policy* 27, 65–73. doi: 10.1016/j.drugpo.2015.03.005

Shima, N., Katagi, M., Kamata, H., Zaitsu, K., Kamata, T., Nishikawa, M., et al. (2008). Urinary excretion of the main metabolites of 3,4-methylenedioxymethamphetamine (MDMA), including the sulfate and glucuronide of 4-hydroxy-3-methoxymethamphetamine (HMMA), in humans and rats. *Xenobiotica* 38, 314–324. doi: 10.1080/00498250701802506

Shimshoni, J. A., Britzi, M., Sobol, E., Willenz, U., Nutt, D., and Edery, N. (2015). 3-Methyl-methcathinone: pharmacokinetic profile evaluation in pigs in relation to pharmacodynamics. *J. Psychopharmacol.* 29, 734–743. doi: 10.1177/0269881115576687

Tovote, P., Fadok, J. P., and Lüthi, A. (2015). Neuronal circuits for fear and anxiety. *Nat. Rev. Neurosci.* 16, 317–331. doi: 10.1038/nrn3945

Tzschentke, T. M. (2007). Measuring reward with the conditioned place preference (CPP) paradigm: update of the last decade. *Addict. Biol.* 12, 227–467. doi: 10.1111/j.1369-1600.2007.00070.x

Volkow, N. D., Wang, G. J., Fowler, J. S., Tomasi, D., and Telang, F. (2011). Addiction: beyond dopamine reward circuitry. *Proc. Natl. Acad. Sci. U.S.A.* 108, 15037–15042. doi: 10.1073/pnas.1010654108

Waterhouse, B. D., and Navarra, R. L. (2019). The locus coeruleus-norepinephrine system and sensory signal processing: a historical review and current perspectives. *Brain Res.* 1709, 1–15. doi: 10.1016/j.brainres.2018.08.032

Xu, P., Qiu, Y., Zhang, Y., Bai, Y., Xu, P., Liu, Y., et al. (2016). The Effects of 4-methylethcathinone on conditioned place preference, locomotor sensitization, and anxiety-like behavior: a comparison with methamphetamine. *Int. J. Neuropsychopharmacol.* 19:yv120. doi: 10.1093/ijnp/pyv120

Yu, Z., Han, Y., Hu, D., Chen, N., Zhang, Z., Chen, W., et al. (2022). Neurocan regulates vulnerability to stress and the anti-depressant effect of ketamine in adolescent rats. *Mol. Psychiatry* 27, 2522–2532. doi: 10.1038/s41380-022-01495-w

Zhao, Y., Sallie, S. N., Cui, H., Zeng, N., Du, J., Yuan, T., et al. (2020). Anterior cingulate cortex in addiction: new insights for neuromodulation. *Neuromodulation* 24, 187–196. doi: 10.1111/ner.13291

Zwartsen, A., Olijhoek, M. E., Westerink, R. H. S., and Hondebrink, L. (2020). Hazard characterization of synthetic cathinones using viability, monoamine reuptake, and neuronal activity assays. *Front. Neurosci.* 14:9. doi: 10.3389/fnins.2020.00009

frontiers | Frontiers in Molecular Neuroscience

TYPE Original Research
PUBLISHED 12 September 2022
DOI 10.3389/fnmol.2022.972798

OPEN ACCESS

EDITED BY
Qi Wang,
Southern Medical University, China

REVIEWED BY
Jessica A. Loweth,
Rowan University School of Osteopathic Medicine, United States
Zayra Millan,
University of New South Wales, Australia

*CORRESPONDENCE
Peng Xu
pengxu750@163.com
Wenhua Zhou
whzhou@vip.163.com

†These authors have contributed equally to this work

SPECIALTY SECTION
This article was submitted to Molecular Signalling and Pathways, a section of the journal Frontiers in Molecular Neuroscience

RECEIVED 19 June 2022
ACCEPTED 18 August 2022
PUBLISHED 12 September 2022

CITATION
Du H, Lai M, Zhuang D, Fu D, Zhou Y, Chen S, Wang F, Xu Z, Liu H, Wang Y, Xu P and Zhou W (2022) A comparison of reinforcing effectiveness and drug-seeking reinstatement of 2-fluorodeschloroketamine and ketamine in self-administered rats. *Front. Mol. Neurosci.* 15:972798. doi: 10.3389/fnmol.2022.972798

A comparison of reinforcing effectiveness and drug-seeking reinstatement of 2-fluorodeschloroketamine and ketamine in self-administered rats

Han Du[1†], Miaojun Lai[1†], Dingding Zhuang[1], Dan Fu[1], Yiying Zhou[1], Shanshan Chen[1], Fangmin Wang[1], Zemin Xu[1], Huifen Liu[1], Youmei Wang[2], Peng Xu[2]* and Wenhua Zhou[1]*

[1]Zhejiang Provincial Key Laboratory of Addiction Research, Ningbo Kangning Hospital, School of Medicine, Ningbo University, Ningbo, China, [2]Key Laboratory of Drug Monitoring and Control, Drug Intelligence and Forensic Center, Ministry of Public Security, Beijing, China

2-Fluorodeschloroketamine (2F-DCK), a structural analog of ketamine, has been reported to cause impaired consciousness, agitation, and hallucination in abuse cases. It has similar reinforcing and discriminative effects as ketamine. However, the reinforcing efficacy and drug-seeking reinstatement of this analog have not been clarified to date. In this study, the effectiveness of 2F-DCK and ketamine was compared using a behavioral economics demand curve. The reinstatement of 2F-DCK- and ketamine-seeking behaviors induced by either conditioned cues or self-priming was also analyzed. Rats were intravenously self-administered 2F-DCK and ketamine at a dose of 0.5 mg/kg/infusion under a reinforcing schedule of fixed ratio 1 (FR1) with 4 h of daily training for at least 10 consecutive days. The elasticity coefficient parameter α and the essential value of the demand curve in the two groups were similar. Both groups of rats showed significant drug-seeking behavior induced either by conditional cues or by 2F-DCK and ketamine priming. Moreover, the α parameter was inversely related to the degree of reinstatement induced by cues or drug priming in both groups. In total, the expression levels of brain-derived neurotrophic factor (BDNF) and phosphorylated cAMP response element-binding protein (p-CREB) in the nucleus accumbens in both extinguished and reinstated rats were significantly lower than those in the control. The expression of total Akt, glycogen synthase kinase (GSK)-3β, mammalian target of rapamycin (mTOR), and extracellular signal-related kinase (ERK) also decreased, but p-Akt, p-GSK-3β, p-mTOR, and p-ERK levels increased in both extinguished and reinstated rats. This is the first study to demonstrate that 2F-DCK has similar reinforcing efficacy, effectiveness, and post-withdrawal cravings as ketamine after repeated use. These data suggest that the downregulation of CREB/BDNF and the upregulation of the Akt/mTOR/GSK-3β signaling pathway in the nucleus accumbens may be involved in ketamine or 2F-DCK relapse.

KEYWORDS

new psychoactive substance, PCP, ketamine, BDNF, GSK-3β

Introduction

Ketamine, a dissociative anesthetic and psychedelic compound, has rapid-acting antidepressant activity in patients with major depression (Berman et al., 2000) and resistant depression (Zarate et al., 2006). Ketamine's efficacy, however, is transient, and repeated clinical use often leads to drug dependence or use disorders (Krystal et al., 1994). Ketamine is known for its abuse liability, which poses a major challenge for its clinical use in depression and other mental disorders (Liu et al., 2016). Preclinical studies have shown that ketamine produces discriminative (Chiamulera et al., 2016) and reinforcing effects in women and men (Wright et al., 2017). 2-Fluorodeschloroketamine (2F-DCK) is a novel psychoactive ketamine derivative that has been detected in wastewater treatment plants (Shao et al., 2021). Sporadic clinical reports have described the use of 2F-DCK to induce a dissociated state (Domanski et al., 2021) and identified the 2F-DCK concentration in the illegal range in forensic blood and hair samples of drivers under the influence of drugs (Davidsen et al., 2020). The clinical effects in patients exposed to 2F-DCK are predominantly impaired consciousness, agitation, abnormal behavior, hypertension, and tachycardia (Tang et al., 2020). 2F-DCK has recently emerged as a substitute for ketamine in drug abusers. However, 2F-DCK has not been controlled or regulated in many countries, which may be partly related to the lack of evidence regarding its abuse potential.

The reinforcing effects of drugs are fundamental to the development of drug addiction and are intrinsic to most rodent models of addiction-like behaviors (Koffarnus et al., 2012). 2F-DCK was recently shown to produce self-administration, generalized to ketamine discriminative stimuli and induce conditioned place preference in rats (Li et al., 2022). Self-administration of ketamine or 2F-DCK determines their functions as reinforcers but does not provide quantitative information about their reinforcing effectiveness (Huskinson et al., 2014). Behavioral economics approaches permit the quantification of reinforcing effects, placing a relative value on different drug reinforcers (Galuska et al., 2011; Koffarnus et al., 2012). Behavioral economics curves are independent of the magnitude (dose) of the reinforcer, allowing each reinforcing stimulus to be assigned a single number that reflects its reinforcing effectiveness (Hursh and Silberberg, 2008). Addicted individuals are highly susceptible to relapse when exposed to the self-administered drug and drug-associated cues even after extensive periods of abstinence (Kuijer et al., 2020). Reinstatement procedures in animal models are thought to resemble drug-seeking and relapse in humans (Epstein and Preston, 2003; Shaham et al., 2003). Preclinical data have shown reinstatement of ketamine-seeking behavior induced by cues and ketamine priming after ketamine self-administration (Huang et al., 2015). However, to date, the reinforcing effectiveness and reinstatement of drug seeking by 2F-DCK are still unclear.

Ketamine is proposed to selectively block *N*-methyl-D-aspartate (NMDA) receptors expressed on GABAergic inhibitory interneurons, which results in the disinhibition of pyramidal neurons, enhancement of brain-derived neurotrophic factor (BDNF) release, and subsequent promotion of protein synthesis (Zanos and Gould, 2018). The antidepressant effects of ketamine are mediated, at least in part, by molecular adaptations, resulting in long-lasting synaptic changes in the mesolimbic brain regions known to regulate natural and drug rewards (Zanos and Gould, 2018). Silencing of glycogen synthase kinase (GSK)-3β in the nucleus accumbens (NAc) increases depression- and addiction-related behavior (Crofton et al., 2017). Ketamine at a lower dose induces behavioral sensitization, which is accompanied by an increase in the spine density in the NAc and changes in protein expression in pathways commonly implicated in addiction (Strong et al., 2017). Three weeks of abstinence from ketamine was associated with increased dendritic mushroom spines in the NAc (Strong et al., 2019). The mammalian target of rapamycin (mTOR) inhibitor rapamycin blocks the effects of ketamine (Sabino et al., 2013). However, much remains to be known about the long-term effects of ketamine and the neurobiological mechanisms underlying its addiction (Kokane et al., 2020; Sial et al., 2020).

In the present study, we used a behavioral economics approach to compare the reinforcing effectiveness of 2F-DCK and ketamine, and compared the reinstatement of 2F-DCK- and ketamine-seeking behaviors induced by either conditioned cues or themselves. The expression of BDNF, CREB, extracellular signal-related kinase (ERK), Akt, GSK-3β, mTOR, and their phosphorylation in the NAc after extinction or reinstatement induced by both cues and priming were measured by Western blotting. These studies will provide evidence for the difference in abuse potential between 2F-DCK and ketamine and the molecular mechanisms underlying the relapse of 2F-DCK and ketamine in rats.

Materials and methods

Subjects

Male Sprague–Dawley rats (280–300 g) purchased from the Experimental Animal Center of Zhejiang Province, China, were housed in a temperature- and humidity-controlled ventilated colony room with a reversed 12-h light/dark cycle (lights onset 20:00 h, offset 8:00 h). The temperature was maintained at 22–24°C, and humidity levels were stable (50–70%). The experimental sessions were performed during the dark period. Food and water were provided *ad libitum* in the home cage. All experiments were conducted in accordance with the Eighth Edition of the Guide for Care and Use of Laboratory Animals

(I.f.L.A. Research., 2011). This study was approved by the Hospital Ethics Committee for Animal Use.

Ketamine crystalline powder was provided by the Drug Intelligence and Forensic Center of the Ministry of Public Security, China. The crystalline 2F-DCK powder was provided by the Drug Laboratory of the Narcotic Control Division of the Nanjing Public Security Bureau, China. All the drugs were dissolved in physiological saline.

Surgery

After acclimation to the environment for 7 days, the animals were anesthetized with sodium pentobarbital (50 mg/kg, i.p.). Each rat was subsequently implanted with a chronically indwelling intravenous catheter (Silastic; length, 3.5 cm; inner diameter, 0.5 mm; outer diameter, 0.94 mm) into the right external jugular vein, and the other end of the catheter (10 cm, PE20) was passed subcutaneously to the dorsal surface of the scapulae. The catheters were flushed daily with 0.3 ml of sterile saline containing heparin (15 units) and penicillin B (60,000 units) to preserve catheter patency and prevent infection. After surgery, the rats were allowed to recover for 1 week prior to drug self-administration training. The catheters were flushed with 0.3 ml of heparinized saline (50 U/ml) every day, and if resistance or exudation was noted while flushing the catheters, we used 10 mg/kg propofol to assess the catheter patency. All catheters remained patent throughout the experiments.

Self-administration

All the experiments were conducted in an operant chamber (AniLab Software Instruments Co., Ltd., Ningbo, China). After ∼7 days of recovery from surgery, the rats ($n = 16$) were divided randomly into two groups, which underwent ketamine and 2F-DCK self-administration training. During the 4-h acquisition phase of self-administration starting with the green light inside the active nose-poke hole, rats were trained to respond under a fixed ratio 1 (FR1) reinforcement schedule for ketamine and 2F-DCK (0.5 $mg{\cdot}kg^{-1}{\cdot}infusion^{-1}$), in accordance with the protocol described in a previous study (Li et al., 2022). To prevent overdose, the number of infusions was limited to 200 per session. Each infusion was paired with a 20-s illumination of the house light in combination with the noise of the infusion pump. A time-out period was imposed for 20 s, during which the response produced no programmed consequences but was still recorded. Responding to inactive nose pokes produced no programmed consequences. Acquisition training under these conditions continued for at least 10 sessions until the animals met the stability criteria (±15% of the mean number of infusions of three consecutive training sessions).

Behavioral economics demand curve

Behavioral economics demand was determined after stable self-administration training (Lai et al., 2022). Briefly, the dose (0.5 mg/kg/infusion) chosen was consistent with the training session, and each daily session was 4 h in duration. Once the number of infusions was stable under the FR1 schedule, the FR value was increased across sessions until zero infusions were delivered in a single session in the following order: 3, 10, 18, 32, 56, 98, 172, and 300 (i.e., each value was 1.75 times the preceding response requirement except in the case of 3 and 10). If the mean number of infusions for 2 consecutive days showed considerable variability at a particular ratio, three or more sessions were conducted, and the most discrepant result was excluded from the data analysis.

Extinction and reinstatement

After the acquisition and determinations of self-administration for 14 days, rats (each group, $n = 7$) underwent an extinction period for seven sessions during which the drug was not available. Both cue- and drug-induced reinstatement tests were conducted for 2 h in operant chambers after extinction training. The cue-induced reinstatement test began with drug-associated conditioned cues (CS), consisting of the house light and the sound of the pump. Nose pokes in both the active and inactive holes were recorded. The only difference between the self-administration sessions and reinstatement tests was the lack of drug infusion. After the CS-induced relapse test was completed, the rats underwent another extinction training for three sessions, following which they were administered either ketamine (10 mg/kg, i.p.) or 2F-DCK (10 mg/kg, i.p.) and placed immediately into the operant chamber for the drug-induced reinstatement test without drug-associated cues. Nose pokes in both the active and inactive holes were recorded.

Western blot

Another group of rats was used to investigate the expression of signaling proteins in the NAc. The groups of rats were divided into the control group (a drug-naive), the ketamine or 2F-DCK extinction group in which they completed 14 days of self-administration followed by 10 days of extinction, and the ketamine or 2F-DCK priming group in which rats were exposed to either acute ketamine (10 mg/kg, i.p.) or 2F-DCK (10 mg/kg, i.p.) injection after extinction with CS rewards. The rats were decapitated within 2 h after the extinction or relapse test. The brains were rapidly removed and dissected to obtain NAc tissue. Tissue samples obtained from individual rats were immediately homogenized on ice in ice-cold RIPA lysis buffer (20 mM Tris, pH 7.5; 150 mM NaCl; 1% Triton X-100;

2.5 mM sodium pyrophosphate; 1 mM EDTA; 1% Na_3VO_4; 0.5 mg/ml leupeptin; and 1 mM phenyl-methanesulfonyl fluoride) containing 1 mM phenyl-methanesulfonyl fluoride and 1 mM phosphatase inhibitor. After immersion for 30 min in RIPA lysis buffer, the homogenized tissue was centrifuged at 12,000 rpm at 4°C for 20 min. Protein concentrations were determined using a bicinchoninic acid protein assay, and the samples were further diluted in RIPA lysis buffer to equalize the protein concentrations. The extracts were then mixed with 5 × loading buffer, boiled for 5 min, centrifuged for 5 min, aliquoted, and stored at −80°C. For Western blot analysis, 20–40 μg of protein was subjected to electrophoresis on sodium dodecyl sulfate (SDS) polyacrylamide mini gels for 20 min at 100 V in the stacking gel and 60 min at 220 V in the resolving gel. After electrophoresis, the separated proteins were transferred to a polyvinylidene fluoride (PVDF) membrane at 100 V for 60 min. To detect the protein of interest, the membranes were blocked in 5% non-fat dried milk in Tris-buffered saline (TBS) for 3 h. Membranes were then probed with different primary antibodies. Antibodies for BDNF (1:1,000; Ab108319, Abcam), CREB (1:1,000; Ab32515, Abcam), p-CREB (1:500; 9198s, Cell Signaling Technology), ERK (1:500; 4695s, Cell Signaling Technology), p-ERK (1:500; 4370s, Cell Signaling Technology), Akt (1:1,000; 9272s, Cell Signaling Technology), p-Akt (1:1,000; 9271s, Cell Signaling Technology), GSK-3β (1:1,000; 12456-R, Cell Signaling Technology), p-GSK-3β (1:500; 5558-R, Cell Signaling Technology), mTOR (1:500; 2972s, Cell Signaling Technology), p-mTOR (1:500; 2971s, Cell Signaling Technology), or β-actin (1:2,000; 4967s, Cell Signaling Technology) were added to TBST (Tris-buffered saline plus 0.05% Tween-20, pH 7.4) containing 5% bovine serum albumin. The blots were incubated in the primary antibody solution overnight at 4°C. The next day, after three 10-min washes in TBST buffer, the membranes were incubated for 1 h at room temperature on a shaker with a 1:5,000 dilution of fluorescent secondary antibody [goat (polyclonal) anti-rabbit IgG (LI-COR Bioscience, Beijing, China)] in TBST in the dark. The blots were then washed three times for 10 min each in TBST and detected using the Odyssey Imaging System Application (Odyssey, USA).

Data analyses

For acquisition studies on the FR1 schedule, results are shown as the mean ± standard error of the mean (SEM) of the number of responses and infusions across 10 sessions. Statistical tests were performed by using repeated measures analysis of variance (ANOVA). For the demand curve, as reported previously (Hursh and Silberberg, 2008), the logarithm of the number of infusions was plotted as a function of the logarithm of the price (FR value) according to the equation $\log Q = \log Q_0 + k\,(e^{-\alpha Q_0 C} - 1)$, where Q is the average number of infusions obtained for a given drug at any FR value, Q_0 is the average number of infusions obtained for a given drug when FR is set to 1, C is the FR value, α is the elasticity coefficient of each drug, and k is a constant. In this study, the k parameter was set to 1, and the log of the maximum number of infusions was obtained under any FR for a particular determination. Because the parameter α is inversely proportional to the reinforcing effectiveness, the equation converts it into an essential value (EV) with $EV = 1/(100\ \alpha\ k^{1.5})$, which is directly related to the reinforcing effectiveness (Hursh and Silberberg, 2008; Maguire et al., 2020). For both normalized and non-normalized analyses, we also fitted the exponential equation to the individual subject data and obtained the best-fitting α and EV parameters for each rat. In cases where individual rats did not earn a reinforcer at a particular ratio, a value of 0.1 was assigned because the log of zero is undefined. For both CS- and drug-induced reinstatement tests, the results were expressed as mean ±SEM of the number of responses per session, and the analysis of differences between groups (ketamine *vs.* 2F-DCK) and tests (extinction *vs.* reinstatement) was performed by using a two-way ANOVA. Western blot data were analyzed using an independent *t*-test between the control and ketamine or 2F-DCK groups. Changes were considered statistically significant when $P<0.05$. Statistical analysis was performed using SPSS 18.0 (SPSS, Inc.) and GraphPad Prism 7 (GraphPad Software, Inc.).

Results

Comparison of reinforcing effectiveness between 2F-DCK and ketamine

Both 2F-DCK and ketamine quickly induced self-administration behavior, as shown in Figure 1. From the first day of training, the number of active responses increased significantly, and the number of injections increased significantly in the first 5 days. Moreover, the mean number of infusions on days 8, 9, and 10 met the stability criteria for acquisition of self-administration. Repeated-measures ANOVA revealed a significant increase in active responses in the 2F-DCK group with an increase in training days [$F_{(9,126)} = 5.513$, $P < 0.001$], along with a significant difference between the active and inactive responses [$F_{(1,14)} = 45.74$, $P < 0.0001$]. We also observed a significant increase in active responses [$F_{(9,126)} = 4.828$, $P < 0.001$] and between active and inactive responses [$F_{(1,14)} = 167.6$, $P < 0.001$]. No significant difference was observed between 2F-DCK and ketamine in active responses [$F_{(1,14)} = 1.949$, $P = 0.184$] and inactive responses [$F_{(1,14)} = 0.128$, $P = 0.726$]. The average number of daily injections in the last 3 days in the 2F-DCK and ketamine groups was 122.62 ± 7.93 and 101.58 ± 4.02, respectively, but the two groups showed no significant difference [$F_{(1,14)} = 1.266$, $P = 0.280$]. Thus, rats in both 2F-DCK and ketamine groups could quickly acquire and maintain self-administration, suggesting that 2F-DCK and ketamine have similar reinforcement and rewarding effects.

In the actual test of economic demand, only FR10 was tested for 3 days and excluded the data on the second day for analysis due to considerable variability. To complete the test within the service life of the intravenous catheter, when the number of infusions of more than half of the rats is 0 and other rats gained ≤10 infusions, each FR value was only tested for 1 day. Figure 2 shows the non-normalized and normalized demand curves for ketamine and 2F-DCK. Subsequent fitting of the exponential equation to the normalized results from each rat individually revealed the α parameter in the ketamine group [2.145E-4 (95% CI: 1.918E-4, 2.365E-4)] and in the 2F-DCK group [2.014E-4 (95% CI: 1.638E-4, 2.588E-4)]. The α parameter was similar, and the 95% confidence interval almost coincided. As shown in Figure 2C, Q_0 and EV values in the ketamine group were 137.63 ± 10.92 and 8.69 ± 2.33, respectively, and the Q_0 and EV in the 2F-DCK group were 138.81 ± 14.56 and 9.40 ± 1.97, respectively. The independent *t*-test revealed no significant differences in Q_0 and EV between the ketamine and 2F-DCK groups ($t = 0.065$, $P = 0.949$ and $t = 0.234$, $P = 0.819$). Together, these results showed that the elasticity coefficient and EV in the 2F-DCK and ketamine groups were very close, suggesting that 2F-DCK and ketamine functioned as reinforcers with similar effectiveness.

Reinstatement of 2F-DCK and ketamine-seeking behaviors

After stable self-administration training for 14 days, the rats completed the 2-h extinction period in self-administration chambers for 7 days. The results of extinction training is shown in Figure 3A. Two-way ANOVA was used to analyze the reinstatement of drug-seeking behavior induced by CS with extinction between 2F-DCK and ketamine-trained rats. As shown in Figure 3B, a significant difference was observed in the number of active responses between the extinction and CS-induced reinstatement ($F = 44.797$, $P < 0.001$); however, no significant difference was observed between 2F-DCK and ketamine groups ($F = 0.098$, $P = 0.756$) and interaction ($F = 0.044$, $P = 0.836$). Moreover, there were no differences in the inactive responses in tests ($F = 0.167$, $P = 0.686$), 2F-DCK and ketamine treated group ($F = 0.306$, $P = 0.585$), and interaction ($F = 0.014$, $P = 0.905$). These results suggest that both 2F-DCK and ketamine groups of rats showed significant drug-seeking behavior when exposed to CS which is associated with previous rewards. The two groups of rats were intraperitoneally injected with the same drugs as the drug-priming-induced reinstatement at doses of 10 mg/kg ketamine or 2F-DCK, and immediately placed into their own administration cages for 2 h. Two-way ANOVA analysis revealed a significant difference between extinction and reinstatement induced by priming ($F = 13.662$, $P = 0.001$), but no difference between 2F-DCK and ketamine groups ($F = 0.441$, $P = 0.513$) and interaction ($F = 0.883$, $P = 0.357$). Moreover, there was no difference in the inactive responses between the tests ($F = 0.239$, $P = 0.629$), 2F-DCK and ketamine treated group ($F = 1.496$, $P = 0.233$), and interaction ($F = 0.135$, $P = 0.717$). Figure 3C shows the frequency of active responses across 2-h reinstatement testing. These results suggest that both 2F-DCK and ketamine priming can produce an increase in drug-seeking behavior after extinction. The results demonstrated relapse and craving in the rats after exposure to the CS or 2F-DCK and ketamine lapse after extinction and withdrawal from 2F-DCK and ketamine self-administration.

Relationship between reinforcing effectiveness and reinstatement

The relationship of the Q_0 and α parameters with extinction, cue-induced, or drug-priming reinstatement behaviors is shown in Table 1. Spearman's rank-order correlation analysis showed that the Q_0 parameter was not associated with the degree of extinction, cues, or drug-priming reinstatement. However, the α parameter was inversely related to the degree of reinstatement induced by cues or drug priming in the ketamine group and 2F-DCK group, but the statistical value in the 2F-DCK group was equal to 0.05.

Signaling protein expression in the NAc

The relative expression of BDNF, CREB, or ERK in the NAc is shown in Figure 4. The independent *t*-test showed a significant decrease in BDNF levels in ketamine extinction ($t = 6.362$, $P < 0.01$), 2F-DCK extinction ($t = 11.507$, $P < 0.01$), and ketamine priming group ($t = 7.907$, $P < 0.01$) compared with the control group, but no difference in the 2F-DCK priming group ($t = 1.907$, $P = 0.075$). Moreover, a decrease in the BDNF levels was observed in the ketamine priming group compared to that of the ketamine extinction group ($t = 2.934$, $P < 0.01$), but an increase in 2F-DCK priming rats was noticed compared to that in 2F-DCK extinction group ($t = 12.773$, $P < 0.01$). The total CREB expression was not different in the ketamine extinction ($t = 0.689$, $P = 0.500$) and priming groups ($t = 0.561$, $P = 0.581$), decreased in the 2F-DCK extinction group ($t = 2.154$, $P = 0.045$), and increased in the 2F-DCK priming rats ($t = 4.407$, $P < 0.01$), in comparison with the control group. Moreover, the p-CREB level decreased in 2F-DCK extinction ($t = 7.564$, $P < 0.01$), ketamine ($t = 3.451$, $P < 0.01$), and 2F-DCK ($t = 9.316$, $P < 0.01$) priming groups, but no difference in the ketamine extinction ($t = 0.313$, $P = 0.759$) group was noted when compared to the control. There was no difference either between ketamine extinction and priming groups ($t = 0.313$, $P = 0.759$) or between 2F-DCK extinction and priming groups ($t = 0.946$, $P = 0.362$). The total ERK levels were decreased

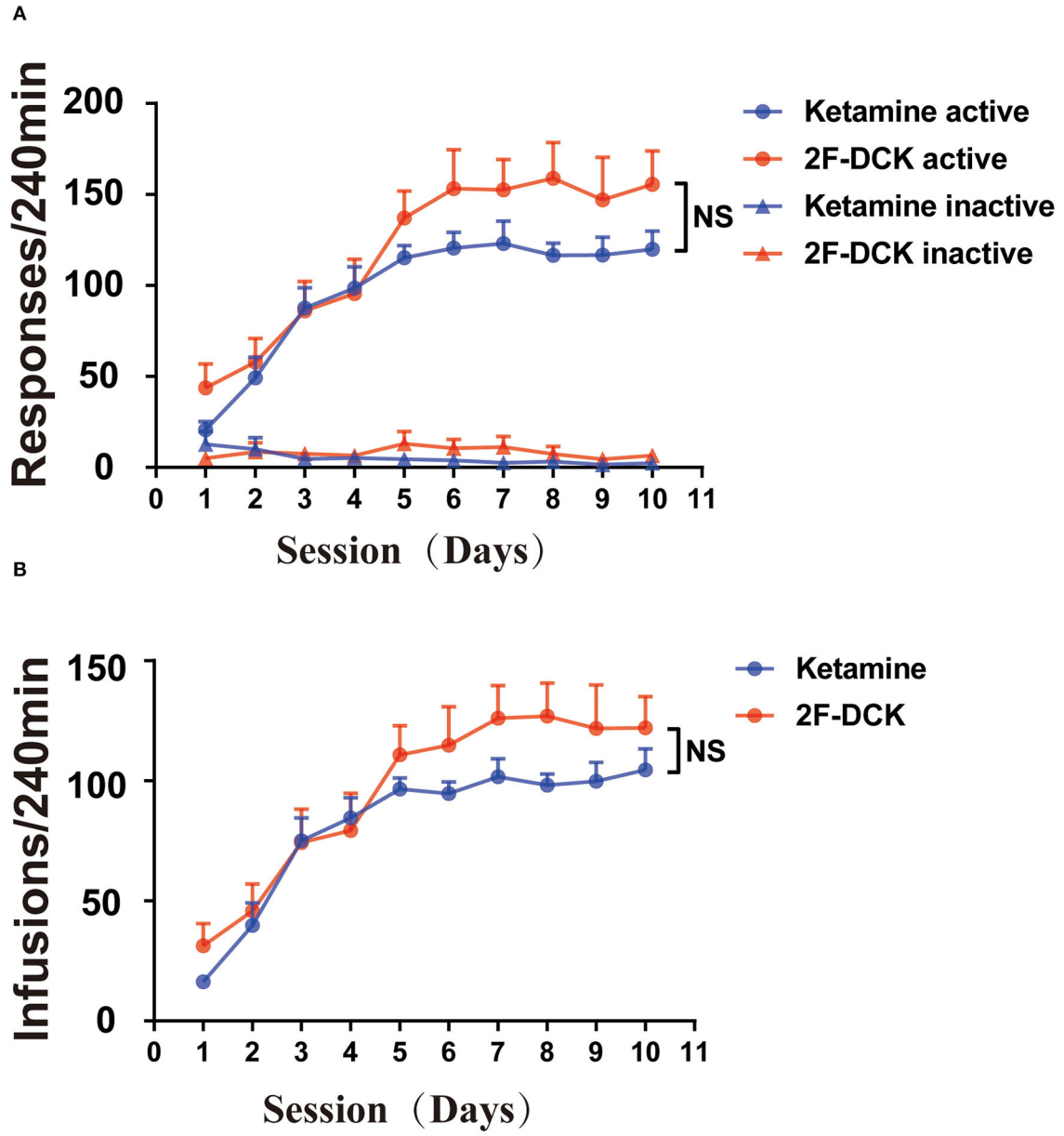

FIGURE 1
2F-DCK and ketamine self-administration. The rats were acquired and maintained at stable 2F-DCK or ketamine self-administration for 10 days. **(A)** The active or inactive response per 4 h of the training session was not different between 2F-DCK and ketamine groups under the FR1 schedule. **(B)** The total infusions per 4 h trained for 10 sessions were also not different between 2F-DCK and ketamine groups. Data are presented as mean ± SEM. NS, not significant.

significantly in four groups (ketamine extinction: $t = 4.513$; ketamine priming: $t = 7.549$; 2F-DCK extinction: $t = 9.366$; 2F-DCK priming: $t = 6.777$), and the relative expression of p-ERK increased significantly in four groups (ketamine extinction: t=2.220, P=0.044; ketamine priming: t=14.546, P<0.01; 2F-DCK extinction: $t = 3.659$, $P < 0.01$; 2F-DCK priming: $t = 15.174$, $P < 0.01$) in comparison with the control group.

As shown in Figure 5, the relative expression levels of Akt, GSK-3β, and mTOR and their phosphorylation in the NAc were analyzed. There was a significant decrease in the t-Akt levels (ketamine extinction: $t = 5.66$, $P < 0.01$; ketamine priming: $t = 11.917$, $P < 0.01$; 2F-DCK extinction: $t = 12.362$, $P < 0.01$; 2F-DCK priming: $t = 2.769$, $P = 0.011$), t- GSK-3β levels (ketamine extinction: $t = 5.645$, $P < 0.01$; ketamine priming: $t = 6.531$, $P < 0.01$; 2F-DCK extinction: $t = 6.702$, $P < 0.01$; 2F-DCK priming: $t = 6.940$, $P < 0.01$), and t-mTOR levels (ketamine extinction: $t = 3.124$, $P = 0.01$; ketamine priming: $t = 8.906$, $P < 0.01$; 2F-DCK extinction: $t = 44.482$, $P < 0.01$; 2F-DCK priming: $t = 6.498$, P

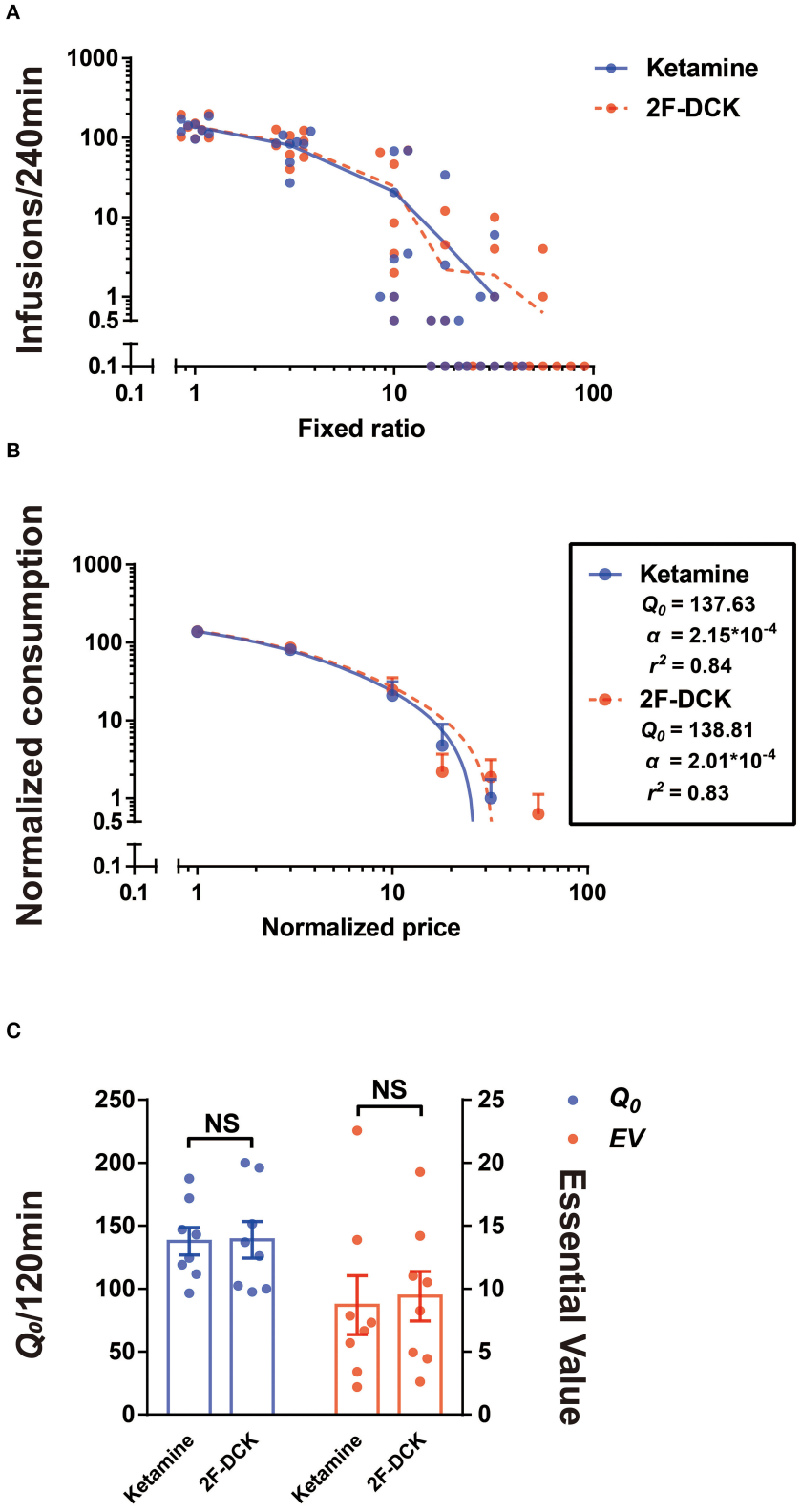

FIGURE 2
Demand curve for 2F-DCK and ketamine. **(A)** Individuals' demand curves for 2F-DCK and ketamine, in which the number of infusions is plotted as a function of the fixed-ratio requirement on a log scale. **(B)** Normalized demand curves for 2F-DCK and ketamine, and the abscissa and ordinate use logarithmic scaling. **(C)** Parameters derived from the demand curve fit for each of the solutions available for self-administration. Estimates of consumption at a minimal cost (Q_0; Equation 1) are plotted in the left ordinate, whereas estimates of essential value (EV; Equation 2) are plotted in the right ordinate. NS, not significant.

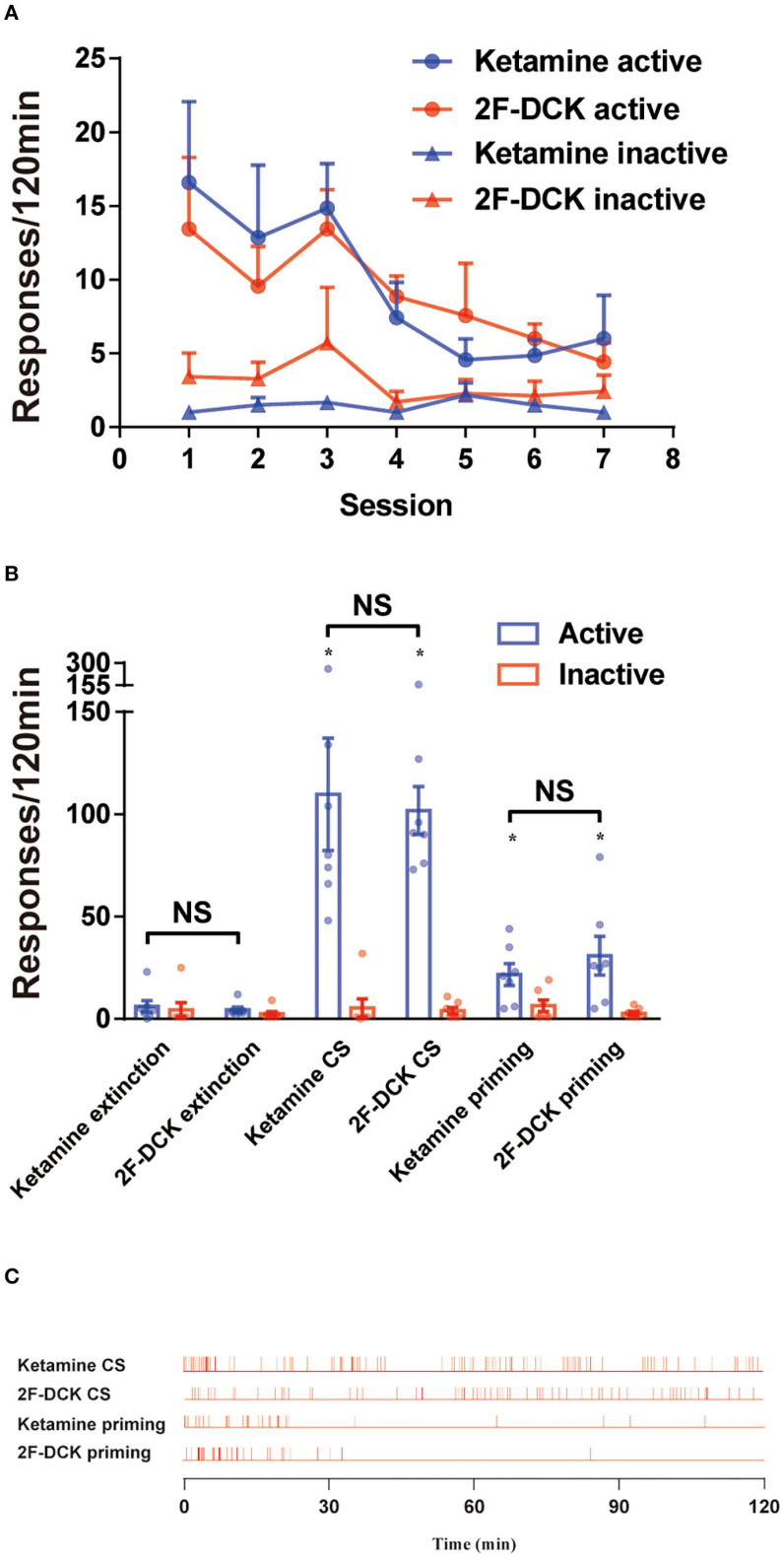

FIGURE 3
The extinction and reinstatement of 2F-DCK and ketamine. **(A)** The active or inactive responses between the 2F-DCK and ketamine groups per 2 h session for 7 days of extinction training were gradually decreased. **(B)** Mean (± SEM) number of responses during the final extinction session, cue-induced, and drug-priming reinstatement tests as a function of the group. There was a relative increase in responses from extinction to reinstatement in both the 2F-DCK and ketamine groups. Each bar represents mean ± SEM ($n = 8$ per group). *$P < 0.05$ in comparison with extinction. **(C)** The representative raster plot for active responses as a function of time during a 2-h reinstatement testing session. Ketamine- or 2F-DCK-associated CS-induced responses were completed across the session, but both ketamine and 2F-DCK priming responses were mostly completed within the first 30 min.

TABLE 1 The relationship of the Q_0 and α parameters with extinction, cue-induced, or drug-priming-reinstatement behaviors.

	2F-DCK ($n = 7$)			Ketamine ($n = 7$)		
	Extinction	CS	Priming	Extinction	CS	Priming
Q_0	0.18 (0.70)	0.61 (0.15)	0.57 (0.18)	−0.58 (0.18)	−0.04 (0.94)	−0.04 (0.94)
α	−0.34 (0.45)	−0.75 (0.05)	−0.75 (0.05)	−0.45 (0.31)	−0.93 (0.003)**	−0.86 (0.014)*

Spearman's rank-order correlations revealed a significant negative correlation between α ranks and reinstatement ranks in the 2F-DCK and ketamine groups (*P < 0.05; **p < 0.01).

< 0.01) in comparison with those in the control; however, there was an increase in the p-Akt levels (ketamine extinction: $t = 3.566$, $P < 0.01$; ketamine priming: $t = 6.854$, $P < 0.01$; 2F-DCK extinction: $t = 9.653$, $P < 0.01$; 2F-DCK priming: $t = 5.394$, $P < 0.01$), p-GSK-3β levels (ketamine extinction: $t = 9.912$, $P < 0.01$; ketamine priming: $t = 7.820$, $P < 0.01$; 2F-DCK extinction: $t = 10.472$, $P < 0.01$; 2F-DCK priming: $t = 17.581$, $P < 0.01$), and p-mTOR expression (ketamine extinction: $t = 6.406$, $P < 0.01$; ketamine priming: $t = 11.544$, $P < 0.01$; 2F-DCK extinction: $t = 1.914$, $P = 0.073$; 2F-DCK priming: $t = 9.939$, $P < 0.01$) in comparison with those in the control. The expression levels of p-Akt, p-GSK-3β, and p-mTOR in the ketamine priming group (p-Akt: $t = 2.352$, $P = 0.028$; p-GSK-3β: $t = 5.667$, $P < 0.01$) or 2F-DCK priming group (p-Akt: $t = 3.597$, $P < 0.01$; p-GSK-3β: $t = 13.092$, $P < 0.01$; p-mTOR: $t = 7.737$, $P < 0.01$) were higher than those of ketamine extinction or 2F-DCK extinction groups, respectively, but no difference in the p-mTOR levels were noted between the ketamine extinction and priming groups ($t = 0.607$, $P = 0.554$).

Discussion

The main findings of the present study are that both the α parameter and the EV of effectiveness between 2F-DCK and ketamine are similar, and the reinstatement of 2F-DCK- and ketamine-seeking behaviors after extinction is also similar. These data, along with the data from previous studies, suggest that 2F-DCK and ketamine have abuse potential and can cause cravings after extinction (Huang et al., 2015; Li et al., 2022]. The value of the α parameter is inversely proportional to the intensity of reinstatement of 2F-DCK- and ketamine-seeking behaviors, which could predict cravings for 2F-DCK and ketamine after withdrawal from self-administration. Interestingly, the expression of BDNF and phosphorylation of ERK, AKT, mTOR, GSK-3β, and CREB decreased in the NAc, while the phosphorylation of ERK, AKT, mTOR, and GSK-3β in the NAc increased after extinction and reinstatement of 2F-DCK and ketamine, suggesting that Akt, ERK, and CREB in the NAc may have different regulatory pathways, and downregulation of CREB/BDNF and upregulation of Akt/mTOR/GSK-3β may be involved in 2F-DCK and ketamine relapse and addiction after withdrawal.

The present study used a behavioral economics approach to compare the reinforcing efficacy of 2F-DCK and ketamine. With respect to drug self-administration, the elasticity of demand in animal self-administration has been suggested to partly correspond to abuse liability in humans (Hursh et al., 2005; Schwartz et al., 2019). The demand curves plot the amount of infusion consumed as a function of the price (response requirement) of 2F-DCK and ketamine. The change in the elasticity of the demand curve as the response increases reflects the reinforcing effectiveness (Hursh and Silberberg, 2008). The α parameter is a free parameter that reflects demand elasticity and is inversely related to the reinforcing effectiveness. It is transformed into an EV, which is directly related to reinforcing effectiveness (Hursh and Romaa, 2016; Zanettini et al., 2018; Maguire et al., 2020). Our previous studies have shown that 2F-DCK produces self-administration, conditions place preference, and generalizes discriminative stimuli effects similar to ketamine (Li et al., 2022). Behavioral economics provides a framework for quantifying 2F-DCK and ketamine abuse potential, while also offering an approach complementary to the self-administration and dose–response curve used previously to characterize the abuse-related effects of 2F-DCK and ketamine (Li et al., 2022). Thus, the α parameter and EV values of 2F-DCK and ketamine were very close, indicating that both have similar reinforcing effectiveness.

Environmental cues associated with rewards can acquire motivational properties (Kuijer et al., 2020). The present results showed that repeated exposure to context could extinguish the ketamine- or 3F-DCK-seeking behavior in their chambers after abstinence, supporting the idea that treatments for ketamine use disorders could be improved by considering drug-associated contexts as a factor in extinction interventions (Kuijer et al., 2020). Several factors, such as the presentation of either drug-associated cues or a single dose of the drug itself, are known to contribute to craving and relapse to drug use in the reinstatement model (Ma et al., 2019). The rats exposed to the CS could induce the elevation of 2F-DCK- or ketamine-seeking responses across a 2-h session after extinction in the present study. When the CS was paired previously with 2F-DCK or ketamine reward, it acquired the incentive properties and its ability to reinstate reward-seeking behavior (Perry et al., 2014). While in the rats exposed to non-contingent 2F-DCK or ketamine injection, the responses were completed mostly

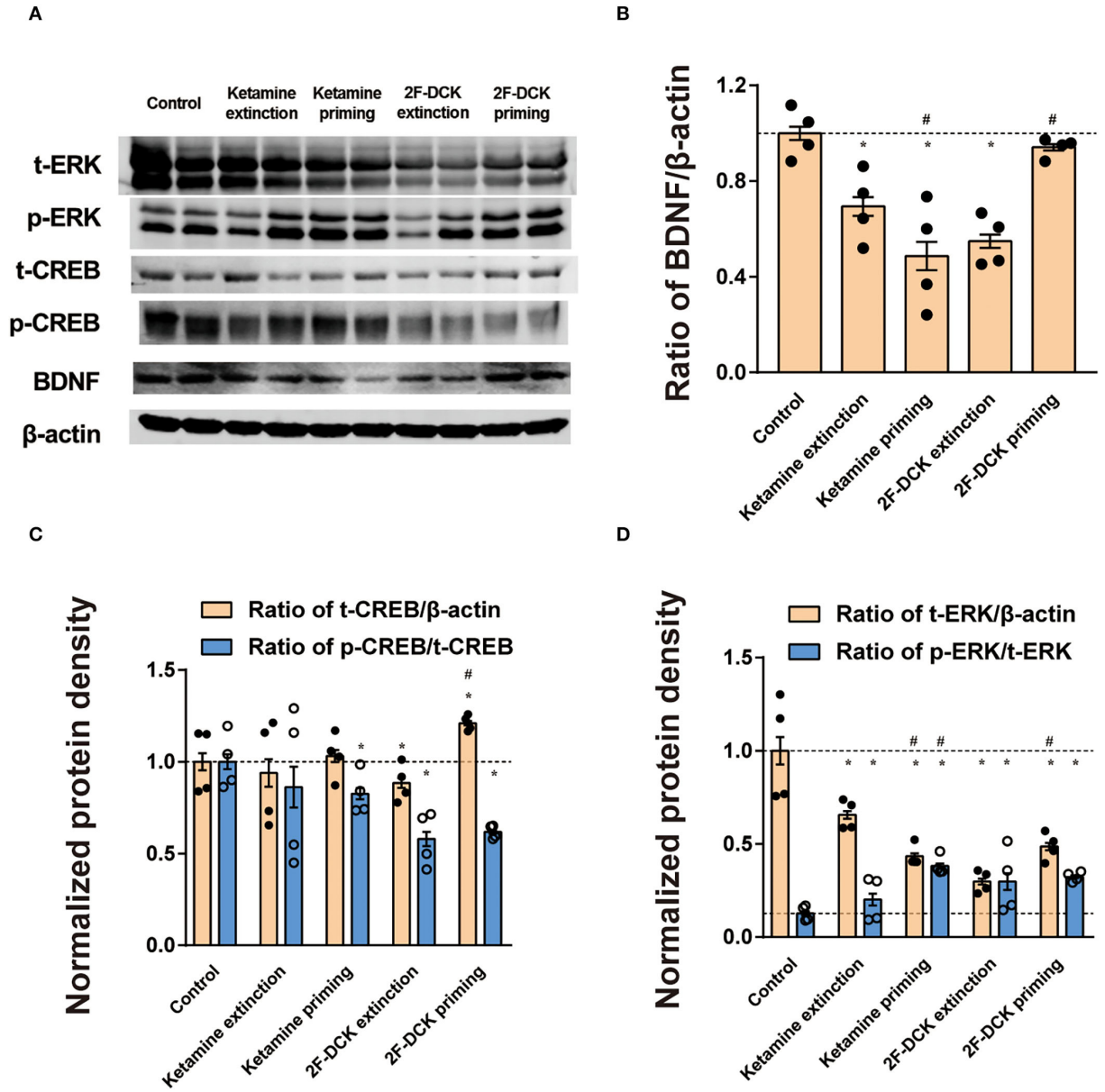

FIGURE 4
Expression of BDNF, CREB, ERK, CREB, and ERK phosphorylation in the NAc during extinction and reinstatement. **(A)** Representative bands of BDNF, CREB, and CREB phosphorylation and β-actin in the NAc, and quantification of Western blot bands, with each bar representing the mean ± SEM (n =4). **(B)** The histogram shows the relative expression of BDNF to β-actin among the groups. **(C)** The histogram shows the relative expression of t-CREB/β-actin and p-CREB/t-CREB. **(D)** The histogram is shown as the relative expression of t-ERK/β-actin and p-ERK/t-ERK. *P < 0.05 in comparison with the control and $^{\#}P$ < 0.05 in comparison with extinction.

within the first 30 min. The intensity and duration of drug-seeking behavior induced by CS are obviously greater than that induced by non-contingent 2F-DCK and ketamine injections, suggesting that both 2F-DCK and ketamine could produce drug cravings or relapse on exposure to drug-associated CS or the drug itself after abstinence. To our knowledge, this is the first study to show a relationship between the economic demand parameter α and the reinstatement of drug seeking. For the self-administered 2F-DCK and ketamine groups, the α parameter was inversely related to the degree of CS-induced or drug-priming reinstatement. These results are consistent with the relationship between the methamphetamine demand curve and relapse (Galuska et al., 2011). Demand elasticity not only provides a metric to rank-order ketamine or 2F-DCK of abuse

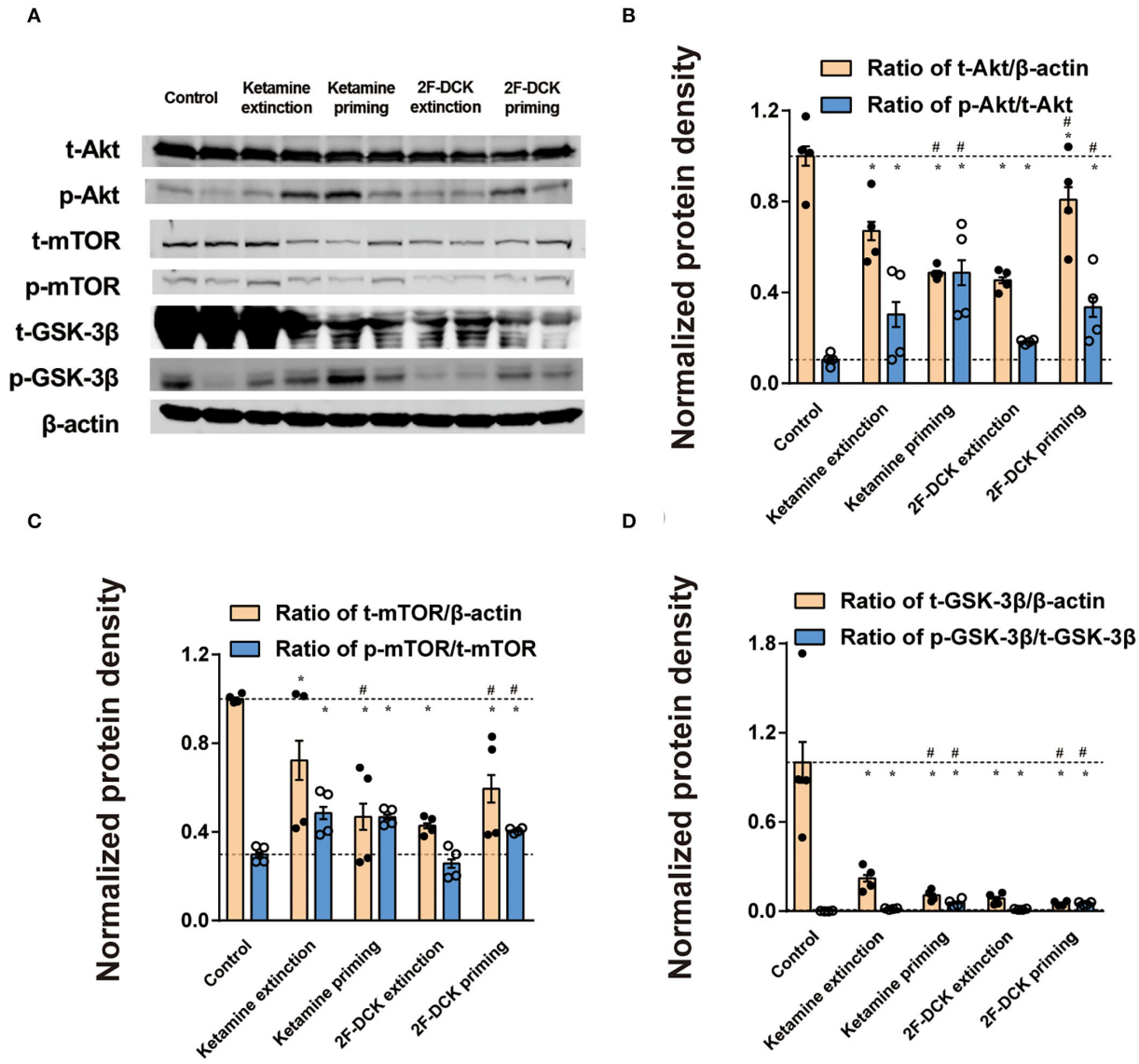

FIGURE 5
Expression of Akt, mTOR, and GSK-3β, and their phosphorylation in the NAc during the extinction and reinstatement. **(A)** Representative bands of Akt, mTOR, GSK-3β, and their phosphorylated forms, and quantification of Western blot bands ($n = 4$), with each bar representing the mean ± SEM. **(B)** The histogram shows the relative expression of t-Akt/β-actin and p-AKT/ t-Akt. **(C)** The histogram shows the relative expression of t-mTOR/β-actin and p-mTOR/ t-mTOR. **(D)** The histogram shows the relative expression of t-GSK-3β/β-actin and p-GSK-3β/t-GSK-3β. $^{*}P < 0.05$ in comparison with control and $^{\#}P < 0.05$ in comparison with extinction.

in terms of abuse liability but may also predict the propensity to ketamine or 2F-DCK relapse.

The CREB is an important transcription factor involved in the regulation of many processes, including synaptic plasticity, memory, and addiction (Nestler, 2004). The CREB family transcription factors are the main regulators of BDNF gene expression after tropomyosin receptor kinase B (TrkB) signaling (Esvald et al., 2020). The present results showed a decrease in the p-CREB/CREB ratio and the BDNF level in the NAc under CS and priming conditions. This result is different from the increased expression of BDNF following a single injection of ketamine (Li et al., 2010; Pham and Gardier, 2019), which may be attributable to long-term exposure and withdrawal from ketamine or 2F-DCK. In a ketamine-induced schizophrenia-like deficit model, ketamine also reduced BDNF levels. These data were further supported by the findings obtained with the PDE1 selective inhibitor vinpocetine, which elevated BDNF expression (Ahmed et al., 2018). Ketamine is proposed to enhance BDNF release and subsequently promote protein synthesis in the mesolimbic brain regions known to regulate natural and drug

rewards (Zanos and Gould, 2018). In the present study, the total protein expression of Akt, GSK-3β, mTOR, and ERK decreased significantly in the NAc and decreased in the NAc parallel to BDNF. BDNF is a CREB-dependent gene that plays a pivotal role in drug addiction (Sun et al., 2015). Neutralizing endogenous BDNF regulation with intra-NAc infusions of antibodies to BDNF subsequently reduced cocaine self-administration and attenuated relapse. Dynamic induction and release of BDNF from neurons in the NAc during cocaine use promote the development and persistence of addictive behavior (Graham et al., 2007). Endogenous BDNF acts on the TrkB receptor to provide an inhibitory tone for reinstated cocaine-seeking, and this effect was recapitulated by exogenous BDNF (Bobadilla et al., 2019). It is reasonable to speculate that downregulation of CREB-BDNF signaling could account for 2F-DCK and ketamine relapse.

Classically, dopamine receptors have been shown to regulate cAMP/PKA and Ca^{2+} pathways through G protein-mediated signaling. A major downstream target of striatal D1R is the ERK pathway. ERK activation by drugs of abuse acts as a key integrator of D1R and glutamate NMDA receptor (NMDAR) signaling (Cahill et al., 2014). NMDARs have been linked with ERK activation in the NAc (Girault et al., 2007). Activation of the NMDAR-D1R/ERK/CREB signal transduction pathway plays a critical role in the control of reward-seeking behavior through reward-predictive cues (Kirschmann et al., 2014). In conjunction with studies showing increased striatal CREB phosphorylation in response to the application of NMDA or activation of D1Rs (Kirschmann et al., 2014), decreased CREB phosphorylation in the NAc may account for the blockage of NMDA receptors by 2F-DCK and ketamine priming. A decrease in phosphorylated CREB and ERK in the NAc is associated with heroin seeking induced by cues after withdrawal (Sun et al., 2015). D1 receptor and ERK/CREB signaling in the ventral hippocampus and medial prefrontal cortex is associated with the formation of opiate-related associative memories (Rosen et al., 2016; Wang et al., 2019). In contrast, an increase in phosphorylated ERK expression in the NAc during 2F-DCK or ketamine relapse was observed. Thus, the molecular mechanism underlying 2F-DCK or ketamine relapse warrants further study.

Dopamine receptor D2 functions through the Akt/GSK-3β signaling cascade (Rosen et al., 2016; Wang et al., 2019). The present results showed upregulation of the Akt/mTOR/GSK-3β pathway, which is consistent with the previous reports (Zhu et al., 2021). Ketamine self-administration decreased the expression of GSK-3β in the NAc (Huang et al., 2015). Silencing of GSK-3β in NAc increases depression- and addiction-related behavior (Crofton et al., 2017). Ketamine at a lower dose induces behavioral sensitization, accompanied by an increase in spine density in the NAc and changes in protein expression in pathways commonly implicated in addiction (Strong et al., 2017). Three weeks of abstinence from ketamine was associated with increased mushroom spines in all the groups (Strong et al., 2019). The upregulation of AKT/mTOR signaling is associated with rapid-acting antidepressant-like effects. This requires AMPA receptor and mTOR activation (Lu et al., 2015) *via* BDNF and protein neo-synthesis (Pham and Gardier, 2019). Depression and addiction may share overlapping neural circuitry and molecular mechanisms; however, there is much that remains to be known about the neurobiological mechanisms underlying ketamine addiction (Kokane et al., 2020; Sial et al., 2020). Evidence has shown that the CREB/BDNF or Akt/GSK-3β signaling pathways may play critical roles in methamphetamine-induced neurotoxicity (Keshavarzi et al., 2019). The Akt/GSK-3β/mTOR signaling pathway is involved in the antidepressant-like effect of atorvastatin in mice (Ludka et al., 2016). According to the obtained data, the reinstatement of ketamine or 2F-DCK could probably be produced by the mediation of the CREB/BDNF or Akt/mTOR/GSK-3β signaling pathways.

In conclusion, the results demonstrated that 2F-DCK has similar reinforcing effectiveness and craving as ketamine after abstinence and suggested that the downregulation of CREB/BDNF and the upregulation of phosphorylation of Akt/mTOR/GSK-3β signaling pathway in the NAc may be involved in ketamine or 2F-DCK relapse.

Data availability statement

The raw data supporting the conclusions of this article will be made available by the authors, without undue reservation.

Ethics statement

The animal study was reviewed and approved by the Ethics Committee of Ningbo University.

Author contributions

HD, ML, DZ, and DF performed research, analysis of the data, and the writing of the paper. YZ, SC, FW, and ZX performed research. HL, YW, and PX were responsible for the maintenance of animal and experimental conditions. WZ was responsible for the study design and revising the paper. All authors contributed to the article and approved the submitted version.

Funding

This work was supported by the National Natural Science Foundation of China (82071499 and 81671321), Ningbo Public Welfare Research Project (202002N3169), the Open Project of

Key Laboratory of Drug Monitoring and Control, Ministry of Public Security (2021-KLDMC-03), and the Zhejiang Medical and Health Leading Academic Discipline Project (00-F06).

Conflict of interest

The authors declare that the research was conducted in the absence of any commercial or financial relationships that could be construed as a potential conflict of interest.

Publisher's note

References

Ahmed, H. I., Abdel-Sattar, S. A., and Zaky, H. S. (2018). Vinpocetine halts ketamine-induced schizophrenia-like deficits in rats: impact on BDNF and GSK-3beta/beta-catenin pathway. *Naunyn Schmiedebergs. Arch. Pharmacol.* 391, 1327–1338. doi: 10.1007/s00210-018-1552-y

Berman, R. M., Cappiello, A., Anand, A., Oren, D. A., Heninger, G. R., Charney, D. S., et al. (2000). Antidepressant effects of ketamine in depressed patients. *Biol. Psychiatry* 47, 351–354. doi: 10.1016/S0006-3223(99)00230-9

Bobadilla, A. C., Garcia-Keller, C., Chareunsouk, V., Hyde, J., Camacho, D. M., Heinsbroek, J. A., et al. (2019). Accumbens brain-derived neurotrophic factor (BDNF) transmission inhibits cocaine seeking. *Addict. Biol.* 24, 860–873. doi: 10.1111/adb.12638

Cahill, E., Salery, M., Vanhoutte, P., and Caboche, J. (2014). Convergence of dopamine and glutamate signaling onto striatal ERK activation in response to drugs of abuse. *Front. Pharmacol.* 4, 172. doi: 10.3389/fphar.2013.00172

Chiamulera, C., Armani, F., Mutti, A., and Fattore, L. (2016). The ketamine analogue methoxetamine generalizes to ketamine discriminative stimulus in rats. *Behav. Pharmacol.* 27, 204–210. doi: 10.1097/FBP.0000000000000221

Crofton, E. J., Nenov, M. N., Zhang, Y., Scala, F., Page, S. A., McCue, D. L., et al. (2017). Glycogen synthase kinase 3 beta alters anxiety-, depression-, and addiction-related behaviors and neuronal activity in the nucleus accumbens shell. *Neuropharmacology* 117, 49–60. doi: 10.1016/j.neuropharm.2017.01.020

Davidsen, A., Mardal, M., Holm, N., Andreasen, A., Johansen, S., Noble, C., et al. (2020). Ketamine analogues: comparative toxicokinetic *in vitro-in vivo* extrapolation and quantification of 2-fluorodeschloroketamine in forensic blood and hair samples. *J. Pharm. Biomed. Anal.* 180, 113049. doi: 10.1016/j.jpba.2019.113049

Domanski, K., Fleming, S. W., Maag, H., Raley, E. B., DeBord, J., Wright, B., et al. (2021). A psychonaut's experience of intoxication with multiple classes of drugs including novel psychoactive substance 2-fluorodeschloroketamine: case report and urinary analysis. *J. Psychoact. Drugs*. doi: 10.1080/02791072.2021.2006373. [Epub ahead of print].

Epstein, D. H., and Preston, K. L. (2003). The reinstatement model and relapse prevention: a clinical perspective. *Psychopharmacology* 168, 31–41. doi: 10.1007/s00213-003-1470-6

Esvald, E. E., Tuvikene, J., Sirp, A., Patil, S., Bramham, C. R., and Timmusk, T. (2020). CREB family transcription factors are major mediators of BDNF transcriptional autoregulation in cortical neurons. *J. Neurosci.* 40, 1405–1426. doi: 10.1523/JNEUROSCI.0367-19.2019

Galuska, C. M., Banna, K. M., Willse, L. V., Yahyavi-Firouz-Abadi, N., and See, R. E. (2011). A comparison of economic demand and conditioned-cued reinstatement of methamphetamine-seeking or food-seeking in rats. *Behav. Pharmacol.* 22, 312–323. doi: 10.1097/FBP.0b013e3283473be4

Girault, J. A., Valjent, E., Caboche, J., and Herve, D. (2007). ERK2: a logical AND gate critical for drug-induced plasticity? *Curr. Opin. Pharmacol.* 7, 77–85. doi: 10.1016/j.coph.2006.08.012

Graham, D. L., Edwards, S., Bachtell, R. K., DiLeone, R. J., Rios, M., Self, D. W., et al. (2007). Dynamic BDNF activity in nucleus accumbens with cocaine use increases self-administration and relapse. *Nat. Neurosci.* 10, 1029–1037. doi: 10.1038/nn1929

Huang, X., Huang, K., Zheng, W., Beveridge, T. J., Yang, S., Li, X., et al. (2015). The effects of GSK-3beta blockade on ketamine self-administration and relapse to drug-seeking behavior in rats. *Drug Alcohol Depend.* 147, 257–265. doi: 10.1016/j.drugalcdep.2014.10.028

Hursh, S. R., Galuska, C. M., Winger, G., and Woods, J. H. (2005). The economics of drug abuse: a quantitative assessment of drug demand. *Mol. Interv.* 5, 20–28. doi: 10.1124/mi.5.1.6

Hursh, S. R., and Romaa, P. G. (2016). behavioral economics and the analysis of consumption and choice. *Managerial Decis. Econ.* 37, 224–238. doi: 10.1002/mde.2724

Hursh, S. R., and Silberberg, A. (2008). Economic demand and essential value. *Psychol. Rev.* 115, 186–198. doi: 10.1037/0033-295X.115.1.186

Huskinson, S. L., Naylor, J. E., Rowlett, J. K., and Freeman, K. B. (2014). Predicting abuse potential of stimulants and other dopaminergic drugs: overview and recommendations. *Neuropharmacology* 87, 66–80. doi: 10.1016/j.neuropharm.2014.03.009

I.f.L.A. Research. (2011). *Guide for the Care and Use of Laboratory animals*. Washington, DC: National Academies Press.

Keshavarzi, S., Kermanshahi, S., Karami, L., Motaghinejad, M., Motevalian, M., Sadr, S., et al. (2019). Protective role of metformin against methamphetamine induced anxiety, depression, cognition impairment and neurodegeneration in rat: the role of CREB/BDNF and Akt/GSK3 signaling pathways. *Neurotoxicology* 72, 74–84. doi: 10.1016/j.neuro.2019.02.004

Kirschmann, E. K. Z., Mauna, J. C., Willis, C. M., Foster, R. L., Chipman, A. M., Thiels, E., et al. (2014). Appetitive cue-evoked ERK signaling in the nucleus accumbens requires NMDA and D1 dopamine receptor activation and regulates CREB phosphorylation. *Learn. Mem.* 21, 606–615. doi: 10.1101/lm.035113.114

Koffarnus, M. N., Hall, A., and Winger, G. (2012). Individual differences in rhesus monkeys' demand for drugs of abuse. *Addict. Biol.* 17, 887–896. doi: 10.1111/j.1369-1600.2011.00335.x

Kokane, S. S., Armant, R. J., Bolanos-Guzman, C. A., and Perrotti, L. I. (2020). Overlap in the neural circuitry and molecular mechanisms underlying ketamine abuse and its use as an antidepressant. *Behav. Brain Res.* 384, 112548. doi: 10.1016/j.bbr.2020.112548

Krystal, J. H., Karper, L. P., Seibyl, J. P., Freeman, G. K., Delaney, R., Bremner, J. D., et al. (1994). Subanesthetic effects of the noncompetitive NMDA antagonist, ketamine, in humans. Psychotomimetic, perceptual, cognitive, neuroendocrine responses. *Arch. Gen. Psychiatry* 51, 199–214. doi: 10.1001/archpsyc.1994.03950030035004

Kuijer, E. J., Ferragud, A., and Milton, A. (2020). Retrieval-extinction and relapse prevention: rewriting maladaptive drug memories? *Front. Behav. Neurosci.* 14, 23. doi: 10.3389/fnbeh.2020.00023

Lai, M. J., Fu, D., Xu, Z. M., Du, H., Liu, H. F., Wang, Y. M., et al. (2022). Relative reinforcing effects of dibutylone, ethylone, and N-ethylpentylone: self-administration and behavioral economics analysis in rats. *Psychopharmacology*. 239, 2875–2884. doi: 10.1007/s00213-022-06173-x

Li, F., Du, H., Wu, B., Wei, J., Qiao, Y., Lai, M. J., et al. (2022). 2-Fluorodeschloroketamine has similar abuse potential as ketamine. *Addict. Biol.* 27, e13171. doi: 10.1111/adb.13171

Li, N. X., Lee, B., Liu, R. J., Banasr, M., Dwyer, J. M., Iwata, M., et al. (2010). mTOR-dependent synapse formation underlies the rapid antidepressant effects of NMDA antagonists. *Science* 329, 959–964. doi: 10.1126/science.1190287

Liu, Y., Lin, D. Y., Wu, B. L., and Zhou, W. H. (2016). Ketamine abuse potential and use disorder. *Brain Res. Bull.* 126, 68–73. doi: 10.1016/j.brainresbull.2016.05.016

Lu, Y., Wang, C., Xue, Z. C., Li, C. L., Zhang, J. F., Zhao, X., et al. (2015). PI3K/AKT/mTOR signaling-mediated neuropeptide vgf in the hippocampus of mice is involved in the rapid onset antidepressant-like effects of GLYX-13. *Int. J. Neuropsychopharmacol.* 18, pyu110. doi: 10.1093/ijnp/pyu110

Ludka, F. K., Constantino, L. C., Dal-Cim, T., Binder, L. B., Zomkowski, A., Rodrigues, A. L., et al. (2016). Involvement of PI3K/Akt/GSK-3beta and mTOR in the antidepressant-like effect of atorvastatin in mice. *J. Psychiatr. Res.* 82, 50–57. doi: 10.1016/j.jpsychires.2016.07.004

Ma, B. M., Mei, D. S., Wang, F. M., Liu, Y., and Zhou, W. H. (2019). Cognitive enhancers as a treatment for heroin relapse and addiction. *Pharmacol. Res.* 141, 378–383. doi: 10.1016/j.phrs.2019.01.025

Maguire, D. R., Minervini, V., Dodda, V., and France, C. P. (2020). Impact of order of fixed-ratio presentation on demand for self-administered remifentanil in male rats. *Behav. Pharmacol.* 31, 216–220. doi: 10.1097/FBP.0000000000000502

Nestler, E. J. (2004). Molecular mechanisms of drug addiction. *Neuropharmacology* 47(Suppl. 1), 24–32. doi: 10.1016/j.neuropharm.2004.06.031

Perry, C. J., Zbukvic, I., Kim, J. H., and Lawrence, A. J. (2014). Role of cues and contexts on drug-seeking behaviour. *Br. J. Pharmacol.* 171, 4636–4672. doi: 10.1111/bph.12735

Pham, T. H., and Gardier, A. M. (2019). Fast-acting antidepressant activity of ketamine: highlights on brain serotonin, glutamate, and GABA neurotransmission in preclinical studies. *Pharmacol. Ther.* 199, 58–90. doi: 10.1016/j.pharmthera.2019.02.017

Rosen, L. G., Zunder, J., Renard, J., Fu, J., Rushlow, W., Laviolette, S. R., et al. (2016). Opiate exposure state controls a D2-CaMKII alpha-dependent memory switch in the amygdala-prefrontal cortical circuit. *Neuropsychopharmacology* 41, 847–857. doi: 10.1038/npp.2015.211

Sabino, V., Narayan, A. R., Zeric, T., Steardo, L., and Cottone, P. (2013). mTOR activation is required for the anti-alcohol effect of ketamine, but not memantine, in alcohol-preferring rats. *Behav. Brain Res.* 247, 9–16. doi: 10.1016/j.bbr.2013.02.030

Schwartz, L. P., Roma, P. G., Henningfield, J. E., Hursh, S. R., Cone, E. J., Buchhalter, A. R., et al. (2019). Behavioral economic demand metrics for abuse deterrent and abuse potential quantification. *Drug Alcohol Depend.* 198, 13–20. doi: 10.1016/j.drugalcdep.2019.01.022

Shaham, Y., Shalev, U., Lu, L., de Wit, H., and Stewart, J. (2003). The reinstatement model of drug relapse: history, methodology and major findings. *Psychopharmacology* 168, 3–20. doi: 10.1007/s00213-002-1224-x

Shao, X. T., Yu, H., Lin, J. G., Kong, X. P., Wang, Z., Wang, D. G., et al. (2021). Presence of the ketamine analog of 2-fluorodeschloroketamine residues in wastewater. *Drug Test. Anal.* 13, 1650–1657. doi: 10.1002/dta.3098

Sial, O. K., Parise, E. M., Parise, L. F., Gnecco, T., and Bolanos-Guzman, C. A. (2020). Ketamine: the final frontier or another depressing end? *Behav. Brain Res.* 383, 112508. doi: 10.1016/j.bbr.2020.112508

Strong, C. E., Schoepfer, K. J., Dossat, A. M., Saland, S. K., Wright, K. N., Kabbaj, M., et al. (2017). Locomotor sensitization to intermittent ketamine administration is associated with nucleus accumbens plasticity in male and female rats. *Neuropharmacology* 121, 195–203. doi: 10.1016/j.neuropharm.2017.05.003

Strong, C. E., Wright, K. N., and Kabbaj, M. (2019). Sex and individual differences in alcohol intake are associated with differences in ketamine self-administration behaviors and nucleus accumbens dendritic spine density. *eNeuro* 6, 31740575. doi: 10.1523/ENEURO.0221-19.2019

Sun, A., Zhuang, D. D., Zhu, H. Q., Lai, M. J., Chen, W. S., Liu, H. F., et al. (2015). Decrease of phosphorylated CREB and ERK in nucleus accumbens is associated with the incubation of heroin seeking induced by cues after withdrawal. *Neurosci. Lett.* 591, 166–170. doi: 10.1016/j.neulet.2015.02.048

Tang, M., Li, T., Lai, C., Chong, Y., Ching, C., Mak, T., et al. (2020). Emergence of new psychoactive substance 2-fluorodeschloroketamine: Toxicology and urinary analysis in a cluster of patients exposed to ketamine and multiple analogues. *Forensic Sci. Int.* 312, 110327. doi: 10.1016/j.forsciint.2020.110327

Wang, Y. P., Zhang, H. Y., Cui, J. J., Zhang, J., Yin, F. Y., Guo, H., et al. (2019). Opiate-associated contextual memory formation and retrieval are differentially modulated by dopamine D1 and D2 signaling in hippocampal-prefrontal connectivity. *Neuropsychopharmacology* 44, 334–343. doi: 10.1038/s41386-018-0068-y

Wright, K. N., Strong, C. E., Addonizio, M. N., Brownstein, N. C., and Kabbaj, M. (2017). Reinforcing properties of an intermittent, low dose of ketamine in rats: effects of sex and cycle. *Psychopharmacology* 234, 393–401. doi: 10.1007/s00213-016-4470-z

Zanettini, C., Wilkinson, D. S., and Katz, J. L. (2018). Behavioral economic analysis of the effects of N-substituted benztropine analogs on cocaine self-administration in rats. *Psychopharmacology* 235, 47–58. doi: 10.1007/s00213-017-4739-x

Zanos, P., and Gould, T. D. (2018). Mechanisms of ketamine action as an antidepressant. *Mol. Psychiatry* 23, 801–811. doi: 10.1038/mp.2017.255

Zarate, C. A., Singh, J. B., Carlson, P. J., Brutsche, N. E., Ameli, R., Luckenbaugh, D. A., et al. (2006). A randomized trial of an N-methyl-D-aspartate antagonist in treatment-resistant major depression. *Arch. Gen. Psychiatry* 63, 856–864. doi: 10.1001/archpsyc.63.8.856

Zhu, H. Q., Zhuang, D. D., Lou, Z. Z., Lai, M. J., Fu, D., Hong, Q. X., et al. (2021). Akt and its phosphorylation in nucleus accumbens mediate heroin-seeking behavior induced by cues in rats. *Addict. Biol.* 26, e12959. doi: 10.1111/adb.13013

frontiers | Frontiers in Molecular Neuroscience

TYPE Original Research
PUBLISHED 13 September 2022
DOI 10.3389/fnmol.2022.1002139

OPEN ACCESS

EDITED BY
Qi Wang,
Southern Medical University, China

REVIEWED BY
Bing Xie,
Hebei Medical University, China
Kai Yuan,
Peking University Sixth Hospital, China

*CORRESPONDENCE
Yixiao Luo
luoyx@hunnu.edu.cn

SPECIALTY SECTION
This article was submitted to Molecular Signalling and Pathways, a section of the journal Frontiers in Molecular Neuroscience

RECEIVED 24 July 2022
ACCEPTED 18 August 2022
PUBLISHED 13 September 2022

CITATION
Qian S, Shi C, Huang S, Yang C and Luo Y (2022) DNA methyltransferase activity in the basolateral amygdala is critical for reconsolidation of a heroin reward memory.
Front. Mol. Neurosci. 15:1002139.
doi: 10.3389/fnmol.2022.1002139

DNA methyltransferase activity in the basolateral amygdala is critical for reconsolidation of a heroin reward memory

Shuyi Qian[1], Cuijie Shi[2], Shihao Huang[3], Chang Yang[2] and Yixiao Luo[2]*

[1]Department of Nephrology and Laboratory of Kidney Disease, Hunan Provincial People's Hospital, Hunan Normal University, Changsha, China, [2]Hunan Province People's Hospital, The First-Affiliated Hospital of Hunan Normal University, Changsha, China, [3]National Institute on Drug Dependence, Beijing Key Laboratory of Drug Dependence, Peking University, Beijing, China

The persistence of drug memory contributes to relapse to drug seeking. The association between repeated drug exposure and drug-related cues leads to cravings triggered by drug-paired cues. The erasure of drug memories has been considered a promising way to inhibit cravings and prevent relapse. The re-exposure to drug-related cues destabilizes well-consolidated drug memories, during which a *de novo* protein synthesis-dependent process termed "reconsolidation" occurs to restabilize the reactivated drug memory. Disrupting reconsolidation of drug memories leads to the attenuation of drug-seeking behavior in both animal models and people with addictions. Additionally, epigenetic mechanisms regulated by DNA methyltransferase (DNMT) are involved in the reconsolidation of fear and cocaine reward memory. In the present study, we investigated the role of DNMT in the reconsolidation of heroin reward memory. In the heroin self-administration model in rats, we tested the effects of DNMT inhibition during the reconsolidation process on cue-induced reinstatement, heroin-priming-induced reinstatement, and spontaneous recovery of heroin-seeking behavior. We found that the bilateral infusion of 5-azacytidine (5-AZA) inhibiting DNMT into the basolateral amygdala (BLA) immediately after heroin reward memory retrieval, but not delayed 6 h after retrieval or without retrieval, decreased subsequent cue-induced and heroin-priming-induced reinstatement of heroin-seeking behavior. These findings demonstrate that inhibiting the activity of DNMT in BLA during the reconsolidation of heroin reward memory attenuates heroin-seeking behavior, which may provide a potential strategy for the therapeutic of heroin addiction.

KEYWORDS

addiction, heroin, amygdala, reconsolidation, DNMT, self-administration

Introduction

A major challenge in treating heroin addiction is relapse and is closely related to the persistence of drug reward memories (Kalivas and Volkow, 2005; Robbins et al., 2008; Torregrossa et al., 2011; Wang et al., 2012; Preller et al., 2013; Chen et al., 2021a; Ewing et al., 2021; Douton et al., 2022; Xie et al., 2022). Drug memories are maladaptive memories that usurp normal memory, leading to craving and relapse (Hyman, 2005; Hyman et al., 2006; Böning, 2009; Alvandi et al., 2017; Stern et al., 2018; Liu et al., 2019; Chen et al., 2021b). Previous studies have reported that memory traces become labile after reactivation and are re-stabilized through a process termed "reconsolidation" (Nader, 2003; Nader and Einarsson, 2010; Alberini and Ledoux, 2013; Tronson and Taylor, 2013). Both human and animal studies demonstrate that drug-seeking behavior is impaired by the pharmacological or non-pharmacological interference in the reconsolidation of drug reward memories (Lee et al., 2005; Xue et al., 2012; Lin et al., 2014; Chen et al., 2021a; Zhang et al., 2021; Xie et al., 2022). Therefore, clarifying the underlying mechanism in the reconsolidation of drug memories will help determine the pharmacological target for the prevention of relapse.

The basolateral amygdala (BLA), a subregion of the amygdala, is closely implicated in learning, memory, and emotional behavior (Davis, 1992; Maren, 2003; See et al., 2003). Substantial evidence indicates that the BLA is a critical brain region involved in the reconsolidation of drug-related associative memories (Hellemans et al., 2006; Wells et al., 2013; Jian et al., 2014; Higginbotham et al., 2021; Ritchie et al., 2021). Two important aspects of memory reconsolidation have been pointed out. One is that *de novo* protein synthesis is required during the reconsolidation process and the other is that reconsolidation occurred within a 6 h time window (Nader et al., 2000). Therefore, previous studies have demonstrated that disrupting protein synthesis for reconsolidation in the BLA reduces relapse of both fear and addiction memory (Fuchs et al., 2009; Wells et al., 2011; Si et al., 2012; Arguello et al., 2014; Ratano et al., 2014). Moreover, the abovementioned effects would not be observed if the intervention occurs out the time window of the reconsolidation or without the reconsolidation process (Chen et al., 2021a; Zhang et al., 2021). In short, these studies indicated that the BLA plays a critical role in the reconsolidation of heroin reward memory.

DNA methyltransferase (DNMT), widely expressed in the nervous system of mammalians, is an enzyme catalyzing DNA methylation that is critical for the formation of amygdala-dependent memory and the maintenance of long-term memory (Feng et al., 2005; Miller and Sweatt, 2007; Day and Sweatt, 2010; Sultan and Day, 2011). In the previous study, infusing the nucleoside analog 5-azacytidine (5-AZA) and DNMT inhibitor RG108 into the lateral amygdala (LA) significantly impaired the reconsolidation of fear memory (Maddox and Schafe, 2011). Our previous study found that a bilateral intra-BLA infusion of the 5-AZA after reactivation decreased subsequent cocaine-seeking behavior, indicating that the activity of DNMT in the BLA is crucial for the reconsolidation of cocaine-associated memory (Shi et al., 2015). However, whether DNMT plays a role in the reconsolidation of heroin reward memory is still unknown (Lüscher and Ungless, 2006).

In this study, we investigated the effect of intra-BLA DNMT inhibition during reconsolidation on the subsequent heroin-seeking behavior of heroin reward memory. We found that a bilateral infusion of the 5-azacytidine (5-AZA) into the basolateral amygdala (BLA) to inhibit the activity of DNMT immediately after heroin reward memory retrieval, but no longer than 6 h after retrieval or with a 5-AZA infusion without retrieval, decreased subsequent cue-induced and heroin-priming-induced reinstatement of heroin-seeking behavior.

Materials and methods

Subjects

The male Sprague Dawley rats weighed 280–300 g on arrival and were placed in a climate-controlled environment with a constant 22 ± 2°C temperature and 60% humidity. Food and water were freely accessible to the rats and they were under a 12-h light/dark cycle. Leading up to the surgeries, the operator handled the rats for 3 min/d for 5 day so that they would be more accustomed to the operator. The current study and all animal procedures were performed following the Guide of Hunan Province for the Care and Use of Laboratory Animals. The experiments were approved by the Local Committee on Animal Care and Use and Protection of the Hunan Normal University. The Dark phase was the time all the experiments were performed.

Surgery

A sodium pentobarbital anesthesia (60 mg/kg, intraperitoneally) was administered to the rats (300–320 before surgery) using catheters inserted into the right jugular vein and terminating at the opening of the right atrium (Lu et al., 2005). The guide cannulae (23 gauge; Plastics One, Roanoke, VA, United States) was implanted bilaterally 1 mm above the BLA. The coordinates of the BLA are as follows (Wu et al., 2011): anterior/posterior: −2.8 mm, medial/lateral: ±5.0 mm from bregma, and dorsal/ventral: −8.5 mm from the surface of the skull. Every 2 days 0.1 ml heparinized saline (30 USP heparin/saline; Hospira) was infused through a patent catheter. As soon as the rats returned from surgery, they were

housed individually and had free access to food and water. They recovered for 5–7 days before the start of the experiment.

Behavioral procedures

Heroin SA training

As reported by Xue et al. (2012) the heroin SA training method and conditions were established with slight modifications. In the chambers (AniLab Software & Instruments, Ningbo, China), there were two nose poke operandi positioned 9 cm above the floor. The active nosepoke lead to an intravenous heroin infusion following a compound 5-s tone-light cue (conditioned stimulates, CS), while the inactive nosepoke had no consequence.

A 10-day training program was conducted to train the rats to self-administer heroin (0.05 mg/kg/infusion) in three 1-h training processes, separated by 5 min breaks. During training, the fixed-ratio 1 reinforcement schedule was implemented at the beginning of each dark cycle. There was a 40-s timeout period following every infusion. The house light was on when each session began. During the training sessions, the rats were deprived of food. To protect the rats from an overdose, the number of heroin infusions was limited to 20 per hour (Xue et al., 2012; Luo et al., 2015). The heroin SA paradigm was performed in all four experiments.

Nose poke extinction

After the SA training, rats received a 9-day nosepoke extinction training for 3 h per day with no illumination or any stimulus in the original training chamber (experiments 1–4). A nosepoke in either operandum would result in no consequences (i.e., no heroin infusion and no tone/light cue).

Reactivation of heroin reward memory

After 24 h, following the last nosepoke extinction (experiments 1, 2, 4), the rats were subjected to conditioned stimulus in the original training chamber for 15 min to reactivate heroin reward memory. The retrieval conditions were similar to the heroin SA training, but a nosepoke in the active operandum caused no heroin infusions.

5-AZA treatment

In experiments 1 and 2, immediately after the reactivation session, the rats received bilateral infusions of the 5-AZA (1 μg/side at 0.25 μl/min for 2 min; Sigma-Aldrich) intra-BLA to inhibit the activity of DNMT. The syringe pump used the 10 μl Hamilton syringes. The syringes were linked to the infusion cannula (28 gauge; Plastics One) by the polyethylene tubing, while the controls had an equal volume infusion of vehicle (0.5% DMSO). The syringes were kept at the injection site for at least 2 min after completing the injection and then slowly withdrawn. In experiment 3, the rats received an infusion of the 5-AZA or vehicle with no light/tone stimuli reactivation. Finally, in experiment 4, the rats received infused 5-AZA or the vehicle 6 h after retrieval. The rats were placed in their home cage after infusion manipulation.

Cue extinction

Daily cue extinction was performed on the rats in experiments 1, 3, and 4 for 3 h. The conditions were the same as the heroin SA session but without heroin infusions following the tone/light cue.

Cue-induced reinstatement test (experiments 1–4)

This test was carried out on the rats 24 h after the 5-AZA or the vehicle intra-BLA infusion. The testing conditions were the same as the heroin SA session except that the active nosepoke did not have any tone-light cues, nor was it reinforced with heroin. The number of nosepokes was recorded for 1 h and the houselight was on for the whole session.

Heroin-induced reinstatement test (experiments 1, 3, 4)

Heroin (0.25 mg/kg, s.c.) was systematically injected into the rats for 5 min before the reinstatement test. The conditions of the test were the same as the SA training except that a nosepoke in the active operandum led to the delivery of a cue (tone/light) but not the heroin. A reinstatement test was performed for 1 h and the number of active nosepokes was recorded.

Spontaneous recovery test (experiment 2)

After withdrawal (28 days), the number of active nosepokes was recorded for 1 h in the spontaneous recovery test with the same conditions as in the reactivation.

Specific experiments

Experiment 1

The role of immediate post-reactivation 5-AZA treatment intra-BLA on subsequent cue-induced and heroin-priming-induced reinstatement of heroin-seeking behavior.

The rats were subjected to the heroin SA training for 10 days in 1 h sessions, 3 times per day. They were then trained for 9 days of daily nosepoke extinction in the original chamber. After 24 h following the last nosepoke extinction, the rats were reactivated for 15 min with heroin reward cues in the training context. After reactivation, the rats were divided into two groups: (1) infusing 5-AZA intra-BLA bilaterally 1 μg in 0.5 μl/side (5-AZA group); (2) infusing vehicle intra-BLA bilaterally 0.5 μl/side (vehicle group). The rats received a bilateral infusion of either 5-AZA or vehicle intra-BLA immediately after the reactivation. After 24 h, we tested the heroin-seeking behavior of cue-induced reinstatement in rats. A priming-induced reinstatement test

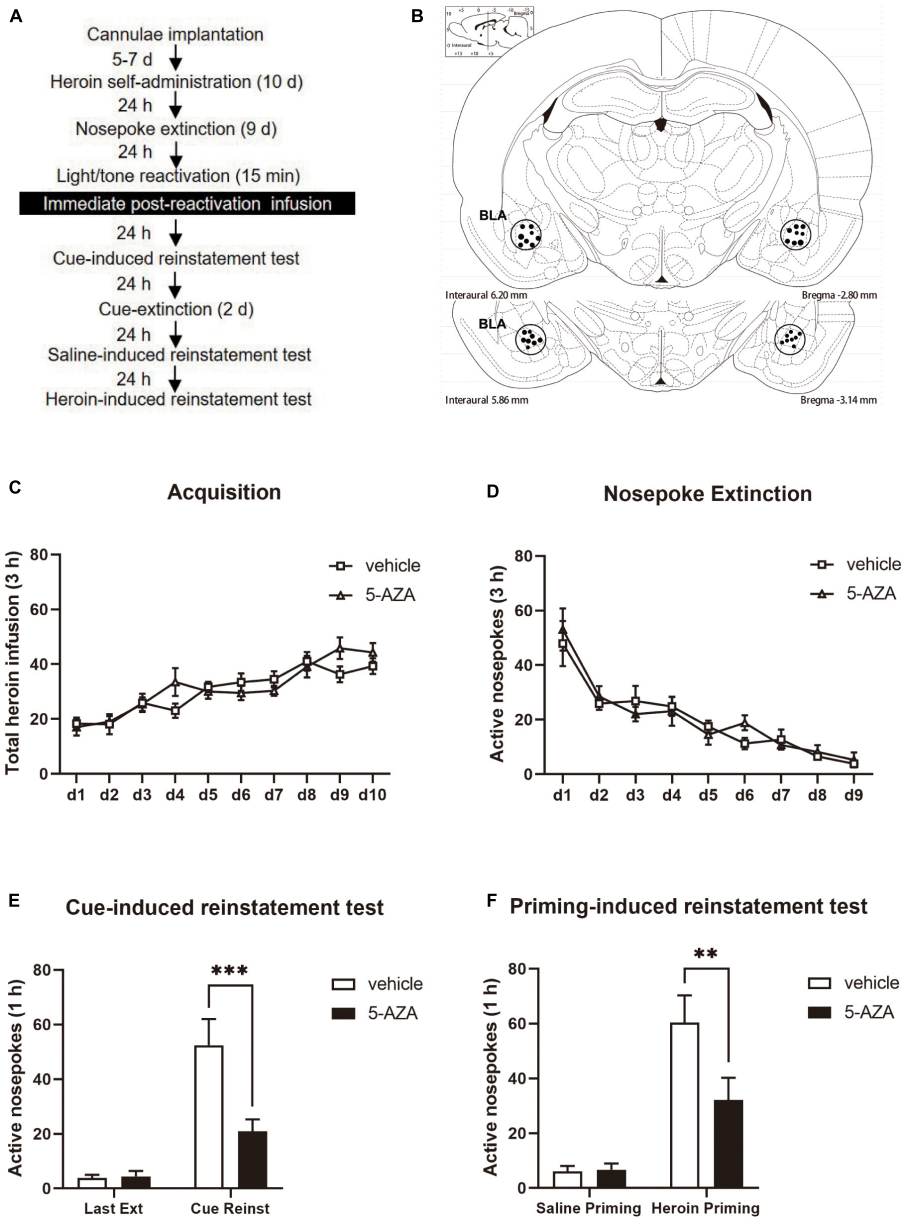

FIGURE 1
Immediate post-reactivation 5-AZA treatment intra-BLA reduces subsequent cue-induced and heroin-priming reinstatement of heroin-seeking behavior. **(A)** Schematic representation of the experimental procedure. **(B)** The regions of the representative cannula placements in the basolateral amygdala (BLA: −2.8 mm from bregma) as shown in the rostral faces of each coronal section. **(C)** Total number of heroin infusions across acquisition of heroin self-administration sessions. **(D)** Total number of active nosepoke responses across nosepoke response extinction sessions. **(E)** Active nosepoke responses during the last extinction session and the cue-induced reinstatement test. **(F)** Active nosepoke responses during the saline- or heroin- priming reinstatement test. $n = 10$ rats per group. Data are means ± SEM, $^{**}p < 0.01$, $^{***}p < 0.001$, compared with the vehicle group. Ext, extinction; Reinst, reinstatement.

was conducted 2 days after the cue extinction session (see Figure 1A).

Experiment 2

The long-term role of immediate post-reactivation 5-AZA treatment intra-BLA on cue-induced reinstatement and spontaneous recovery.

For the heroin self-administration session and nosepoke extinction session, the conditions and tone/light reactivation in Experiment 2 were the same as in Experiment 1. The rats were subjected to the 5-AZA treatment of 1 μg in 0.5 μl/side and the controls received the vehicle immediately after a 15-min tone/light reactivation. The cue-induced reinstatement test was performed 24 h later to assess the heroin-seeking behavior. After

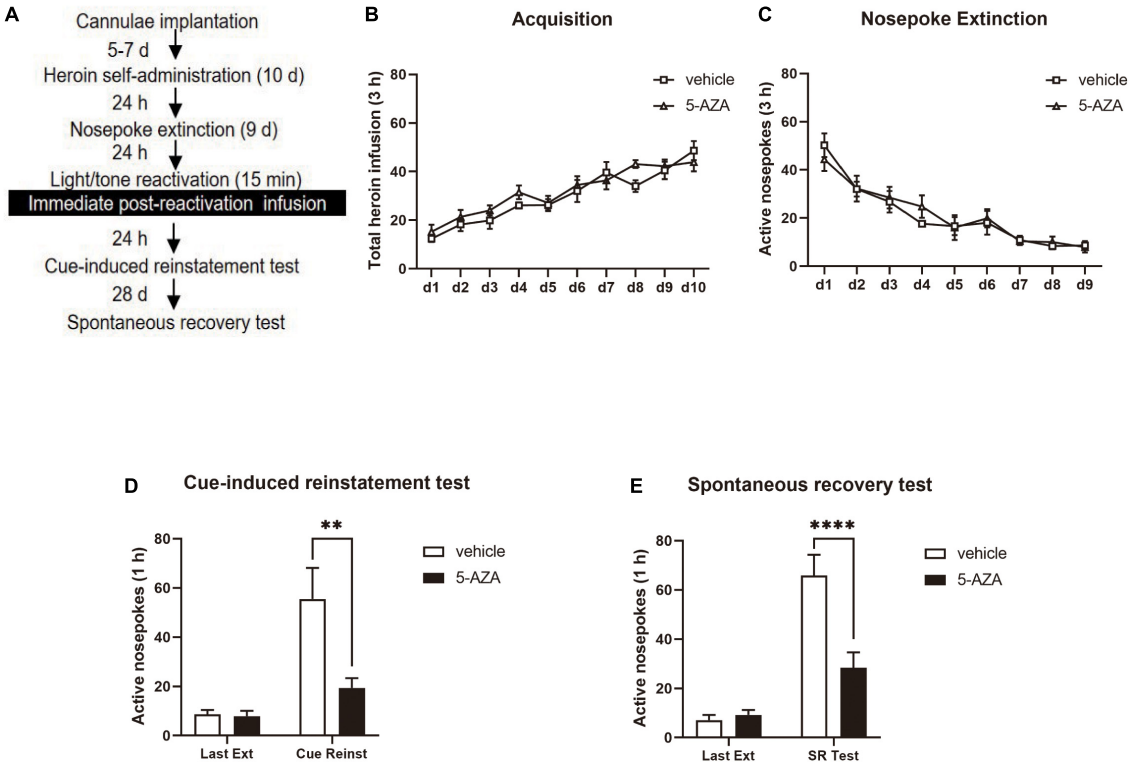

FIGURE 2
Immediate post-reactivation 5-AZA treatment intra-BLA reduces subsequent cue-induced heroin seeking and the spontaneous recovery of heroin seeking behavior. **(A)** Schematic representation of the experimental procedure. **(B)** Total number of heroin infusions across acquisition of heroin self-administration sessions. **(C)** Total number of active nosepoke responses across nosepoke response extinction sessions. **(D)** Active nosepoke responses during the last extinction session and the cue-induced reinstatement test. **(E)** Active nosepoke responses during the last extinction session and spontaneous recovery test. $n = 8$ rats per group. Data are means ± SEM, $^{**}p < 0.01$, $^{****}p < 0.0001$, compared with the vehicle group. Ext, extinction; Reinst, reinstatement; SR, spontaneous recovery.

28 days of withdrawal, the spontaneous recovery was tested (Figure 2A).

Experiments 3

The role of immediate post-reactivation 5-AZA infusion intra-BLA on subsequent cue-induced and heroin-priming-induced reinstatement of heroin-seeking behavior without reactivation.

During Experiment 3, the experimental protocol was similar to Experiment 1, except that the rats were subjected to the infusion of 5-AZA or vehicle intra-BLA bilaterally without reactivation (see Figure 3A).

Experiment 4

The role of delayed 5-AZA treatment intra-BLA post-reactivation on subsequent cue- and heroin-priming-induced reinstatement of heroin-seeking behavior.

During Experiment 4, the experimental protocol was the same as in Experiment 1 except that the rats were subjected to the infusion of 5-AZA or vehicle intra-BLA bilaterally 6 h after the 15-min retrieval (see Figure 4A).

Statistical analysis

The results were reported as mean ± SEM and analyzed using the two-way/repeated measures ANOVAs in GraphPad, v.9.0. Each experiment had a between-subjects factor for the infusion treatment (5-AZA vs. vehicle) and a within-subjects factor for the test (last nosepoke extinction day vs. cue-induced reinstatement test or saline-priming reinstatement test vs. heroin-priming-induced reinstatement test) (see section "Results"). We used Tukey's *post hoc* tests to analyze the two-way ANOVAs for specific pair-wise comparisons and examine any significant main effects or interactions ($p < 0.05$, two-tailed).

Results

Experiment 1

Immediate post-reactivation 5-AZA treatment intra-BLA reduced subsequent cue-induced and heroin-priming-induced reinstatement of heroin-seeking behavior.

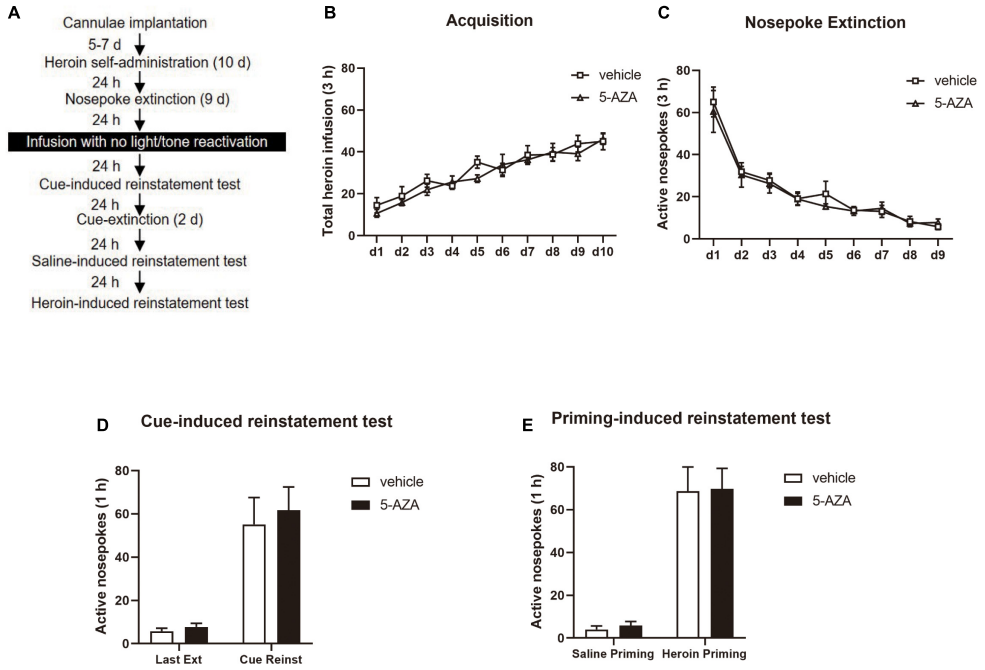

FIGURE 3
5-AZA infusion intra-BLA without reactivation has no effect on subsequent cue-induced and heroin-priming reinstatement of heroin-seeking behavior. **(A)** Schematic representation of the experimental procedure. **(B)** Total number of heroin infusions across acquisition of heroin self-administration sessions. **(C)** Total number of active nosepoke responses across nosepoke response extinction sessions. **(D)** Active nosepoke responses during the last extinction session and the cue-induced reinstatement test. **(E)** Active nosepoke responses during the saline- or heroin-priming reinstatement test. n = 8 rats per group. Data are means ± SEM. Ext, extinction; Reinst, reinstatement.

Two groups of rats were used in experiment 1 to examine the effects of post-reactivation 5-AZA infusion intra-BLA on cue-induced and heroin-priming-induced reinstatement of heroin-seeking behavior (Figure 1A). According to the schematic representation of the BLA regions, all cannula placements were within the BLA boundaries (Figure 1B). Analysis of the behavioral data of a mixed two-way ANOVA with the training date as a within-subjects factor, and the treatment (5-AZA vs. vehicle) as a between-subjects factor showed that the rate of heroin self-administration did not differ between the rats in the 5-AZA group (N = 10) and the rats in the vehicle group (N = 10), indicated by the total number of heroin infusions [main effect of acquisition date: $F_{(9,\ 162)} = 16.55$, $p < 0.0001$; infusion treatment: $F_{(1,\ 18)} = 0.4890$, $p = 0.4933$; acquisition date × infusion treatment: $F_{(9,\ 162)} = 1.556$, $p = 0.1327$; Figure 1C]. Furthermore, there was no difference between the 5-AZA group and the vehicle group in the nosepoke extinction session as shown in the total number of nosepokes [main effect of extinction date: $F_{(8,\ 144)} = 23.21$, $p < 0.0001$; infusion treatment: $F_{(1,\ 18)} = 0.2118$, $p = 0.6508$; extinction date × infusion treatment: $F_{(8,\ 144)} = 0.4913$, $p = 0.8609$; Figure 1D].

We found that the active nosepokes of the 5-AZA group significantly differed from the vehicle group in both the cue-induced and heroin-priming-induced reinstatement tests. A two-way ANOVA with the treatment (5-AZA vs. vehicle) as the between-subjects factor and test day (last extinction day vs. cue reinstatement day) as the within-subjects factor revealed a main effect of treatment [$F_{(1,\ 18)} = 7.236$, $p = 0.0150$], a main effect of test day [$F_{(1,\ 18)} = 40.91$, $p < 0.0001$], and a significant treatment × test day interaction [$F_{(1,\ 18)} = 9.947$, $p = 0.0055$] during the cue-induced reinstatement test. The *post hoc* analysis revealed that the number of active nose pokes of the 5-AZA group was significantly decreased compared with the vehicle group during the cue-induced reinstatement test ($p < 0.01$) (Figure 1E right column). Furthermore, a two-way ANOVA with treatment (5-AZA vs. vehicle) as the between-subjects factor and test day (last extinction day vs. cue reinstatement day) as the within-subjects factor revealed a main effect of treatment [$F_{(1,\ 18)} = 4.570$, $p = 0.0465$], a main effect of test day [$F_{(1,\ 18)} = 35.33$, $p < 0.0001$], and a significant treatment × nosepokes interaction [$F_{(1,\ 18)} = 4.675$, $p = 0.0443$] during the heroin reinstatement test. The *post hoc* analysis showed that the number of active nosepokes in the 5-AZA group was significantly lower than the vehicle group during the heroin-induced reinstatement test ($p < 0.01$) (Figure 1F right column).

These findings suggest that inhibiting the activity of DNMT with infusions of 5-AZA in the BLA immediately following the heroin cue retrieval significantly reduced cue-induced and heroin-priming-induced heroin-seeking behavior.

Experiment 2

Immediate post-reactivation 5-AZA treatment intra-BLA reduced subsequent cue-induced heroin seeking and the spontaneous recovery of heroin-seeking behavior.

In experiment 2, we aimed to test the effect of immediate post-reactivation 5-AZA treatment intra-BLA on cue-induced heroin seeking reinstatement and the long-term effect on heroin reward memory in two groups of rats (Figure 2A). No difference was observed in the total heroin infusion after achieving heroin self-administration between the rats infused with either 5-AZA (N = 8) or the vehicle (N = 8) [main effect of acquisition date: $F_{(9,\ 126)} = 22.31$, $p < 0.0001$; infusion treatment: $F_{(1,\ 14)} = 2.671$, $p = 0.1245$; acquisition date × infusion treatment: $F_{(9,\ 126)} = 0.8167$, $p = 0.6018$; Figure 2B]. Likewise, no differences were found between groups in extinction training [main effect of extinction date: $F_{(8,\ 112)} = 23.59$, $p < 0.0001$; infusion treatment: $F_{(1,\ 14)} = 0.08584$, $p = 0.7738$; extinction date × infusion treatment: $F_{(8,\ 112)} = 0.4240$, $p = 0.9045$; Figure 2C].

Similar to the results obtained in experiment 1, there was a significant difference in the active side nosepoke between the 5-AZA group and the vehicle group in the cue-induced reinstatement test [main effect of test: $F_{(1,\ 14)} = 19.98$, $p = 0.0005$; infusion treatment: $F_{(1,\ 14)} = 6.843$, $p = 0.0203$; test × infusion treatment: $F_{(1,\ 14)} = 7.339$, $p = 0.0170$; Figure 2D]. The *post hoc* analysis showed that active nosepokes were significantly reduced in the 5-AZA group compared with the vehicle group in the cue-induced reinstatement test ($p < 0.01$) (Figure 2D right column). In addition, in the spontaneous recovery test, active nosepokes significantly differed between the 5-AZA group and the vehicle group [main effect of test: $F_{(1,\ 14)} = 63.00$, $p < 0.0001$; infusion treatment: $F_{(1,\ 14)} = 8.866$, $p = 0.0100$; test × infusion treatment: $F_{(1,\ 14)} = 16.31$, $p = 0.0012$; Figure 2E]. The *post hoc* analysis revealed that drug-seeking in the 5-AZA group was significantly reduced compared to the vehicle group in the spontaneous recovery test ($p < 0.01$) (Figure 2E right column).

The findings of experiment 2 suggest that the immediate post-reactivation 5-AZA treatment intra-BLA reduced subsequent cue-induced heroin seeking reinstatement and this effect lasted for 28 days.

Experiment 3

5-AZA infusion intra-BLA with no reactivation had no effect on subsequent cue-induced and heroin-priming-induced reinstatement of heroin-seeking behavior.

In experiment 3, we examined whether the effect of DNMT in the BLA on the reconsolidation of heroin reward memory depended on retrieval by using the 5-AZA group (N = 8) and vehicle group (N = 8) of rats. Following the acquisition session of heroin self-administration and extinction session which is the same as experiments 1, rats were infused with 5-AZA or the vehicle intra-BLA immediately after exposing to the training chamber for 15 min with no cue exposure (Figure 3A). We did not find differences in the acquisition session of heroin [main effect of acquisition date: $F_{(9,\ 126)} = 25.84$, $p < 0.0001$; infusion treatment: $F_{(1,\ 14)} = 0.7240$, $p = 0.4091$; acquisition date × infusion treatment: $F_{(9,\ 126)} = 0.6614$, $p = 0.7423$; Figure 3B] or the extinction session [main effect of extinction date: $F_{(8,\ 112)} = 37.20$, $p < 0.0001$; infusion treatment: $F_{(1,\ 14)} = 0.2503$, $p = 0.6246$; extinction date × infusion treatment: $F_{(8,\ 112)} = 0.2094$, $p = 0.9887$; Figure 3C] between the two groups of rats.

In cue-induced reinstatement test, we did not find a difference in active nosepokes between the groups [main effect of test: $F_{(1,\ 14)} = 43.38$, $p < 0.0001$; infusion treatment: $F_{(1,\ 14)} = 0.2478$, $p = 0.6264$; test × infusion treatment: $F_{(1,\ 14)} = 0.08683$, $p = 0.7726$; Figure 3D]. Furthermore, in the priming-induced reinstatement test, the groups did not differ from each other in active nosepokes [main effect of test: $F_{(1,\ 14)} = 71.04$, $p < 0.0001$; infusion treatment: $F_{(1,\ 14)} = 0.04099$, $p = 0.8425$; test × infusion treatment: $F_{(1,\ 14)} = 0.002420$, $p = 0.9615$; Figure 3E].

Thus, these results indicated that the 5-AZA treatment intra-BLA without reactivation had no effects on the subsequent cue-induced and heroin-priming-induced reinstatement of heroin-seeking behavior, indicating that the effect of DNMT in the BLA on the reconsolidation of heroin reward memory was reactivation-dependent.

Experiment 4

Delayed 5-AZA treatment intra-BLA following reactivation had no effect on subsequent cue-induced and heroin-priming-induced reinstatement of heroin-seeking behavior.

Finally, in experiment 4, we investigated whether the role of 5-AZA treatment intra-BLA in the reconsolidation of heroin reward memory had a time window by using two groups of rats infused with either 5-AZA (N = 9) or vehicle (N = 9) (Figure 4A). In line with experiments 1–3, no difference was found in total heroin infusion between the two groups in the acquisition sessions [main effect of acquisition date: $F_{(9,\ 144)} = 35.09$, $p < 0.0001$; infusion treatment: $F_{(1,\ 16)} = 0.4635$, $p = 0.5057$; acquisition date × infusion treatment: $F_{(9,\ 144)} = 0.5624$, $p = 0.8260$; Figure 4B]. Furthermore, no group difference in the extinction session was found for active nosepokes [main effect of extinction date: $F_{(8,\ 128)} = 38.71$, $p < 0.0001$; infusion treatment: $F_{(1,\ 16)} = 0.03292$, $p = 0.8583$; extinction date × infusion treatment: $F_{(8,\ 128)} = 0.6184$, $p = 0.7612$; Figure 4C].

However, intra-BLA 5-AZA treatment 6 h after the reactivation did not affect the subsequent cue-induced reinstatement of heroin seeking behavior, indicated by the number of active nosepokes had no difference between groups

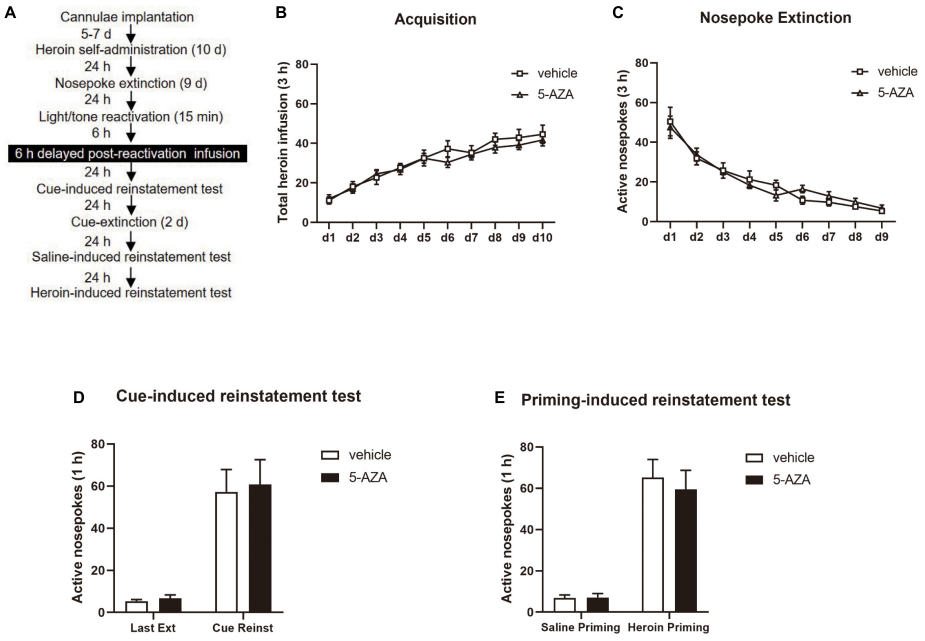

FIGURE 4
Delayed 5-AZA treatment intra-BLA following reactivation has no effect on subsequent cue-induced and heroin-priming reinstatement of heroin-seeking behavior. **(A)** Schematic representation of the experimental procedure. **(B)** Total number of heroin infusions during acquisition of heroin self-administration sessions. **(C)** Total number of active nosepoke responses across nosepoke response extinction sessions. **(D)** Active nosepoke responses during the last extinction session and the cue-induced reinstatement test. **(E)** Active nosepoke responses during the saline- or heroin-priming reinstatement test. n = 9 rats per group. Data are means ± SEM. Ext, extinction; Reinst, reinstatement.

[maineffect of test: $F_{(1,16)}$ = 48.29, p < 0.0001; infusion treatment: $F_{(1,16)}$ = 0.08935, p = 0.7689; extinction date × infusion treatment: $F_{(1,16)}$ = 0.01919, p = 0.8915; **Figure 4D**]; or the priming- induced reinstatement, as the number of active nosepokes had also no difference between groups [main effect of test: $F_{(1,16)}$ = 72.48, p < 0.0001; infusion treatment: $F_{(1,16)}$ = 0.1839, p = 0.6737; test × infusion treatment: $F_{(1,16)}$ = 0.2131, p = 0.6506; **Figure 4E**].

These experiments indicated that the role of 5-AZA on heroin-seeking behavior was time-specific, and inhibiting the activity of DNMT should be within 6 h after reactivation to suppress the heroin-seeking behavior.

Discussion

Our study examined the role of DNA methyltransferase (DNMT) in the BLA on the reconsolidation of heroin reward memory. The main findings are as follows: (1) DNMT inhibition in the BLA immediately after light/tone cue reactivation reduces subsequent cue-induced and heroin-priming-induced reinstatement of heroin-seeking behavior; (2) a 5-AZA infusion in the BLA without reactivation has no effect on the subsequent cue-induced reinstatement of heroin-seeking behavior; (3) the inhibitory effect of a 5-AZA infusion in the BLA immediately after the reactivation session on heroin-seeking behavior lasts at least 28 days. These findings indicate that the activity of DNMT in the BLA is required for the reconsolidation of the heroin reward memory and inhibiting the DNMT in the BLA attenuates heroin-seeking behavior by disrupting the reconsolidation of heroin reward memory.

A relapse caused by persistent heroin reward memory is a major challenge to the therapy of heroin addiction (Kalivas and Volkow, 2005; Robbins et al., 2008; Economidou et al., 2011; Torregrossa et al., 2011; Ma et al., 2012; Ewing et al., 2021). Studies on drug addiction in both humans and animals have demonstrated that either pharmacological or non-pharmacological intervention in reconsolidation has a great potential to prevent relapse (Lee et al., 2005; Xue et al., 2012; Lin et al., 2014; Chen et al., 2021a; Zhang et al., 2021; Xie et al., 2022). In our present study, we find that DNMT inhibition in the BLA disrupts reconsolidation and attenuates the subsequent heroin-seeking behavior of heroin reward memory. Our results are consistent with our previous study, further confirming the role of DNMT in the reconsolidation of heroin reward memory, and indicate that DNMT inhibition during reconsolidation may be a general way to prevent relapse across drug classes (Shi et al., 2015). In addition, the present results verify two aspects of reconsolidation that have been reported by previous studies, namely the requirement of new protein synthesis during the process and the need to be maintained for approximately 6 h (Valjent et al., 2006; Li et al., 2010; Wu et al., 2011;

Lin et al., 2014; Chen et al., 2021a; Zhang et al., 2021; Xie et al., 2022). Overall, we find that immediate post-reactivation intra-BLA DNMT inhibition reduces subsequent cue-induced and heroin-priming-induced reinstatement of heroin-seeking behavior by disrupting the reconsolidation of heroin reward memory and this inhibitory effect depends on the reactivation session and has a limited time window.

It has been reported that the memory reconsolidation process involves DNA transcription and *de novo* protein synthesis (Nader et al., 2000; de la Fuente et al., 2015). DNA transcription is regulated by the epigenetic mechanisms of chromatin restructuring and DNA methylation, which play critical roles in the reconsolidation of memory (Levenson and Sweatt, 2005; Duvarci et al., 2008; de la Fuente et al., 2015; Gonzalez et al., 2019; Liu et al., 2022). DNMT, a widely expressed DNA methylation enzyme in the mammalian adult nervous system (Feng et al., 2005; Rahn et al., 2013), suppresses the transcription process by catalyzing the methylation of cytosine residues in DNA, causing the chromatin structure to compact and abolishing the transcription factors binding to the specific site of DNA (Miller and Sweatt, 2007; Selvakumar et al., 2012; Lyko, 2018; Shi et al., 2021). Thus, DNMT is thought to disrupt reconsolidation by inhibiting the binding between transcription factors and DNA. In this way, the inhibiting activity of DNMT is argued to positively regulate the reconsolidation of memory (Maddox and Schafe, 2011; Selvakumar et al., 2012). However, some studies show that the inhibition of DNMT disrupts the consolidation and reconsolidation of memory. This is inconsistent with aforementioned positive effect of DNMT inhibiting activity on the reconsolidation of memory (Miller and Sweatt, 2007; Miller et al., 2008; Zhao et al., 2010; Maddox and Schafe, 2011; Monsey et al., 2011; Pearce et al., 2017). One of the reasons for this discrepancy may due to the fact that the DNA needs to be re-repressed for memory re-stabilization. Thus, if the activity of DNMT is inhibited, the re-repression of gene transcription will be blocked and the memory may remain in a labile state and be impaired easily (Miller and Sweatt, 2007; Miller et al., 2008; Zhao et al., 2010; Shi et al., 2015). Moreover, DNMT inhibition may influence other epigenetic mechanisms such as histone acetylation to regulate reconsolidation of memory (Maddox and Schafe, 2011). This may explain the aforementioned inconsistency. In addition, a similar study found that DNA methylation in the LA is required for the reconsolidation of fear memory (Maddox and Schafe, 2011). Our previous study also revealed that the activity of DNMT in the BLA is required in the reconsolidation of cocaine reward memory (Shi et al., 2015). Thus, the present study is consistent with the findings of recent studies that indicate the role of DNMT in the reconsolidation of drug memory (Shi et al., 2015; Brown and Feng, 2017; Cannella et al., 2018; Urb et al., 2020). However, our study also has some limitations such as the lack of molecular evidence to explain the alteration of the activity of DMNT during/after the manipulation in the study. More experiments are needed in the future that focus on the specific molecular alterations and related signaling pathways during/after retrieval of heroin reward memory. Furthermore, as the epigenetic mechanisms involving DNA methylation and histone acetylation are complex (Mahan et al., 2012), other potential epigenetic mechanisms of the DNMT in the reconsolidation of drug memory need to be investigated in the future (Jarome and Lubin, 2014).

In conclusion, our study demonstrated that DNA methylation regulates the reconsolidation of heroin reward memory in the BLA. Our study also highlights the significant effect of epigenetic regulation, specifically DNA methylation, in the reconsolidation of heroin reward memory. Our findings provide theoretical support for the molecular mechanisms of reconsolidation of drug memory in the BLA and the development of potential therapies for heroin addiction.

Data availability statement

The raw data supporting the conclusions of this article will be made available by the authors, without undue reservation.

Ethics statement

The animal study was reviewed and approved by the Local Committee on Animal Care and Use and Protection of the Hunan Normal University.

Author contributions

SQ, CY, and YL: conceptualization. CS and SH: data curation. SQ and CS: writing of original draft preparation. CS and CY: review and editing. YL: funding acquisition. All authors contributed to the article and approved the submitted version.

Funding

This work was financially supported from Natural Science Foundation of China (no. 81771434) and Outstanding Innovative Youth Training Program of Changsha (kq2106032) for YL.

Conflict of interest

The authors declare that the research was conducted in the absence of any commercial or financial relationships that could be construed as a potential conflict of interest.

The reviewer BX declared a past co-authorship with the author YL to the handling editor.

Publisher's note

References

Alberini, C. M., and Ledoux, J. E. (2013). Memory reconsolidation. *Curr. Biol.* 23, R746–R750. doi: 10.1016/j.cub.2013.06.046

Alvandi, M. S., Bourmpoula, M., Homberg, J. R., and Fathollahi, Y. (2017). Association of contextual cues with morphine reward increases neural and synaptic plasticity in the ventral hippocampus of rats. *Addict. Biol.* 22, 1883–1894. doi: 10.1111/adb.12547

Arguello, A. A., Hodges, M. A., Wells, A. M., Lara, H., Xie, X., and Fuchs, R. A. (2014). Involvement of amygdalar protein kinase A, but not calcium/calmodulin-dependent protein kinase II, in the reconsolidation of cocaine-related contextual memories in rats. *Psychopharmacology* 231, 55–65. doi: 10.1007/s00213-013-3203-9

Böning, J. (2009). Addiction memory as a specific, individually learned memory imprint. *Pharmacopsychiatry* 42(Suppl. 1), S66–S68. doi: 10.1055/s-0029-1216357

Brown, A. N., and Feng, J. (2017). Drug addiction and DNA modifications. *Adv. Exp. Med. Biol.* 978, 105–125. doi: 10.1007/978-3-319-53889-1_6

Cannella, N., Oliveira, A. M. M., Hemstedt, T., Lissek, T., Buechler, E., Bading, H., et al. (2018). Dnmt3a2 in the nucleus accumbens shell is required for reinstatement of cocaine seeking. *J. Neurosci.* 38, 7516–7528. doi: 10.1523/JNEUROSCI.0600-18.2018

Chen, L., Huang, S., Yang, C., Wu, F., Zheng, Q., Yan, H., et al. (2021a). Blockade of β-adrenergic receptors by propranolol disrupts reconsolidation of drug memory and attenuates heroin seeking. *Front. Pharmacol.* 12:686845. doi: 10.3389/fphar.2021.686845

Chen, L., Yan, H., Wang, Y., He, Z., Leng, Q., Huang, S., et al. (2021b). The mechanisms and boundary conditions of drug memory reconsolidation. *Front. Neurosci.* 15:717956. doi: 10.3389/fnins.2021.717956

Davis, M. (1992). The role of the amygdala in fear and anxiety. *Annu. Rev. Neurosci.* 15, 353–375.

Day, J. J., and Sweatt, J. D. (2010). DNA methylation and memory formation. *Nat. Neurosci.* 13, 1319–1323. doi: 10.1038/nn.2666

de la Fuente, V., Federman, N., Zalcman, G., Salles, A., Freudenthal, R., and Romano, A. (2015). NF-κB transcription factor role in consolidation and reconsolidation of persistent memories. *Front. Mol. Neurosci.* 8:50. doi: 10.3389/fnmol.2015.00050

Douton, J. E., Horvath, N., Mills-Huffnagle, S., Nyland, J. E., Hajnal, A., and Grigson, P. S. (2022). Glucagon-like peptide-1 receptor agonist, liraglutide, reduces heroin self-administration and drug-induced reinstatement of heroin-seeking behaviour in rats. *Addict. Biol.* 27:e13117. doi: 10.1111/adb.13117

Duvarci, S., Nader, K., and LeDoux, J. E. (2008). De novo mRNA synthesis is required for both consolidation and reconsolidation of fear memories in the amygdala. *Learn. Mem.* 15, 747–755. doi: 10.1101/lm.1027208

Economidou, D., Dalley, J. W., and Everitt, B. J. (2011). Selective norepinephrine reuptake inhibition by atomoxetine prevents cue-induced heroin and cocaine seeking. *Biol. Psychiatry* 69, 266–274. doi: 10.1016/j.biopsych.2010.09.040

Ewing, S. T., Dorcely, C., Maidi, R., Paker, G., Schelbaum, E., and Ranaldi, R. (2021). Low-dose polypharmacology targeting dopamine D1 and D3 receptors reduces cue-induced relapse to heroin seeking in rats. *Addict. Biol.* 26:e12988. doi: 10.1111/adb.12988

Feng, J., Chang, H., Li, E., and Fan, G. (2005). Dynamic expression of de novo DNA methyltransferases Dnmt3a and Dnmt3b in the central nervous system. *J. Neurosci. Res.* 79, 734–746. doi: 10.1002/jnr.20404

Fuchs, R. A., Bell, G. H., Ramirez, D. R., Eaddy, J. L., and Su, Z.-I. (2009). Basolateral amygdala involvement in memory reconsolidation processes that facilitate drug context-induced cocaine seeking. *Eur. J. Neurosci.* 30, 889–900. doi: 10.1111/j.1460-9568.2009.06888.x

Gonzalez, M. C., Rossato, J. I., Radiske, A., Pádua Reis, M., and Cammarota, M. (2019). Recognition memory reconsolidation requires hippocampal Zif268. *Sci. Rep.* 9:16620. doi: 10.1038/s41598-019-53005-8

Hellemans, K. G. C., Everitt, B. J., and Lee, J. L. C. (2006). Disrupting reconsolidation of conditioned withdrawal memories in the basolateral amygdala reduces suppression of heroin seeking in rats. *J. Neurosci.* 26, 12694–12699. doi: 10.1523/JNEUROSCI.3101-06.2006

Higginbotham, J. A., Jones, N. M., Wang, R., Christian, R. J., Ritchie, J. L., McLaughlin, R. J., et al. (2021). Basolateral amygdala CB1 receptors gate HPA axis activation and context-cocaine memory strength during reconsolidation. *Neuropsychopharmacology* 46, 1554–1564. doi: 10.1038/s41386-020-00919-x

Hyman, S. E. (2005). Addiction: A disease of learning and memory. *Am. J. Psychiatry* 162, 1414–1422.

Hyman, S. E., Malenka, R. C., and Nestler, E. J. (2006). Neural mechanisms of addiction: The role of reward-related learning and memory. *Annu. Rev. Neurosci.* 29, 565–598.

Jarome, T. J., and Lubin, F. D. (2014). Epigenetic mechanisms of memory formation and reconsolidation. *Neurobiol. Learn. Mem.* 115, 116–127. doi: 10.1016/j.nlm.2014.08.002

Jian, M., Luo, Y.-X., Xue, Y.-X., Han, Y., Shi, H.-S., Liu, J.-F., et al. (2014). eIF2α dephosphorylation in basolateral amygdala mediates reconsolidation of drug memory. *J. Neurosci.* 34, 10010–10021. doi: 10.1523/JNEUROSCI.0934-14.2014

Kalivas, P. W., and Volkow, N. D. (2005). The neural basis of addiction: A pathology of motivation and choice. *Am. J. Psychiatry* 162, 1403–1413.

Lee, J. L. C., Di Ciano, P., Thomas, K. L., and Everitt, B. J. (2005). Disrupting reconsolidation of drug memories reduces cocaine-seeking behavior. *Neuron* 47, 795–801.

Levenson, J. M., and Sweatt, J. D. (2005). Epigenetic mechanisms in memory formation. *Nat. Rev. Neurosci.* 6, 108–118.

Li, F.-Q., Xue, Y.-X., Wang, J.-S., Fang, Q., Li, Y.-Q., Zhu, W.-L., et al. (2010). Basolateral amygdala cdk5 activity mediates consolidation and reconsolidation of memories for cocaine cues. *J. Neurosci.* 30, 10351–10359. doi: 10.1523/JNEUROSCI.2112-10.2010

Lin, J., Liu, L., Wen, Q., Zheng, C., Gao, Y., Peng, S., et al. (2014). Rapamycin prevents drug seeking via disrupting reconsolidation of reward memory in rats. *Int. J. Neuropsychopharmacol.* 17, 127–136. doi: 10.1017/S1461145713001156

Liu, J.-F., Tian, J., and Li, J.-X. (2019). Modulating reconsolidation and extinction to regulate drug reward memory. *Eur. J. Neurosci.* 50, 2503–2512. doi: 10.1111/ejn.14072

Liu, P., Liang, J., Jiang, F., Cai, W., Shen, F., Liang, J., et al. (2022). *Gnas* promoter hypermethylation in the basolateral amygdala regulates reconsolidation of morphine reward memory in rats. *Genes* 13:553. doi: 10.3390/genes13030553

Lu, L., Hope, B. T., Dempsey, J., Liu, S. Y., Bossert, J. M., and Shaham, Y. (2005). Central amygdala ERK signaling pathway is critical to incubation of cocaine craving. *Nat. Neurosci.* 8, 212–219.

Luo, Y.-X., Xue, Y.-X., Liu, J.-F., Shi, H.-S., Jian, M., Han, Y., et al. (2015). A novel UCS memory retrieval-extinction procedure to inhibit relapse to drug seeking. *Nat. Commun.* 6:7675. doi: 10.1038/ncomms8675

Lüscher, C., and Ungless, M. A. (2006). The mechanistic classification of addictive drugs. *PLoS Med.* 3:e437. doi: 10.1371/journal.pmed.0030437

Lyko, F. (2018). The DNA methyltransferase family: A versatile toolkit for epigenetic regulation. *Nat. Rev. Genet.* 19, 81–92. doi: 10.1038/nrg.2017.80

Ma, X., Zhang, J.-J., and Yu, L.-C. (2012). Post-retrieval extinction training enhances or hinders the extinction of morphine-induced conditioned place preference in rats dependent on the retrieval-extinction interval. *Psychopharmacology* 221, 19–26. doi: 10.1007/s00213-011-2545-4

Maddox, S. A., and Schafe, G. E. (2011). Epigenetic alterations in the lateral amygdala are required for reconsolidation of a Pavlovian fear memory. *Learn. Mem.* 18, 579–593. doi: 10.1101/lm.2243411

Mahan, A. L., Mou, L., Shah, N., Hu, J.-H., Worley, P. F., and Ressler, K. J. (2012). Epigenetic modulation of Homer1a transcription regulation in amygdala and hippocampus with pavlovian fear conditioning. *J. Neurosci.* 32, 4651–4659. doi: 10.1523/JNEUROSCI.3308-11.2012

Maren, S. (2003). The amygdala, synaptic plasticity, and fear memory. *Ann. N. Y. Acad. Sci.* 985, 106–113.

Miller, C. A., Campbell, S. L., and Sweatt, J. D. (2008). DNA methylation and histone acetylation work in concert to regulate memory formation and synaptic plasticity. *Neurobiol. Learn. Mem.* 89, 599–603.

Miller, C. A., and Sweatt, J. D. (2007). Covalent modification of DNA regulates memory formation. *Neuron* 53, 857–869.

Monsey, M. S., Ota, K. T., Akingbade, I. F., Hong, E. S., and Schafe, G. E. (2011). Epigenetic alterations are critical for fear memory consolidation and synaptic plasticity in the lateral amygdala. *PLoS One* 6:e19958. doi: 10.1371/journal.pone.0019958

Nader, K. (2003). Memory traces unbound. *Trends Neurosci.* 26, 65–72. doi: 10.1016/S0166-2236(02)00042-5

Nader, K., and Einarsson, E. O. (2010). Memory reconsolidation: An update. *Ann. N. Y. Acad. Sci.* 1191, 27–41. doi: 10.1111/j.1749-6632.2010.05443.x

Nader, K., Schafe, G. E., and Le Doux, J. E. (2000). Fear memories require protein synthesis in the amygdala for reconsolidation after retrieval. *Nature* 406, 722–726.

Pearce, K., Cai, D., Roberts, A. C., and Glanzman, D. L. (2017). Role of protein synthesis and DNA methylation in the consolidation and maintenance of long-term memory in *Aplysia*. *eLife* 6:e18299. doi: 10.7554/eLife.18299

Preller, K. H., Wagner, M., Sulzbach, C., Hoenig, K., Neubauer, J., Franke, P. E., et al. (2013). Sustained incentive value of heroin-related cues in short- and long-term abstinent heroin users. *Eur. Neuropsychopharmacol.* 23, 1270–1279. doi: 10.1016/j.euroneuro.2012.11.007

Rahn, E. J., Guzman-Karlsson, M. C., and David Sweatt, J. (2013). Cellular, molecular, and epigenetic mechanisms in non-associative conditioning: Implications for pain and memory. *Neurobiol. Learn. Mem.* 105, 133–150. doi: 10.1016/j.nlm.2013.06.008

Ratano, P., Everitt, B. J., and Milton, A. L. (2014). The CB1 receptor antagonist AM251 impairs reconsolidation of pavlovian fear memory in the rat basolateral amygdala. *Neuropsychopharmacology* 39, 2529–2537. doi: 10.1038/npp.2014.103

Ritchie, J. L., Walters, J. L., Galliou, J. M. C., Christian, R. J., Qi, S., Savenkova, M. I., et al. (2021). Basolateral amygdala corticotropin-releasing factor receptor type 1 regulates context-cocaine memory strength during reconsolidation in a sex-dependent manner. *Neuropharmacology* 200:108819. doi: 10.1016/j.neuropharm.2021.108819

Robbins, T. W., Ersche, K. D., and Everitt, B. J. (2008). Drug addiction and the memory systems of the brain. *Ann. N. Y. Acad. Sci.* 1141, 1–21. doi: 10.1196/annals.1441.020

See, R. E., Fuchs, R. A., Ledford, C. C., and McLaughlin, J. (2003). Drug addiction, relapse, and the amygdala. *Ann. N. Y. Acad. Sci.* 985, 294–307.

Selvakumar, T., Gjidoda, A., Hovde, S. L., and Henry, R. W. (2012). Regulation of human RNA polymerase III transcription by DNMT1 and DNMT3a DNA methyltransferases. *J. Biol. Chem.* 287, 7039–7050. doi: 10.1074/jbc.M111.285601

Shi, H.-S., Luo, Y.-X., Yin, X., Wu, H.-H., Xue, G., Geng, X.-H., et al. (2015). Reconsolidation of a cocaine associated memory requires DNA methyltransferase activity in the basolateral amygdala. *Sci. Rep.* 5:13327. doi: 10.1038/srep13327

Shi, J., Xu, J., Chen, Y. E., Li, J. S., Cui, Y., Shen, L., et al. (2021). The concurrence of DNA methylation and demethylation is associated with transcription regulation. *Nat. Commun.* 12:5285. doi: 10.1038/s41467-021-25521-7

Si, J., Yang, J., Xue, L., Yang, C., Luo, Y., Shi, H., et al. (2012). Activation of NF-κB in basolateral amygdala is required for memory reconsolidation in auditory fear conditioning. *PLoS One* 7:e43973. doi: 10.1371/journal.pone.0043973

Stern, C. A. J., de Carvalho, C. R., Bertoglio, L. J., and Takahashi, R. N. (2018). Effects of cannabinoid drugs on aversive or rewarding drug-associated memory extinction and reconsolidation. *Neuroscience* 370, 62–80. doi: 10.1016/j.neuroscience.2017.07.018

Sultan, F. A., and Day, J. J. (2011). Epigenetic mechanisms in memory and synaptic function. *Epigenomics* 3, 157–181. doi: 10.2217/epi.11.6

Torregrossa, M. M., Corlett, P. R., and Taylor, J. R. (2011). Aberrant learning and memory in addiction. *Neurobiol. Learn. Mem.* 96, 609–623. doi: 10.1016/j.nlm.2011.02.014

Tronson, N. C., and Taylor, J. R. (2013). Addiction: A drug-induced disorder of memory reconsolidation. *Curr. Opin. Neurobiol.* 23, 573–580. doi: 10.1016/j.conb.2013.01.022

Urb, M., Niinep, K., Matsalu, T., Kipper, K., Herodes, K., Zharkovsky, A., et al. (2020). The role of DNA methyltransferase activity in cocaine treatment and withdrawal in the nucleus accumbens of mice. *Addict. Biol.* 25:e12720. doi: 10.1111/adb.12720

Valjent, E., Corbillé, A.-G., Bertran-Gonzalez, J., Hervé, D., and Girault, J.-A. (2006). Inhibition of ERK pathway or protein synthesis during reexposure to drugs of abuse erases previously learned place preference. *Proc. Natl. Acad. Sci. U.S.A.* 103, 2932–2937.

Wang, G.-B., Zhang, X.-L., Zhao, L.-Y., Sun, L.-L., Wu, P., Lu, L., et al. (2012). Drug-related cues exacerbate decision making and increase craving in heroin addicts at different abstinence times. *Psychopharmacology* 221, 701–708. doi: 10.1007/s00213-011-2617-5

Wells, A. M., Arguello, A. A., Xie, X., Blanton, M. A., Lasseter, H. C., Reittinger, A. M., et al. (2013). Extracellular signal-regulated kinase in the basolateral amygdala, but not the nucleus accumbens core, is critical for context-response-cocaine memory reconsolidation in rats. *Neuropsychopharmacology* 38, 753–762. doi: 10.1038/npp.2012.238

Wells, A. M., Lasseter, H. C., Xie, X., Cowhey, K. E., Reittinger, A. M., and Fuchs, R. A. (2011). Interaction between the basolateral amygdala and dorsal hippocampus is critical for cocaine memory reconsolidation and subsequent drug context-induced cocaine-seeking behavior in rats. *Learn. Mem.* 18, 693–702. doi: 10.1101/lm.2273111

Wu, P., Xue, Y.-X., Ding, Z.-B., Xue, L.-F., Xu, C.-M., and Lu, L. (2011). Glycogen synthase kinase 3β in the basolateral amygdala is critical for the reconsolidation of cocaine reward memory. *J. Neurochem.* 118, 113–125. doi: 10.1111/j.1471-4159.2011.07277.x

Xie, Y., Zhang, Y., Hu, T., Zhao, Z., Liu, Q., and Li, H. (2022). Inhibition of glycogen synthase kinase 3β activity in the basolateral amygdala disrupts reconsolidation and attenuates heroin relapse. *Front. Mol. Neurosci.* 15:932939. doi: 10.3389/fnmol.2022.932939

Xue, Y.-X., Luo, Y.-X., Wu, P., Shi, H.-S., Xue, L.-F., Chen, C., et al. (2012). A memory retrieval-extinction procedure to prevent drug craving and relapse. *Science* 336, 241–245. doi: 10.1126/science.1215070

Zhang, F., Huang, S., Bu, H., Zhou, Y., Chen, L., Kang, Z., et al. (2021). Disrupting reconsolidation by systemic inhibition of mTOR kinase via rapamycin reduces cocaine-seeking behavior. *Front. Pharmacol.* 12:652865. doi: 10.3389/fphar.2021.652865

Zhao, Z., Fan, L., and Frick, K. M. (2010). Epigenetic alterations regulate estradiol-induced enhancement of memory consolidation. *Proc. Natl. Acad. Sci. U.S.A.* 107, 5605–5610. doi: 10.1073/pnas.0910578107

frontiers | Frontiers in Molecular Neuroscience

TYPE Original Research
PUBLISHED 10 November 2022
DOI 10.3389/fnmol.2022.1020098

OPEN ACCESS

EDITED BY
Qian Ren,
Hebei Medical University, China

REVIEWED BY
Ying Han,
Peking University, China
Le Shi,
Peking University Sixth Hospital, China

*CORRESPONDENCE
Si Chen
chendd0522@163.com
Zihua Chen
zihuac@outlook.com

SPECIALTY SECTION
This article was submitted to Molecular Signalling and Pathways, a section of the journal Frontiers in Molecular Neuroscience

RECEIVED 15 August 2022
ACCEPTED 20 September 2022
PUBLISHED 10 November 2022

CITATION
Li H, Hu T, Zhang Y, Zhao Z, Liu Q, Chen Z and Chen S (2022) Extracellular signal-regulated kinase in the basolateral amygdala is required for reconsolidation of heroin-associated memory.
Front. Mol. Neurosci. 15:1020098.
doi: 10.3389/fnmol.2022.1020098

Extracellular signal-regulated kinase in the basolateral amygdala is required for reconsolidation of heroin-associated memory

Haoyu Li[1,2,3], Ting Hu[1,2,3], Yanghui Zhang[4], Zijin Zhao[1,2,3], Qing Liu[1,2,3], Zihua Chen[3,5]* and Si Chen[3,6,7]*

[1]Department of Neurosurgery, Xiangya Hospital, Central South University, Changsha, China, [2]The Institute of Skull Base Surgery and Neurooncology at Hunan Province, Changsha, China, [3]National Clinical Research Center for Geriatric Disorders, Xiangya Hospital, Central South University, Changsha, China, [4]Center of Medical Genetics, Jiangmen Maternity and Child Health Care Hospital, Jiangmen, China, [5]Department of General Surgery, Xiangya Hospital, Central South University, Changsha, China, [6]Department of Ophthalmology, Xiangya Hospital, Central South University, Changsha, China, [7]Hunan Key Laboratory of Ophthalmology, Changsha, China

Reconsolidation of heroin-associated memory is an independent memory process that occurs following retrieval, which is essential for the sustained capacity of an associative drug stimulus to precipitate heroin-seeking. Extracellular signal-regulated kinase (ERK) in the basolateral amygdala (BLA) mediates the reconsolidation of drug memory. In the present study, we utilized a rat model of drug craving and relapse to verify the hypothesis that the reconsolidation of heroin-associated memory requires ERK in an instrumental heroin-seeking behavior, focusing on the BLA brain region, which is crucial for synaptic plasticity and memory processes. We found that bilateral intra-BLA infusions of U0126 (1 μg/0.5 μl), an ERK inhibitor, immediately after retrieving heroin-associated memory significantly reduced cue-induced and drug-induced reinstatement and spontaneous recovery of heroin-seeking compared to the vehicle. Furthermore, this inhibitory effect was related to the characteristic of reconsolidation. Conversely, no effect was observed on the heroin-seeking behavior when the intra-BLA infusion of U0126 was administered 6 h after the heroin-associated memory retrieval or without memory retrieval. Together, these data suggest that disrupting the reconsolidation of heroin-associated memory *via* an ERK inhibitor may serve as a promising option for treating relapse in opiate addicts.

KEYWORDS

heroin, reconsolidation, ERK, BLA, relapse

Introduction

The associative memory formed by repeated drug use usurps standard reward-related memory, leading to substance-related and addictive disorders that result from a disturbance in learning, emotional, decision-making, and response systems (Gardner, 2011; Volkow et al., 2019). Such aberrations lead addicts to reemerge with compulsive drug-seeking behavior and even relapse (Hyman et al., 2006; Gardner, 2011). Exposure to environmental cues or contexts associated with drug elicits craving and relapse, which is the core primary clinical problem in drug addicts (Childress et al., 1999; Crombag et al., 2008; Chen et al., 2021b). To address the persistent propensity for relapse, an increasing number of studies suggest that disrupting drug-associated memory, which maintains conditioned reinforcing properties through various manipulations, is a promising strategy to prevent relapse (Milton and Everitt, 2010; Jian et al., 2014; Barak and Goltseker, 2021).

The memory reconsolidation supposes the hypothesis that the consolidation memory underwent retrieval *via* reexposure to the conditioned stimulus (CS) and becomes labile during a time window. It requires a *de novo* protein synthesis-dependent reconsolidation process to subsist (Nader et al., 2000; Kida et al., 2002; Tronel et al., 2005; Fukushima et al., 2014; Chen et al., 2021a; Zhang et al., 2021). Disrupting the reconsolidation of drug memory would limit relapse susceptibility. Studies in animal models and human addicts find that intervening in the reconsolidation of drug memory subsequently attenuates drug-seeking behaviors (Milton and Everitt, 2010; Sorg, 2012; Liang et al., 2017; Lin et al., 2021). Therefore, elucidating the molecular mechanism of reconsolidation is of great significance for developing a highly selective drug therapy to prevent relapse.

The mitogen-activated protein kinase (MAPK) ERK is essential for synaptic plasticity, learning, and memory, which is especially involved in the reconsolidation of some memory forms (Lu et al., 2006; Peng et al., 2010; Leal et al., 2014). ERK activation in neurons significantly integrates signaling for the reconsolidation of drug memory, including N-methyl D-aspartate receptors (NMDARs; Brown et al., 2008; Milton et al., 2008), the activation of β-adrenergic receptor, and the stimulation of protein kinase A (PKA; Sweatt, 2001; Fricks-Gleason and Marshall, 2008; Milton and Everitt, 2010; Sanchez et al., 2010). Furthermore, studies suggest that ERK is critical for the reconsolidation of auditory fear memory (Duvarci et al., 2006), object recognition memory (Kelly et al., 2003; Silingardi et al., 2011), and cocaine memory in both Pavlovian cocaine-related memory of the conditioned place preference (CPP) model and response-outcome associative cocaine-related memory of the self-administration (SA) model (Miller and Marshall, 2005; Valjent et al., 2006; Wells et al., 2013). Nevertheless, several gaps remain in our understanding of the effect of ERK on the memory reconsolidation. More specifically, the effect of ERK on the reconsolidation of heroin-associated memory has not been investigated in the response-outcome paradigm, since studies show that the reconsolidation of drug memory in Pavlovian and instrumental patterns involves distinct neuroanatomical mechanisms (Wells et al., 2016; Bender and Torregrossa, 2020).

In the present study, we used the classical heroin SA model of relapse to confirm whether ERK is required for the reconsolidation of heroin-associated memory in the brain regions of the BLA that have been demonstrated to critically regulate reconsolidation of drug memory (Li et al., 2010; Sanchez et al., 2010; Xie et al., 2022). We also tested the effect of ERK inhibition during reconsolidation on subsequent cue-induced and heroin-induced reinstatement and spontaneous recovery of heroin-seeking behavior.

Methods

Subjects

Male Sprague-Dawley rats (260–280 g on arrival) were placed in a 23 ± 2°C temperature and 50% humid environment with free access to food and water under a 12-h light/dark cycle. The rats were handled for 3 min/day for 5 days before surgery. All experimental procedures were performed under the Guidelines of the Xiangya Hospital Ethics Committee, Xiangya Hospital (Changsha, China).

Surgery

After 60 mg/kg of sodium pentobarbital anesthesia was administered intraperitoneally (ip) to rats, the rats received an implantation with intravenous (iv) jugular catheters and bilateral guide cannulae (23 gauge; Plastics One, Roanoke, VA, USA) surgically (Xue et al., 2012; Xie et al., 2022). The implantation region of the guide cannulae was 1 mm above the BLA (anterior/posterior:−2.8 mm, medial/lateral: ±5.0 mm from bregma, and dorsal/ventral: −8.5 mm from the surface of the skull; Wu et al., 2011; Xie et al., 2022). Then, the animals received 5–7 days of recovery. The regions of the representative cannula placements in the basolateral amygdala as shown in the rostral faces of each coronal section (see Figure 1).

Behavioral procedures

Heroin SA training

Heroin SA training procedures were established in previous studies (Xue et al., 2012; Luo et al., 2015). Two nosepoke operandi (active/inactive) were placed 9 cm above the floor of the chambers (AniLab Software and Instruments Co., Ltd., Ningbo, China). As a result of nosepoke into the

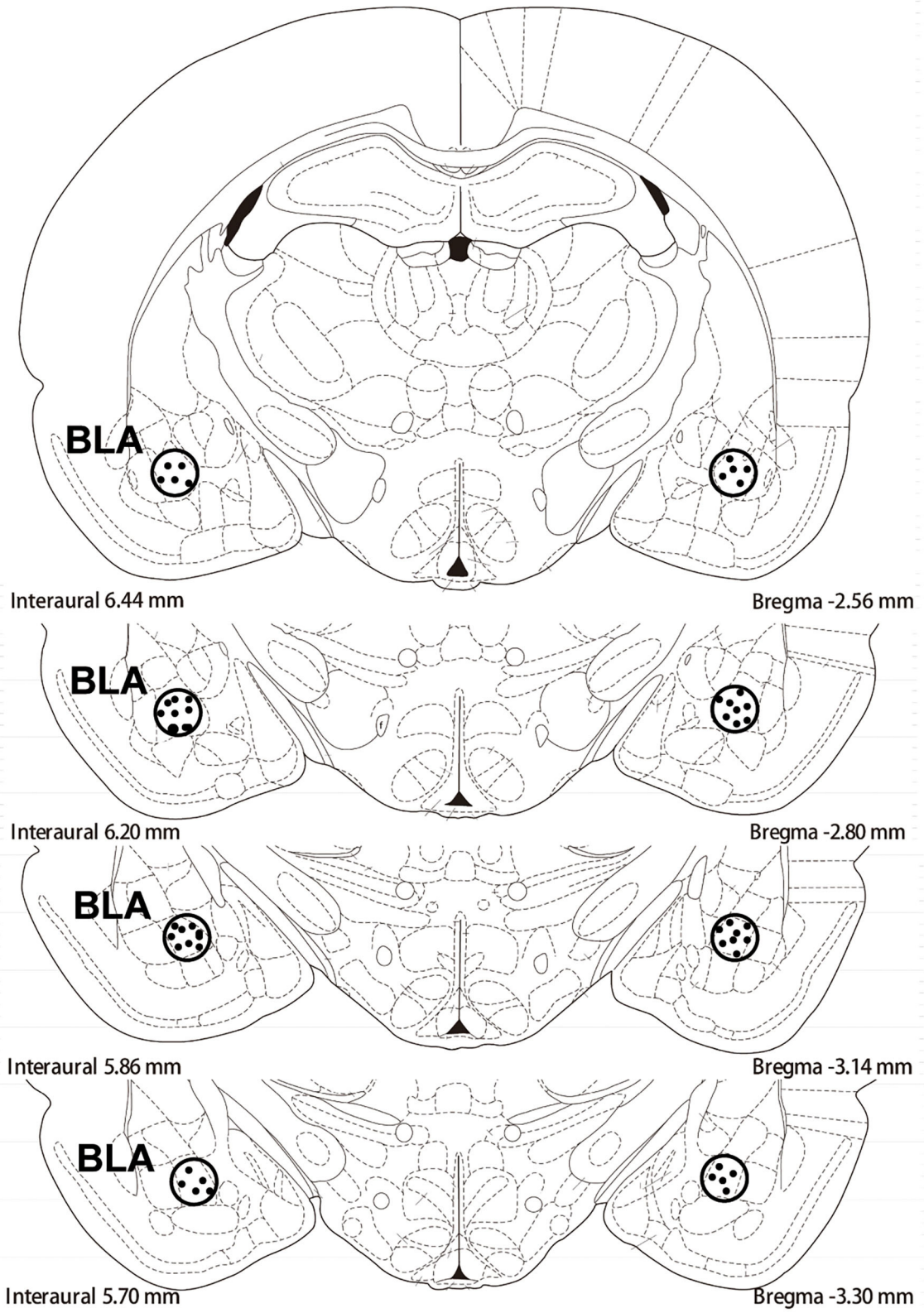

FIGURE 1
The schematic depiction of the region basolateral amygdala (BLA) of cannula placements: −2.8 mm from bregma.

active operandum, rats received heroin infusions paired with tone/light cues for 5 s. As a result of nosepoke into the inactive operandum, there was no consequence.

The heroin SA training session was carried out every 10 days, and the rats received three 1-h training sessions separated by 5 min. The training used a 1:1 fixed-ratio reinforcement schedule at the start of each dark cycle. Every infusion was followed by a 40 s period that had no consequence of nosepoke. The house light was turned on at each session. A maximum of 20 heroin infusions per hour were permitted (Xue et al., 2012; Luo et al., 2015).

Nosepoke extinction

Rats then underwent extinction training in the original environment for 10 days with no illumination or stimulation after SA in all four experiments. In this situation, nosepoke (active/inactive) resulted in no heroin infusion or tone/light cue consequences.

Heroin reward memory retrieval

A 15-min reactivation experiment was conducted 24 h after the last extinction session under conditions that were similar to those for SA training, except no heroin infusions occurred following active nosepoke (experiments 1, 2, and 4).

U0126 treatment

Immediately after retrieval, U0126 was infused bilaterally (1.0 μg/0.5 μl/side for 2 min; Calbiochem) into the BLA of rats (experiments 1 and 2; Wells et al., 2013). The 10 μl Hamilton syringes were linked to the 28-gauge infusion cannulae (Plastics One). An equal volume of 5% dimethyl sulfoxide (DMSO) was infused into the control rats. In experiment 3, infusions of U0126 or vehicle were administered to rats without reactivating light/tone stimuli. In experiment 4, we infused rats with U0126 or vehicle 6 h after retrieval.

Cue extinction

The cue extinction conditions were the same as those during heroin SA sessions, except for the absence of heroin infusions after the tone/light cue. For experiments 1, 3, and 4, rats were subjected to a 3-h daily cue extinction.

Cue-induced reinstatement test (experiments 1–4)

Twenty-four hours after U0126 or vehicle infusion into the BLA, rats were subjected to this test. The conditions were the same as those for the SA, except that the active nosepoke had contingent tone-light cues but without heroin infusions. The number of active and inactive nosepokes was recorded for one hour.

Heroin-induced reinstatement test (experiments 1, 3, and 4)

After the 5-min heroin infusion [0.25 mg/kg, subcutaneously (sc)], rats were subjected to heroin-induced reinstatement. Conditions were the same as those for the SA, except that active nosepoke was paired with tone/light cues but not heroin. The number of active and inactive nosepokes was recorded for 1 h.

Spontaneous recovery test (experiment 2)

After 28 days of withdrawal, the number of nosepokes (active and inactive) was recorded for 1 h in the same condition as reactivation.

Specific experiments

Experiment 1

The role of immediate post-CS ERK inhibition in the BLA in the subsequent cue-induced and heroin-induced reinstatement of heroin-seeking behavior.

Following the 10-day heroin SA training sessions, the rats received 9 days of nosepoke extinction in the original environment. Twenty-four hours after the last nosepoke extinction, heroin-associated cues were presented for 15 min to reactivate the drug-associated memory. Immediately after retrieval, one group of rats was infused with U0126 intra-BLA bilaterally at 1.0 μg/0.5 μl/side, termed the U0126 group, and another group of rats was infused with vehicle intra-BLA bilaterally at 0.5 μl/side, termed the vehicle group. Twenty-four hours after infusion, a cue-induced reinstatement test was carried out to investigate heroin-seeking behavior in rats. Then, we tested priming-induced reinstatement after 2 days of cue extinction (see Figure 2A).

Experiment 2

The role of immediate post-CS ERK inhibition in the BLA in subsequent cue-induced heroin seeking and spontaneous recovery of heroin-seeking behavior after long-term (28 days) withdrawal.

After heroin SA and nosepoke extinction sessions (same as Experiment 1), rats were allowed to be infused with U0126 (1 μg/0.5 μl/side), and the control group of rats was infused with an equal volume of vehicle following retrieval. Twenty-four hours later, a cue-induced reinstatement test was performed. After 28 days of withdrawal, we tested spontaneous recovery in rats (see Figure 3A).

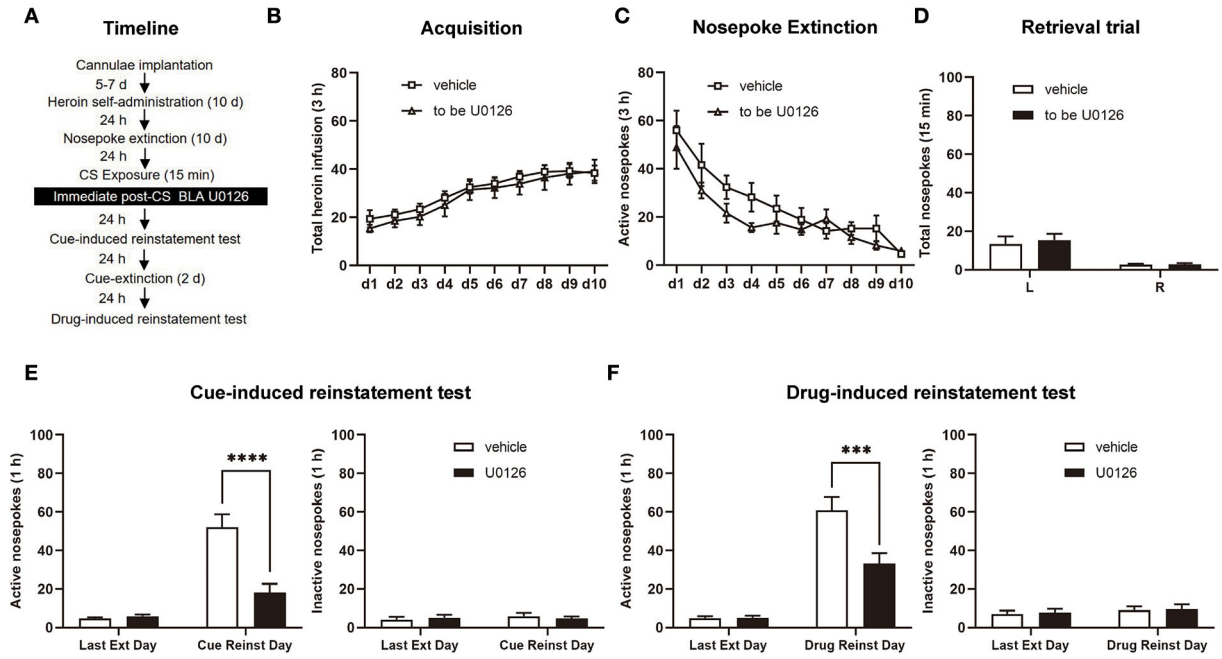

FIGURE 2
Immediate post-CS (conditioned stimulus) U0126 intra-BLA (basolateral amygdala) treatment reduces subsequent cue-induced and heroin-induced reinstatement of heroin seeking. **(A)** Schematic depiction of the experimental procedure. **(B)** Total number of heroin infusions during the acquisition of heroin self-administration. **(C)** Active nosepoke responses during extinction training. **(D)** Total nosepoke responses during a retrieval trial. **(E)** Active **(left)** and inactive **(right)** nosepokes during the last extinction session and cue-induced reinstatement test. **(F)** Active **(left)** and inactive **(right)** nosepokes during the last extinction session and heroin-induced reinstatement test. $n = 8$ rats per group. Data are means ± SEM, ***$p < 0.001$, ****$p < 0.0001$, compared with the vehicle group. CS, conditioned stimulus; Ext, extinction; Reinst, reinstatement.

Experiment 3

The role of ERK inhibition in the BLA without retrieval in subsequent cue-induced and heroin-induced reinstatement of heroin-seeking behavior.

In Experiment 3, the same experimental procedure was performed as in Experiment 1, except that U0126 or vehicle infusion was performed without retrieval (see Figure 4A).

Experiment 4

The role of delayed ERK inhibition in the BLA after retrieval in subsequent cue-induced and heroin-induced reinstatement of heroin-seeking behavior.

We used the same experimental procedure as Experiment 1 in this experiment, except that infusion of U0126 and vehicle was delayed by 6 h after retrieval (see Figure 5A).

Statistical analysis

Two-way/repeated-measures ANOVAs of GraphPad, v.9.0. were used to analyze the results, which are presented as the mean ± SEM (standard error of mean). Treatment type (U0126 or vehicle) was the between-subjects factor, and test type was the within-subjects factor (last extinction day or cue/heroin-induced reinstatement test; see "**Results**"). Tukey's *post hoc* tests were used to analyze significant differences in specific paired comparisons ($p < 0.05$).

Results

Experiment 1: Immediate post-CS ERK inhibition in the BLA reduces subsequent cue-induced and heroin-induced reinstatement of heroin-seeking behavior

To test the role of ERK in the BLA on cue-induced and heroin-induced reinstatement of heroin-seeking behavior, we trained rats in the SA paradigm in experiment 1 (Figure 2A). As the number of total heroin infusions showed, no significant differences were shown between the rats of the vehicle group ($n = 8$) and U0126 group ($n = 8$) in the SA training [main effect of training session: $F_{(9, 126)} = 20.96$, $p < 0.0001$; treatment type: $F_{(1, 14)} = 0.3410$, $p = 0.5685$; training session × treatment type: $F_{(9, 126)} = 0.1519$, $p = 0.9978$; Figure 2B]. In the extinction session, the two groups did not differ from each other in the active nosepoke responses either [main effect of training session:

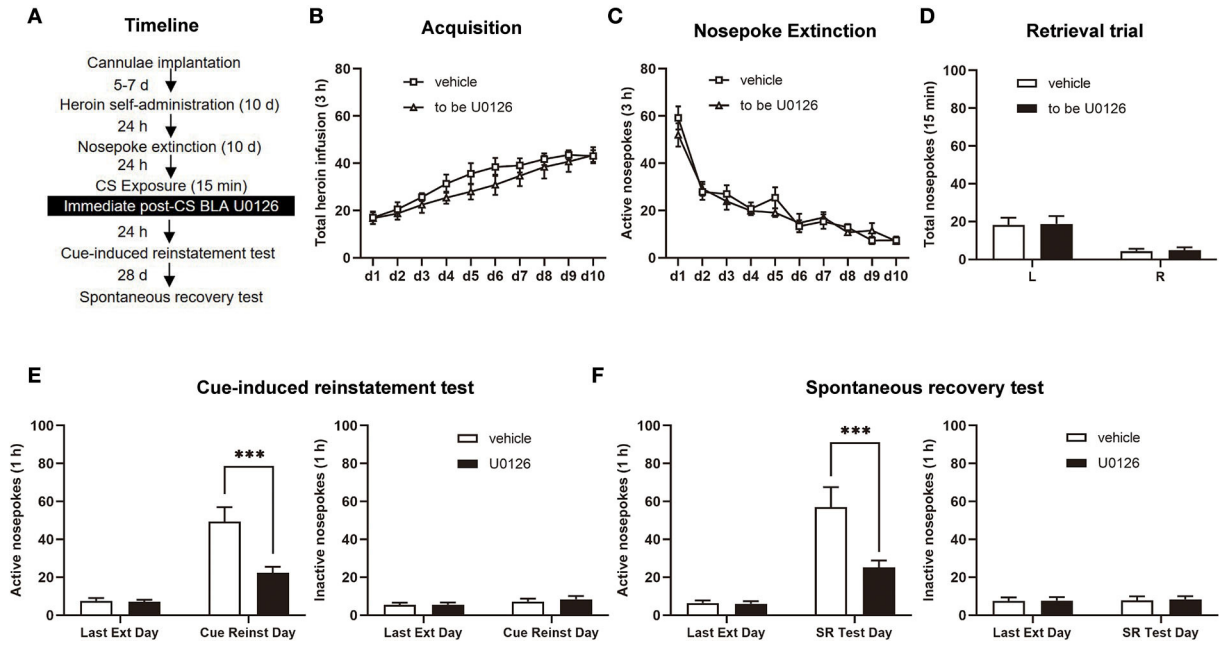

FIGURE 3
Immediate post-CS (conditioned stimulus) U0126 intra-BLA (basolateral amygdala) treatment reduces subsequent cue-induced heroin seeking and the spontaneous recovery of heroin-seeking behavior. **(A)** Schematic depiction of the experimental procedure. **(B)** Total number of heroin infusions during the acquisition of heroin self-administration. **(C)** Active nosepoke responses during extinction training. **(D)** Total nosepoke responses during a retrieval trial. **(E)** Active **(left)** and inactive **(right)** nosepokes during the last extinction session and cue-induced reinstatement test. **(F)** Active **(left)** and inactive **(right)** nosepokes during the last extinction session and spontaneous recovery test. $n = 9$ rats per group. Data are means ± SEM, ***$p < 0.001$, compared with the vehicle group. CS, conditioned stimulus; Ext, extinction; Reinst, reinstatement; SR, spontaneous recovery.

$F_{(9, 126)} = 23.95$, $p < 0.0001$; treatment type: $F_{(1, 14)} = 1.645$, $p = 0.2205$; extinction training × treatment type: $F_{(9, 126)} = 0.9701$, $p = 0.4680$; Figure 2C]. For the retrieval trial, no difference was noticed between the vehicle and U0126 groups in the nosepoke responses [main effect of nosepoke type: $F_{(1, 14)} = 21.23$, $p = 0.0004$; treatment type: $F_{(1, 14)} = 0.1658$, $p = 0.6900$; nosepoke type × treatment type: $F_{(1, 14)} = 0.1366$, $p = 0.7172$; Figure 2D].

A significant difference between the two groups in active nosepokes was revealed by the reinstatement test [main effect of test type: $F_{(1, 14)} = 54.55$, $p < 0.0001$; treatment type: $F_{(1, 14)} = 15.45$, $p = 0.0015$; test type × treatment type: $F_{(1, 14)} = 18.93$, $p = 0.0007$; Figure 2E, left] but not in inactive responses [main effect of test type: $F_{(1, 14)} = 0.6215$, $p = 0.4437$; treatment type: $F_{(1, 14)} = 0.004233$, $p = 0.9490$; test type × treatment type: $F_{(1, 14)} = 1.398$, $p = 0.2567$; Figure 2E, right]. *A post hoc* test was carried out to show a significant reduction in heroin-seeking behavior in the U0126 group compared to the vehicle group ($p < 0.01$; Figure 2E, left). In addition, there was a significant difference between the vehicle and U0126 groups in active responses in the heroin-induced reinstatement test [main effect of test type: $F_{(1, 14)} = 80.27$, $p < 0.0001$; treatment type: $F_{(1, 14)} = 10.79$, $p = 0.0054$; test type × treatment type: $F_{(1, 14)} = 8.866$, $p = 0.0100$; Figure 2F, left] but not inactive nosepoke [main effect of test type: $F_{(1, 14)} = 0.9777$, $p = 0.3396$; treatment type: $F_{(1, 14)} = 0.07692$, $p = 0.7856$; test type × treatment type: $F_{(1, 14)} = 0.004345$, $p = 0.9484$; Figure 2F, right]. A significant reduction in heroin-seeking behavior in the U0126 group compared to the vehicle group was shown by a *post hoc* test ($p < 0.01$; Figure 2F, left column). Therefore, the findings in this experiment suggested that immediate post-CS ERK inhibition in the BLA reduces subsequent cue-induced and heroin-induced reinstatement of heroin-seeking behavior.

Experiment 2: Immediate post-CS ERK inhibition in the BLA reduces subsequent cue-induced heroin-seeking and the spontaneous recovery of heroin-seeking behavior

In experiment 2, we aimed to investigate whether immediate post-CS ERK inhibition in the BLA has an attenuating effect on the subsequent cue-induced heroin seeking and spontaneous recovery of heroin-seeking behavior after long-term withdrawal (28 days; Figure 3A). Between the vehicle group ($n = 9$) and

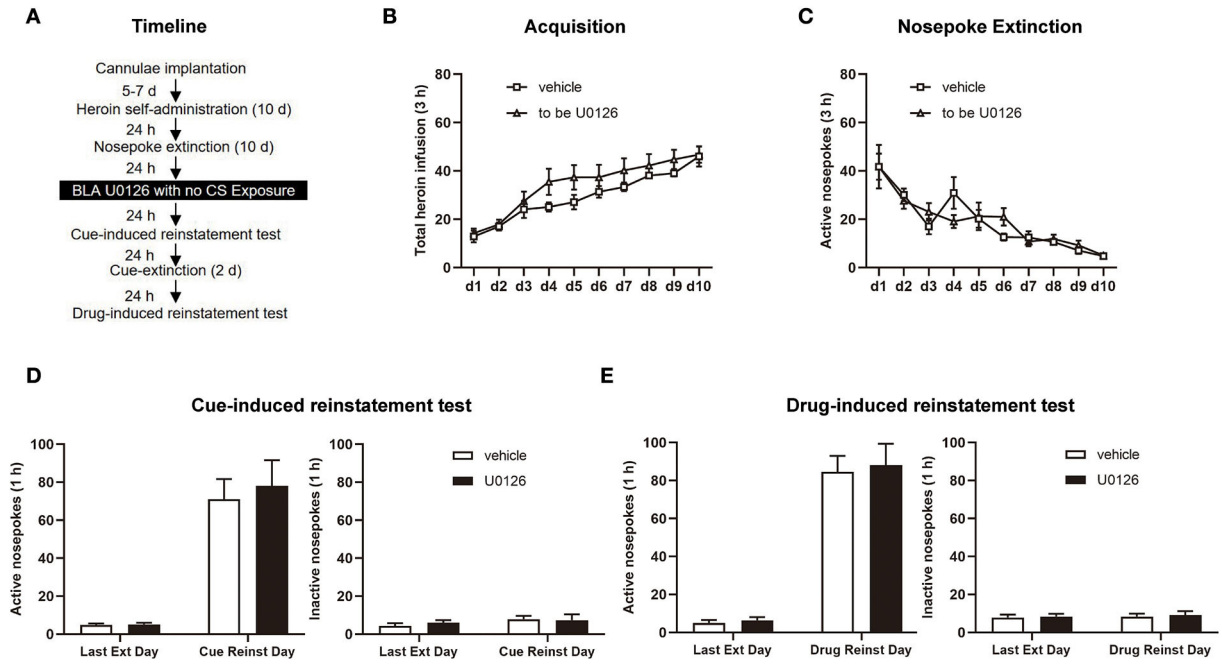

FIGURE 4
U0126 intra-BLA (basolateral amygdala) treatment without retrieval has no effect on subsequent cue-induced and heroin-induced reinstatement of heroin-seeking behavior. **(A)** Schematic depiction of the experimental procedure. **(B)** Total number of heroin infusions during the acquisition of heroin self-administration. **(C)** Active nosepoke responses during extinction training. **(D)** Active **(left)** and inactive **(right)** nosepokes during the last extinction session and cue-induced reinstatement test. **(E)** Active **(left)** and inactive **(right)** nosepokes during the last extinction session and heroin-induced reinstatement test. $n = 8$ rats per group. Data are means ± SEM. CS, conditioned stimulus; Ext, extinction; Reinst, reinstatement.

U0126 group ($n = 9$), no significant difference was observed in heroin SA training [main effect of training session: $F_{(9, 144)} = 32.17$, $p < 0.0001$; treatment type: $F_{(1, 16)} = 1.036$, $p = 0.3240$; training session × treatment type: $F_{(9, 144)} = 0.7004$, $p = 0.7077$; Figure 3B], extinction procedure [main effect of extinction training: $F_{(9, 144)} = 44.50$, $p < 0.0001$; treatment type: $F_{(1, 16)} = 0.5014$, $p = 0.4891$; extinction training × treatment type: $F_{(9, 144)} = 0.7585$, $p = 0.6548$; Figure 3C], or retrieval trial [main effect of nosepoke type: $F_{(1, 16)} = 25.30$, $p = 0.0001$; treatment type: $F_{(1, 16)} = 0.01829$, $p = 0.8941$; nosepoke type × treatment type: $F_{(1, 16)} = 1.035$, $p > 0.9999$; Figure 3D].

In the cue-induced reinstatement test, a significant difference in the two groups was revealed by active nosepoke [main effect of test type: $F_{(1, 16)} = 55.49$, $p < 0.0001$; treatment type: $F_{(1, 16)} = 8.851$, $p = 0.0089$; test type × treatment type: $F_{(1, 16)} = 12.10$, $p = 0.0031$; Figure 3E, left] but not inactive responses [main effect of test type: $F_{(1, 16)} = 1.884$, $p = 0.1888$; treatment type: $F_{(1, 16)} = 0.2839$, $p = 0.6015$; test type × treatment type: $F_{(1, 16)} = 0.09078$, $p = 0.7671$; Figure 3E, right]. The *post hoc* test suggested that there was a significant decrease in active nosepoke in the U0126 group compared to the vehicle group ($p < 0.01$; Figure 3E, left column). In addition, the active nosepoke of the U0126 group in the spontaneous recovery test significantly differed from that of the vehicle group [main effect of test type: $F_{(1, 16)} = 45.77$, $p < 0.0001$; treatment type: $F_{(1, 16)} = 6.844$, $p = 0.0187$; test type × treatment type: $F_{(1, 16)} = 9.361$, $p = 0.0075$; Figure 3F, left] but not inactive nosepoke [main effect of test type: $F_{(1, 16)} = 0.06534$, $p = 0.8015$; treatment type: $F_{(1, 16)} = 0.04214$, $p = 0.8399$; test type × treatment type: $F_{(1, 16)} = 0.007260$, $p = 0.9332$; Figure 3F, right]. A *post hoc* test demonstrated that the active nosepoke of the U0126 group was significantly reduced compared to that of the vehicle group ($p < 0.01$; Figure 3F, left column). The results of experiment 2 suggested that immediate post-CS ERK inhibition in the BLA reduces subsequent cue-induced heroin seeking and spontaneous recovery of heroin-seeking behavior after 28 days of withdrawal.

Experiment 3: ERK inhibition in the BLA without retrieval has no effect on subsequent cue-induced and heroin-induced reinstatement of heroin-seeking behavior

In experiment 3, we examined the role of ERK in the BLA in cue-induced and heroin-induced reinstatement of

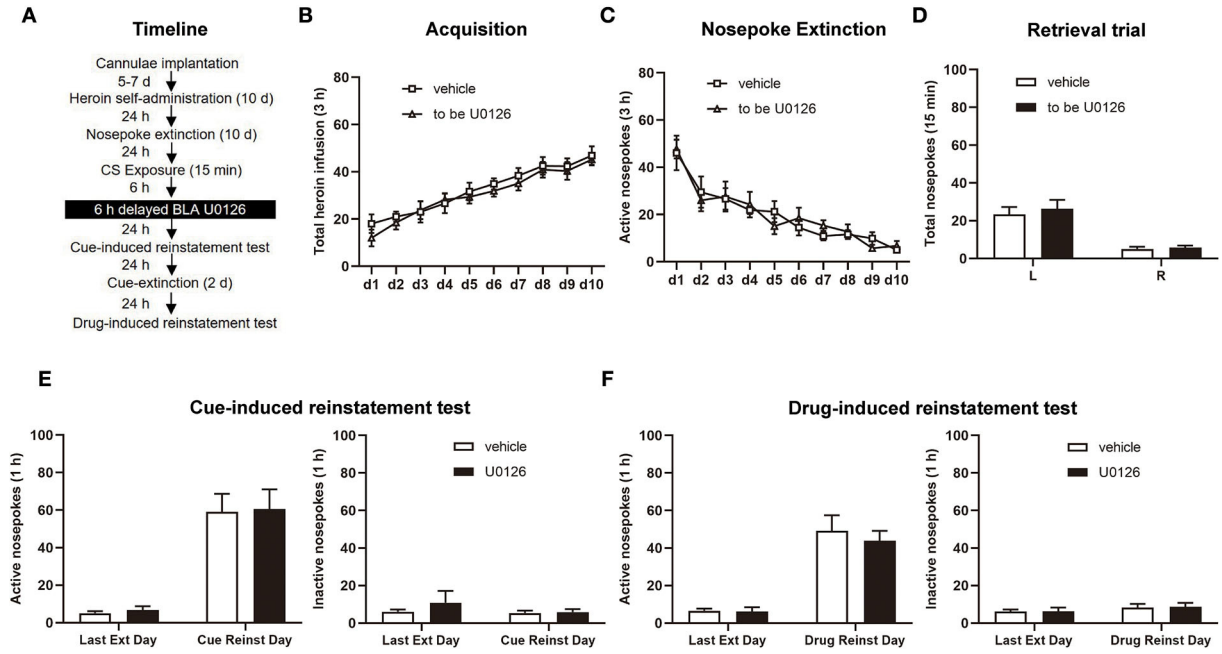

FIGURE 5
Delayed U0126 intra-BLA (basolateral amygdala) treatment following retrieval has no effect on subsequent cue-induced and heroin-induced reinstatement of heroin-seeking behavior. **(A)** Schematic depiction of the experimental procedure. **(B)** Total number of heroin infusions during the acquisition of heroin self-administration. **(C)** Active nosepoke responses during extinction training. **(D)** Total nosepoke responses during a retrieval trial. **(E)** Active **(left)** and inactive **(right)** nosepokes during the last extinction session and cue-induced reinstatement test. **(F)** Active **(left)** and inactive **(right)** nosepokes during the last extinction session and heroin-induced reinstatement test. $n = 8$ rats per group. Data are means ± SEM. CS, conditioned stimulus; Ext, extinction; Reinst, reinstatement.

heroin-seeking behavior with or without retrieval sessions to investigate whether the attenuating effect of ERK inhibition on reconsolidation of heroin-associated memory is retrieval-dependent (Figure 4A). Consistent with experiments 1 and 2, no significant difference was displayed between the vehicle group ($n = 8$) and U0126 group ($n = 8$) groups in SA training [main effect of training session: $F_{(9, 126)} = 38.97$, $p < 0.0001$; treatment type: $F_{(1, 14)} = 1.740$, $p = 0.2084$; training session × treatment type: $F_{(9, 126)} = 1.110$, $p = 0.3606$; Figure 4B] and extinction [main effect of extinction training: $F_{(9, 126)} = 17.83$, $p < 0.0001$; treatment type: $F_{(1, 14)} = 0.02481$, $p = 0.8771$; extinction training × treatment type: $F_{(9, 126)} = 1.067$, $p = 0.3915$; Figure 4C].

However, different from the results of experiment 1, no significant difference was found in the cue-induced reinstatement test [active nosepoke: main effect of test type: $F_{(1, 14)} = 63.98$, $p < 0.0001$; treatment type: $F_{(1, 14)} = 0.1758$, $p = 0.6813$; test type × treatment type: $F_{(1, 14)} = 0.1503$, $p = 0.7040$; Figure 4D, left; inactive nosepoke: main effect of test type: $F_{(1, 14)} = 1.072$, $p = 0.3180$; treatment type: $F_{(1, 14)} = 0.1481$, $p = 0.7061$; test type × treatment type: $F_{(1, 14)} = 0.2171$, $p = 0.6484$; Figure 4D, right] and the drug-induced reinstatement test [active nosepoke: main effect of test type: $F_{(1, 14)} = 128.9$, $p < 0.0001$; treatment type: $F_{(1, 14)} = 0.1220$, $p = 0.7320$; test type × treatment type: $F_{(1, 14)} = 0.02509$, $p = 0.8764$; Figure 4E, left; inactive nosepoke: main effect of test type: $F_{(1, 14)} = 0.1982$, $p = 0.6630$; treatment type: $F_{(1, 14)} = 0.1114$, $p = 0.7435$; test type × treatment type: $F_{(1, 14)} = 0.007928$, $p = 0.9303$; Figure 4E, right] between two groups. The findings of experiment 3 indicated that the attenuating effect of ERK inhibition in the BLA on reconsolidation of heroin-associated memory is retrieval dependent.

Experiment 4: Delayed ERK inhibition in the BLA following retrieval has no effect on subsequent cue-induced and heroin-induced reinstatement of heroin-seeking behavior

Finally, experiment 4 tested whether ERK inhibition out the time window of memory reconsolidation attenuates heroin-seeking behavior in the vehicle group ($n = 8$) and U0126 group ($n = 8$; Figure 5A). Consistent with experiments 1 and 2, there was no significant difference in the heroin SA training [main effect of training session: $F_{(9, 126)} = 26.29$, $p < 0.0001$; treatment type: $F_{(1, 14)} = 0.4818$, $p = 0.4989$; training session × treatment

type: $F_{(9, 126)} = 0.2792$, $p = 0.9793$; Figure 5B], extinction procedure [main effect of extinction training: $F_{(9, 126)} = 20.64$, $p < 0.0001$; treatment type: $F_{(1, 14)} = 0.009984$, $p = 0.9218$; extinction training × treatment type: $F_{(9, 126)} = 0.4540$, $p = 0.9025$; Figure 5C], and retrieval trial [main effect of nosepoke type: $F_{(1, 14)} = 28.74$, $p = 0.0001$; treatment type: $F_{(1, 14)} = 1.661$, $p = 0.2183$; nosepoke type × treatment type: $F_{(1, 14)} = 0.8740$, $p = 0.3657$; Figure 5D].

There was no significant difference between the two groups in cue-induced reinstatement test [active nosepoke: main effect of test type: $F_{(1, 14)} = 55.11$, $p < 0.0001$; treatment type: $F_{(1, 14)} = 0.04952$, $p = 0.8271$; test type × treatment type: $F_{(1, 14)} = 0.0002967$, $p = 0.9865$; Figure 5E, left; inactive nosepoke: main effect of test type: $F_{(1, 14)} = 0.5720$, $p = 0.4620$; treatment type: $F_{(1, 14)} = 0.8282$, $p = 0.3782$; test type × treatment type: $F_{(1, 14)} = 0.3460$, $p = 0.5658$; Figure 5E, right] and the drug-induced reinstatement test [active nosepoke: main effect of test type: $F_{(1, 14)} = 57.05$, $p < 0.0001$; treatment type: $F_{(1, 14)} = 0.3426$, $p = 0.5677$; test type × treatment type: $F_{(1, 14)} = 0.2215$, $p = 0.6452$; Figure 5F, left; inactive nosepoke: main effect of test type: $F_{(1, 14)} = 1.336$, $p = 0.2671$; treatment type: $F_{(1, 14)} = 0.01948$, $p = 0.8910$; test type × treatment type: $F_{(1, 14)} = 0.004124$, $p = 0.9497$; Figure 4F, right]. Thus, the findings of experiment 4 indicated that the attenuating effect of ERK inhibition in the BLA on the reconsolidation of heroin-associated memory is time specific.

Discussion

Available literature has linked the molecule of the neural mechanism to the behavioral effects of repeated drug administration on learning and memory. Our results demonstrated that inhibition of ERK in the BLA immediately after retrieval interferes with heroin-associated memory in an operant heroin SA paradigm.

Our study first identified that ERK in the BLA is critical for reconsolidation of heroin-associated memory in the classical heroin SA paradigm of relapse. The main findings are as follows: (1) Intra-BLA infusion of U0126 immediately after retrieval significantly attenuated the heroin-seeking behavior induced by cues or heroin in rats. (2) The negative regulation of intra-BLA infusion of U0126 immediately after retrieval on heroin-seeking behavior lasting at least 28 days in rats. (3) Intra-BLA infusion of U0126 but with no retrieval manipulation or infusion with a 6-h delay postretrieval blocked the disruption of the reconsolidation of heroin-associated memory by U0126. In summary, our data showed that intra-BLA infusion of U0126 immediately after retrieval of heroin-associated memory has an inhibitory effect on subsequent heroin-seeking behavior, and the inhibitory effects of U0126 are retrieval-dependent and time-limited.

First, we investigated the role of ERK in the reconsolidation of heroin-associated memory. The results showed that intra-BLA infusion of U0126 during reconsolidation (immediately after retrieval of memory) attenuated cue-induced reinstatement test and lasted at least 28 days relative to vehicle rats (Figures 2, 3), the significance of the current results extending the knowledge of the effect of ERK that interference with the reconsolidation of heroin-associated memory produces a long-lasting effect on heroin-seeking behavior. Consistent with these results, previous studies have revealed the negative effect of ERK inhibition on other forms of memory reconsolidation, including conditioned fear memory (Duvarci et al., 2006), object recognition memory (Kelly et al., 2003; Silingardi et al., 2011), and cocaine memory in both Pavlovian cocaine-related memory and response-outcome associative cocaine-related memory (Miller and Marshall, 2005; Valjent et al., 2006; Wells et al., 2013). Notably, intra-BLA infusion of U0126 exerted a lasting attenuation of the retrieval-dependent heroin-associated memory, which can be interpreted as disrupting reconsolidation that reflects interference by the ERK inhibitor with transcription during the time window when memory is reactivated and is labile (Figure 3). In support of this, in experiment 4, we found that an ERK inhibitor does not affect the consequent cue-induced and heroin-induced reinstatement test 6 h after the retrieval session, the time when reconsolidation presumably occurs (Nader et al., 2000). Our experimental results suggest that the activity of ERK in the BLA regulates the reconsolidation of heroin-associated memory, thus disrupting reconsolidation by the ERK inhibitor U0126 significantly reduces heroin-seeking behavior and prevents relapse.

ERK, a mitogen-activated protein kinase, is activated by various cell growth factors and plays an essential role in cell proliferation and differentiation, leading to meaningful connections to higher learning and memory functions (Adams and Sweatt, 2002; Peng et al., 2010). English and Sweatt (1997) were the first to find the role of ERK signaling in synaptic plasticity that inhibited LTP *via* the ERK inhibitor PD98059 (English and Sweatt, 1997). In support of this in drug addiction, the activity of ERK plays a critical role in the incubation, a phenomenon that enhances cue-induced drug seeking after withdrawal period and demonstrates that ERK phosphorylation increased in the central amygdala (CeA) but not the BLA (Lu et al., 2005; Li et al., 2008). In our study, we did not examine the possible role of the CeA in the effect of ERK inhibition on heroin-seeking behavior since the role of the CeA in the reconsolidation of drug memory has been investigated and was not supported (Wang et al., 2008; Wu et al., 2011). Fortunately, our data suggest that the inhibitory effect of U0126 depends on the BLA, which is consistent with Wells et al. (2013) study that ERK in the BLA is critical for context-response–cocaine reconsolidation (Wells et al., 2013). Consolidation of new drug-related memories is ERK dependent (Lu et al., 2006; Jia et al., 2021). Similar findings have been reported that activation of the ERK pathway results in long-term changes in synaptic activity that underlie the consolidation of new memories (Schafe et al.,

2000; Rodrigues et al., 2004; Feld et al., 2005; Lai et al., 2014). Most relevant to our study is that ERK has been reported to be required for memory reconsolidation. In Kelly et al. (2003) demonstrated that ERK in the hippocampal circuitry is required for the reconsolidation of object recognition memory (Kelly et al., 2003). Since then, many laboratories have tested the ability of ERK inhibition to disrupt reconsolidation in other forms of memory, such as auditory fear memory, Pavlovian cocaine-related memory, and instrumental associative cocaine-related memory (Miller and Marshall, 2005; Duvarci et al., 2006; Valjent et al., 2006; Wells et al., 2013). In brief, the above studies hypothesize that ERK may mediate the reconsolidation of heroin-associated memory, regulating various gene expressions to change addictive behavior. Moreover, our data showed that the negative effects of ERK inhibitors on reconsolidation across drug classes are exciting for treating substance use disorders.

Recently, researchers have investigated the role of ERK in reconsolidation-related phenomena. In Rabinovich Orlandi et al. (2020) found that memory reconsolidation is mediated by a "behavioral tagging" process, a behavioral analog of the capture hypothesis and synaptic tagging (Frey and Morris, 1997; Rabinovich Orlandi et al., 2020). Behavioral tagging, whether it acts as a fundamental mechanism underlying drug memory reconsolidation, needs further investigation. Interestingly, a recent study demonstrated that activation of the ERK signaling pathway can change the memory process from reconsolidation to extinction and act as a switch that controls the reconsolidation of fear memory (Fukushima et al., 2021). Furthermore, the ERK 1/2 pathway participates in synthesizing plasticity-related proteins required for spatial memory reconsolidation but is not involved in the tag-setting process. These findings suggest a new strategy that prevents the induction of reconsolidation by activating the ERK signaling pathway.

Together, our data suggest that disruption or modulation of the reconsolidation of heroin-associated memory *via* an ERK inhibitor may serve as a promising option for treating relapse in opiate addicts. This study extends earlier studies showing that ERK activity affects the reconsolidation of drug-related memory, yet its effectiveness in treating clinical populations remains to be tested. It is important to understand further the molecular and cellular mechanisms underlying the reconsolidation of heroin-associated memory to develop target-specific methods for the treatment of opiate addicts.

Data availability statement

The raw data supporting the conclusions of this article will be made available by the authors, without undue reservation.

Ethics statement

The animal study was reviewed and approved by the Xiangya Hospital Ethics Committee, Xiangya Hospital (Changsha, China).

Author contributions

ZC, SC, and HL designed and supervised this study. HL, TH, YZ, ZZ, and QL carried out the main experiments. HL, TH, and YZ prepared the manuscript. ZZ and QL analyzed the data. ZC and SC contributed to manuscript revision with contributions from the other authors. All authors contributed to the article and approved the submitted version.

Funding

This work was financially supported by National Natural Science Foundation of China (Grant No. 82101247) and the Natural Science Foundation of Hunan Province, China (Grant No. 2021JJ40999).

Conflict of interest

The authors declare that the research was conducted in the absence of any commercial or financial relationships that could be construed as a potential conflict of interest.

Publisher's note

References

Adams, J. P., and Sweatt, J. D. (2002). Molecular psychology: roles for the ERK MAP kinase cascade in memory. *Annu. Rev. Pharmacol. Toxicol.* 42, 135–163. doi: 10.1146/annurev.pharmtox.42.082701.145401

Barak, S., and Goltseker, K. (2021). Targeting the reconsolidation of licit drug memories to prevent relapse: focus on alcohol and nicotine. *Int. J. Mol. Sci.* 15, 22. doi: 10.3390/ijms22084090

Bender, B. N., and Torregrossa, M. M. (2020). Molecular and circuit mechanisms regulating cocaine memory. *Cell. Mol. Life Sci*. 77, 3745–3768. doi: 10.1007/s00018-020-03498-8

Brown, T. E., Lee, B. R., and Sorg, B. A. (2008). The NMDA antagonist MK-801 disrupts reconsolidation of a cocaine-associated memory for conditioned place preference but not for self-administration in rats. *Learn Mem*. 15, 857–865. doi: 10.1101/lm.1152808

Chen, L., Huang, S., Yang, C., Wu, F., Zheng, Q., Yan, H., et al. (2021a). Blockade of beta-adrenergic receptors by propranolol disrupts reconsolidation of drug memory and attenuates heroin seeking. *Front. Pharmacol*. 12, 686845. doi: 10.3389/fphar.2021.686845

Chen, L., Yan, H., Wang, Y., He, Z., Leng, Q., Huang, S., et al. (2021b). The mechanisms and boundary conditions of drug memory reconsolidation. *Front. Neurosci*. 15, 717956. doi: 10.3389/fnins.2021.717956

Childress, A. R., Mozley, P. D., McElgin, W., Fitzgerald, J., Reivich, M., O'Brien, C. P., et al. (1999). Limbic activation during cue-induced cocaine craving. *Am. J. Psychiatry*. 156, 11–18. doi: 10.1176/ajp.156.1.11

Crombag, H. S., Bossert, J. M., Koya, E., and Shaham, Y. (2008). Review. Context-induced relapse to drug seeking: a review. *Philos. Trans. R. Soc. Lond B. Biol. Sci*. 363, 3233–3243. doi: 10.1098/rstb.2008.0090

Duvarci, S., Mamou, C. B., and Nader, K. (2006). Extinction is not a sufficient condition to prevent fear memories from undergoing reconsolidation in the basolateral amygdala. *Eur J Neurosci.*;24, 249–260. doi: 10.1111/j.1460-9568.2006.04907.x

English, J. D., and Sweatt, J. D. (1997). A require ment for the mitogen-activated protein kinase cascade in hippocampal long term potentiation. *J. Bio.l Chem*. 272, 19103–19106. doi: 10.1074/jbc.272.31.19103

Feld, M., Dimant, B., Delorenzi, A., Coso, O., and Romano, A. (2005). Phosphorylation of extra-nuclear ERK/MAPK is required for long-term memory consolidation in the crab Chasmagnathus. *Behav. Brain. Res*.158, 251–261. doi: 10.1016/j.bbr.2004.09.005

Frey, U., and Morris, R. G. (1997). Synaptic tagging and long-term potentiation. *Nature*. 385, 533–536. doi: 10.1038/385533a0

Fricks-Gleason, A. N., and Marshall, J. F. (2008). Post-retrieval beta-adrenergic receptor blockade: effects on extinction and reconsolidation of cocaine-cue memories. *Learn Mem*. 15, 643–648. doi: 10.1101/lm.1054608

Fukushima, H., Zhang, Y., Archbold, G., Ishikawa, R., Nader, K., Kida, S., et al. (2014). Enhancement of fear memory by retrieval through reconsolidation. *Elife* 3, e02736. doi: 10.7554/eLife.02736

Fukushima, H., Zhang, Y., and Kida, S. (2021). Active transition of fear memory phase from reconsolidation to extinction through erk-mediated prevention of reconsolidation. *J Neurosci*. 41, 1288–1300. doi: 10.1523/JNEUROSCI.1854-20.2020

Gardner, E. L. (2011). Addiction and brain reward and antireward pathways. *Adv. Psychosom. Med*. 30, 22–60. doi: 10.1159/000324065

Hyman, S. E., Malenka, R. C., and Nestler, E. J. (2006). Neural mechanisms of addiction: the role of reward-related learning and memory. *Annu. Rev. Neurosci*. 29, 565–598. doi: 10.1146/annurev.neuro.29.051605.113009

Jia, W., Kawahata, I., Cheng, A., and Fukunaga, K. (2021). The role of CaMKII and ERK signaling in addiction. *Int. J. Mol. Sci*. 20, 22. doi: 10.3390/ijms22063189

Jian, M., Luo, Y. X., Xue, Y. X., Han, Y., Shi, H. S., Liu, J. F., et al. (2014). eIF2alpha dephosphorylation in basolateral amygdala mediates reconsolidation of drug memory. *J Neurosci*. 34, 10010–10021. doi: 10.1523/JNEUROSCI.0934-14.2014

Kelly, A., Laroche, S., and Davis, S. (2003). Activation of mitogen-activated protein kinase/extracellular signal-regulated kinase in hippocampal circuitry is required for consolidation and reconsolidation of recognition memory. *J. Neurosci*. 23, 5354–5360. doi: 10.1523/JNEUROSCI.23-12-05354.2003

Kida, S., Josselyn, S. A., de Ortiz, S. P., Kogan, J. H., Chevere, I., Masushige, S. et al. (2002). CREB required for the stability of new and reactivated fear memories. *Nat. Neurosci*. 5, 348–355. doi: 10.1038/nn819

Lai, T. W., Zhang, S., and Wang, Y. T. (2014). Excitotoxicity and stroke: identifying novel targets for neuroprotection. *Prog. Neurobiol*. 115, 157–188. doi: 10.1016/j.pneurobio.2013.11.006

Leal, G., Comprido, D., and Duarte, C. B. (2014). BDNF-induced local protein synthesis and synaptic plasticity. *Neuropharmacology* 76, 639–656. doi: 10.1016/j.neuropharm.2013.04.005

Li, F. Q., Xue, Y. X., Wang, J. S., Fang, Q., Li, Y. Q., Zhu, W. L., et al. (2010). Basolateral amygdala cdk5 activity mediates consolidation and reconsolidation of memories for cocaine cues. *J. Neurosci*. 30, 10351–10359. doi: 10.1523/JNEUROSCI.2112-10.2010

Li, Y. Q., Li, F. Q., Wang, X. Y., Wu, P., Zhao, M., Xu, C. M., et al. (2008). Central amygdala extracellular signal-regulated kinase signaling pathway is critical to incubation of opiate craving. *J. Neurosci*. 28, 13248–13257. doi: 10.1523/JNEUROSCI.3027-08.2008

Liang, J., Li, J. L., Han, Y., Luo, Y. X., Xue, Y. X., Zhang, Y., et al. (2017). Calpain-GRIP signaling in nucleus accumbens core mediates the reconsolidation of drug reward memory. *J. Neurosci*. 37, 8938–8951. doi: 10.1523/JNEUROSCI.0703-17.2017

Lin, X., Deng, J., Yuan, K., Wang, Q., Liu, L., Bao, Y., et al. (2021). Neural substrates of propranolol-induced impairments in the reconsolidation of nicotine-associated memories in smokers. *Transl. Psychiatry*. 11, 441. doi: 10.1038/s41398-021-01566-6

Lu, L., Hope, B. T., Dempsey, J., Liu, S. Y., Bossert, J. M., Shaham, Y., et al. (2005). Central amygdala ERK signaling pathway is critical to incubation of cocaine craving. *Nat. Neurosci*. 8, 212–219. doi: 10.1038/nn1383

Lu, L., Koya, E., Zhai, H., Hope, B. T., and Shaham, Y. (2006). Role of ERK in cocaine addiction. *Trends Neurosci*. 29, 695–703. doi: 10.1016/j.tins.2006.10.005

Luo, Y. X., Xue, Y. X., Liu, J. F., Shi, H. S., Jian, M., Han, Y., et al. (2015). A novel UCS memory retrieval-extinction procedure to inhibit relapse to drug seeking. *Nat. Commun*. 6, 7675. doi: 10.1038/ncomms8675

Miller, C. A., and Marshall, J. F. (2005). Molecular substrates for retrieval and reconsolidation of cocaine-associated contextual memory. *Neuron*. 47, 873–884. doi: 10.1016/j.neuron.2005.08.006

Milton, A. L., and Everitt, B. J. (2010). The psychological and neurochemical mechanisms of drug memory reconsolidation: implications for the treatment of addiction. *Eur. J. Neurosci*. 31, 2308–2319. doi: 10.1111/j.1460-9568.2010.07249.x

Milton, A. L., Lee, J. L., Butler, V. J., Gardner, R., and Everitt, B. J. (2008). Intra-amygdala and systemic antagonism of NMDA receptors prevents the reconsolidation of drug-associated memory and impairs subsequently both novel and previously acquired drug-seeking behaviors. *J. Neurosci*. 28, 8230–8237. doi: 10.1523/JNEUROSCI.1723-08.2008

Nader, K., Schafe, G. E., and Le Doux, J. E. (2000). Fear memories require protein synthesis in the amygdala for reconsolidation after retrieval. *Nature*. 406, 722–726. doi: 10.1038/35021052

Peng, S., Zhang, Y., Zhang, J., Wang, H., and Ren, B. (2010). ERK in learning and memory: a review of recent research. *Int. J. Mol. Sci*. 11, 222–232. doi: 10.3390/ijms11010222

Rabinovich Orlandi, I., Fullio, C. L., Schroeder, M. N., Giurfa, M., Ballarini, F., Moncada, D., et al. (2020). Behavioral tagging underlies memory reconsolidation. *Proc. Natl. Acad. Sci. USA*. 117, 18029–18036. doi: 10.1073/pnas.2009517117

Rodrigues, S. M., and Schafe, G. E., LeDoux, J. E. (2004). Molecular mechanisms underlying emotional learning and memory in the lateral amygdala. *Neuron*. 44, 75–91. doi: 10.1016/j.neuron.2004.09.014

Sanchez, H., Quinn, J. J., Torregrossa, M. M., and Taylor, J. R. (2010). Reconsolidation of a cocaine-associated stimulus requires amygdalar protein kinase A. *J. Neurosci*. 30, 4401–4407. doi: 10.1523/JNEUROSCI.3149-09.2010

Schafe, G. E., Atkins, C. M., Swank, M. W., Bauer, E. P., and Sweatt, J. D., LeDoux, J. E. (2000). Activation of ERK/MAP kinase in the amygdala is required for memory consolidation of pavlovian fear conditioning. *J. Neurosci*. 20, 8177–8187. doi: 10.1523/JNEUROSCI.20-21-08177.2000

Silingardi, D., Angelucci, A., De Pasquale, R., Borsotti, M., Squitieri, G., Brambilla, R., et al. (2011). ERK pathway activation bidirectionally affects visual recognition memory and synaptic plasticity in the perirhinal cortex. *Front. Behav. Neurosci*. 5, 84. doi: 10.3389/fnbeh.2011.00084

Sorg, B. A. (2012). Reconsolidation of drug memories. *Neurosci. Biobehav. Rev*. 36, 1400–1417. doi: 10.1016/j.neubiorev.2012.02.004

Sweatt, J. D. (2001). The neuronal MAP kinase cascade: a biochemical signal integration system subserving synaptic plasticity and memory. *J. Neurochem*. 76, 1–10. doi: 10.1046/j.1471-4159.2001.00054.x

Tronel, S., Milekic, M. H., and Alberini, C. M. (2005). Linking new information to a reactivated memory requires consolidation and not reconsolidation mechanisms. *PLoS Biol*. 3, e293. doi: 10.1371/journal.pbio.0030293

Valjent, E., Corbille, A. G., Bertran-Gonzalez, J., Herve, D., and Girault, J. A. (2006). Inhibition of ERK pathway or protein synthesis during reexposure to drugs of abuse erases previously learned place preference. *Proc. Natl. Acad. Sci. USA*. 103, 2932–2937. doi: 10.1073/pnas.0511030103

Volkow, N. D., Michaelides, M., and Baler, R. (2019). The neuroscience of drug reward and addiction. *Physiol. Rev*. 99, 2115–2140. doi: 10.1152/physrev.00014.2018

Wang, X. Y., Zhao, M., Ghitza, U. E., Li, Y. Q., and Lu, L. (2008). Stress impairs reconsolidation of drug memory *via* glucocorticoid receptors in the basolateral amygdala. *J. Neurosci.* 28, 5602–5610. doi: 10.1523/JNEUROSCI.0750-08.2008

Wells, A. M., Arguello, A. A., Xie, X., Blanton, M. A., Lasseter, H. C., Reittinger, A. M., et al. (2013). Extracellular signal-regulated kinase in the basolateral amygdala, but not the nucleus accumbens core, is critical for context-response-cocaine memory reconsolidation in rats. *Neuropsychopharmacology.* 38, 753–762. doi: 10.1038/npp.2012.238

Wells, A. M., Xie, X., Higginbotham, J. A., Arguello, A. A., Healey, K. L., Blanton, M., et al. (2016). Contribution of an SFK-mediated signaling pathway in the dorsal hippocampus to cocaine-memory reconsolidation in rats. *Neuropsychopharmacology* 41, 675–685. doi: 10.1038/npp.2015.217

Wu, P., Xue, Y. X., Ding, Z. B., Xue, L. F., Xu, C. M., Lu, L., et al. (2011). Glycogen synthase kinase 3beta in the basolateral amygdala is critical for the reconsolidation of cocaine reward memory. *J. Neurochem.* 118, 113–125. doi: 10.1111/j.1471-4159.2011.07277.x

Xie, Y., Zhang, Y., Hu, T., Zhao, Z., Liu, Q., Li, H., et al. (2022). Inhibition of Glycogen Synthase Kinase 3beta Activity in the Basolateral Amygdala Disrupts Reconsolidation and Attenuates Heroin Relapse. *Front. Mol. Neurosci.* 15, 932939. doi: 10.3389/fnmol.2022.932939

Xue, Y. X., Luo, Y. X., Wu, P., Shi, H. S., Xue, L. F., Chen, C., et al. (2012). A memory retrieval-extinction procedure to prevent drug craving and relapse. *Science* 336, 241–245. doi: 10.1126/science.1215070

Zhang, F., Huang, S., Bu, H., Zhou, Y., Chen, L., Kang, Z., et al. (2021). Disrupting reconsolidation by systemic inhibition of mTOR kinase *via* rapamycin reduces cocaine-seeking behavior. *Front. Pharmacol.* 12, 652865. doi: 10.3389/fphar.2021.652865

Frontiers in
Molecular Neuroscience

Leading research into the brain's molecular structure, design and function

Part of the most cited neuroscience series, this journal explores and identifies key molecules underlying the structure, design and function of the brain across all levels.

Discover the latest Research Topics

See more →

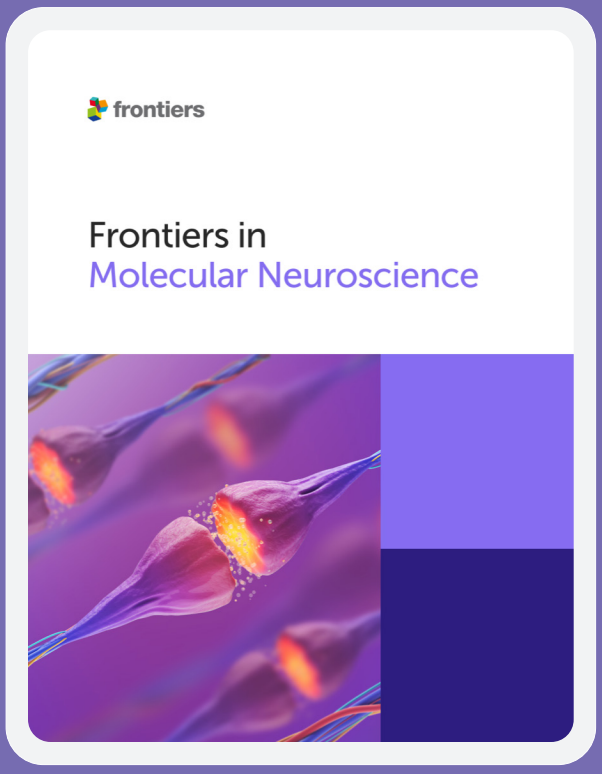

Frontiers

Avenue du Tribunal-Fédéral 34
1005 Lausanne, Switzerland
frontiersin.org

Contact us

+41 (0)21 510 17 00
frontiersin.org/about/contact